Proceedings of the 1st WSEAS International Conference on
ENVIRONMENTAL and GEOLOGICAL
SCIENCE and ENGINEERING (EG'08)

ENVIRONMENT and GEOSCIENCE

Published by WSEAS Press www.wseas.org

Malta, September 11-13, 2008

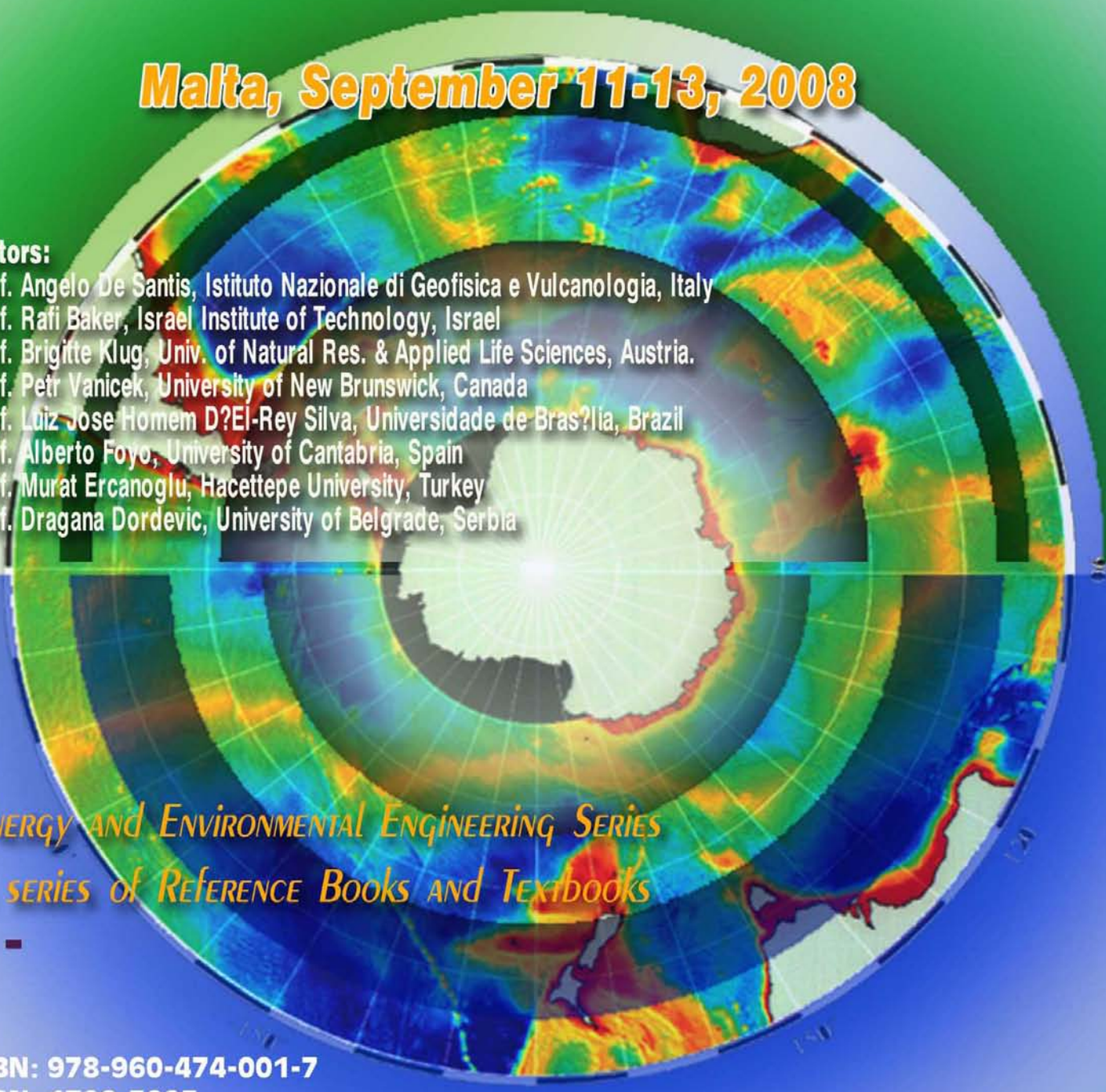

Editors:
Prof. Angelo De Santis, Istituto Nazionale di Geofisica e Vulcanologia, Italy
Prof. Rafi Baker, Israel Institute of Technology, Israel
Prof. Brigitte Klug, Univ. of Natural Res. & Applied Life Sciences, Austria.
Prof. Petr Vanicek, University of New Brunswick, Canada
Prof. Luiz Jose Homem D?El-Rey Silva, Universidade de Bras?lia, Brazil
Prof. Alberto Foyo, University of Cantabria, Spain
Prof. Murat Ercanoglu, Hacettepe University, Turkey
Prof. Dragana Dordevic, University of Belgrade, Serbia

Energy and Environmental Engineering Series
A series of Reference Books and Textbooks

ISBN: 978-960-474-001-7
ISSN: 1790-5095

ENVIRONMENT and GEOSCIENCE

Proceedings of the 1st WSEAS International Conference on ENVIRONMENTAL and GEOLOGICAL SCIENCE and ENGINEERING (EG'08)

Malta, September 11-13, 2008

Energy and Environmental Engineering Series
A series of Reference Books and Textbooks

Published by WSEAS Press
www.wseas.org

ISSN: 1790-5095
ISBN: 978-960-474-001-7

ENVIRONMENT and GEOSCIENCE

Proceedings of the 1st WSEAS International Conference on ENVIRONMENTAL and GEOLOGICAL SCIENCE and ENGINEERING (EG'08)

Malta, September 11-13, 2008

Energy and Environmental Engineering Series
A series of Reference Books and Textbooks

Published by WSEAS Press
www.wseas.org

All papers of the present volume were peer reviewed by two independent reviewers. Acceptance was granted when both reviewers' recommendations were positive.
See also: http://www.worldses.org/review/index.html

ISSN: 1790-5095
ISBN: 978-960-474-001-7

World Scientific and Engineering Academy and Society

ENVIRONMENT and GEOSCIENCE

Proceedings of the 1st WSEAS International Conference on ENVIRONMENTAL and GEOLOGICAL SCIENCE and ENGINEERING (EG'08)

Malta, September 11-13, 2008

Editors:

Prof. Angelo De Santis, Istituto Nazionale di Geofisica e Vulcanologia, Italy
Prof. Rafi Baker, Israel Institute of Technology, Israel
Prof. Brigitte Klug, Univ. of Natural Res. & Applied Life Sciences, Austria.
Prof. Petr Vanicek, University of New Brunswick, Canada
Prof. Luiz Jose Homem D´El-Rey Silva, Universidade de Brasília, Brazil
Prof. Alberto Foyo, University of Cantabria, Spain
Prof. Murat Ercanoglu, Hacettepe University, Turkey
Prof. Dragana Dordevic, University of Belgrade, Serbia

International Program Committee Members:

Kelvin S. Rodolfo, USA
Phaedon C. Kyriakidis, USA
Carlo Vandecasteele, BELGIUM
P De Bievre, BELGIUM
Jean-Paul Bravard, FRANCE
Erick Carlier, FRANCE
Thomas Kohl, SWITZERLAND
Randy Seright, USA
An Li, USA
Hikari Fujii, JAPAN
Yuh-Shan Ho, CHINA
Hasan Tosun, TURKEY
Ahmet Sasmaz, TURKEY
Jean-Yves Parlange, USA
Viney P. Aneja, USA
Marco Mucciarelli, ITALY
Chris Cramer , USA
Tom Rockwell, USA
John Carranza, THE NETHERLANDS
Levent Yilmaz, USA
Hong-Kai Chen, CHINA
Jianmin Chen, CHINA
David Gomez, SPAIN
Julia Lu, CANADA
Stefano Gresta, ITALY
Shiyong Zhou, CHINA
Shaofeng Liu, CHINA
Alberto Foyo, SPAIN
Mandal Prantik, INDIA
Tae-Kyung Hong, SOUTH KOREA
Maria Belarmina Diaz Aguado, SPAIN
André Jasper, BRASIL
Vikrant Chitnis, INDIA
Xiyuan Zhou, CHINA
Paul Fitzgerald, USA
Yoram Eckstein, USA
Eser Durukal, TURKEY
Alfred Stein, THE NETHERLANDS
Zengxi Ge, CHINA
Mustafa Erdik, TURKEY
Hing-Ho Tsang, HONG KONG
Sergei Stanchits, GERMANY
David Schaff, USA
Maria Stella Giammarinaro, ITALY
Fares M. Howari, UAE
Efthimios Karymbalis, GREECE
Tamaz Chelidze, GEORGIA
Gulum Birgoren Tanircan, TURKEY
Rui Pedro Juliao, PORTUGAL
Christos Chalkias, GREECE
Yanbin Wang, CHINA
Mustafa Aktar, TURKEY
Menas Kafatos, USA
Philippe de Donato, FRANCE
Jacek Namiesnik, POLAND
Dimitris Dermatas, USA
W.W.-S. Yim, HONG KONG
Chun-Ho Liu, CHINA
Murat Ercanoglu, TURKEY
Mohamed Obeid, EGYPT
Pasquale Steduto, Italy
Richard Glen, AUSTRALIA
M.F. Loutre, BELGIUM
Serena Pastore, ITALY
Francisco J. Moral, SPAIN
Miguel A. Sánchez, SPAIN
Aurelian Pantea, ROMANIA
Tamara Polubesova, ISRAEL
Angelo De Santis, ITALY
Petr Vanicek, CANADA
Boris Berri, CANADA
Alok Porwal, AUSTRALIA
Sabah A. Abdul-Wahab Al-Sulaiman, OMAN
Giovanni Martinelli, ITALY
Daniele Contini, ITALY
Hung-Yu Chen, TAIWAN
Kees Stigter, CHINA
Francisco H.R. Bezerra, BRAZIL
Saif Ud Din, KUWAIT
R. Latha, INDIA
Suzanne Hecker, USA
Olav Slaymaker, CANADA
Jeff Collett, USA
Samuel Ortega-Farias, CHILE
R. P. Kane, BRAZIL
Hebe Carreras, ARGENTINA
Alexander Rabinovich, CANADA
Tat Leung Chan, HONG KONG
Yang Deng, USA
Concettina Nunziata, ITALY
Jimmy Jiao, HONG KONG
Renato Lancellotta, ITALY
Daniel E. McNamara, USA
Stefan Florin Balan, ROMANIA
Mircea Radulian, ROMANIA
Vladimir Graizer, USA
Ernst D. Schmitter, GERMANY
Constantin Ionescu, ROMANIA
Andrei Bala, ROMANIA
J. R. Kayal, INDIA
Mihaela Popa, ROMANIA

Preface

This book contains the proceedings of the 1st WSEAS International Conference on ENVIRONMENTAL and GEOLOGICAL SCIENCE and ENGINEERING (EG'08) which was held in Malta, September 11-13, 2008. This conference aims to disseminate the latest research and applications in Renewable Energy, Mineral Resources, Natural Hazards and Risks, Environmental Impact Assessment, Urban and Regional Planning Issues, Remote Sensing and GIS, and other relevant topics and applications.

The friendliness and openness of the WSEAS conferences, adds to their ability to grow by constantly attracting young researchers. The WSEAS Conferences attract a large number of well-established and leading researchers in various areas of Science and Engineering as you can see from **http://www.wseas.org/reports**. Your feedback encourages the society to go ahead as you can see in **http://www.worldses.org/feedback.htm**

The contents of this Book are also published in the CD-ROM Proceedings of the Conference. Both will be sent to the WSEAS collaborating indices after the conference: **www.worldses.org/indexes**

In addition, papers of this book are permanently available to all the scientific community via the WSEAS E-Library.

Expanded and enhanced versions of papers published in this conference proceedings are also going to be considered for possible publication in one of the WSEAS journals that participate in the major International Scientific Indices (Elsevier, Scopus, EI, ACM, Compendex, INSPEC, CSA .... see: www.worldses.org/indexes) these papers must be of high-quality (break-through work) and a new round of a very strict review will follow. (No additional fee will be required for the publication of the extended version in a journal). WSEAS has also collaboration with several other international publishers and all these excellent papers of this volume could be further improved, could be extended and could be enhanced for possible additional evaluation in one of the editions of these international publishers.

Finally, we cordially thank all the people of WSEAS for their efforts to maintain the high scientific level of conferences, proceedings and journals.

Table of Contents

Plenary Lecture I

Critical Review of the Physical Foundations of Unsaturated Soil Mechanics

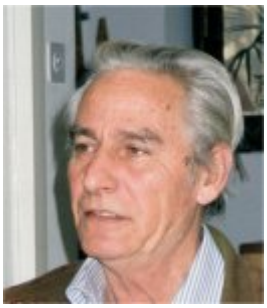

Professor Rafi Baker
Co-author: Professor S. Frydman
Department of Structural Engineering & Construction Management
Faculty of Civil & Environmental Engineering
Technion - Israel Institute of Technology
Haifa, 32000,
ISRAEL

Abstract: Most constitutive models for unsaturated soils are based on identification of matrix (or metric) potential (energy per unit volume) ψ with it's the capillary component $\psi cpl = (ua - uw)$ where {ua, uw} are the pore air pressure and (negative) pore water pressure receptivity. This identification ignores the contribution of adsorption potential ψad to ψ. Identification of a potential with stress (or suction), is questioned, since these quantities have different physical significance despite their common dimensions. Moreover, (ua - uw) is a valid expression for capillary potential only in the simplified and non realistic model of a pore space consisting of a collection of cylindrical capillaries. In reality however the structure of clay soils consists of collection of pods built up of closely spaced parallel plates, and the pods themselves are arranged randomly in space. The water inside these pods is well within the range of adsorption forces, and the adsorption potential should not be ignored. It is noted that unlike the capillary potential, the adsorption potential has no direct interpretation in terms of pressures, and it can not be incorporated directly into mechanical constitutive equations.

Note also that (ua - uw) are not measurable quantities and the only measurable variable is the potential ψ which to a first approximation can be considered as a sum of capillary and adsorption potential, i.e. $\psi = \psi ad + (ua - uw)$. Therefore, neglecting the adsorption potential results in an over estimation of the capillarity component, for a given measured ψ value.

All techniques for measuring ψ are based on the principle that at equilibrium it is the water potentials rather than water pressures that are equal in the soil and the measuring device. It is impossible to measure water tension greater than approximately 0.8-1.0 atm due to cavitation of the water in the measuring device. In order to overcome this technical difficulty, most potential tests in geotechnical engineering utilize the axis translation technique which applies an external air pressure to the sample. This technique "translates" water pressure to the positive range thus preventing cavitation and making it possible to perform the measurement of uw.

Both thermodynamic considerations and direct measurement of ψ using psychrometeric techniques indicate that at low water content ψ is of the order of 10.000 atm. Moreover under usual field conditions air pressure is atmospheric (i.e. ua = 0). Combining the above considerations yields uw = -10.000 atm. In a heterogeneous and cavitation nuclei rich medium like unsaturated clays, the tension stress in the water can not exceed 0.8-1.0 atm due to cavitation of the soil water. Consequently the extremely large tensile stresses in the water implied by the geotechnical approach, are not realistic, and result from neglecting the adsorption potential which does not have a mechanical interpretation, and from the use of the axis translation technique. Introducing such unrealistic water tensions into mechanical constitutive equations is not justified, resulting with various conceptual problems. It is noted that preventing cavitation by applying an elevated air pressure to an unsaturated soil sample, modifies its behavior. Consequently it is doubtful whether constitutive formulations based on experimental information obtained by the axis translation technique are relevant to actual field behavior.

Capillary potential is shown to account for only a small part of matrix potential, the major contribution resulting from water adsorption inside the soil pods, particularly in soils having large specific surface areas. Consideration of double porosity models as well as the adsorption potential appears essential for proper interpretation of unsaturated soil behavior.

The present talk does not present a complete framework overcoming the above mentioned difficulties. However, reference to the strength of unsaturated clay soils supports the above criticism, resulting also with an alternative and simpler formulation than the conventional geotechnical approach. The main purpose of the present talk is to emphasize the distinction between the terms water potential ψ (energy per unit volume), and the stress variable (ua - uw). The confusion between these two terms in the common geotechnical framework is probably the main element preventing the construction of rational and consistent theory describing the mechanical behavior of unsaturated clay soils.

Brief Biography of the Speaker: Baker completed his first and second degrees in the faculty of Civil Engineering of the Technion I.I.T. The 2nd degree was done in the Geotechnical Engineering Department. He did his PhD in the faculty of Agriculture of McGill University, Montreal Canada, in the Dept. of Soil Physics. The subjects of the speaker's 2nd and 3rd degrees dealt with the interface between soil mechanics and soil physics. As a result, of this history he follows both the geotechnical and soil physics literature. The present talk is a result of this dual interest. He received the G.J. Zeitlen price from the Israeli Association of Engineers and Architects, and twice delivered the Kassiff memorial lecture, which is the most prestigious geotechnical lecture in Israel (some of the previous distinguish lecturers include: G.A. Leonards from Purdue Univ., J. Bear from the Technion, S. Marchetti from L'Aquila Univ., D. Fredlund from Saskatchwan Uni., J.B. Burland from Imperial College, R. Goodman from Berkley, M. Randolh from the Univ. of Western Australia, F.H. Kulhawy from Cornell Univ., and I. Moore from Queen's Univ.).

During 1995-1998 he was a member of the International subcommittee on Slope Stability. During 2000-2002 he served as the head, of the Division. of Geotechnical Engineering at the Technion I.I.T.

During 1980-1981 he was a Visiting Professor at VPI & SU. Virginia, USA. During the summer of 1981 he was a Visiting Scholar, in the Geotechnical Research Center of McGill Univ. Montreal, Canada. During the summer of 1983 he was a Visiting Scholar in the Univ. of Arizona, Tucson, Arizona, USA. During 1985-1986 he was Visiting Professor in Carleton Univ. Ottawa, Canada. During the summer of 1997 he was a Visiting Professor, at Kobe Univ. Kobe. Japan. During 2004 he was a visiting professor in North-Carolina University at Chapel-Hill USA (interrupted due to sickness).

Plenary Lecture II

Natural Hazards Induced by Large Intermediate Vrancea Earthquakes in SE Europe

Professor Andrei Bala
Co-author: Mircea Radulian
National Institute for Earth Physics
P.O. Box MG-2, Bucharest-Magurele, Romania

Abstract: Bucharest, the capital of Romania, with more than 2 million inhabitants, is considered after Istanbul the second-most earthquake-endangered metropolis in Europe. It is identified as a natural disaster hotspot by a recent global study of the World Bank and the Columbia University (Dilley et al., 2005). Four major earthquakes with moment-magnitudes between 6.9 and 7.7 hit Bucharest in the last 65 years. The most recent destructive earthquake of 4. March 1977, with a moment magnitude of 7.4, caused about 1.500 casualties in the capital alone. All disastrous earthquakes are generated within a small epicentral area – the Vrancea region - about 150 km north of Bucharest (Fig. 1). Thick unconsolidated sedimentary layers in the area of Bucharest amplify the arriving seismic shear-waves causing severe destruction. Thus, disaster prevention and mitigation of earthquake effects is an issue of highest priority for Bucharest and its population.

The studies done after this earthquake had shown the importance of the surface geological structure upon ground motion parameters. New seismic measurements are performed in Bucharest area with the purpose of defining better elastic and dynamic properties of the shallow sedimentary rocks. Down-hole seismic measurements were performed in a number of 10 cased boreholes drilled in the Bucharest City area. Processing and interpretation of the data lead to the conclusion that shallow sedimentary rocks can be considered weak in the area, down to 150 - 200 m depth. Seismic wave velocity values and bulk density values presented in the paper associated with local geology are useful primary data in the seismic microzonation of Bucharest City. They are used as 1D models to derive transfer functions and response spectra for the stack of sedimentary rocks in several parts of Bucharest area, leading to a better knowledge of the local site amplification and associated frequency spectra. The last chapter is dedicated to the data acquired in 20 sites in Bucharest City and to compute the spectral ratio of the noise. The obtained ratios confirm the previous results, showing a dominant resonance in the period range of 1.25 - 1.75 seconds. The average period of these maxima is 1.47 ± 0.20 s, while the average amplitude is 2.5. Our results bring evidence of the applicability of the ambient noise measurements for the risk assessment studies.

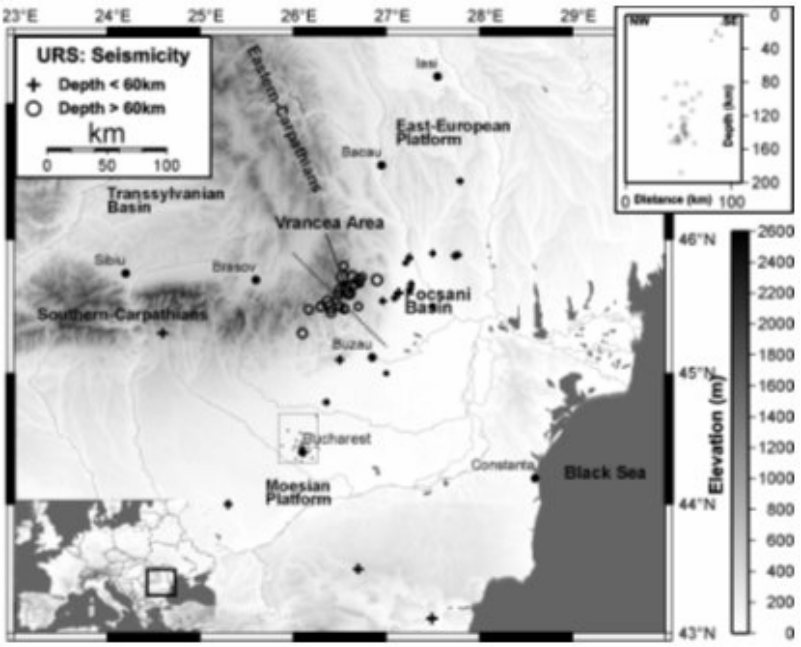

Fig. 1: General map of study region. Strong earthquakes occur at depth below the Vrancea area which corresponds roughly to the southeastern bend of the Carpathian mountains. The seismic waves cause severe damage in Bucharest, about 150 km to the south. The map shows the distribution of epicenters during the URS (URban Seismology) experiment. The cross-section in the upper right corner shows the distribution of hypocenters along a NW-SE cross-section (dotted line in the map).

Plenary Lecture III

The Paleontological History of Wildfire: An Important Tool to Define Fluctuations in the Atmospheric Composition

Professor André Jasper
Botanica, Paleobotanica e Evolucao de Biomas
PPG - Ambiente e Desenvolvimento
Centro de Ciencias Biologicas e da Saude
Museu de Ciencias Naturais
Setor de Botanica e Paleobotanica
Rua Avelino Tallini, 171
Bairro Universitario, Lajeado
Rio Grande do Sul, Brasil
E-mail: ajasper@univates.br
URL: http://www.univates.br

Abstract: The study of the actual biomes is more and more connected to the environmental processes occurred in its genesis. The actual stability, for the human conditions, is fragile and correlated with an important element: the composition of the atmosphere. In this way, we can observe the recent discussions about the global warming, correlate with the upgrade of the concentration of Carbon in the atmosphere. It is obvious that the human activities have a great influence in the global climatic changes. However, the study of the geological and paleontological registers, can confirm that these changes normally occurred in the Earth's history. One of the most important forms of control of the atmosphere composition is the presence of the "Fire Window", an interval of atmospheric oxygen level (13 to 35%) that permits the occurrence of wildfire. Moreover, if we accept that, over the geologic time, fluctuations in atmospheric gases levels have influenced biological evolution and had an integral role in the feedback mechanisms that governing Earth's biogeochemical cycles, the study of the events is fundamental to establish models for the future. Thus, the evaluation of occurrence, frequency and conditions of palaeowildfires, through study of charcoal (Fig. 1 and 2), a proxy for fire, can contribute for the construction of models that enable a planning of future actions of environmental management.

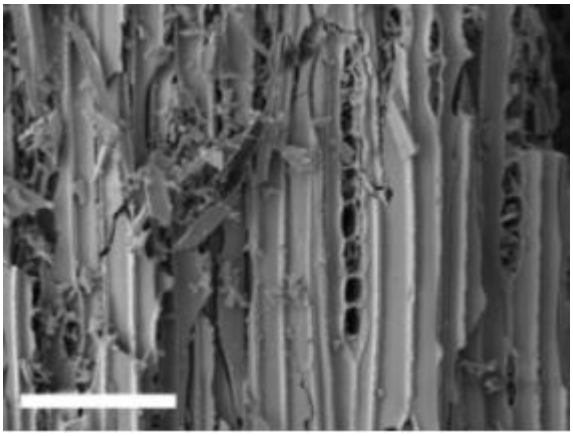

Figure 1: Scanning Electron Micrograph of a charcoal with gimnospermic affinity from the Early Permian of South America (scale bar = 40 μm).

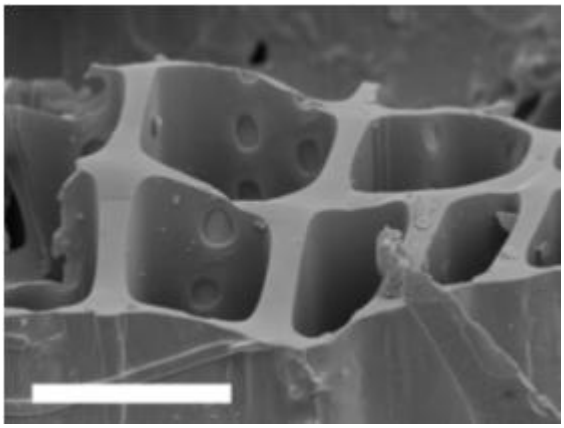

Figure 2: Scanning Electron Micrograph of a charcoal from the Early Permian of South America with the cellular walls indicating a fire of 230 – 340ºC (scale bar = 15 μm).

Brief Biography of the Speaker: Jasper is Biologist in its first degree formation and developed it Master and PhD degrees in Paleobotany at the Geosciences Institute of the Federal University of Rio Grande do Sul (UFRGS), Brazil. Made the Postdoctoral stage at the Geosciences Institute of the University of Tübingen, Germany. His main areas of interest are Paleobotany, Evolution of Terrestrial Biomes and Study of Paleowildfires. In addition he compares the Paleoecological data with the actual situation of the environments to be able to determine differences between the planetary events with natural origin and those caused by human action. Actually he works at the Museum of Natural Sciences of the UNIVATES, Brazil, and is Titular Professor for Paleontology in the same University. He is also Guest Professor at the UNICAMP, Brazil, and at the Halmstad University, Sweden.

Plenary Lecture IV

Evaluating and Planning Waste Landfill Top Covers with the Help of Vegetation and Population Ecology

Professor Brigitte Klug1
Co-authors: Johannes Tintner2, Marion Huber-Humer2
1: Department of Integrative Biology and Biodiversity Research
2: Department of Water, Atmosphere, and Environment
University of Natural Resources and Applied Life Sciences (BOKU)
Gregor-Mendel-Stra?e 33, 1180 Vienna
AUSTRIA

Abstract: The accumulation of solid waste has caused remarkable problems for environment and public health, and authorities have to tackle the costly recycling, reduction, and management of solid waste. Nevertheless, the area occupied by landfills is steadily growing. It is an urgent need to avoid toxic impacts such as landfill gas or leachate arising from old landfills, and to find environmentally friendly after-uses for the sites. The co-operation of botany and waste management shows viable practices for the future: Phytosociological releves of the (spontaneous or seeded) vegetation on old landfills can indicate not only the quality of the top cover, but also gaps in the cover where methane or leachate emerges. This information helps companies and authorities to take appropriate steps of sanitation. Well-kept old landfills may be re-integrated into the production of energy plants or fibre plants. Another possible after-use would be a park for recreation. In this case, special care has to be taken for selecting local tree and shrub species with suitable demands and a superficial root system. In regions where rare ecosystems in the vicinity of a landfill are threatened by extinction, one can think of a re-establishment of those ecosystems. By providing a suitable top cover and introducing species of the threatened ecosystem, it is possible to trigger a succession towards this. Nevertheless, steady monitoring of the vegetation development and the soil seed bank is necessary to guarantee success. A new experimental field for botanists and ecological engineers is re-vegetation on combustion slag. To reduce the volume of waist, some municipalities have chosen this method recently instead of mechanical-biological waste treatment. Re-cultivating combustion slag causes many ecological problems, and this is one of the challenges for the future.

Brief Biography of the Speaker:

Date and place of birth: Jan 6,1947, Innsbruck, Tyrol, Austria.
Studies of botany and zoology, University of Innsbruck, 1966-1973.
Additional studies of forestry, University of Applied Life Sciences and Renewable Resources (BOKU), Vienna, 1973-1974.
1974-1980: Researcher, Austrian Academy of Sciences, Vienna: MaB-High Mountain Project Hohe Tauern
1978: Birth of 1st son
1980-1982: Research Assistant, Institute of Game Research, Veterinary University of Vienna.
1982: Birth of 2nd son.
1986-1991: Research assistant, Institute of Botany, BOKU.
1991: Habilitation.
1991-2007: Assistant professor, Institute of Botany, BOKU.

Fields of research:
Ecology of alpine plants, restoration ecology, diaspore ecology, phenology, production ecology

Latest projects:
2001-…:Symphenology of oak-hornbeam forests in the “Wienerwald” (Vienna forest)
2005: Plant ecological research as a basis for a restoration concept at the landfill site Rautenweg (Vienna)
2005: Actual above ground vegetation and diaspore communities on re-vegetated ski runs in the Austrian Alps.
2006-2007: Diaspore communities in successional states of an oak-hornbeam forest in Lower Austria
2006-2007: Above ground vegetation and diaspore communities on an artificially greened solid waste landfill and in the surrounding semi-dry meadows in Lower Austria.
2007: Influence of pasturage on herbaceous and woody successional plants in the Kamp valley 4 years after the flood disaster.

Plenary Lecture V

An Overview on the Landslide Susceptibility Assessment Techniques

Professor Murat Ercanoglu
Hacettepe University Geological Engineering Department
06800 Beytepe, Ankara
TURKEY

Abstract: Natural disasters and their consequences have considerable and destructive effects on human life, properties, infrastructures, and, of course, on environment. One of the most important natural hazards, landslides play a very important role in these effects throughout the world. Therefore, many countries, particularly the developed ones, invest huge amount of money either in mitigation or in prevention of landslides. The first, and probably the most important, stage of mitigation an/or prevention efforts is to assess landslide susceptibility by obtaining data related to landslides, i.e. preparation of landslide inventory and database. If taken into consideration, results of these assessments, i.e. landslide susceptibility maps, will provide useful information and economic benefits for urban planning, development plans, engineering applications, land use potential planning, and so on. When the international scientific literature related to landslide assessments is examined, there has been an increasing interest in landslide susceptibility mapping studies in the last decades, instead of evaluating hazard and/or risk. Particularly, in recent years, depending upon the breakthroughs in computer technology, GIS (Geographic Information System), and RS (Remote Sensing) techniques, very important developments were achieved in these studies. This can be concluded as one of the most promising efforts with respect to combat with natural hazards since they opened wide range of opportunities for analysing, evaluating, and assessing earth processes, notably for landslides. Thus, there are a multitude of studies carried out by different researchers in different parts of the world with the aid of these technological items.

In this study, it was aimed at assessing landslide susceptibility techniques by means of a detailed literature survey based on an overview including twenty years' experiences. The techniques were categorized into two distinct groups such as qualitative and quantitative ones, and examined individually. By doing so, a historical development of the techniques and actual trends in landslide susceptibility assessments were evaluated. It was revealed that some traditional methods seemed to have disappeared, while the new ones, particularly included in the GIS softwares, became very popular. However, at present, there seems to be no agreement on these techniques which is the most effective among the researchers.

Brief Biography of the Speaker: Murat Ercanoglu is a Geological Engineer, PhD. His main areas of interest are Landslides and Engineering Geology. In addition, he has got experience of utilization GIS, Remote Sensing, and Artificial Intelligence techniques such as fuzzy logic and neural networks for his research. He has been studying on landslides more than 10 years, and he has got national and international papers commonly on this subject. He is working at Hacettepe University Geological Engineering Department (Ankara, Turkey) as an Associate Proffessor in Applied Geology Division.

Plenary Lecture VI

The Method of Sequence Stratigraphy

Professor Octavian Catuneanu
Department of Earth and Atmospheric Sciences
University of Alberta
1-26 Earth Sciences Building
Edmonton, Alberta, T6G 2E3
CANADA

Abstract: Sequence stratigraphy is a modern method of stratigraphic analysis, whereby stratal stacking patterns and facies relationships of sedimentary rocks are studied within a time framework. Sequence stratigraphy is now routinely employed in both academic and industry research, to understand local to global changes in the geological record, to improve the predictability of petroleum, coal and mineral resources exploration, and to optimize the development of petroleum-producing reservoirs.

In spite of its popularity, the sequence stratigraphic method tends to be confusing and hence difficult to apply because of the proliferation of an unnecessarily complicated terminology, with several synonymous terms for the same concept, or similar terms for different concepts. In addition to this, the existence of several different approaches to sequence stratigraphy complicates further its applicability. This paper takes a balanced approach to explaining what is the relationship between all existing approaches, what are the reasons for having this diversity of opinions, and what is the logical way that would help one select the optimum approach for each case study. Ultimately, all current approaches are correct in the context under which they were proposed. The proponents of each model have often used case studies from different sedimentary basins to support their methodology, which explains the difference of opinions that is observed today. The applicability of the sequence stratigraphic model varies with the data set that is available for analysis (e.g., seismic data versus well logs or outcrop), tectonic setting, depositional setting, and the scale of observation. Taking the right decision regarding the method that provides the optimum approach under specific circumstances requires an emphasis on depositional processes rather than terminology or other model-dependent assumptions. This promotes flexibility in the application of sequence stratigraphy, and guides the practitioner through a process-based, model-independent approach.

The lack of formal inclusion of sequence stratigraphy in the current international stratigraphic codes may be attributed largely to trivial differences in terminology and the style of conceptual packaging of the rock record into sequences and systems tracts. The choice of how we name the packages of strata between specific sequence stratigraphic surfaces varies with the model, which is why the systems tract nomenclature becomes less important than the correct identification of the stratal stacking pattern which defines that particular package of strata. Even the selection of what surface (or set of surfaces) should serve as the 'sequence boundary' becomes subjective and trivial to some extent, as the correct interpretation of all sequence stratigraphic surfaces and of the origin of strata that separate them is far more important for the success of the sequence stratigraphic method. Irrespective of the model of choice, the 'pulse' of sequence stratigraphy is fundamentally represented by shoreline shifts, whose type and timing control the formation of all genetic packages of strata (systems tracts) and bounding surfaces. Beyond nomenclatural preferences, each stage of shoreline shift (normal regression, forced regression, transgression) corresponds to the formation of a systems tract with unique characteristics in terms of stratal architecture, sediment dispersal patters and distribution of depositional elements across a sedimentary basin. These fundamental principles are common among all models, and allow for a unified sequence stratigraphic approach. Finding the common ground between the various 'schools' is the key for making real progress towards standardizing the concepts of sequence stratigraphy (Catuneanu, 2006).

Reference:

Catuneanu, O. (2006) Principles of Sequence Stratigraphy. First Edition, Elsevier, Amsterdam, 375 pp.

Brief Biography of the Speaker: Octavian Catuneanu is Professor in the Department of Earth and Atmospheric Sciences at the University of Alberta, with Ph.D. degrees from the University of Toronto (1996) and the University of Bucharest (1992). He is the recipient of several distinctions in the field of Geology, including best paper awards from the Geological Society of America (2002) and the Romanian Academy (1994). Octavian Catuneanu has served as the Chair of the North American Commission on Stratigraphic Nomenclature (2005-2006), the Chair of the Canadian Sedimentology Research Group (a division of the Geological Association of Canada; 2004-2007), and he is the current Chair of the International Working Group on Sequence Stratigraphy (working towards the standardization of sequence stratigraphy in the International Stratigraphic Guide and in the North American Stratigraphic Code). He is the Editor-in-Chief of the Journal of Marine and Petroleum Geology, and also serves on the editorial board of the Journal of African Earth Sciences and as an Associate Editor of the Bulletin of Canadian Petroleum Geology. He is the author of Elsevier's textbook titled "Principles of Sequence Stratigraphy" (Elsevier's best seller in Earth Sciences, and recipient of a CHOICE Award for one of the best reference titles), co-editor or senior editor of several books and special issues, and author of numerous publications in the fields of sedimentology, stratigraphy and basin analysis. He is currently involved in several international research programs and as an instructor of sequence stratigraphy and basin analysis workshops for conferences and companies worldwide.

Plenary Lecture VII

Climate Change (in Sweden)- Geotechnical and Contaminated Land Consequences

Professor Yvonne Andersson-Skold
Co-authors: Carina Hulten, Louise Simonsson-Forsberg, Sofie Storbjork
Swedish Geotechnical Institute (SGI)
Goteborg,
SWEDEN

Abstract: According to climate scenarios the global mean temperature will increase the nearest 50 to 100 year. Based on regional climate models the annual precipitation and heavy rain events in most parts of Sweden will consequently increase. The risks for flooding will increase. Also the risks of erosion and landslide are expected to increase as well changed behaviour and increased mobility of soil contaminants. The summer season in general is expected to become drier. There consequently is expected to be larger fluctuations of groundwater levels further enhancing risks of erosion, land slides and mobility of soil contaminants. One of the areas expected to be among the most affected in Sweden is the Lake Vanern and the Gota alv river system.
The Swedish geotechnical institute has, together with other agencies and universities in Sweden, contributed in the national climate and vulnerability inquiry (SOU 2007:60, Sverige infor klimatforandringarna - hot och mojligheter). The individual contributions are presented in separate appendixes. Here the results from the following reports will be presented:

Impact of Flooding on soil pollutants, Andersson-Skold, Nyberg, Goransson, 2007, Varia 576 & Varia 577, SGI, Statens geotekniska institut 2006. (In Swedish)

Hulten C, Edstam T, Arvidsson O, Nilsson G. 2006. Increased tapping from lake Vanern and related geotechnical conditions in the Gota alv valley. (Geotekniska forutsattningar for okad tappning fran Vanern till Gota alv. Underlag till klimat och sarbarhetsutredningen.) SGI, Statens geotekniska institut 2006. (In Swedish)

Fallsvik, J, Hageryd, A-C, Lind, B, Alexandersson, H, Edsgard, S, Lofling, P, Nordlander, H, 2007, Assessment of erosion and landslides in a changing climate (Oversiktlig bedomning av jordrorelser vid forandrat klimat, preliminar version Dnr 1-0611-0652) (In Swedish)

Based on the results from the national climate and vulnerability inquiry research projects have been initiated. One project focuses on the vulnerability and adaption capacity among municipalities along the Gota alv river system. The project includes eco social, environmental and geotechnical aspects and is done in co-operation by Linkoping University and Swedish Geotechnical Institute. The aim is to present some preliminary results from this project.

Plenary Lecture VIII

The Role of Engineering Geology in the Identification and Evaluation of Geological Risk and their Application in Prehistoric Cave Areas. Three Case Histories

Professor Alberto Foyo
Civil Engineering School
University of Cantabria
SPAIN
E-mail: foyoa@unican.es

Abstract: By means of the traditional geologic approaches as they are the characterization of geologic estratigraphical and structural discontinuities, the petrographic and geomorphological characteristic, the conditions of stability and the elaboration of geological maps, it is possible to define such parameters of geological risk as Natural Risk Index (NRI) and the Safety Factor (SF), and through them, to establish the corresponding protection areas and their characteristics about the different human uses, be already industrial, urbanistic or touristic, to prevent and avoid the geological deterioration of the cavities and, in consequence, of the samples of prehistoric art that content.
The experience and research works in the Altamira Cave and El Castillo Cave Areas in Cantabria, and in the Tito Bustillo Cave Area in Asturias, North of Spain, carried out by the Engineering Geology Group, will be presented.

Brief Biography of the Speaker: Was born on 1949 in Lugo, Galicia, North of Spain. Graduate in Geology (1976) and Doctorate in Geology (1980) in the University of Oviedo, Asturias.

Since 1977, as a member of the Applied Geology Group of the University of Cantabria, participate in many civil engineering projects, mainly in motorways, large dams foundations, geological risk in hydraulic works and, finally, since 1999, in the geological risk research around the main prehistoric caves in the North of Spain. Since 1983, Professor of Engineering Geology in the Civil Engineering School of the University of Cantabria, and since 1993 Prof. of Dam Geology in the Master of Engineering Geology, Geological Faculty of the University of Madrid. Member of the Cantabria International Institute for Prehistoric Research. Actually, Director of the Ground Engineering and Material Sciences Department of the Cantabria University.

Plenary Lecture IX

Are we going towards a Global Planetary Magnetic Change? Possible Scientific Perspectives and Consequences to our Everyday Life

Professor Angelo De Santis
Director of Research
Istituto Nazionale di Geofisica e Vulcanologia, Roma, Italy
and
Professor of Geophysics at
University G. D'Annunzio, Chieti,
ITALY

Abstract: The dipolar part of the geomagnetic field has been decaying rapidly during the last few hundreds of years. In addition to this classical argument, from Information theory applied to geomagnetism, there are some evidences that the recent Earth magnetic field is showing characteristics typical of a reversal in progress. If this is true, many scientific and environmental questions will arise. For instance, it will be of particular interest to monitor the time-space dynamics the South Atlantic Anomaly, where the magnetic field is strongly reduced (a sort of "planetary magnetic hole"). Here we find one of the most favourite places where Low Earth Orbiting (LEO) satellites are lost or present some damages, due to the vicinity of "clouds" of electric particles (Van Allen belts) to the Earth's surface. The decay of the field will also decrease the screening effect to the solar wind and cosmic charges, so enhancing the cosmic radiation illuminating our planet: possible negative consequences are expected in terms of increase of skin cancers. Also important will be the study of the possible evolution of the core dynamics that will be generating this specific condition of the geomagnetic field.

Brief Biography of the Speaker: I have been working since 1977 in the National Institute of Geophysics and Vulcanology of Italy (INGV). I took my Doctor Degree in Physics (1984) at University of Rome (Italy). My main interests are in: a) Models in Earth sciences, with particular attention to geomagnetism; b) Search for nonlinearities in Geophysics; c) Geomagnetic Deep Sounding; d) Potential Field Theory; e) Magnetometry and Riometry. My present position at INGV is as Director of Research (since 1999). I have been Head of Geomagnetism Group for 5 years (from 2000 to 2005). I received a Royal Society 5-month Grant visiting the British Geological Survey (1987). Former Member of INGV Scientific Committee 1999-2005 and former Member of ESA Swarm satellite Mission Advisory Group Phase A. I am presently formal member of INGV and INFN (National Institute of Nuclear Physics of Italy) Committee. Professor of Solid Earth Physics and then Geophysics at Chieti University (from 1998 to present). I have been member of 5 Italian expeditions in Antarctica and I coordinated all scientific activities during the XI Antarctic expedition. I have been responsible of many National and International Projects: Riometry, ARM I, II, REM within the “ItaliAntartide” Program, 1993-2006; bilateral Cooperation Italy-Spain 1994-1996; bilateral Cooperations: Italy-Czech Rep. 1996-1999, Italy-Albania 2002-2004; NATO 1999-2001. Vice-Responsible of Space Weather Project within the “ItaliAntartide” Program, 1996-1999. I coordinate some programmes of research in the framework of Oersted and Champ satellite missions 2001- present. I cooperate with many Italian Universities following graduates and PhD for theses. I also teach some PhD Courses in Geophysics (2000- present). I count around 140 scientific publications (70% are International) and 150 scientific communications at national and international conferences.

Plenary Lecture X

Source Identification using CMB Models and Effects of Emission Control on Reducing Ambient Air Pollution in Industrial City

Professor Dragana Dordevic
Institute for Chemistry, Technology and Metallurgy
Centre of Chemistry
Department of Environment
University of Belgrade
Studentski trg 12 - 16
11001 Belgrade
SERBIA
E-mail: dragadj@chem.bg.ac.yu

Abstract: Harmful substances in the ambient air can be reduced only on condition that their emitters are kept under control. For that purpose it is necessarily to know key points in technological processes that are emitting specific pollutants, the nature of emitters, the link between the emission fluxes on the emitters, meteorological base of the region and the concentration of pollutants at the receptors of ambient air. Atmospheric surface temperature inversions play a significant role in the problem of ambient air pollution since their upper edge acts as a natural barrier to the vertical dispersion of pollutants. In many cases of pollution, there are no prior knowledge of the emission sources, hence Chemical Mass Balance models (CMB) are applied to extract information concerning the sources using minute by minute continuous measurements data of ambient air pollution at the receptors. The results of calculated fingerprints of possibly sources are connecting to real emission sources. Model of investigation was highly industrial city in Serbia (Pančevo), with over 80.000 habitants, where among the rest industries are located oil refinery, petrochemistry and fertilizer factory. The investigated region is characterized by maximum number of surface temperature inversions of atmosphere during the night times and their furlough during the day times in August. Analysis of daily variations contents of pollutants in ambient air show that concentrations of the pollutants from the low altitude emission sources were higher two times and more during the night than daytimes vice verse for pollutants from the high altitude sources. The daily variations of their concentrations show the minimums in the afternoons when is boundary layer at the top point. NH3 in this case origin from high altitude source in fertilizer factory, which is only one in the region, therefore was chosen as a tracer of industrial area influence. CMB models showed the highest associations of pollutants that are constituents of volatile organic compounds from low altitude sources in industrial area. The measures of control of identified emission sources, such as extinguishing key sources, planning of emiters' activities in harmony with meteorological conditions, and at a low rate and simple reconstruction one part of sources in both the refinery and petrochemistry had as the result the reduction of VOCs concentrations in the receptor's part of ambient air for more than twice. The benzene concentrations at the receptors which are under high influence of industrial sources reached in the years 2004 and 2005 the values acceptable with regard to the limit value of the Directive 2000/69/EC.

Brief Biography of the Speaker:
Graduation: 1990, Faculty of Physical Chemistry, University of Belgrade
M.Sc. Thesis: 1996, Faculty of Physical Chemistry, University of Belgrade
Ph.D. Thesis: 2004, Faculty of Chemistry, University of Belgrade

Professional background: Between 1990 and 1991 part-time worked in Institute of General and Physical Chemistry in Belgrade as a Research Assistant. From 1992 to 1999 worked in Institute of Workers Safety, Fire and Environmental Protection, Belgrade as a research associate. Since 1999 has been working in Centre of Chemistry of Institute for chemistry, technology and metallurgy. Present position is scientific research and head of the Environment department of the Laboratory of IHTM-Centre of chemistry. She is familiar with GC, FAS and GF-AAS laboratory techniques. The scientific research evolves investigation in environment; air pollution and their physicochemical transformations, emission sources and atmospheric transport as well as interactions between aquatic systems and soils. The whole scientific research of Dr. Dragana Đorđević published in 20 scientific articles, 7 contributions to books and over 60 published contributions to academic conferences.

Plenary Lecture XI

How a Horizontal Surface is Traced

Professor Petr Vanicek
Department of Geodesy and Geomatic Engineering,
University of New Brunswick,
Fredericton, NB,
CANADA
E-mail: vanicek@unb.ca
Web Page: http://gge.unb.ca/Personnel/Vanicek/Vanicek.html

Abstract: What is a horizontal surface and who needs it? Whoever is determining or using heights uses it, implicitly or explicitly: one particular horizontal surface, the geoid, is the reference surface for heights, the "heights above the sea level". These heights are used exclusively in engineering practice as well as in other applications. A horizontal surface is realized, more or less, by a surface of a water body, but how about dry land; what is needed for tracing a horizontal surface on land? What is needed, are gravity data observed on the surface of the earth, earth topography, some idea about topo-density, some idea about long-wavelength features of gravity field (derived from satellite tracking), and a conventional reference system with respect to which the tracing and the display should be done. The tracing is done through solving a non-linear boundary value problem for gravity potential with the boundary (the geoid) being itself a function of the potential. The solution is obtained by finite element or finite difference techniques, after transforming the boundary value problem into Green's form. The solution uses a vast amount of data irregularly distributed on the surface of the earth.

Brief Biography of the Speaker: Petr Vanícek, P.Eng., Ph.D., Dr.Sc, is Professor Emeritus of geodesy in the Department of Geodesy and Geomatics Engineering at UNB. He retired in 1999, after 28 years of teaching and is now involved only in post-graduate student supervision and in research. His research interests cover the whole spectrum of geodesy, geophysics and applied mathematics. He is a fellow of AGU, IAG, Senior Distinguished Scientist Humboldt awardee (1989), and recipient of CGU 1996 Tuzo J. Wilson medal. He is also author and co-author of about 450 publications including the comprehensive textbook "Geodesy: the concepts" used world-wide.

Plenary Lecture XII

Heterogeneous Photo-Fenton Process for Effective Removal of Organic Pollutants Contaminated in Wastewater

Professor Xijun Hu
Department of Chemical Engineering,
Hong Kong University of Science and Technology,
Clear Water Bay, Kowloon,
Hong Kong,
E-mail: hu@ust.hk
Fax: (852) 2358 0054
Tel: (852) 2358 7134

Abstract: Civilization and industrialization have resulted in serious problems with water supply. Industrial water effluents contain a variety of highly toxic organics such as dye pollutants. Numerous processes have been investigated for treating such pollutants. Among them, photo-Fenton's reaction is effective for the organics mineralization with the hydroxyl radical generated from the Fenton's reagents (Fe2+ and H2O2). However, there are two major problems with the application of photo-Fenton process. One is that a separation system is required to recover the homogeneous ferrous ion in the treated wastewater and the other is that the oxidation performance deteriorates quickly as the solution pH goes up above 4. The working pH range can be broadened by replacing Fe with Cu and the secondly pollutant (metal ions in the treated water) can be eliminated by immobilizing active metal onto the surface of porous solids. In this study, a heterogeneous Cu catalyst supported on bentenite clay was synthesized using a chemical vapor deposition (CVD) technique. To resolve the copper leaching problem during the catalyst's application in aqueous reaction, a critical pretreatment step, acid activation by H2SO4, was applied to the original bentonite clay. Such manufactured Cu/clay catalyst was characterized and evaluated in the photo-Fenton-like degradation of an azo organic dye, Acid Black 1 (AB1). It was found that the acid activation process of clay could significantly reduce the leaching problem by almost 72% and improve the catalytic activity. These improvements came from the active site and the addition of sulfonate functional group on the clay surface. Moreover, in order to provide a best catalyst over a broad pH range, the pH insensitive Cu was integrated together with the typically affirmed Fenton (Fe) reagent to form a bimetallic catalyst. The metals (Cu and Fe) were deposited onto the acid-activated bentonite clay by CVD to form a heterogeneous bi-functional catalyst. The developed bimetallic catalyst is able to sustain the activity in catalysing the total organic carbon (TOC) removal of organic dye in a wide range of pH, viz acidic and alkaline condition. To further minimize metal leaching, another highly porous solid, MCM-41, was used as the catalyst support. An in-situ oxidation technique was developed to stabilize the metals on the support. The bimetallic MCM-41 supported catalyst, FeCu/MCM-41, was found to achieve an extremely low leaching level (~0.3 ppm) and have an excellent degradation power of organics over a wide pH range, achieving TOC removals of 93%, 83%, and 78% at pHs of 3, 5.5, and 7, respectively. Furthermore, this catalyst can maintain its high catalytic activity after 10 consecutive runs. .

Brief Biography of the Speaker: Xijun Hu is Associate Professor of Chemical Engineering at the Hong Kong University of Science and Technology. He received his B.S. in chemical engineering from South China University of Technology (1982) and his Ph.D. from the University of Queensland, Australia (1993). After two years postdoctoral work at the University of Queensland, he joined the faculty of the Hong Kong University of Science and Technology in 1994.

Professor Hu is associate editor of two journals, has edited 1 book, published over 90 technical articles and presented more than 50 conference papers. He also has 3 patents.

Professor Hu has been active in international conferences. For example, He was the secretariat of 17th International Symposium on Chemical Reaction Engineering (ISCRE17, 2002), technical chairman of 3rd Asia Pacific Conference on Sustainable Energy and Environmental Technologies (2000).

Professor Hu's research covers the development of novel heterogeneous catalysts by chemical vapour deposition (CVD) and their applications in air pollution control and wastewater treatment; Continuous wastewater treatment by catalytic wet oxidation using a trickle bed reactor; Modified nanoporous materials for efficient storage and rapid release of hydrogen; Multicomponent adsorption equilibrium and kinetics in heterogeneous porous media; Characterization of microporous solids; fabrication of Meso-Structured Crystals for Electrical and Optical Applications.

Professor Hu is the first person to introduce the concept of micropore size distribution (MPSD) to describe the surface heterogeneity of adsorbents for the study of multicomponent adsorption equilibrium and kinetics, which has now been widely adopted by other researchers. The synthesis of a high performance heterogeneous bimetallic (Fe+Cu) catalyst by his group is one of the most important contributions in the Fenton process, which successfully solved the problems of stability (metal leaching in acidic solution) and narrow working pH range of Fenton catalyst, which have puzzled the scientists for a long time.

Plenary Lecture XIII

Collision Mountain Belts as Crustal-Scale Pop-Up Structures due to Underthrusting: The case of the Brasília Belt, Central Brazil

Professor Luiz Jose Homem D´El-Rey Silva
Instituto de Geociências
Universidade de Brasília
Campus Darcy Ribeiro,
Asa Norte, CEP 70910-900, Brasília,
DF - BRAZIL
E-mail: ldel-rey@unb.br

Abstract: Because collision-related mountain chains form above sites of mantle down welling (= mantle convection), contractional deformation in general must be governed by the mechanism of underthrusting, mainly, and the inner parts of mountains should correspond to crustal-scale pop-up structures. In fact, convective cells and underthrusting are the basis for a new understanding (termed Suction Tectonics) on lithosphere deformation. The Brasília Belt (BB) is the most complex of the three fold-and-thrust belts that constitute the Tocantins Province of central Brazil, a Neoproterozoic orogen situated between the Amazonian and São Francisco cratons. The Araguaia and Paraguay Belts are the other two. The Araguaia-Brasilia Belt records the evolution of a Meso-Neoproterozoic ocean and the collision between the Amazonian and São Francisco paleo-continents, during the ~750-590 Ma Brasiliano orogeny. The Paraguay Belt records the 620-510 Ma evolution of a rift-oceanic basin opened within the Amazonian paleo-continent, adjacent to the southern half of the BB. The results of a research carried out in the last 15 years and focused on the operation of the underthrusting mechanism in the BB are summarized, and a brief review of the up-to-date literature supporting the new understanding on lithosphere deformation is presented. Due to underthrusting, the inner part of the BB evolved such as a crustal-scale pop-up structure, and the evidence presented herein must be found in other collision-related mountain chains on Earth.

Brief Biography of the Speaker: PhD geologist, educator, born in Itabuna-BA, Brazil, 1947, son of José Silva and Mary Alice H. D'el-Rey, married Irene Ordine Lopes H. D'el-Rey, three children: Manuela, Alexandre, and Henrique O.L.H. D'el-Rey. Diploma in Geology, University of Brasília (Brazil), 1971; MSc in Geology, Federal University of Bahia (Brazil), 1984; PhD in geology, Royal Holloway University London (UK), 1992; Post-doctor in geology, Geological Survey of Finland (Finland), 2001. Biography included in Marquis Who´s Who in Science and Engineering (2005, 2006, 2007-2008), and Who´s Who in the World (2007).

Associate Professor of structural geology and tectonics in the Institute of Geosciences of the University of Brasília, since 1993, where has been developing a research program focused on the controls exerted by age- and scale-independent convection cells on the deformation of the lithosphere and formation of tectonic features such as mountain belts, basins, plateaus, with special attention on the tectonic evolution of the Neoproterozoic fold belts that surround the São Francisco Craton, Brazil. Scientific publications include 64 pieces or work, being 34 full papers (25 in indexed periodicals, 9 in congresses). Large working experience in mine geology and on the structural controls of ore deposits, with special achievements in the detailed study of highly deformed ore deposits of copper, gold, emerald, and base sulfides, in Brazil and in Canada.

Plenary Lecture XIV

Monitoring Land Degradation by the Integration of in Situ and Remote Sensed Data: Badlands in Basilicata Region

Professor Maria Francesca Macchiato
CNISM – Dipartimento di Scienze Fisiche, Universita "Federico II",
Complesso Universitario di Monte Sant'Angelo, I-80126, Napoli,
ITALY

E-mail: macchiat@na.infn.it

Abstract: The complexity of land degradation phenomena leads to a large number of definitions and to the use of terminologies often having distinct disciplinary-oriented meanings. Although land degradation is under a debate on terminology and is still difficult to grasp in its totality, some individual processes of degradation such as soil erosion, wind erosion, salinization and desert expansion are properly described and defined. Human activities enter in this framework through the uncontrolled and irrational exploitation of natural resources. Overgrazing of rangeland, over-cultivation of cropland, waterlogging and salinization of irrigated land, deforestation and pollution, intensive change of land use are some of unsustainable human practices that in recent years undermined the environmental balance, causing accelerated forms of land degradation. These processes act on lands at different spatial and temporal scales, making the understanding and the characterization of land degradation processes quite arduous. In this talk we present a multidisciplinary research work carried out through the integration of different monitoring techniques carried out in an area of Basilicata region in Southern Italy where badland landforms ("calanchi") are found in fine-grained clastic sedimentary bedrock. Badlands consist of deeply-dissected, non vegetated or poorly-vegetated landforms of high relative relief and high drainage density; they are conventionally considered areas of extreme soil erosion. In this work, we focus on the development of a suitable approach for remote identification of areas interested by "calanchi" formations by means of the analysis of Landsat ETM images for mapping badlands area. Contemporaneously we selected some chemical physical parameters (soil magnetic susceptibility, electrical conductivity, and pH) suitable for the characterization of erosive processes that took place in the "calanchi" formations.

Brief Biography of the Speaker: Maria Macchiato Biography. Maria Macchiato, is full professor of Physics at the University "Federico II" of Naples. She is responsible of research activities related to environmental modelling at DSF (Department of Physical Sciences) of the University "Federico II". She is also responsible of research activities related to the development of integrated technologies in situ and in remote sensing for the study of land degradation and of research activities related to energetic-environmental planning at IMAA/CNR (Institute of Methodologies for Environmental Analysis). Her main areas of interest are in the field of land degradation with a particular attention to those scientific issues that are related to climate change and sustainable development. The research lines can be summarized as in the following: study of vegetation cover dynamics observed from satellite for desertification and climate studies; soil and air monitoring by means of integrated chemical and geophysical techniques for pollution studies; development of integrated methodologies and multicriteria models for environmental planning. In recent years, she has been responsible of many National and International projects. At now she is Project Manager of the project INTERREG III B ARCHIMED "Methodology integration of EO techniques as operative tool for land degradation management and planning in Mediterranean areas" and she is responsible of the Integrated Project "New Energy Externalities Developments for Sustainability - NEEDS". She counts around 150 scientific international publications and 140 scientific communications at national and international conferences.

978-960-474-001-7

Stress Strain Modeling by Transformed equations of Ultrasonic wave

ARASH ZIAIE
Civil Engineering Department
University of Kerman
22th of Bahman Ave, Kerman University, Kerman
IRAN
ZIAIE111@YAHOO.COM
KAVEH KUMARCI
Sama Organization (Affiliated With Islamic Azad University), Shahr-e-Kord Branch
IRAN
KUMARCIKAVEH@YAHOO.COM
ARASH KIYOUMARSI
Electric Engineering Department, Faculty of Engineering
University of Isfahan
Hezar Jerib Ave., University of Isfahan, Isfahan
IRAN
Kiyoumarsi_arash@yahoo.com

Abstract: - The equations of ultrasonic wave propagation in Cartesian coordinates are functions of 27 partial displacement derivatives, which first derived and then transformed into cylindrical coordinates. The new obtained functions are functions of 27 partial displacements of first and second order derivatives in cylindrical coordinates too and they will be linearized using a perturbation method based on the Taylor series expansion. A displacement wave, which propagates in a body, composed of two general part; static displacement part, and also small dynamic displacement part. Happening of the small dynamic displacement of a particle around its static situation, Taylor series expansion can be written around this point. Using this determined static situation and considering only the two first components of Taylor series expansion, the equations of motion will be linearized. Tremendously lengthy algebraic operations involved in the derivation and linearization process, all of the mathematical manipulations are performed using Mathematica [8].

Key-Words: perturbation- acoustoelasticity- strained cylindrical solids- ultrasonic- wave propagation- Mathematica

1 Introduction

One of the most useful nondestructive methods for stress analyzing, is using Ultrasonic wave propagation in bodies, which is based on difference of wave propagation properties in different stress fields. Using theoretical methods the relation between velocity of wave propagation and strain (stress) value can be obtained. Considering the importance of this object many scientists are focusing on theoretical and experimental stress analyzing methods with Ultrasonic waves. Biot[1] in 1940 was the first person who considered the subject scientifically. Hughes and Kelly [2], Henneke[3] and Green[4] are the other pioneers of this method. The most perfect form of equations governing the wave propagation in strained (stressed) bodies that ever obtained is named general motion equation.

2 Problem Formulation

These equations in isotropic elastic solids for limited deflections have been derived by several authors [6], using tensorial notation in a continuum mechanics media [7] and supposing Cartesian coordinates (x_1, x_2, x_3), the motion equation component in 1 direction (u-direction) derived as:

$$\begin{aligned}\rho_0\ddot{u}_1 = {} & (2\mu+\lambda)[u_{1,11}+u_{2,12}+u_{3,13}+u_{1,1}(3u_{1,11}\\ & +u_{1,22}+u_{1,33}+u_{2,12}+u_{3,13})+u_{2,1}u_{2,11}+u_{3,1}u_{3,11}\\ & +u_{1,2}(u_{2,22}+2u_{1,12}+u_{3,23})\\ & +u_{2,2}(u_{1,11}+u_{1,22}+u_{1,33}+u_{2,12})+u_{3,2}u_{3,12}\\ & +u_{1,3}(u_{3,33}+2u_{1,13}+u_{2,23})+u_{2,3}u_{2,13}\\ & +u_{3,3}(u_{1,11}+u_{1,22}+u_{1,33}+u_{3,13})]\\ & +\mu[u_{1,22}+u_{1,33}+u_{2,12}-u_{3,13}-u_{1,1}(u_{2,12}+u_{3,13})\\ & +u_{2,1}(u_{2,22}+u_{2,33}+2u_{1,12})\\ & +u_{3,1}(u_{3,22}+u_{3,33}+2u_{1,13})+u_{1,2}(u_{2,11}+u_{2,33}-u_{3,23})\\ & +u_{2,2}(-2u_{1,11}-2u_{1,33}-u_{2,12})\end{aligned}$$

$$+u_{3,2}(2u_{1,23}-u_{3,12})+u_{3,3}(-2u_{1,11}-2u_{1,22}-u_{3,13})]$$
$$+2(l+2m)[(u_{1,1}+u_{2,2}+u_{3,3})(u_{1,11}+u_{2,12}+u_{3,13})]$$
$$+m[u_{1,1}(u_{1,22}+u_{1,33}-3u_{2,12}-3u_{3,13})$$
$$+(u_{1,2}+u_{2,1})(u_{2,11}+u_{2,22}+2u_{1,12}+2u_{3,13})$$
$$+u_{3,1}(u_{3,11}+u_{3,33}+2u_{1,13}+2u_{2,23})$$
$$+u_{2,2}(-4u_{1,11}+u_{1,22}-u_{1,33}-5u_{3,13}-3u_{2,12})$$
$$+u_{3,2}(u_{2,13}+u_{3,12})+u_{1,3}(+u_{3,11}+u_{3,33}+2u_{1,13}+u_{2,33})$$
$$+u_{2,3}(u_{2,13}+u_{3,12})$$
$$+u_{3,3}(-4u_{1,11}+u_{1,33}+3u_{3,13}-5u_{2,12})]$$
$$+(n/4)[(u_{1,2}+u_{2,1})(u_{2,33}-u_{3,23})+(u_{1,3}+u_{3,1})(u_{3,22}-u_{2,23})$$
$$+(u_{2,3}+u_{3,2})(2u_{1,23}-u_{2,13}-u_{3,12})$$
$$+2u_{2,2}(u_{3,13}-u_{1,33})+2u_{3,3}(u_{2,12}-u_{1,22})]$$

Where ρ_0 is density of the body before deflection, (1, 2, 3) are principal direction in Cartesian coordinates system, (,) is the partial derivative and u_i is the component of displacement in i direction.

The equations of motion in the other two directions, 2 and 3 can be obtained by a circular permutation of the subscripts 1, 2 and 3 in equation (1).There are 27 partial derivatives($U_{1,1},U_{1,2},...,U_{3,33}$) of displacement functions in each of these non-linear partial differential equations. These equations are achieved in Cartesian coordinates system and they could be derived in other coordinates system. Here, because of the main purpose of the paper, the relation between Ultrasonic waves velocity and strain (stress) in cylindrical shells, the motion equations convert to cylindrical coordinate system.

3 Problem Solution

3.1 The Principals of Transforming From Cartesian Coordinates System in to Cylindrical

As it mentioned before, the cylindrical coordinates system is proper to derive the properties of cylindrical and cone shells which have curvature in one direction and because the equations of motion are functions of partial first and second order derivatives, we need to change them from Cartesian into cylindrical coordinates system. By using the relation between independent parameters in cylindrical coordinates (θ, z) and Cartesian coordinates(x, y, z), transforming relations are determined. Because of writing in tensorial form in many equations, the triplet (x_1, x_2, x_3) is used instead of (x, y, z) [7]. The relations of a point coordinate in Cartesian and cylindrical systems may be written as below;

$$x_1 = r\cos\theta, \quad (1)$$
$$x_2 = r\sin\theta,$$
$$x_3 = z$$

And so the variables of cylindrical coordinate system are as follows:

$$r = (x_1^2 + x_2^2)^{1/2}, \quad \theta = \arctan\left(\frac{x_2}{x_1}\right), \quad z = x_3 \quad (9)$$

So:

$$\frac{\partial r}{\partial x_1} = \frac{x_1}{r} = \cos\theta, \ \frac{\partial r}{\partial x_2} = \frac{x_2}{r} = \sin\theta, \ \frac{\partial r}{\partial x_3} = 0$$

And also:

$$\frac{\partial \theta}{\partial x_1} = \frac{-\sin\theta}{r}, \quad \frac{\partial \theta}{\partial x_2} = \frac{\cos\theta}{r}, \quad \frac{\partial \theta}{\partial x_3} = 0$$
$$\frac{\partial z}{\partial x_1} = 0, \quad \frac{\partial z}{\partial x_2} = 0, \quad \frac{\partial z}{\partial x_3} = 1$$

So where f is a function of first order partial derivatives in Cartesian coordinate, by using the chain rule of differentiation we can derive the first order partial derivatives in cylindrical coordinate as follow:

$$\frac{\partial f}{\partial x_1} = \frac{\partial f}{\partial r}.\frac{\partial r}{\partial x_1} + \frac{\partial f}{\partial \theta}.\frac{\partial \theta}{\partial x_1} + \frac{\partial f}{\partial z}.\frac{\partial z}{\partial x_1}$$

Substituting the above values in this equation we can write:

$$\frac{\partial f}{\partial x_1} = \cos\theta\frac{\partial f}{\partial r} - \frac{\sin\theta}{r}\frac{\partial f}{\partial \theta} \quad (2)$$

At the way the principal of other first order partial derivatives may achieved:

$$\frac{\partial f}{\partial x_2} = \sin\theta\frac{\partial f}{\partial r} + \frac{\cos\theta}{r}\frac{\partial f}{\partial \theta} \quad (3)$$

$$\frac{\partial f}{\partial x_3} = \frac{\partial f}{\partial z} \quad (4)$$

For deriving the second order partial derivatives principals in cylindrical coordinate system, we suppose that f is a function of second order partial in Cartesian coordinate system, so we have:

$$\frac{\partial^2 f}{\partial x_1^2} = \frac{\partial}{\partial x_1}\left(\frac{\partial f}{\partial x_1}\right)$$

Now using equation (3), $\frac{\partial^2 f}{\partial x_1^2}$ in cylindrical coordinate system may be written as follows:

$$\frac{\partial^2 f}{\partial x_1^2} = \frac{\partial}{\partial x_1}\left(\cos\theta.\frac{\partial f}{\partial r} - \frac{\sin\theta}{r}.\frac{\partial f}{\partial \theta}\right)$$

$$= \cos\theta\frac{\partial}{\partial x_1}\left(\frac{\partial f}{\partial r}\right) - \frac{\sin\theta}{r}.\frac{\partial}{\partial x_1}\left(\frac{\partial f}{\partial \theta}\right)$$

$$= \cos\theta\left(\frac{\partial^2 f}{\partial r^2}.\frac{\partial r}{\partial x_1} + \frac{\partial^2 f}{\partial r\partial\theta}.\frac{\partial\theta}{\partial x_1} + \frac{\partial^2 f}{\partial r\partial z}.\frac{\partial z}{\partial x_1}\right)$$

$$-\frac{\sin\theta}{r}\left(\frac{\partial^2 f}{\partial r\partial\theta}.\frac{\partial r}{\partial x_1} + \frac{\partial^2 f}{\partial\theta^2}.\frac{\partial\theta}{\partial x_1} + \frac{\partial^2 f}{\partial\theta\partial z}.\frac{\partial z}{\partial x_1}\right)$$

Substituting the value of $\frac{\partial r}{\partial x_1}$, $\frac{\partial\theta}{\partial x_1}$ and $\frac{\partial z}{\partial x_1}$ in above relation and summarizing the equation we have:

$$\frac{\partial^2 f}{\partial x_1^2} = \cos^2\theta\frac{\partial^2 f}{\partial r^2} + \frac{\sin 2\theta}{r^2}.\frac{\partial f}{\partial\theta} + \frac{\sin^2\theta}{r}.\frac{\partial f}{\partial r}$$

$$-\frac{\sin 2\theta}{r}.\frac{\partial^2 f}{\partial r\partial\theta} + \frac{\sin^2\theta}{r^2}.\frac{\partial f}{\partial\theta^2}$$

And for the other instance $\frac{\partial^2 f}{\partial x_1\partial x_2}$ in cylindrical coordinate system will be:

$$\frac{\partial^2 f}{\partial x_1\partial x_2} =$$

$$\left(\sin\theta\left(\frac{\partial^2 f}{\partial r^2}.\frac{\partial r}{\partial x_1} + \frac{\partial^2 f}{\partial r\partial\theta}.\frac{\partial\theta}{\partial x_1} + \frac{\partial^2 f}{\partial r\partial z}.\frac{\partial z}{\partial x_1}\right)\right.$$
$$\left.+\frac{\cos\theta}{r}\left(\frac{\partial^2 f}{\partial r\partial\theta}.\frac{\partial r}{\partial x_1} + .\frac{\partial^2 f}{\partial\theta^2}.\frac{\partial\theta}{\partial x_1} + \frac{\partial^2 f}{\partial\theta\partial z}.\frac{\partial z}{\partial x_1}\right)\right)$$

Substituting the value of $\frac{\partial r}{\partial x_1}, \frac{\partial\theta}{\partial x_1}, \frac{\partial z}{\partial x_1}$, and summarizing the equation we have:

$$\frac{\partial^2 f}{\partial x_1\partial x_2} = \frac{1}{2}\sin 2\theta\frac{\partial^2 f}{\partial r^2} - \frac{\cos 2\theta}{r^2}\frac{\partial f}{\partial\theta} - \frac{\sin 2\theta}{2r}\frac{\partial f}{\partial r}$$

$$+\frac{\cos 2\theta}{r}\frac{\partial^2 f}{\partial r\partial\theta} - \frac{\sin 2\theta}{2r^2}\frac{\partial^2 f}{\partial\theta^2}$$

And at the same way all of the 27 partial derivatives may be obtained. By substituting these partial derivatives in Cartesian motion equation, the cylindrical form of motion equation will obtained. And also motion equation in other direction of cylindrical coordinates ($\rho_0\ddot{u}_\theta, \rho_0\ddot{u}_z$), will be derived. Each of these motion equation components in cylindrical coordinate system are contain of 27 partial derivatives of first and second order. Due to the tremendously lengthy form of the resulting equations, however, they cannot be presented here in their original form, because of the limited space. Nevertheless, it is possible to change their form to make them shorter. To accomplish this, the following change of notation is adopted:

$(r,\theta,z) \rightarrow (1,2,3)$

And by using tensorial notation in a continuum mechanics media [7] we will have:

$$u_r = u_{1,},\quad u_\theta = u_2,\quad \frac{\partial u_r}{\partial\theta} = u_{1,.2},\quad \frac{\delta^2 u_z}{\delta r\partial\theta} = u_{3.12}$$

3.2 Linearization Process in Cylindrical Coordinate System

Motion equations in cylindrical coordinate system are equations with nonlinear partial derivatives which for extension and solving some special method should be used. To accomplish this, cylindrical forms of motion equations are changed to linear form using Taylor series expansion around the displaced static situation. The total displacement at any moment at any point in the elastic medium is composed of two parts: the static part caused by the applied stress and the dynamic part due to the propagating stress wave. Assuming a low amplitude plane wave propagating in an initially isotropic elastic medium, the displacement components in cylindrical coordinates can written as:

$$u_n = \eta_n a_n + m_n A\exp\left[i(\omega t - k_j x_j)\right], n = 1,2,3 \quad (5)$$

Where u_n are the total displacement components (u_1 ,u_2 , u_3) along the initial coordinates a_n, η_n are the principal strains(η_1 ,η_2 , η_3), m_n are the direction cosines of the polarization vector(m_1 ,m_2 , m_3), A is the amplitude of the wave, $i = \sqrt{-1}$, ω is the circular frequency of the wave, t is the time, k_j are components of the wave vector (k_1 ,k_2 , k_3) and x_j are the current coordinates (x_1 , x_2 , x_3), related to the initial coordinates a_j; (a_1 ,a_2 , a_3) and at this equation the summing convention refer to the dummy index j only.

Short form of equation (5) is as: $u_n = U_n^s + u_n^d$

Where $U_n^s = \eta_n.a_n$ is static displacement and $u_n^d = m_n A\exp[i(\omega t - k_j x_j)]$ is the small dynamic part of displacement. The first term in equation (5) denotes the large static displacement u_n^s of an initially isotropic medium subjected to a triaxial strain (stress) field. The second term represents the very small dynamic deformation u_n^d due to the elastic plane wave

propagating through the then anisotropic medium, because the isotropy in wave propagation is already removed by the applied strains (stresses).

The first sentence of equation (5) is supposed from initial coordinates without any deformation (Lagrangian coordinates), but the second term is not so and for transferring of this part to the initial coordinates we have:

$$x_j = a_j + u_j$$

In this equation the components of displacement vector u_j related to the initial coordinates a_j as bellow:

$$u_j = \eta_j . a_j , \qquad j = 1,2,3$$

(Summing convention dose not refer to j),So:

$$x_j = (1+\eta_j) a_j$$

(Summing convention dose not refer to j) (6)

The components of the wave vector (k_j) may also be written in terms of the wave number (k) and the direction cosines of the wave normal (l_j) as:

$$k_j = \frac{2\pi}{\lambda} l_j = k_j l_j \qquad j = 1,2,3 \qquad (7)$$

Where λ is the wavelength. Substituting from equations (6) and (7) into equation (5), the three components of the total displacement (u_1 , u_2 , u_3) in cylindrical coordinates related to strain components (η_1 , η_2 , η_3), the direction cosines of the wave normal (l_1, l_2, l_3) and the direction cosines of the polarization vector(m_1 , m_2 , m_3), that all referred to the initial cylindrical coordinates, as:

$$u_1 = \eta_1 a_1 + m_1 e^{i\omega t} . A \exp\left\{ -ik \left[\begin{array}{l} (1+\eta_1) a_1 l_1 \\ +(1+\eta_2) a_2 l_2 + (1+\eta_3) a_3 l_3 \end{array} \right] \right\}$$

$$= \eta_1 a_1 + m_1 e^{i\omega t} . F$$

$$u_2 = \eta_2 a_2 + m_2 e^{i\omega t} . F \ , u_3 = \eta_3 a_3 + m_3 e^{i\omega t} . F \qquad (8)$$

Where:

$$F = A \exp\left\{ -ik \left[(1+\eta_1) a_1 l_1 + (1+\eta_2) a_2 l_2 + (1+\eta_3) a_3 l_3 \right] \right\}$$

Equation (8) then represents the superposition of a very small dynamic displacement upon a large static deformation. Equation (8) may, therefore, be written in short as:

$$\begin{array}{ll} u_1 = U_1^S + u_1^d & u_1^d << U_1^s \\ u_2 = U_2^S + u_2^d & u_2^d << U_2^s \\ u_3 = U_3^S + u_3^d & u_3^d << U_3^s \end{array} \qquad (9\text{-a})$$

With the above considerations, it is now possible to proceed with the linearization process. Referring bake to the first component of the equation of motion, it can be written in the following general form in terms of the 27 variables $u_{i,j}$ and $u_{i,jk}$ as:

$$\rho_0 \ddot{u}_1 = f(u_{1,1}, u_{1,2}, u_{1,3}, u_{2,1}, u_{2,2}, ...,$$

$$u_{3,3}, u_{1,11}, u_{1,12}, u_{1,13}, u_{1,22}, ..., u_{3,32}, u_{3,33}) \quad (9)$$

Or, in short form, as

$$\rho_0 \ddot{u}_1 = f(u_{i,j}, u_{i,jk})$$

Noting that $u_{i,jk} = u_{i,kj}$ similarly, for the two remaining components of the equation of motion,

$$\rho_0 \ddot{u}_2 = g(u_{i.j}, u_{i,jk}) \qquad (10)$$

$$\rho_0 \ddot{u}_3 = h(u_{i,j}, u_{i,jk})$$

$$+ \left[(\xi \partial / \partial u_{1,1} + \zeta \partial / \partial u_{1,2} + \gamma \partial / \partial u_{1,3} \right.$$

$$\left. + ... + \varepsilon \partial / \partial u_{1,11} + ... + \rho \partial / \partial u_{3,33}) \ f \right]_{stat} . \qquad (11)$$

The three functions f, g and h in equations (9), (10) and (11) are analytic functions and may be expanded Taylor series around bellow static deformation values:

$$(U_{1,1}^S, U_{1,2}^S, U_{1,3}^S, U_{2,1}^S, ..., U_{1,11}^S, U_{1,12}^S, ..., U_{3,33}^S)$$

So Taylor series will be written as:

$$\rho_0 \ddot{u}_1 = f(u_{1,1}, u_{1,2}, u_{1,3}, u_{2,1}, u_{2,2}, ..., u_{1,11}, u_{1,12}, ..., u_{3,33})$$

$$= f(u_{1,1}^s, u_{1,2}^s, u_{1,3}^s, u_{2,1}^s, u_{2,2}^2, ..., u_{1,11}^s, u_{1,12}^s, ..., u_{3,33}^s)$$

$$+ \left[(\xi \partial / \partial u_{1,1} + \zeta \partial / \partial u_{1,2} + \gamma \partial / \partial u_{1,3} \right.$$

$$\left. + ... + \varepsilon \partial / \partial u_{1,11} + ... + \rho \partial / \partial u_{3,33}) \ f \right]_{stat} . \qquad (12)$$

$$+ \frac{1}{2!} \left[(\xi \partial / \partial u_{1,1} + \zeta \partial / \partial u_{1,2} + \gamma \partial / \partial u_{1,3} \right.$$

$$\left. + ... + \varepsilon \partial / \partial u_{1,11} + ... + \rho \partial / \partial u_{3,33})^2 \ f \right]_{stat} .$$

+Negligible HOT

Where we use equation (9), to expanded Taylor series as bellow:

$$\xi = u_{1.1} - U_{1.1}^s = u_{1,1}^d$$

$$\zeta = u_{1,2} - U_{1,2}^s = u_{1,2}^d$$

$$\gamma = u_{1,3} - U_{1,3}^s = u_{1,3}^d$$

.

.

.

$$\varepsilon = u_{1,11} - U_{1,11}^s = u_{1,11}^d$$

.

.

.

$$\rho = u_{3,33} - U_{3,33}^s = u_{3,33}^d$$

The symbol $\big|_{stat}$ implies evaluation of the partial derivatives for the static values u_n^s and f, g functions in equation (10), (11) may be extend at the same way. Saving the two first sentences of right part of equation (12) we can substitute related derivatives and using

equation (8) the static displacements and their derivatives are obtained as follow:

$$U_1^s = \eta_1\alpha_1,\quad U_2^s = \eta_2\alpha_2,\quad U_3^s = \eta_3\alpha_3$$

$$U_{1,1}^s = \eta_1,\quad U_{2,2}^s = \eta_2,\quad U_{3,3}^s = \eta_3$$

$$U_{1,2}^s = U_{1,3}^s = 0, U_{2,1}^s = U_{2,3}^s = 0, U_{3,1}^s = U_{3,2}^s = 0$$

Thus the values of all second order derivatives in static situation are equal to zero. Now considering the mentioned points and equation (12) the equation of motion will be achieved. First term of this equation is related to motion equation in static deformation state and is equal to zero. Thus:

$$f(U_{1,1}^s, U_{1,2}^s, U_{1,3}^s, U_{2,1}^s, ..., U_{1,11}^s, U_{1,12}^s, ..., U_{3,33}^s) = 0$$

This point could be deduced from the physics of the problem, so equation (12) wall be summarized as:

$$\rho_0\ddot{u}_1 = \left[\begin{array}{l}(u_{1,1}^d\frac{\partial}{\partial u_{1,1}} + u_{1,2}^d\frac{\partial}{\partial u_{1,2}} + u_{1,3}^d\frac{\partial}{\partial u_{1,3}} + \\ ... + u_{1,11}^d\frac{\partial}{\partial u_{1,11}} + ... + u_{3,33}^d\frac{\partial}{\partial u_{3,33}})f\end{array}\right]_{stat} + \text{NegligibleHOT} \quad (13)$$

At the same way the motion equations in other two directions (2, 3) will be summarized and the results are similar to equation (13). The 27 partial derivatives required in the second part of equation (13) are all determined and substitute in the equation at static position to linearizing the equation. Ensuring the correctness, the software package Mathematica is employed for determination of these derivatives.

For example,

$$\frac{\partial f}{\partial u_{1.1}}\Big|_{stat} = \eta_3\lambda\cos^2\theta + \eta_3 m\cos^2\theta + \mu\cos^2\theta - \frac{\eta_3 n\cos^2\theta}{2}$$
$$+ 2\eta_1\lambda\cos^3\theta + 2\eta_1 m\cos^3\theta + 4\eta_1\mu\cos^3\theta + 2\eta_3 l\sin^2\theta$$
$$+ \lambda\sin^2\theta + \eta_3\lambda\sin^2\theta + 2\mu\sin^2\theta + 4\eta_1 l\cos\theta\sin^2\theta$$
$$+ 2\eta_1\lambda\cos\theta\sin^2\theta + 4\eta_1 m\cos\theta\sin^2\theta + 4\eta_1\mu\cos\theta\sin^2\theta$$
$$+ 3\eta_1 m\cos\theta\sin^2\theta + \eta_2\mu\cos\theta\sin^2\theta$$

The other derivates in this direction and the other directions are also determined at the same way. For substituting $u_{1,1}^d$ to $u_{3,33}^d$ in equations (13) we use equation (8) as follow:

$$u_{1,1}^d = m_1\left[-ik(1+\eta_1)l_1\right]e^{i\omega t}.F$$

$$u_{1,2}^d = m_1\left[-ik(1+\eta_2)l_2\right]e^{i\omega t}.F \quad (14)$$

.

.

.

$$u_{1,12}^d = m_1\left[-k^2(1+\eta_1)(1+\eta_2)l_1l_2\right]e^{i\omega t}.F$$

.

$$u_{3,33}^d = m_3\left[-k^2(1+\eta_3)^2 l_3^2\right]e^{i\omega t}.F$$

At the other hand time-rate of change of deformation is achieved from equation (8) as:

$$\ddot{u}_1 = -m_1\omega^2 e^{i\omega t}.F \quad (15)$$

Substituting from equations (14) to (15) into equation (13), canceling the common multiplier $(-Fe^{i\omega t})$ from both sides, dividing the resulting equation by k^2 and taking $\omega^2/k^2 = V^2$, the end result will be as:

$$\rho_0 m_1 V^2 = F(\eta_1, \eta_2, \eta_3, l, m, n, \lambda, \mu, l_1, l_2, l_3, m_1, m_2, m_3, \theta)$$

Because of being extremely lengthy, one more summarizes process is applied on the equation before of presentation. Considering a perfect symmetric shell, stress, strain and the related equations are independent from the value of θ, so we can suppose $\theta = 0$ for more simplification. And finally the linearized equation of motion in 1 direction, after the simplification and neglecting of the higher order strain statements, will be as bellow:

$$m_1\rho_0 V^2 = m_1\left[(\lambda + ml_2^2 + ml_3^2 + 2ll_1^2)\gamma\right]$$
$$+ 4ml_1^2\eta_1 + \lambda l_1^2(l + 4\eta_1) + 2\mu l_1^2(1 + 5\eta_1)$$
$$+ \mu l_2^2(l + 2\eta_1 + 4\eta_2) + \mu l_3^2(l + 2\eta_1 + 4\eta_3)$$
$$- \frac{n}{2}(l_2^2\eta_3 + l_3^2\eta_2)]$$
$$+ m_2[l_1l_2(2\mu + 2\lambda + 4l\gamma + 2m\gamma - 4m\eta_3 + 4\lambda\eta_1$$
$$+ 4\lambda\eta_2 + 4\lambda\eta_1 + 4\mu\eta_2 + n\eta_3)]$$
$$+ m_3[l_1l_3(2\mu + 2\lambda + 4l\gamma + 2m\gamma - 4m\eta_2 + 4\lambda\eta_1$$
$$+ 4\lambda\eta_3 + 4\mu\eta_1 + 4\mu\eta_3 + n\eta_3)] \quad (16)$$

Where

$$\gamma = \eta_1 + \eta_2 + \eta_3$$

The new quantity V is the velocity of wave propagation in the strained (stressed) solid and the last equation is linearized in 1 direction. Performing the same lengthy process as above, the other two linearized components of the equation of motion in (2 , 3) direction are obtained:

$$m_2\gamma_0 V_2^2 = m_1[l_1l_2(2\mu + 2\lambda + 4l\gamma + 2m\gamma - 4m\eta_3$$
$$+ 4\lambda\eta_2 + 4\mu\eta_1 + 4\mu\eta_2 + n\eta_3)] \quad (17)$$
$$+ m_2[(\lambda + ml_1^2 + ml_3^2 + 2ll_2^2)\gamma$$
$$+ 4ml_2^2\eta_2 + \lambda l_2^2(l + 4\eta_2) + 2\mu l_2^2(1 + 5\eta_2)$$
$$- n/2(l_1^2\eta_3 + l_3^2\eta_1)]$$

$$+\mu l_1^2(l+2\eta_2+4\eta_1)+\mu l_3^2(l+2\eta_2+4\eta_3)$$
$$+m_3[l_2l_3(2\mu+2\lambda+4l\gamma+2m\gamma-4m\eta_1+4\lambda\eta_2$$
$$+4\lambda\eta_2+4\mu\eta_2+4\mu\eta_3+n\eta_1)]$$

And:

$$m_3\gamma_0V_3^2=$$
$$m_1[l_1l_3(2\mu+2\lambda+4l\gamma+2m\gamma-4m\eta_2$$
$$+4\lambda\eta_3+4\mu\eta_1+4\mu\eta_3+n\eta_3)]$$
$$+m_2[l_2l_3(2\mu+2\lambda+4l\gamma+2m\gamma-4m\eta_1$$
$$+4\lambda\eta_2+4\lambda\eta_3+4\mu\eta_2+4\mu\eta_3+n\eta_1)]$$

4 Conclusion

As it mentioned before, because the vibration of particles is happened due to wave propagation around the static position of it, the Taylor series expansion and the partial nonlinear derivatives may be written around this point. Considering the two first terms of Taylor series the equations are changed to linear form. The next exact numerical calculations imply that linearizing error of these equations and neglecting of the next terms of Taylor series is so tiny. For example the value of this error for a steel cylinder is less than 1×10^{-5} and for an aluminum cylinder is less than 1.5×10^{-5}.

The obtained linearized equation of this paper can be used widely in physics, mathematics and engineering. For example the equations (16) to (18) are applied to stress analyzing by ultrasonic waves transmitting as the following form:

$$\begin{cases}(\lambda_{11}-\rho_0V^2)m_1+\lambda_{12}m_2+\lambda_{13}m_3=0\\ \lambda_{21}m_1+(\lambda_{22}-\rho_0V^2)m_2+\lambda_{23}m_3=0\\ \lambda_{31}m_1+\lambda_{32}m_2+(\lambda_{33}-\rho_0V^2)m_3=0\end{cases}$$

So the solution of motion equations for measuring of the wave velocities from elasticity constants and strains (stresses) affects will tend to determination of eigen values of the following matrix:

$$\begin{bmatrix}\lambda_{11}-\rho_0V^2 & \lambda_{12} & \lambda_{13}\\ \lambda_{21} & \lambda_{22}-\rho_0V^2 & \lambda_{23}\\ \lambda_{31} & \lambda_{32} & \lambda_{33}-\rho_0V^2\end{bmatrix}\begin{bmatrix}m_1\\ m_2\\ m_3\end{bmatrix}=0$$

Thus for any $\begin{bmatrix}m_1\\ m_2\\ m_3\end{bmatrix}$ vector the determinant of the matrix should be equal to zero:

$$\begin{vmatrix}\lambda_{11}-\rho_0V^2 & \lambda_{12} & \lambda_{13}\\ \lambda_{21} & \lambda_{22}-\rho_0V^2 & \lambda_{23}\\ \lambda_{31} & \lambda_{32} & \lambda_{33}-\rho_0V^2\end{vmatrix}=0$$

At the general form there are three roots of (ρ_0V^2) for this equation, so ρ_0V^2 and the resulting value of propagated wave's velocity will achieved. One of the three mentioned values is related to quasi-longitudinal and the other two roots are belonged to quasi-transverse wave. So obtaining of this determinant the relation between wave velocity and the related strain (stress) will achieved.

References:

[1] Biot. M. A., *The influence of initial stress on elastic waves*, J.App.Phys.,1940.

[2] Hughes, D.S. and Kelly, J.L., *Second-Order elastic deformation of solids*, Phys. Rev., 1953.

[3] Henneke II. E.G. and Green Jr., R.E., *Light-wave/elastic- wave analogies in crystals*, J. Acoust. Soc. Amer., 1968.

[4] Green Jr., R. E., *Ultrasonic Investigation of Mechanical properties*,Vol. 3, Treatise on Materials Science and Technology ,Ed. H. Herman, 1973.

[5] Toupin, R. A. and Bernstein, B., *Sound waves in deformed perfectly elastic materials, acoustoelastic effect*. J. Acoust. 1961.

[6] Murnaghan, T. D., *Finite Deformation of an Elastic Solid, John Wiley*, New York, 1951.

[7] Chung, T.J., *Continuum Mechanics, Prentice-Hall International*, Inc.,1988.

[8] Wolfram, S. Mathematica 3.1, 1997.

[9] Sinaie.A., Ziaie.A., General linearized equations of wave propagation in strained elastic solids of cylindrical shapes using a simple perturbation method, *Journal of Mechanical Engineering Science*, Vol 216, 2002.

Using Neural Network in Plate Frequency Calculation

ARASH ZIAIE
Civil Engineering Department
University of Kerman
22th of Bahman Ave., Kerman University, Kerman
IRAN
ZIAIE111@YAHOO.COM
ISSA MAHMOUDI
Sama Organization (Affiliated With Islamic Azad University), Shahr-e-Kord Branch
IRAN
MAHMOUDI.ISSA@GMAIL.COM
ARASH KIYOUMARSI
Electric Engineering Department, Faculty of Engineering
University of Isfahan
Hezar Jerib Ave., University of Isfahan, Isfahan
IRAN
Kiyoumarsi_arash@yahoo.com

Abstract: -The general goal of this research is the determination natural regular frequency of a plate by artificial neural network with various supporting conditions. For the subject of neural network, training or learning algorithms are applied the most famous of which is back propagation algorithm. This algorithm is a systematic method for training multi layer artificial neural network. Back propagation algorithm is based on gradient descant which means that it moves downward on the error declination and regulates the weights for the minimum error. In this research, the real frequency is calculated first using ANSYS program and is defined as a goal function for neural network, so that all outputs of the network can be compared to this function and the error can be calculated. Then, a set of inputs including dimensions or specifications of plate are made using MATLAB program. After the determination of algorithm and quantification of the network, the phases of training and testing of the results are carried out and the output of the network is created. It is concluded that according to results, the performance of the neural network is optimum, and the errors are less than 7%, so the network can perform training in different manner. Furthermore the time of frequency calculations in neural network is less than real analysis time that calculated by ANSYS software, and it's precision is acceptable(less than 10%).

Key-words: -Frequency- Artificial intelligence- Plate- Excitement function- Training function- Learning function.

1 Introduction

Providing a program to answer to multivariate problem as input and output is hard or impossible because we can ´t considers all of variables and their effects. But it is practicable by artificial neural network and use a software .Also modern programming methods are the methods which are sensitive to error in input data, because in artificial neural network, the training is on the base of experience and it can tolerate against errors. Artificial neural networks are used in different researching fields and professions, and are made by cooperation of scientists in different fields such as computer engineering, electronic, structure and biology. Some of the important usages of neural network are classification of data, recognition of letters and figures, estimation of functions and etc. use of neural network in the structure engineering is developing and will develop more and more. In the field of structure engineering, it used for optimization, analysis and designing, anticipate of results for soil and concrete, graphs theory and etc.

2 Problem Formulations

2.1 Elements of Plates in Flexural State

It's probable that isoparameter hexahedron limited, so a dimension is small versus two other dimensions. In this case, hexahedron changed to shell element or plane. For analysis of flat plane, it's necessary to limit reformed dimensions to put them in a single area. This part allocated to isoparametric hexahedron H20, which change to flexural tetrahedral plane, PBQ8.

The figure (1-1a) shows the main member of H20.It defined by geometrical interpolated quadratics .For perceive of required constraints for change it to flexural elements, we make a flat cuboids with natural coordinates, ζ ,η, ξ with small dimension , ζ , perpendicularly. Obtained element is shown in (1-1b) and is as a rectangular pattern, PQR8, from PBQ8 element before constriction. It must be remembered that that three nodal groups are located in angles, but two nodal groups are in the middle of side in PQR8 element. In the figure 1, we see that with special constraints instigation, we can change each group and twin nodal to single nodal in the middle of area.

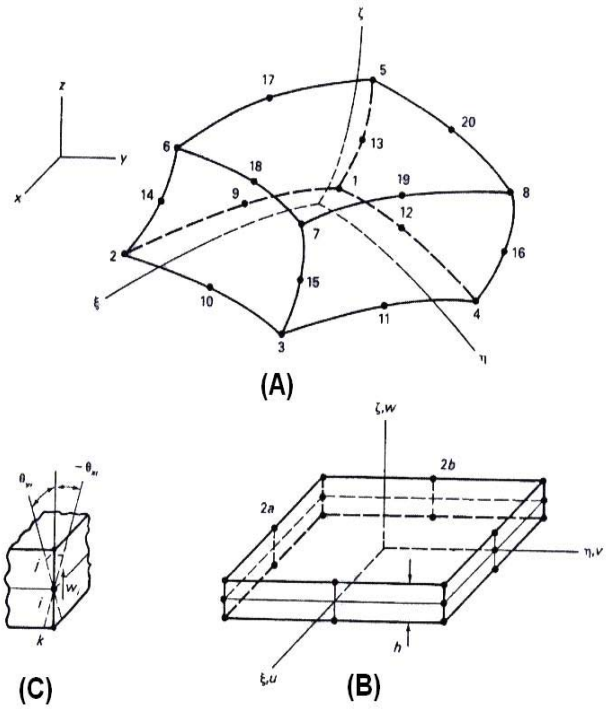

Fig.1: special manner of hexahedron

2.2 Making an artificial neural network for approximation of plate's frequency

For network training, 160 plates were chose. Each of them had six parameters: length, width, thickness, Young's modulus, Poisson's ratio and density. Three of them (length, width, thickness) are based on plate dimensions and another (Young's modulus, Poisson's ratio and density) are based on plate quality. The alteration for plate length is 0/5 to 12 m and for width is 0/5 to 4 m. Also, the alteration for thickness is 0/002 to 0/22.Because plates are steel, their quality coefficients are fixed. So, Young's modulus is 2×10^6 kg/cm^2, Poisson's ratio is 0/3 and density is 7850 kg/m^3. Because mapping range for input parameters should be 0 and 1, the units changes for decrease of dispersion in input parameter, so we consider micrometer, nanometer, kg/cm^2, μg /hectometer^3 for length, width, thickness, elastomer and density , respectively. Poisson's ratio is multiplied in 10^6.All of input parameters are divided to square of sum of square separately to network input mapping estimates between 0 to 1.All of results which obtained by plate analysis in ANSYS11 software chose as an objective function, to compare obtained output network with objective function and all errors can calculated In this formula:

Net= newff(PR,[$S_1S_2\ldots S_i$] ,{$TF_1TF_2\ldots TF_n$},BTF)

Where; *PR* is matrix of R×2 with minimum and maximum input elements, *si* is the size of i layer, *TFi* is the excitation of i layer (obtained by transfer function) with tansgin presupposition and *BTF* is the network conversion function with trainlm presupposition.

Network specifications are defined by network structures, number of layers, number of neuron in each layer, transfer function in layers, learning function and performance evaluation .With regard to back propagation neural network that used for plate frequency calculation, we should study newff , newcf, newelm structure and the best of them chose. In this paper, each of them is made separately, and has different layer (2-5 layers), and the structure with less error is used for optimum network. In each structure we choose 6 plates for test, and their specifications are in table 1. one of the test samples is part of training input and others are new inputs.

Table 1: dimensions of plates for network test

Plate sample	Dimensions(m)			Natural frequency (hertz)
	length	width	thickness	
(1)	0/5	0/5	0/002	22/73
(2)	0/8	0/7	0/005	25/06
(3)	1/3	1	0/008	17/91
(4)	1/8	1/2	0/01	14/4

(5)	2/5	2	0/05	28/56
(6)	4	3	0/1	24/28

2.3 The study of newff, newcf, newelm neural network

Here, the neural network with 2-5 layers with newff structure is studied, and 20 networks with different neurons are analyzed for each plate. Modulus network had 6 fixed neurons in input layer (plate variable parameters) and a neuron in output layer (plate frequency). The neural network with newelm and newef structure is studied and results are provided in table 2.

Table 2: results of neural network with 2 to 5 layers

network	Two layer network		Three layer network		Four layer network		Five layer network	
	Error percent	Test time average	Error percent	Test time average	Error percent	Test time average	Error percent	Test time average
Newff	8/27	0/04	8/04	0/041	6/67	0/042	6/86	0/044
Newcf	13/22	0/026	10/39	0/027	7/88	0/039	10/27	0/058
newelm	9/39	0/032	4/74	0/031	5/34	0/029	5/4	0/038

According to newelm, newcf and newff neural network output with 2 to 5 layers , , we found that by mathematical complex relations for regulation of interplay weight, we can't anticipated that with increase of layers, the network precision increases, but we should get optimum network by trail and error. newelm neural network with 3 layers and error of 4/74 % has the best performance, so another stages will continue.

2.4 Effect on neuron number (neural cell) in newelm neural network layers

Neuron number in each layer is important, so if the number of layer is low, neural network can't reflect nonlinear mapping for input and output .On the other hand, if they are more than required, the network produces nonlinear mapping with unsatisfactory performance. Because neurons number get by trial and error, so newelm three layer neural networks has studied, separately.

It's clear that three layer newelm neural network and 8 neurons in input layer and 8 neurons in the middle layer has less error. Figure 2 shows the error percent and neuron number in inner layer.

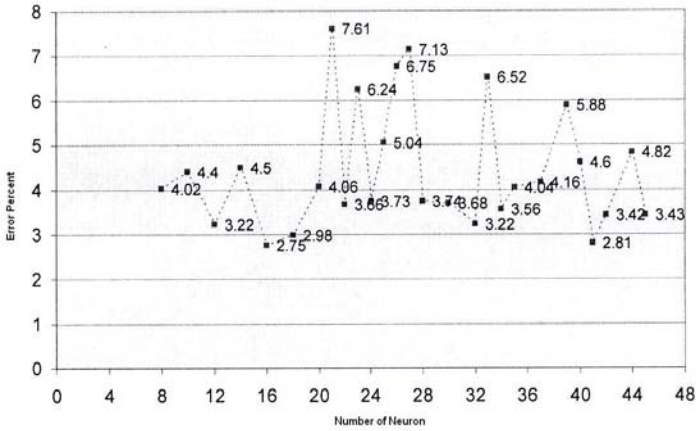

Fig.2: effect of neuron number in inner layer on amount of error

2.5 The effect of excitement functions in newelm three layer neural networks

Usually, network processing is by excitement and is as a logical or crescent (sigmoid).Although it's not necessary to choose excitation function for all neurons in layer, but the excitement function is same for neurons in layer and most of the time, nonlinear excitement function is used to maximize efficiency of multilayer networks. In this paper, excitement functions such as purelin, logsig and tansig are back propagation algorithm that have studied (table 3).

Table 3: effect of excitation function in newelm three layer networks

Excitation function composition	Average error percent	Average testing time(s)
Tansig-logsig-purelin	2/8	0/031
Tansig- Tansig -purelin	3/38	0/026
logsig -Tansig -purelin	3/21	0/031
Logsig- logsig -purelin	5/96	0/023

2.6 Effect of training function on newlem three layer neural network

The goal of training is finding an optimum answer of network, so that output arises from real answer. In network training, each input vector and opposite output vector make a couple. Usually, a neural network trains with more couple. In neural network, primary weights

are important because this comparison is depended on different elements such as input data, weights number, goal error parameter and the aim of network usage.
In table 4, the results of comparison between different training function in newelm network are shown.
So, we found that Train cgb has less error (2/32%) and it's performance is better than other functions.

Table 4: effect of training function

Kind of training function	Average error percent	Average testing time(s)
Train lm	5/76	0/047
Train bfg	3/98	0/032
Train cgb	2/32	0/028
Train cgf	5/11	0/034
Train cgp	5/42	0/029
Train oss	2/64	0/026
Train rp	10/78	0/029
Train scg	3/54	0/031

2.7 Effect of learning function on newlem three layer neural network

In the neural network, all of calculations are related to each layer, and the output can estimated. At first, output of neural cells in a layer calculated and the result used as an input for another layer. After that, according to input, the second layer output is calculated. This process continues to output make output vector. Learning functions are important, so the effect of learning function on newelm neural network is studied (figure 5).

Table 5: effect of learning function

Kind of training function	Average error percent	Average testing time(s)
Learn gdm	5/84	0/031
Learn gd	7/82	0/034
Learn som	3/8	0/036
Learn p	2/32	0/029
Learn os	6/45	0/031
Learn lv_1	7/2	0/026
Learnlv_2	5/74	0/032
Learn con	6/11	0/034
Learn k	5/69	0/039
Learn I_s	6/51	0/047
Learn h	2/81	0/096
Learn hd	4/30	0/089
Learn wh	16/05	0/016

According table 5, learn P function (error=2/32%) has better performance. In this function, training input functions binary. After training, the network accepts continuous input and produces output.

2.8 Effect of performance evaluation on newelm three layer neural network

In performance evaluation, we want to study how a network performs by trained and new (untrained) input. Amount of training and network performance calculated by different parameters and methods .Each of them studied separately and the best functions chose.(Table 6)

Table 6: effect of error function

Kind of training function	Average error percent	Average testing time(s)
mae	41/13	0/016
mse	7/82	0/013
Msereg	39/45	0/013
sse	3/88	0/013

According the results, sse function has the best performance.

2.9 Proposed neural network

By analysis, this neural network is suggested for calculation of plate frequency:
net= newelm (maxmin(p),[8 8 1],{′tansig' ′logsig' 'purelin'};'traincgb','learn p', 'sse')

3.1 Network testing for different plates

Plates with different models (according to place of supports and fixed supports) analyzed by ANSYS11 software, and their real frequency determined. They tested by proposed network and their efficiency determined by errors. Some samples of output results are given in table 7and fig. 2, 3, 4 and 5.

Table 7: plate analysis by support in around the plate

Plate No.	Real frequency	Analysis time(s)	Network frequency	Training time(s)	Testing time(s)	Error percent
1	22/73	0/6	21/48	28/47	0/062	6/95
2	25/06	1/37	26/91	16/34	0/031	0/04
3	17/91	3/21	18/19	21/11	0/016	7/65
4	14/4	5/36	14/11	12/47	0	2/01
5	28/56	12/46	28/07	31/73	0	2/87

6	24/28	30	25/1	17/56	0/016	3/79

Hitherto, according to different supports for plate, the first frequency output in neural network has been studied. Now, we study the first and second frequency output for plates with support in the corners, and first to fifth frequency output for plates with supports in the opposite side to calculated proposed network power for higher frequency (tables 8 and 9)and (fig. 6 and 7).

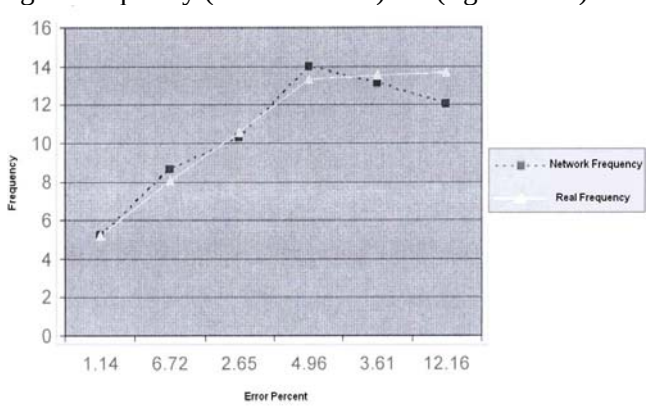

Fig.2: compare of calculated and approximate (support on two opposite side)

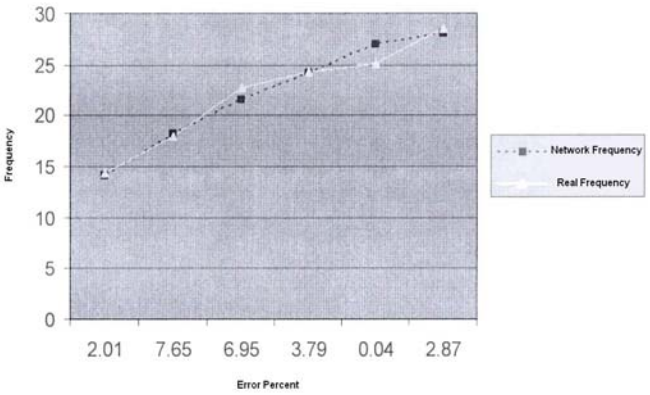

Fig.3 Diagram 3: compare of calculated and approximate (around support plate)

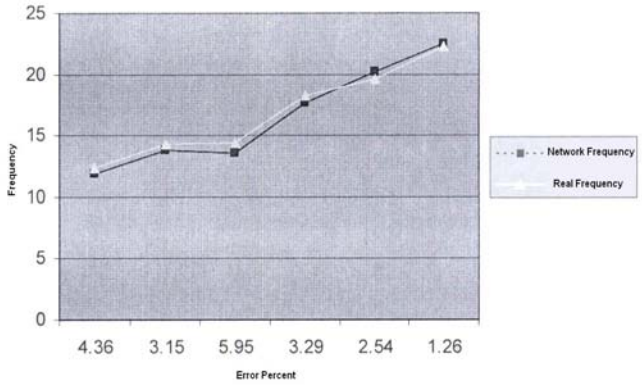

Fig 4: compare of calculated and approximate (punched plate)

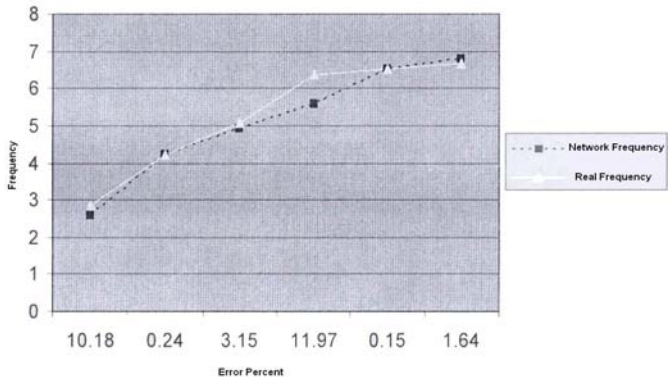

Fig.5: compare of calculated and approximate (Plate support at corners)

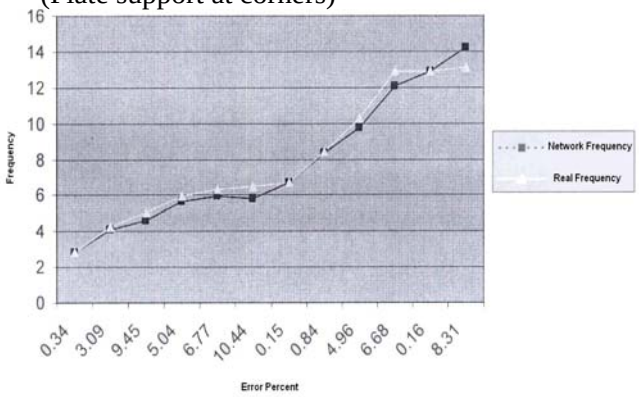

Fig.6: compare of calculated and approximate results (first and second frequency)

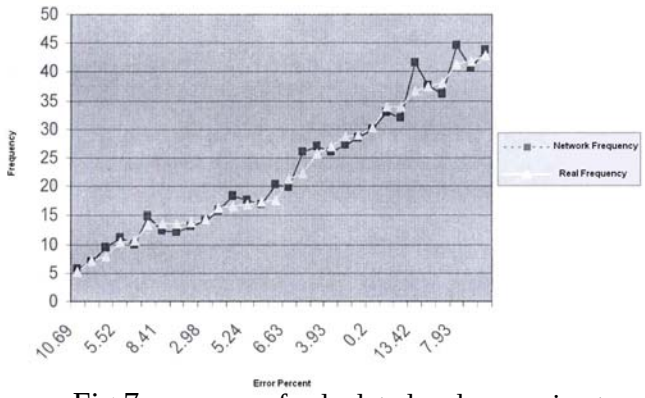

Fig.7: compare of calculated and approximate results (first to fifth)

Table 8: the results of first and second frequency

Average error percent	Average testing time in network(s)	Average real analysis time(s)	Plate support
4/68	0/039	8/99	Support in the angles

Table 9: first and second frequency output results for plate with support in corners

Plate No.	Real frequency	Analysis time(s)	Network frequency	Training time(s)	Testing time(s)	Error percent
1	6/35	0/65	5/92	68/05	0/047	6/77
	12/88		12/02			6/68
2	6/69	1/44	6/68	32/69	0/032	0/15
	13/11		14/2			8/31
3	4/21	3/32	4/08	59/27	0/031	3/09
	8/38		8/31			0/84
4	2/85	5/5	2/86	41/89	0/047	0/34
	5/95		5/65			5/04
5	6/51	12/68	5/83	31/41	0/046	10/44
	12/89		12/91			0/16
6	5/08	30/34	4/6	52/97	0/031	9/45
	10/27		9/76			4/96

4 Conclusions

Regarded to complex mathematical relations for regulation of weights in neural network output optimization, we can't anticipated that increasing of layers improve the network output. So, after study of 2 to 5 layer network, three layer networks with newlem function has the best answer. Usually, network data processes by excitement function and neural output signal produce. Change of structure functions can change the network output. With regard to effect of excitement functions combination in neural network, tansig, logsig and porelin are suitable for the firs, second and third hidden layer, respectively. During network training, network weights converge, so with regard to input vector, the out put vector produced and network output convergence with goal function (real frequency) obtained by traincgb training function. Powerful network can answer to trained and new (un trained) input. It calculated by learning function and performance evaluation function, sse, are the best output for neural network. The research shows that kind of plate and its condition are ineffective for final results of network. With change of support conditions, we found natural frequency. According to analysis, estimation of frequency with neural network is unlimited and outputs are accessible, but because structure elementary frequencies have more effects on dynamical analysis, they have studied. With artificial neural network, structure neural frequencies are estimated rapidly and exactly (less than 10%). So, after network training, we don't need plate analysis.

References:

[1] Talylor JG., Mannion clt., *Theory and Application of Neural Networks*, Springer-Verlag, New York, 1992.

[2] Wasserman PD., *Neural Computing (Theory and Practice)*, Van Nostrand Rrinhold, New York, 1989.

[3] Fausset L, *Fundamental of Neural Networks*, Prentice hall company, New York, 1994.

[4] Szewczyk Z., Hajela P., Neural Network Approximation in a Simulated Annealing, Based Optimal, *Structure Design*, Vol.5, 1993, PP.159-165.

[5]- MATLAB6P5/toolbox/nnet/nnet.

[6] Grandhi RV, structural optimization with frequency constrains-a review, *AIAAJ.,Vol 31*1993,*PP.2296-2303.*

[7] Moore GJ., Vanderplaats GN., Improved Approximations for Static Stress Constraints in Shape Optimal Design of Shell Structures, *Long Beach,CA, AIAA/ASME/ASCE/AHS/ASC, 31nd structures, Struct .Dyn, Mater.Conf.*Vol.1, 1999, PP. 161-170.

GIS BASED LANDSLIDE SUSCEPTIBILITY MAPPING: KARABÜK PROVINCE CASE in TURKEY

Ahmet Temiz
General Directorate of Disaster Affairs
Earthquake Research Department, Ankara, Turkey
temiz@deprem.gov.tr

Abstract:- Landslide constitutes one of the major hazards of NW Turkey including Karabük province. Recently, a large number of landslides have occurred and caused considerable damage on the buildings, infrastructures and agricultural lands. Geological and topographical conditions in the most part of the region are extremely favorable for occurrence of landslides. Landslide susceptibility mapping is the basic study for all landslide mitigation projects. "Past is the key to the present and future" is the fundamental idea of landslide susceptibility mapping. Hence, it is assumed that future landslides are most likely to follow the spatial patterns of the past landslides. This study consists of: 1) detailed field works to produce landslide inventory map at 1: 25,000 scale, 2) establishing spatial relationship between existing landslides and landslide contributing factors using GIS. In this framework, landslide factor maps were generated from digital elevation model (DEM) in raster format with a grid spacing of 10m to 10m. Digital geological map at 1:25.000 scale was also employed. Logistic regression as a multivariate statistical method was used to evaluate landslide susceptibility. The results of spatial analyses have revealed that Upper-Cretaceous and Eocene flysch units in certain terrain conditions have the primary influence on landsliding. The produced landslide susceptibility map distinguishes the areas that have different potentials for landsliding. Consequently, it can be used for engineering and planning purposes to predict the relative degree of landslide hazard.

Key Terms: Geographic Information System(GIS), Landslide, Susceptibility Map, Karabük(Turkey), Geology, DEM, Spatial Analysis.

1 Introduction

Landslides are a complex natural phenomenon that constitutes a serious natural hazard in many countries (Brabb and Harrod, 1989). Landslides also play a major role in the evolution of landforms. The term landslide denotes " the movement of a mass of rock, debris or earth down a slope" (Cruden 1991,27).

Landslide susceptibility mapping is based on a extensive study of slope movements and their contributing factors. "Past is the key to the present and future" is the fundamental idea of landslide susceptibility mapping. Therefore, landslide susceptibility mapping is based on an assumption that future landslides are most likely to follow the spatial patterns of the past landslides.
Quantitative methods are based on numerical expressions of the relationship between controlling factors and landslides. There are two types of quantitative methods: deterministic and statistical (Aleotti and Chowdhury, 1999). Deterministic quantitative methods mainly employ engineering principles of slope instability expressed in terms of the factor of safety. Among various multivariate statistical approaches discriminant analyses and logistic regression stand out. Logistic regression has been applied for landslide susceptibility mapping by various researchers including Bernknopf et al. (1988), Wieczorek et al. (1996), Atkinson and Massari (1998), Guzzetti et al. (1999), Dai et al. (2001), Lee (2007), Ayalew and Yamagishi (2004).

Since GIS provides an efficient framework for preparing landslide factor maps and spatial analysis, it has been widely employed in this study.

2 Study area

The Study area (Fig. 1), Karabük province, is located about 200 km of capital Ankara, and covers 4.105 km^2.

Compared to the other regions, North-West of Turkey is known more prone to landslide occurrence (Fig. 2).

Recently, landslides in the region have caused heavy damage on a large number of buildings, disrupted the roads and severed the pipelines. Totally 1800 houses from 40 different residential areas had to be relocated by the government due to landslide activity.

Vegetation is dense throughout the mountains but scarce in the residential areas and their surroundings. The climate of the study area is generally humid. Precipitation is heavy and occasionally intense and often causes flooding. The annual mean precipitation is around 1200 mm and the annual mean moisture is measured as %76.

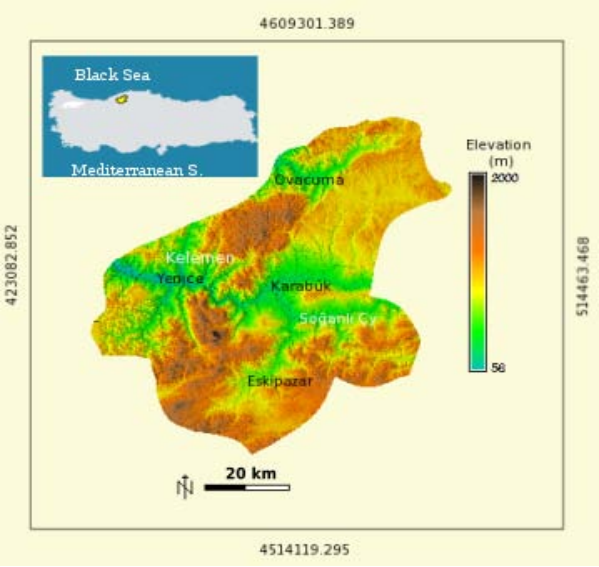

Fig. 1. The study area and its geographic location.

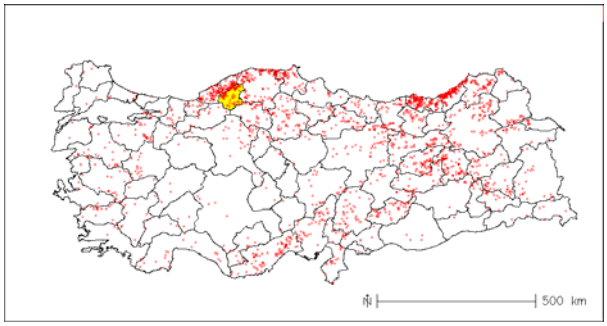

Fig. 2. General distribution of landslides in Turkey, which have affected residential areas (1950-2004) and the study area.

2.1 Geological Setting

The region geologically is mainly composed of:
1- Paleozoic granadiorites;
2- Jurassic limestones;
3- Upper-Cretaceous flysches and olisthostroms,
4- Tertiary sedimentary units (Fig. 3).

Precambrian and Paleozoic rocks are mainly represented by metamorphosed intrusive rocks. Jurassic rocks are composed of limestones and recrystallized limestones.

Upper Cretaceous flysch is in turbiditic character and has deposited originally in deep-sea facies.

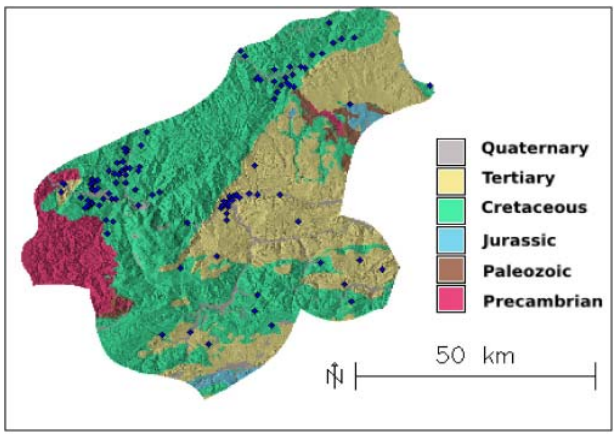

Fig 3. The simplified geological map of the area. Blue points stand for residential areas stricken by landslides in the past (1950-2004).

This flysch unit consists of an alternation of

predominantly shale and sandstone (Fig. 4). It is known that a lot of debris flows in depositional era occurred (Tüysüz,1999). Consequently, a large number of olistholiths mostly derived from older Jurassic limestones and are embedded in this unit (one example can be seen in Fig. 7).

Fig. 4. A typical view of Upper-Cretaceous flysch.

Upper-Cretaceous flysch seems to be the most susceptible rocks in terms of landsliding.

Cretaceous olistostrome unit looks chaotic mass and mostly consists of various green and carbonate rocks.

Tertiary units are composed of various rock groups as: flysch, marlstone - sandstone and limestones.

Due to influence of intensive north-south post-tectonic compression, these rocks are observed as heavily folded and faulted. Besides, meteorological conditions of the region bring about considerable decomposition in the rock units.

Major active fault of Turkey, namely North Anatolian Fault, crosses southern part of the province. In addition to tectonic disruption, a large amount of deformation in the rock masses is originated from mass movements which have occurred in the depositional era.

2.2 Landslide types and general characteristics

The landslides of the region can be classified according to terminology of Cruden and Varnes (1996) as 1- rotational rock slides, 2- translational rock slides, 3- debris slides-flows.

Deep seated rotational landslides constitute the dominant type of landslide mechanism of the region (Fig. 5).

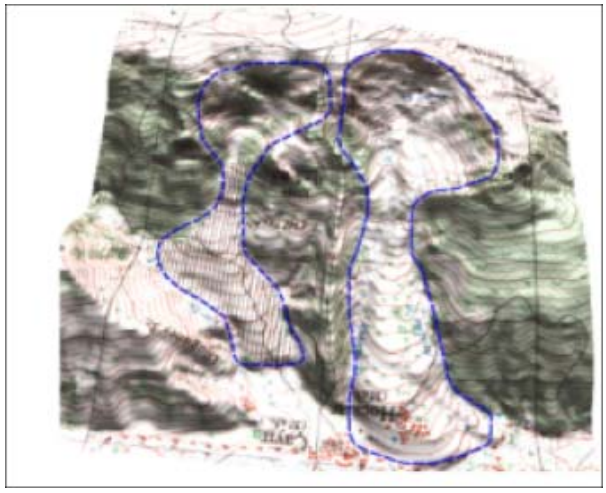

Fig 5. A typical 3D view of a landslide of the region: complex rotational rock slide - earthflow on the topographical map. Approximate length: 2300 m. and width: 900 m.; location: around Eskipazar-Hocakoy.

They generally involve bedrock (Fig. 6). Their depth of slip surfaces are more than 20 m. In terms of style of activity of landslides, they can be called as “complex rotational rock slide - earth flow”. They have material flow at their accumulation zones, and they are usually getting more complex as they have rockfall components with olistholith blocks and very hard quartzite rocks (Fig. 7).

Fig. 6. Left flank of an active landslide in the region. Location: Yenice Derebaşı village.

Fig. 7. An olistholith block in a landslide body.

In terms of state of activity, most of the slides are old and in dormant stage. Their accumulation zones either have been eroded or removed by streams. They are mostly observed in gentle and moderate slopes. Because of their large size and taking place on gentle slopes, it can be said that these slides show slow movement activity.

However, landslides with flow or rockfall components may take place in quick form. The types of the landslides are primarily governed by some geological features of the region:

1- Because of outcropping of bedrocks in the most part of the region, surficial material flows have taken place in limited numbers.
2- Densely folded layers of the flyschs are rarely seen parallel to free faces of the topography, which is a prerequisite for initiation of translational rock slides. For this reason, translational landslides are not frequently observed, and
3- Extensive forest coverage of the region has significantly inhibited occurrence of all shallow movements including flows and translational slides. Consequently, it can be said that favorable geologic conditions for development of shallow movements don't widely exist. But, in comparison of number of landslides with respect to their types, it should be kept in mind that surficial movements occurred in the past might have easily been absorbed by nature and obliterated in time, whereas head scarps of old deep rotational slides still remain and that may appear to be dominant. However, since most of the fresh looking landslides were observed to have occurred as deep seated rotational landslides, this type was accepted to reflect dominant landslide type of the region. The recent landslides were primarily triggered by extreme climatic events of melting of snow packs and prolonged heavy rainfalls. In the region, landslides usually occur locally. But, landslides that took place in 1985 and 1998 are somewhat exceptional. In 1985 spring, landslides in the whole region including Karabük, Bartın, Zonguldak, Kastamonu and Sinop provinces were simultaneously triggered in the whole NW Turkey in response to groundwater buildup from sudden melting of winter snow packs. In 1998, extreme rainfall resulted in both new slope failures and the activation of slope movements of earlier origin.

Earthquake represents secondary triggering mechanism for the region. 1944 Gerede earthquake that occurred at North Anatolian Fault is known to have induced some gigantic landsides (see Fig. 3).

Upper Cretaceous flysch in turbiditic facieses is actually a depositional product of displaced masses of landslides. As it is well known, subsequent mass movements occurred in the whole period of Cretaceous period and these movements led to heavy deformations on the rock units. These deformations are one of the major causes of today's landslides. Besides, post-tectonic related intense folding and faulting bring about tremendous strength reduction in the rock masses. Susceptibility to sliding is also increased by the heterogeneity of slope sediments, which in some places are permeable, composed of sand and rock fragments, and in others consist predominantly of clay layers.

Topographical conditions are also an important factor which largely controls the course and extent of shallow landslides. Angles of slopes abruptly change and steepen as a result of strong compressional post-tectonism.

Delicate equilibrium state of the slopes is continuously disturbed by the lateral erosion of Filyos, Soğanlı and Kelemen rivers which carry

away the front margins of the slopes. Frequent flood occurrences originated from these rivers have also intensified this situation in the recent past.

3 Landslide inventory

Landslide inventory is the basis for landslide susceptibility mapping. As generally accepted, landslide inventory maps are in two classes: 1- inventory map built based on certain landslide-event associated with a trigger 2- historical landslide inventories which include events that have occurred over periods of tens, hundreds or even thousands of years (Malamud et al., 2003). Knowing from our past studies, the current landslides of the region are mainly results of reactivation of the old landslides, therefore historical landslide inventory was preferred to use for this study.

At the initial stage of building inventory, existing databases of General Directory of Disaster Affairs (GDDA) were compiled. “General distribution map of landslides that affected residential areas" was used to get initial idea about the locations where past landslides have concentrated (Temiz, 2005, see Fig. 2).

A series of field trips were carried out to identify the types of movements, the materials involved, and determine the activity (active, dormant, etc.) of failed slopes.

1/25000 scaled digital topographic contour maps of General Mapping Command was used as the base map of landslide inventory.
Since the lack of aerial photos and satellite imageries for the whole region, mostly shaded relief map was used to check the landslide boundaries which had been originally determined during field studies.

In total, 250 landslides were mapped, digitized and rasterized in GRASS-GIS environment (Fig. 8).

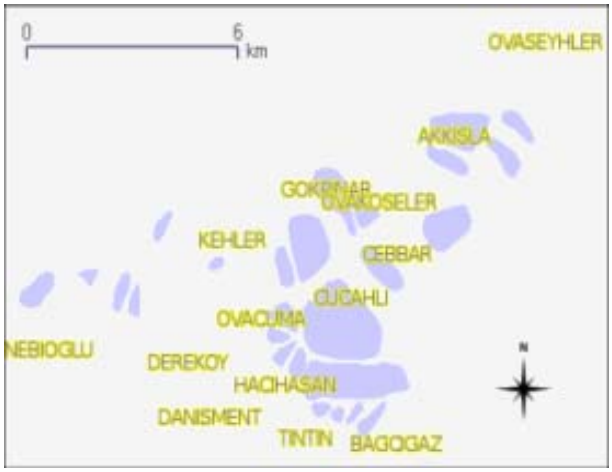

Fig. 8. A part of landslide inventory map of the study area.

As is known, there are some limitations in using historical landslide inventory: One of them is that some small shallow landslides might have been obliterated in time or obscured by the forest cover. Hence, they cannot be easily recognized and counted in lower numbers than their real numbers.

Regarding the complex manner of the large landslides, different part of the landslides were distinguished and only the failed part of these landslides were stored in the inventory to include the model. Since they don't represent the geologic and topographic cause of the occurrences, accumulation zones of the landslides were excluded from the inventory.

Inventory data was stored in PostgreSQL- PostGis spatial database and connected to GRASS for GIS implementations.

4 Modeling and GIS studies

The modeling is based on an assumption that future landslides are most likely to occur in same environmental conditions of the past landslides. Hence, establishing the spatial relationship between existing landslides and landslide influencing factors was accepted the core of the modeling.
The main idea of the modeling can be explained as understanding reason-result relationship. In this context, factors leading to landslide can be categorized in two folds: 1: static factors which

remain constant in both pre-landslide and post-landslide stage such as lithology and aspect of slope. Therefore, their current values also indicate their pre-failure values. 2: dynamic factors which mainly refer to triggers. They abruptly change in time. Their pre-failure values cannot be estimated correctly. Since we need to know pre-sliding values of all factors, we can only take static factors into consideration. By thinking current conditions of land use related parameters (i.e. roads, agricultural lands, etc.) may not have existed at the time of initial movement, they were refrained to include to the modeling.

In spite of the fact that trees have stability increasing effect, they also have somewhat adverse effects on stability. Besides, their positive effects on stability can be negligible for deep seated landslides. Therefore, forest coverage as a factor was not included to the model either.

GIS is the integral part of the project. 1/25000 scaled topographical contour and geological maps were employed as the base maps.

Landslide factor maps were prepared in GIS environment mostly in raster structure. Since different type of landslides occur in different terrain conditions, each type of landslide of the region was modeled separately.

Rock type, slope gradient, slope aspect, and slope shape were accepted input parameters for the model. Geological conditions of the region are very conducive to landsliding. One to one relationship between existing landslides in the inventory and rock type indicated that most of the existing landslides have developed in certain rock group, namely Upper Cretaceous flysch and Eocene flysch units. Digital Elevation Model (DEM) was constructed with a grid size of 10*10 m. using regularized spline tension interpolation technique in GRASS-GIS environment. Slope gradient, slope aspect, and slope form maps as landslide influencing factor maps were derived from the DEM.

Slope gradient is one of the most significant cause of landslides. It was derived from DEM. But, since we need to know their pre-failure value of existing landslides, slope angle of existing landslides were estimated from height differences between crown and tip altitudes and axis length of landslides. Slope gradient map map was categorized into eight classes as 0-10, 10-20, 20-30, 30-40, 40-50, 50-60, 60-70, 70-90.

Aspect of slope may be an important factor to be taken into account in terms of landslide susceptibility, because it may indicate changing conditions of wetness of the ground. Slope aspect was categorized in 8 equal classes.

Profile curvature is also an important factor because it influences accumulation and transport process of materials. Slope form map was produced from profile curvature map as concave, straight and convex.

Modeling was carried out in three separate modeling areas and extrapolated to the larger areas of the region for generalization purposes.

Multivariate statistical analysis, namely logistic regression was adopted to determine spatial relationship between existing landslides and landslide contributing factors.

4.1 Application of Logistic Regression

Binary logistic regression is a form of regression which is used when the response variable is a dichotomy and the predictor variables are continuous, categorical, or both. Logistic regression applies maximum likelihood estimation after transforming the response occurring or not. In this way, it estimates the probability of a certain event occurring. Logistic regression calculates changes in the logodds of the response, but not changes in the response itself. The advantage of logistic regression analysis is that it does not require any assumption about the distribution of the predictor variables. They do not have to be normally distributed, linearly related or of equal variance. The other strength of logistic regression lies in the fact that an entire set of variables can simultaneously be taken into account.

The general formula of logit can be expressed as:

$$\ln[p/(1-p)]=a+b1x1+b2x2... \quad (1)$$

where p / (1-p) is called odds ratio that refers to the likelihood of a given event occurring compared to the likelihood of the same event not occurring.
Probability of the given event (p) can be defined as:

$$p = \exp(a+b1x1+b2x2 ...) / (1+ \exp(a+b1x1+b2x2 ...)) \quad (2)$$

All the statistical analyses in this study were conducted using the "R-Stat" package.
First, single models in which each predictor variable was modeled alone with response variable were constructed. These models had lower deviance values than null model in which no predictor variable was included to model except intercept (Table 1). These results indicated that each variable had certain effect on landsliding. But, because deviance values of each parameter weren't significantly different from null model, interactions of predictor variables were needed.

Table 1: Deviance values of single models of predictor variables and null value.

	Deviance
NULL	27733.79
Rock Type	8284.431
Slope Gradient	25941.69
Slope Form	27591.91
Slope Aspect	27576.35

Selection of model with interactive parameters was carried out on the basis of likelihood-ratio test, particularly AIC (Akaike Information Criterion) which is a measure of goodness of fit. StepAIC method facilitated model selection with stepwise process removing redundant variables. The final model with lowest AIC value was inferred as better model fit.

The final model was obtained as in Table 2:

Table 2. Initial model and final model obtained after stepwise process.

Stepwise Model Path
Analysis of Deviance Table

Initial Model:
*cbind(hv, hy) ~ as.factor(geo) * as.factor(slp) * as.factor(con) * as.factor(asp)*

Final Model:
cbind(hv,hy)~as.factor(geo)+
as.factor(slp)+as.factor(con)+
as.factor(asp)+as.factor(geo):as.factor(slp) +
as.factor(geo):as.factor(con) +
as.factor(slp):as.factor(con)+
as.factor(geo):as.factor(asp)+
as.factor(slp):as.factor(asp)+
as.factor(con):as.factor(asp)+
as.factor(slp):as.factor(con):as.factor(asp)

In this table (hv,hy): response variable (landslide presence/absence), geo:rock type, slp:slope angle, con:slope form, asp=aspect,":"factor interaction.
Since the model was complex, interpretation from coefficients wouldn't be informative. For this reason, model interpretation was carried out on predicted values of group combinations.

The model results revealed that all parameters independently and interactively had certain effect on susceptibility.

In Table 3, the highest susceptibility was represented by: Rock type (geo,10) is Upper Cretaceous flysch; Slope gradient (slp,2) is $10\text{-}20^0$; Slope form (con,3) is the concave slope form; Aspect (asp,4) is the north-west facing slopes.
The fact that combinations of Upper Cretaceous flysch as rock type, gentle slopes, North-west facing slopes and concave forms of first order basins represented high susceptibility in analyses substantiated our field interpretations.
These predicted values were reclassified as 1- low 2- moderate 3- high 4- very high susceptibility zones and used for portraying landslide

susceptibility map (Table 3 and Fig. 9).

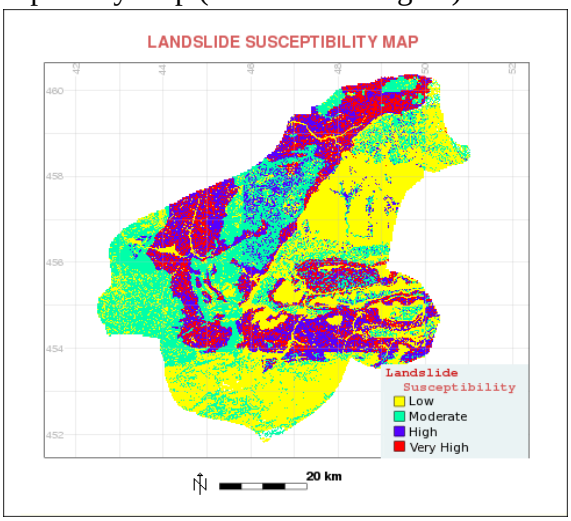

Fig.9. Landslide susceptibility map of Karabük province.

Table 3: A part of the model. Predicted values of group combinations and susceptibility categories. (Predicted values below 0.2 is not shown in the table).

geo	slp	con	asp	hy	hv	pred.	cat	suscept.
10	2	1	1	1043	43	0.8111702	(0.8,1]	very high
10	2	1	2	1147	74	0.7538953	(0.6,0.8]	high
10	2	1	3	1317	55	0.5387751	(0.4,0.6]	moderate
10	2	1	4	1156	89	0.7805885	(0.6,0.8]	high
10	2	1	7	1087	41	0.7192940	(0.6,0.8]	high
10	2	1	8	1157	39	0.5994329	(0.4,0.6]	moderate
10	2	3	4	1012	77	0.8491421	(0.8,1]	very high
10	3	1	1	2492	59	0.2477749	(0.2,0.4]	low
10	3	1	2	2719	77	0.2840192	(0.2,0.4]	low
10	3	1	3	2415	72	0.2945130	(0.2,0.4]	low
10	3	1	5	2046	73	0.3475790	(0.2,0.4]	low
10	3	1	6	1748	88	0.4705882	(0.4,0.6]	moderate
10	3	2	1	254	75	0.2917842	(0.2,0.4]	low
10	3	2	2	237	52	0.2372769	(0.2,0.4]	low
10	3	2	3	247	55	0.2369729	(0.2,0.4]	low
10	3	2	4	229	71	0.3059063	(0.2,0.4]	low
10	3	2	5	196	47	0.2732003	(0.2,0.4]	low
10	3	2	6	144	39	0.3900000	(0.2,0.4]	low
10	3	2	7	170	41	0.3033885	(0.2,0.4]	low
10	3	2	8	180	30	0.2222209	(0.2,0.4]	low
10	3	3	1	1878	46	0.2967466	(0.2,0.4]	low
10	3	3	2	1629	18	0.2059995	(0.2,0.4]	low
10	3	3	5	1559	70	0.4501836	(0.4,0.6]	moderate
10	3	3	7	2128	84	0.3663115	(0.2,0.4]	low
10	3	3	8	1882	32	0.2358315	(0.2,0.4]	low
10	4	3	1	3626	68	0.2148923	(0.2,0.4]	low
10	4	3	2	3205	90	0.2601402	(0.2,0.4]	low
10	4	3	5	3613	76	0.2287582	(0.2,0.4]	low
10	4	3	8	3957	67	0.2036120	(0.2,0.4]	low
10	5	2	3	1051	12	0.5215828	(0.4,0.6]	moderate
10	5	2	4	1200	46	0.5696115	(0.4,0.6]	moderate
10	5	2	7	1179	99	0.7674085	(0.6,0.8]	high
10	5	2	8	1512	47	0.4016958	(0.4,0.6]	moderate
10	5	3	6	4295	91	0.2275000	(0.2,0.4]	low
10	7	1	1	2012	37	0.2189343	(0.2,0.4]	low
10	7	1	2	1997	61	0.3269761	(0.2,0.4]	low
10	7	1	4	2792	91	0.3148716	(0.2,0.4]	low
10	7	1	5	2624	77	0.2883073	(0.2,0.4]	low
10	7	1	8	2031	49	0.2677552	(0.2,0.4]	low
10	7	2	5	356	73	0.2225209	(0.2,0.4]	low
10	7	2	7	592	99	0.2008110	(0.2,0.4]	low
10	7	3	1	2798	67	0.2506166	(0.2,0.4]	low
10	7	3	2	3303	72	0.2259597	(0.2,0.4]	low
10	7	3	4	2083	68	0.2788237	(0.2,0.4]	low
10	7	3	5	1777	27	0.2040999	(0.2,0.4]	low

5 Conclusions

For North-West of Turkey, landslides constitute one of the major natural hazards and account for considerable property damage in terms of both direct and indirect costs. Geological and topographical conditions of the region are extremely favorable for landsliding.

Landslide susceptibility mapping is the fundamental step to reduce effects of landslide hazard.

GIS is a powerful tool for evaluating spatial relationship between existing landslides and landslide contributing factors.

This study adopted logistic regression as statistical analysis method. Logistic regression results revealed that Upper Cretaceous flysch unit in certain terrain conditions is very conducive to landsliding.

References:

Aleotti, P., Chowdhury, R., 1999. Landslide hazard assessment:summary review and new perspectives. *Bulletin of Engineering Geology and the environment 58, 21– 44.*

Atkinson, P.M., Massari, R., 1998. Generalized linear modeling of susceptibility to landsliding in the central Apennines, Italy. *Computers and Geosciences 24,* pp 373–385.

Ayalew, L., Yamagishi, H. 2004. The application of

GIS-based logistic regression for landslide susceptibility mapping in the Kakuda-Yahiko Mountains, Central Japan. *www.elsevier.com/ locate/geomorphology*.

Bernknopf, R.L., Cambell, R.H., Brookshire, D.S., Shapiro, C.D.,1988. A probabilistic approach to landslide hazard mapping in Cincinnati, Ohio, with applications for economic evaluation. *Bulletin of the International Association of Engineering Geology 25,* pp. 39–56.

Brabb, EE, Harrod B.L (eds). 1989. Landslides: Extent and Economic Significance: *Proc.,28th International Geological Congress : Symposium on Landslides, A.A. Balkema: Rotterdam, Netherlands,385 pp*.

Cruden, D.M. 1991. A Simple Definition of a Landslide. *Bulletin of the International Association of Engineering Geology, No.43,*pp. 27-29.

Cruden, D.M., Varnes, D.J., 1996. Landslide types and processes. In: Turner, K.A., Schuster, R.L. (Eds.), Landslides: investigation and mitigation, *Transport Research Board Special Report,* vol. 247, pp. 36– 75.

Guzzetti, F, Cardinali M, Reichenbach P, Carrara A. 1999. Comparing landslide maps: A case study in the upper Tiber River Basin, central Italy. *Environmental Management 25:* pp. 247–363.

Lee, S., 2007. Comparison of landslide susceptibility maps generated through multiple logistic regression for three test areas in Korea. *www,interscience.wiley.com* DOI: 10.1002 / esp.1517

Malamud, B., Donald L., Guzzetti F., Reichenbach P. 2003. Landslide Inventories and Their Statistical Properties. *Published online in WileyInterScience (www.interscience.wiley.com)*.DOI: 10.1002/esp.1064.

Varnes DJ. 1978. Slope movement, type and processes. In special report 176: Landslides: Analysis and Control (R.L Schuster RL and RJ Krizek, eds.), *TRB, National Research Council, Washington, D.C.*, pp. 11-33.

Temiz, A. 2005. Landslide Distribution Map of Turkey, which Affected Residential Areas. General Directory of Disaster Affairs, unpublished.

Tüysüz,O.1999. Geology of the Cretaceous sedimentary basins of the Western Pontides. *Geological Journal geol. J. 34:* pp 75-93.

Wieczorek GF. 1984. Preparing a detailed landslide-inventory map for hazard evaluation and reduction. Bulletin Association of Engineering Geologists 21: pp 337–342.

Climate change in Sweden – geotechnical and contaminated land consequences

YVONNE ANDERSSON-SKÖLD, JAN FALLSVIK,
CARINA HULTÉN, ANNA JONSSON[1], MATTIAS HJERPE[1], ERIK GLAAS[1]
Swedish Geotechnical Institute (SGI), SE 412 Göteborg
SWEDEN
yvonne.andersson-skold@swedgeo.se, http://www.swedgeo.se

Abstract: - According to climate scenarios the global mean temperature will increase the nearest 50 to 100 year. Regional climate scenarios show increases in annual precipitation and heavy rain events in most parts of Sweden. Accordingly, the risks for flooding will increase. Also the risks of erosion and landslides are expected to increase as well as changed behaviour and increased mobility of soil contaminants. The summer season in general is expected to become drier and there consequently larger fluctuations of groundwater levels is expected further enhancing the risks of erosion, land slides and mobility of soil contaminants. One of the areas expected to be among the most affected in Sweden is the Lake Vänern and the Göta älv (river) system. The Swedish geotechnical institute has, together with other agencies and universities in Sweden, contributed in the national climate and vulnerability inquiry [1]. Here the results from three of those reports are presented, i.e. impact of flooding on soil pollutants [2], increased tapping from lake Vänern and related geotechnical conditions in the Göta älv valley [3] and overview assessment of land slide changes in a changing climate [4]. Based on the results from the national climate and vulnerability inquiry research projects have been initiated. One project focuses on the vulnerability and adaptive capacity among municipalities along the Göta älv system. The project includes socioeconomic, environmental and geotechnical aspects. The aim is to present some preliminary results from this project.

Key-Words: - Climate change, Sweden, land slides, geotechnical aspects, contaminant mobility

1 Background

Global temperature has increased during the last century, and according to climate change scenarios the increase will continue [5]. A sea level rise is expected due to the global temperature increase. The magnitude of changes will vary geographically and seasonally also in Sweden [6]. In Sweden the temperature increase will be more pronounced in winter than summer, and the snow season will be shorter. Apart from the south east parts of Sweden the annual precipitation is expected to increase in all of Sweden, in some areas by up to 25 % during the nearest century. More rain days are expected, and heavier rain falls. The precipitation increases even over autumn, winter and spring. During those seasons the rain falls will be heavier, but not more than expected from the general increase. During summer the precipitation will be more intense despite the total precipitation decrease. The increased sea water levels, the increased annual precipitation in most parts of Sweden and the changes in precipitation pattern will, of course, also have impacts on water flows and ground water levels, and more flooding events can be expected [1], [6]. During periods with large precipitation both the water flow and the ground water level will increase. The ground water already today is fluctuating between long rain and draught periods, but the frequency is likely to increase. Increased ground water level and increased fluctuations may result in increased leaching and spreading of pollutants from contaminated sites. Heavy water flow may result in large run off from the top layer bringing increased amounts of humus to surface waters. The result is increased turbidity and darker water. The humus may also carry pollutants [7]. The changes in ground water level and the increased fluctuation will also alter the soil conditions such as the oxygen availability, biological activity, redox and weathering conditions, which alter the risks since the toxicity and the mobility may change by changing the chemical conditions, the sorption processes and the degradation routes and times. Increased probability of erosion and land slides may

[1] Linköping University, SE 581 83 Linköping, SWEDEN, http://www.liu.se

result in accidents where high amounts of pollutants to air, soil or water may be released. For example dam ruptures and erosion and land slides in contaminated areas will result in the release of contaminated masses. Here the results from a study of the potential release of pollutants due to flooding of contaminated land and in areas with ongoing industrial activities will be presented based on the work in [2].

Vulnerability to climate change is a critical factor for the possibilities to achieve sustainable development. A changing climate will also affect city planning in that areas may become unsuitable for development due to increased risks for flooding and landslides. Cities and regions, thus, will increasingly get a key role in assessing the requirements for adaptation [8].

2 Mapping potential changes in landslide events

To find areas with prerequisites for landslides in areas covered by fine-grained soils, nationwide survey hazard mapping is performed, e.g. in Norway and Sweden. In Sweden this mapping is based on overview information on the slope inclinations and the soil conditions in the mapped areas, roughly the existence of clay and silt layers in the terrain coinciding with slope inclinations greater than a certain angle, primarily 1:10. Especially riverbank slopes can be unstable, and in quite many cases prone for devastating landslides also impacting built-up areas. During the first period of time after flooding, the landslide hazard in the riverbank slopes is increased due to remaining high pore water pressures in low permeable soil layers. Therefore, a further hazard mapping method, where flooding and landslide hazard digital maps have been combined to a map indicating sub-areas with prerequisites for landslides which also can be flooded has been done.

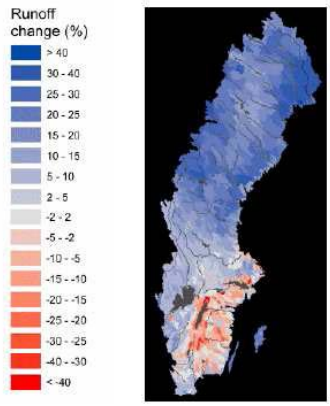

Fig. 1 Simulated increase of the annual runoff in Sweden 2071-2100 compared to reference period 1961-1990 [6].

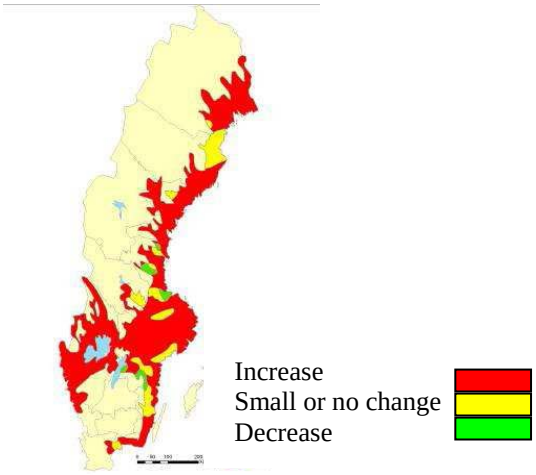

Fig. 2 Overview estimation of the landslide hazard change in Sweden due to the expected climate change during the coming 70-80 years [4].

2.1 National overview

Built up areas adjacent to rivers, lakes and sea shores will be exposed to flooding, waves and erosion related to the climate changes, in their turn triggering landslides. An overview estimation how the landslide hazards will change during the coming 70- 80 years, is presented in Fig.2. The map is performed by overlay between two index maps indicating the change in expected runoff [6] (Fig. 1) and erosion respectively, and presented in detail in [4].

3 Case studies of landslide risks – the Göta älv valley

In addition to the overview mapping, a case study area, the Göta älv (Göta river) valley in south-west Sweden was chosen for calculations of potential change in land slide probability. The Göta älv valley runs from Lake Vänern in the north to Göteborg in the south and is one of the most frequent landslide valleys in Sweden. A number of landslides occur every year but in general they are fairly small, shallow and caused by erosion. Limited slides under the water table occasionally also occur. An aerial photo scanning survey conducted in 1982 revealed 150 slide scars in the river valley. Larger landslides have also occurred in the river valley such as Surte, 1950 and Göta, 1957 where one or more people were killed, e.g. [3]. The high frequency of landslides in the river valley is due to the geological history, which has resulted in deep clay layers. Most of the clays have been deposited in a marine environment and quick clay is therefore common in the area. Quick clay is a soil where the skeleton collapses due to vibrations, or stirring, and the clay

thereafter behaves as a liquid. When a landslide occurs in a quick clay area the process is very rapid and the extent of the slide can be very large, with major consequences. In the northern part of the Göta älv valley the soil depths are moderate. Bedrock is common together with and mixed with sediment areas. The slopes towards the river are in general high and steep. The clays are firm and often contain water-permeable layers. Towards the south of the valley the clays are soft and homogenous and the clay and soil depths increase. In the southern part, riverside shelves and slopes under the water table often occur between the shoreline and the deepest part of the river [3 and references therein].
In 1938, a regulation of Lake Vänern, and thereby also the river (Göta älv) was done to optimise the use of the power stations along the river. The water flow in the river prior the regulation varied between 200 and 850 m3/s and the deviation between normal water flow and high water flow was moderate. After the regulation, water flows higher than 1000 m3/s occur more and more frequently, and also lower water flows (< 200 m3/s) have been permitted. This may have a great impact on the erosion processes and the of slope stability conditions along the river. First attempts to investigate the possible impact of increased precipitation and tapping on slope stability have been made based on tests and sensitivity analysis using methods developed for past and present climatic conditions.

Table 1 Case study scenarios to investigate the possible impact of increased precipitation and water flow in the Göta älv valley. F = Safety factor (> 1 the slope is regarded as safe, < 1 the slope is not regarded as safe, i.e. high probability of slope failure (land slide).

	Conditions	*Calculated safety factor, F*[1]	*Changes in safety factor, F*
Cross-section in the south-west of the Göta älv (Bäckebol, Göteborg)			
1	Present conditions	1.23	
2	Change (increase) in groundwater level (1m) and erosion	1.13	8-10% reduced risk margin
Cross-section in the north-east of the Göta älv (Lilla Edet)			
1	Present conditions	1.04	
2	Change (increase) in groundwater level (1m) and erosion	0.95	9% reduced risk margin, the slope can not be regarded safe.
3	Change (increase) in the groundwater level (1 m). The river water level is assumed to decrease 0.5 m.	0.93	11% reduced risk margin , the slope can not be regarded as safe

The rise in groundwater level due to increased precipitation is, in this scenario, set 1 m in the clay layer. This may be realistic for precipitation increase of ≥ 40%, which also may occur under present climatic conditions. The scenario with changed tapping and increased maximum flow is expected to result in 50 % increase in the erosion rate, depending on local conditions. The different scenario conditions for Göta älv valley and the impact on the slope stability (defined as the change in safety factor, F) are described in Table 1 and further details are presented in [3].

4 Contaminated sites and ongoing activities in flood risk areas

The Swedish MIFO (Methodology for inventory of contaminated land) database and the national Emission Register (EMIR) data base has been used to identify the number of contaminated sites and ongoing activities in the areas which have been identified as flood risk areas by the National mapping of the Swedish Rescue Service. At present around 10 % of the water coarse areas have been flood risk invented [9]. In Sweden around 83 000 potentially contaminated sites have been identified, among those about 15000 have been classified and among those all have not yet been communicated to the land owners [10]. The MIFO inventory is conducted by the 24 county administration boards in Sweden. The data base has been, and still is continuously updated. During the course of this investigation the relative amount of the sites investigated, classified and communicated varied among the counties. The data obtained from the county administration boards are most often the ones communicated but in some cases the ones classified have been reported. The EMIR database includes ongoing A activities (e.g Larger Airports, Refineries, Medical and Chemical Industries) and B activities (e.g. larger oil tanks, manufacturing industry, garages,). In total 376 ongoing A and B activities and 932 of the communicated contaminated sites have been identified in the flood risk areas [2]. The variation and difference among them is large and constitutes of previous and/or present activities and the thousands of landfills in Sweden.

4.1 Landfills

The old landfills can contain anything varying from domestic waste to mining waste [11]. Since 1994 the amount of active landfills has decreased and demands have increased. The landfills in use today have been designed to fulfil the national waste directive criteria (SFS 2001:512, NFS 2004:10) based on the climate today. Calculations show that there will be both an increased evapotranspiration and increased water leaching. The relative leaching may increase by more than twice the relative

increase of precipitation for the old landfills. The increased leaching in landfills in use today is around 10 % or less under the same conditions. Under conditions were the landfill is designed to the criteria of 50 mm per year, the increase is however that significant that the criteria can not be fulfilled under conditions with increased precipitation and consequently higher demands on the water collecting systems will have to be taken [11].

4.2 Contaminated land

In order to investigate the potential impact on increased precipitation on contaminated land some calculations have been done. The calculations are based on available information from investigations of contaminated sites of a chemical industry – mercury found above national guideline values at some locations inside the site, wood impregnation – creosote, copper and arsenic found above guideline values at some locations inside the site and an area with mixed industrial land – lead, copper and zinc found above guideline values at some locations inside the site. The soil and water guideline values (Swedish EPA, 2002) are not exceeded outside the sites for any of the activities and this is also the basis for the calculations. The calculations include the following scenarios; i) Today conditions, ii) Increased ground water level and increased water flow – hard surface, no contact between surface and ground water, iii) Increased ground water level and increased water flow – contact between surface and ground water, iv) Land slides to three different waters: one river with a flow of 150 m^3/s, a water coarse 37 m3/s and a lake 90 000 000 m^3 with water residence time 3.1 year.
The calculations including changes in ground water level and water flows were done using Bioscreen®. The landslide calculations are based on a land slide that took place in Ballabo, along the Göta älv in southwest of Sweden, in April 1996 [12]. The slide masses covered 110 meters along the Göta älv and reached around 50 to 70 meters up from the river. The size of the slide is not the largest that have occurred in the area (e.g. Surte, 24 ha, 1950, and Göta, 32 ha, 1957). The landslide lasted around 10 minutes and that is also assumed to be the case in the calculations. The contaminated masses are assumed to follow the water in the river and the water coarse. In reality parts of the masses will deposit just outside and downstream the location of the landslide area. The calculations also include the total amounts of contaminants, i.e. the amount in the contaminated massed, and not the dissolved chemicals. The results of the calculations therefore present the highest possible amount of contaminants to be found in for example the drinking water reservoir downstream.

4.2.1 Increased ground water levels

Increased ground water level may increase the transport by groundwater to surrounding areas significantly due to changes in chemical conditions. For mercury and the contaminants at the impregnation site, the increase initially is more than ten times and 40% respectively. The increased mobility is mainly due to higher contaminant concentrations and lower Kd (distribution coefficient between adsorbed and dissolved compounds) value in the vadose zone (today). The effect is expected to be reduced if the ground water level stays high, since then the Kd value is expected to become similar Kd in the saturated zone today. Increased water flow further increase the leaching, but the guideline values are not exceeded outside the contaminated site despite the increased leaching. Flooding with increased ground water level and increased water flow with contact between surface and ground water over three days, however, result in a more significant transport to nearby areas. The water speed at the surface has been set to 1 m/s and the flooding event has been assumed to last for three days. The impact on the nearby areas depends on the available amount of pollutant by the surface at the site. When the total amount of contaminant by the surface is limited the flooding event will cause a pollution plume. The highest concentration is rather limited to the front of the plume and follows the water flow. If the amount available is set identical to the total amount at the site, the impact is larger. The maximum concentration is higher, and more even in the water that has passed the site. The surface water concentrations can be well above the guideline values for drinking water. In both cases the concentration depends on the Kd values assumed, the available non hard surface allowing the surface water to get in contact with the contaminated masses in addition to the concentration in the ground and amount available at the surface. The calculations do not include spreading through cracks or particulate bound transport in the soil, nor changes of those due to the flooding events. Nor are changes in the ground conditions due to changes in vegetation and biological activity considered.
Not calculated, but maybe of larger importance, is the impact in a longer perspective. Repeated flooding may spread pollutants to surrounding areas where they are accumulated on the surface between

each event. By time high surface concentrations may be built up causing risks for grazing animals and oral intake by children.
Calculations of the annual discharge to the Göta älv shows that the pollution discharge, both nutrients and chemical contaminants, will increase in the same order as the increase in precipitation in the area. An increase in precipitation by 25 % results in a discharge increase of 23 %. The pollution load to the river, its sediment and the estuary will be increased to the same extent. The full study includes further case study scenarios and overviews.

4.2.2 Land slide events

More severe impact also in a short time perspective is the occurrence of landslides in contaminated masses. The calculated concentrations of mercury from the chemical industry site is calculated to temporary reach a value of 6 mg/l which is 600 times the drinking water guideline value (Swedish EPA, 2002) and the guideline value will be exceeded for more than 50 minutes after the landslide. The concentrations will be found in principle all the way downstream the river, but at different times. The same event but to the smaller water coarse will lead to higher maximum concentration but the time for the exceeded drinking water guideline will be the same. Similar results were obtained for the other contaminated sites and contaminants. The same type and size of slide, releasing contaminated mercury masses, but to the lake, will result in total concentration of 0,009 mg/l mercury in the lake and the total concentration will remain over hundred of years. It has to be noted that the calculations are based on one land slide scenario. If the water flow is higher than assumed for the rivers considered here, the concentration will decrease and the time for the guideline value being exceeded will also decrease. On the other hand, the size of the land slide is relatively small compared to the worst land slide events in Sweden. The larger the slide and the more contaminated the masses the higher the maximum concentration in the waters and the longer time the guideline values are exceeded. In reality all the masses will not be transported with the water as the landslide occurs. Some of the masses will be deposited by the slide area and downstream. By time the masses will be eroded from the bottom and transported down the river. Further details and information about the full study can be found in [2].

5 Cities capacity to manage vulnerability to climate change

Vulnerability does not only depend on physical risks related to climate change. Localisation and quality of the infrastructure as well as the impacts of socioeconomic change interplay with the biophysical changes [13]. Accordingly, to estimate vulnerability and adaptive capacity among municipalities, socioeconomic processes need to be incorporated. A case study based project has been initiated to investigate the vulnerability and adaptive capacity along the Göta älv system by using three methods developed by international research emphasizing different aspects of vulnerability: downscaled socioeconomic scenarios, e.g. [14], climate vulnerability indices, e.g. [15], and double exposure analysis, e.g. [13], as well as a number of tools that are used to project bio geophysical impacts of climate change. The project includes socioeconomic, environmental and geotechnical aspects and aims at investigating the institutional capacity to assess society's vulnerability to climate change of cities and regions. The project also uses participatory methodology, i.e. it studies how key officials at municipal level interpret the different methods in order to discuss how they could be used to support decision-making on adaptation. Two groups of key-stakeholders from Göteborg and Lilla Edet participates in a series of four workshops / stakeholder meetings. The workshops will cover for instance: selection of common case; discussion and selection of climatic and non-climatic aspects, sectors and activities and factors affecting adaptive capacity to include in the decision support; presentation and interpretation of decision support and application to other cases. The key officials include representatives from inter alia: city planning, water and sanitation, railway, traffic, park and environmental administration. The two groups have selected two interesting cases. One major change of the city communication centre in Gothenburg, Sweden's second largest city, located very low, i.e. highly exposed to high water levels in the Göta älv. The second case involves the construction of a new residential area in the proximity of Göta älv outside Lilla Edet, a small municipality about 55 km north of Gothenburg.
The expected project outcomes are elements that could constitute an integrated vulnerability tool and criteria for robust decision making tailored for planners within municipal and regional administration.
Primary results indicate that rising sea level, high water flows caused by increased precipitation

tapping from Lake Vänern or both and increased probability for storm events are the climate aspects of most concern in the two case studies. In the case studies road and railway infrastructure as well as building and water supply, sanitation and drainage will be subject for deeper studies of vulnerability and adaptive capacity. The temperature increase itself will affect the rail way system. There is, already today, a need of more (frequent and secure) weather prognosis and related warning systems as well as increased organisation capacity to handle crisis situations such as extreme water levels.
The further study will include an analysis of how number of already selected economic, political, social as well as demographic and technological factors interplay to create vulnerability to multiple stressors. Climate change adaptation measures are also discussed both in Göteborg and Lilla Edet as part of ongoing planning discussions. To what extent these decisions depend on several factors such as the political will and the financial situation is however unclear.
The key participating stakeholders point to the importance of national, regional and internal economy both regarding the vulnerability, the adaptive capacity and the long term adaptation strategy. Further the awareness, competence and opinion on different political levels (local, regional, national and EU) play an important role on the available funding for implementing adaptation measures and for sustainable municipal planning solutions in general.

6 Acknowledgement

Three studies presented here were funded by the Governmental Climate and Vulnerability Inquiry (M 2005:3) which is gratefully acknowledged. These projects would not have been possible to perform without the data from all county administration boards and other experts which are also gratefully acknowledged. The study enhancing cities capacity to manage vulnerability to climate change depends on the key stake involvement and the participants from Göteborg and Lilla Edet and the funding by Formas which are all gratefully acknowledged.

References:

[1] SOU 2007:60 *Sverige inför klimatförändringarna - hot och möjligheter (Sweden and climate change*, in Swedish), SOU 200/:60, Ministry of the Environment, Stockholm, Sweden.
[2] Andersson-Sköld, Y, Nyberg, H, Nilsson, G, Gustafsson, M., 2008, Flooding and potential risks for pollutants spreading - emissions related to climate, Proceedings *International FZK/TNO conference on soil-water systems*, 10, ConSoil 2008, Milan, June 3-6, 2008.
[3] Hultén C, Andersson-Sköld, Y. Ottosson, E., Edstam, T., Johansson, Å., Case studies of landslide risk due to climate change in Sweden, *Proceedings Landslides and Climate change - challenges and solutions*, May 21-24 2007 on the Isle of Wight, UK
[4] Fallsvik, J, Hågeryd, AC, Lind, B, Edsgård, S, Alexandersson, H, Löfling, P, Nordlander, H, Thunholm, B, 2007, *Impact of the climate change in Sweden. Overview assessment of soil movements due to climate change*. In Swedish, SGI. Varia 571
[5] IPCC, 2007, Climate Change 2007: *Impacts, Adaptation and Vulnerability Working Group II Contribution to the Intergovernmental Panel on climate Change Fourth Assessment Report Summary for Policymakers*, Brussels, April 2007.
[6] Rossby Centre, SMHI, 2007, http://www.smhi.se/sgn0106/leveranser/sverigeanalysen/ (2007-07-19)
[7] Johansson, L., 2003, *Evaluation of trends in Mälaren- A studie of the water quality at Lovö water agency 1935-2002*, in Swedish, Stockholm Vatten R 23.
[8] Bulkeley, H and Betsill, M (2006) Cities and the multilevel governance of global climate change. *Global Governance* 12(2):141-159.
[9] Näslund-Landemark, B., 2007., Contact person General flood risk mapping, SRV, www.srv.se
[10] Färnqvist, K., 2008, *Contaminated land, climate change, planning*, in Swedish), Workshop, Göteborg, Sweden, January 21 2008, http://www.renaremark.se/arkiv/ws080122/
[11] Nilsson, G, Rosqvist, H, Andersson-Sköld, Y, Starzec, P, Norrman, J, 2005, *Contaminants and climate change a basis for action plan to predict and prevent natural hazards in Sweden*, in Swedish, SGI. Varia 560:3
[12] Andersson, H, Ottosson, E, Sällfors, G (1999) *Skredet i Ballabo, Västerlanda*, SGI. Rapport 57
[13] Leichenko, R and O'Brien, K. (2002). *The dynamics of rural vulnerability to global change:the case of southern Africa. Mitigation and Adaptation Strategies for Global Change* 7:1-18.
[14] Kaivo-oja J, Luukkanen J and Wilenius M (2004) Defining alternative national-scale socio-economic and techno-logical futures up to 2100: *SRES scenarios for the case of Finland.Boreal Environment Research* 9(2): 109-125.
[15] Sullivan CA and Meigh JR (2005) Targeting attention on local vulnerabilities using an integrated indicator approach: the example of the Climate Vulnerability Index. *Water Science and Technology* 51(5): 69–78.

Water Quality Assessment in the Restoration of the Meirama Open Pit Mine, NW Spain. Part I. Hydrochemistry

J. DELGADO, R. JUNCOSA, A. VAZQUEZ, F. PADILLA,
P. VELLANDO, H. HERNÁNDEZ and S. FERNÁNDEZ-BOGO
Water and Environmental Engineering Group
University of A Coruña
Campus de Elviña s/n – 15192, A Coruña
SPAIN
jdelgado@udc.es http://www.geama.info/

Abstract: - In December, 2007, after 30 years of operations, the mine of Meirama finished the extraction of brown lignite. Since then operations have begun which will lead to the formation of a big mining lake (~2 km^2 surface and up to 180 m depth) after the controlled flooding of the open pit. In the process of flooding are involved both surface and ground waters, each one of them, with their corresponding chemical fingerprints. The future Meirama lake sits at the headwaters of Barcés River, which brings its waters to the Cecebre reservoir, which is responsible for the drinking water supply of A Coruña (~250.000 inhabitants) and neighboring municipalities. From the point of view of supply to the population, there are some doubts concerning the quality of the water in the future lake and it is being considered the hypothetical case that these were of poor quality, what could adversely affect the quality of the Cecebre reservoir waters. Also, the diversion of the river flow in order to flood the Meirama pit could affect also the water supply. Moreover, the introduction of the Water Framework Directive determined that by the year 2015 surface and groundwater must meet strict quality requirements, which may not be true in the case of the Meirama lake. This contribution focuses on the predictive modelling of the hydrochemistry of the future lake based on the currently available database of surface and ground water compositions. Results suggest that the future lake water will meet the high quality standards prescribed by the environmental legislation.

Key-Words: - Acid mine drainage, hydrochemical modelling, flooding, open-pit lake

1 Introduction

The treatment and remediation of acid mine drainage is a major environmental challenge in many countries of the European Union. In fact, in a given setting, pollutant discharges may persist for decades or even centuries after the mining activity have ceased [1], [2]. Banks et al. [3] have provided a review of the different types of acid discharges from abandoned mines in EU member countries as well as an examination of the environmental and economic repercussions on aquifers and water courses.

Discharges of acid mine drainage associated with coal mining exhibit a particular typology, as opencast mining and mining activities in large sandy areas are quite common (for example the Niederlausiz district in E Germany) with the consequent impact on surface and groundwater resources [4].

Coal mining in Galicia (NW Spain) has been an important activity which came to an end in December, 2007. Hence, for different reasons, the two large brown coal mines in Galicia (the As Pontes mine, run by ENDESA GENERACIÓN, and the Meirama mine, owned by Lignitos de Meirama, S.A., LIMEISA), have started closure procedures, both of which are considering the flooding of the mine pits to create two large lakes (~8 km^2 in As Pontes and ~2 km^2 in Meirama). They will be unique in Galicia (a lake-free territory) and singular in the whole of Spain.

An important point to consider as regards the flooding of the lignite mine pits in Galicia is how the process of the creation of a body of artificial water will adapt to the strict legal demands put forth in the Water Framework Directive (WFD). This problem has been carefully examined by different authors in other countries ([5], [6], [7], [8], [9]) and it raises the question of the need to adapt sampling surveys to monitor a number of key parameters –priority substances, physical and chemical parameters, biological indicators, …– that cannot be overlooked.

This paper focuses on the Meirama pit lake, whose flooding is scheduled to begin in the autumn/winter of 2008.

2 Pit Lake Context

The extraction of lignite in the Meirama basin began in 1980 under the management of LIMEISA. The

suspension of this activity, owing to the exhaustion of the resources both technically and economically recoverable, took place in December, 2007. Over the course of nearly 30 years, roughly 81 million m^3 of clay, ~50 million m^3 of granite, ~44 million m^3 of schist and ~93 million m^3 of lignite have been removed from the mine pit. The total volume of material moved or used for profit amounts to a total of some 268 million m^3, although it must be noted that part of this material has been returned to the pit, reducing the excavation volume to roughly 150 million m^3 at elevation level 177 (Fig. 1).

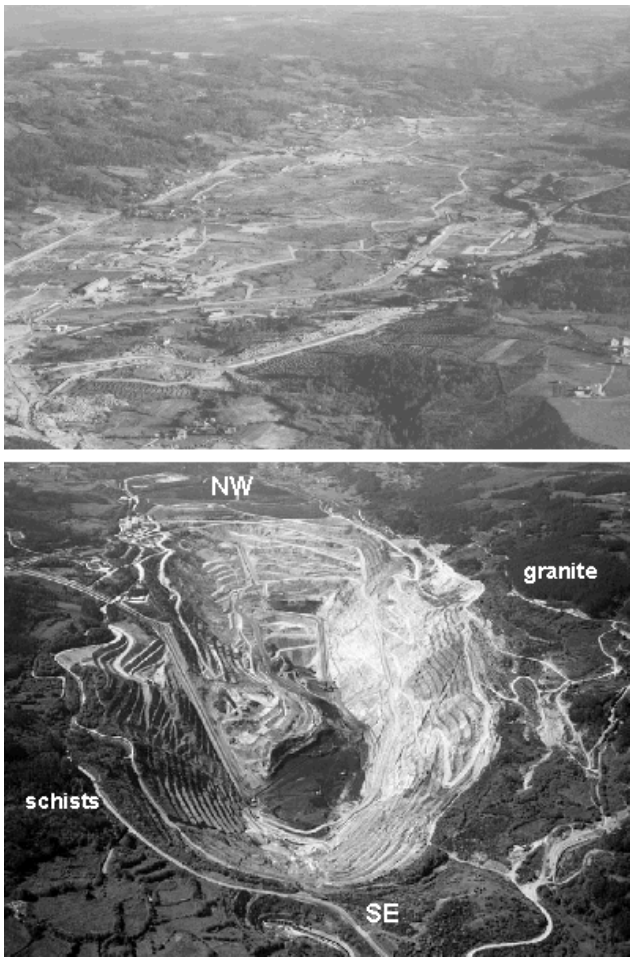

Figure 1. Aerial photograph of the Meirama basin in the mid seventies (top) and 2004 (bottom). The left slope of the open pit is made of schists. Rocks outcroping at the right slope are granites.

The suspension of the mining activity entails a series of activities related to the closure and rehabilitation of the mine area, among which we may cite the creation of a large lake –through a flooding process regulated with natural waters– which will occupy the physical space of the current mine pit. In accordance with preliminary estimations, it is predicted the filling of the pit will last at least 7 years.

The waters that will flow into the mining hole have different origins and their runoff may be separated into different types: surface, ground and rain waters. Each one of them has their own hydrochemical characteristics. Thus, while the natural waters not affected by the mining operations (regardless of their origin), contribute good quality waters, opencast runoff and those flowing through some geologic units (schist, mine dumps, etc.) take up a load of pollutants and acidity with an overall negative impact.

2.1 Geological and Climatic Context

Geologically speaking the mine is located in the Central Iberian Zone, specifically in a *pull-apart* type sedimentary Tertiary basin which is encased in the contact between the rocks of the Órdenes Schist Formation and the Monte Xalo granitic intrusive. The province of A Coruña, where this mine is located, is situated in a typical Atlantic climate zone. Rainfall is high all year round, with minimum values in summer and maximum values in winter. Temperatures are mild with a markedly limited thermal range (~10 ºC).

Since 1976 LIMEISA has recorded the monthly rainfall around the mine. That provides with an extensive series of historical data. Thus, the maximum rainfall recorded was in 2000, with an accumulated annual value of 2069.6 L/m^2. By contrast, the driest period of the series occurred in 1988, with an accumulated rainfall of only 1037.6 L/m^2. The average rainfall in the mine area hovers around 1500 L/m^2.

2.2 Hydrologic Context

Given the proximity of the water table to the original surface of the land, over the course of 30 years of extraction and to this day, LIMEISA had to build an extensive hydraulic system comprising two channels to divert the surface waters in addition to wells to pump groundwater to prevent the pit from flooding during mining operations. Owing to the high mean rainfall, it was determined necessary to install a series of well points located following the perimeter of the open pit, a collaborative peak pumping capacity of ~12.000 m^3/h.

The mine hole covers the upper third area of the Barcés river catchment, which is a major source of water for the Cecebre reservoir. That reservoir constitutes the only supply of drinking water for the city of A Coruña (~250.000 inhabitants) and the surrounding towns.

From a hydrogeological point of view, the characteristics of the different outcrops in the basin where the Meirama mine is located are strongly affected by the lithology and tectonics of the existing

material. The granite massif and schist formations of the Órdenes Series are materials with very low hydraulic conductivity and little porosity, which means that the flow of deep waters is of little consideration. More specifically, the granite massif has been substantially disturbed and fractured in the area around the NE border of the mine pit, coinciding with the fault, which, to a certain extent, has individualized the tertiary sedimentary basin. The hydrogeological behavior of the granite is, therefore, highly varied. By contrast, the schist to the south of the basin has a very low permeability and a small storage coefficient.

In the area surrounding the mine, ground water is pumped out owing mainly to the dewatering of the mine hole during the extraction operations. On the other hand, surface waters that could enter into the pit are diverted through a system of channels that follow the outer perimeter of the mine. Apart from that, water is also used for other, less important purposes in terms of consumed volume: pumping out of groundwater and diversion of surface waters by means of irrigation ditches. In addition, small discharges of wastewater from return waters –mainly from agricultural and livestock-related activities- or from small industries enter into the Barcés river downstream the mine. As a whole, they are of little importance as compared with the uses originating from the mining activity itself.

A number of scenarios are being considered in relation with the flooding process. The one preferred by the managers of the mine considers the partial diversion of surface waters from the upper part of the catchment along the wet season or rainy periods. A preliminary assessment based on water balances and coupled ground and surface water modelling suggests that the minimum time needed to fully flood the pit would be around seven years [10]. This study has served to significantly broaden and improve our knowledge of the hydrology of the high basin of the Barcés River, and in particular, the work carried out by Golder Associates Limited on the initiative of LIMIESA in 2002. It also provides the preliminary basis for the design of predictive models on the water quality of the future pit lake.

3 Hydrochemistry

The waters that will flow into the mining hole have different origins and their contributions may be separated into the categories of surface, ground and rain waters. Each one of them has its own chemical fingerprint and will affect, to different extent, the intermediate and final quality of the lake. Therefore, a close scrutiny of their chemical composition, variability and availability (i.e. fluxes) is required to set the local natural background values, to forecast lake quality and to design adequate management strategies. Hence, while the unaffected natural waters (regardless of whether they are surface waters, groundwater or rainwater) contribute good quality waters, those flowing along the inside of the pit or interacting with some of their geological units or materials (schist walls, waste rock dumps, etc.) take up a significant load of metals and acidity that may challenge the overall quality of the lake (endangering ecosystems) and its discharge (owing to overflow) into the lower Barcés River. This contribution focuses in the chemical characteristics of pre-flooding surface and ground waters with the aim of setting up the above mentioned background levels needed to proceed with the predictive modelling of lake quality.

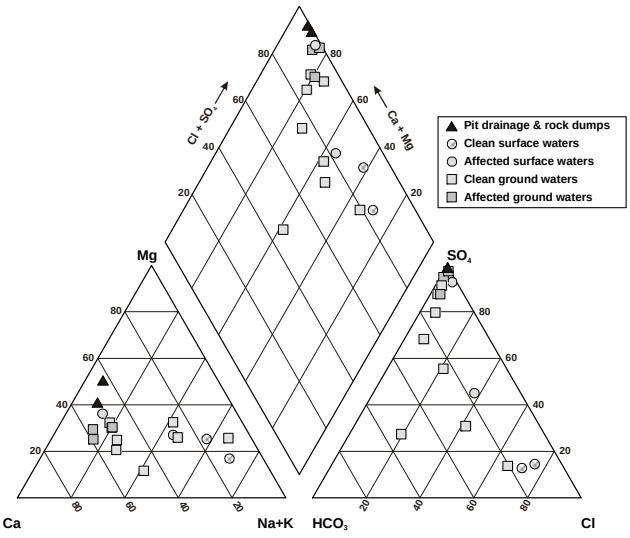

Figure 2. Piper-Hill diagram showing the most significant hydrochemical features of the ground and surface waters

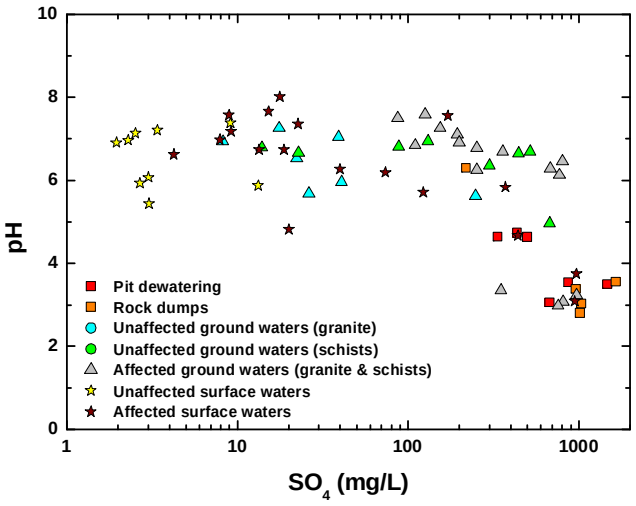

Figure 3. pH vs. sulfate concentration in the analyzed ground and surface waters around the Meirama open pit

From a hydrochemical standpoint, the information available to date comes from sampling surveys carried out by LIMEISA and the authors between 2002 and 2008. A summary of them are presented in the Piper-Hill diagram of figure 2. The unaffected surface waters tend to be of the Na/Cl-type, in agreement with the main chemical characteristics of local precipitation. Ground waters coming from granitic or schistose substrates have different chemical signatures. While granitic lithologies tend to be slightly alkaline and of the Na/HCO_3-type, schistose rocks waters have more variable pH's (from slightly alkaline to mildly acidic) and belong to the Ca/SO_4-type. That suggests the more or less conspicuous presence of sulfide minerals (pyrite/pyrrhotite) in the schists and meteoric carbonates in the igneous rocks. On the other hand, the waters sampled at the deepest point of the pit hole (dewatering pond) as well as those draining the crushed rock dumps and the broken pit slopes are moderately to highly acidic (pH~3) and of the Ca-Mg/SO_4-type (Fig. 3).

The Ficklin diagram shown in figure 4 illustrates the base metal content of the waters associated to the Meirama open pit. It is interesting to observe that the worse quality waters of the area (coming from pit dewatering and rock dumps), although having high metal contents and being acidic, they do not attain the extreme values sometimes reported in the literature for similar systems.

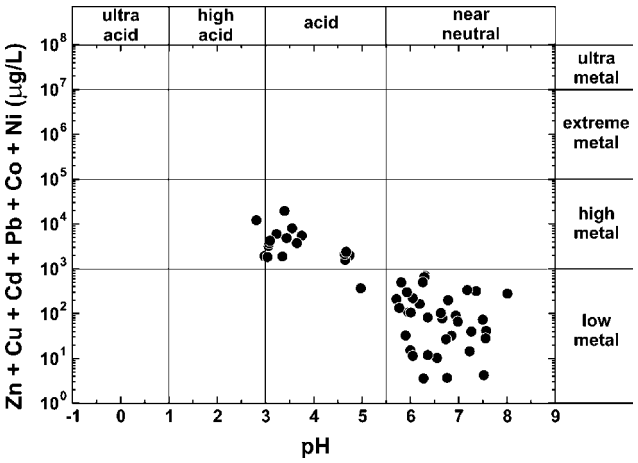

Figure 4. Ficklin diagram showing the the sum of disolved base metals from affected and unaffected waters of the Meirama open pit.

The currently available water database has allowed us to conduct a detailed analysis on the chemical characteristics of each type of water eventually involved in the flooding of the Meirama open pit. This is important in order to establish a scientific frame amenable of helping in the prediction of pollutant discharges from the future lake towards the Barcés River, and to assess the hypothetical affection of the Cecebre potable water reservoir.

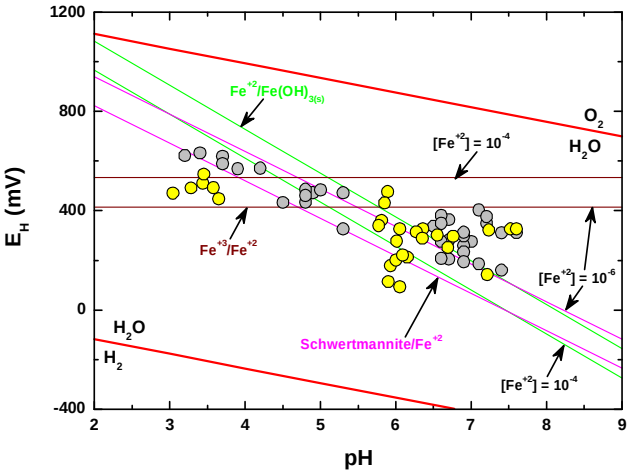

Figure 5. pH-E_H diagram showing field measured values for ground and surface waters and the stability field of relevant iron-bearing mineral phases

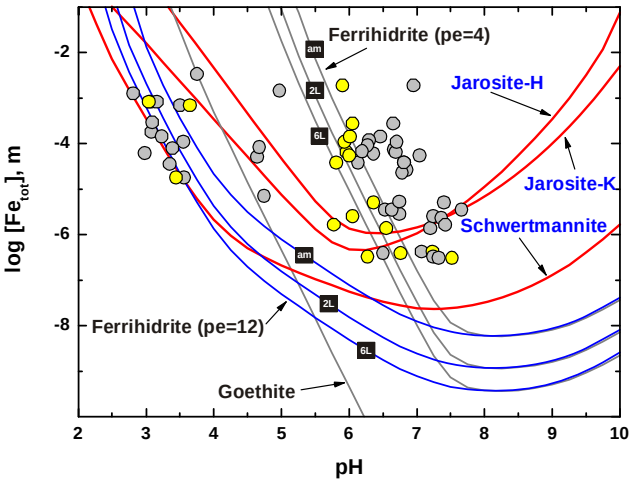

Figure 6. Solubility diagram of Fe-bearing phases and measured iron concentrations in the Meirama ground and surface waters

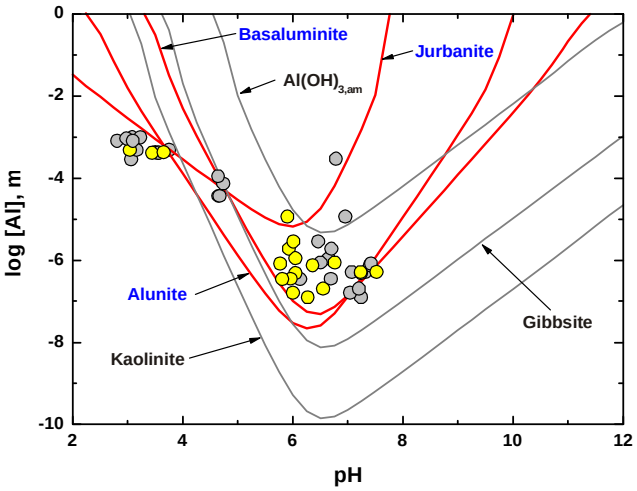

Figure 7. Solubility diagram of Al-bearing phases and measured aluminum concentrations in the Meirama ground and surface waters

Accordingly, we have performed a comparison of the composition of the different mine waters and the maximum acceptable limits for pollutant discharge towards natural waters, according to the Spanish and European legislation. Result indicate that, in general, only the most acidic waters exceed the regulatory limits, although the excess is limited to pH, Al, Fe, Mn, Ni, Se, Cu and Zn. The concentration of some other potential contaminants like As, Ba, B, Cd, Cr, Hg, Pb, Co, Mo, V, Sb, Sn, F, Cl, NH_4, NO_3, NO_2 and Ti are always below the mandatory concentration or exceeding the limit in a statistically non-significant number of samples (i.e. one sample among the entire dataset).

3.1 Hydrochemical Modelling

The hydrochemical database allows us to perform a series of theoretical computations that help us to understand the natural constrains of each water type.

Plausible mineral solubility constrains have been identified for the local Meirama ground and surface waters. Thus, the Fe-content of the most acidic waters seems to be associated to solubility of K-jarosite and schwertmannite (Figs. 5, 6 and 7) while the aluminum in the same waters would be limited by the precipitation of jurbanite.

On the other hand, figure 8 shows the computed fugacities of oxygen and CO_2 from surface and ground waters of the Meirama mine. It is interesting to observe that, while surface waters are nearly saturated with respect to oxygen (log fO_2 = ─0.7), ground waters, as it might be expected, have significantly lower values. In turn, the CO_2 content of surface waters is close to equilibrium with the atmospheric reference value (log fCO_2 = ─3.5) and significantly over that value in ground waters. This observation becomes important when considering which hydrochemical conditions prevail in order to set up any predictive lake chemistry assessment.

Figure 9 shows the computed saturation index of gypsum from the chemical composition of the Meirama surface and ground waters. The solubility of this mineral phase is important as far as sulfate constitutes the largest contributor to the chemical composition of the mine waters. As it can be observed, although there is a clear tendency of waters to become saturated with respect to gypsum, this mineral appears to never attain saturation. However, it is likely that gypsum may form in the rock slopes and mine dumps following periods of low precipitation.

In figure 10 has been represented the computed saturation index of calcite. It is interesting to observe that the most calcite-subsaturated waters are these more acidic while unaffected ground waters (either from granites or schists) are closer to saturation, evidencing its scarce presence in the local rock formations.

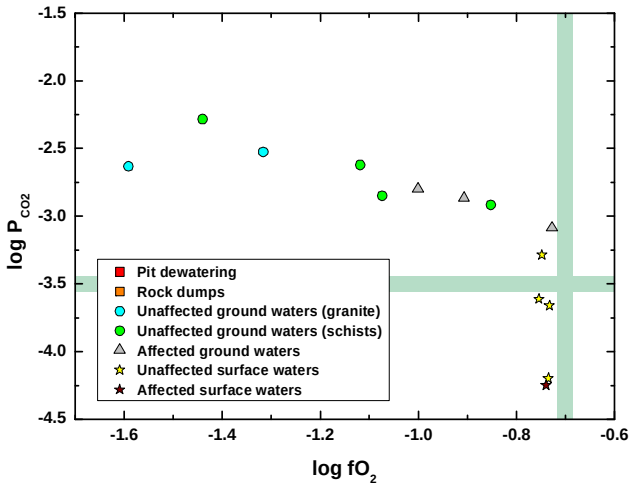

Figure 8. Computed oxygen and CO_2 fugacities in ground and surface waters and comparison with the atmospheric equilibrium condition

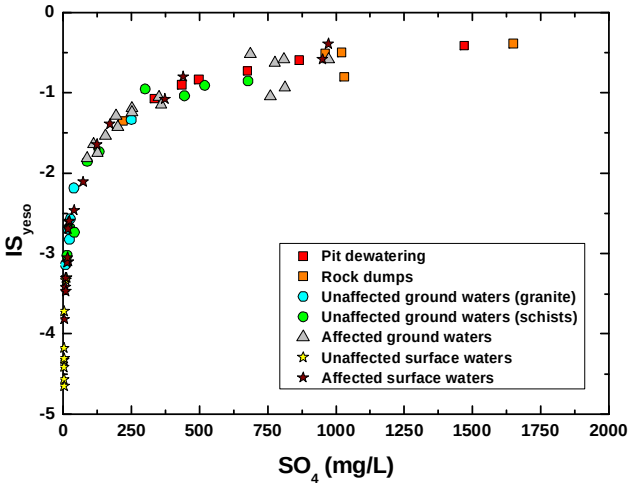

Figure 9. Gypsum saturation index computed for the surface and ground waters of the Meirama open pit

This is an important input to evaluate the future hydrochemistry of the lake. Hence, the lack of effective pH-buffering minerals coupled to the oxidation of sulfides present in the pit slope rocks and dumps conducts to the development of acid drainage, whose chemical characteristics have been evidenced in this paper. Therefore, a management strategy by which the flooding of the mine makes exclusive use of ground waters, direct rain fall and pit slope runoff/infiltration will conduct to the formation of an acidic water body. However, if the flooding process is controlled and natural –unaffected- local surface waters are employed to flood the mine hole, the likely result will be a moderately acidic to circumneutral lake [11]. Both management strategies have been tested via computer modelling.

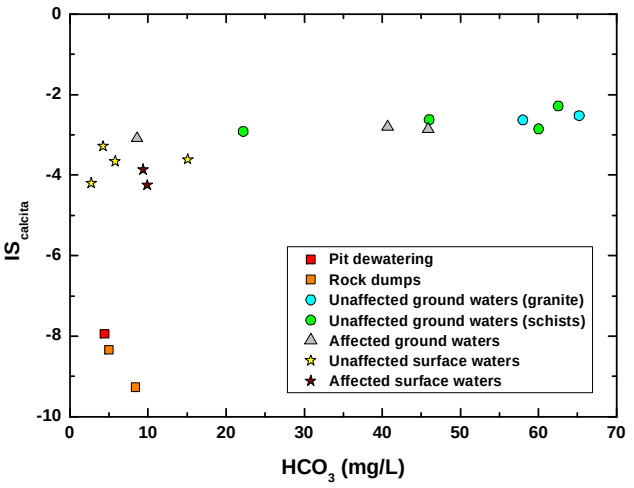

Figure 10. Calcite saturation index computed for different surface and ground waters of the Meirama open pit

4 Conclusions

According to the chemical characteristics of the waters around and in the Meirama open pit and the bundle of plausible geochemical processes that would operate during the flooding of the mine, the planned strategy of diverting surface waters towards the pit hole should conduct to a water body of acceptable to good quality. However, because the highest metal contents are associated to the waters draining the pit slopes and rock dumps, it is expected that a natural flooding process including only ground and rain waters may led to an acidic water body. The chemical characteristics of waters transitorily impounded at the bottom of the pit (tens of thousands of cubic meters) during low pumping/high precipitation periods as well as predictive modelling of the described scenario confirm this perception.

Acknowledgements: Funds for this work have been provided by the projects CGL2006-01452HID, BIA2005-07916, PGIDIT06PXIC176002PN, the European Regional Development Funds 2007/2013 and LIMEISA

References:

[1] Strömberg, B., and Banwart, S., Kinetic modelling of geochemical reactions at the Aitik mining waste rock site in northern Sweden, *Applied Geochemistry*, Vol. 9, 1994, pp 583-595

[2] Castro, J.M. and Moore, J.N., Pit lakes: their characteristics and the potential for their remediation. *Environmental Geology*, Vol. 39, No 11, 2000, pp. 1254 – 1260

[3] Banks, D., Younger, P.L., Arnesen, R.T., Iversen, E.R., and Banks, S.D., Mine-water chemistry: the good, the bad and the ugly. *Environmental Geology*, Vol. 32, No 3, 1997, pp. 157 – 174

[4] Werner, F., Bilek, F. and Luckner, L., Implications of predicted hydrologic changes on Lake Senftenberg as calculated using water and reactive mass budgets, *Mine Water and the Environment*, Vol. 20, 2001, pp. 129-139

[5] Kroll, A., Amezaga, J. M., Younger, P. L. and Wolkersdorfer, C., Regulation of Mine Waters in the European Union: Contribution of Scientific Research to Policy Development. *Mine Water and the Environment*, Vol. 21, No 4, 2002, pp.

[6] Working Group 2.2 – HMWB, Guidance Document nº 4. Identification and designation of heavily modified and artificial water bodies, *Common implementation strategy for the Water Framework Directive (2000/60/EC).* European Communities, 2003

[7] Graupner, B.J., Benthausb, F.C., Bürger, S. and Werner, F., Implications of EU-Water Framework Directive for the East German Postmining Landscape Lausitz: Coping with a sparse knowledge of the underground, *Limnologica*, Vol 35, 2005, pp. 199-205

[8] Nixdorf, B., Lessmann, D. and Deneke, R., Mining lakes in a disturbed landscape: Application of the EC Water Framework Directive and future management strategies, *Ecological Engineering*, Vol. 24, 2005, pp. 67-73

[9] Wolkersdorfer, C., Mine Water Management and the Water Framework Directive. S. 1-8 (CD), (Proceedings, Post-Mining 2005).

[10] Padilla, F., Vellando, P., Delgado, J.L., Juncosa, R., Delgado, J. and Fernández, J., Surface and ground water flow modelling in the restoration of the Meirama open pit mine. In Water in Mining Environment. R. Cidu & F. Frau (Eds.), 2007, 5 pp.

[11] Castendyk, D., Webster-Brown, J., Sensitivity analysis in pit lake prediction, Martha Mine, New Zealand 1: Relationship between turnover and input water density, *Chemical Geology*, Vol. 244, 2007, pp. 42-55

Water Quality Assessment in the Reclamation of the Meirama Open Pit Mine, NW Spain. Part II. After-Flooding Assessment

R. JUNCOSA, J. DELGADO, P. VELLANDO, F. PADILLA
A. VÁZQUEZ, H. HERNÁNDEZ and S. FERNÁNDEZ-BOGO
Water and Environmental Engineering Group
University of A Coruña
Campus de Elviña s/n – 15192, A Coruña
SPAIN
rjuncosa@udc.es http://www.geama.info/

Abstract: - The mining activities in Meirama open pit coal mine (NW Spain) were halted in December 2007 and the mine pit is to be restored as a lake with ~180 m in its deepest point. The flooding is to be carried out with surface waters coming from the upper section of the Barcés river catchment. It is expected that the flooding process will be completed in about 7 years. In 2006, LIMEISA, the company in charge of the mining activities since 1980, entrusted the *Water and Environmental Engineering Group* of the University of A Coruña the assessment of the lake water quality during and after completion of the flooding process. The present paper presents a summary of the work done to assess the water quality parameters in the future lake, carried out with the finite element FREECORE^{2D} software, developed within the group. As a final conclusion, the water quality parameters obtained for the post-flooding conditions will apparently fulfill the requirements set by the environmental authorities.

Key-Words: - Water quality assessment, mine pit restoration, solute transport, hydrochemistry, finite elements, FRECORE^{2D}.

1 Introduction

The coal mining activities in the Meirama open pit mine (A Coruña, NW Spain) finished in December 2007. LIMEISA (*LIgnitos de MEIrama Sociedad Anónima*), the company in charge of the lignite mine since 1980 used the mined coal for supplying of the nearby 550 *Mw* Meirama power station. Since the interruption of coal extraction, the flooding process has started in the pit, with ground and rain waters and still awaits the administrative authorization for the detraction of surface fluxes from the surface waters of the upper Barcés River catchment. According to modeling, it is expected that flooding process will last, at least for some 7 years.

Over the last decade, LIMEISA has entrusted certain institutions and consultants the drafting of different environmental studies associated with the mine reclamation activities and to meet the demands of the environmental authorities and laws in force. A significant part of these reports are concerned with the geological, hydrological, hydrochemical, and geotechnical characterization of the future lake and its surroundings. Several models seeking to assess the environmental effects over the Barcés River catchment have also been developed. The first of these reports on water quality was entrusted to Golder Associates [2] in 2002.

In 2005 to the *Water and Environmental Engineering* Group (GEAMA) evaluated the surface and ground water flow balances associated to the reclamation of the open pit to conform a lake [1]. This report shows the hydrodynamic balance of the surface and ground waters in the basin and provides an accurate assessment of the water flows arriving to the pit. In addition, water flows are not only quantitatively featured but also characterized in terms of the geologic materials they go through or upon.

Taking the results obtained in the former report as an input value, a second assessment was carried out in 2007 to subsequently evaluate the lake water quality parameters and to check its eventual accomplishment with respect the different legal and environmental constrains. This water quality assessment was arranged into two different parts. The first part focuses on the water quality assessment associated to the pre-flooding and flooding stages. To achieve so, a comprehensive sampling survey was performed to complete previously acquired data [2].

In that study, a comprehensive analysis of the natural controls for acidity and metal concentration in the waters surrounding the pit was carried out [3].

With these data, several models that evaluate the hydrochemistry in the lake were developed, based upon the previously mentioned surface and ground water balance model. Thus, the flows of surface and ground water arriving at the pit, were assigned different reference water qualities that were used to make mixing models taking into account several hydrological hypothesis, processes and chemical reactions, so resulting in a prediction of water quality in the future lake. Among the factors that showed the greatest impact over the quality of the lake was the volume of water that interacted with the rock waste dumps inside the pit. Several realistic hydrogeological scenarios were considered, and it was concluded that the quality of the future Meirama Lake would progressively improve as far as the flooding process advances. According to the model, once the lake becomes full, it chemical quality would meet nearly all the regulatory requirements in force. The particulars regarding the first part of this report have been summarized in a companion paper [4].

This second part is devoted to assess the hydrochemical evolution and the reactive solute transport processes taking place in the lake after its flooding. That condition represents the achievement of the quasi-steady flow conditions in the catchment basin and with respect to the discharge flows from the lake towards the Barcés River. In order to evaluate the effect of different processes and scenarios over the chemical evolution of the lake, we developed two approaches. First, a thermo-hydrochemical model was elaborated to check the importance an extent of thermal stratification in the lake. Then, a two-dimensional reactive solute transport model of upper layer of the flooded lake helped us to understand hydrodynamic homogenization processes.

In that contribution we also present the code FREECORE^{2D} [5], with which we performed the numerical simulations.

2 Model Description

Based on the available hydrochemical information, its interpretation and modelling, a series of constraining geochemical reactions (aqueous speciation, acid/base, oxidation/reduction, mineral dissolution/precipitation and ion adsorption) were defined [4]. In addition, because dissolved mass transport in the free surface of any water body is mainly associated to water flow, it was necessary to carry out a hydrodynamic model of the lake. With this data at hand and combining it with the previously defined hydrogeochemical framework, a numerical model was elaborated and it is summarized next.

2.1 Code and Equations

The finite element code FREECORE^{2D} [5] has been used to assess the reactive solute transport in the Meirama Lake after flooding the pit hole. The model is based upon the resolution of the equation of the solute transport, which takes into account advection, molecular diffusion and hydrodynamic dispersion. Advection refers to the solute migration associated to water flow. If water flows at a specific discharge **q** (volumetric water flux), and c is the solute concentration, the advective solute flux $\mathbf{F}_A$ is given by

$$F_A = qc \tag{1}$$

On the other hand, molecular diffusion is a transport mechanism related to the continuous brownian motion of microscopic particles (ions, aqueous complexes, ion pairs, molecules, etc.) within the realm of the water phase. Its mathematical expression is given by Fick´s law as

$$F_D = -D_0 \nabla c \tag{2}$$

where D_0 is the molecular diffusion coefficient in water.

In addition to molecular diffusion, there is another mixing phenomenon known as hydrodynamic dispersion which is caused by the turbulent water motion and produces both longitudinal and transverse solute spreading. It is broadly accepted that this mass transport mechanism can also be evaluated in terms of a formulation analogue to the Fick´s law, that is

$$F_H = -D_h \nabla c \tag{3}$$

where $\mathbf{D}_h$ is the hydrodynamic dispersion tensor. Further details on the formulation can be found in [3]. The equation governing the free surface solute transport is directly derived from the mass conservation equation and can be written as

$$-\nabla \cdot \left(F_A + F_D + F_H\right) = \frac{\partial (c)}{\partial t} \tag{4}$$

Substituting equations (1), (2), and (3) into equation (4) the following expression is obtained

$$\nabla \cdot \left(D \nabla c\right) - q \cdot \nabla c + w\left(c^* - c\right) + \theta R = \frac{\partial c}{\partial t} \tag{5}$$

where w is the fluid source of water flux having a concentration c*, R is the solute sink/source term, and **D** is the diffusion/dispersion tensor.

2.2 Physical Model

The numerical formulation has been applied to a two-dimensional finite element mesh with more than 3000 nodes representing the after flooding surface of the lake. The reactive solute transport model is highly affected by the shallow flow at the lake surface, that constantly moves and rinses solutes (Fig. 1).

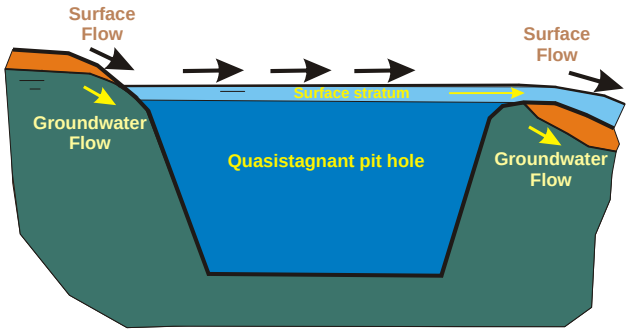

Figure 1. Sketch illustrating a vertical section of the lake and the conceptual model for the post-flooding condition

It is interesting to stress that it should be expected that the advective component of the flow is going to be considerably higher than the diffusive one, although diffusion cannot be neglected. On the other hand, it is likely to find a certain stratification of solutes, with a more or less diluted upper, surficial layer. The mixing and homogenizing of the water will depend upon the eventual vertical velocities induced by a potential thermocline inversion associated to density gradients (Fig. 2).

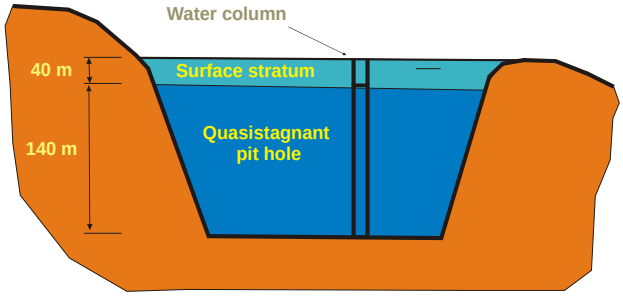

Figure 2. Conceptual model for the thermal analysis of the lake

2.3 Thermal Model

In order to evaluate the likely thermal stratification of the future Meirama Lake and the eventual thermocline inversion, we conducted a thermal study in the nearby Eume River reservoir. This water body has a maximum depth of 90 m and it is located close to our filed area and affected by similar hydro-meteorological conditions. Results of the field survey shows that, at least in the year 2006, there was no thermocline inversion in the reservoir, and that the temperature in its surface stratum (that in winter may achieve a thickness of about 40 m) remained slightly higher than the temperature at the bottom layer. Taking this evidence as a proxy for the Meirama Lake, we developed a numerical thermal model trying to assess the behaviour of the water column with respect to its eventual thermal inversion. In the computations we have assumed a surface and bottom layer thicknesses of 40 and 140 m, respectively and a temperature of 8 ºC for the top water body and 10 ºC for the bottom (Fig. 2). Taking into account that the density gradient that causes the temperature inversion varies not only with temperature, but also with pressure and solute concentration, it can be shown that water density decreases with temperature but increases with the hydrostatic water weight and the solute concentration. This is illustrated in figure 3, where it can be observed that the density variations are not expected to be larger than 0.04%. This should not constitute a significant driving force for thermal inversion. Based on the empirical evidence of the Eume River reservoir and the previous computations, we can assume that, according to the conceptual model depicted in figure 1, the advective vertical solute transport processes can be safely neglected.

2.4 Reactive Solute Transport Model

FREECORE^{2D} allows for the evaluation of flows with heat transfer, and reactive solute transport including equilibrium and kinetic processes. In this work, we have elaborated a 2-D unstructured finite element mesh (6160 triangular elements and 3189 nodes) to model a 20 m thick lake surface stratum in the after-flooding and pouring of lake waters towards the Barcés River. The chemical composition of water flowing to the lake is those derived from the preliminary stages of the study (rain, surface, ground and runoff waters, [2], [4]) and they are taken as boundary conditions. The perimeter of the lake has been divided in 18 regions, each one of them contributing different amounts of water types and qualities.

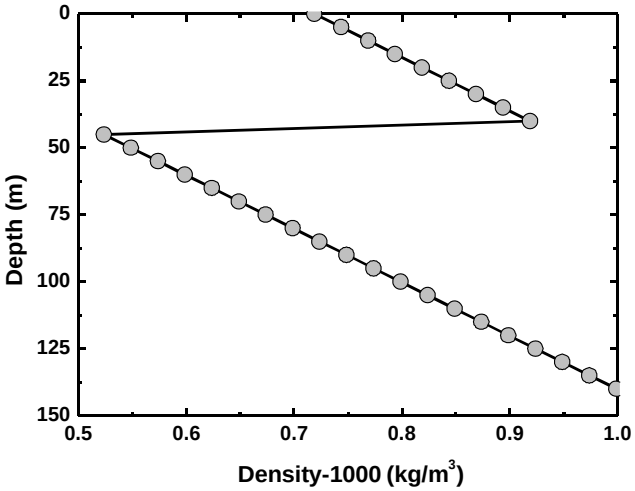

Figure 3. Density variation as a function of pressure (depth) and temperature

A number of hypotheses have been considered in order to construct the reactive transport model: a) The

hydrometeorologic situation corresponds the mean of the dry 2014/2015 period; b) 2 injection points for water associated to surface water derivations; c) Constant chemical composition for the inflow waters (including the injection points); d) Allowance of a spillway point towards the Barcés River and possibility for of ground water flowing outwards in the unsteady input values at the rest of model regions; e) Heterogeneous reactions were not considered; and f) 12 unsteady (0.1 days time step) hydrodynamics variations (one per month) associated to the 18 perimeter model regions of the lake (Fig. 4).

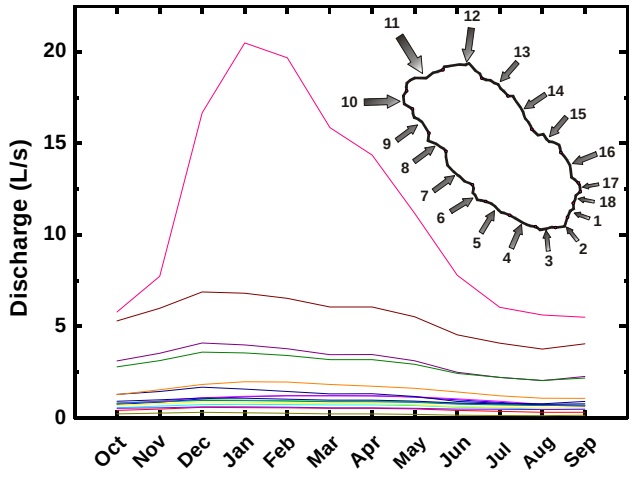

Figure 4. Yearly-distributed discharge through different perimeter sections (numbers in the inset) of the future Meirama lake

Each one of the modelling regions was featured with the parameters of their predominant materials (being schist, sedimentary, rock dump or granite). Neumann boundary conditions (i.e. solute transport associated to water discharge) have been prescribed in all the regions.

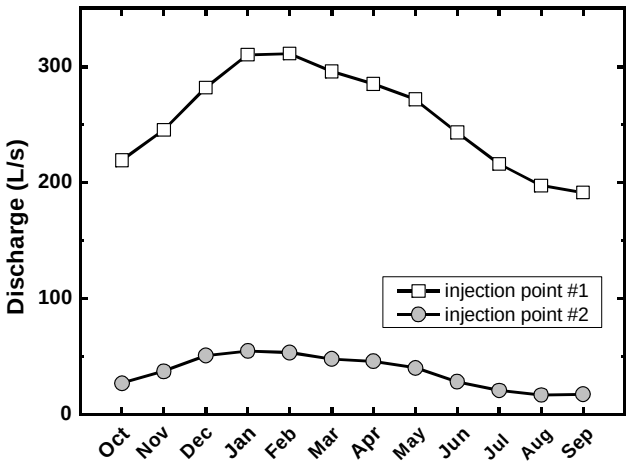

Figure 5. Time-dependent water discharges at the injection points

The hydrodynamic parameters considered for the reactive solute transport model have been the following: Molecular diffusion 10^{-9} m^2/s; Longitudinal and transversal dispersivities 100; Manning coefficient 0.03 $m^{-1/3}$·s. The chemical components considered in the model include H_2O, H^+, HCO_3, Na, Ca, Mg, Mn, Cl, SO_4, K, Al, Fe, NO_3, Co, Ni, Cu, Zn, Ba, As, Cr, Hg, Cd and Pb. More details concerning the initial and boundary conditions assigned to each particular node are given in [1].

3 Results

Reactive solute transport results have been obtained for all the spices considered. For the sake of brevity, only a few of them will be covered here. Figures 6 to 9 show the surface distribution of Al^{+3} and pH at the second (october) and last month (august) of the hydrological year.

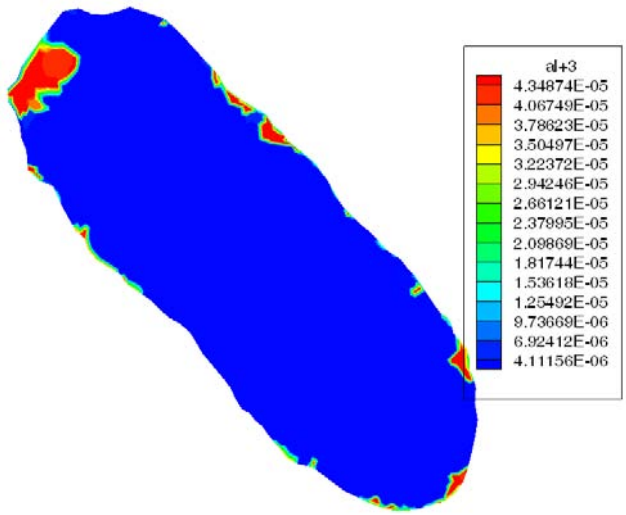

Figure 6. Computed total Al concentrations in the lake in October

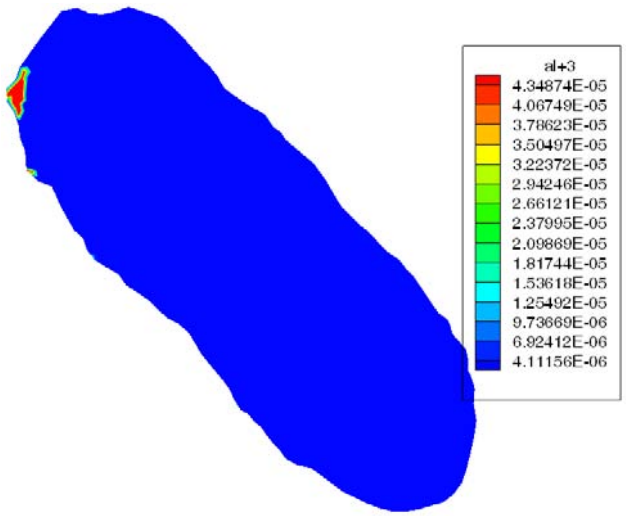

Figure 7. Computed total Al concentrations in the lake in August

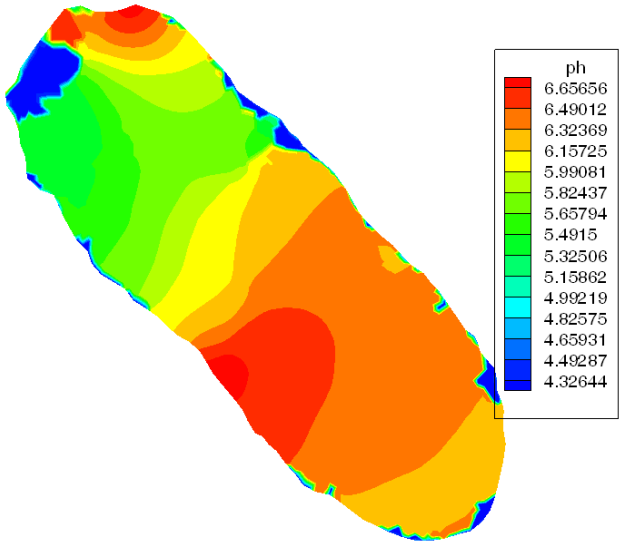

Figure 8. Computed pH of the lake in October

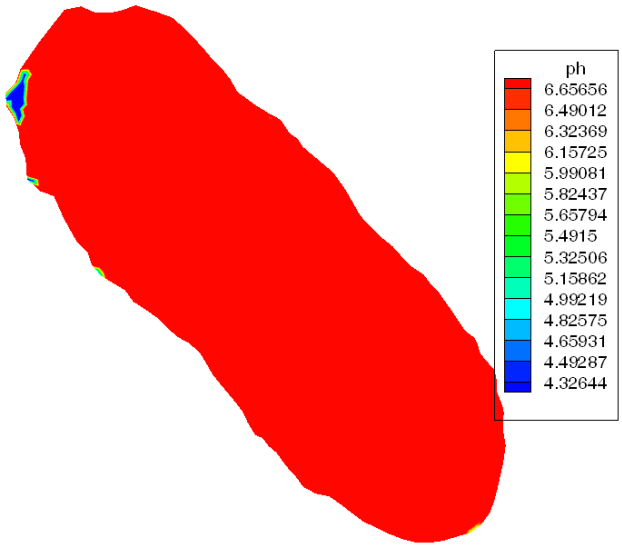

Figure 9. Computed pH of the lake in August

At first glance, it can be observed that an almost complete chemical dilution and homogeneization of species and pH has taken place in the lake, except for some water pockets located at certain points of the perimeter. There, homogenization is to be based on dispersion (which is slower) and not advection.

Figures 10, 11 and 12 show the time evolution of the concentrations of manganese, iron, potassium, aluminum, sodium, calcium, magnesium, total carbonate and pH in the region where the water is spilt towards the Barcés River basin. It can be seen how the Mn, Al and Fe decrease in their concentration with time due to the fact that the inflow water concentration for these species is bigger than the initial concentration of in the lake. On the contrary, the concentration of K becomes greater due to its greater concentration in the inflow waters.

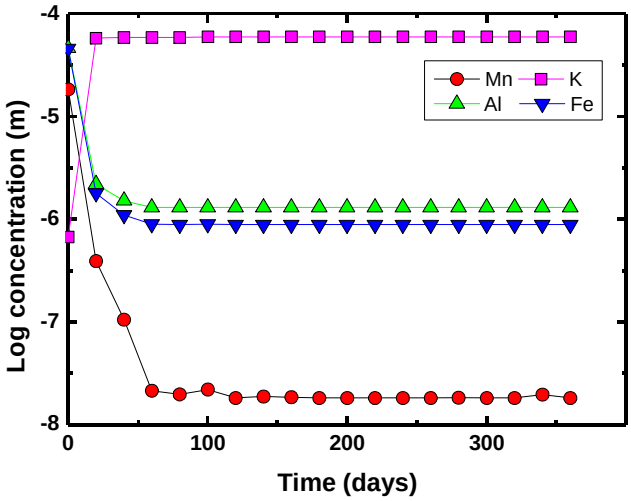

Figure 10. Time evolution of manganese, potassium, aluminium and iron at the lake spill point

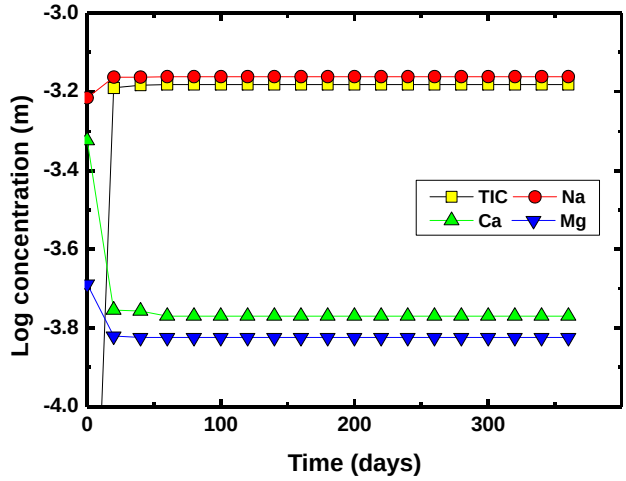

Figure 11. Time evolution of bicarbonate, sodium, calcium and magnesium at the spill point

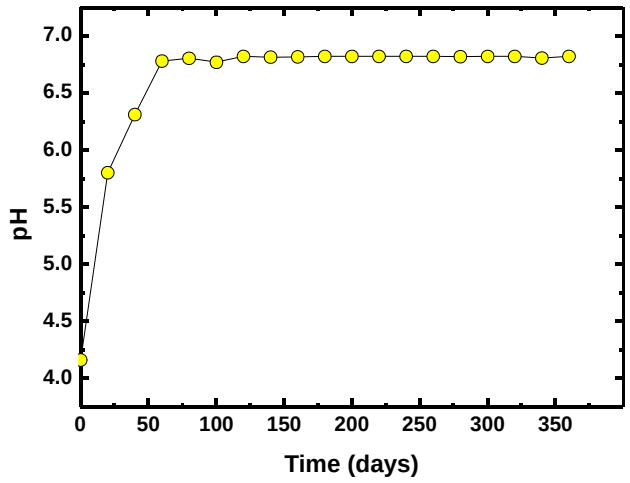

Figure 12. Time evolution of pH at the lake spill point

Calcium and bicarbonate behave differently. While the concentration of bicarbonate increases, the

calcium decreases with time due to the reaction leading to the formation of dissolved carbonate, what contributes to the increase of pH (4.16 at the beginning and 6.5/6.9 at the end of simulation). In the overall, the chemical composition of the upper layer of the lake meets the environmental and other legal objectives.

3.1. Sensitivity analysis

A sensitivity analysis has been carried out in order to determine the influence of the variation in certain parameters in the final results. First, the molecular diffusion coefficient has been increased by an order of magnitude because this is the most relevant transport parameter in the nearly-stagnant water pockets. Second, ground water discharge out off the modelling perimeter was not considered as they are very small compared to the localized surface inflows. Results indicate that no major differences with respect the original model occur.

4 Conclusions

In a first approach to assess the quality of the waters that will spill out off the future Meirama Lake, we have developed a detailed two-dimensional reactive transport surface water model. The model is based on previous studies that include comprehensive surface and ground water balances, hydrochemical characterization and geochemical modeling. In order to reduce the uncertainty associated to the need of defining the verisimilitude of a 2-D versus a 3D approach and, considering that lake overturn due to density gradients and/or thermal stratification, field and theoretical analyses have been performed. As a first conclusion, it appears that lake overturn is not a likely scenario as far as thermal stratification tends to remain constant throughout the entire year and density changes are small.

FREECORE^{2D} modelling shows that, along a complete year, the chemical composition of the water of the upper layer of the lake tends to be homogenized and diluted due to the inflow of relatively diluted surface waters. The effect over the top layer surface is to decrease the concentration of the major part of components although some of them slightly increase due to the fact that the concentration of the inflowing waters is higher than in the lake. Small pockets of water in the top layer of the lake may retain certain initial characteristics (nearly stagnant regions) due to geometric constrains.

In general, the chemical composition of the top surface waters, that eventually will spill out towards the Barcés River basin, meet the criteria given in the environmental regulations in force. That means that, on a steady state basis, the inflow of surface waters will tend to improve or maintain the good water quality of the top layer of the lake.

The sensitivity analyses performed do not affect significantly these results. Nonetheless, it is recommended to conduct a water quality monitoring survey during the flooding and after flooding conditions so as to being able to calibrate the model in order to corroborate the results obtained so far.

Acknowledgements: Funds for this work have been provided by the projects CGL2006-01452HID, BIA2005-07916, PGIDIT06PXIC176002PN, the European Regional Development Funds 2007/2013 and LIMEISA

References:

[1] Padilla, F., Vellando, P., Fernández, J., Juncosa, R. and Delgado, J. (2006) El flujo de las aguas durante el régimen hídrico de la excavación minera de Meirama. University of A Coruña unpublished report. 215 pp.

[2] Golder (2002) Mina de Meirama. Investigaciones para el cierre. Calidad del agua del lago. Golder Associates unpublished report. 37 pp.

[3] Delgado, J., Juncosa, R., Padilla, F., Vellando, P., Vázquez, A., Hernández, H. and Fernández, J. (2007) Clausura y llenado de la Corta Minera de Meirama. Parte I – Estudio y Modelización de la Calidad Química del Futuro Lago. University of A Coruña unpublished report. 234 pp.

[4] Delgado, J., Juncosa, R., Vazquez, A., Padilla, F., Vellando, P., Hernández, H. and Fernández-Bogo, S. (2008) Water quality assessment in the reclamation of the Meirama open pit mine, NW Spain. Part I. Hydrochemistry. This volume.

[5] Juncosa, R., Delgado, J., Vellando, P. and Padilla, F. (2006) FREECORE^{2D}: Código para resolver transporte de solutos reactivos en lámina libre en condiciones no isotermas. Manual del usuario v.0

[6] Juncosa, R., Delgado, J., Vellando, P., Padilla, F., Vázquez, A. and Hernández, H. (2007) Estudio de la influencia del hueco lleno de la mina sobre la cuenca del río Barcés (La Coruña). University of A Coruña unpublished report.

Why the Rio Quente is a special spring within The Caldas Novas Thermal Aquifer, central Brazil?

LUIZ JOSÉ HOMEM D´EL-REY SILVA,
DETLEF HANS-GERD WALDE,
JOSÉ ELÓI GUIMARÃES CAMPOS
RODRIGO ÁVILA CIPULLO
Instituto de Geociências
Universidade de Brasília
Campus Darcy Ribeiro, Asa Norte, CEP 70910-900, Brasília, DF
BRAZIL
ldel-rey@unb.br; detlef@unb.br; eloi@unb.br; racshalom@gmail.com

Abstract: - Thermal waters up-rise through Precambrian rocks in the inner part of the Neoproterozoic Brasília Belt (Tocantins Province, central Brazil) and make of the town of Caldas Novas an outstanding tourism place. They have fed a boom in the economy of the region around the Caldas Novas dome, a tectonic structural window ~20 km-long and ~12 km-wide cored by sub-greenschist facies quartzite, metasiltite, meta-argillite, slate, phyllite, and metarhythmite (Paranoá Group) and mantled by a nappe of biotite-quartz schist and garnet-bearing chlorite-muscovite schist (Araxá Group). Multidisciplinary geology studies have been supported from the local community of tourism entrepreneurs concerned with environmental issues, the quality of the underground aquifers, and with the possibility of artificial recharge. Rocks of the Paranoá Group record a passive margin-like basin developed 1300 – 900 Ma ago along the western coast of the São Francisco paleo-continent, and rocks of the Araxá Group record sedimentation/volcanism in a 900-800 Ma back arc basin developed between the paleo-continental margin and an intra-oceanic island arc to the west. Amalgamation of the arc and back-arc rocks to this margin led to ESE-driven transport of a nappe of Araxá Group rocks over the Paranoá Group rocks. All these rocks exhibit evidence of D_1-D_2 ductile deformation and metamorphism according to regional contraction in the WNW-ESE direction, during the first (~750-650 Ma old) stage of the Brasiliano orogeny. A new tectonic pulse (D_3) shortened all D_1-D_2 tectonites, 630-620 Ma ago, and developed, in the southern segment of the belt, km-scale and NNW-trending F_3 folds, such as the Caldas Novas dome F_3 braquiantiform. The anomalous thickness of 1,000 m of quartzite in the core of the dome (geophysical evidence) is likely due to a duplex of basal quartzite layers of the Paranoá Group. In the western margin of the dome the thermal waters flow within Paranoá basal quartzite at a rate of 1.6 m^3/s and reach surface as hot as 50 ^{0}C, forming a true river of hot waters. To the E-NE of the dome, in the Araxá schist flooring the town of Caldas Novas, the water flows at a much smaller rate. Hydrogen, carbon and oxygen isotopes data point to the thermal waters as being meteoric in origin, and the temperature indicates up-rise from depths of about 1,000 m. Data from detailed structural studies strongly suggest that the path for up-rise is controlled by a net of open surfaces that include the S_3 axial planar foliation and fractures associated mostly to the D_3 compression, combined with the stiffness of basal rocks of both the Paranoá and Araxá Groups. The 1.6 m^3/s flow of thermal waters in the western margin of the dome relates to a combination of the thickness and asymmetry of the D_3 duplex with the effects of late-D_3 gravity slide in the area.

Key-words: - Thermal water aquifer; Caldas Novas dome, Brasília Belt, Neoproterozoic, Brasiliano orogeny, central Brazil.

1 Introduction

The area of Caldas Novas, Goiás State – central Brazil, is part of the Internal Zone of the Brasília Belt. This one forms, together with the Araguaia and Paraguay belts, a Neoproterozoic geotectonic unit known as the Tocantins Province (Fig. 1).

The province is bounded by the Parnaíba and Paraná Phanerozoic sedimentary basins, and results from the collision of the paleo-continents precursors of the Amazonian and São Francisco cratons, as recorded by poly-deformed and metamorphosed Archean-Neoproterozoic rocks.

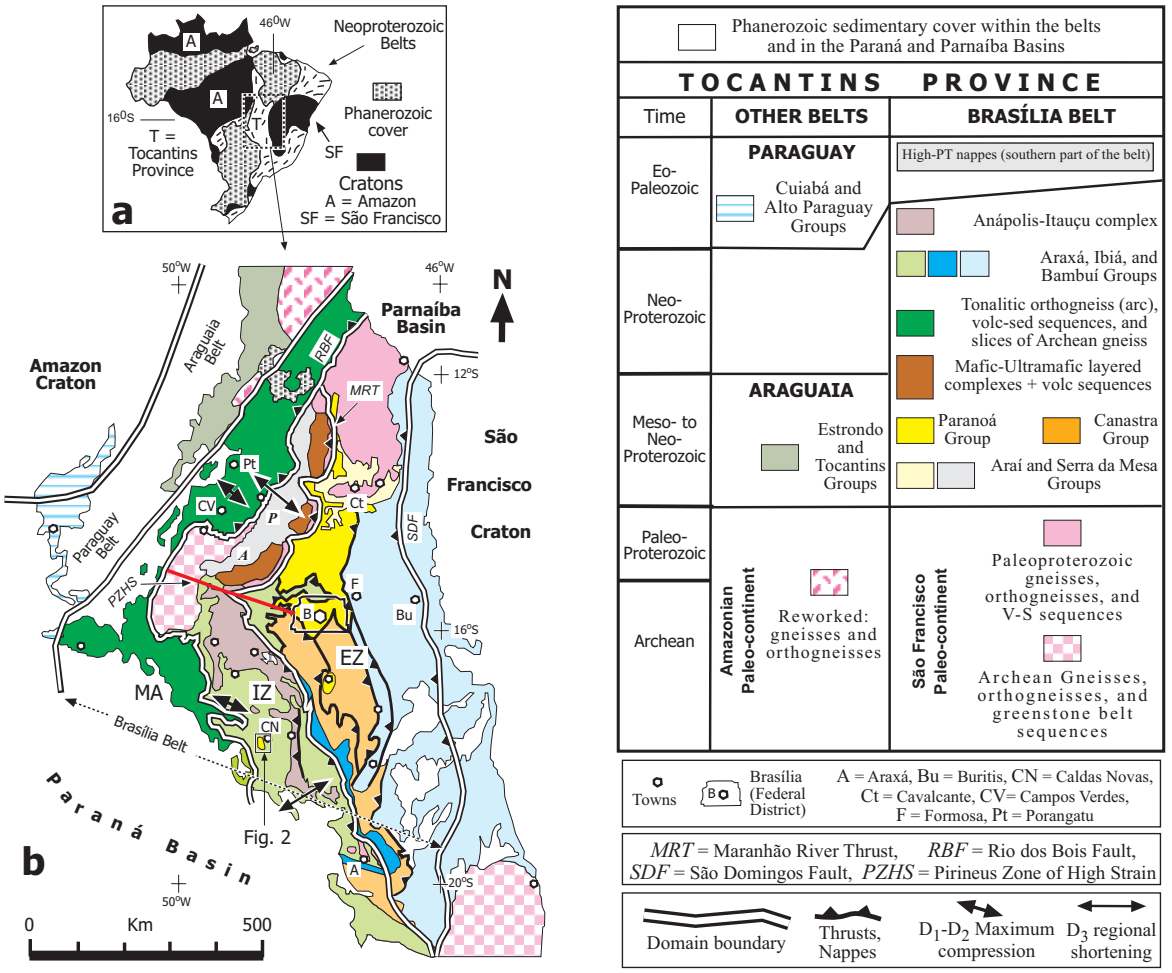

Fig. 1: Summary map displaying the main tectonic provinces in Brazil (**a**) and the central part of the Tocantins Province, as well as the three main lithotectonic units of the Brasília Belt (**b**; legend to the right): the Magmatic Arc – MA; the Internal Zone – IZ; and the External Zone – EZ. The EZ includes part of the Neoproterozoic sedimentary cover of the São Francisco craton. *A* = Araxá, and *P* = Paranoá. Adapted from [1] and [2].

The relevance of the Caldas Novas area rests on a structural dome and on the Rio Quente, Caldas Termas Clube, and Lagoa Quente springs of thermal waters (Fig. 2). The exploration of the thermal waters for tourism and leisure purposes has improved dramatically the economy in Caldas Novas and other two towns in the surroundings (Fig. 2a).

A boom in the economy of the area has been possible in the last twenty years because of an exponential growth in the volume of pumped thermal waters from artificial wells, but also brought to light a crescent concern about the capacity of the underground reservoir to maintain the current volume and temperature of the thermal waters.

For this reason, since about two years ago, the local association of entrepreneurs that explore the thermal waters (AMAT) has supported an international and multi-disciplinary scientific project destined to study the area and understand better the geological controls of the thermal aquifer, aiming to find alternatives for future planning.

The Caldas Novas dome is an elliptical structure with a NNW-trending axis as long as 20 km, and minor axis of ~10 km. Since [3] the dome is known as a structural window, as it exhibits a core of sub-greenschist facies quartzite and finer grained siliciclastics rocks of the Meso-Neoproterozoic Paranoá Group tectonically juxtaposed by a nappe of greenschist-amphibolite facies mica schist of the Neoproterozoic Araxá Group.

Nevertheless, solely more recently the area has been the locus of detailed geological studies: [4] described the Paranoá Group lithostratigraphy units; [5] and [6] described the rocks of the Araxá Group, as well as the tectonic structures and the structural-tectonic evolution of the whole area surrounding the Caldas Novas dome, whereas [7], [8], and [9]

have studied the main physical and chemical parameters and other aspects directly linked to the thermal waters and underground aquifers.

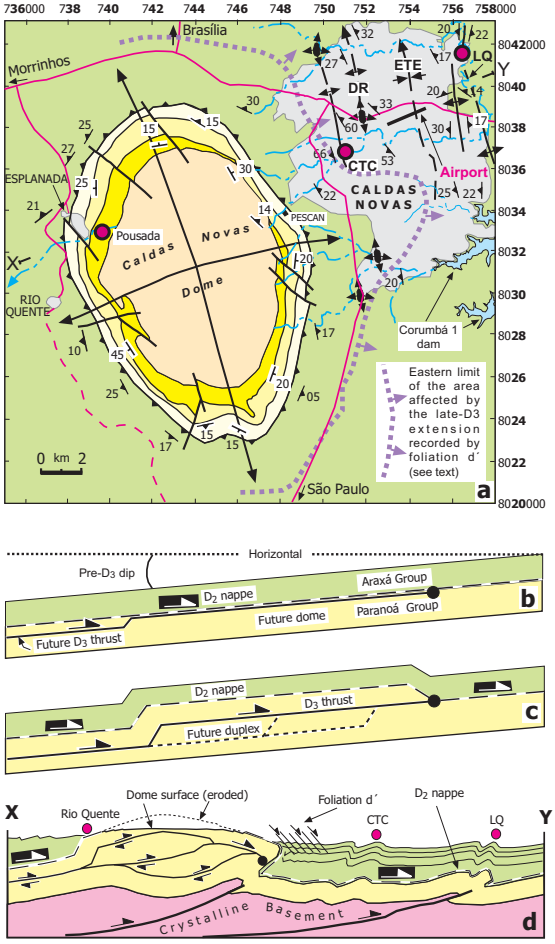

Fig. 2: The main geological features of the surroundings of Caldas Novas (modified from [5], and [6]): a summary geological map (**a**) and one cross-section (XY) explained in three cartoons (**b-d**). A small body of Cretaceous conglomerate mapped by [4] is omitted in the map. See legend to the right and other details in text.

This paper presents the recent advances in the geological knowledge of the Caldas Novas area and the consequences for the origin of the springs of thermal waters. Because of its distinct characteristics, one of the springs is geologically special and more important economically, thus we firstly describe the springs, secondly we focus on the basic geology of the study area and on the origin of the springs, and finally we present a geological model capable to justify their basic differences.

2 The springs of thermal waters

The springs of thermal waters (herein termed TWs) are known for over a century [5].

Among them, the **Rio Quente** (or Hot River) is a 10 m-wide natural stream that starts to flow in the upper part of the western flank of the Caldas Novas dome. The TWs rise on surface at a temperature of ~50 ^{0}C and total rate of 1 m^3/s, from a series of open spaces (described ahead) in the basal layers of quartzite of the Paranoá Group, within the artificial pools of the Pousada Park (Fig. 3).

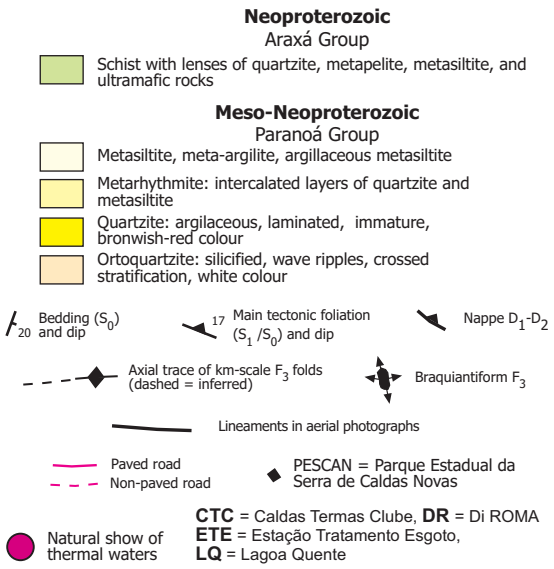

The Rio Quente is unique, and there is not another natural spring of TWs in Paranoá quartzite layers elsewhere around the dome. The TWs of the Rio Quente start to flow at 700 m above sea level and remain relatively warm down stream, until the town of Esplanada (Fig. 2). The chemical composition indicates high Ca and Mg contents, suggesting interaction of the TWs with carbonate rocks at depth, according to U. Tröger [9].

The other two springs occur within the Araxá schist of the town of Caldas Novas. Historical data about the **CTC** spring indicate a flow of 0,1 m^3/s, but it stopped flowing since ~25 years ago [9]. The **LQ** spring also flows at a rate of 0,1 m^3/s [9] and consists of three much focused brines enclosed in a 1000 m^2 site. Two of these are 1 m^2 each, and occur just beside the western margin of a voluminous river of cold waters. The third brine occurs in the bottom of a hot pool.

3 Summary regional geology

The Araguaia and Brasília Belts record the time life of a large ocean. Its spreading from ~1.3 to 0.9 Ga is recorded by sedimentary rocks of two passive margin-like sequences represented by the Paranoá (and Canastra) and

the Estrondo (and Tocantins) Groups, respectively mapped in the Brasília and Araguaia Belts.

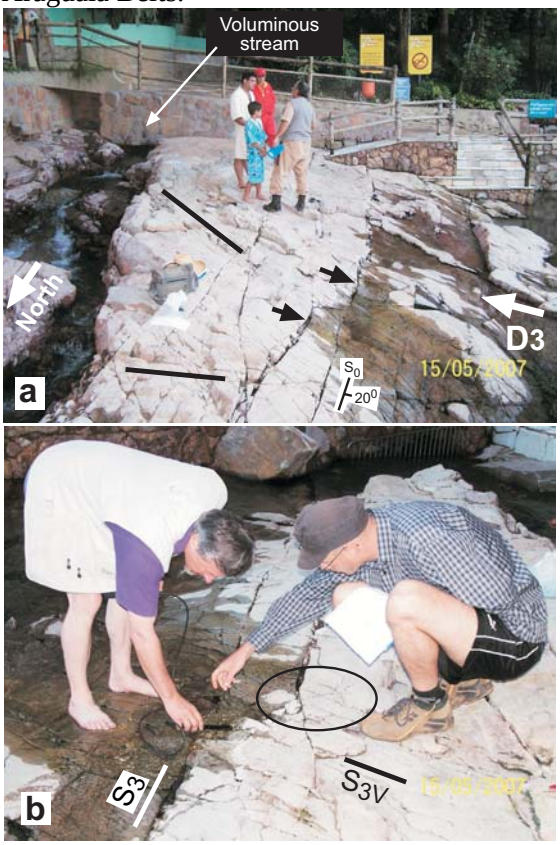

Fig. 3: Partial view of the TWs spring in two of the artificial pools in the upper part of the Pousada Park. The pools were deliberately emptied for direct observation of the TWs show on the bedrock. (**a**) The quartzite layers dip 20^0 to the west and exhibit a superb set of open surfaces. The longer of these form an anastomosed array of N-S trending and sub-vertical surfaces (S_3 foliation) along which the water comes up from depth (black arrows). The voluminous stream shown to the left corresponds to a mixture of hot (~50 ^{0}C) and normal waters (25 ^{0}C) that come up mostly along the contact between quartzite layers, along open S_3 surfaces, and along sub-vertical oblique fractures (black lines) related to D_3 shortening (indicated to the right). (**b**) U. Tröger (left) and J. Fornaçón measuring the temperature of TWs flowing up along S_3 surfaces. Note the S_{3V} surfaces sub-perpendicular to S_3 and, in the ellipse, the oblique fractures.

From 0.8 to 0.65 Ga a multi-stage intra-oceanic magmatic arc formed and was amalgamated, together with at least two back-arc basins adjacent to the western margin of the São Francisco paleo-continent [2], consequently nappes of the back-arc basin-like rocks (Araxá Group) propagated onto the Paranoá Group rocks (Fig. 1). From ~750 to 650 Ma all the rocks in the belt were shortened in the NW-SE direction, under D_1-D_2 deformation events typified by frontal ramps (summary of data in [2] and [5]).

Final closuring of the ocean brought the paleo-continents into collision 650 to 590 Ma, and led to D_3 deformation. The event D_3 shortened regionally the nappes, but shortening is recorded in two nearly orthogonal directions, relative to the Pirineus Zone of High Strain (*PZHS*) that separates, in the Brasília Belt, a NE-trending northern segment from a SE-trending southern segment.

The D_3 event is responsible for the evolution of regional faults such as the Maranhão River Thrust and the São Domingos Fault (Fig. 1), as well as the *PZHS*. As discussed in [2], there are strong and multi-disciplinary evidence for a time-kinematic compatibility between D_3 and the event of opening/infilling of the basin that originated the Paraguay Belt.

The D_1-D_3 evolution is the record of the Neoproterozoic Brasiliano orogeny and, in the southern segment of the belt, it is quite evident in the Caldas Novas area, and further to the south [5].

4 The Caldas Novas area

4.1 – Lithostratigraphy

The Paranoá Group in the core of the Caldas Novas dome is a low-greenschist facies sequence of four units. These consist of basal quartzite, siliciclastic metarhythmite made of cm- to dm-thick layers of quartzite and metasiltite, white to gray phyllite, and brownish to red meta-argillite (Fig. 2; [4]).

The Araxá Group comprises basal biotite-quartz schist and biotite quartzite, topped by garnet-bearing mica-chlorite schist with thin lenses of quartzite and mafic-ultramafic rocks. Wells data indicate a thickness of ~250 m for the Araxá rocks ([5] and [6]).

Two facts are important for understanding the Rio Quente spring: a - the basal unit consists of 1 m-thick layers of quartzite intercalated with cm- to dm-thick layer of finer-grained siliciclastic material. The thinner intercalations are suitable for inter-layer slip during deformation and also for erosion by the underground waters, thus the bedding is marked by opened spaces between the 1 m-thick quartzite layers (Fig. 4); and b – gravity data indicate anomalous thickness of ~1000 m for the Paranoá quartzite exactly beneath the Caldas Novas dome [5].

The high mechanical resistance of the basal layers of the two groups ([3] and [4]) allows a concentration of strain that is also important for understanding the TWs.

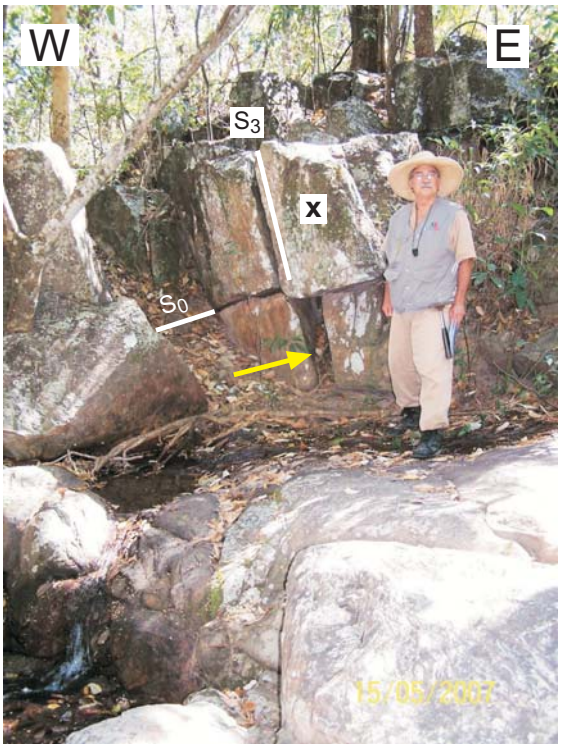

Fig. 4: Thick layers of Paranoá quartzite in the head waters of the Rio Quente, Pousada Park. Note the open space along the bedding (S_0) that dips gently to the west, and along surfaces of the steep-E-dipping S_3 foliation. Differential movement of block **X** during further gravity slide of the upper layer closed the along-S_3 wide space still seen in the lower layer (yellow arrow).

4.2 – Tectonic structures

After [3] and [4]) it is known that the geometry of the rocks in the area is controlled by regional-scale, double-plunging, and NNW-trending, normal to steeply inclined F_3 folds, verging to ENE such as the Caldas Novas dome itself and the CTC, DiRoma, and LQ antiforms, and intervening synform such as the ETE (Fig. 2). Cross-sections based on contrasting electricity resistance [10] fully support the fold interpretation for the Araxá rock layers underneath Caldas Novas (Fig. 2d).

The pre-D_3 structures indicate a ESE-driven tectonic transport along gently-dipping frontal ramps (Fig. 2b), particularly the asymmetry of the S-C pair within the S_1 mylonitic foliation, the S_2/S_1 asymmetry, and the vergence of F_2 folds (Fig. 2b). The ESE-driven tectonic transport during D_1-D_2 is strongly indicated by a pervasive stretching lineation (L_x) that is defined by sheath folds and stretched minerals. L_x trends systematically WNW-ESE across the area, in despite of all the F_3 folds ([5] and [6]).

The F_3 folds and the pervasive axial planar foliation S_3 affect all D_1-D_2 structures. Because strain was also taken-up by foliations S_{3V} and S_{3H} (respectively sub-vertical and sub-horizontal spaced cleavages related to the **b** and **a** tectonic axes of F_3) as well as oblique fractures and 1 m-wide shear zones sub-parallel to S_3, we assume that D_3 likely records a kind of transpression. The shear zones developed R, R´, P, and Y fractures in the resistant basal layers of the Paranoá and Araxá Groups, and are particularly evident in the western limbs of the Caldas Novas dome (Pousada pools), the CTC, and the LQ folds, coincidently the site of the natural springs.

Moreover, the Araxá D_1-D_3 tectonites adjacent to the southern, eastern, and northern margins of the dome are affected by a late-D_3 cm-spaced extensional crenulation cleavage (d´; Fig. 2; [3] and [4]) due to gravity slide of the schist layers during the uplift of the dome.

During the uplift, the Paranoá layers around the dome and the Araxá schist adjacent to the western margin of the dome were also affected by gravity slide in the form of late F_3 folds, not the d´ foliation. The reasons for d´ to exist in the Araxá schist are discussed in detail by [3].

5 Origin and up-rise of the TWs

A meteoric origin is well accepted for the TWs, based on the stable isotopes and other geochemical data [9]. The temperature indicates that the TWs must rise quickly from depths of about 1000 m, therefore a very efficient structural pathway must exist in the rocks. It demands explanation.

The detailed structural analysis has shown that all the fracture surfaces that can be observed in the outcrops are fully compatible with D_3 deformation, the last event to affect the area during orogeny ([5] and [6]).

The intersection of the planar structures existing in the area may have formed narrow and vertically continuous corridors across the competent basal layers, producing channels suitable for the fast up-rise of the TWs (Fig. 5). Such template is quite feasible because the western limbs of the F_3 antiforms are the locus of strain concentration, specially considering that the d´ gravity sliding of the schist implies further tightening the F_3 folds to the east of the extensional front (Fig. 2). The concentration of strain explains the onset of shear zones in the

CTC and LQ areas, and is also, theoretically, a positive factor for the multi-layer propagation of open brittle fractures through resistant rocks (see analogy in [12]).

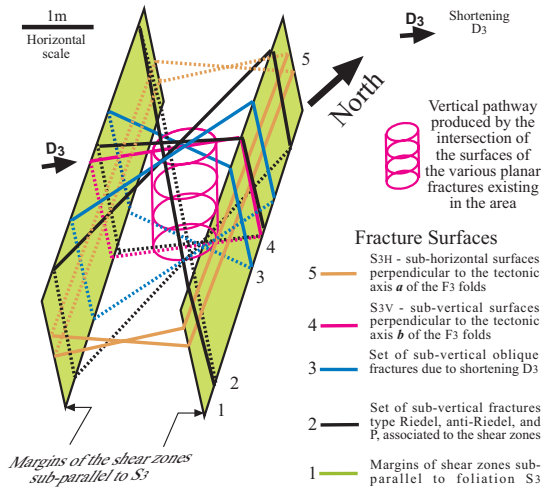

Fig. 5: Mechanical porosity that may exist in the Caldas Novas area. Details in text.

A duplex structure that likely formed underneath the dome (Fig. 2c-d; [3]) explains the anomalous thickness of quartzite and, together with the west-dip of the horses, explains the largest flow of TWs in the Pousada Park. The flow is likely facilitated by a combination of voids opened along S_0 and S_3 (Fig. 4). Actually, because the S_3 surfaces were sub-perpendicular to the direction of gravity slide, the along-bedding slip in the basal quartzite easily opened S_3-controlled large separations (yellow arrows) across the layers.

6 Conclusions

The TWs of Caldas Novas are meteoric waters heated at depth and forced to move up quickly when the temperature creates a sufficiently low density. The upward flow is likely facilitated by channels built along the intersection of syn- to late-D_3 brittle fractures related to the tectonic evolution of the Brasília Belt. A D_3 duplex in the core of the Caldas Novas dome antiform makes thicker the quartzite (= good aquifer) there. The west-dipping horses and better fracturing in more resistant rocks allow the flow of 1 m^3/s that make of the Rio Quente a special spring.

Where is the main area for recharging the aquifers? The answers are still being looked for. They will provide a key for preventing pollution in the aquifer and for future planning.

References:

[1] Fuck, R.A., Pimentel, M.M., D'el-Rey Silva, L.J.H., Compartimentação Tectônica na Porção Oriental da Província Tocantins, in XXXVIII Congresso Brasileiro de Geologia, Camboriú, SBG, Bol. 1, 1994, pp. 215-217.

[2] D'el-Rey Silva, L.J.H, Vasconcelos, M.A.R., Gonçalves, D.V., Timing and role of the Maranhão River Thrust in the evolution of the Neoproterozoic Brasília Belt and Tocantins Province, Central Brazil, Gondwana Research 2007, doi:10.1016/j.gr.2007.09.004.

[3] Drake Jr., A.A., The Serra de Caldas Window, Goiás, Tectonic Studies in the Brazilian Shield, Geological Survey of America Professional Paper 1119-A, 13p.

[4] Campos, J.E.G., Fortes, P.F., Santos, R.V., Geologia do Domo de Caldas Novas, 2000, Relatório Interno, UnB – IG, 80p.

[5] D'el-Rey Silva, L.J.H., Klein, P.B.W., Walde, D.G.H., The Caldas Novas Dome, Goiás: Structural evolution and implications for tectonics in the Brasília Belt, Brazil, Jour. of S. Ame. E. Sciences Vol.17, No. 2, pp. 153-169, 2004, doi:10.1016/j.sames.2004.03.001

[6] D'el-Rey Silva, L.J.H., Walde, D.H-G., Campos, J.E.G., Cipullo, R.A.A., Mapa Geológico da região de Caldas Novas, Goiás, $10^{0.}$ Simpósio de Geologia do Centro Oeste, Pirinópolis, poster, 2007.

[7] Tröger, U., Costa, J.F.G., Haesbaert, F.F. & Zschoche, A., Novas contribuições aos aquíferos termais de Caldas Novas, in VII Simpósio de Geologia do Centro-Oeste e X Simpósio de Geologia de Minas Gerais, Brasília, Boletim de Resumos, SBG-DF / MG / CO, 1999, p.131.

[8] Tröger, U. , Peixoto Filho, S., Lacerda, H., Thermal Water Springs in Central Brazil – Hydrogeology, Chemical Composition, and Isotope Studies, XXXIII IAH Congress, Zacatecas-Mexico, 2004, ISBN970-32-1749-4.

[9] Tröger, U., Structure conditioning thermal springs in Central Brasil in Groundwater in fractured rocks, Krásný, J. & Sharp, J.M.Jr. Editors, Taylor & Francis London, 2007 pp355-371.

[10] Cunha, L.S., Caracterização geoelétrica por eletroresistividade na área urbana da cidade de Caldas Novas–GO, Internal Report, AMAT-Caldas Novas, 2007, 11p.

[11] Gross, M.R. and Eyal, Y., Throughgoing fractures in layered carbonate rocks, Geological Society of America Bulletin, Vol. 119, No.11/12, pp.1387-1404; doi:10.1130B26049.1.

Evaluating and planning waste landfill top covers with the help of vegetation and population ecology

Brigitte Klug[1], Johannes Tintner[2], Marion Huber-Humer[2],
Katharina Meissl[2]
[1] Department of Integrative Biology and Biodiversity Research
[2] Department of Water, Atmosphere, and Environment
Universität für Bodenkultur (BOKU)
Gregor-Mendel-Straße 33, 1180 Vienna
AUSTRIA
brigitte.klug@boku.ac.at, johannes.tintner@boku.ac.at, http://www.boku.ac.at

Abstract:-The accumulation of solid waste has caused remarkable problems for environment and public health, and authorities have to tackle the costly recycling, reduction, and management of solid waste. Nevertheless, the area occupied by landfills is steadily growing. It is an urgent need to avoid toxic impacts such as landfill gas or leachate arising from old landfills, and to find environmentally friendly after-uses for the sites. The co-operation of waste management and botany shows viable practices for the future: Phytosociological relevés of the (spontaneous or seeded) vegetation on old landfills can indicate not only the quality of the top cover, but also gaps in the cover where methane or leachate emerge. This information helps companies and authorities to take appropriate steps of sanitation. Well-kept old landfills may be re-integrated into the production of energy plants or fibre plants. Another possible after-use would be a park for recreation. In this case, special care has to be taken for selecting local tree and shrub species with suitable demands and a superficial root system. In regions where rare ecosystems in the vicinity of a landfill are threatened by extinction, one can think of a re-establishment of those ecosystems. By providing a suitable top cover and introducing species of the threatened ecosystem, it is possible to trigger a succession towards this. Nevertheless, steady monitoring of the vegetation development and the soil seed bank is necessary to guarantee success. A new experimental field for botanists and ecological engineers is re-vegetation on combustion slag. To reduce the volume of waist, some municipalities have chosen this method recently instead of mechanical-biological waste treatment. Re-cultivating combustion slag causes many ecological problems, and this is one of the challenges for the future.

Key-Words: - After-use, Bio-indication, Phytosociological relevés, Re-vegetation, Soil seed bank

1 Introduction

In Central European societies the so-called "Wirtschaftswunder" (miracle of economics) after World War II has led not only to wealth for almost everybody, but also to environmental problems caused by the steadily growing amounts of waste. Official statistics name a total production of waste in Vienna in 2001 of 5,25 million tons of solid waste, 5% of which are dangerous [1]. The municipalities, however, have learned their lessons and have released laws and orders to reduce, recycle, and manage whatever is thrown away [2]. Urgent aims behind all these measures are to raise the recycling rates and thus to reduce the space needed for the deposition of not recyclable leftovers, and to minimize hazards for the environment [3, 4]. Moreover, in times with growing need of recreation parks for the public and with shrinking refugial areas for rare animal und plant species in urban areas, well-kept and re-vegetated former landfills might be considered as stepstones or valuable niches for nature (even if "second-hand") [5].

Waste management and botany can co-operate in a fruitful way to reach these goals, as already shown in the past decades [e.g. 6, 7, 8].

The legal situation in Austria does not allow solid waste from households to be deposited without either mechanical-biological pre-treatment or combustion. Vienna has chosen the latter possibility, and nowadays the slag and ashes from the incineration plants are mixed with cement and deposited in a landfill in the north-eastern outskirts of Vienna. Compared to the former situation, the volume of the deposits is smaller, but the re-cultivation of the landfill surface has become a challenge for everyone involved.

Another urgent problem – especially with old solid waste landfills in the provinces - is the fact

that substances in the waste body might still cause noxious leachate and/or landfill gas. Areas where these substances emerge are usually either completely unvegetated or show a typical composition of the plant cover that can - to a certain extent - cope with the noxious impact, or avoid a direct contact with the poison thanks to their adapted life traits [9].

The top cover of the landfill must therefore be selected very carefully and with respect of local demands and eventual future after-uses.

2 Materials and methods

Three examples in Vienna and Lower Austria (all in a pannonian climate with warm summers and cold winters and a yearly precipitation of 400 - 600 mm) can highlight today´s situation and challenges for re-vegetation and sanitary demands of landfills.

2.1 Vienna – Rautenweg

In 2003, the managers of Vienna´s biggest landfill stated serious re-vegetation failures on the superficially applied substrate on the eastern slope where slag-cement was going to be built in.

Fig. 1 shows the construction concept [10] of the slope in question where big bare areas were the reason of complaints. Especially on the uppermost slope neither planted trees nor seeded grasses and herbs showed vital growth. Therefore we checked every planted tree by noting its position by GPS, identified the species, and classified its vitality in a 3 steps scale [11].

Secondly, we performed phytosociological relevés using a combined scale after Braun-Blanquet 1964 and Londo 1976 in the most characteristic sections of the 3 uppermost slopes of the landfill [12, 13]. Thus we assessed cover percentages of seeded grasses and herbs as well as of naturally growing ruderal species. The cover data were then used to calculate average indicator values for moisture, nutrients and soil reaction as well as salinity. These data characterized the site quality and were adapted from Ellenberg et al. 1992 to the Austrian situation by Karrer and Kilian [14, 15].

Thirdly, we performed germination tests with the seed mixture used for the re-cultivation of the slope. The tests were performed in the greenhouse for 20 days and continued in the open air for further 45 days. As a substrate we took the soil that had been provided as a plant bed on top of the ash-slag-cement of the slope. Additionally we took the original ash-slag-cement and mixed it 1:1 with the soil mentioned before. As a control a peat substrate for plant cultivation was also used in the germination tests. The 3 plant groups tested were the same as used at the landfill, namely a grass mixture, vetch (*Vicia* spp.), and sainfoin (*Onobrychis viciifolia*). In the experiment these plants were sown in exactly the same density as for practical re-vegetation; thus we used a known number of seeds and could calculate the percentage of surviving seedlings after the experiment. Furthermore we measured shoots length and total dry weight of the seedlings.

2.2 Breitenau

The situation at Breitenau was different concerning the history of the landfill: It had been installed as a test area to compare different top covers and their ability to avoid the emission of landfill gas. Fig.2. shows the 3 test cells and their cover characteristics. These test cells were divided into 2 and 3 relevé fields, respectively, according to the obviously different cover layers and different plant covers in cell 1 and 2, and according to different plant species composition despite a more or less uniform top cover in cell 3. Relevés and calculations of average indicator values were performed here as well.

2.3 Mannersdorf

Constructed in 2 consecutive periods, this 3rd landfill reveals its history and frequent disturbances in the low-quality top cover very well by the actual plant cover. The landfill is surrounded by a thermophilous oak forest and the last remainders of formerly widespread semi-dry meadows containing some rare and endangered plants like members of the orchid family. None of these rare species can cope with the compacted and periodically wet substrate of the landfill, but large parts of the top cover are dominated by short-lived weeds.

To offer those rare species the possibility to immigrate into the landfill we started a little experiment where - on top of the former top cover - α) a layer of sand and, in the second variant, β) also a thin layer of meadow soil was spread. On top of this, mulch material and seeds from the meadow outside the landfill was spread in comparably low density [16]. We performed relevés and calculations of indicator values and life forms on the old parts and on the experimental plots as described for site 1.Two years after seeding, we took soil samples from the experimental plot as well as from the 2 parts of the old landfill cover to assess the soil seed bank of the 3 plots. 20 samples from each plot were taken to a depth of 10 cm.

They were divided into 2 soil depths, namely from 0 to 5 cm soil depth and to 5 – 10 cm soil depth. The samples were kept in the cool for almost 3 months for vernalization, and then, in the green-house, spread on styropore trays and exposed to 16 hr light, summer temperatures, and regular water supply for 100 days. Emerging seedlings were counted at least every second or third day, and identified to species level as soon as possible.

3 Results

3.1 Vienna-Rautenweg

Fig. 2 and Fig. 3 show that on the uppermost (youngest) slopes the greatest deficiencies were noted. These slopes were by far the steepest (over 30°), and from their surface the soil layer had partly been eroded together with the seeds of herbs and grasses. Thus especially trees [11] but also the few remaining grasses and herbs had to root in almost pure slag cement [17].

As Fig. 4 confirms, pure slag cement with a pH of 11 is a serious problem for germination and development of young seedlings. Only short-lived weeds with a rapid development and a high seed production can survive for some months on the uppermost slope (Fig. 3), and one year later the same group of species will develop a new generation. Only within some years - when at least the superficial layers of the slag cement have aged - the situation will improve; but the superficial erosion of soil on the steep slopes has to be stopped at once by measures of ecological engineering.

On the more or less horizontal berms, however, where enough substrate can be applied to isolate plant roots from the slag, even the production of fibre plants or energy plants is possible shortly after the construction.

3.2 Breitenau

Fig. 5 demonstrates that top covers on solid waste without any compost or soil layer do not suppress landfill gas emissions completely. On the other hand, the vegetation on thick compost layers will always stay dominated by nitrophytes, i.e. very common ruderal plants with different life spans; it would not develop towards a semi-dry meadow or a thermophilous forest in a reasonable period of time (Fig. 6). In Test Cells I and II with gravel and silt as main top covers, the number of perennial plants was more than doubled between 1990 and 2002; in that period of time it stayed almost unchanged in Test Cell 3 (compost top cover). The number of short-lived plants, however, shrunk in tall 3 test cells. While in I and II the perennials had taken over, in Test Cell III only very few competitive annual nitrophytes dominated at last on the pure compost.

The contrasting results of test cells I and II demonstrate that gravel and/or silt without any humus (soil) addition will not stop the emission of landfill gas, but the plant cover on these fields shows more similarities with the traditional dry and nutrient-poor meadows and forests of the region (Fig. 7). The combination of compost with gravel layers on top proved to be best of all.

3.3 Mannersdorf

This landfill also exhibits its history with the help of relevés and maps referring to indicator values and life spans. We learn that the top cover material is compacted to different degrees; this can be deducted from indicator plants for changing moisture (Fig. 8a). Some parts must have been disturbed recently; this can be assumed by the accumulation of short-lived plants in certain areas (Fig. 8b).

The experiment with the aim to install a semi-dry meadow on top of the former top cover gives hope for the future. The averaged N-values (indicating the nutrient demands), plotted against the F-values (indicating moisture demands), clearly separate the data of the old landfill parts from the relevés of the adjacent meadow, and the experimental plots are found in between the two groups (Fig. 9).

Regardless of the very short existence of the experimental plot, this site has already built up a very interesting and promising soil seed bank. Especially the species number (Fig. 10) of perennial plants in the seed bank (indicating similarities with the adjacent semi-dry meadow) is high in the experimental plots; typical ruderals, mainly short-lived grasses and herbs, prevail in the seed store of the old landfill parts where they are also well presented in the above ground vegetation.

4 Conclusion

Vegetation and population ecology helps us
*to find out the reasons of failures in recultivation,
*to deduct information about possible emissions,
*to learn about possible plant communities on different landfill top covers,
*to distinguish parts with a different history within one landfill,

*to get insight in the quality and quantity of soil seed banks in landfill top covers, and
*to initiate a vegetation development on landfill top covers towards a plant community of higher ecological value.

In times of shrinking physical and natural resources, future landfill management should take these aspects into account.

5 Acknowledgments

We are grateful to all who contributed to the success of our work, be it financially, or via permissions, or by physical and/or intellectual co-operation.

References:

[1] Municipality of Vienna: Abfallstatistik (Waste Statistics; latest visit at web site: May 9th 2008), www.wien.gv.at/ma22/abfall/abfallstatistik.htm

[2] Bundesminister für Umwelt (Austrian Minister of Environment), Deponieverordnung, BGBl. Nr. 164/1996, ST0049

[3] Gomiscek, T., *Rekultivierung von Deponien mit abfallbürtigen Substraten und Energiepflanzen im Hinblick auf Wasserhaushalt und Biomasseertrag*. PhD Thesis, Universität für Bodenkultur (BOKU) Vienna, 1999

[4] Maurice, Chr., Bergman, A., Ecke, H., Lagerkvist, A., Vegetation as a biological indicator for landfill gas emissions: initial investigations. *Proceedings from Sardinia '95: Fifth International Landfill Symposium, October, 2-6, 1995, St. Margherita di Pula, Cagliari, Italy*, Vol. III, 1998, pp. 481-494

[5] Simmons, E., Restoration of landfill sites for ecological diversity. *Waste Management and Research* 17 (6), ISWA, 1999, pp. 511-519

[6] Konold, W, Zeltner, G. H., Untersuchungen zur Vegetation abgedeckter Mülldeponien. *Beihefte Veröff. Naturschutz und Landschaftspflege Ba den-Württ.* 24, 1981, pp. 7-83

[7] Neumann, U., *Untersuchungen über die Begrü nung und Entwicklung von Vegetationsdecken auf Mülldeponien*. PhD Thesis, Technical University Berlin, Germany, 1976

[8] Handel, S. N., Robinson, G. R., Parson, W. F. J., Mattei, J. H., Restoration of Woody Plants to Capped Landfills: Root Dynamics in an Engineered Soil. *Restoration Ecology* 5 (1), 1997, pp. 178-186

[9] Huber-Humer, M., Klug-Pümpel, B., The vegetation on different top covers of an abandoned solid waste landfill. *Die Bodenkultur* 55 (4), 2004, pp. 155-163

[10] Kotal, C., *Untersuchungen über die Standsi cherheit einer Deponieböschung* (Investigations on the stability of a landfill slope; in German), Diploma thesis, Universität für Bodenkultur (BOKU) Vienna, 1998

[11] Taschil, V., *Entwicklung von Gehölzpflanzungen auf der Wiener Mülldeponie Rautenweg in Abhängigkeit von Substrat und Umgebungs-vegetation*. (Development of wood plantations at the Viennese landfill Rautenweg in relation to substrate and adjacent vegetation; in German), Diploma thesis, Universität für Bodenkultur (BOKU) Vienna, 2005

[12] Braun-Blanquet, J., *Pflanzensoziologie*, 3rd ed., Springer Wien, 1964

[13] Londo, G., The decimal scale for relevés of permanent quandrats. *Vegetatio* 33, 1976

[14] Ellenberg,H., Weber, H., Düll, R., Wirth, V., Werner, W., Paulissen, D., Zeigertwerte von Pflanzen in Mitteleuropa. *Scripta Geobotanica* Vol.. 18, 2nd ed., Goltze, Göttingen, 1992

[15] Karrer, G., Kilian W., Standorte und Waldgesellschaften im Leithagebirge, Revier Sommerein (incl. 2 tables, 1 map), *Mitt. Forstl. Bundesversuchsanst.*, Wien, 1990, pp. 165-244

[16] Tintner, J., Meissl, K., Klug, B., *Possible vegetation successions on landfill top covers in the Pannonian region – an example from Eastern Austria* (see this volume)

[17] Taschil, U., *Die aktuelle Pflanzendecke des Ostabhangs der Wiener Mülldeponie Rautenweg – ein Ergebnis von Standortsfaktoren, Einsaat und natürlichen Sukzessionsprozessen* (The actual plant cover on the Eastern slope of the Viennese Landfill Rautenweg; in German), Diploma thesis, Universität für Bodenkultur (BOKU), Vienna, 2005, 116 pp. + appendix

[18] Walter, J., *Flora und Sukzessionsverhältnisse auf Mülldeponien in verschiedenen Gebieten Österreichs* (Flora and successional relations at landfill sites in different regions of Austria), Diploma thesis, University of Vienna, 1992, 241 pp.

Figures:

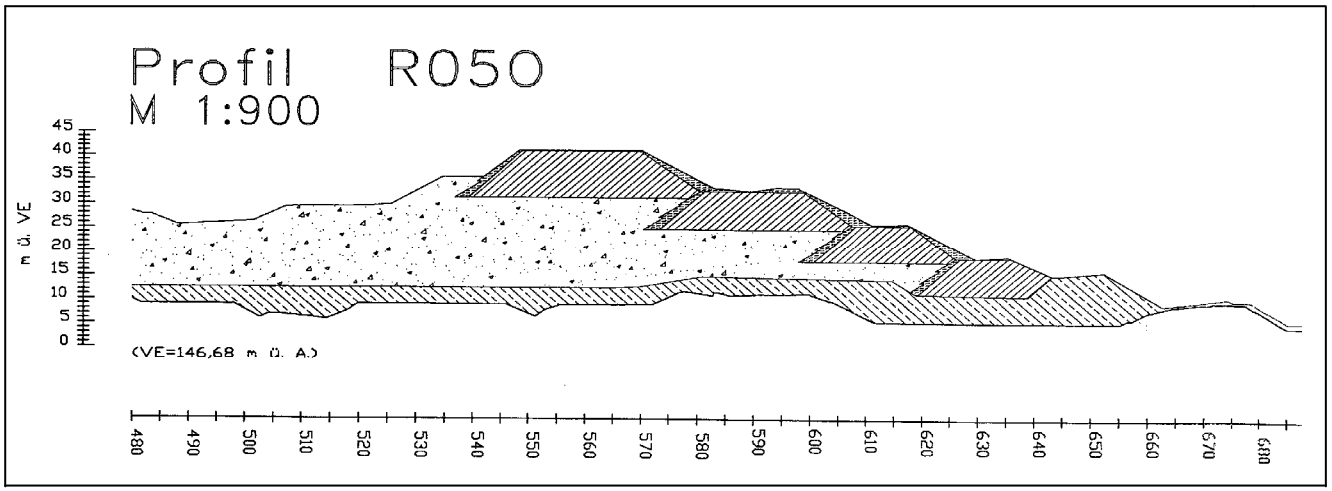

Fig. 1: Cross section through the eastern ash-and-slag-cement slope of the solid waste landfill Rautenweg (Vienna). Source: C. Kotal [10].

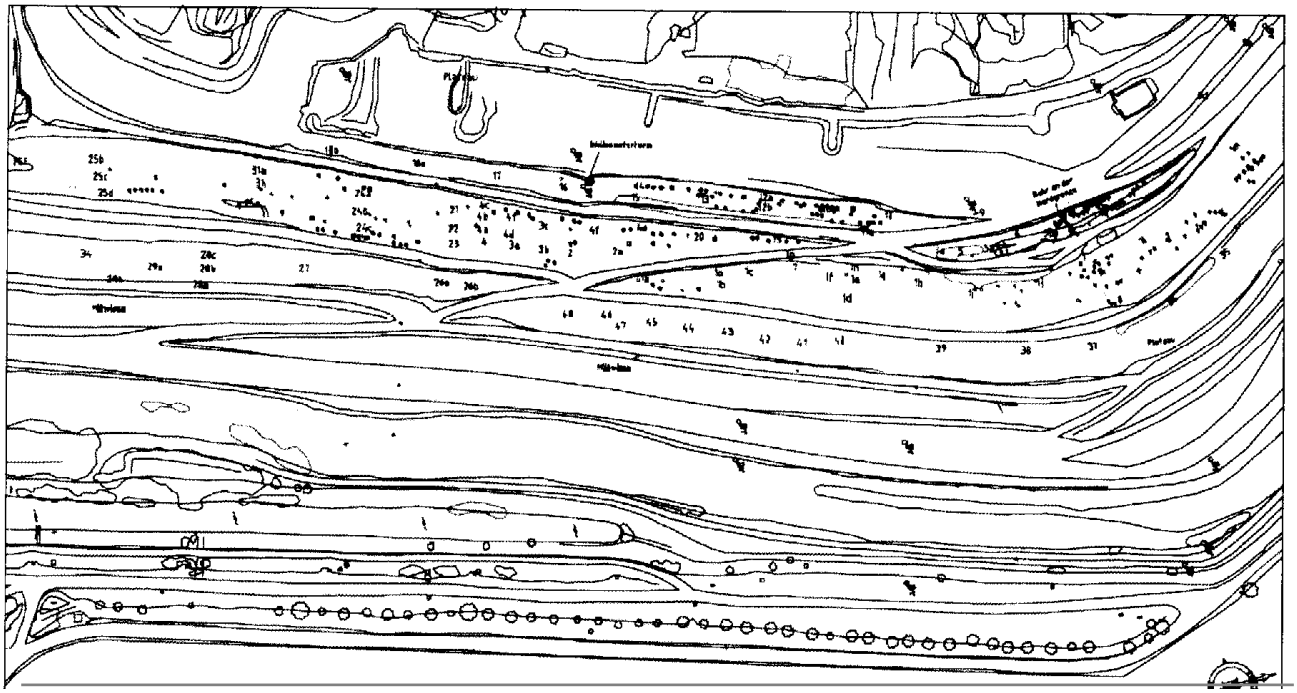

Fig. 2: Position of dead young trees (black dots) of various species planted one year earlier in the eastern slope of the landfill Rautenweg. Source: V. Taschil [11].

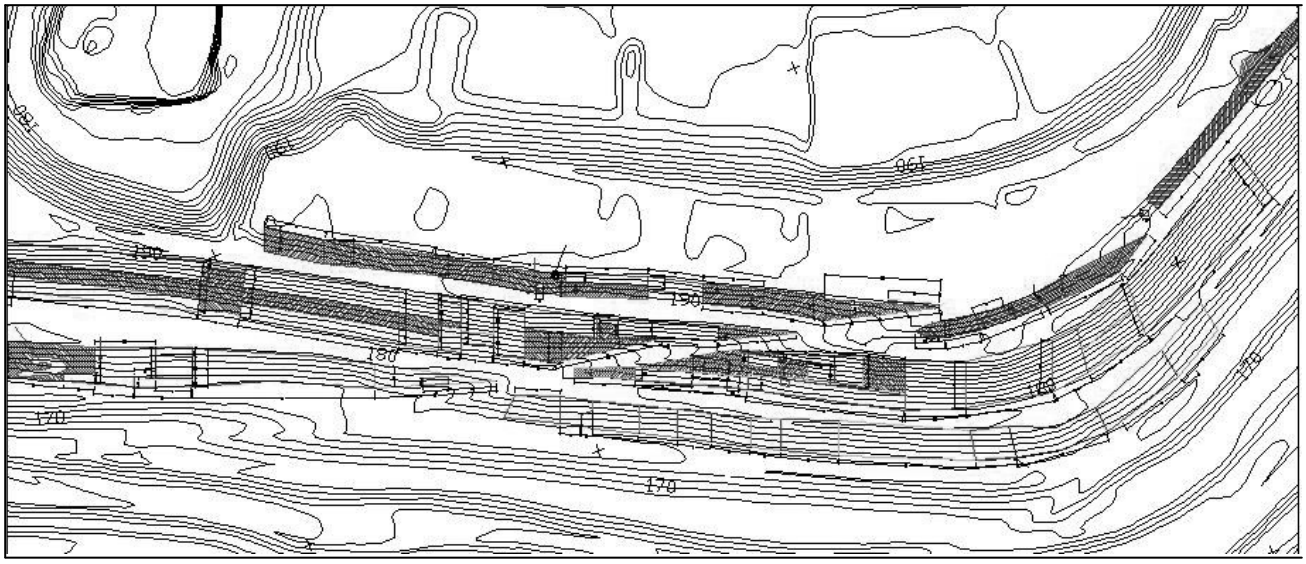

Fig. 3: Plant communities on the eastern slope of the landfill Rautenweg with an especially high portion of short-lived (annual) species. Data source: U. Taschil [16].

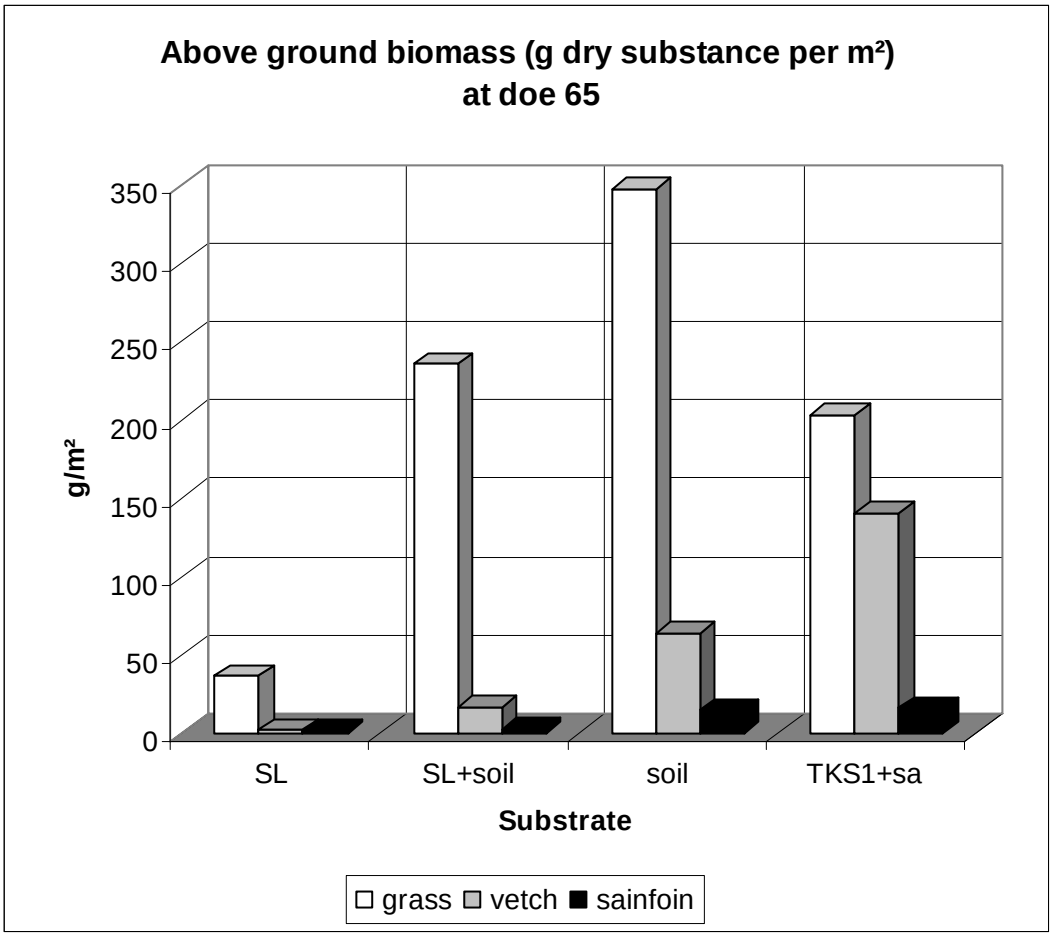

Fig. 4: Results of a germination test of conventional seed mixtures on different substrates. 65 days after the start of the experiment (20 days in the greenhouse, 45 days in the open air), the grasses, vetches and sainfoin plants on pure slag cement (SL) had developed only very little biomass compared to plants in soil or the cultivation substrate (TKS1+sa).

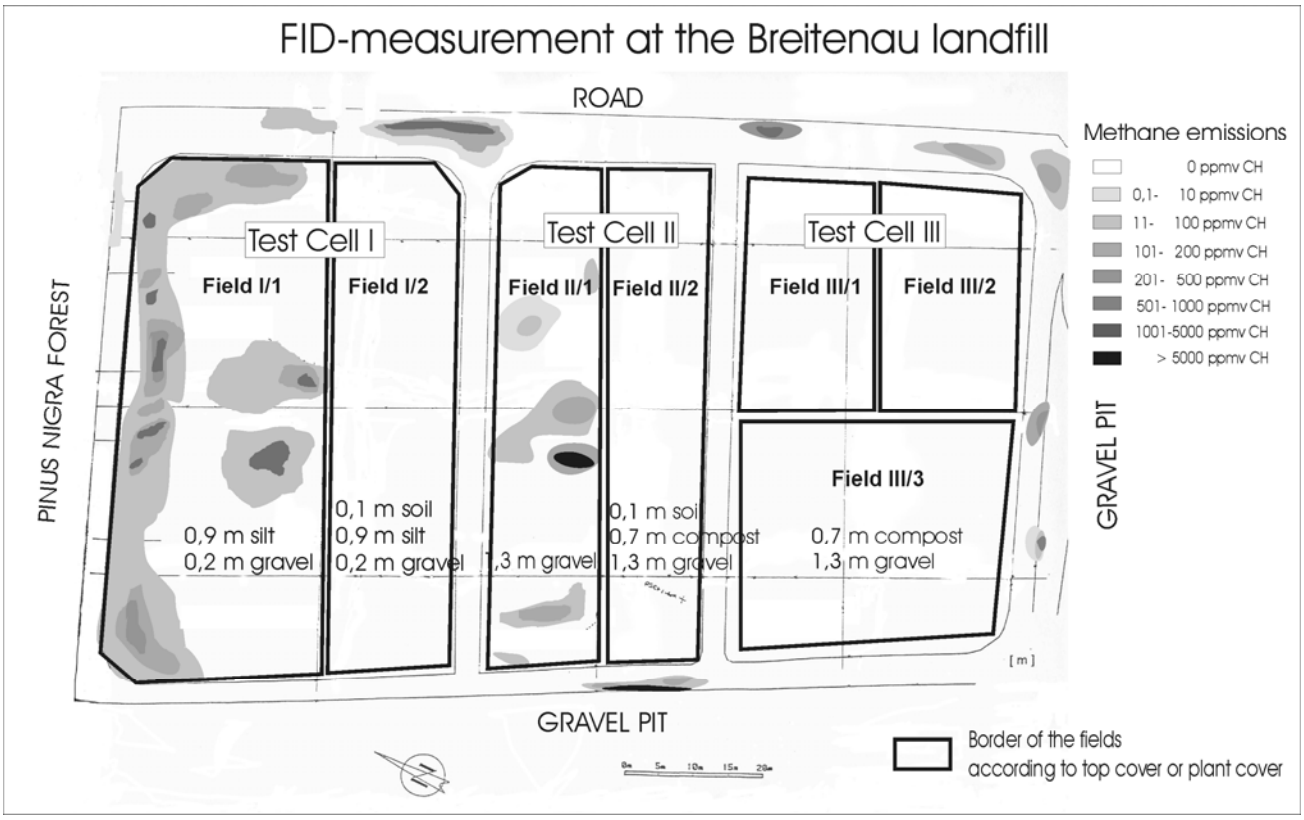

Fig. 5: Experimental solid waste landfill Breitenau. In 3 test cells (each divided into 2 and 3 experimental fields, respectively), phytosociological relevés documented the plant covers on characteristic layers of top cover 10 years after the closure of the landfill. Patches with methane emissions are shown in different shades of grey, according to gas concentration. Source: Huber-Humer and Klug-Pümpel [9].

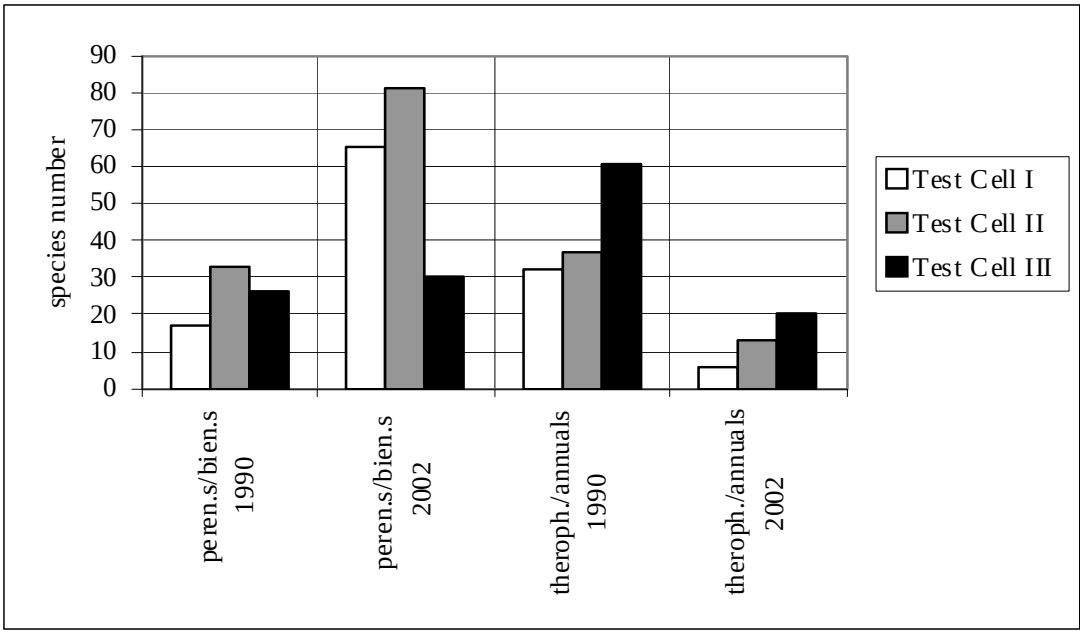

Fig 6: Development of the species numbers in the 3 test cells between 1990 and 2002. Data for 1990 from Walter [18].

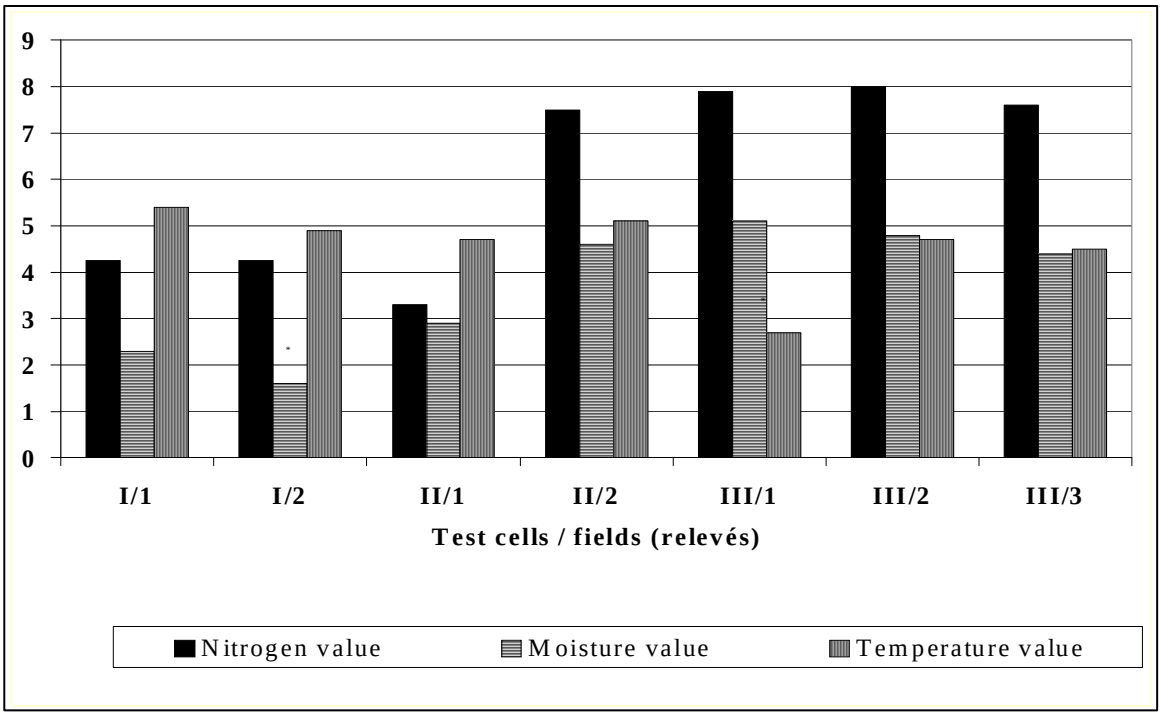

Fig. 7: Average indicator values for nutrition (nitrogen), moisture, and temperature in the test cells and fields, respectively. Low nitrogen and moisture supply is indicated in the fields without compost; in the compost fields, the high N-values of the nitrophytes are reflected. Temperature values seem to be unaffected by the different top covers in this case.

(a) 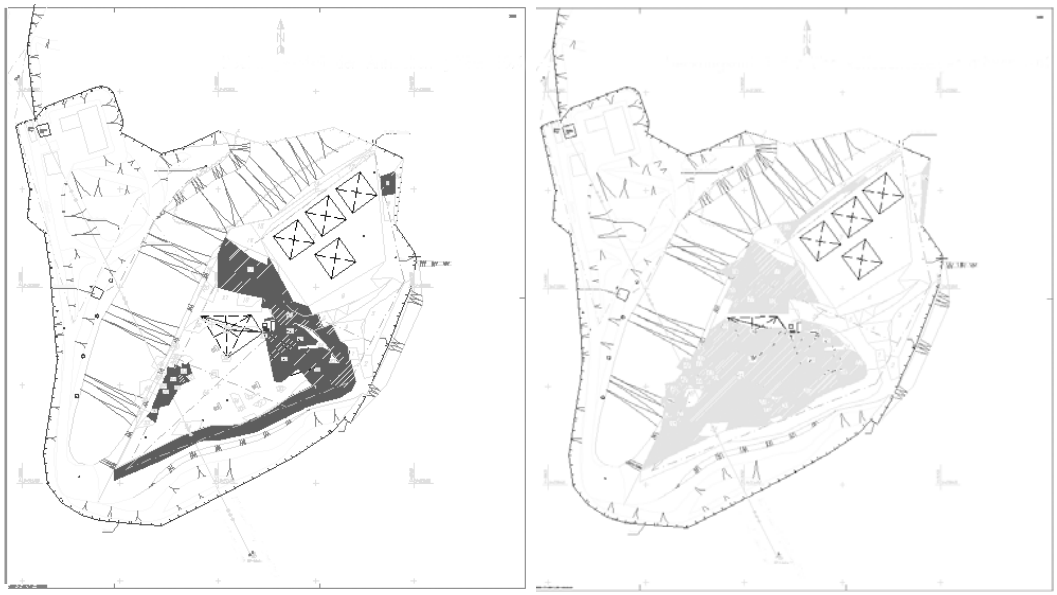 (b)

Fig. 8: Landfill Mannersdorf. Phytosociological relevés and indicator values allow a distinction of areas with changing moisture (a) and disturbances, the latter expressed by high cover percentages of annual plants (b). Source: Tintner et al. [16].

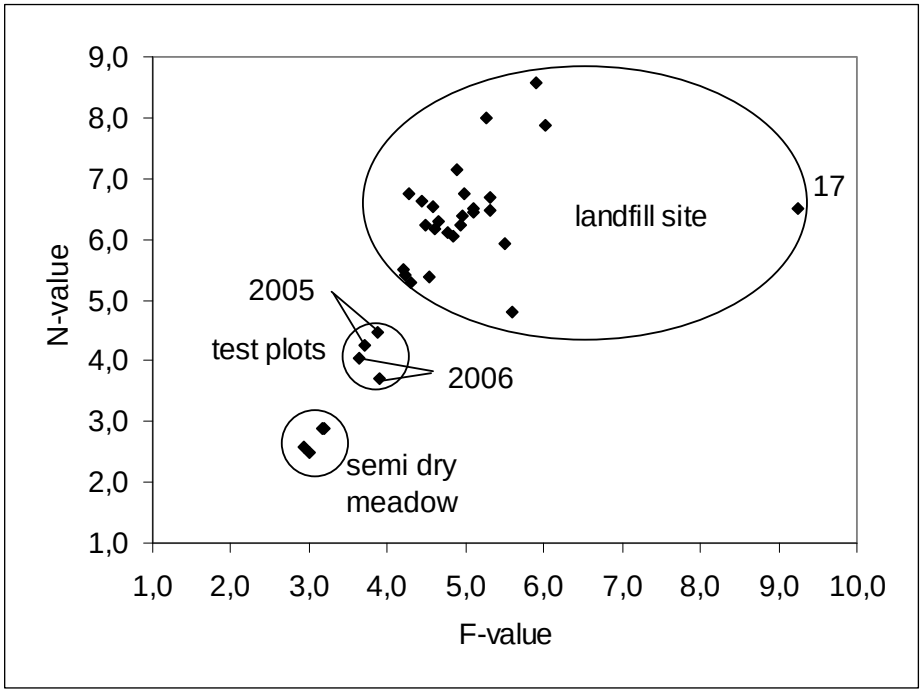

Fig. 9: The F and N indicator values of the plant communities on the old landfill cover are clearly separated from those of the adjacent semi-dry meadow, whereas the test plots with the meadow species on the sand/soil layer are positioned between the 2 groups, showing a tendency to develop towards the meadow only 2 years after the start of the experiment. Source: Tintner et al. [16].

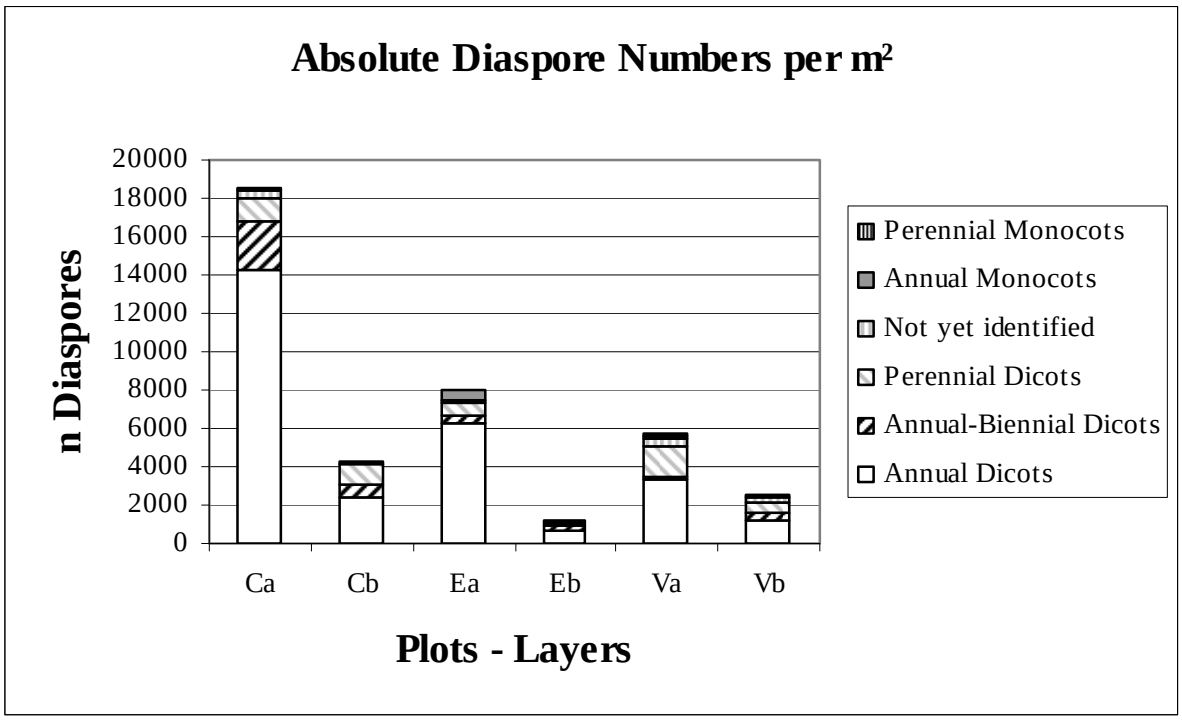

Fig. 10: Diaspore (seed) pool on 2 differently vegetated areas of the landfill top cover and in the experimental plots. C, E: landfill area; V: experimental plot.
a: Soil layer 0-5 cm; b: soil layer 5-10 cm. Each column represents means of 20 replicates.

Amaranth Food Dye Photochemical and Photoelectrochemical Degradation

CRISTIANO P. SILVA, SANDRO MARMITT, CLAUS HAETINGER AND SIMONE STÜLP
Programa de Pós-Graduação em Ambiente e Desenvolvimento (PPGAD), Univates, Avelino Tallini, 171, Lajeado/RS, BRAZIL. stulp@univates.br

Abstract: - This paper studied the photochemical and photoelectrochemical degradation of food dye (red dye - amaranth). The investigation aimed at the assessment of alternative treatments, focusing the use of clean technologies. The photochemical and photoelectrochemical degradation experiments were performed in a compartment with UV radiation (mercury lamp – 125W). For the amaranth dye, the photoelectrochemical method has shown itself to be more efficient than the photochemical one. The photoelectrochemical treatment pointed to a 92% color reduction in the dye solution, and Chemical Oxygen Demand (COD) removal reached up to 57%.

Key-Words: - food dye, photoelectrochemical degradation, azo group

1 Introduction

Advanced oxidation processes (AOPs) which involve in situ generation of highly potent chemical oxidants, such as the hydroxyl radical (•OH), have emerged as an important class of technologies for accelerating the oxidation (and hence contaminant removal) of a wide range of organic contaminants in polluted water and air [1].

In general, the methods of advanced oxidation[2] include application of the following agents: ozone, hydrogen peroxide, UV radiation [3], ozone and UV radiation together [4], hydrogen peroxide and UV radiation [5], Fenton [6] reagent and hydrogen peroxide, and photocatalysis on titanium dioxide. All the methods listed above were used in the investigation of the oxidation, and some of them were applied in the treatment of various kinds of wastewater [7].

Although the removal and eventual mineralization of organic contaminants through advanced oxidation processes can be complex, and involves a number of elementary chemical steps, the overall kinetics or rate of removal of a specific component, can often be described phenomenologically by simple rate expressions that are either zero-order or first-order in the organic contaminant [1].

Over the last decades, the increasing industry demand for dyes has shown a high pollutant potential, specially the use of azo dyes [8], for example, tartrazine [9], amaranth [10] and others. Decolouration is one of the basic indicators that describe the quality of water [11].

Photolysis (UV irradiation) is an alternative method for the degradation azo dyes [12, 13].

Photodegradation of amaranth has been reported in the literature [12, 13, 14]. The degradation has been investigated using UV radiation in the presence of TiO_2. The results show the efficiently degradation through photocatalytic treatment.

The aim of this work was to verify the possibility of use of the photochemical and photoelectrochemical techniques to degradate amaranth dye (FD&C Red No. 2) [15] and compared the degradation efficiency. In some countries this food dye is not permitted, for example in Russian [12]. On the other hand, the dye is still allowed in other countries, including Brazil [16]. The photoelectrochemical degradation of dye solutions was investigated using DSA (Dimensionally Stable Anodes) [17, 18]. This is a type of anode where oxidation reactions usually will be acting on dye via HO• radicals on the surface, which can lead to better performance in organic and inorganic species degradation [19].

2 Experimental

2.1 Reagents

Red amaranth (95%) dye (C.I. 16185) [20] was acquired from Duas Rodas (Santa Catarina, Brazil) as a commercially available dye formulation and used without further purification. This dye is an azo type dye as represented by the chemical structure in Fig. 1. The concentration aqueous solution was 100 mg L^{-1}. The water employed in all the studies was deionized. The dye solution was studied using

KNO_3 0.1 mol L^{-1} as the support electrolyte.

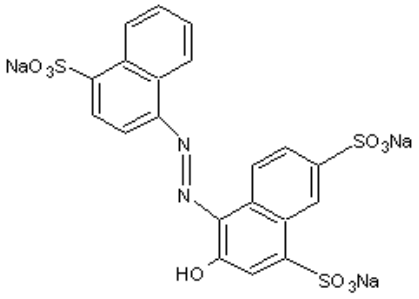

Fig. 1. Amaranth dye chemical structure.

2.2 Photoelectrochemical and photochemical treatments

Experiments were performed in an open batch system [20]. The system consisted of 200 mL quartz cell and the solution was irradiated with an ultraviolet lamp (125 W) [21] during 90 minutes. In photoelectrochemical treatment were used DSA $Ti/Ru_{0,3}Ti_{0,7}O_2$ electrodes (11.2cm^2) and a potentiostat CIDEPE EQ030C. The photoelectrochemical experiments were performed at a current density of 20mA cm^{-2}.

2.3 Mathematical modelling

The mathematical treatment of the experimental data was made using the LAB Fit Curve Fitting software [22]. The tolerance of the non-linear regressions, accomplished by the least square method, was fixed by $1 \cdot 10^{-6}$, and the quality of the fittings was indicated by the determination and the reduced χ^2 coefficients [23].

2.4 Analytical methodology

The analytical analyses in aqueous dye solutions were realized before and after the photochemical and photoelectrochemical treatments.

The UV/Vis spectrophotometer used for the determination of dye disappearance kinetics was a "Perkin Elmer Lambda 25" UV/Vis Spectrometer recording the spectra over the 190-900 nm.

Chemical Oxygen Demand (COD) was made using a method described in Standard Methods [24].

The Chromatographic experiments were performed using an Agilent Technologies 1200 Series Quaternary LC System and Diode-Array Detector (DAD). The mobile phase used was a mixture of water and methanol in the volumetric proportion of 70:30 [25]. The flow rate used was 0.5 mL min^{-1} and detection was monitored at λ = 525 nm and λ = 260 nm [26, 27]. The analytical column [9] was Zorbax Eclipse XDB-C18 4.6 mm diameter and 150 mm length, 5μm.

3 Results and Discussion

The efficiency of photoelectrochemical and photochemical degradation of amaranth dye was first investigated using UV-Vis spectra and monitored the disappearance of this compound. Amaranth dye absorved in the visible region (λ = 525nm) [25]. Fig. 2 and 3 show the absorbance spectra (scan) during photoelectrochemical and photochemical treatments, respectively.

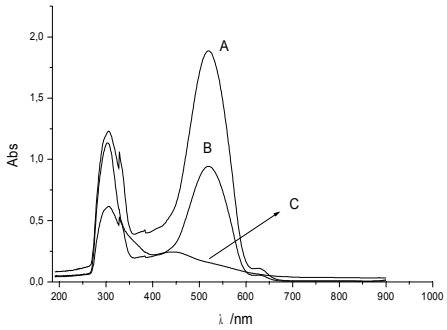

Fig. 2. UV-Vis absorption spectra of 100mg L^{-1} amaranth before (A) and after photoelectrochemical treatment time 45 min (B) and time 90 min (C).

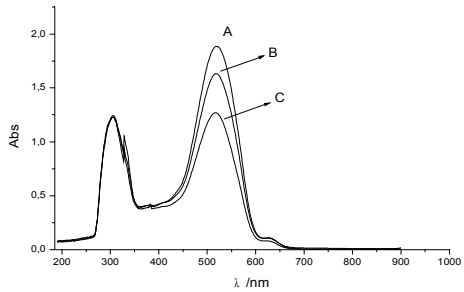

Fig. 3. UV-Vis absorption spectra of 100mg L^{-1} amaranth before (A) and after photochemical treatment time 45 min (B) and time 90 min (C).

In these treatments (photochemical and photoelectrochemical) times, the disappearance of long wavelength absorbing chromophores in the dye structure was around 34% and 92%, respectively. Fig. 4 shows the absorbance (Abs_t/Abs_o) during the degradation period, in both treatments, photochemical and photoelectrochemical degradation.

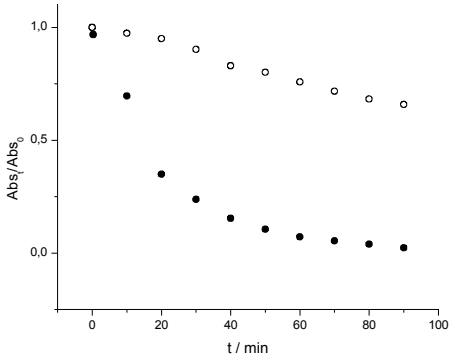

Fig. 4. Amaranth absorbance reduction as a function of photochemical (○) and photoeletrochemical (●) treatment time (λ = 525nm).

For the photoelectrochemical degradation, the best mathematical modelling indicated by the LAB Fit software was the exponential model $y(t) = 1.01538 \cdot 0.954557^{t}$, where y indicated Abs_t/Abs_0, with coefficients R^2= 0.99263 and reduced χ^2=0.000885426. This comportment indicates a first order reaction.

When a $\ln\left(\frac{[A]_t}{[A]_0}\right)$ is plotted against t, then a first-order reaction will give a straight line [28, 29] ($[A]_t = [A]_0 \cdot e^{-kt} = a \cdot b^{t}$), the value of k may be obtained from the slope (the slope is – k).

Let now a=1.01538, b=0.954557 and $[A]_0 = 1$. In particular, for t=1, an easy calculation gives $k = -\ln\left(\frac{a \cdot b}{[A]_0}\right) = -0.031245$. The Fig. 5 shows $y(t) = \ln\left(\frac{Abs_t}{Abs_0}\right)$ for the photoelectrochemical treatment.

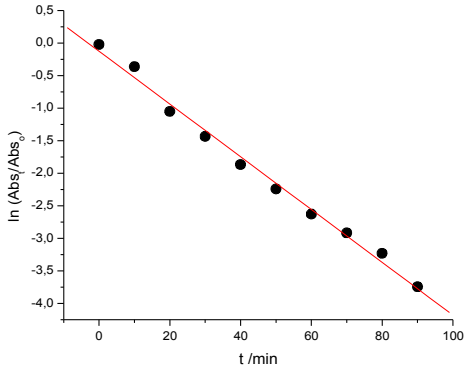

Fig. 5. Kinetics of amaranth dye disappearance during photochemical(○) and photoelectrochemical (●) degradation process.

The photoelectrochemical degradation exhibit first order decay, with a linear dependence of $\ln\left(\frac{Abs_t}{Abs_0}\right)$ on time, given by $y(t) = -0.04065 \cdot t - 0.1182$; therefore, the observed first order rate. This result is in according to literature [30]. The constant k was 0.04065 min^{-1} for this treatment. However, others authors [14] explain the amaranth dye degradation and in this case the k was around 0.006 min^{-1}, approximately one order greater.

On the other side, the best mathematical model for the photochemical degradation of Fig. 4 was the linear one, given by $y(t) = -0.0040834 \cdot t + 1.01145$, with R= -0.9946991 and reduced χ^2=0.000183776. Therefore, the photochemical degradation indicates a zero-order reaction [31, 32], where $\frac{d[A]}{dt} = k$. This can also occur in a photochemical reaction if the rate is determined by the light intensity; in this case k may be proportional to the light intensity [29].

The figure-of-merit [1] *Electric Energy per Order* (E_{EO}) is best used for situations where the mechanism involves first-order reaction. For the photoelectrochemical treatment the E_{EO} was 854.99 $kWh.m^{-3}$. The Electric Energy per Mass (E_{EM}) is most useful when were zero order reactions. For the photochemical treatment the E_{EM} was 14204.54 $kWh.kg^{-1}$. These results demonstrate the photoelectrochemical efficiency.

In Chemical Oxygen Demand (COD) measurements, occur a percentage reduction, 47% and 57% for the photochemical and photoelectrochemical treatments, respectively. These results indicate a organic material degradation beyond the colour decrease of amaranth dye solution.

The Fig. 6 shows the chromatographic amaranth dye behaviour before and after photochemical and photoelectrochemical treatments at 260 nm, and the Fig. 7 before and after degradation treatments at 525 nm.

In regions near 260 nm, a peak decrease after the photochemical and photoelectrochemical treatment (Fig. 6). This may indicate the presence of aromatic amines [33, 34, 35] in according with the COD results (47% - 57%), showing a not complete degradation (mineralization) of organic material.

The Fig. 7 shows a peak decrease in 2.87 minutes (retention time) at 525 nm [36, 37]. The concentrations were 100 mg L^{-1} (before treatment), 49.23 mg L^{-1} (after photochemical treatment) and 19.81 mg L^{-1} (after photoelectrochemical treatment). The photoelectrochemical treatment was more efficient, in according with the absorbance and COD results.

These results suggest that the chromophore degradation step followed the same mechanism in both treatments (photochemical and photoelectrochemical), probably involving –N=N– group reduction.

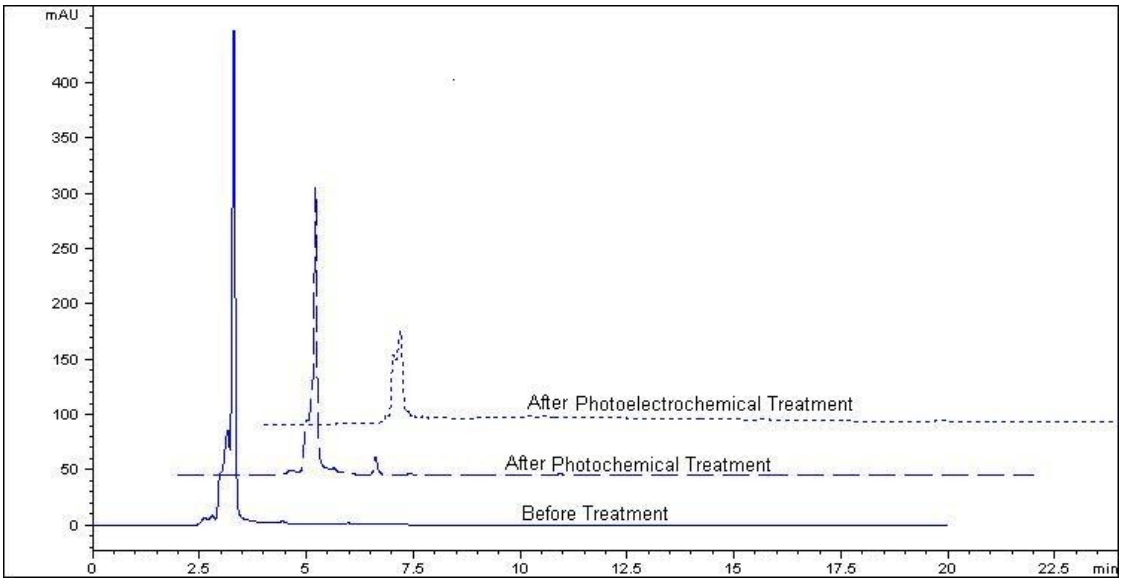

Fig. 6. Chromatogram of the separation in a C18 column of amaranth. The chromatographic conditions are given in the text. λ = 260 nm.

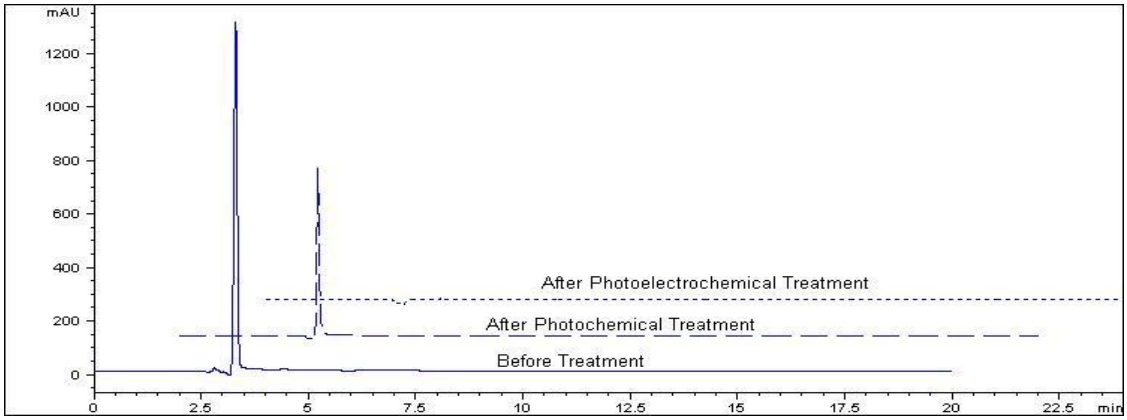

Fig. 7. Chromatogram of the separation in a C18 column of amaranth. The chromatographic conditions are given in the text. λ = 525 nm.

4 Conclusion

The results presented here show that for the amaranth dye, the photoelectrochemical method was considered more efficient than the photochemical one. The photochemical treatment showed a 92% color reduction in the dye solution, and Chemical Oxygen Demand (COD) removal reached 57%.

These results suggest that photoelectrochemical process may be envisaged as a method for treatment of colored waste waters for decolorization and degradation, in particular food industries.

5 Acknowledgments

The authors would like to acknowledge financial support from FAPERGS.

References:

[1] J. R. Bolton, K.G. Bircher, W. Tumas, C.A. Tolman, Figures-of-merit for the technical development and application of advanced oxidation technologies for both electric- and solar-driven systems, *Pure and Applied Chemistry*, Vol. 73, No. 4, 2001, pp. 627-637.

[2] J. Perkowski, S. Ledakowicz, Decomposition of Antraquinone dye in the aqueous solution during advanced oxidation processes, *Fibres & Textiles in Eastern Europe*, Vol. 10, 2002, pp. 68-72.

[3] R. Bertazzoli, R. Pelegrini, Photoelectrochemical discoloration and degradation

of organic pollutants in aqueous solutions, *Química Nova*, Vol. 25, No3., 2002, pp. 477-482.
[4] M. Dilmeghani, K.O. Zahir, Kinetics and mechanism of chlorobenzene degradation in aqueous samples using advanced oxidation processes, *Journal of Environmental Quality,* Vol. 30*,* 2001, pp. 2062-2070.
[5] F. V. F. Araújo, L. Yokoyama, Color removal in reactive dye solutions by UV/H_2O_2 Oxidation, *Química Nova*, Vol. 29, No. 1, 2006, pp. 11-14.
[6] A. CK. Yip, F. LY. Lam, X. Hu, A novel heterogeneous acid-activated clay supported copper catalyst for the photobleaching and degradation of textile organic pollutant using photo-Fenton-like re-action, Chemical Communications, Vol. 25, 2005, pp. 3218-3220.
[7] L.S. Andrade, E.A. Laurindo, R.V. Oliveira, R.C. Rocha-Filho, Q.B. Cass, Development of a HPLC method to follow the degradation of phenol by electrochemical or photoelectrochemical treatment, *Journal of the Brazilian Chemical Society*, Vol. 17, No. 2, 2006, pp. 369-373.
[8] W.S. Pereira, R.S. Freire, Azo dye degradation by recycled waste zero-valent iron powder, *Journal of the Brazilian Chemical Society*, Vol. 17, No. 5, 2006, pp. 832-838.
[9] E.C. Vidotti, M.C.E. Rollemberg, Derivative spectrophotometry: A simple strategy for simultaneous determination of food dyes, *Química Nova*, Vol. 29, No. 2, 2006, pp. 230-233.
[10] A. Keck, J. Klein, M. Kudlich, A. Stolz, H-J. Knackmuss, R. Mattes, Reduction of azo dyes by redox mediators originating in the naphthalenesulfonic acid degradation pathway of *Sphingonomas sp.* Strain BN6, *Applied and Environmental Microbiology*, Vol. 63, No. 9, 1997, pp. 3684-3690.
[11] J. Perkowski, L. Kos, Decolouration of model dyehouse wastewater with advanced oxidation processes, *Fibres & Textiles in Eastern Europe*,Vol. 11, No.3, 2003, pp. 67-71.
[12] M. Karkmaz, E. Puzenat, C. Guillard, J.M. Herrmann, Photocatalytic degradation of the alimentary azo dye amaranth mineralization of the azo group to nitrogen, *Applied Catalysis B: Environmental*, Vol. 51, 2004, pp. 183-194.
[13] C-H. Wu, Comparison of azo dye degradation efficiency using UV/single semicondutor and UV/coupled semicondutor systems, *Chemosphere*, Vol. 57, 2004, pp. 601-608.
[14] M. Abu Tariq, M. Faisal, M. Munner, Semiconductor-mediated photocatalysed degradation of two selected azo dye derivatives, amaranth and bismark brown in aqueous suspension, Journal of Hazardous Materials, Vol. 58, No. 1, 2005, pp. 172-179.
[15] http://www.fda.gov/default.htm, accessed in September 2007.
[16] http://www.anvisa.gov.br, accessed in September 2007.
[17]B. Wang, W. Kong, H. Ma, Electrochemical treatment of paper mill wastewater using three-dimensional electrodes with Ti/Co/SnO2-Sb2O5 anode, *Journal of Hazardous Materials*, Vol. 146, 2007, pp. 295-301.
[18] G.R.P. Malpass, A.J. Motheo, Cyclic Voltammetric behaviour of Dimensionally Stable Anodes in the presence of C1-C3 Aldehydes, *ournal of the Brazilian Chemical Society*, Vol. 14, No. 4, 2003, pp. 645-650.
[19]P.A. Carneiro, Fugivara, C.S., R.F.P. Nogueira, N. Boralle, M.V.B. Zanoni, A comparative study on chemical and electrochemical degradation of reactive blue 4 dye, *Portugaliae Electrochimica Acta*, Vol. 21, 2003, pp. 49-67.
[20] C.P. Silva, S. Marmitt, C. Haetinger, S. Stülp, Assessment of red dye degradation through photochemical process, *Engenharia Sanitária e Ambiental*, Vol. 13, No. 1, 2008, pp. 222-226.
[21] S. Stülp, C. P. Silva, S. Marmitt, The use of electrochemical techniques in the treatment of food industry effluents: a tool for the environmental management systems, *Estudo & Debate*, Vol. 12, No. 2, 2005, pp. 109-123.
[22] http://www.labfit.net, accessed in September 2007.
[23] P.R. Bevington, D.K. Robinson, Data reduction and error analysis for the physical sciences. Boston: WCB/McGraw-Hill, second edition, 328p, 1992.
[24] APHA. American Public Health Association. Standard Methods for the Examination of Water and Wastewater. 21st Ed., USA, Ed. American Public Health Association, 2005.
[25] M.A. Prado, H.T. Godoy, Contents of synthetic in foods determined by high performance liquid chromatography, *Química Nova,* Vol. 30, No. 2, 2007, pp. 268-273.
[26] J. M. Cleaves, S L. Miller, Oceanic protection of prebiotic organic compounds from UV radiation, *Proceedings of the National Academy of Sciences of the United States of America*, Vol. 95, 1998, pp. 7260-7263.
[27] J. B. Souza, L. A. Daniel, Comparison between sodium hipoclorite and peracetic acid for *E. coli*, coliphagis and *C. perfringes* inactivation of high organic matter concentration water, *Engenharia Sanitária e Ambiental,* Vol. 10, No. 2, 2005, pp. 111-117.
[28] P.W. Atkins, *Physical Chemistry*, Oxford, 3rd edn, 1988.
[29] R.J. Silbey, R.A. Alberty, *Physical Chemistry*, New York, Third Edition, 2001.
[30] E. Puzenat, H. Lachheb, M. Karkmaz, A. Houas, C. Guillard, J.M. Herrmann, Fate of nitrogen atoms in the photocatalytic degradation of industrial (congo red) and alimentary (amaranth) azo dyes. Evidence for mineralization into gaseous

dinitrogen, *International Journal of Photoenergy*, Vol. 5, 2003, pp. 51-58.
[31] N. Genç, Photocatalytic oxidation of a reactive azo dye and evaluation of the biodegradability of photocatalytically treated and untreated dye, *Water SA*, Vol. 30, No. 3, 2004, pp. 399-405.
[32] M.M. Tauber, G.M. Guebitz, A. Rehorek, Degradation of azo dyes by laccase and ultrasound treatment, *Applied Environmental Microbiology*, Vol. 71, No. 5, 2005, pp. 2600-2607.
[33] J.-W. Wegener, H. Schulz, Characterization of leather candidate certified reference materials for their mass fractions of aromatic amines, Accred Qual Assur, Vol. 12, 2007, pp. 12-20.
[34] P.P. Vijaya, S. Sandhya, Decolorization and Complete Degradation of Methyl Red by a Mixed Culture, *The Environmentalist*, Vol. 23, 2003, pp. 145–149.
[35]S.-A. Ong, E. Toorisaka, M. Hirata, T. Hano, Treatment of methylene blue-containing wastewater using microorganisms supported on granular activated carbon under packed column operation *Environmental Chemistry Letters*, Vol. 5, 2007, pp. 95-99.
[36] J. Kirschbaum, C. Krause, H. Brückner, Liquid chromatographic quantification of synthetic colorants in fish roe and caviar, *European Food Research Technology*, Vol. 22, 2005, pp. 572-579.
[37] M.A. Prado, H.T. Godoy, Determination of synthetic dyes by high performance liquid chromatography (HPLC) in jelly powder, *Química Nova*, Vol. 27, No. 1, 2004, pp. 22-26.

Waste management towards zero emissions approach in the fruit juice processing industry

Uyen Nguyen Ngoc and Hans Schnitzer

Institute for Process Engineering (IPE)
Graz University of Technology
Inffeldgasse 21a, A8010, Graz, AUSTRIA
uyennn@sbox.tugraz.at , hans.schnitzer@tugraz.at

Abstract

On the one hand we reuse and recycle more waste from the manufacturing and processing industry than before, but on the other hand we also create more waste. In the recent years since the amount of waste generated is increasing, the demand of energy is pressed, and availability of resources is limited, the use of whole crop residues has become a main field of interest. Waste can be a resource if it is put in the right place.

The fruit juice processing industry is an important part in a linked group of the food processing industry. Its contribution can be a significant point for the economic development of a country and also serves for our quality of life. However, it is unfortunately a processing industry which also generates high amounts of organic waste. That high amount of waste can be a serious concern in case of unsanitary conditions of waste, more especially it will be serious if waste is simply left at the open-site landfills.

From waste prevention towards a zero emissions system approach is an expectation since the twenties. The fruit juice is an example where the concept of zero emissions approach can actually be applied successfully with today's possibilities. An outline of the concept of zero emissions systems approach related to waste management regarding the aim of sustainability will be started in the paper. Further on, an agro-based zero emissions system (AIZES) model will also be displayed by a deep-dive case study of the mango juice processing industry – reaching from the analysis on material balances, energy balances to wastewater treatment system or the use of waste for the other process, etc. The model can be shown as a clustering of an industry eco-system which permits an identification of opportunities for reducing environmental impacts at process level. The utilization of renewable energy and economic points are in consideration to adapt to environmental issues and the aim of eco-efficiency. Also, the opportunities of waste management under a zero emissions approach in the fruit juice processing industry will be discussed.

Keywords: Zero emissions system, fruit juice processing, energy, and biogas.

1. Introduction

Mango is a fruit which has many varieties and is grown in many places all over the world *[1]*. Mango processing is a traditional activity, production began to produce juice from the mango without intending to satisfy the demands of the international fresh fruit market. These processes can be done in a factory after mango is harvested at the plantation. In an operation of the mango processing industry, only 50% of the mango becomes juice and the rest is seed, skin, or fruit pulp which is removed during the process *[2]*. This kind of waste is not only a problem for tropical production, but also an issue of waste management for the society. The waste decomposes rapidly, and gives rise to the hatching of many fly larvae. Because of this it has to be quickly removed from the production areas to be buried. The expense connected to the problem of hygiene and odor of the fruit waste could possibly be turned into an advantage by transforming fruit waste to renewable energy through anaerobic digestion and the remains into fertilizer and irrigation in agriculture.

The idea of zero emissions agro-based industrial systems also provides the phenomenon of the industrial metabolism in a closed loop of recycling of materials. By this way, a perfectly integrated process management produces no waste, for example solid waste and wastewater, because waste can be fully matched with the input requirements of the other processes in total production. More especially, the generation of gaseous carriers can be an efficient factor as the mango is harvested only during a

couple of months per year but mango juice production processes can be operated all year around.

2. Zero emissions systems concepts

As a rule of nature the natural cycles function without producing waste. The sun provides the energy for the system, which drives the photosynthesis processes that order atoms and molecules to higher value such as forest and food products. Dead matter is processed by microbes in the soil to become food for the next cycle. A popular expression of this concept is that 'Waste = Food' [3]. The comprehensive nature of zero emissions systems is shown in the following diagram of Figure 2.1.

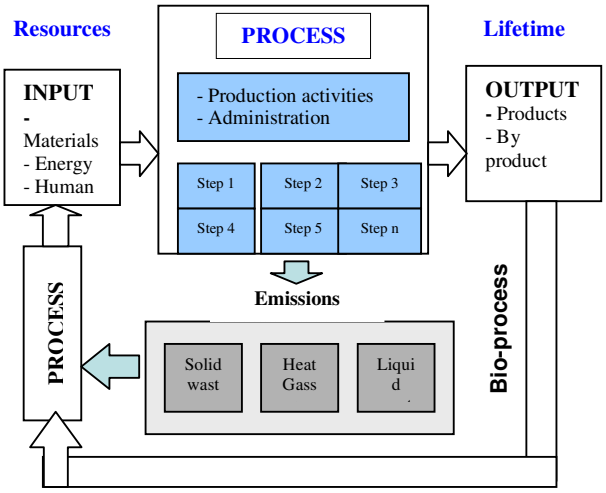

Figure 2.1 Flow-diagram considered for zero emissions systems approach.

From a systems viewpoint, any processing production has waste, but the concept of zero emissions systems approach is employed when returning these residual products as inputs to further processes in industrial closed loop systems. This may involve redesigning both products and processes in order to eliminate hazardous properties that make them unusable and unmanageable in quantities that overburden both industry and the environment. So, a foundation of zero emissions systems is provided by the concept of the industrial metabolism, which stands for the whole integrated collection of physical processes that convert raw materials and energy, plus labor, into finished products and wastes in a steady state condition. Because of this, zero emissions systems represents the conversion and use of process outputs as inputs for other processes and therefore an increase in eco-efficiency and elimination of waste as well. Zero emissions strategies can also consider the entire life-cycle of products, processes and systems in the context of a comprehensive system of interactions with nature and search for inefficiencies at all stages. It also offers a chance that waste can be prevented through designs based on the full life cycle of the product. Instead waste should, like any residues of processes, be thought of as potential inputs for starting new processes. The opportunities for reduced costs and reduced negative environmental impacts will be possible. Also, a zero emissions system strategy leads to look for inefficiencies in the use of materials, energy and human resources to achieve a sustainable future, extreme efficiency in the use of all resources, and in order to meet the needs of human.

3. The fruit juice processing industry and applying model of a zero emissions agro-based industrial system (AIZES)

3.1. Mango juice processing industry

Mango is a fruit crop grown in many different countries. It is available only during 4-5months, and has a short post-harvest shelf life because of its highly perishable nature [4]. Because of its popularization, mango juice processing industry can be found in many places all over the world. Mango juice production is basically divided into four stages, including preliminary, primary, secondary, and final stage. All process is shows in Figure 3.1.

Preliminary stage - Raw material preparation: Mango is harvested during 4-5months. After harvesting, it is transported to the factory for production. Here mango is load for weighing, washing, and shaping peel. Then, it is washed again.

Primary stage: the operation in this stage is coring, extraction, heating and processing. Extraction is an important step in juice making. It can be done in ways of blending, milling, hammering, pressing, centrifugation, or soaking in water. Heating is involved after the extraction step. The fruit is heated to inactivate the pectic enzymes. Then, juice is transferred into a syrup tank for the processing step. The juice is mixed with sugar, gelatin, acid citric, pectic enzymes, and vitamin C in a syrup tank for couple of hours to obtain the best quality of mango juice.

Secondary stage: After the syrup tank, juice is processed again at the temperature of 60-65^{o}C. Blending is one of the key steps for the quality of juice. In this operation, juice must flow through sieves. Filling and bottling are the following two steps at this stage. Then, the mango juice bottles are transferred to the seamier step.

The final stage: this stage provides for sterilization, cooling, labeling, packing, and storing. The temperature to pasteurize is 87°C-92°C. The packing material varies with the process. In conventional canning, metal or glass containers are usually used.

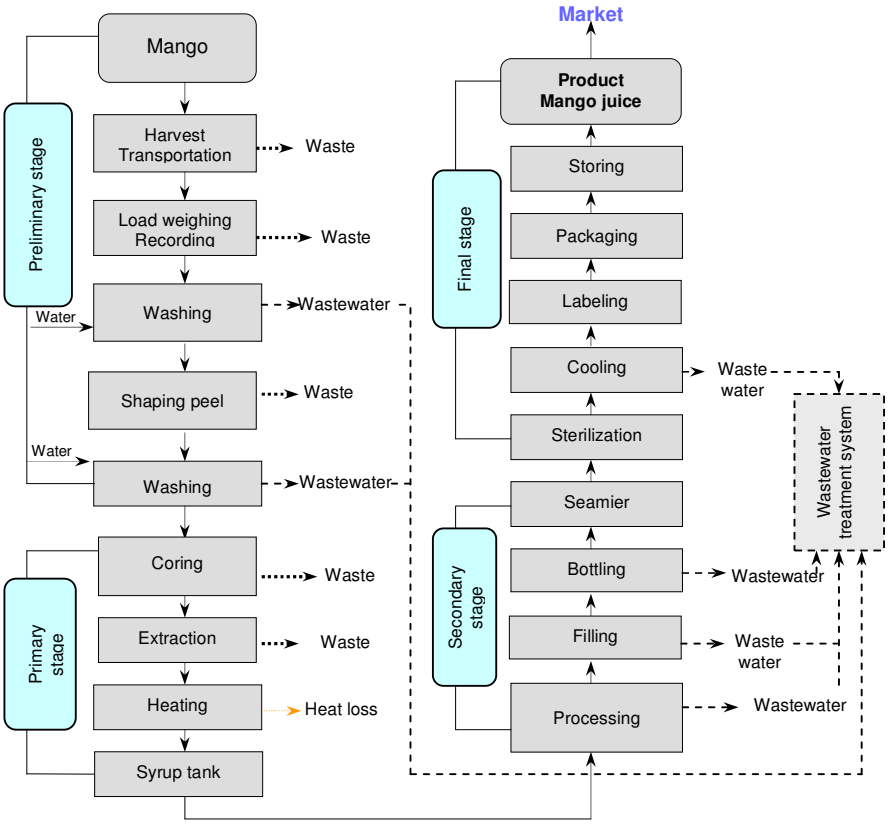

Figure 3.1. Flow diagram considered for mango juice processing industry.

3.2. A zero emissions agro-based industrial system model

3.2.1. Method of AIZES

A methodology towards a model of a zero emissions agro-based industrial system is established including three basic steps. It starts with analyzing the material and energy flows that run through the agro-based industrial systems and partly end up in wastes (solid and liquid) and energy, followed by analyzing various possibilities and modification to prevent the generation of wastes in the second step. The third step concentrates on identifying, analyzing and designing potential offsite recovery and reuse options. Also it entails the modifications of remaining wastes in this step to treat them. This Methodology follows a reasonable method toward zero emissions approach.

3.2.2. Input - output analysis of AIZES model

The AIZES model is introduced on a case study of mango juice production at a food and vegetable company (COFIDEC) in Thoi An in Vietnam. The production capacity in the factory is 30 - 40ton/day depending on the season of the year. A chain route of the production originates continuously from raw material, primary, secondary to final product processors for the consumer market. Production activities require input materials for the process, including mango, white sugar, water, chemicals (acid citric, pectic enzymes, and vitamin C) and energy (electricity, oil, and heat). The AIZES model starts from the analysis of the amount of Mango residues generated during the production. The material flow model is simulated in Figure 3.2. In the model, water is supplied partly for production from the located well. Wastewater which is discharged from the process is treated in the model in a wastewater treatment plant. Water, after treatment, meets the standard for discharge of industrial wastewater backer -used for irrigation in agriculture. Electricity powers all stages of processing. Organic waste which is collected every day and thrown into landfill is used as an input material for a digester in anaerobic digestion. The

product of the digestion is fertilizer; it could be used as plant fertilizer. Biogas, which is also the product of fermentation, can be used directly as an Energy source for lighting and boiler demand in the factory. The fertilizer as digestive from fermentation may find an attractive market for using it in agriculture.

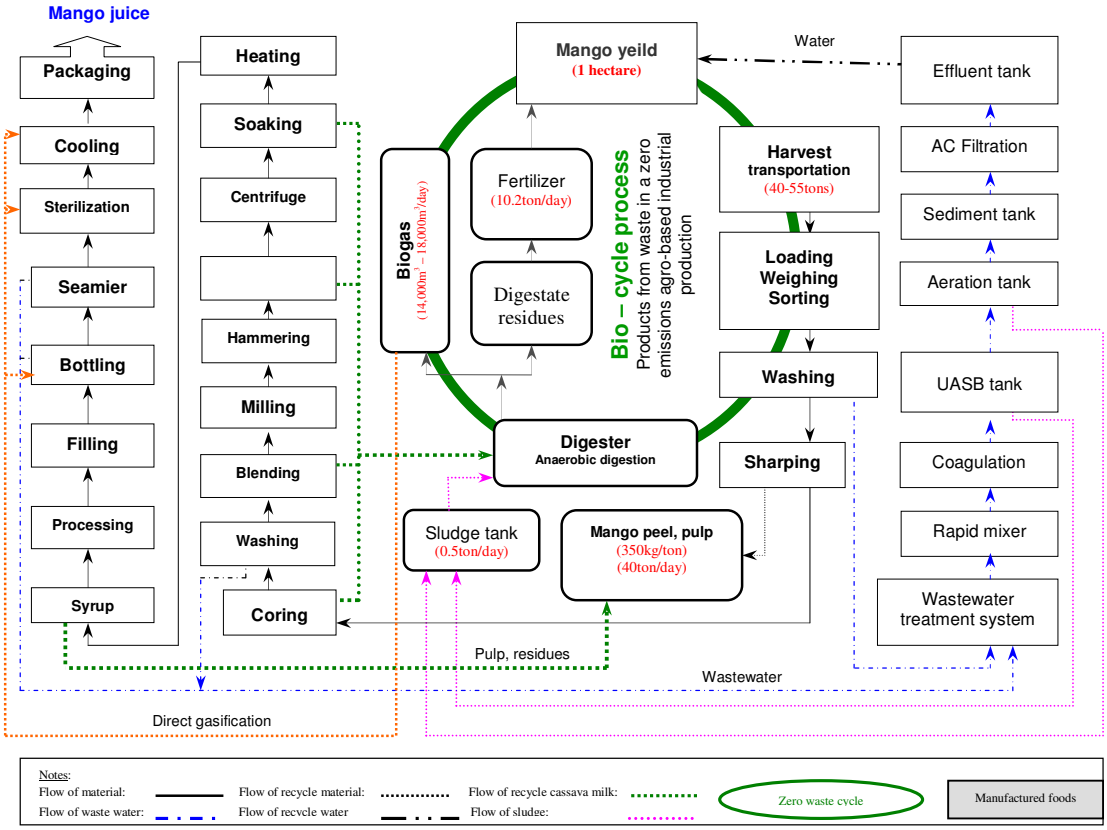

Figure 3.2 AIZES model on mango juice processing industry.

Inputs: The amount of input materials for a mango juice processing plant depends partly on the capacity of the production processes, for example the equivalent kind of small-scale, medium-scale or large-scale enterprises. However, inputs consist of crop, white sugar, energy, water, and chemicals.

Non-waste: In our AIZES model, mango waste (peel) generated from the production is collected, gathered and put into a digester for anaerobic fermentation. Digester is obtained from mango waste, livestock manure, sludge from wastewater treatment plant, and organic waste from the factory. In the case of the plant considered here there was approximately 350kg of waste generated when 1ton of fresh mango to process. The products of anaerobic digestion are biogas used as renewable energy and fertilizer for agriculture.

Water and Non-wastewater: to process 1 ton of mango juice, water consumption demand is approximately 20 - 25m^3. It is used for all processes, mainly supplied from the local well, pumped of at 350 - 400m^3/day. Wastewater is discharged as much as 400m^3/day. In the model it is to be collected, and then piped directly to the wastewater treatment system. A part of the wastewater after treatment is used to mix the substrates in the digester for biogas production. The wastewater treatment system applies a combination of physical, biological and chemical treatment methods, to remove suspended solids, organic matters, and bacteria population. Treated water meets to industrial standard B of discharged water and is used back as water for irrigation system or is satisfied for pouring plant.

Energy demand: energy for cassava production processes consists of electricity 136KWh/ton mango, and oil (FO, DO) of 20 liter/ton.

Outputs: *Fertilizer and biogas*: output of the mango production is mango juice and emissions (waste, gas, and wastewater). The compositions of solid waste consist of waste from the mango juice production (14ton/day) and from other productions in the

factory (20ton/day). The system in AIZES model outperforms its design goals by a significant margin, for instance all waste from the production is used as input substrates. Also the use of treated wastewater as supply water for mixing substrates (waste, manure) is a significant advantage. Biogas conversion was efficient throughout our experiments regarding mango substrate (methane concentration of biogas of 70 - 80.5% was generating more than anticipated) [5]. If it is possible, inside the factory gas is combusted. Such reduction in energy cost is a further advantage of AIZES. Furthermore the sludge from the fermentation can be used as plant fertilizer.

3.3.3. Materials and energy balances

Material balances are fundamental to control production processes, particularly in the control of product yields. The calculation of material balances is based on material, waste, wastewater and energy in the process. Material balance in this case study is formulated as the law of conservation of mass. The basic formula is:

$Mass_{in} = Mass_{out} + Mass_{stored} + Mass_{lost}$

Raw materials = products + wastes + stored materials + losses

$\Sigma m_R = \Sigma m_p + \Sigma m_w + \Sigma m_s + \Sigma m_L$

$\Sigma m_P = m_{P1} + m_{P2} + m_{P3} + \ldots + m_{Pn}$: Total products

$\Sigma m_w = m_{w1} + m_{w2} + m_{w3} + \ldots + m_{wn}$: Total wastes

$\Sigma m_s = m_{s1} + m_{s2} + m_{s3} + \ldots + m_{sn}$: Total stored products

$\Sigma m_P = m_{L1} + m_{L2} + m_{L3} + \ldots + m_{Ln}$: Total losses are unidentified materials

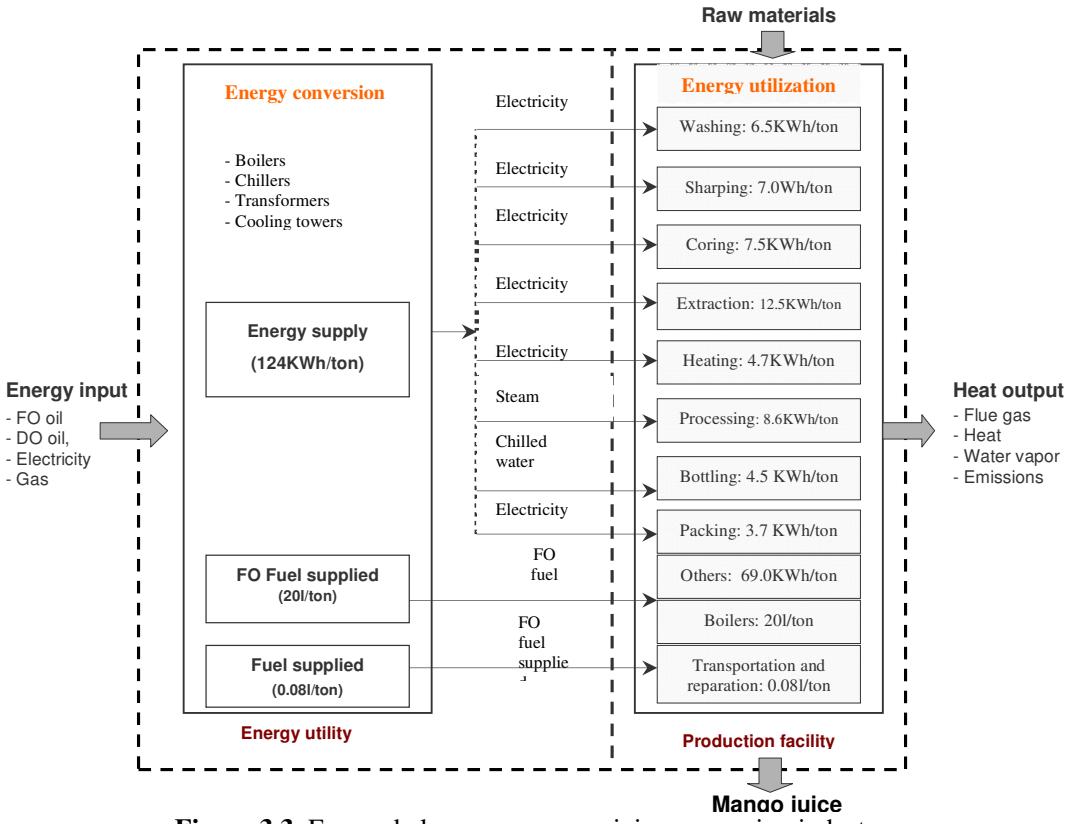

Figure 3.3. Energy balances on mango juice processing industry.

Material balances: The balances for the AIZES model are calculated for *mass-in* and *mass-out* in the mango production processes, simulated in Fig. 3.3.

Mass in

Mango = Σm_R = 40ton/day.

Loading waste for digester = $\Sigma m_R = m_{mango} + m_{organic}$ = 35% x 40 + 20 = 34ton/day

Lemon waste = Σm_R = 2ton/day

Acid citric = Σm_R = 2ton/year

Water = $\Sigma m_{Water} = m_{washing1} + m_{washing2} + m_{washingbottles} + m_{cooling} + m_{others} = 400m^3$/day

Mass out

Mango waste = $\Sigma m_{w\ peel} + m_{wextraction} + m_{others}$ = 34ton/day

Water for digester = $\Sigma m_{mixing} = 100m^3$/day

Wastewater = $\Sigma m_{Water} = m_{washing1} + m_{washingbottles} + m_{cooling} + m_{others} = 400m^3$/day

Organic waste = $\Sigma m_{organic\ waste}$ = 34ton/day

Fertilizer mass=30%x$m_{loading}$=0.30x34 = 10.2ton/day

Energy balances: Energy balances are normally not simple because they can be inter-converted, for

instance mechanical energy to heat energy, but overall the quantities must be balanced. As mass is conversed, energy coming into a unit should be balanced by energy coming out and energy stored.

$Energy_{in} = Energy_{stroed} + Energy_{out}$

$Energy_{stored} = \Sigma E_E + \Sigma E_S$

$Energy_{out} = \Sigma E_L + \Sigma E_P$

In which: ΣE_e: Total energy entering the process

ΣE_S: Total energy stored

ΣE_P Total energy leaving with the products

ΣE_L: Total energy lost to surroundings.

Then: $\Sigma E_{In} = \Sigma E_e + \Sigma E_L + \Sigma E_s + \Sigma E_P$

Total energy entering for the process

$\Sigma E_e = E_{washing} + E_{sharping} + E_{coring} + E_{extraction} + E_{heating} + E_{processing} = 55.0$KWh/ton

Total energy leavings with products

$\Sigma E_P = E_{P1} + E_{P2} + E_{P3} \ldots + E_{Pn} = E_{P1} + E_{Plighting} + E_{Pother\ act} =$ 0.84 KWh/ton

Total energy lost to surrounds

$\Sigma E_L = E_{L1} + E_{L2} + E_{L3} + E_{Ln} = E_{Lboilers} + E_{Lprocess} = E_{Lprocess} =$ 10%x42.5 = 4.25KWh/ton

Total energy to process each ton product:

$\Sigma E_{In} = \Sigma E_e + \Sigma E_L + \Sigma E_s + \Sigma E_P + \Sigma E_{other} =$ 124KWh/ton.

3.3.4. Wastewater treatment system

The mango juice processing industry generates substantial amount of wastewater that is characterized by a high organic content, high strength chemical oxygen demand (13,500mg/l), biochemical oxygen demand (19,000mg/l), total suspended (4,400mg/l), temperature of 30-45^{o}C.

A physical treatment method is applied firstly in the mango wastewater system to remove coarse by letting the wastewater flow through bar rack. Then the wastewater flows into an equalization tank to control for hydraulic velocity, or flow rate. Wastewater is then pumped into the mixing tank and coagulation tank to increase the removal of solids because with the addition of specific chemicals, solids become heavier than water gravity and will settle down. The aeration tank can be considered as a biological phase in the system to remove up to 90% of organic matter in the wastewater. Sedimentation tank is also called settling tank, a vessel in which solids settle out of water by gravity through pulling particles to the bottom of the tank. It is installed after aeration tank. Effluent from sedimentation tank is pumped into an activated carbon tower to pure contaminant concentration through a bed of activated carbon. Effluent will thereby be disinfected from many types of human enteric organisms.

3.3.5. Anaerobic digestion – biogas production

A primary method introduced in our AIZES model is anaerobic digestion. In the digestion progress, organic matter is digested in the absence of air to produce biogas (methane, carbon dioxide, and trace compounds). The digester consists of a mixing tank, sludge tank, an engine generator set and liquid storage. The digester is an in-ground concrete tank and coated by epoxy. When gas production has ceased, the digester is emptied and refilled with a new batch. Retention time of fermentation is within 28 - 32 days. Digester is sealed from the inside to prevent biogas leakage and insulated to maintain temperature. The calculation on biogas yield in our case study of mango wastes was 14,000m^3-18,000m^3/day. The separated liquids will flow to the storage by gravity, where a liquid is centrifuged, and then the liquid is used as a fertilizer.

3.3.6. Economic calculation

The decision to implement a system like ours is for a production company dependent on economic considerations, which includes both amount of investment necessary and operation costs. However, from an environmental aspect, those costs must be compared to environmental issues although economic efficiency, monetary flow back, or the possibilities of cost savings are put on the top. Economic calculations are described in table 3.1.

Table 3.1. Cost benefit analysis of AIZES model on mango juice production.

Items	Unit	Unit cost	Total cost
W.W.T.P	€/year	99,640	22,580.0
Digester Star-up	€/year		14,720.5
Total costs			36,350.5
Fertilizer	Kg/day	0.04€/kg	12,240.0
Biogas	kwh/mon	0.01€/kwh	30,720.0
Profit	€/year		42,960.0
Profit per day	€/day		6669.5
Profit per kg	€/ton		6.3

4. The opportunities of waste management towards an approach of zero emissions systems in the fruit juice processing industry

The opportunity for applying zero emissions system on the citrus processing industry is supported by its benefits. Gains from implementing AIZES will be:

(*i) Saving money*, since waste is a sign of inefficiency, the reduction of waste usually reduces costs. The criteria also include reductions in solid and hazardous waste, emissions, energy consumption, and increased recycling.

(ii) Faster progress. It can be recognized that a zero emissions systems concept improves upon cleaner production and pollution prevention

concepts by providing a visionary endpoint that leads us to take larger, more innovative steps. Because of the final goal, zero emissions system strategies lead to breakthrough improvements. This not only results in significant cost savings, greater competitiveness and reduced environmental negative impacts, but also will move more quickly toward the term of 'sustainable development'.

(iii) Supports sustainability. The concepts as well as strategy of zero emissions system support all three of the generally accepted goals of sustainability including the ability of environmental protection, an economic aspect and social aspect of human well being. It means that the model will enable organizations to identify the inefficiencies in production processes thereby to find cost saving solutions to them. Enhances further enhancement is the replacement of fossil energy sources by renewable ones. The Zero emissions approach is proposing to improve materials flow throughout the production processes.

Previously our industrial system was primarily linear, with a 'take-make-waste' process. It means the use of materials being extracted from the earth's crust, transported to manufacturing sites, used to produce products, and then products are transported to users and finally, at the end-of-life, discarded as waste. Not only is this inefficient and costly, but also these products often contain persistent or toxic materials that negatively impact the environment when they are incinerated or disposed of in landfills. In the recent years, forward ways to fulfill the equation 'waste = resource', the term of 'zero emissions' gained popularity. Therefore, the opportunities of waste management towards a zero emissions approach can be applied successfully because of its advantages. For instance, implementation will reduce high amounts of both liquid and solid waste besides the products. It can also use waste from processing enterprises or by-products as input for the fermentation. It can also use livestock manure and sludge to feed the fermentation. Biogas yield produced can burn back for the steam requirements and lighting during the production. Biogas could also be converted to fit the firing system. This promises CO_2-free production and minimization of greenhouse effect gases. Also wastewater which is treated in the wastewater treatment plant can be used to improve fruit yields, mango again for example.

5. Conclusions

We will have to deal with the difficulties in waste management as well as the limits of natural resources if we do not think about the solutions to control waste as well as replacing the utilization of resources from the environment. The vision of zero emissions systems can offer a solution which will be a key to our grandchildren's future such as zero solid waste, zero wastewater, zero hazardous waste, zero toxic emissions, etc. More especially, the use of an endpoint goal of 'zero' can promote not only ideas of material reuse and recycling, but also prevention and redesign along the entire product life cycle. These new designs will strive for reduced materials use, use of recycled materials, renewable energy and more benign materials. Therefore zero emissions systems can be applied throughout production, manufacturing and consumption of goods and services; defining positively the beneficial environmental, social, as well as economic traits. It can also empower waste to gain the status of a resource by establishing a coherent network of process chains. Although it is not easy to change routines in existing situations, the concept of AIZES can find that it is a good connection of the control of input and output approaching 'zero' waste, because the concept proposes on the one hand an industrial closed-loop and on the other hand it reaches towards the final goal of overall sustainability.

References

[1]M.E. Dauth. Food and vegetable processing, Food and agriculture organization of United Nations, Rome, 1995.

[2] B. L. Amla and V. H. Potty. Development of energy-saving technologies for the food processing industry. Food technological research Institute, India, 2001.

[3] W. McDonough and M. Braungart. Cradle to cradle-Remaking the way we make thing,2003.

[4] Jim Neitzel. Mango growing in California. Journal of the California Rare Fruit Growers, 1986, pp 22-30.

[5] Nguyen Ngoc U, Berghold H, SchnitzerH. Utilization of agro-based industrial by products for biogas production in Vietnam, proceedings of (560) Asian Power and Energy Systems, 2007.

[6] Yuichi Moriguchi. Establishing a Sound Material Cycle Society in Asia, National Institute for Environmental Studies, Japan, 2002.

[7] F. W. Popenoe. The Mango in Southern California. Journal of Economic Botany, Vol. 1, pp. 153-200.

[8] A Cleaner Production Handbook for Local Government, Centre for Resource and Environmental Studies Australian National University, 1996.

[9] Gravitis J. Zero techniques and systems – ZETS strength and weakness, Journal of Cleaner production, Vol.15, 2007, pp.1190 – 1197.

[10] Kuehr R. Towards a sustainable society: United Nations University's Zero emissions approach, Journal of Cleaner production, Vol.15, pp.119 –1204.

[11] Mango juice processing. U.S. Dept. of Agriculture. Yearbook, 1907, 1910.

Using an Environmental Information System to present the states of the streamlets for the residents

ZS. KOVÁCS, I. MAGYAR, G. KOHLRUSZ, J. KOVÁCS and Á. RÉDEY
Institute of Environmental Engineering
University of Pannonia
Veszprém, P.O.B. 158, H-8201
HUNGARY
zsofiakovacs@vipmail.hu, http://uni-pannon.hu

Abstract: - In the previous years the environmental consciousness of the society has become stronger also in Hungary. The bottleneck of this process is the lack of public information on environmental data. The Institute of Environmental Engineering, University of Pannonia has undertaken this challenge and developed an online environmental information system. This system is able to receive and process the collected environmental data via Internet. The aim of project to define physical and chemical parameters of surface waters and to support the hydro-geochemical elements of the typology with the analysis of the main ions and to the streams for pollution and apply Water Framework Directive (WFD) for examined water bodies further goal is to display result analysis via internet in Environmental Information System by its authors. In the first phase of mapping surface waters Hungarian streamlets were charted. Streams were categorized according to typology. The field measurement (temperature, pH, conductivity, chlorophyll-a, PAH) and laboratory texts *(COD_t, PO_4^{3-}, NH_4^+, NO_3^-, NO_2^-, SO_4^{2-}, Na^+, Ca^{2+}, Mg^{2+}, K^+, Si^{4+} Cd^{2+}, Co^{2+}, Cr^{3+}, Ni^{2+}, Zn^{2+})* has been taken. Measured results have been compared with MSZ 12749 standards and accordingly streams were classified. Bedrock has taken effect via main ions of the water so this element of the typology has been proved by main ions. In the case of N and P forms only polluted sites were significantly different. On the homepage bar charts show measured values at different sampling sites of the streams. On the Google Map distances between two sampling sites were coloured according to water quality colour scale. The developed homepage contains such a techniques of visualization that makes it easily understandable for everybody.

Key-Words: - surface water, water quality, Water Framework Directive (WFD), Environmental Information system, GIS, visualization

1 INTRODUCTION

The society has been playing more and more significant role in EU's and Hungary's environmental policy considering that environmental consciousness of the people raised increasing demand on environmental information. Therefore it is essential that the residents of small regions may easily access information on the state of their narrower environment and have the possibility to take part in the decision process.

The Institute of Environmental Engineering, University of Pannonia has undertaken this challenge and has developed an online environmental information system. This system is able to receive and process the collected environmental data via Internet. These data on the environmental elements (air, surface water, noise) are then available to the public as a web service displayed by GIS and graphical tools. The system had to meet simplicity and comprehensibility. The database can be efficiently used in areas where displaying spatial information on maps is important.

Aim of the project to define physical and chemical parameters of surface water and to support the hydro-geochemical elements of the typology with the analysis of the main ions and to the streams for pollution and apply Water Framework Directive (WFD) for examined water bodies further goal is to display results via internet in

Environmental Information System developed by its authors. As the load to our surface water become greater, it created increasing demand for adequate quality and quantity waters. A good condition is available with prevention of the quality ruin and provides sustainable water management. The WFD was created as a long-term water policy of the European Union. Member States are required to achieve good ecological and chemical status in all bodies of surface water by 2015 [1]. Not only is the chemical water classification important but also the ecological water classification made by biological indicator groups [phytoplankton, phytobenthos (diatoms), aquatic macrophytes, macroinvertebrates and fish]. Currently the most important issue of WFD is to establish a well-prepared monitoring system in Hungary. Comparing this new system with the existing system the basic difference is that WFD is able to provide information about condition of water bodies entirely and not only about sampling sites. Working out of the river basin management plans by 2009 is demanded by WFD and national laws. Measured results have been compared to MSZ 12749 standards and based on these measurements streams got classified. The bedrock has its effects through the main ions of the water thus typology had been proved by main ions. According to results of the examined water the followings were determined: nitrate, nitrite and phosphate-ion from the gardens, cultivated lands and sewage significantly pollute the surface water. Traffic means further pollution, in this case organic compounds or heavy metals can solve into the water. After processing these data are available to the public as a web service displayed by GIS and graphical tools. Important viewpoints were automatic data visualization-, and the development of methods that help creating easily understandable graphical objects for the target audience. The database can be efficiently used in areas where displaying spatial information on maps is important.

2 Material and methods

One part of this project was to examine physical and chemical parameters of surface water in accordance with the WFD. The following streams were examined (Fig.1) Csenkő (1), Tolcsva (2), Hór (3), Eger (4), Csörgő (5), Cuha (6), Torna (7), Veszprémi Séd (8), Kösély (9), Tócó (10).

Fig.1, Sampling sites (–)

Calibrated and portable Consort C535 was used to take outside measurement. Temperature, pH-value and conductivity were measured in the field.

UV-fluorescens and spectrofotometry sensors (Fig.2) can provide information directly about clorophyll-a, PAH, COD_t and nitrate concentrations in the surface water (rivers, lakes).

Fig.2, Sensors used

Sensors can help monitoring of surface water as there is the possibility to receive information directly that can speed up the process of interference. The 8 main ions and N and P forms were analyzed by titrimitry (COD_t, HCO_3^-, CO_3^{2-}, SO_4^2 [2] and Cl^- [3] by spectrophotometry PO_4^{3-}, NH_4^+, NO_3^-, NO_2^-, by AAS (Cd^{2+}, Co^{2+}, Cr^{3+}, Ni^{2+}, Zn^{2+}, Pb^{2+}) by ICP-OES Na^+,

K^+, Ca^{2+}, Si^{4+}, Mg^{2+}). For estimation of the results SYNTAX 2000 [4] program package was used.
So far on the base of the results of field and laboratory measurements surface water has been qualified according to MSZ 12749 standards in the Environmental Information System. Represents colour scale for water qualification (Table 2).

	I. Excellent
	II. Good
	III. Tolerable
	IV. Polluted
	V. Extremely polluted

Table 2, Colour scale for water qualification

The homepage created for the project runs under Windows 2003 operation system, but all of its components are platform independent and free to use.
Components:
Database: Oracle Database 10g Express Edition (http://www.oracle.com/technology/products/database/xe/index.html)
Webserver: Apache/Tomcat/5.5.17 (http://tomcat.apache.org/)
MapScript and GIS data: Google Maps Api (http://www.google.com/apis/maps/)
Own GIS data: ArcView 3.2: (http://www.esri.com/software/arcview/)

3 Results and Conclusion

The choice fell on Oracle database because of the support and experience provided by its company. This version is free to use, and it will allow us the easy switch for a version with greater performance if needed.
Apache was an obvious option for its platform independency. This is the reason for the use of Java programs, too. These components allow installing the system on almost any platform.

The integration of Google Maps API enables using a solid interface known by many for in-map data visualization. Its further advantage is that storing project-independent map data does not demand any resources from the university. Data is stored by Google and the users get them from their databases.
GIS information supplementing measured data (i.e. streams and coordinates) were digitized using Arcview 3.2. These files are stored on server of the project. In Fig.3, the connections of these elements are shown.

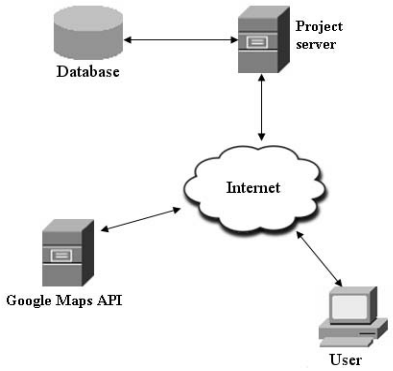

Fig.3, Connection of components

Any information concerning the system and the project is easily accessible via drop-down menus from the index page (Fig.4). Elements of the drop-down menu are static HTML 4.01 pages. Using the dynamic pages users can reach the "Map" menu serving as the first step of data visualization.

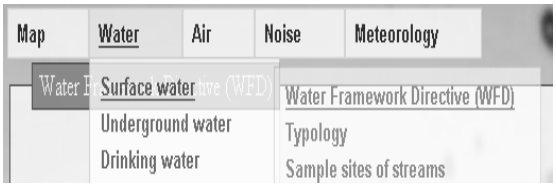

Fig.4, Structure of index page

Popup windows (Fig.5) show only basic information from data collected on the site.

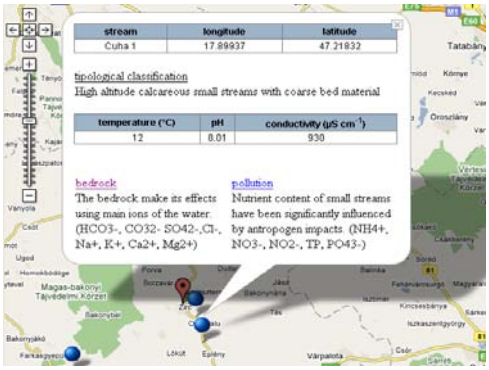

Fig.5, Generic information about upper reach of Cuha stream

Other possibility for users is receiving information about effect of bedrock to water and pollutants level of watercourses. These data were stored in a database after manual screening. The aim of this step is to select and discard faulty data. Faulty data could significantly slow down, complicate, or in some cases make interpretation impossible of the outcome given by automatic processing.
In the popup window (Fig.5) the user may choose to go to a new page where measured essential chemical parameters (8 main ions and N and P forms) are displayed (Fig. 6).

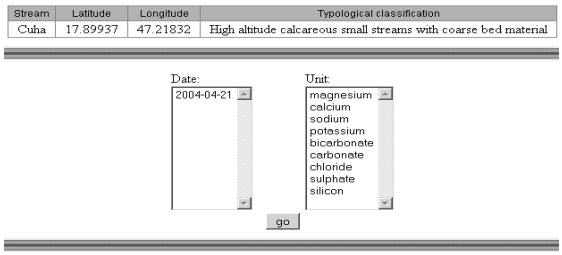

Fig.6, Searching according to measurement periods and chemical parameters

3.1 Appearance of results

With cluster analysis based on the main ions calcareous and siliceous waters were distinguished. Dendogram on the main ions have supported the hydrogeochemical differentiation of the typology. High sulphate and chloride concentrations were measured at the lower reach of the Kösély stream. This proves that it does not belong to either of the two categories (Fig.7).

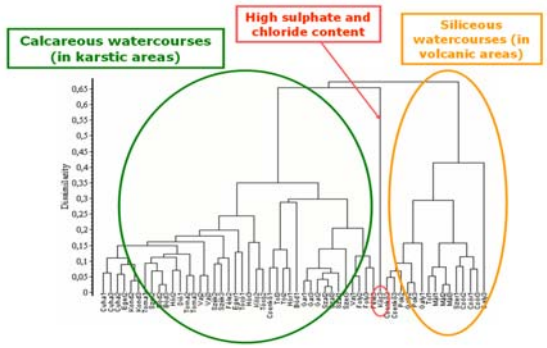

Fig.7, Dendogram (Bray-Curtis) of streams based on the main ionic (Ca^{2+}, K^{+}, Mg^{2+}, Na^{+}, HCO_3^{-}, CO_3^{2-}, SO_4^{2-}, Cl^{-}) composition

In the case of N and P forms only polluted sites were significantly different (Fig.8). Figure clearly shows that the middle reach of the Kösély and Tócó streams were different from the other streams as the measured N and P forms level were extremely high.

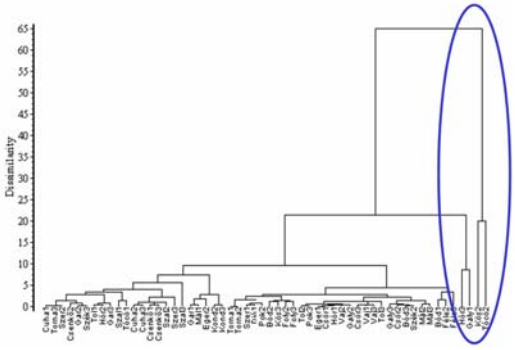

Fig. 8, Dendogram according to nitrogen and phosphorus forms (Euclides)

3.2 Measurement of displayed

On the homepage bar charts show measured values at different sampling sites of the streams. These provide generic information about condition of watercourse comprehensible for everyone. The system relieves users to query data since those bar charts and figures may be inquired from the database, which provide the needed information.
Examined values were presented on map due to easier evaluation and introduction of water quality.

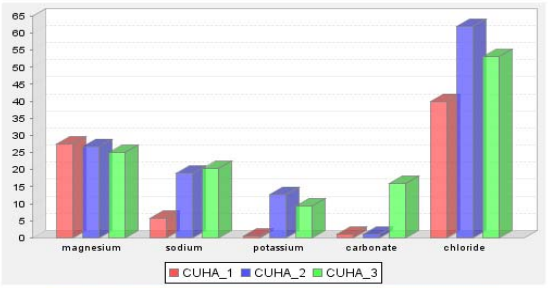

Sampling sites	magnesium	sodium	potassium	carbonate	chloride
Cuha 1	27.5	5.77	0.53	<1	40
Cuha 2	26.8	18.9	12.75	<1	62
Cuha 3	25	20.22	9.36	16	53

Fig.9, Representation of some chemical parameters of Cuha stream using a bar chart

The polygon of the river was divided into to five parts resembling the different quality classes (from to down A-B-C-D-E) surface water was divided into small sections short by sample sites as well (fig.10).

Fig.10, Fractional water qualification of Veszprém Séd stream (homepage)

On the map it is clearly visible that according to measured concentration components in group A are categorised as excellent. Components (NO_3^-, NO_2^-, NH_4^+, PO_4^{3-}) in group B are categorised as strongly contaminated water. Components in group C group were not tested therefore the line stayed coloured i.e. white. In group D the following micro-pollutants (Cd^{2+}, Co^{2+}, Cr^{3+}, Ni^{2+}, Zn^{2+}, Pb^{2+}) were measured. According to measured values the Cadmium concentration was high so D was categorised as extremely contaminated water quality. Components (pH, conductivity, temperature, Na^+-, K^+-, Ca^{2+}-, Mg^{2+}-, Mn^{2+}-, $Fe^{2+/3+}$-, SO_4^{2-}) in group E are categorised as tolerable in accordance to the measured concentrations.

4 Conclusion

Cluster analysis on the main ions supported the hydrogeochemical differentiation of the typology: streams with calcareous and siliceous bedrock appeared in different group. According to the water quality measurement results can be stated that the quality of watercourses is mostly influenced by artificial or human impact pollution forms like sewage or cultivated lands and gardens. The main road is the other pollution source as organic compounds or heavy metals can be washed into the streams. Not only is the prevention of surface water from pollutants important but it is very crucial to inform people (both experts and residents) about state of streams using Environmental Information System. To introduce the results in an informative way by bar charts and cluster analysis. Displaying the results on coloured scale helps to understand water condition for users. The developed homepage contains such techniques of visualization that makes it easily understandable for everybody.To provide an entire state assessment on the environment the measurements and results are needed to be permanently available. Tendencies of figures, bar charts, diagrams only provide useful information if they are based on sufficient data. Therefore the structure of the system allows further expansion and is able to measure other environmental elements such as meteorology data, air pollution and noise map.

References

[1] Directive 2000/60/EC of the European Parliament and of the Council

[2] Incédy J. (1981): Analytic laboratory practice I. Publishing of University of Veszprém, Veszprém

[3] Németh J. (1998): Methods of biological water, Aquatic, Nature- and Environmental protection (7. volume), Budapest

[4]Podani J. (2000): Introduction to the exploration of multivariate biological data. Backhuys, Leiden.

Possible successions on landfill top covers in the Pannonia area – an example from eastern Austria

JOHANNES TINTNER[1], KATHARINA MEISSL[1], BRIGITTE KLUG[2]
[1:] Department of Water, Atmosphere, and Environment,
Muthgasse 107, 1190 Vienna
[2:] Department of Integrative Biology and Biodiversity Research,
Gregor-Mendel-Straße 33, 1180 Vienna
Universität für Bodenkultur (BOKU)
AUSTRIA
johannes.tintner@boku.ac.at, brigitte.klug@boku.ac.at, http://www.boku.ac.at/

Abstract: - Main goals of landfill re-cultivation are minimization of leachate and - in most cases - a simple optical greening effect. The composition and quality of the vegetation cover, however, is not included in the evaluation of the re-cultivation success. On the other hand, the necessity of different after-use concepts is arising. One of these concepts is the creation of habitats for endangered vegetation types and species. The typical semi-dry meadows of pannonian Eastern Austria, for instance, have already become rare. In the light of this situation, methods of vegetation ecology were used on a closed landfill at the eastern border of the Vienna basin to assess the actual plant communities on the landfill top cover. Additionally, an experiment was run to establish a plant cover on the landfill similar to a neighbouring semi-dry meadow which was endangered by the landfill site and by building activities. The experimental re-cultivation plots in the landfill area were covered with sand; half of the test plot area was additionally covered with soil from nearby. The plots were then covered with mulch originating from the semi-dry meadow. 5 $g*m^{-2}$ of hand-collected fruits from there were also added, and the plots were inoculated with turf sods. The landfill and the plots were monitored over two years by phytosociological relevés. By statistical analysis of ecological indicator values and species life traits, two parts of different age and/or top cover quality could be distinguished on the landfill. Furthermore the decrease of ruderal species and the increase of species characteristic for semi-dry meadows were shown on the experimental plots.

Key-Words: Ellenberg indicator values; Landfill monitoring; Landfill re-cultivation; Landfill vegetation; Life traits

1 Introduction

Landfill re-cultivation in the past was often a matter of trial and error. The success of the efforts depended on the type of waste deposit and its top cover, and was influenced by in the intended after use of the landfill site. Under different climatic conditions and possible impacts of emissions, the seeded plant species often failed partly or even completely. Well adapted, highly competitive ruderals or short-lived segetal species came to dominance instead [9].

Prach and Pysek describe the possibilities of spontaneous succession to restore habitats after human disturbances, but they restrict this to cases where site conditions had not changed completely by the disturbances [19].

In Eastern Austria semi-dry meadows have become rare due to intensification or abandonment, whereas in the meantime the number of landfill sites has increased ([10], [11]).

In the light of this situation, a closed landfill southeast of Vienna offered us a possibility to investigate the plant communities on different top covers by methods of vegetation ecology, especially with the help of 34 phytosociological relevés on the artificially greened top covers. We tried to prove that the actual top covers would not allow a spontaneous succession towards a semi-dry meadow, even when it seems to reach the aims of minimizing gas and leachate emissions. To complete the picture given by the vegetation analyses, additional soil data were assessed and compared to literature.

Furthermore a small-scale experiment was started to study the effect of an additional autochthonous cover layer and the application of local plant material for the re-establishment of a semi dry meadow. As an after use concept such a

semi dry meadow has lots of advantages on that landfill site. Even if some studies suggest that trees and shrubs do not destroy landfill caps [7], they often are not accepted by owners of landfills. However, the maximization of evapotranspiration is a demand, as leachate treatment causes the biggest costs for a landfill runner after the closure of the landfill.

2 Materials and Methods

The closed landfill lies in an old limestone mine in the foothills of the Leitha Mountains at the borders of the Vienna basin. Average annual precipitation amounts to 570 mm, and average annual temperature to 10 °C. The landfill is divided in two parts, the older one closed more than 20 years ago, the younger one 10 years ago.

In large parts the top cover consists of compacted soil only; in one section of the old landfill part sewage sludge compost was tested (Relevés No. 26, 28, 29).

Decrees of the Federal Government prescribe a re-cultivation of top covers, but in this case the recent vegetation cover suggests that only very few seeded species have survived.

The landfill is surrounded by a mixed thermophilous oak forest, remainders of semi-dry meadows, arable fields, and meadows. The recent vegetation on roughly one hectare of landfill area and the adjacent meadow was assessed by 30 phytosociological relevés. Every relevé was performed in an area of homogeneous structure and species composition. The relevé size amounted to about 25 to 40 m². The site of the relevé, however, represents a bigger total area of comparable characteristics. The Londo [15] scale for estimations of cover percentages was slightly modified: A finer scale of cover was introduced for rare species with low cover [22].

The relevés were performed in 2004, 2005 and 2006. Species nomenclature follows Fischer et al. [6]. By the program VegePro (© Irene Ahamer 2003) the ecological site indicator values of the species (Ellenberg et al. [5], adapted by Karrer and Kilian [12]) were weighted by the respective cover values. The relevés were the input data, the cover percentage was used as weight. Weighted indicator values were the results. The following values were used: The F value indicates the moisture conditions, the R value the soil reaction and the N value the nutrient supply. The weighted and species specific indicator values were then summed up for every relevé. This sum, related to (divided by) the total cover of the respective species, makes up the average indicator value of the plant community. The use of indicator values in ruderal habitats has many restrictions [4]. Therefore the density of relevés on the landfill site was chosen rather high in order to enable satisfactory interpretation. The indicator values are valid only for a certain climatic region. Several authors developed values for other regions almost all over Europe (cf. [3], [24], [25]). For the pannonian region Karrer and Kilian developed values for the south eastern part of the Vienna basin, where the landfill is situated [12].

The relevès of the different parts, the experimental plots, and the semi-dry meadow were evaluated separately. The relative frequency of the species was calculated as number of relevès containing a certain species divided by the total number of relevès of the corresponding part. The mean cover of a certain species was calculated by averaging the cover of that species in all relevès of the corresponding part (Tables 1-4).

The experimental plot was divided into two subplots. Sand was spread in layers of different dimensions (50 cm and 100 cm) on top of the current landfill top cover. In subplot 1, pure sand was used (Cut A-A). In subplot 2, an additional layer of meadow soil was added (Cut B-B). The sand originated from a sandpit near the landfill site. Half the meadow soil was mixed with the sand in a 5 cm layer and then topped with an additional 5 cm of pure soil. The design of the subplots is shown in Fig. 1.

Soil analyses complete the picture of the vegetation analyses. The two meadow soil samples and the compost sample were taken as mixed samples consisting of material from 5 subsamples each. The samples from the landfill site were taken from the uppermost 20 cm of the top cover, but only one from each subplot. Photos of 20 boreholes in the top cover were additionally evaluated. The photos had been taken in the course of a previous study in 2003 (before the authors had access to the site).

All parameters were measured according to the Austrian Standards, with the exception of NH_4-N. In the latter case H_2O was taken instead of $CaCl_2$ as eluation medium. In the resulting eluate both pH and NH_4-N were measured. The results of the soil analyses are shown in Table 7. The sand of the experimental plots was not analysed as we assumed that its nutrient content and especially the organic content were negligible.

On the experimental plots the new top cover was mulched with a layer of 5 - 10 cm of hay clippings from the neighboring semi-dry meadow assessed in relevés no. 2, 3, 4, and 10 Table 4.

Hay transfer has positive effects also for soil temperature, for the stabilization of the surface, and as a seed trap. The impact on restoration is therefore positive even if there are few amounts of seeds in the mulch material ([1], [13]). The time of cutting was October, so only late ripening species were still providing seeds. Therefore the plots were inoculated with 30 to 30 cm turf sods (one per 5 m²), and 5 g of hand collected fruits per m² were applied. These fruits originated from the adjacent semi-dry meadow. In the following June this procedure was repeated with the fruits of the early flowering species, mainly *Brachypodium pinnatum* and *Bromus erectus*. The use of site specific plant material increases the success in such experiments ([16], [23]). One and two years after seeding, the vegetation on the two experimental subplots was documented by relevés. After such a short period of time the plant community of the experimental plot certainly was still in an early stage of development.

Multivariate data analysis (Principal Component Analysis PCA) was carried out using the Unscrambler 9.2 software (© Camo). PCA was used in order to detect "hidden phenomena" in the data set.

The information of the original data matrix X is reduced to the minimum number of dimensions needed to describe the relevant information contained in the original observation. The original data matrix Z is divided in a Scores matrix (T), a Loadings matrix (P) and an Errors matrix (E), mathematically explained as Z = T * P + E. [2]

These analyses had already been carried out on various ecological questions [17].

3 Results

In the old part of the landfill the total species number amounted to 151. On average, 32 species (maximum 61, minimum 18) were found per relevé. Most of the frequent species were biennial or perennial ruderals. 122 species (81 %) of all species found were ruderals or segetals. Only 2 species (1 %) – occurring only in one relevé each - were typical species of semi-dry meadows. 27 species (18 %) had an unspecific, wide ecological range. The 12 most important species of the old part of the landfill with a mean cover of almost or over 2% are combined in

Tables:

Table 1. Two remarkable species were *Erigeron canadensis* and *Erigeron annuus*, which were frequent in the old part but much rarer in the new part.

In the new part of the landfill site, total species number was 102, or 25 species per relevé (maximum 51, minimum 14; see Table 2).

This is significantly fewer than in the older part. Perennial and annual species were most frequent. The high number of annual species originates from one-year-old disturbances by sampling of waste material from the landfill body. 75 % of the species were ruderals or segetals. Only 2 % of the species originated from semi-dry meadows, and they were rare in the relevés. The 12 most important species of the new part of the landfill with a mean cover higher 2 % are shown in Table 2.

The main species outside the landfill were perennial species characteristic for semi-dry meadows. Two of these frequent species (*Helianthemum ovatum*, *Scabiosa canescens*) were indicated as threatened species in the Red List of Lower Austria [21]. Furthermore some other threatened taxa like orchids (*Orchis purpurea*, *Orchis militaris*, *Ophrys spegodes*, *Ophrys insectifera*, *Ophrys holosericea*, *Anacamptis morio*, *Gymnadenia conopsea*) and *Lilium martagon* were found beside the relevés. The threatened species give motivation to think about re-cultivation with such a semi-dry meadow. All relevés together comprised 79 species. In relation to the number of relevés this meant 20 different species per relevé (79 species/ 4 relevés), a figure much higher than on the landfill site. In the old part 151 different species were found in 13 relevés which would mean 12 new species per relevé. In the new part this relation was only 8. Average species number per relevé was 33, with a maximum of 43 and a minimum of 23. Ruderals were much less frequent than at the landfill site. Only 15 % (12 species) belonged to this group. 62 % (49 species) were typical for semi-dry and dry meadows. 18 species (23 %) were indifferent. The species with the highest average cover were mainly species of semi-dry meadows, even when they were not the most frequent ones. All species of the semi-dry meadow with a mean cover >1 % are shown in Table 3.

The relevés no.31 – 34 originated from the experimental plots (see Table 3). Relevés no. 31 and 32 were taken in 2005, 33 and 34 in 2006. The total number of species amounted to 115 (90 in 2005 and 69 in 2006). Averaging all relevés of both years, 58 species were found per relevé (maximum 71, minimum 46). In the relevés of 2005 this average was 66, in 2006 49. Compared with

vegetation on the landfill or at the semi dry meadow, this was significantly higher, being explained by the low total coverage on the experimental plots. 56 species (49 % of 115) were characteristic of ruderal sites. 40 (35 %) species originated from semi-dry meadows. 19 (17 %) species were indifferent. These ratios were derived from the 2006 data (Table 5). All species of the experimental plots with a mean cover higher 1 % are shown in Table 4.

Table 5 displays the decrease of ruderal and segetal species in the experimental plots within two vegetation periods. As the number of semi-dry meadow species remained rather stable, this led to a decrease of the total species number (the slight increase of indifferent species cannot compensate this decrease).

The most frequent species in the experimental plots were well mixed with respect to their life traits – ruderals (5 species), species from semi-dry meadows (5), and indifferent species (4 species).

In Table 6 the mean Ellenberg indicator values for F, R, and N, adapted to Austrian environmental conditions by Karrer and Kilian [12], are listed for the three types of vegetation (old part, new part, semi-dry meadow) as well as for the experimental plots. Furthermore the cover percentage for annual, biennial, herbaceous perennial and woody perennial species are shown. At the experimental plots the cover of herbaceous perennials had increased in the second year of investigations, whereas the annual species had become less important. This indicates an undisturbed succession process. The total cover on the pure sand increased from only 20 % in 2005 to 65 % in 2006. On the subplot with additional soil the total vegetation cover rose from 50 % to 80 % in the same period of time. Such covers seem to be normal for successions on areas totally free of vegetation (cf. [14]).

Fig. 2 shows results obtained by PCA of the life span data of the species. The loadings (2 c) illustrate that the old part (▲) of the landfill site was dominated by annual and biennial species although this part of the landfill was older than 20 years. The new part of the landfill site (△) and the semi dry meadow (◆) were mainly covered by perennial species. Relevés 21, 22, 24, and 25 of the new part had been disturbed by former samplings in the waste deposit. Therefore they comprised mostly annual species. Furthermore, relevés 26, 28, and 29 in the old part were mainly covered by perennial species. Compost had been used as top cover in these three areas to foster methane oxidation (Fig. 2 b).

The varying levels of disturbances on the sites had led to different cover percentages of annual and biennial species (Fig. 2). The high percentage of annual species in the test plots can be explained by the fact that the succession process had started only one year ago. Relevés no. 32 and 31 had been taken in the first year, while relevés no. 33 and 34 were generated in the second year. The loading plot (Fig. 2 c) explains the shift of these relevés from the top left-hand corner of the diagram, where annual species cover was responsible for the separation of the relevés, to the mid-right side, where herbaceous perennial species exerted the main influence.

The old part seems to have followed an underdeveloped or disturbed succession as it puts up a high portion of short-lived plant species. Possible reasons could be landfill gas emissions or deficits in the top cover material [17].

The results assessed from soil samples (Table 7) and photos of boreholes suggested that the cover material of the old and of the new part was quite homogenous. In the new part the material was more compacted than in the old part (photos not shown).

The meadow soil from subplot 2 and the top cover of the landfill site were comparably poor in nutrients and organic content (cf. TOC, Table 7). Due to a higher compaction rate of the top cover (especially in the new part of the landfill), nutrients were locally stabilized. The loamy and cohesive material may have inhibited water drainage. In the sand, on the other hand, water runs off fast and the substrate dries more quickly. Nutrients could be washed out faster, the residuals being hardly available for the plants.

All the results confirmed the higher ecological N-indicator values (for nutrient supply) in the relevés with the landfill vegetation on the top cover material. The vegetation on the experimental plots was growing on pure sand or sand with a thin layer of poor soil. Therefore, also its N- and F-values were lower. As reported by [5] or [4], the N-value does neither correlate particularly well with total nitrogen content, nor with ammonium nor nitrate. It is rather a response to general nutrient supply [8]. Therefore, soil measurements were taken only roughly for the confirmation of the Ellenberg values obtained.

4 Conclusion

The main driving force for vegetation dynamics on the landfill site in Eastern Austria was the top cover material used to minimize emissions. The ecological site indicator values (mainly for

moisture and nutrients) derived from phytosociological relevés on the landfill proved to be helpful in prospecting the quality of the cover material. Disturbances originating from the landfill itself led to higher frequency of species with a short life span (biennials, annuals). Species with short life-spans quite often remain longer in succession than only one or two years (cf. [18]), but their persistence after more than twenty years is remarkable. As the cover material seemed to be less compacted than in the new part, gaseous emissions such as methane could have been responsible for this unusual situation. Further investigations are needed to prove this hypothesis. Even after more than 20 years, the plant cover on the landfill comprised high numbers of ruderal species and showed no similarities with the semi-dry meadow outside the landfill. The reason is the typical top cover material which differs strongly from the surrounding soil type, a nutrient poor and sandy soil.

The statistical analysis of phytosociological relevés has proved to be a proper tool for monitoring and interpreting the succession of the landfill vegetation. The quality of the cover material and changes in the landfill cap can be assessed. Compared with chemical or physical analyses, the vegetation analysis is not only quicker but also much cheaper. The two parts of the landfill could easily be distinguished by this method. It may be useful especially in the planning phase of landfill monitoring and controlling. The history of the development and management of old and closed landfills is often badly documented. In the present case, the plant cover of the landfill reflected the historical development of the landfill in two phases. For future planning this must be taken into consideration.

The application of a sand layer on top of the actual landfill cover seems to be appropriate to establish a semi-dry meadow similar to the small rest of a meadow that represents a threatened plant community and contains rare species. Thus the landfill site could be considered as a target area for future ecological restoration. The restoration of a semi-dry meadow does not guarantee the re-immigration of threatened species. But the chances for the re-establishment of these species are incomparably higher than without a proper restoration.

5 Acknowledgments

This research was funded by the NUA Company (Niederösterreichische Umweltanstalt).

References:

[1] Athy, E. R., Keiffer, C. H., Stevens, M. H., 2006: Effects of Mulch on Seedlings and Soil on a Closed Landfill. Restoration Ecology 14(2), pp. 233-241.

[2] Brereton, R., 2003: Chemometrics: data analysis for the laboratory and chemical plant. John Wiley & Sons Ltd., Chichester, West Sussex.

[3] Diekmann, M., 1995: Use and improvement of Ellenberg's indicator values in deciduous forests of the Boreo-nemoral zone in Sweden - Ecography 18, pp. 178-189.

[4] Diekmann, M., 2003: Species indicator values as an important tool in applied plant ecology – a review. Basic and Applied Ecology 4, pp. 493-506.

[5] Ellenberg, H., Weber, H. E., Düll, R., Würth, V., Weber, W., Paulißen, D., 1992: Zeigerwerte von Pflanzen in Mitteleuropa. Scripta Geobotanica 18, pp. 3–258, Goeltze, Göttingen.

[6] Fischer, M. A., Adler, W., Oswald, K., 2005: Exkursionsflora von Österreich, Liechtenstein und Südtirol. – 2nd ed. – Land Oberösterreich, Biologiezentrum der OÖ Landesmuseen, Linz.

[7] Handel, S. N., Robinson, G. R., Parson, W. F. J., Mattei, J. H., 1997: Restoration of Woody Plants to Capped Landfills: Root Dynamics in an Engineered Soil. Restoration Ecology 5(1), pp. 178-186.

[8] Hill, M. O., Carey P. D., 1997: Prediction of yield in the Rothamsted Park Grass Experiment by Ellenberg indicator values. Journal of Vegetation Science 8: pp. 579-586.

[9] Huber-Humer, M., Klug-Pümpel, B., 2004: The vegetation on different top covers of an abandoned solid waste landfill. Bodenkultur 55(4), pp. 155-163.

[10] Jacquemyn, H., Brys, R, Hermy, M, 2003: Short-term effects of different management regimes on the response of calcareous grassland to increased nitrogen. Biological Conservation 119, pp. 137-147.

[11] Kahmen, S., Poschlod, P., Schreiber, K. F., 2002: Conservation management of calcareous grasslands. Changes in plant species composition and response of functional traits during 25 years. Biological Conservation 104, pp. 319-328.

[12] Karrer, G., Kilian, W., 1990: Standorte und Waldgesellschaften im Leithagebirge Revier Sommerein. - Mitt.Forstl.Bundesversuchsanst. Wien, 165, pp. 1-244.

[13] Kiehl, K., Wagner, C, 2006: Effect of hay transfer on long-term establishment of

vegetation and grasshoppers on former arable fields. Restoration Ecology 14, pp. 157-166.

[14]Lin, W., Lin, C., Chou, W., 2006: Assessment of vegetation recovery and soil erosion at landslides caused by a catastrophic earthquake: A case study in Central Taiwan. Ecological Engineering 28(1), pp. 79-89.

[15]Londo, G., 1976: The decimal scale for relevés of permanent quadrats. Vegetatio 33, pp. 61-64.

[16]Martinez-Ruiz, C., Fernandez-Santos, B., Putwain, P., Fernandez-Gomez, M. J., 2007: Natural and man-induced revegetation on mining wastes: Changes in the floristic composition during early succession. Ecological Engineering 30(3), pp. 286-294.

[17]Maurice, Chr., Bergman, A., Ecke, H., Lagerkvist, A., 1998: Vegetation as a biological indicator for landfill gas emissions: initial investigations. Proceedings from Sardinia '95: Fifth International Landfill Symposium, October, 2-6th, 1995, St Margherita di Pula, Cagliari, Italy, Vol. III, pp. 481-494.

[18]Prach, K., Pysek, P., Smilauer, P., 1999: Prediction of Vegetation Succession in Human-Disturbed Habitats Using an Expert System. Restoration Ecology 7(1), pp. 15-23.

[19]Prach, K., Pysek, P., 2001: Using spontaneous succession for restoration of human-disturbed habitats: Experience from Central Europe. Ecological Engineering, 17(1), 55 - 62.

[20]Scheffer, F., 1998: Lehrbuch der Bodenkunde: Scheffer/ Schachtschabel. 14th ed., Stuttgart, Enke.

[21]Schratt, L, 1990: Rote Liste gefährdeter Farn- und Blütenpflanzen Niederösterreichs. 1st ed., Institut für Botanik der Universität Wien.

[22]Smidt, E., Tintner, J., Meissl, K., 2007: New Approaches of Landfill Assessment and Monitoring. In: Velinni, A (Ed.): Landfill Research Trends. NOVA Publisher, pp. 191-225.

[23]Tinsley, M. J., Simmons, M. T., Windhager, S., 2006: The establishment success of native versus non-native herbaceous seed mixes on a revegetated roadside in Central Texas. Ecological Engineering 26 (3), pp. 231-240.

[24]Zólyomi, B., Baráth, Z., Fekete, G., Jakucs, P., Kárpáti, I., Kovács, M., Máthe, I., 1967: Einreihung von 1400 Arten der ungarischen Flora in ökologische Gruppen nach TWRZahlen. Fragmenta Botanica Musei Historico-Naturalis Hungarici 4, pp. 101–142.

[25]Zarzycki, K., 1984: Ekologiczne liczby wskaz´nikowe ros´lin naczyniowych Polski [Indicator Values of Vascular Plants in Poland]. Polska Akademia Nauk-Instytut Botaniki, Kraków, Poland.

Tables:

Table 1: Mean relative frequency and cover percentage of the 12 most important species in the old landfill part.

	Species	Mean cover [%]	Relative frequency
1	*Urtica dioica*	11.69	0.46
2	*Tripleurospermum perforatum*	9.42	1.00
3	*Erigeron canadensis*	8.81	0.46
4	*Elymus repens*	6.04	0.92
5	*Cirsium arvense*	5.81	0.69
6	*Anthriscus sylvestris*	4.85	0.38
7	*Erigeron annuus*	4.35	0.62
8	*Galium aparine*	2.70	0.38
9	*Echinochloa crus-galli*	2.65	0.23
10	*Plantago lanceolata*	2.13	0.62
11	*Bromus sterilis*	1.96	0.38
12	*Calamagrostis epigejos*	1.92	0.31

Table 2: Mean relative frequency and cover percentage of the most important species on the new landfill part.

	Species	Mean cover [%]	Relative frequency
1	*Elymus repens*	29.08	1.00
2	*Plantago lanceolata*	9.46	0.85
3	*Poa angustifolia*	8.58	0.85
4	*Achillea millefolium* agg.	6.31	1.00
5	*Calamagrostis epigejos*	5.42	0.15
6	*Phragmites australis*	5.12	0.46
7	*Polygonum aviculare*	2.46	0.62
8	*Arrhenatherum elatius*	2.38	0.23
9	*Cirsium arvense*	2.31	0.46
10	*Buphthalmum salicifolium*	2.31	0.08
11	*Atriplex patula*	2.15	0.38
12	*Chenopodium album*	2.00	0.54

Table 3: Mean relative frequency and cover percentage of species of the semi-dry meadow covering >1%.

	Species	Mean cover [%]	Relative frequency
1	*Festuca rupicola ssp. rupicola*	17.50	0.75
2	*Bromus erectus*	13.50	0.75
3	*Brachypodium pinnatum*	8.75	1.00
4	*Anthericum ramosum*	7.50	0.25
5	*Origanum vulgare*	5.50	0.50
6	*Centaurea scabiosa*	5.50	1.00
7	*Teucrium chamaedrys*	3.50	0.75
8	*Helianthemum ovatum*	2.88	0.75
9	*Scabiosa canescens*	2.65	0.75
10	*Sanguisorba minor*	2.63	0.50
11	*Peucedanum alsaticum*	2.53	0.50
12	*Geranium sanguineum*	2.50	0.25
13	*Avenula pubescens*	2.50	0.25
14	*Pimpinella saxifraga*	1.50	1.00
15	*Dorycnium germanicum*	1.50	0.50
16	*Plantago media*	1.13	0.50
17	*Galium verum agg.*	1.13	0.50
18	*Carex humilis*	1.13	0.50
19	*Quercus cerris*	1.03	0.50
20	*Stipa capillata*	1.00	0.25
21	*Corylus avellana*	1.00	0.25
22	*Potentilla arenaria*	1.00	0.25

Table 4: Mean relative frequency and cover percentage of the most important species at the test plots.

Species	Mean cover [%]	Relative frequency
1 *Securigera varia*	7.75	1.00
2 *Origanum vulgare*	6.25	1.00
3 *Erigeron canadensis*	5.75	1.00
4 *Bromus erectus*	3.75	1.00
5 *Carlina biebersteinii*	3.50	1.00
6 *Elymus repens*	3.13	0.75
7 *Carex hirta*	2.75	0.50
8 *Odontites luteus*	1.78	1.00
9 *Achillea millefolium* agg.	1.75	1.00
10 *Verbascum chaixii*	1.50	0.75
11 *Dactylis glomerata*	1.38	0.75
12 *Lotus corniculatus*	1.25	1.00

Table 5: Development of the life type numbers of the species of the experimental plots

	Total	Ruderals, Segetals		Semi-dry meadows		Indifferent	
	Number	Number	% of total	Number	% of total	Number	% of total
2005	90	51	57	28	31	11	12
2006	69	22	32	30	43	17	25

Table 6: Average F-, R-, and N- values and cover percentages, attributed to species groups with different life (span) traits. Data comprise all relevés made in the respective plots.

Part of the (landfill) area	Indicator values			Cover (%) of species groups			
	F	R	N	annual	biennial	perennial	woody
Old part	5.0	6.8	6.6	18.2	34.7	46.9	0.1
New part	5.2	7.0	6.2	11.8	7.6	80.5	0.1
Semi-dry meadow	3.1	7.8	2.7	0.6	1.8	87.3	10.3
Experimental plots 2005	3.8	7.7	4.4	24.1	20.9	54.5	0.5
Experimental plots 2006	3.8	8.0	3.9	4.5	17.2	75.4	0.7

Table 7: Parameters of the meadow soil in subplot 2, the compost (sewage sludge compost) at the relevés no. 26, 28, and 29, and the top cover of the rest of the landfill site (**1:** taken in uppermost 5 cm, **2:** taken in 30 cm depth), compared with various sewage sludge composts and soil [20]. (TOC = Total Organic Carbon)

	Meadow soil (n = 2)	Compost (n = 2)	Landfill cover, **1** (n = 2)	Landfill cover, **2** (n = 3)	Sewage sludge composts	Soil [20]
Loss of ignition (% DM)	3.9	16.0	6.5	4.5	30.0	4 - 6
TOC (% DM)	1.3	5.6	2.1	1.1	14.8	1.2 - 3.0
pH-value $_{H2O}$	8.1	7.5	7.6	7.7	7.5	5.5 - 7.5
Conductivity (mS/cm)	0.17	0.35	0.27	0.29	2.70	0.30 - 0.70
NH_4-N $_{H2O}$ (mg/kg DM)	2.5	9	13	6	10 – 4,000	0.2 - 4

N_{tot} (% DM)	0.10	0.53	0.68	0.07	1.50

Figures:

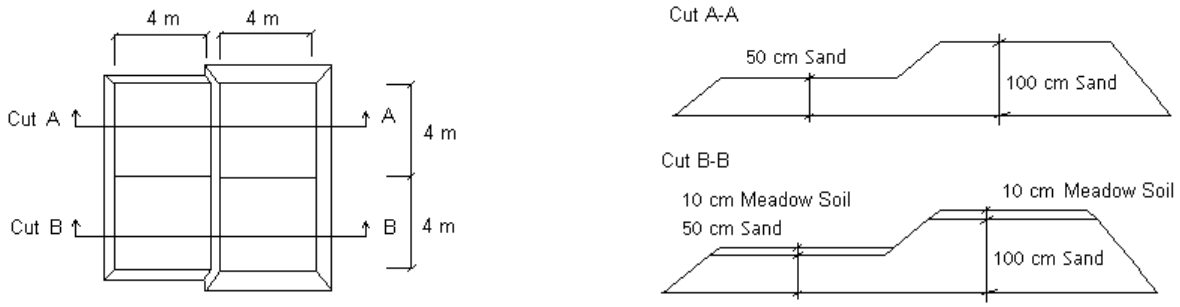

Fig. 1: Draft of the subplot design, the supreme 5 cm of the sand in cut B are mixed with meadow soil (not marked separately). Cut A-A shows subplot 1 and cut B-B shows subplot 2.

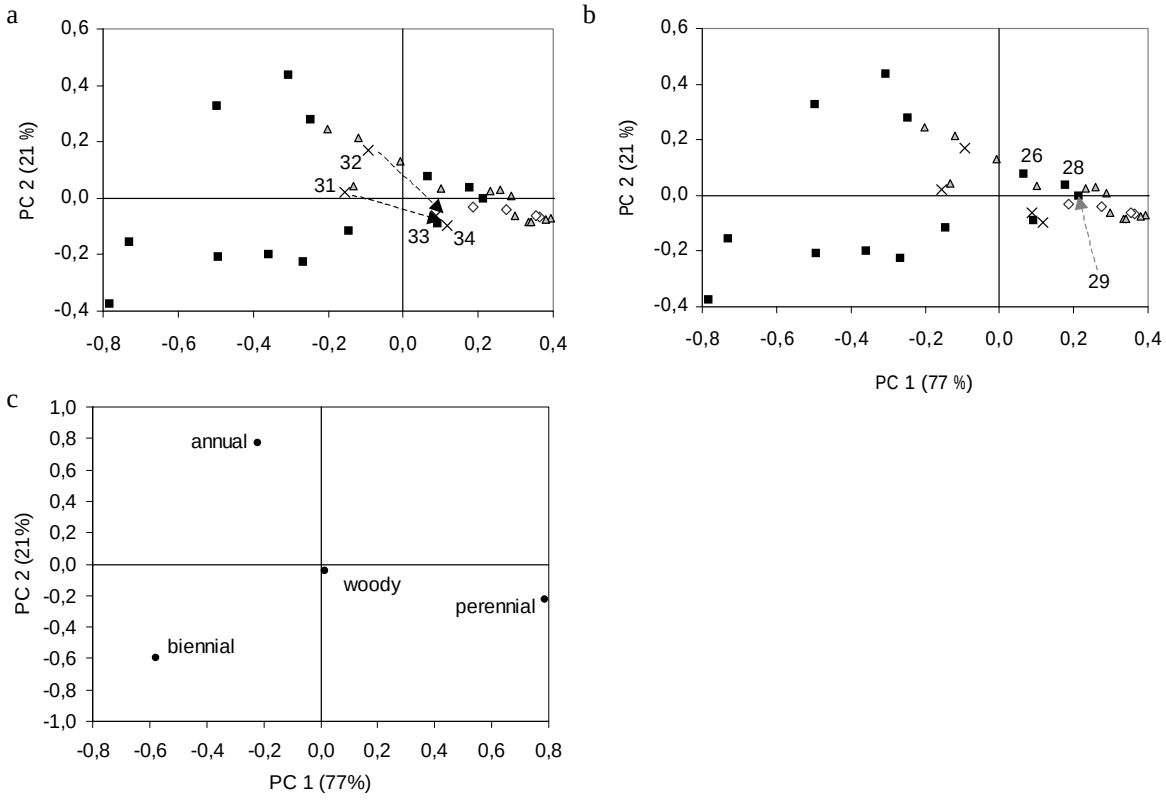

Fig. 2: PCA of the life traits from old (▲■) and new part (△) of the landfill, and semi dry meadow (◆);

(a,b) Scores plot and (c) Loadings plot, showing PC 1 and PC 2; in brackets: the respective contribution to variance

Exploratory point pattern analysis for modeling earthquake data

S. ZIMERAS
University of the Aegean
Department of Statistics and Actuarial-Financial Mathematics
G.R.832 00, Karlovassi, Samos,
GREECE
e-mail: zimste@aegean.gr

Abstract: Geostatistics is a collection of statistical methods which were traditionally used in geo-sciences. These methods describe spatial autocorrelation among sample data and use it in various types of spatial models. Spatial statistics is concerned with statistical methods that explicitly analyses spatial arrangement of the data. When analyzing these kinds of data, we might be interested investigating the temporal data process that generated the data. Typically spatial point patterns are data that made up of the location of point events. We are interested in whether or not their relative locations represent a significant pattern. For example, seismologists have been showing the distribution of earthquakes in a region. They would like to known if there is any pattern that might help them make predictions about future earthquakes. In this work, an investigation of earthquakes spatial data is analyzed, using specific statistical modeling techniques.

Keywords: Spatial point analysis, earthquakes data, spatial statistics, Geostatistical analysis, GIS.

1. Introduction

Spatial statistics is concerned with the study of spatially referenced data combined with appropriate statistical models and process. For many researchers, point pattern analysis has been a powerful tool, to investigate the relationship between different locations of a particular event (earthquake) applying specific statistical technique (estimation of the intensities using measures like nearest neighbors distance). Few works have been introduced spatial statistical methods to evaluate earthquake data and reproduce predictions for the future [1, 2, 3, 4, 5].
Spatial background rates are commonly estimated by seismologists by smoothing the larger events only. For instance [2, 3, 4] suggests anisotropic kernel smoothing of larger events in order to estimate the spatial background intensity for all earthquakes. In this application, we investigate various spatial background seismicity rate estimates involving kernel smoothings of only the 2030 earthquakes of magnitude 3:5 and higher, by using K-Ripley function to assess their fit to the earthquake data set.
Spatially data consist of measurements for a stochastic process at a set of sampled locations. The objective of the analysis is to model the variability of the associated random variable over space and to examine statistically factors that explain this behaves. Models are also used to predict the values of the random variable at locations in the study area that were not sampled (this is called spatial interpolation) [6, 7].
A stochastic process that takes place over space gives rise to events, which are represented by their locational coordinates. The epicenters of earthquakes, for example, can be considered as events in space. The stochastic process that gives rise to these events is governed by a variety of complex geological phenomena. A collection of events in a study region constitutes a point pattern. The object of point pattern analysis is to study the stochastic process that gives rise to the observed point pattern. To this end, it is important to determine in a statistical sense whether the events in the point pattern under study are regularly spaced or clustered. The former implies repulsion between events while the latter implies attraction. If none of those cases applies then we say that the pattern is random.
Most recently, statistical techniques applying to point patterns are considered because of the developments of geographical information systems

(GIS). Under these systems, it could be generated predictions of the spatial location for predictions about the future phenomena. Finally they provide a variety of tools for the visualization of point data. They allow us simultaneously to view the point patterns, explore structure in data by estimations appropriate models and test hypothesis relating to the process considering the observed event distribution.
In this work, an investigation for earthquake data is analyzed, using specific statistical modeling techniques. Statistical models could be useful for the prediction of the earthquake locations in the future.

2. Spatial statistics modeling

Spatial modelling is dealing with separate, broadly defined areas of spatial statistics: **1**. geostatistical data, **2**. lattice data, and **3**. point patterns. However, they are unified in one general model as it is given in Figure 1.

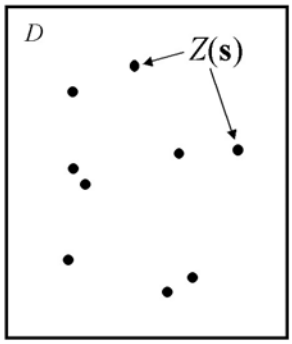

Figure 1. General spatial model

The notations that will be used throughout this work are based on [6, 8]. The domain, or the "study area," is given by *D*. Usually *D* is a subset of 2-dimensional space, but it could be 1-dimensional or 3-dimensional or even beyond. Thus, we will say that $D \subset \Re^d$, for whatever dimension *d* we choose. The vector **s** contains information on the data location. Locations in *D* are denoted by the vector **s**. For example, in 2-dimensional space, **s** will have 2 components containing the coordinates (x, y) , such as latitude and longitude. At location **s**, we obtain some value *z*. Because we are applying spatial statistics techniques, using spatial information for our models, we need to keep track of where values occur. Thus, we show that the value *z* came from location **s** by attaching the location to each value *z*(**s**). Finally, because we will study stochastic models for data, we will assume that *Z*(**s**) is a random variable at each location. Note the usual convention; an upper case letter indicates a random variable, while a small case letter indicates and observed value from the random variable. Usually, texts on statistics keep track of data and random variables with a subscript, such as Z_i; notice that here we have essentially replaced that subscript with the spatial location. With this background, we can define the general spatial model as, $\{\mathbf{Z}(\mathbf{s}) : \mathbf{s} \in D\}$. Basic models in spatial statistic are: **1**. ***Geostatistical data*** (for example temperature values taken at weather stations): Here *D* is a continuous fixed subset of $\Re^d$; **Z**(**s**) is a random vector at location $\mathbf{s} \in D$. **2**. ***Lattice data*** (for example counts of accidents per road segment in a road system): Here *D* is a fixed but countable subset of $\Re^d$ such as a grid some representation with nodes; **Z**(**s**) is a random vector at location $\mathbf{s} \in D$. **3**. ***Point Patterns*** (for example The epicentres of earthquakes): Here *D* is a random subset of $\Re^d$ and is called a point process; if **Z**(**s**) is a random vector at location $\mathbf{s} \in D$ then it is a *marked spatial point process*; if **Z**(**s**) ≡ 1 so that it is a degenerate random variable, then only D is random and it is called a *spatial point process*.
A spatial point process (SPP) differs from the first two types of spatial data in that the domain D is a random set containing location s of events. Whereas interest with geostatistical and lattice data lies in studying the properties of Z(s) or E[Z(s)], for spatial point processes studying the properties of the set D is the primary focal point.
A process where Z(s) = 1 $\forall$s $\in$ D is called a simple point process to emphasize that only the random locations at which events occur are of interest. A second class of point processes allows Z(.) to vary randomly in addition to the stochastic nature of
D. Examples of such marked point processes, that derives its denomination from labeling Z(.) the mark variable, would be recording the location and magnitude of earthquakes.

3. Point Pattern analysis

Point Pattern Analysis is an investigation focused on finding patterns in data comprised of points in a spatial region. A spatial point pattern is probably the simplest example of spatial data. The data set only consists of n locations $s_1 \ldots s_n$, each consisting of an (x,y) co-ordinate. It is often advantageous to refer to a point pattern as a set of event locations because the general objective is an analysis of the

pattern of thee events. The word 'event' suggests some consideration of the probabilistic mechanism involved. We're also interested in the intensity of the events over the region. it is possible for the data to contain spatial location plus additional information. For example, earthquake data typically gives the location of earthquakes along a fault line and will often have the size and the time of each earthquake. Data that contains spatial data plus additional information is often referred to as *marked spatial data*. In our analysis, we will be concerned with only the spatial information and we will disregard any additional information associated with the data. Moreover, the examples we will work with are limited to two-dimensional data. Our interest will lie in quantifying the dispersion of objects within a confined geographical area. We try to understand the interaction of pattern and process and use point pattern analysis as a mechanism for detecting patterns associated as compared to random processes. Our main goal of point pattern analysis is to find out whether the distribution of the spatial data is random, clustered or regularly dispersed especially in earthquake data. For example, if the pattern is clustered, the seismologists may conclude that natural factors in that region with high intensities encourage the seismic behave and promote unnatural phenomena.

There are several methods and algorithms that endeavor to describe pattern for a collection of points. The most common methods discovered for spatial pattern analysis are as follows [6]: **1.** Quadrant Count Method, **2.** Kernel Density Estimation (K means), **3.** Nearest Neighbor Distance (G function, F function, K function). The above list of techniques for Point Pattern Analysis is among the most popular and best established mathematical and statistical methods used in the literature [6, 7, 9, 11]. Since Point Pattern Analysis can take several forms and can be applied in a variety of settings we will present a list of criteria in order to determine if a data set is suitable for our Point Pattern Analysis. The criteria we will use to determine if a data set is appropriate for our type of point patter analysis is given by the following:

- Spatial data must be mapped on a plane; both coordinates are needed.
- Point data should not be a selected sample, but rather the entire set of data to be analyzed.
- There should be 1-1 correspondence between objects in study area and events in pattern.
- Points must be true incidents with real spatial coordinates.

As mentioned the basic interested in analyzing spatial point data is the investigation of the pattern. Overall, this investigation may be whether or not it is systematic (clustered or regular) or it may be a consideration of whether or not there are more (or less) events in a particular sub-region than one would expect by chance alone. Figure 2 illustrates different type of clusters.

For the cluster pattern, the data set has one or more groups of points in clusters and large areas of maps without points. For the regular pattern the events are distributed more or less regularly over the region. For the random pattern, the data set has no dominant trend towards clustering or dispersion.

Clustered pattern

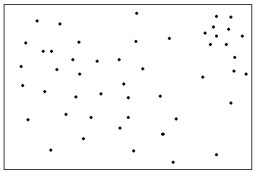

Regularly Dispersed Pattern

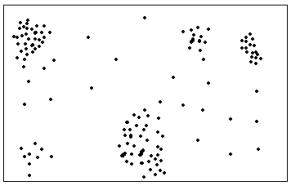

Random Pattern

Figure 2. Types of clustre patterns

The most effective way to visualise spatial pattern data is to plot them as a dot map. A dot map is a region over which the events are observed as points. The dot map has long been one of the most popular cartographic tools of geographers. It is popular since it displays spatial distributions with both clarity and simplicity. Figure 3 represents the locations of the epicenters of the earthquakes where observations in this data frame are 2049 earthquake epicenters in the San Francisco Bay area for the time period 1962-1981. Obviously the pattern appears clusters.

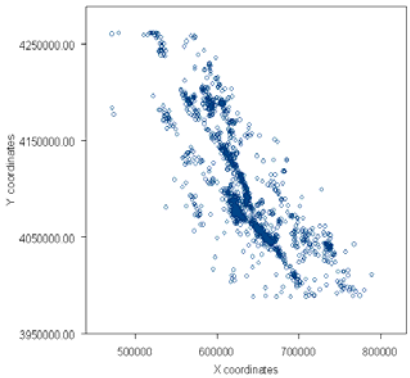

Figure 3. Spatial locations of the epicenters of earthquakes

4. Simulating Point Patterns

From a probabilistic standpoint, complete spatial randomness or CSR is associated with a Poisson random variable (i.e. a homogeneous spatial Poisson process). A homogeneous spatial Poisson process is one in which the events occur uniformly throughout the region. In other words there is a constant expected intensity for a given spatial unit. Events of the process are assumed to have equal probability of occurring anywhere in the region A. The events are assumed to be independently and uniformly distributed over A. An exploratory analysis of the plot locations should reveal something as an initial overview. However, we need something more formal to decide on whether clustering exists.

A point process is a process of locations of events taking place in some space *X*. Each event has associated with a mark, taking place in some mark space *Y* [12]. The term event (points) can refer to any spatial phenomena that occur at a point location. The epicenters of earthquakes, for example, can be considered as events in space A point pattern is a set of point locations $\mathbf{s}=\{s_1, s_2,\ldots,s_n\}$ in a specific sub-region A. [4]. The random variable N(A) is the number of events in the set $A\subset X$ introducing a random process. Since a random process have been considered, the analysis of patterns in terms of first-order (related to expected values) and second-order properties (related to the covariance) could be analyzed [6]. In the case of point pattern analysis, second-order properties are perhaps less informative [7] but are still important factor for the analysis of point patterns [8, 11]. First-order properties are described in terms of intensity $\lambda(\mathbf{s})$, of the process, which is the mean number of events per unit at the point **s** [6, 7, 11].

This is defined as $\lambda(s)=\lim_{ds\to 0}\left\{\frac{E(N(ds))}{|ds|}\right\}$, where d(**s**) is a small region around the point **s**, E(.) is the expected value, and N(d(**s**)) is the number of events in the small region. The second-order properties, of a spatial point process introduce the relationship between numbers of events in pairs of sub-regions as

$$\gamma(s_i, s_j)=\lim_{ds_i, ds_j\to 0}\left\{\frac{E\left(N(ds_i)N(ds_j)\right)}{|ds_i||ds_j|}\right\},$$

with similar notations. This is equivalent to saying $\lambda(s)\cong\lambda$ so that the expected number of events at an arbitrary location s is constant for all $s\in D$; and $\gamma(s_i,, s_j)\cong\gamma$ (d) so that the dependence between events at two arbitrary locations s_i and s_j depends only on the difference d.

A point process is stationary if the intensity is constant over A, so $\lambda(\mathbf{s})=\lambda$ and $\gamma(s_i,s_j)=\gamma(s_i-s_j)=\gamma(d)$ (depending only on direction and distance). Finally, the process is defined as isotropic if the second-order intensity depends only on the distance between s_i and s_j (does not depend on the direction).

The random model that will serve as our standard of comparison is the *Complete Spatial Randomness* (CSR) model [6, 7, 11, 12]. The CSR model has two basic characteristics: 1. the number of events in any planar region *A* is with area |*A*| follows a Poisson distribution with mean $\lambda|A|$. 2. given there are n events in A, those events are independent and form a random sample from a uniform distribution on A. The constant λ is the intensity, or the mean number of events per unit area. Also, by (1), the intensity of events does not vary over the plane. According to (2), CSR also implies the events are independent of each other and there is no interaction between them.

The mathematical construct that we will use to simulate a CSR model is the homogenous Poisson process. The Poisson process is suitably defined by the following postulates: 1. If $\lambda>0$, and any finite planar region A, N(A), follows a Poisson distribution with mean $\lambda|A|$. 2. Given N (A) =n, the n events in *A* form an independent random sample from the uniform distribution on A. (In our case, n is the number of trees in the region)

The importance of the CSR process lies in the fact that it is often used as a null hypothesis for testing a spatial point pattern. Under CSR, a spatial point pattern has no structure and thus failing to reject

such a hypothesis warrants no further examination of the data [7]. Thus, concluding a spatial point pattern is CSR implies uniformity of events ($E[N(A)] = \lambda|A|$) as well as independence ($cov[N(A),N(B)] = 0$ if $A \cap B = \varnothing$). It follows then that a test for CSR acts as a dividing hypothesis between regular and aggregated processes.

As stated above, the CSR corresponds to the homogenous Poisson distribution. Please recall that the Poisson distribution can be used in place of the Binomial distribution in the case of very large samples. In a binomial distribution, all eligible phenomena are studied, whereas in the Poisson distribution only the cases with a particular outcome are studied. The Poisson distribution can also be used to study how "events" are distributed on the level of a population. If having one "event" has no influence on the chance of having another accident, the "event" is put back into the population immediately after an "event"; people may have one, two, three, or more events during a certain period of time. One assumption in this application of the Poisson distribution is that the chance of having an event is randomly distributed: every individual has an equal chance. Mathematically, this is expressed in the fact that for a Poisson distribution, the variance of the sample is equal to its mean. Figure 4 illustrates simulated coordinated (x,y) of 100 points of a CSR process simulated on the unit square.

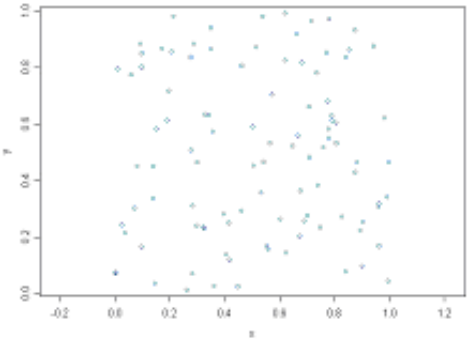

Figure 4. Simulated coordinated (x,y) of 100 points

One way to summarised the events in a spatial point pattern is to divide the regions into sub-regions of equal areas (quadrants). By counting the number of events inside each quadrant, we end with a measure (frequency or histogram) that summarizes the spatial pattern. The intensity of a point pattern is the mean number of points per unit area. Intensity plots display a smooth estimate of intensity for a spatial point pattern. One can see how dependent the visual display is on some of the options when one considers the intensity image via the binning method. Figure 5 illustrates two cases for simulating Poisson cluster process using different fraction of the area values.

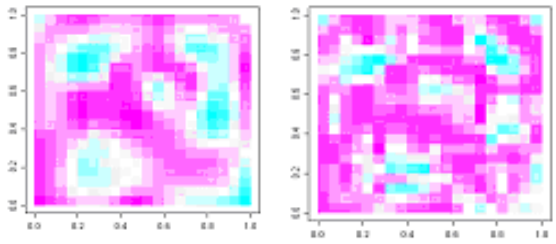

Figure 5. Simulation of a Poisson cluster process with different fractions of area values.

5. Intensity measures of Spatial point patterns

One major approach for point pattern analysis through the years has involved the physical distances between (neighbouring) points. The distance from the i^{th} event and the nearest other event is the most common basis for analysis in nearest neighbour methods. If the event-to-event nearest neighbour distances tend to be small (relative to what would be expected by chance under CSR), then there is evidence of clustering. Suppose we denote the random variable W to be a variable representing the event to event distance. The cumulative probability distribution of W is P(W =w) and estimated as $\hat{G}(w) = \frac{\#(Wi \le w)}{n}$, meaning that the probability of other inter-event distances less than or equal to w is estimated as $\hat{G}(w)$. The numerator of the right-hand side is the number of values of W less than or equal to the specific value W (hence the right hand fraction is the cumulative empirical probability).

A similar quantity to be considered is the event-point cumulative distribution. In this situation, m points are randomly chosen within the region and the distance H from points {1,…, m} to the nearest existing event is the random variable of interest. We look at $\hat{F}(h) = \frac{\#(Hi \le h)}{m}$ which is the number of event-point distances over all such points.

If we consider the random variable H with respect to CSR (and the associated spatial Poisson process with mean intensity of events per unit area as λ), we know that the number of events in any area a is distributed as Poisson (λa) so the probability of no events falling in a circle of radius d around the randomly chosen point is (from the Poisson model with mean per area of $\lambda\pi d^2$):

$$\frac{[(\lambda\pi d^2)^0\left(\exp\left[-\lambda\pi d^2\right]\right)}{0!} = \exp\left(\lambda\pi d^2\right)$$

By definition, F(d) = P(D = d), hence the probability of the distance being less than d is the complement of this probability, so F(d) = 1- exp(-$\lambda\pi d^2$). The quantity πd^2 is a random variable which follows an exponential distribution with parameter λ with $E(d)=\frac{1}{(2\sqrt{\lambda})}$ and $Var(d)=\frac{4-\pi}{4\lambda\pi}$.

We also take the same distributional form as H under CSR and hence the formulas are the same as given above and hence under CSR, a plot of $\hat{G}$ versus $\hat{F}$ should be approximately straight. For simulated data example the corresponding empirical distribution functions for the point to point and origin to point distances are given by Figure 6.

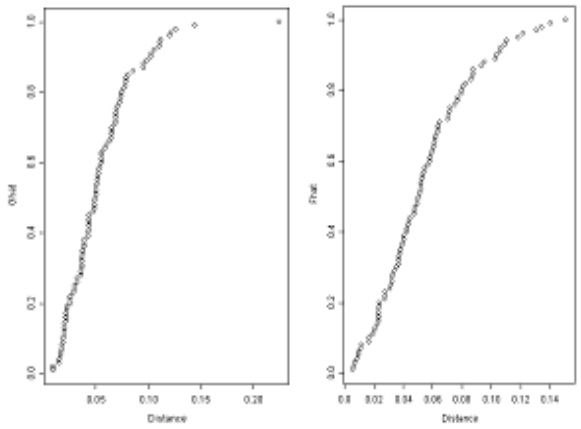

Figure 6. The $\hat{G}$ and $\hat{F}$ graphs for 100 simulated Poisson point data.

Note that the distance range is only up to 0.2, so the plots are not really increasing that quickly in probability with distance. As expected, the plot of $\hat{G}$ versus $\hat{F}$ is a straight line (Figure 7):

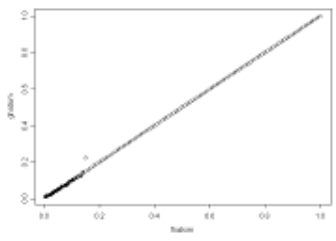

Figure 7. Plot $\hat{G}$ versus $\hat{F}$

For the eaurthquake data, Figure 8 iluustrates the corresponding empirical distribution functions for the point to point and origin to point distances

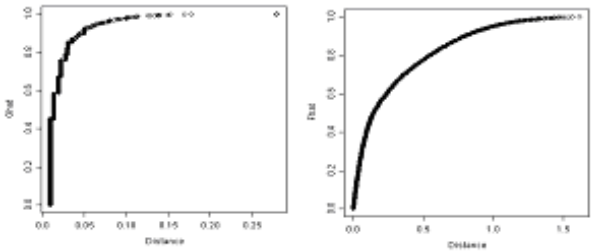

Figure 8. The $\hat{G}$ and $\hat{F}$ graphs for earthquake data.

Note that, the event-event EDF is probably more useful due to the irregular shape of the land. There won't be any points in some of the corners of the region, even with re-sizing to a square. The excess of short distances (i.e. most of the empirical probability has been used up before the distance is .05) suggests the short distances that we expected for the clustered events.

In the case of a point pattern, we are concerned with the *intensity*. *First order intensity* refers to the mean number of points per unit area. *Second order intensity* refers to the spatial relationship/dependence among the number of events in different areas of the region. The most basic is a simple point estimate which counts the number of points and divides by the total area. Units will be points/events per area so the ground scale becomes important. Other methods give local estimates and hence the intensity is likely to vary across the region.

The three most common techniques for estimating the first-order intensity $\lambda(s)$ are: 1. the **Basic estimator**, which assumes $\lambda(s) = \lambda$ for some constant λ; 2. the **Binning estimator**, which is simply a smoothed two-dimensional histogram; and 3. the **Kernel estimator** that employs methods from kernel density estimation to obtain an estimate of λs). Estimators of intensity over a study region A are given by:

$$Basic\ \hat{\lambda}=\frac{n}{|A|}$$

$$Binning\ \hat{\lambda}(s)=\sum_{j=1}^{bins}k\left(\frac{s-s_j}{b}\right)\sum_{j=1}^{n}\frac{I(s_i\in ds_j)}{|ds_j|}$$

$$Kernel\ \hat{\lambda}_b(s)=\frac{1}{p_b(s)}\sum_{i=1}^{n}k\left(\frac{s-s_j}{b}\right)$$

$I(\cdot)$ is an indicator function, $|ds_j|$ the size of the bin centered at s_j , $\kappa(\cdot)$ is a kernel function, and b is an bandwidth satisfying standard conditions [Scott, 1992], b is a bandwidth, and p_b is an edge-

correction factor given by $p_b(s)=\int_A \frac{1}{b^2} k\left(\frac{s-u}{b}\right)du$, $s \in A$. [6] provides details on the choice of $\kappa(\cdot)$ and suggestions for selecting the bandwidth b. A recommended choice for the bandwidth is $h=0.68n^{-0.2}$ [7].

Binning via nonparametric smoothing is a tool for intensity estimation. Rectangular bins are formed within the region. A moving window or 'span' is used to estimate the local intensity through the local nonparametric regression function loess. Figure 9, illustrates the binning smoothing technique with a bandwidth 20x20 (approximate 45 numbers of points).

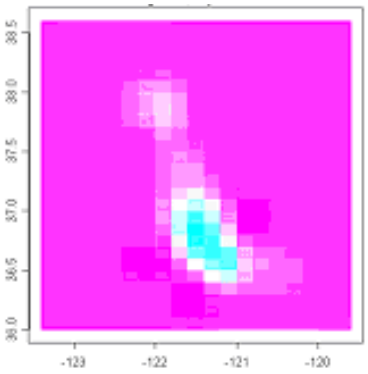

Figure 9. Binning smoothing with a bandwidth 20x20

With the concentrations of earthquakes in just two areas, changing the fraction of region would not accomplish much here visually. Widening the fraction will result in a much smoother/coarser image (Figure 10).

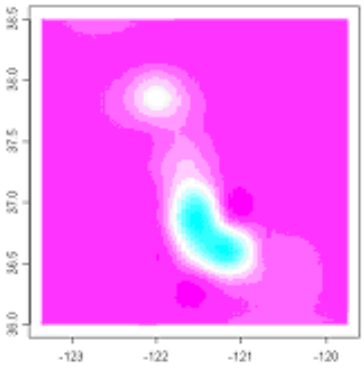

Figure 10. Binning smoothing

Figure 11, illustrates various images using kernel smoothings considering different bandwidth values.

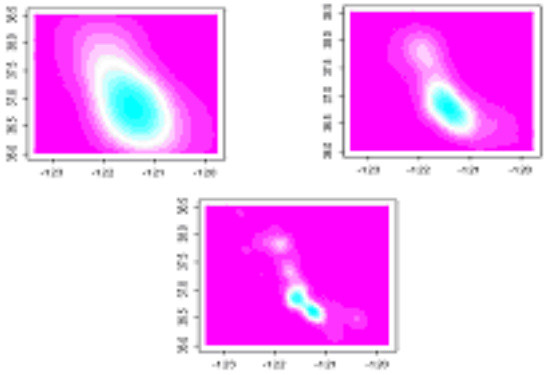

Figure 11. Kernel estimation using different bandwidth values

The choice of the bandwidth (d) is purely subjective. It is up to the researcher to investigate the results using several different bandwidths and selecting the one that best represents the pattern. However, it is important to remember that when d is large, the kernel estimator produces a smooth estimate of the density function (i.e. small variance, large bias). If d is small, the kernel estimator produces a rough estimate of the density function (i.e. large variance, small bias). Considering the results, it is clear that the data are clusters (introducing a cluster pattern) with two strong pattern concentrations.

Second order properties of a spatial point process are investigated further through Ripley's K-function [8]. It is a function that involves a form of quadrant counting and inter-event distances by

$K(d) = \lambda^{-1}E[$ number of points distance d of an arbitrary point$]$

Under CSR, the expected number of event locations within a distance d is $\lambda\pi d^2$ (where λ is the Poisson (intensity) parameter), so $K(d) = \pi d^2$. If there is clustering in the point pattern, we would expect an excess of points at short distances from another arbitrary point. This leads to $K(d) > \pi d^2$ for short distances. If there is more space than could be expected among points at short distances (eg. cyclic regularity, repulsion), then $K(d) < \pi d^2$.

Ripley's K is usually estimated as: $\hat{K}(d)=\frac{\sum\sum_{i\neq j} I_d(d_{ij}) / w_{ij}}{N^2 A}$ where: d_{ij} is the distance between the i-th and j-th observed event locations, which can be viewed as the radius of a circle centred at event point i and passing through j; w_{ij} is a weighting term equal to this circle's proportion of the entire area A For specific distance/lag value d,

$I_d(d_{ij})$ is an indicator function which is 1 if $d_{ij} = d$. The above estimate of K(d) is 'edge–corrected'. The weight w_{ij} accounts for the fact that an event j may not be in A given that it is a distance d_{ij} from the point i. A valuable investigation for a point pattern is a plot of $\hat{K}(d)$ versus πd^2. If $\hat{K}(d) > \pi d^2$ then there is evidence of clustering. Figure 12, represent the graph between Ripley K-function and theoretical one, where clearly there is evidence of clustering for earthquake data.

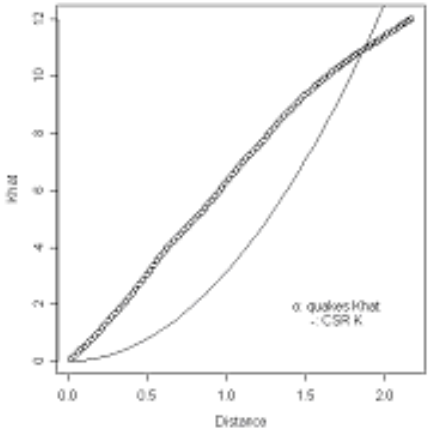

Figure 12. Graph between Ripley K-function and theoretical one

Another useful function to consider is $L(d) = \sqrt{K(d)/\pi}$. $\hat{L}$ can be plotted versus the 45 degree line to evaluate CSR (Figure 13)

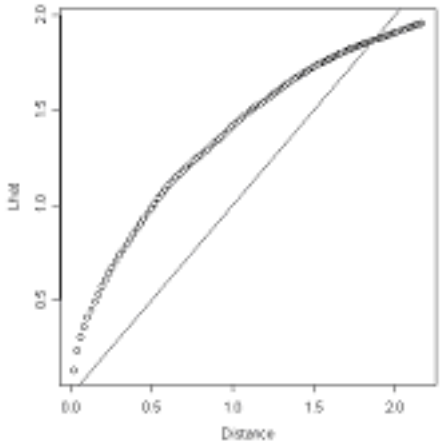

Figure 13. Graph between $\hat{L}$-function and theoretical one

[6] also refers to a more general K-function as the reduced second-order measure. If we assume the process is completely random then the extra number of events within a distance d will be uniform on a disc. From this we see that

$$K(d) = \int_0^{2\pi}\int_0^{d} \left\{ \lambda_2(x) \Big/ \lambda \right\} x\,dx\,d\theta = \frac{2\pi}{\lambda}\int_0^{d} \lambda_2(x)\,x\,dx$$

with $\lambda_2(d) = \dfrac{\lambda^2}{2\pi d}\dfrac{\partial K(d)}{\partial d}$

Several approaches for estimation and interpretation of the K-function are given by [6, 7]. However, it must be noted that K(d) is not unique for similar reasons that disallow identification of a distribution from only the first two moments. Different point processes can produce identical K-functions [14]. Furthermore, though the K-function is used to analyze second-order properties of a spatial point pattern, it cannot distinguish between deviations from CSR due to lack of uniformity or lack of independence of events. However, since K(d) is defined only for first-order stationary processes, uniformity is a requirement of K-function analysis. Under CSR, $\lambda_2(d) = \lambda^2$, $K(d)=\pi d^2$. Testing a point pattern for CSR can be accomplished by comparing the empirical K-function to πd^2. Quite often, inference is based on the L-function defined by $L(d) = \sqrt{K(d)/\pi} = d$ and a plot of L(d) − d versus h is obtained. Because the probability distribution of the K function (or the L-function) is intractable, inference about a process is based on simulated K-functions. An envelope is constructed by simulating the hypothesized point process B times and constructing the K-function for a set of distances d. For every simulation $(K_{min}(d), K_{max}(d))$ is stored. The upper and lower envelopes are then overlaid on the observed K-function $\hat{K}(d)$. Inference can be obtained by comparing the observed K-function to the simulated envelope. If $\hat{K}(d) > K_{sim}(d)$ then the number of events within a distance d of an arbitrary event is greater than expected under the hypothesized process. If the hypothesized process is CSR then this would imply an aggregated process if d is small or a regular process if h is large. Conversely, if $\hat{K}(d) < K_{sim}(d)$ then the number of events within a distance d of an arbitrary event is less than expected under the hypothesized process. Reversing our conclusion we would infer that the observed process is regular if d is small or aggregated if h is large. If $\hat{K}(d) > K_{sim}(d)$ or $\hat{K}(d) < K_{sim}(d)$, the hypothesis is rejected for that particular distance.

6. Conclusions

Statistics for spatial data is a rapidly growing field. Only recently has more methodology for analyzing spatial dependencies been proposed in the literature. However, there is more to be done.

Spatial statistics is a powerful tool, either for presentation of existing spatial phenomena like earthquakes, or investigating relationships between different locations of a particular event (earthquake) applying specific statistical technique. In this work, we have described how spatial point patterns can be represented statistically through first and second order properties. Extensive analysis of spatial point patterns has been illustrated using simulated and real earthquake data. Properties of spatial models are analyzed combined with spatial statistical techniques.

Kernel estimation was suggested as an appropriate method for prediction of mean intensities for earthquake data. The application of the weighted *K*-function to spatial background rate estimates for S-F seismicity shows the power of K(d) function in testing for goodness-of-fit. The K-function is easily able to detect the major departures from the data for simple kernel or Poisson estimates of the spatial distribution of earthquakes.

However, further research is needed in order to identify what types geological or tectonic features may be most important for an accurate modeling of earthquake occurrences as a point process.

Reference:

1. Choi E. and Hall P. (1999): Nonparametric approach to analysis of space-time data on earthquake occurrences, *Journal of Computational and Graphical Statistics*, 8: 733-748.

2. Ogata Y. (1999): Seismicity analysis through point-process modeling: a review, *Pure and Applied Geophysics, 155: 471-507.*

3. Zhuang, J., Y. Ogata, and D. Vere-Jones (2002): "Stochastic declustering of space-time earthquake occurrences," *Journal of American Statistical Association*, 97(458), 369–380.

4. Zhuang, J., Y. Ogata, AND D. Vere-Jones (2004): Analyzing earthquake clustering features by using stochastic reconstruction, *Journal of Geophysical Research*, 109, B05301, doi:10.1029/2003JB002879.

5. Zhuang, J., Y. Ogata, AND D. Vere-Jones (2005): Diagnostic Analysis of Space-Time Branching Processes for Earthquakes, in *Case Studies in Spatial Point Process Modeling*, ed. by A. Baddeley, P. Gregori, J. Mateu, R. Stoica, and D. Stoyan, vol. 185 of *Lecture Notes in Statistics*, pp. 275–292. Springer.

6. Cressie, Noel A. (1993): "Statistics for Spatial Data (revised edition)", John Wiley & Sons.

7. Diggle, Peter J (2003): "Spatial Analysis of Spatial Point Patterns", 2nd Edition, Arnold Publishers.

8. Ripley B.D. (1981): Spatial Statistics, N.Y. John Wiley and Sons

9. Dale, Mark R. T. (1999): "Spatial Pattern Analysis in Plant Ecology", Cambridge University Press.

10. Stoyan, Dietrich, and Helga Stoyan (1994): "Fractals, Random Shapes and Point Fields (Methods of Geometrical Statistics)", John Wiley & Sons.

11. Upton, Graham J.G., and Bernard Fingleton (1985): "Spatial Data Analysis by Example (Point Pattern and Quantitative Data)", volume 1, John Wiley & Sons.

12. Daley and Vere-Jones (1988): An introduction to the Theory of point processes, Springer-Verlag, N.Y.

13. Bailey T.C. and Catrell A.C. (1992): Interactive spatial data analysis, London, Longman Scientific and Technical.

14. Baddeley A.J. and Silverman B.W (1984): A cautionary example of the use of second order methods for analyzing point patterns, Biometrics, 40, 1089-1093.

Annual energetic behavior of buildings and the typical meteorological year

IOLANDA COLDA
FLORINELA ARDELEAN
VIOREL PETREHUS
LIDIA NICULITA
Faculty of Installations
Technical University of Civil Engineering Bucharest
B-dul Lacul Tei nr. 124, sector 2
ROMANIA
iolcolda@yahoo.fr; http://www.utcb.ro/
ardelean@333.org; http://www.utcb.ro/
vpetrehus@yahoo.com; http://www.utcb.ro/
niculita@gmail.com; http://www.utcb.ro/

Abstract: - Assuring interior comfort in the attempt to realize an energy economy is a task, without which, the design of a new modern building is not even conceivable. The climate factors have a big influence on the energy consumptions of buildings. The annual variations have determined the necessity for creating a typical meteorological year for different zones [1], [2], [3]. With this data base and using a specific software (CoDyBa) [8], a simulation was realized regarding the energy necessary for heating and cooling (air-conditioning) of buildings situated in four important cities in Romania (including the capital).

Key-Words: - Energy, building, thermal comfort, air-conditioning, typical meteorological year (TMY), simulation.

1 Introduction

Buildings are an important energy consumer because of specific functions of maintaining thermal comfort and interior air quality. From a thermal point of view, a building is a tried entity on one side from the exterior by meteorological factors and on the other side, from the interior, by heat and humidity generating sources (people, light, equipment), which are variable in time. So, the energy consumption of the building at one moment depends on the values of meteorological parameters and interior demands. But, in order to make a prognosis of energy consumption, climate factors, resulted in statistic processing of meteorological data, are required.

So, through national approaches done in a building energy economic direction, a data base with climatic data, for major cities in the country, covering it's entire geographical area, was established. In this paper, the action realized by us, in our goal to create a national climatic data base, is synthetically presented, as well as an application for it's use in a building's energetic behavior, the building being situated in 4 different locations in Romania.

2 The climatic data base development

A typical meteorological year (TMY) is a collation of selected weather data for a specific location, generated from a data bank much longer than a year in duration. It is specially selected so that it „showcases" the range of weather phenomena for the location in question: normal conditions, the coldest typical conditions, the hottest typical conditions, the strongest rainfall, etc. Through this, a meteorological parameters (timetables, year average values, long term average values) calculation for the specific location chosen for analysis, can be done.

The typical meteorological year (TMY) was invented in Sandia laboratories and the construction method was later modified [1], [2] for an optimization of the importance of environment indexes, so a preferred selection of the months which form a typical meteorological year, can be done, with the measurement of solar radiation, and the study of missing data. The method used in different European countries, for establishing a typical year, method we used in this research is standardized in [3].

The construction of a typical meteorological year, needs choosing of main characteristics, which can

be followed through hour values at least for 10 years, like temperature, humidity, solar radiation, pressure, wind speed etc. In order to keep as many correlations between different meteorological indexes, as possible, in the typical year, time portions of real years are inserted. The standard portion of a real year taken in a typical year is the month.

The construction is done in two stages:

A. In the first stage, for every month of the typical year, a typical month is chosen based on meteorological data, recorded in several real years. For example, a typical January will be a real January from the observation years taken into account.

B. In the second stage, the data between two typical months (which can be from two different years) are adjusted, in order to do a smooth transition between months. There are a lot of smoothing variants, like, for an example, a local mediation with Gaussian variables or interpolation with cubic spline functions [6].

The construction of a standard meteorological year is done in order for the average values, the frequency distribution and the correlations between different meteorological characteristics to maintain as well as possible. For a certain meteorological parameter, identified with "p", choosing of a typical month is done using the following algorithm:

1. Daily averages are created based on the same parameter's time values, measured in that exact month, for a period of 10 years.

2. The cumulative empiric probability function $\mathrm{CDF}_{\mathrm{L,A,p}}$ is built for daily averages of the climatic parameter p in question, calculated for that month, for every year (L-index for month, A for year, p is the climatic parameter: temperature, humidity etc.). The calculating formula is (1):

$$CDF_{L,A,p}(t)=\frac{no.of.average\ values\le t,\ for\ p\ in\ month\ \ L\ from\ year\ A}{1+tot.no.of\ average\ values.for\ p.in\ month\ \ L\ from\ year\ A} \quad (1)$$

3. The cumulative probability function $\mathrm{CDF}_{\mathrm{L,p}}$ is built for daily averages of the climatic parameter, based on daily averages of the month in question from all the years taken into account, using the formula (2):

$$CDF_{L,p}(t)=\frac{no.of.average\ values\le t,\ for\ p\ in\ month\ \ L\ from\ all\ the\ years}{1+tot.no.of\ average\ val.for\ p.in\ \ month\ \ L\ from\ all\ the\ years} \quad (2)$$

Like $\mathrm{CDF}_{\mathrm{L,A,p}}$, this function is also bounded, increasing from 0 to 1.

4. For the considered L month, the Finkelstein-Schafer statistics $\mathrm{FS}\left(\mathrm{CDF}_{\mathrm{L,A,p}},\mathrm{CDF}_{\mathrm{L,p}}\right)$ is calculated as in [3], [4] :

$$\mathrm{FS}\left(\mathrm{CDF}_{\mathrm{L,A,p}},\mathrm{CDF}_{\mathrm{L,p}}\right)=\frac{\sum_{\mathrm{i}}|\,\mathrm{CDF}_{\mathrm{L,A,p}}(\mathrm{p_i})-\mathrm{CDF}_{\mathrm{L,p}}(\mathrm{p_i})\,|}{\mathrm{n}} \quad (3)$$

where p_i is the average value of the parameter p in the day i from the month L in question and n is the number of days in that month.

Basically, a typical month L is chosen from the year A, for which the Finkelstein-Schafer statistics is minimal. This expresses the fact that from the chosen statistic climatic parameter's point of view, the information supplied by the data in the chosen month from the year A are best approaching the information supplied by measurements taken in all the years of observation from that specific month.

In case a typical year is built from more climatic parameter's points of view, we have to take in mind every p parameter. In [3] it is recommended that, after the steps 1-4 above for all A years, L months and p parameters, to order the years according to increasing values of $FS\left(CDF_{L,A,p},CDF_{L,p}\right)$ for given L and p, and to give a value to the year A $r_{LAp}=the\ rank\ of\ A\ year\ in\ the\ enumeration\ above$ and to calculate $\mathrm{D_{LA}}=\sum_{\mathrm{p}}\mathrm{r_{LAp}}$. The procedure is different from the one recommended for TMY [2], where the following formula is used $\mathrm{D_{LA}}=\sum_{\mathrm{w_p}}\mathrm{w_p}\mathrm{FS}\left(\mathrm{CDF}_{\mathrm{L,A,p}},\mathrm{CDF}_{\mathrm{L,p}}\right)$, with the weights w_p associated to every parameter, based on the importance given to that meteorological parameter.

Mainly, the month of reference for the L calendar month is the month for which D_{LA} is minimum. But the standard also stated that we have to notice, in the

secondary, another meteorological characteristic, wind speed, in the following manner:

a) For every L calendar month, the months from the first three years are taken, ordered from small to large after D_{LA}.

b) For every L month from the three months, the difference modules between the average wind speed for L month from that specific year and the average speed calculated for L month from all the years. As a typical L month, the month from these three years with the smallest difference is chosen.

The meteorological characteristics used by us were: temperature, dew point temperature, relative humidity, absolute humidity, direct radiation, diffuse solar radiation, and in the secondary, wind speed.

After choosing a typical month for every calendar month, we skip to the second stage, because the typical months might be from different years, and, so, it is a possibility for some discontinuities to appear between the considered climate parametric values. The second stage consists of smoothing the transition on the basis of the at least 8 hours measured observations starting from the moment of passing from one month to another [1].

The practical calculation of a typical meteorological year was done in Scilab, the dates being available under the form of text files, which had on the columns: the year, the month, the day, hour, characteristic 1, characteristic 2,…, for 10 years, the date of 29th of February being eliminated from the bisect years and the typical year was given under the form of a text file like in the entry dates, for 365 days.

As an example, with hour meteorological data for the city of Constanta, from 1991 to 2000, the typical year using the TMY2 method and the ISO standard 15927-4/2005 was built. The meteorological characteristics used were the ones mentioned above. The values used in the TMY2 method were wFS=[0.4, 0.2, 0.1, 0.05, 0.05, 0.05, 0.05]. In the tables and graphics that follow you can easily see, by comparison, the differences between the two methods of calculation for typical years.

Years from which typical months are in table 1.

Month	TMY	ISO 15927-4/2005
Jan.	1995.00	1991.00
Feb.	1994.00	1998.00
Mar.	1997.00	1995.00
Apr.	1991.00	1991.00
May	1999.00	1999.00
Jun.	1997.00	1991.00
Jul.	2000.00	1991.00
Aug.	1999.00	1996.00
Sep.	1995.00	1995.00
Oct.	2000.00	1999.00
Nov.	1997.00	1992.00
Dec.	1997.00	1995.00

Table 1 Typical months and convenient years

In figures 1, 2, 3, 4 a comparison is made between the values of some meteorological parameters from the typical years built with the two methods and the data for the year 2000.

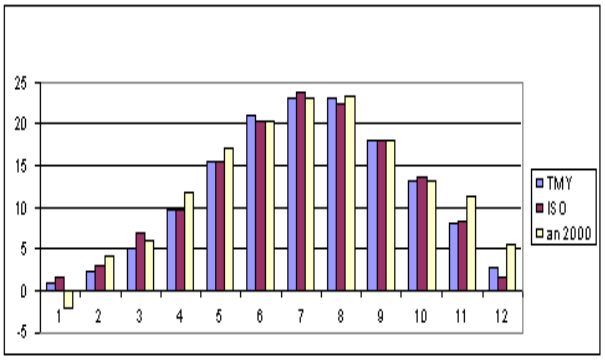

Fig. 1 Average monthly temperatures

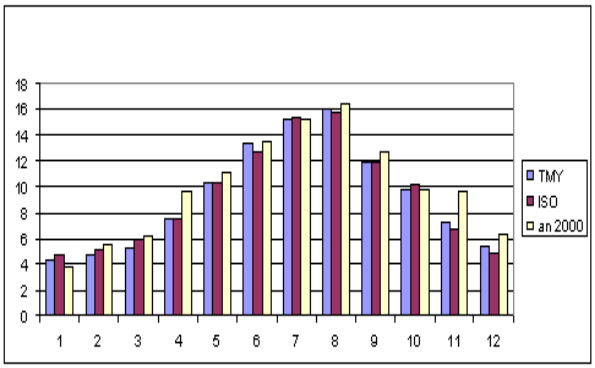

Fig. 2 Absolute humidity in average months

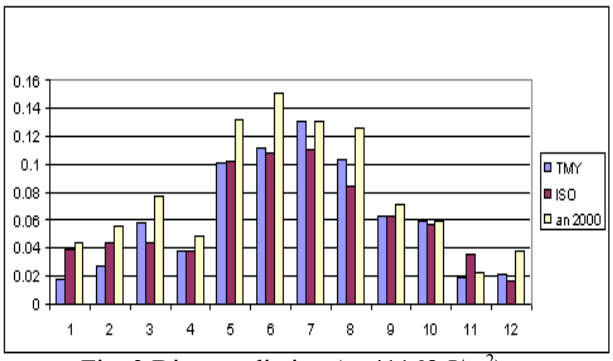

Fig. 3 Direct radiation (x 41168 J/m^2)

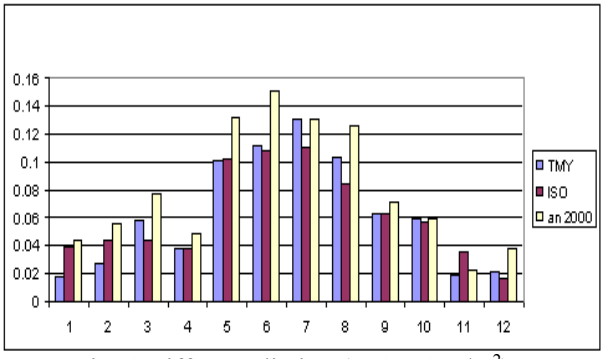

Fig. 4 Diffuse radiation (x 41168 J/m^2)

You can see that, although only April, May and September come from the same calendar year for the two typical years, the differences concerning the average temperature, absolute humidity and dispersed glare aren't that high.
Through the collaboration with the National Meteorological Administration, typical years were created using the ISO 15927-4/1005, method for all the cities, which are state capitals (department) and for the Romanian capital, Bucharest.

3 The simulation of the energy need for heating and cooling of buildings.

3.1 Importance of the climate data for the main issues of buildings energy

The existence of climatic data allows the calculation of building energy consumption, with the purpose of:

- choosing the most advantageous solution from an energetic point of view, of the building's envelope (thermal isolation, window coverage, solar protection),
- choosing the solution for supplying a building with heating, ventilating and air-conditioning equipment,
- adopting some systems, which use, in an economical way, regenerative energy sources,
- establishing the working strategy of energy systems within the endowment of buildings (automatic tuning, nocturnal over ventilation, reducing or interrupting heating/cooling systems when the building is not occupied etc)
- establishing the possibility of avoiding air-conditioning during the summer.

Such studies are required for the conception of new, economical buildings, as well as establishing economical solutions for thermal rehabilitation.

3.2 Simulation conditions in the present study

In this publication, on the basis of processed climatic data, a study has been realized, referring to energy consumption for heating and air-conditioning an office area from a building placed in 4 major cities, from different geographic areas: Bucharest (capital), Iasi (East), Timisoara (West), Cluj (center). The analyzed building area has a 1000 sq. meters (m^2), with a South oriented wall, of 320 sq. meters (m^2), windowed in a proportion of 40 %, a 32 sq. meters (m^2) East wall and the terrace. The building is occupied for 10 hours/day by 50 people. The interior calculation temperatures were 20^{0}C for heating and 26^{0}C for cooling. The air flow for ventilation was considered to be at a rate of 0.5 changes/hour. The ventilating and cooling are realized only in the period when the building is occupied; heating is reduced during the night, at a temperature level of 10^{0}C.
The introduced climate parameters were : the outside air's temperature and relative humidity, direct and diffuse solar radiation on a horizontal surface, the calculated solar azimuth and height angles, the air temperature and wind speed. In fig.5 the hour variation of exterior temperature is presented, calculated for winter time, for the four cities.

3.3 Results

Some of the results are presented as follows: in figure 6 the energy necessary variation for heating is presented, for a 300 hour period from January. Although in the calculations, the effect of solar radiation was taken into consideration, because the degree of solar radiation is some what reduced because of the high coverage degree of the sky (

different for every city), you can observe that the influence of outside air temperature is directly reflected in the heat necessary.

For the summer period, in figure 7, the energy necessary variation for cooling of the building is presented.
Based on the hour energy necessary, the annual energy necessary has been calculated for heating and cooling.

These values represent very important indicators for evaluating different closing solutions of the envelope of the building, conception of new buildings, as well as thermal rehabilitation phases when solutions need evaluating from an economic point of view and establishing the damping time of the investment. The results are presented in figure 8. The differences in energy necessaries reflect the differences between climatic parameters characteristic to every zone, because the simulated building was identical in all 4 locations.

For realizing the simulations, the CoDyBa [9] software was used, established on an analog thermo-electric pattern. The program evaluates the heat transfer through the building , in a dynamic regime and establishes, based on the interior-exterior thermal balance, the power sources needed for heating/cooling. The conception of the program allows input of specific climate data, thermal characteristics of the building's envelope's elements, the usage timetable and the suitable heat sources, as well as usage scenarios of different heating, ventilating and air-conditioning systems.

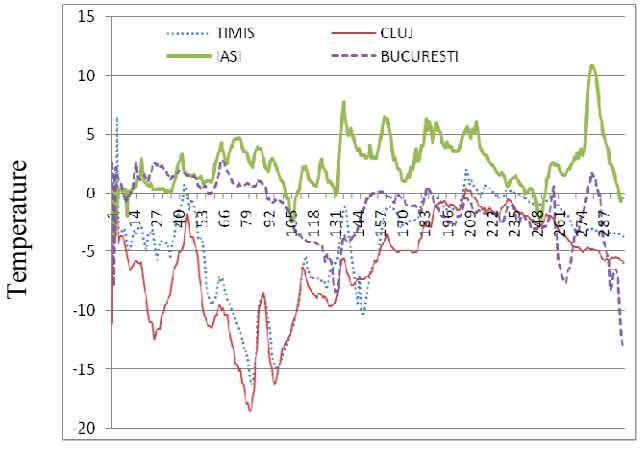

Fig 5 Exterior temperature variation for a simulation period in winter.

The simulations were done with an hour time step, during the entire calculation year.

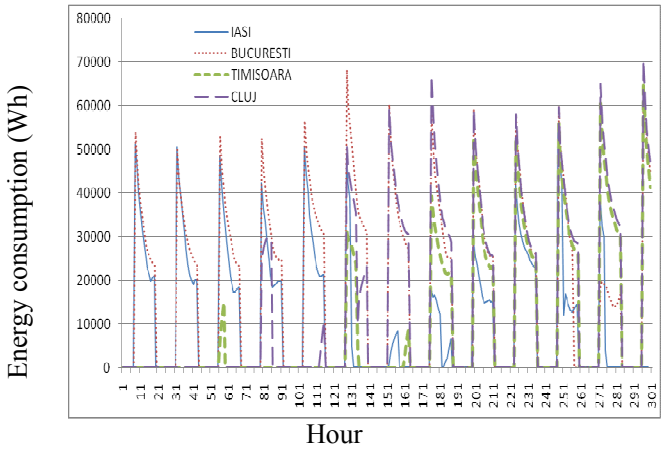

Fig. 6 The hour energy requirement for heating in a simulation period in January

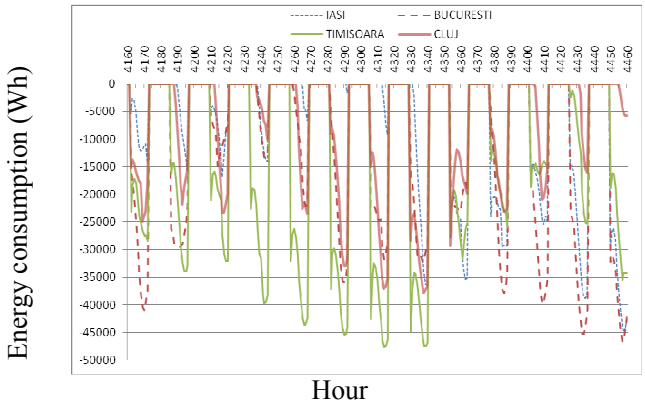

Fig. 7 The hour energy requirement for cooling for a simulation period in June

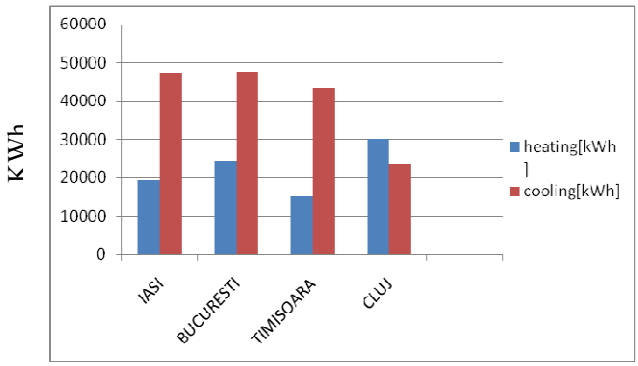

Fig. 8 The annual energy consumption for cooling and heating

4 Conclusion

- The climate factors have a big influence on the coupled system building – installation, as well as in establishing energy consumptions from the installations from within a building.
- Building a typical meteorological year is important for a certain location, as the climate factors vary from one year to another, where a building is going to be built or where a modernization of an existing one is taking place, even when a regenerative energy source is used.
- The data in the TMY can be used in the thermal and energy behavior simulation of buildings, in an estimate of necessary energy resources for heating and cooling the building. Also, it can be used for the calculation of economic solar energy systems, realized by usage of regenerative systems, especially of solar, thermal or photovoltaic energy systems. Therefore, the possibility of realizing a comparison in economic and environment protection terms, between different energy sources, exists.
- An example of a simulation program, which requires TMY type data is CoDyBa, with whom you can make evaluations of the required energy for buildings, necessary which must be provided by installation systems. Using such a program, you can give a qualified answer to different problems summoned by energy consumption in new buildings as well as buildings in rehabilitation process.

References:

[1] I. Hall, R. Prairie, H. Anderson, E. Boes, *Generation of Typical Meteorological Years for 26 SOLMET Stations*, SAND78-1601. Albuquerque, NM: Sandia National Laboratories, 1978

[2] William Marion, Ken Urban, *User's Manual for TMY2s Typical Meteorological Years*, National Renewable Energy Laboratory, Golden, Colorado, 1995

[3] ISO 15927-4/2005 – *Calcul et présentation des données climatiques*

[4] J.M. Finkelstein, R.E. Schafer, *Improved Goodness-of-Fit Tests*, Biometrika, 58(3), 1971, pp. 641-645

[5] Iolanda Colda, Florinela Ardelean, *Meteorology and climatology*, Conspress, Bucharest, 2004

[6] Viorel Petrehuş, Florinela Ardelean, *An analytic approach of climate parameters variation whichform the typical meteorological year*, The Efficiency, Comfort, The conservation of energy and Environment Protection Conference, Faculty of Installations, Bucharest, 2006

[7] Florinela Ardelean, Viorel Petrehuş, Iolanda Colda, *Theoretical considerations regarding the typical meteorological year*, The Efficiency, Comfort, The conservation of energy and Environment Protection Conference, Faculty of Installations

[8] CoDyBa software – INSA Lyon, 2008 version.

[9] M. Slavu, L. Serres, J. Miriel, I. Colda, *Simulation thermique et hydraulique d'une installation de chauffage a eau. Validation experimentale du modele numerique d'un robinet thermostatique de radiateur,* VII-ème Colloque Interuniversitaire Franco-Québécois, Saint Malo (France), 2005

[10] C. Teodosiu, I. Colda, C.Lungu, A. Damian, *Simulation of HVAC Systems Energy Consumption*, International Symposium on Environment Identities and Mediteranean Area, Corte-Ajaccio, IEEE France, 2006

[11] A.Damian, I. Colda, C. Teodosiu, *Modelling an air conditioning plant within the TRNSYS environment*, Scientific Bulletin of University Politehnica of Bucharest, vol 69, nr 4, 2007

[12] I.Colda, A. Damian, C. Teodosiu, *Calculation of the energy efficiency of ventilated and air-conditioned buildings*, REHVA World Congress Clima 2007 „WellBeing Indoors", Helsinki, Finlanda; 10-14 june 2007

[13] Akasaka, H., Nimiya, H., Soga, K., Matsumoto, S., Emura, K., Miki, N., Emura, E. and Takemasa, K. *Development of expanded AMeDAS weather data for building energy calculation in Japan*. *ASHRAE Trans.*, 2000, 106, 455–465.

[14] Targo Kalameesa, Jarek Kurnitskib, *Estonian test reference year for energy calculations,* Proc. Estonian Acad. Sci. Eng., 2006, 12, 1, 40–58

[15] V. Petrehuş, I. Armeanu, *On the construction of the typical meteorological year*, International Conference "Trends and Challenges in Applied Mathematics", ICTCAM 2007, UTCB, Bucureşti, 2007

Geological risk assessment of the area around the Tito Bustillo Prehistoric Cave. Human Heritage (UNESCO, 2008). Asturias, North of Spain

A. FOYO, M.A. SÁNCHEZ, C. TOMILLO & E. IRIARTE
Applied Geology Group. Dpt. of Ground and Materials Sciences
Civil Engineering School
University of Cantabria
Avda. de Los Castros, s/n. 39005 Santander.
SPAIN
foyoa@unican.es

Abstract: - The massif of Ardines is an uplifted wave-cut platform developed over Upper Carboniferous limestones, and contains the Tito Bustillo and La Lloseta caves, two important prehistoric cave sites. The main geomorphological features are controlled by the structural pattern: sinkholes are aligned along fractures and they have an oval morphology and the San Miguel river valley flows parallel to the El Carmen-Collera fault. The geological and geomorphological characterization has been used as the basis for the protection area definition. The Natural Risk Index, NRI, has been used for determining the geological risk level in different zones of the study area and to propose the protection area in order to prevent and mitigate the level risk and to protect the cave and the rock mass containing it. The main geological risk affecting the Tito Bustillo cave is located in the blind valley of the San Miguel river, sinking into the cave it provoke the leakage of the farm activity products throughout the cave galleries. Furthermore, many sinkholes which they are other evident absorption zone of the karstic system, are included in the protection area. This method results significant for geological risk assessment and engineering geology, because it can be used in the planning and development of engineering works near of prehistoric caves, and it also can act as a useful tool for land uses management.

Key-Words: geological risk assessment, protection areas, prehistoric caves, Natural Risk Index

1 Introduction

In addition to the usually conservation works carried out around the Human Heritage monuments, the studies concerning to develop methods to prevent damage are whenever more necessary [1]. The geological risk assessment, as the provided in this study for Tito Bustillo prehistoric cave, can act as a useful tool in damage protection.

Nevertheless, in the karstic areas they are many difficulties to the geological risk evaluation, due to the multiple factors that can have an influence in its protection. Consequently, get a strategy that provides flexibility to adjust specific methods according to the conditions of the different regions is recommendable [2].

A method for geological risk assessment must be based on a detailed knowledge of the geological features in the area around and within the cave, since they are different geological processes that could affect the cave conservation. On the other hand, will must be defined, a protection area to restrict and even forbid such human activities which can modify the natural evolution of the geological process.

The Tito Bustillo prehistoric cave is located in the massif of Ardines, a calcareous hill near the Ribadesella village, in the Asturias province, North of Spain (Fig. 1). The cave is included in a karstic complex composed of three main cavities, Tito Bustillo, La Lloseta and La Cuevona caves, which they contain excellent samples of parietal art and several archaeological sites.

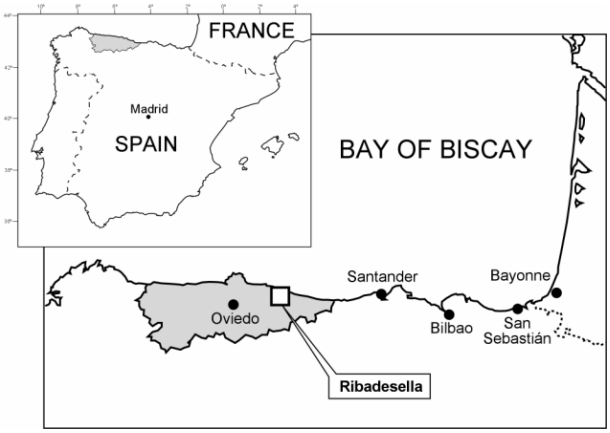

Figure 1. Location map of the Ribadesella village. Asturias, Spain.

The main geological processes affecting the cave, which suppose a risk, they are: the possibility of rock falls within the cave, the landslides and the periodical floods caused by the San Miguel river, and the contaminated water infiltration throughout the sinkholes. Furthermore, the leakage of farm residual toward the cave, must be always taken into account.

2 Geological environment

The Ardines massif is composed by Carboniferous limestones which pass to a formation composed by a succession of sandstones and mudstones through a mechanical contact, the Carmen-Collera thrust fault (Fig. 2). The massif is bordered to the north by the San Pedro river sediments and beach sediments. To the east it limits with the fluvial sediments of the Sella river estuary.

The structural pattern controls the presence and orientation of many geomorphological features [3], e.g. the San Miguel river valley is controlled and flows parallel to the El Carmen-Collera fault, even through the karst of the Ardines massif.

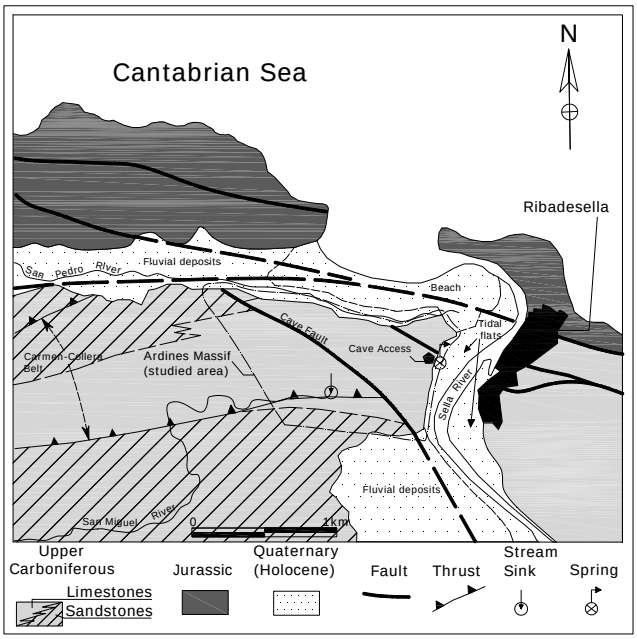

Figure 2. Geological context of the Tito Bustillo prehistoric cave.

These structural pattern controls the presence and orientation of many geomorphological features [3], e.g. the San Miguel river valley is controlled and flows parallel to the El Carmen-Collera thrust fault like this through the karst of the Ardines massif.

Finally, the hercinian main thrust faults structures, are compartmented by three fault sets (Fig. 3) related with the last Alpine orogeny.

3 Geomorphological features

The Ardines massif shows some different geomorphological environments and forms:

1) The uplifted wave-cut littoral platforms are present along the Asturian coast [4], related with the Flandrian transgression sea. The plane surface of the Ardines massif is a typical example. The northern limit of the massif corresponds to a paleocliff that today limits the San Pedro river valley.

2) Karstic, exokarstic and endokarstic features, are the most abundant geomorphological forms in the massif. Their formation is controlled by the structural features zones that act as main fluid-flow pathways. The most common exokarstic features are the sinkholes. They are oval and reach to about 50 m in width and appear aligned along fracture zones. The endokarstic system, with more than 1.500 m long complex karstic network, has two main manifestations, the Tito Bustillo and La Lloseta caves.

3) Finally, fluvial features, as flood plains and terraces, are present in the limits of the massif related to the presence of many fluvial systems: the San Pedro river in the north, the Sella river in the east and the San Miguel river in the southeast, the latter penetrates into the karstic system and flows through the Tito Bustillo cave (Fig. 3).

4 Determination of the NRI index

The Natural Risk Index determination, NRI geological risk, is based on the evaluation of nine parameters which are empirical rated from zero to 10, in agreement with the particularities of the studied area and according to the criteria exposed in [5]. The expression used to estimate the NRI index is:

$$NRI = \frac{P \cdot (0.1 \cdot S \cdot Ed + 2 \cdot Pt + W + Sp + 2 \cdot Ls + 2 \cdot Sd + 2 \cdot Ps)}{110} \quad (1)$$

where:

P, proximity, is the minimum distance between the study zone and the picture gallery into the cave.
S, slope angles, and *Ed*, elevation difference, contemplate the possibility of landslides and consequently are evaluated together.
Pt, position, reflects the influence of geological processes or structures on the cave based on its location.
W, weathering, expresses the degree of weathering using the recommendations exposed in [6].
Sp, seepage, take into account water flow from the analysed zone toward the cave.

Ls, landslide, estimates the presence and type of landslide affecting the zone.
Sd, are the structural discontinuities, considers the possibility that a landslide affects to a structural discontinuity, which determine and control the cave morphology.
Ps, proximity structures, take into account the distance between the actual geological processes and the discontinuity considered.

studied area. As a result, they have been adjusted with a value of two. Slope angle and elevation difference are evaluated together and their contribution is corrected by a decimal number, 0.1.

Considering a hypothetically extreme situation, the total value of the numerator will be 1.100.

Usually, the rank values without units of a security index in Engineering Geology must be from one to 10, consequently, the denominator of the NRI expression take de value of 110.

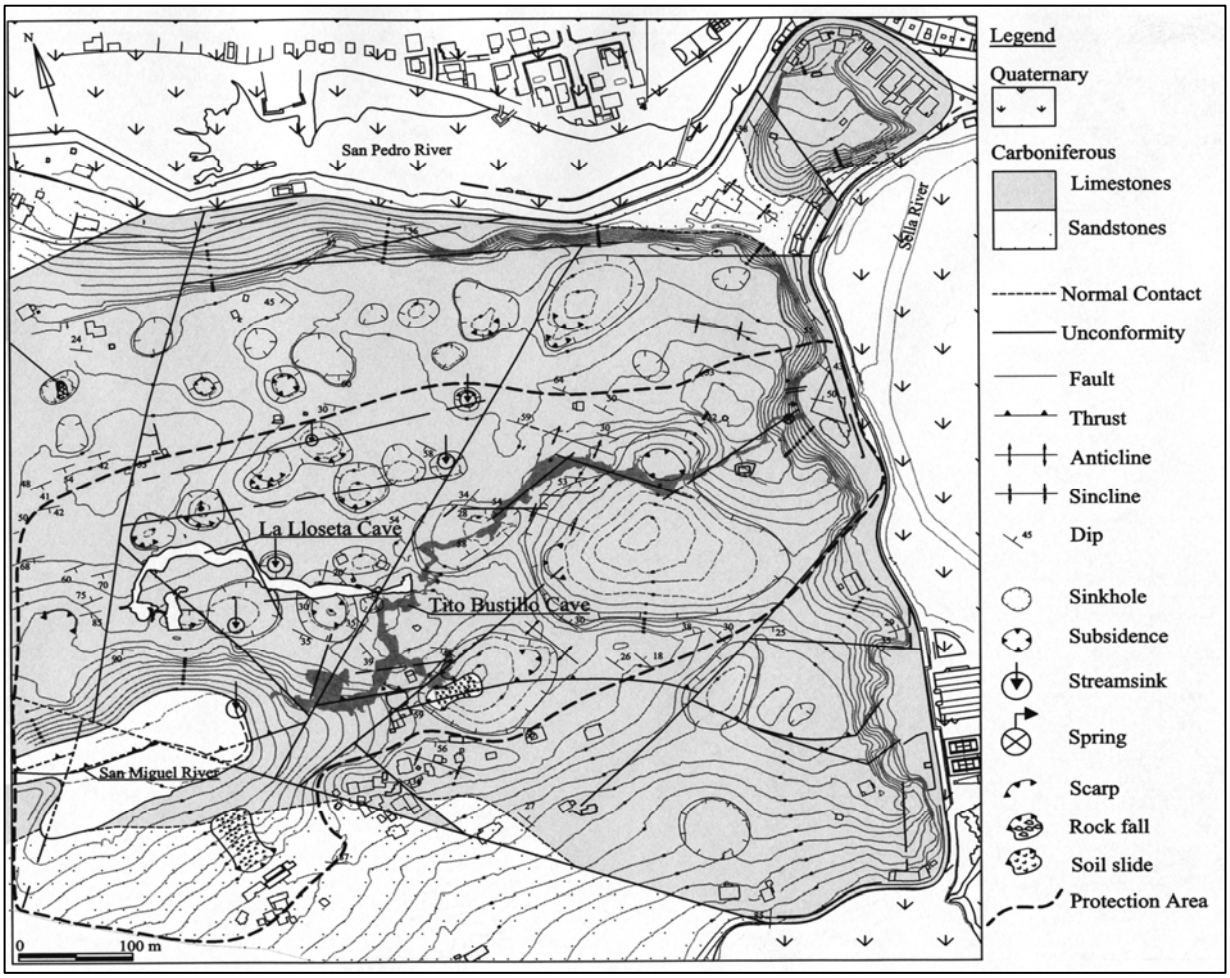

Figure 3. Geological Map around the Tito Bustillo Cave and Protection Area.

According to this proposal, the risk level will be very high when a zone located above the cave can suffer a rock fall, because the slope angle and the elevation difference are high or water could drain toward the cave through a fault which defines a gallery of the cavity and the weathering degree is high. The NRI value could decrease if this zone has the same characteristics, but is far away of the cave.

The NRI has been developed in an empirical way in order to evaluate the significance of each parameter in the geological risk. Position, landslide and structural discontinuities are the most important parameters concerning the geological risk in the

The risk level is expressed as a numerical value which also is classified in a category, Table I, and indicates the risk level related to geological processes without direct human intervention, affecting at well-defined point or zone of the study area around the Tito Bustillo Cave.

	NATURAL RISK INDEX "NRI"			
	0-2	**3-5**	**6-8**	**9-10**
RISK LEVEL	LOW	MEDIUM	HIGH	VERY HIGH

Table 1. Risk levels based on the NRI value.

5 Conclusions

The proposed methodology permit:

a) Taken into account the previous analysis of the geological and geomorphological characteristics, the geological processes which are actives in the studied zone, can be checking.

b) The Protection Area based on the geological risk assessment can be defined. This area will imply the restriction of any activity that can directly or indirectly modify the natural evolution of geological processes and therefore increase the risk level therein.

c) It is useful for geological risk assessment around the prehistoric caves and could be also applied for natural or historical monuments.

Acknowledgments

The authors are grateful to the Government of Asturias Principate, Spain, for their cooperation in the development of this investigation.

References:

[1] Catani, F., Fanti, R., & Moreti, S.,. Geomorphologic Risk Assessment for Cultural Heritage Conservation. Applied Geomorphology: theory and practice. Edit. by R.J. Allison. John Wiley & Sons, LTD. West Sussex, England. 2002 480 pp

[2] IGME, 1986. Mapa y memoria explicativa de la Hoja 31 (Ribadesella) del Mapa Geológico de España a escala 1:50.000 (2º Serie). IGME, Madrid.

[3] Alberto Foyo, Juan L. Suárez, Carmen Tomillo, Miguel A. Sánchez, Análisis previo de la relación entre la estructura geológica y el desarrollo del modelado cárstico en el Macizo de Ardines, Ribadsella, Asturias. Primer Symposium Internacional de Arte Prehistórico de Ribadesella. Edición Rodrigo Balbín y Primitiva Bueno. 2003, Asturias, España, pp. 153-160.

[4] J. Alvarez-Marrón, R. Hetzel, S. Niedermann, R. Menéndez, J. Marquínez, Origin, structure and exposure history of a wave-cut platform more than 1 Ma in age at the coast of norther Spain: A multiple cosmogenic nuclide approach. *Geomorphology*, 93, 2008, pp 316-334

[5] Miguel A. Sánchez Alberto Foyo, Carmen Tomillo, & Eneko Iriarte, Geological risk assessment of the area surrounding Altamira Cave: A proposed Natural Risk Index and Safety Factor for protection of prehistoric caves. *Engineering Geology*, 94, 2007, pp. 180-200.

[6] Geologycal Society Engineering Group Working Party Report, The description and classification of weathered rocks for engineering purposes. *Quaterly Journal of Engineering Geology*, 28 (3), pp 207-242.

[7] Derek Ford & Paul Williams, Karst hydrogeology and geomorphology, Wiley, 2007, 562.

An Overview on the Landslide Susceptibility Assessment Techniques

MURAT ERCANOGLU
Geological Engineering Department
Hacettepe University
06800 Beytepe/Ankara
TURKEY
murate@hacettepe.edu.tr http://yunus.hacettepe.edu.tr

Abstract: Natural disasters and their consequences have considerable and destructive effects on human life, properties, infrastructures, and, of course, on environment. One of the most important natural hazards, landslide plays a very important role in these effects throughout the world. Therefore, many countries, particularly the developed ones, invest huge amount of money either in mitigation or in prevention of landslides. The first, and probably the most important, stage of mitigation and/or prevention efforts is to assess landslide susceptibility by obtaining data related to landslides, i.e. preparation of landslide inventory and database. If taken into consideration, results of these assessments, i.e. landslide susceptibility maps, will provide useful information and economic benefits for urban planning, development plans, engineering applications, land use potential planning, and so on. When international scientific literature related to landslide assessments is examined, there has been an increasing interest in landslide susceptibility mapping studies in the last decades, instead of evaluating hazard and/or risk. Particularly, in recent years, depending upon the breakthroughs in computer technology, GIS (Geographic Information System), and RS (Remote Sensing) techniques, very important developments were achieved in these studies. This can be concluded as one of the most promising efforts with respect to combat with natural hazards since they opened wide range of opportunities for analyzing, evaluating, and assessing earth processes, notably for landslides. Thus, there are a multitude of studies carried out by different researchers in different parts of the world with the aid of these technological items. In this study, it was aimed at assessing landslide susceptibility techniques by means of a detailed literature survey based on an overview including twenty years' experiences. The techniques were categorized into two distinct groups such as qualitative and quantitative ones, and briefly examined individually. By doing so, a historical development of the techniques and actual trends in landslide susceptibility assessments were evaluated. It was revealed that some traditional methods seemed to have disappeared, while the new ones, particularly included in the GIS software, became very popular. However, at present, there seems to be no agreement on these techniques which can be the most effective one among the researchers.

Key-Words: Landslide, landslide susceptibility, GIS, hazard, risk, remote sensing.

1 Introduction

As is well known, natural disasters such as earthquakes, landslides, floods have dramatic effects on human life, infrastructures, environment, and so on. However, there has been an increasing interest in natural hazard assessments within the scientific community. Particularly in the last two decades, there is also an increasing trend in using the outcomes of the results of these assessments. In other respect, important organizations such as UN (United Nations), EU (European Union), and NATO (North Atlantic Treaty Organization) have been encouraging scientists and governments to focus on assessing natural hazards by supporting workshops, projects, conferences, and so on. Declaration of IDNDR (International Decade for Natural Disaster Reduction) by the UN between the decade 1990 and 2000 could be considered as one of the most important events in this issue.

However, recently, natural disasters and their consequences have still been one of the most problematic issues for many countries. Growing population and expansion of settlements and lifelines over hazardous areas have largely increased the impact of natural disasters both in industrialized and developing countries. Third world countries have difficulty in meeting the high costs of controlling natural hazards through major engineering works and rational land-use planning. On the other hand, industrialized societies are increasingly reluctant to invest money in structural measures that can reduce natural risks [1]. Indeed, landslides are one of the most destructive natural hazards in the world, and casualties and property damage caused by landslides are high. In respect of landslides, assessment of landslide susceptibility, hazard or risk evaluations has become a topic of major interest for both

geoscientists and engineering professionals as well as for the community and the local administrations in many parts of the world. But, assessing landslide susceptibility is much more common when compared with hazard and risk assessments, as discussed in the next section.

This study aims at evaluating the history of landslide susceptibility assessment techniques considering their pros and cons and presents a brief overview about their development. It should be noted that this study is based on the detailed literature review [2] which takes into consideration papers published in scientific journals.

2 Background and Terminology

The term landslide is defined as the movement of a mass of rock, debris or earth down a slope [3]. Varnes's landslide classification system [4] is the most widely used one to explain the mechanisms of landslides and to provide communication among the researchers throughout the world, based on the type of movement and material.

Although the landslide studies date back to 1950's, initiation of landslide mapping was at the beginning of 1970's [5]. Then, particularly in 1980's, in line with the achievements in computer technology and GIS (Geographic Information Systems), there was a "boom" related to the landslide mapping in the scientific literature. The beginning of 1990's, with the exception of a very few cases, witnessed the GIS applications for mapping in landslide regions. In some cases, the majority of the analyses and map modeling were fully achieved through a given GIS package, but in other cases, the use of GIS was only partial [6]. However, in 1990's, utilization of GIS was indispensible tool for mapping and evaluating landslides, particularly for regional or medium scale studies.

As for the terminology related to landslides and their mapping, there was a little bit conflict among the users for susceptibility, hazard, and risk. Of course, a lot of definitions can be made with respect to their meanings, but the most recent ones are defined by JTC (Joint Technical Committee) on landslides and engineered slopes as follows [5]:

Landslide Susceptibility: A quantitative or qualitative assessment of the classification, volume (or area), and spatial distribution of landslides which exist or potentially may occur in an area. Susceptibility may also include a description of the velocity and intensity of the existing or potential landsliding. Although it is expected that landsliding will occur more frequently in the most susceptible areas, and in the susceptibility analysis, time-frame is explicitly not taken into account. Landslide susceptibility includes landslides which have their source in the area, or may have their source outside the area but may travel onto or regress into the area.

Hazard: A condition with the potential for causing an undesirable consequence. The description of landslide hazard should include the location, volume (or area), classification and velocity of the potential landslides and any resultant detached material, and the probability of their occurrence within a given period of time.

Risk: A measure of the probability and severity of an adverse effect to health, property or the environment. Risk is often estimated by the product of probability of a phenomenon of a given magnitude times the consequences. However, a more general interpretation of risk involves a comparison of the probability and consequences in a non-product form. For Quantitative Risk Assessment the use of the landslide intensity is recommended.

In general and in some cases, the major problem was that the hazard term was used incorrectly instead of susceptibility. As can be seen from the definitions above, the term susceptibility covers the intrinsic/conditioning landslide parametrs, while the term hazard, in addition to the intrinsic ones, includes extrinsic/triggering parameters. Therefore, any attempt to determine landslide hazard did not comply with and cover the time concept, can only represent landslide susceptibility. In other respect, since it is not always easy to assess and obtain data related to the triggers of landslides, researchers generally prefer to produce landslide susceptibility maps. For this reason, only lanslide susceptibility term is taken into consideration in order to make a more common assessment in this study.

3 Parameters and Techniques

To develop a method for the assessment of landslide susceptibility, determination of the causes of the landslides is crucial. In other words, selection of the parameters is very important for the occurrence of landslides. Indeed, it may be possible by determining the parameters conditioning actual or old landslides to forecast where future possible landslides may occur. Whatever methodology is adopted, the input data for an assessment must only be selected for the possible causes of potential future unstable areas after carefully considering the causes of actual and past instabilities. Under these conditions, analysis of cause-effect relationships is not always simple, however, as a landslide is seldom linked to a single cause [7]. The discussion of cause-effect relationship is complicated because although landslides can have several causes, including geological, morphological, physical, and human. By definition a trigger is an external stimulus such as intense rainfall, earthquake shaking, volcanic eruption, storm waves, or rapid stream erosion that causes near-immediate response in the form of landslide by reducing the strength of slope materials. In some cases landslides may occur without any apparent

attributable trigger because of a variety of causes, such as chemical or physical weathering of materials that gradually bring the slope to failure [8]. Besides, the difficulties in determining the causal factors; the scale of the study, financial conditions, time, experience can also affect the parameters to be used potentially. Moreover, these parameters and the weight of their importance may change from region to region. Thus, at present, there is no agreement either on the methods for or on the scope of producing landslide susceptibility or hazard maps [9]. Although it is true that there is no universally accepted method of producing landslide susceptibility maps, recent works in this field have shown considerable improvement since [9].

To date, a number of different methods have been developed to predict landslide occurrences. They can be divided into two major groups as qualitative methods and quantitative methods. These vary from experience-based analyses to complex mathematical, logical, and/or computer-based systems to analyze landslide susceptibility. Geomorphologic analyses and direct field mapping methods are considered qualitative methods because they are based on judgment and are more subjective than quantitative methods. Quantitative methods such as deterministic analyses, probabilistic approaches, statistical methods, and artificial intelligence techniques closely rely on mathematical models and, as a result, much less human judgment and experience is needed to produce and run such models. However, no general agreement has yet been reached about the best method for producing landslide susceptibility maps [10]. Although all known methods have their advantages and disadvantages, utilization of quantitative methods has become preferred and more commonly used in recent years. In addition, utility of GIS has been emphasized in almost every landslide study published in recent years. Therefore, it can be concluded that the general trend related to landslide assessments is the utilization of quantitative methods and specifically, GIS based ones.

In the last two decades, a great deal of research concerning landslide susceptibility mapping techniques has been done. When compared with the former ones before the 1990's, the investigation trend was solving the landslide problem for a specific site. Thus, in the great majority of the studies, deterministic and probabilistic models were popular. However, the heterogeneity of the natural conditions at the regional scale and the large variability in geotechnical properties such as cohesion and internal friction angle are in sharp contrast to the homogeneity required by deterministic models. This contrast, coupled with the costly and time consuming site investigation techniques required to obtain property values, makes the engineering approaches unsuitable for application over large areas [11]. Then statistical approaches such as bi-variate and/or multivariate have become popular for landslide analyses. Perhaps the most important reason for this situation was that the GIS packages were containing these statistical approaches. Instead of using external statistical software, the users preferred these analyses, which have already been included in the GIS packages. And, thus, statistical techniques have become popular in that time, and even today since they provide quick and no time consuming procedures. However, uncertainty exists in almost every stage of landslide susceptibility modeling. Also, because of the complex nature of landslide phenomena, some of the landslide contributing parameters cannot be modeled. It is well recognized that the various factors contributing to landslides in a region are complexly interrelated [12] and the relationships between these factors and the landslides are nonlinear in nature. Hence, improvement of existing methods or the application of new techniques, which are concerned with or represent the nonlinearity of landslide susceptibility assessments, has become indispensable. Under such conditions, use of nonlinear models that can be applied to the multi-source data analysis and classification with respect to landslide assessments may be more suitable. Therefore, AI (Artificial Intelligence) techniques such as fuzzy logic, artificial neural networks, and genetic algorithms were used, and are still popular when considering complex nature of landslide phenomena. They seem to be one of the most effective ways to cope with the problems stemmed from uncertainty in materials and parametric interrelationships in landslide susceptibility mapping.

RS (Remote Sensing) techniques also constitute an important part of landslide suscetibility studies due to the fact that it can be easily integrated to a GIS environment and provides valuable information about the territories to be studied in a short time. Furthermore, achievements in RS techniques have opened a wide range opportunities for analyzing, evaluating, and assessing; in particular, earth processes such as landslides. Periodical possibility of obtaining detailed representations of Earth's surface allows, with a quite good precision, analyzing landslide dynamics and modeling landslide susceptibility of the territories [13]. Up to ten years's of time, air photo interpretations were very common in landslide investigation. But, recently, satellite images with high resolutions such as IKONOS, QUICKBIRD supersede the time-consuming and subjective air photography interpretations. Although they cost a lot of money when compared with the air photographs, these satellite images have been proven to be more effective and powerful in determining landslide locations. There is another outstanding RS product, namely LIDAR (Light Detection and Ranging) imagery, one of the newest data sources. Its main advantage is that it is quite difficult to use the other RS products in landslide assessments in particularly rugged terrains with

dense vegetation [14]. However, although the LIDAR is a promising application, it is still the most expensive technique and needs huge amount of money for accurate and reliable assessments.

4 Conclusion

Today, in general, it can be concluded that the importance of combating natural disasters is well understood among the public, NGOs (Non Governmental Organizations), and the scientists, and new technologic opportunities and techniques are always coming. Governments and international organizations take positive steps to prevent natural hazards for all over the world. However, natural disasters and their consequences are still one of the most problematic issues for many countries, notably the developing and/or underdeveloped ones. But, the promising issue is that the being awareness of this phenomenon.

Conceptually, with respect to landslides, the same conclusions can be made. But, it should be noted that the investigations will continue. At present, it is revealed that some traditional methods seemed to have disappeared, while the new ones, particularly included in the GIS software, are very popular. Furthermore, there seems to be no agreement on the techniques which are more effective among the researchers. However, one should know that the statistical and AI techniques are more popular than the others. In addition, whatever the methodology is employed, utilization of GIS and RS techniques become more and more important regardless of their costs.

References:

[1] Guzzetti, F., Carrara, A., Cardinali, M, Reichenbach, P., Landslide Hazard Evaluation: A Review of Current Techniques and Their Application in a Multi-Scale Study, Central Italy, *Geomorphology*, Vol. 31, 1999, pp. 181-216.

[2] Ercanoglu, M., Yorgun, C., Ozben, M., Heyelan Duyarlilik Degerlendirmelerinde Kullanilan Yontemler: Gecmis ve Bugun, *60. Türkiye Jeoloji Kurultayı, Bildiri Özleri*, 2007, pp: 309 (in Turkish).

[3] Cruden, D.M., A Simple Definition of a Landslide, *Bulletin of the International Association of Engineering Geology*, Vol. 43, 1991, pp. 27-29.

[4] Varnes, D. J., Slope Movement Types and Processes, *In: Landslides Analysis and Control, (Ed. R.L. Schuster and R.J. Krizek), Transportation Research Board, National Academy of Sciences, Special Report,* No.176, 1978, pp.12-33.

[5] Corominas, J., Guidelines for Landslide Susceptibility, Hazard, and Risk Zoning for Land Use Planning, *Engineering Geology*, 2008, (in press).

[6] Chacon, J., Irigaray, C., Fernandez, T., El Hamdouni, R., Engineering Geology Maps: Landslides and Geographic Information Systems, *Bulletin of Engineering Geology and Environment*, Vol. 65, 2006, pp. 341-411.

[7] Aleotti P., Chowdhury, R., Landslide Hazard Assessment: Summary Review and New Perspectives, *Bulletin of Engineering Geology and Environment*, Vol.58, 1999, pp. 21-44.

[8] Wieczorek, G.F., Landslide Triggering Mechanisms, *In: Landslides: Investigations and Mitigations, A.K. Turner and R.L. Schuster (Eds.), Transportation Research Board, Special Report 247,* 1996, pp.76-90.

[9] Brabb, E.E., Innovative Approaches to Landslide Hazard and Risk Mapping, *In: Proceedings of 4th International Symposium on Landslides, Canadian Geotechnical Society, Toronto, Canada*, Vol. 1, 1984, pp. 307-374.

[10] Guzzetti, F., Cardinali, M., Reichenbach, P., Carrara, A., Comparing Landslides Maps: A Case Study in the Upper Tiber Basin, Central Italy, *Environmental Management*, Vol. 25, No. 3, 2000, pp. 247-263.

[11] Soeters, R.S., Van Westen, C.J., Slope Instability Recognition, Analysis and Zonation, *In: Landslides: Investigation and Mitigation. Turner, A.K. and Schuster, R.L. (Eds.), Transportation Research Board, Special Report 247, National Academy Press, Washington D.C.*, 1996, pp. 129-177.

[12] Jade, S., Sarkar, S., Statistical Models for Slope Instability Classification, *Engineering Geology*, Vol. 36, 1993, pp.91-98.

[13] Sarkar S., Kanungo, D.P., An Integrated Approach for Landslide Susceptibility Mapping Using Remote Sensing and GIS, *Photogrammetric Engineering and Remote Sensing*, Vol. 70, 2004, pp. 617–625.

[14] McKean, J., Roering, J., Objective Landslide Detection and Surface Morphology Mapping Using High-Resolution Airborne Laser Altimetry, *Geomorphology,* Vol. 57, 2004, pp. 331-351.

Monitoring climatic changes and carbon cycle in canyons and caves: the C6 project.

PAOLO MADONIA
Istituto Nazionale di Geofisica e Vulcanologia, Sezione di Palermo
Via Ugo La Malfa 153, 90146 Palermo
ITALIA
p.madonia@pa.ingv.it, http://www.c-six.org
Associazione Italiana Canyoning, Commissione Scientifica
Piazza della Libertà 1, 05039 Stroncone
ITALIA
commissione.scientifica@canyoning.it, http://www.canyoning.it

Abstract: - The acronym C6 means "Climatic Changes and Carbon Cycle in Canyons and Caves". It is a monitoring project, for the evaluation of climate change signals, based on measuring sites located inside canyons and caves; it merged in the year 2005, under the scientific supervision of the Palermo Branch of the Italian National Institute for Geophysics and Volcanology (I.N.G.V.), two different monitoring programs active since 1999.
The choice of these environments is based on their morphological structure: being them more or less segregated respect the outer atmosphere, they act as low-pass filters respect the variations of the monitored parameters, which are rainfall and dropping water amounts and rates, air temperatures and relative humidity and carbon dioxide concentrations in the atmosphere.
On the basis of the preliminary data, reported and discussed in the paper, the C6 network seems to be capable to give useful information on the local effects of global changes, even if at the moment the monitored parameters concern only the abiotic components of the studied ecosystems.

Key-Words: - Air temperature**,** Canyon, Carbon Dioxide, Cave, Climatic Change, Infiltration, Rainfall

1 Introduction

The acronym C6 means "Climatic Changes and Carbon Cycle in Canyons and Caves". It is a monitoring project for the evaluation of climate change signals, based on measuring sites located inside canyons and caves. The choice of these environments is based on their morphological structure: being more or less segregated respect the outer atmosphere, they act as low-pass filters respect the variations of the monitored parameters, suppressing or strongly lowering the high frequency noise, like the circadian thermal cycles.
The C6 project merged in the year 2005, under the scientific supervision of the Palermo Branch of the Italian National Institute for Geophysics and Volcanology (I.N.G.V.), two different monitoring programs, active since 1999,
The former, devoted to environmental monitoring of canyons, was promoted by the Scientific Commission of the Italian Canyoning Association (A.I.C.) and the no-profit association Al Qantara (Palermo, Italy); it was based on three continuous monitoring sites in Wadi al Ghurab (Southern Jordan, since 1999), in the Rio Grande Canyon (Northern Appennines, Italy, since 2001) and in the Rio Grande Canyon (Vulcano Island, Southern Italy, since 2003). In the year 2005 the Royal Society for the Conservation of Nature of Jordan joined the C6 program, and a new site, substituting the Whadi Al Ghurab station, was established inside the Shagher Daghleh Canyon (Wadi Dana Reserve).
The latter, active since the year 1999, was focused on environmental monitoring of karst caves; the Italian NGO Legambiente, managing the natural reserves of Santa Ninfa, Carburangeli and Sant'Angelo Muxaro caves, all three located in Sicily (Southern Italy), promoted a monitoring program focused to verify the existence of a possible environmental negative feedback of human fruition. Continuous and discontinuous meteorological parameters and carbon dioxide concentrations, inside and outside the caves, have been collected since that time.
The network was further developed on October 2006, after the Speleological Federation of Bosnia Herzegovina joined the project, with a site inside a cave not far from the city of Sarajevo.
Finally, on December 2007 a new measuring point was established inside the Corleone Creek Canyon (Sicily, Italy).
The map in Fig.1 shows the location of all the sites.

2 Structure and aims of the monitoring network

The C6 network is nowadays articulated into 8 sites, equally distributed among canyons and caves; Table 1 shows

names, localities and monitored parameters for each of them.
Measures may be subdivided into three main groups:
1) Air temperature and relative humidity are continuously acquired by miniature-low power consumption dataloggers, except the sites located inside caves, where humidity is measured during discrete sessions. Continuous stations are not used inside caves due to the condensation of water vapor on the surface of the capacitive sensors used by this kind of loggers.
2) Rainfall and dropping water rates (inside caves only) continuously measured by the same kind of loggers
3) Static concentrations of carbon dioxide, measured by infrared spectrometers coupled with miniature loggers. The sampling frequency is not higher than 1 measure per day, in order to reduce the maintenance of these stations, located in underground environments characterized by a difficult access.
Three different research lines are based on the abovementioned parameters, with the common goal of identifying local evidences of global climatic changes:

2.1 Air temperatures

Caves have to be considered as very complex thermal systems lying at the interface atmosphere-hydrosphere-lithosphere, described under the theoretical point of view by Badino [1] in a very exhaustive way.
In general, underground air temperatures show values more or less equal to the outside yearly averages, modulated by small (few degrees) seasonal oscillations. Particular morphologic conditions may influence the thermal equilibrium of the caves. Inner average temperatures colder then the outer (the so called “cold trap” effect) are recorded in blind caves with a dominant vertical development and/or lying at the bottom of closed surface morphologies, like dolines or blind-valleys.
The analysis of the dynamic relationships between inner and outer air temperatures, as better explained in the examples reported in the next chapter, may allow the recognition of climatic change signals.
Microclimatic data recorded inside canyons are not very common in the literature, especially because of the very difficult access to these environments. Some preliminary data from Jordan have been reported by Bellanca et al. [2], whereas Madonia [3] illustrated two study cases in Italy.
Canyons are less isolated than caves respect the outer atmosphere, so their intra-annual microclimatic variability is higher; for this reason, as explained in the next chapter, possible climatic changes may be reflected by indicators more sensible than rough parameters as the simple yearly averages of air temperatures.

2.2 Rainfall dynamic

One of the most evident signals of the climatic change processes is the increase in rainfall intensity. Being the dimension of rock permeability a velocity (m/s), an increase in rainfall intensity (commonly expressed in mm/hour) causes a faster saturation of the first soil horizons, increasing runoff and depleting infiltration; at least, this process is responsible of an acceleration of soil erosion and a depletion of the recharge of underground aquifers.
A contemporary measurement of rain intensity at the surface and of dropping water rate inside a cave, this last being a direct measurement of infiltration, allows to directly monitor these kind of climatic changes phenomena under a quantitative point of view, giving useful information for the calibration of more complex theoretical models.
Moreover, the isotopic composition measurements of Oxygen and Hydrogen in rains and underground waters are indicative of possible alteration in the hydrological cycle, as reported by Gat and Gonfiantini [4].

2.3 Carbon dioxide cycle

The primary source for carbon dioxide in underground environments, with the only exception of the anthropic contribution, is linked to the interaction processes between infiltrating waters and organic matter contained into the soil. As already evidenced by Madonia and Di Pietro [5], release of carbon dioxide from dropping waters may lead to static concentrations in cave atmosphere up to more then 1%vol.
The monitoring of underground carbon dioxide cycle is then an useful tool in better understanding the soil respiration phenomena, which have been studied until now without taking into account the amount of CO2 produced by the soil and not released in the atmosphere because fixed in underground water circulation

The research lines active nowadays within the C6 project are dedicated to micro-meteorology and geochemistry, with specific reference to the abiotic components of the cave and canyon ecosystems.
These activities have to be considered only as an initial step of a more complex and extended path, providing for the next future an expansion to eco-hydrological themes .
As an example of a possible bridge from micrometeorology to eco-hydrology, let us to consider the effect of a modification of rainfall dynamics on bedrock channels in a riverine ecosystem. An increment in rainfall rates, favoring the surface runoff respect to the infiltration, causes enhanced erosion and transportation of sediments along the river.
The negative eco-hydrological feedback of such phenomenon is the obliteration, caused by deposition of sediments, of the residual water-pools on the rocky river beds. The disappearance of these micro-environments, very common inside canyons, is a strong disturbance for those living communities needing the constant presence of water for their vital cycles. .Then, the coupled monitoring of the rainfall dynamic (abiotic component) and of the water-pool living communities (biotic component) represents a

paradigmatic example of how copying with climatic changes studies under the light of a holistic perspective.
In the next chapter some preliminary results from C6 project will be described, in order to better explain the above mentioned skills.

3 Preliminary results

The below reported graphs illustrate some preliminary data from the C6 network: the relationships between rainfall and infiltration and among the inner and outer air temperatures and the static concentrations of carbon dioxide, measured in the Carburangeli Cave, are illustrated in Figures 2 and 3 respectively. On the contrary, Figure 4 describes the relationships between the inner and outer microclimates in the Rio Grande Canyon (Vulcano Island).
Data reported in Fig.2 account for a dynamic approach in the analysis of the infiltration coefficient, highlighting the different response of the same hydro-geologic circuit to rainfall events occurred with different rates and under different seasonal conditions. The amount of the effective infiltration, that is the amount of rain available for the recharge of the underground aquifers after the evapo-transpiration process, is slightly different in spring rather than in summer.
Rainfall events characterized by low intensities and occurred between March and April 2003 (main graph) generated a fast infiltration (less than 24 hours of delay), testified by a huge increase in the dropping water rate inside the cave, from 5 to 40 mm/hour. On the contrary (inserted graph) a heavy rain in August 2004 was completely transformed into surface run-off: the total absence of infiltration is testified by the invariance of the dropping water curve.
These data, derived from a direct measure and not from a theoretical model, clearly highlight the negative feedback on the underground water resources of the incoming hydrologic scenario, characterized by concentration of the same amount of rain into a smaller number of much more intense events. Under these conditions, the main part of precipitation is transformed into surface run-off, causing a progressive depletion of the underground water resources.
Figure 3 illustrates air temperatures and relative humidity measured between September and November 2005 in the Rio Grande Canyon at Vulcano Island (Italy). The comparison between the inner and the outer stations clearly demonstrate that the daily thermal variability is much more reduced inside the canyon than outside, with a sensible diminution of the maxima and a more reduced lowering of the minima.
Moreover, during the hottest hours of the day, a more humid atmosphere is maintained inside the canyon, due to the reduced solar insolation on its own provoked by the shield effect of the side rock-walls closely facing each other.
Especially in arid regions, stable conditions of air temperature and relative humidity are fundamental for the maintenance of ecological niches inhabited by sensible living specimens, including the human settlements. One of the most famous and splendid example in the world of what just described, not only by the ecological but also by the artistic and architectural point of view, is represented by Petra, the city carved into the rock inside a canyon system in Southern Jordan.
According to these preliminary data, canyons seem to be sites strongly resistant to climatic variations. So, they represent a good location for microclimatic measurements in the frame of long term climatic change monitoring programs: recording sensible variations inside canyons means that climatic changes are so evident to modify one of the much resistant ecological niche in the continental environment.
Finally, the role of karst environments in the governance of the carbon dioxide global cycle is evidenced in the graph reported in Fig.4, illustrating the relationships between outer and inner air temperatures and carbon dioxide static concentrations in the Carburangeli Cave.
Static concentrations of carbon dioxide, up to 1%, are recorded in the cave atmosphere when the inner air temperature is lower than the outer. Under this condition, the outflow of underground air is inhibited because of the density differential respect to the outside atmosphere: the colder and denser air is trapped inside the cave.
The primary source for carbon dioxide is the diffusion from dropping water, which is strongly enriched in CO2 during the percolation trough the soil. Excess CO2 is fixed in speleothemes under vadose conditions, while it interacts with carbonatic aquifers in the phreatic zone. In both cases carbon dioxide is subtracted to the respiration budget of the soil; if this amount is not measured or modeled, the effects of climatic changes on soil respiration can't be correctly evaluated**.**

4 Conclusions

At the moment, data acquired in the behalf of the C6 project refer to its initial step, whose aim has been the acknowledgement of its performances as a climatic changes long term monitoring network.
On the basis of the preliminary acquired data, partially reported and discussed in the previous chapter, our opinion is that the C6 network is capable to give useful information on the local effects of global changes, even if only at the level of the abiotic components of the studied ecosystems.
Next steps of the C6 project will copy with the acquisition of data series more consistent under the statistical point of view and, at the same time, the development of researches more properly dealing with ecological skills.
Further information on the future developing of the C6 project may be obtained at the URL www.c-six.org.

Aknowledgments

Data presented in this paper have been acquired in part on the behalf of researches financed by the Territory and Environment Department of the Sicilian Government (Regione Siciliana, Assessorato Territorio ed Ambiente), in the framework of the contract with the NGO Legambiente Comitato Regionale Siciliano for the management of the Natural Reserve “Riserva Naturale Integrale Grotta di Carburangeli”.

References:

[1]. Badino G., *Fisica del Clima Sotterraneo*, Mem. dell'Ist. Italiano di Speleologia, Vol.7, serie II, Bologna, 1995.

[2].Bellanca, A., Madonia, P., Canali, S., Geodiversità e biodiversità indotte da fattori geomorfologici in un ambiente arido della Giordania meridionale: il caso dell’area di Beidha, *S.It.E. Atti*, Vol. XXV, 2001, annexed CD.

[3].Madonia, P., Il programma di monitoraggio C6: Climatic Changes and Carbon Cycle in Canyons and Caves, *Atti XVI Congresso Società Italiana di Ecologia*, 2006, Available on line at

[4].Gat, J.R., Gonfiantini, R., (1981) *Stable Isotope Hydrology. Deuterium and Oxygen-18 in the Water Ctcle*, Technical Report Series No.210, International Atomic Energy Agency, Vienna, 1981.

[5].Madonia, P., Di Pietro, R., Concentrations of carbon dioxide in the atmosphere of two limestone and gypsum karst caves in Sicily, Italy (EU): considerations about human impact., *Primera convencìon cubana de ciencias de la tierra, GEOCENCIAS 2005, La Habana, 5-8 de Abril del 2005*, 2005, Memorias en CD-Rom, GEO17-7.

Table 1: Name, description, geographic localization and monitored parameters of the C6 network; the letters between brackets indicate the sampling frequencies (**h**our, **d**ay).

Site name (Id)	Type (start)	Lat, Long, Altitude	OUT Air t	OUT Rh	Rain rate	IN air t	IN Rh	CO_2	Drop. water
Carburangeli (CAR)	Cave (1999)	38°10'00" N 13°09'30" E 22 m	1 h	1 h	1 h	1 h	NO	1 d	1 h
Santa Ninfa (SNI)	Cave (1999)	37°47'00" N 12°54'00" E 400 m	1 h	1 h	1 h	1 h	NO	NO	NO
Rio Grande (RGA)	Canyon (2002)	44°40'00" N 09°24'00" E 600 m	1 h	1 h	NO	1 h	1 h	NO	NO
Rio Grande (RGS)	Canyon (2003)	38°24'00" N 14°28'30" E 100 m	1 h	1 h	1 h	1 h	1 h	NO	NO
Sant'Angelo (SAM)	Cave (2005)	37°28'42" N 13°32'45" E 170 m	1 h	1 h	1 h	1 h	NO	NO	NO
Bijambare (BIJ)	Cave (2006)	44° 5'43" N 18°30'14" E 990 m	1 h	1 h	NO	1 h	NO	NO	NO
Shagher Daghleh (SDA)	Canyon (2005)	30°40'47" N 23°15'09" E 700 m	1 h	1 h	NO	1 h	NO	NO	NO
Corleone Creek (COR)	Canyon (2007)	37°48'33" N 13°18'40" E 630 m	1 h	1 h	1 h	1 h	1 h	NO	NO

Figure 1: Location of C6 measuring sites

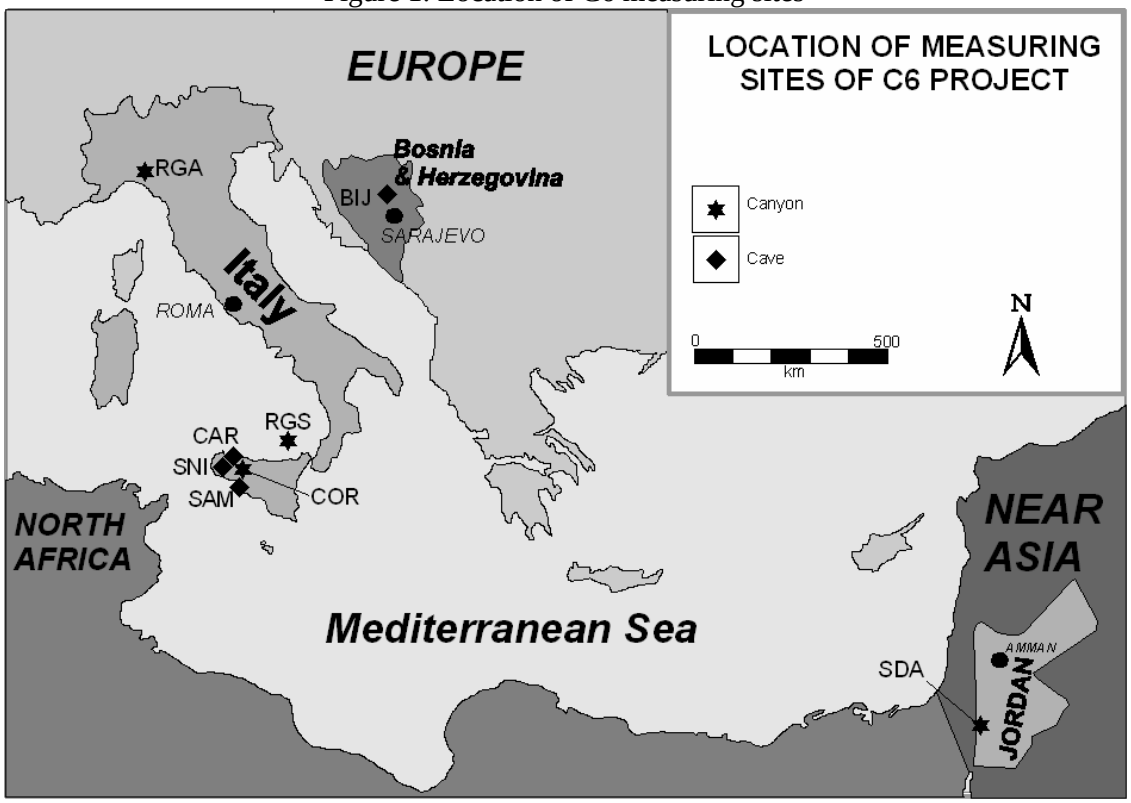

Figure 2: Daily rainfall amounts (grey bars) and dropping water rates (black line with filled circles) measured in the Carburangeli Cave (Italy); for two events the rainfall maximum rate is also reported. The main graph refers to the period comprised between February and April 2003, the insert to the month of July 2004.

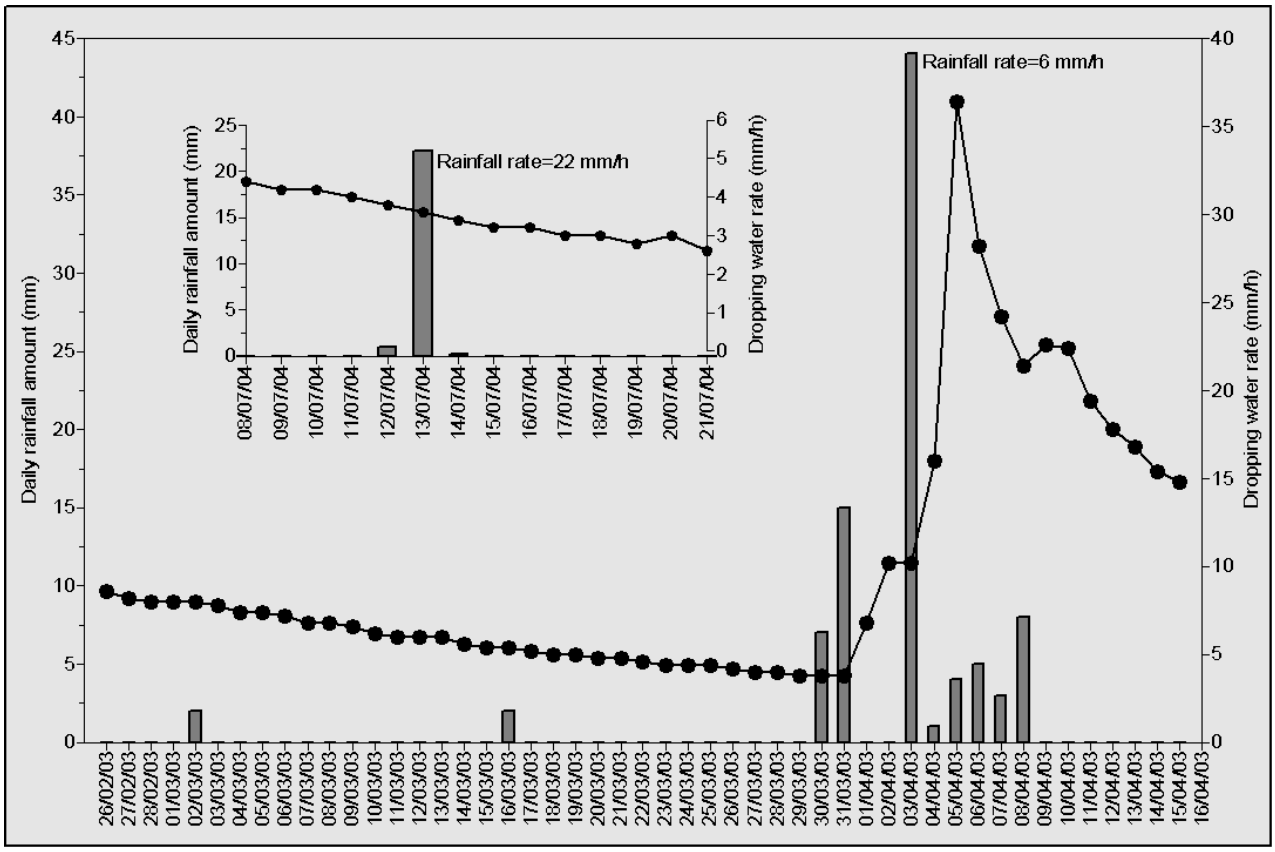

Figure 3: Hourly values of air temperature (lower graph) and relative humidity (upper graph) measured inside (black lines) and outside (grey lines) the Rio Grande Canyon at Vulcano Island (Italy). The graph refers to the period comprised between September and November 2005.

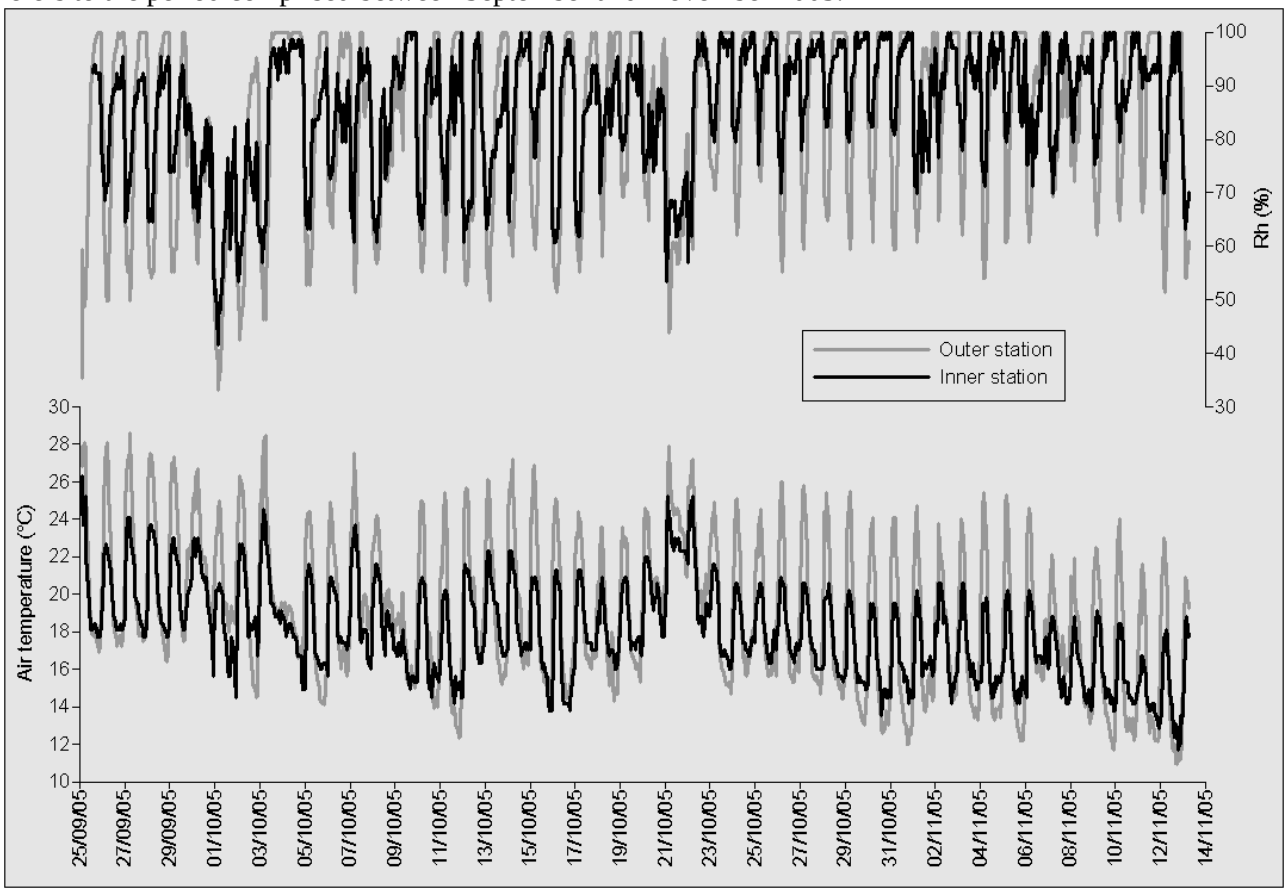

Figure 4: Daily values of outside air temperature (black line with filled diamonds), spot values of underground air temperature (black line with grey triangles) and spot values of carbon dioxide static concentration (black line with grey circles). Graph refers to the period comprised between March and July 2002.

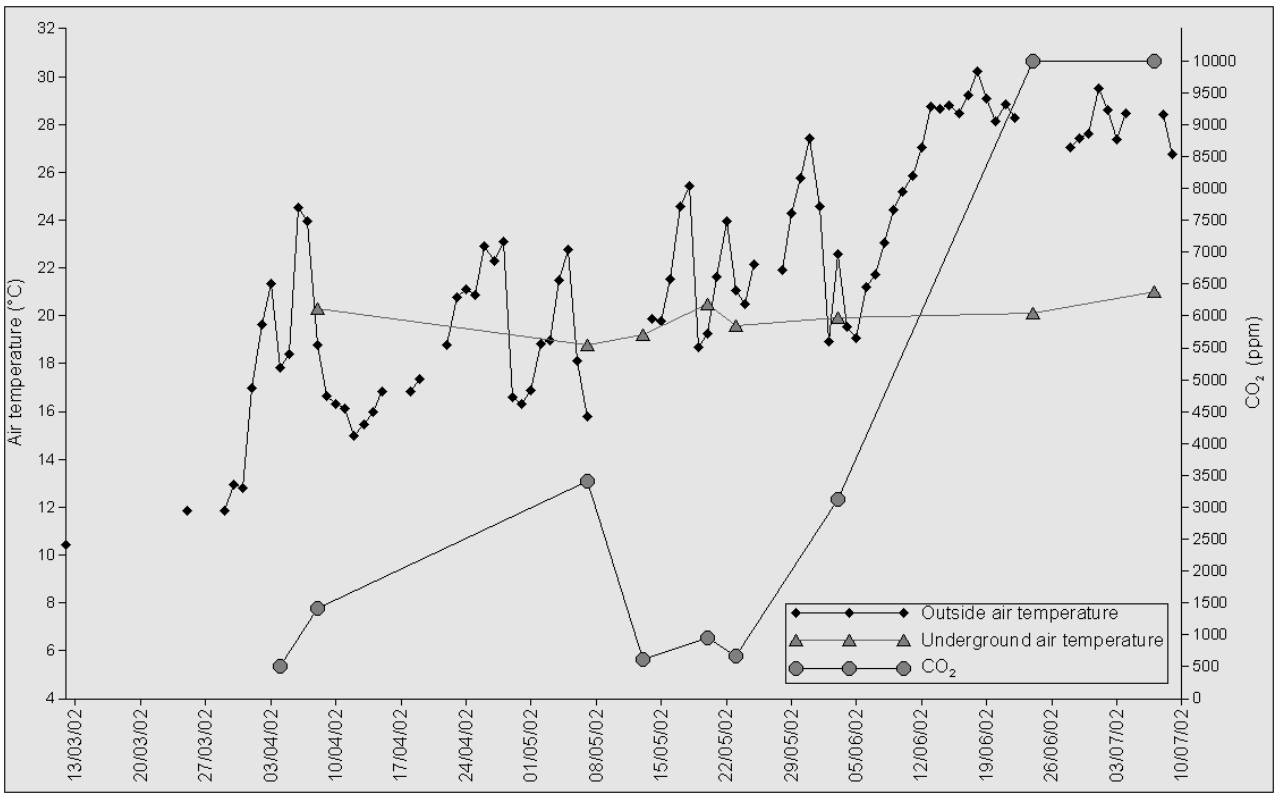

Underthrusting and Late Proterozoic Crustal-Scale Pop-Up in the Brasília Belt, central Brazil

LUIZ JOSÉ HOMEM D´EL-REY SILVA,
Instituto de Geociências
Universidade de Brasília
Campus Darcy Ribeiro, Asa Norte, CEP 70910-900, Brasília, DF
BRAZIL
ldel-rey@unb.br & luizhomemsilva@yahoo.com.br

Abstract: Because collision-related mountain chains form above sites of mantle down welling (= mantle convection), contractional deformation in general must be governed by the mechanism of underthrusting, mainly, and the inner parts of mountains should correspond to crustal-scale pop-up structures. In fact, convective cells and underthrusting are the basis for a new way (termed Suction Tectonics) to understand lithosphere deformation. The Brasília Belt (*BB*) is the most complex of the three fold-and-thrust belts that constitute the Tocantins Province of central Brazil, a Neoproterozoic orogen situated between the Amazonian and São Francisco cratons. The Araguaia and Paraguay Belts are the other two. The Araguaia-Brasilia Belt records the evolution of a Meso-Neoproterozoic ocean and the collision between the Amazonian and São Francisco paleo-continents, during the ~750-590 Ma Brasiliano orogeny. The Paraguay Belt records the 620-510 Ma evolution of a rift-oceanic basin opened within the Amazonian paleo-continent, adjacent to the southern half of the *BB*. The results of a research carried out in the last 15 years and focused on the operation of the underthrusting mechanism in the *BB* are summarized, and a brief review of the up-to-date literature supporting the new approach on lithosphere deformation is presented. Due to underthrusting, the inner part of the *BB* evolved such as a crustal-scale pop-up structure, and the evidence presented herein must be found in other collision-related mountain chains on Earth.

Key-words: - Underthrusting; Pop-Up; Brasília Belt; Brasiliano orogeny; Tocantins Province; central Brazil; Maranhão River Thrust; Granulite Exhumation.

1 Introduction

Since about two decades it is well-accepted that collision-related mountain chains float above two basal detachments that dip in opposite directions [1], towards the site where the mantle lithosphere undergoes down welling [2] or suction. Because the continental crust is carried together with the down welling mantle lithosphere, collision-related mountains are kept high as a kind of crustal-scale pop-up structure, since their Andean-type stage of formation (e.g. [3], [4]). If so, underthrusting must be a key part of the process required to build collision-related mountains and is due to operate in both sides of their inner zones.

Nevertheless, although there is plenty of geophysical evidence for mantle down welling under the main modern mountain chains of Earth, such as the Andes (e.g. [5] and [6]), the Canadian Cordillera (e.g. [7]), the Himalayas (e.g. [8]and [9]), and the Alps (e.g. [10]), and in despite of the fact that much experimental work in laboratories (e.g. [11], [12], [13], [14]) and computer modeling (e.g. [15], [16]) have shown the importance of the mechanism of underthrusting for building contractional fronts and mountains chains, the literature lacks reference to scientific works devoted to show direct field evidence of the operation of such mechanism to deform natural rocks.

The Brasília Belt (Fig. 1a-b) is a collision-related mountain displaying plenty of such evidence (e.g. [17], [18], [19], [20]). This paper summarizes the results of a research carried out in the last fifteen years, pointing to the mechanism of underthrusting as being responsible for making of the inner zone of the Brasília Belt a crustal-scale pop-up.

2 Summary Regional Geology

2.1 – Tectonic Setting

The Brasília Belt (*BB*) is part of the Tocantins Province, a major Neoproterozoic tectonic unit also comprising the Araguaia and Paraguay Belts, and bounded by the Parnaíba and Paraná

Phanerozoic sedimentary basins, in central Brazil.

Archean to Neoproterozoic rocks (see legend to the right of Fig. 1) that underwent poly-phase deformation and metamorphism during the ~750-590 Ma Brasiliano orogeny, indicate that the Araguaia-Brasilia Belt results from the collision of two paleo-continents, remnants of which are the Amazonian and São Francisco cratons, whereas the Paraguay Belt records the evolution of a rift-oceanic basin within the Amazonian craton, coevally with 620-510 Ma tectonic events also recorded in the *BB*, mainly in the southern part.

The crystalline basement includes Archean rocks (previously involved in the 2.2-1.8 Ga Transamazonian orogenesis) and remnants of Paleoproterozoic juvenile crust in the *BB*.

According to R.A. Fuck and co-workers (as in [21] and more recent works - summary as in [17]) the *BB* can be subdivided into three main lithotectonic domains (Fig. 1b):

- The Magmatic Arc consists of ~940-640 Ma amphibolite-greenschist facies tonalitic orthogneisses and metavolcanic-sedimentary rocks. Its western limit hides the ~650-590 Ma collision suture that was reworked by transcurrency in the 590-550 Ma interval.

- The Internal Zone comprises crystalline basement rocks, metavolcanic-sedimentary rocks of the Araxá, Paranoá, and Serra da Mesa Groups, and granulites rocks forming a belt along the boundary (the Maranhão River Thrust – MRT) with the External Zone (Fig. 1b). The Pirineus Zone of High Strain (PZHS) coincides with the axial plane of the regional fold hinge around which the *BB* changes from a NNE-striking northern segment to a SSE-striking southern segment.

- The External Zone comprises basement rocks including metavolcanic-sedimentary rocks of the Araí Group; (meta)-sedimentary rocks of the Paranoá and Bambuí Groups; and nappes of Araxá schist and Canastra phyllite.

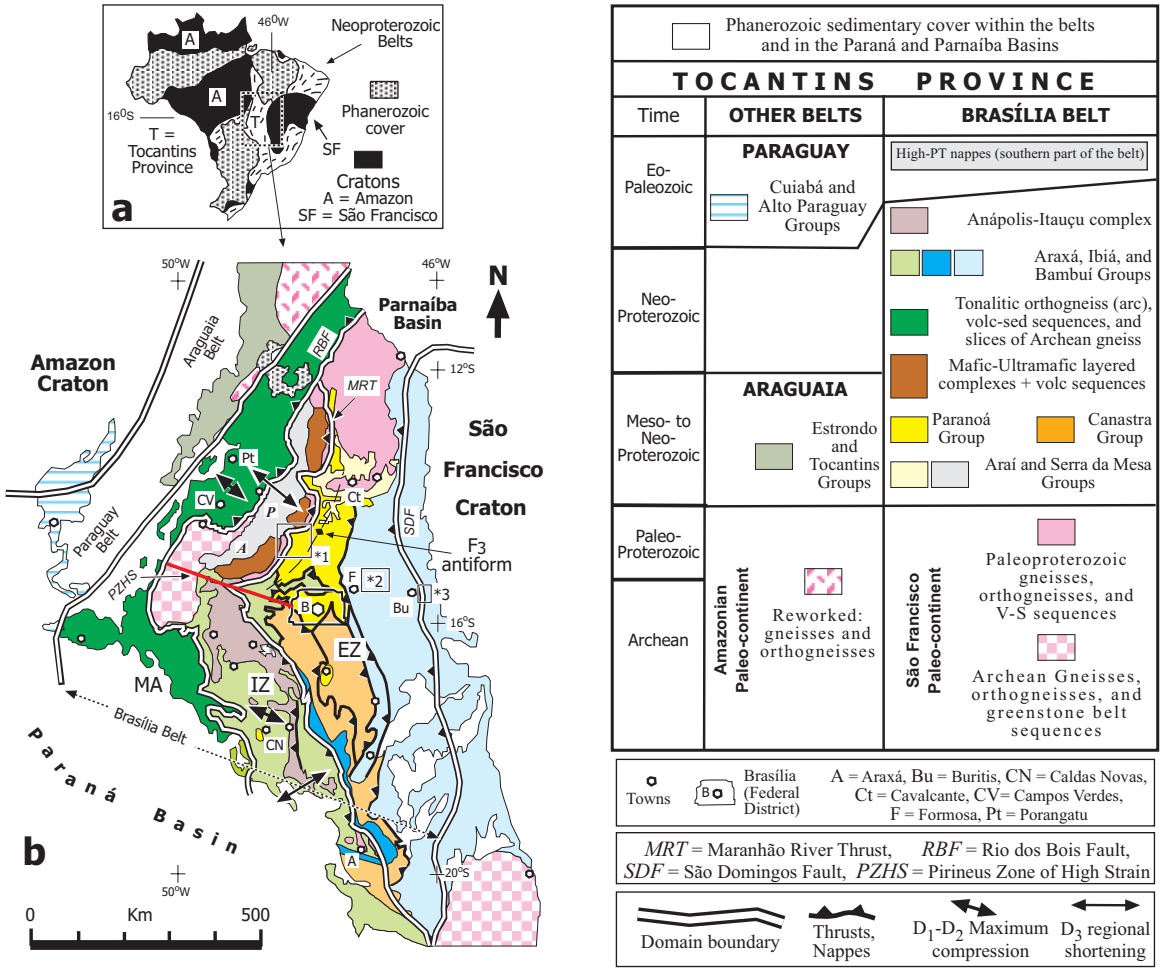

Fig. 1: Summary map displaying the main tectonic provinces in Brazil (**a**) and a summary geological map of the central part of the Tocantins Province (**b**; legend to the right; adapted from [21], [22], and [17]).

According to a vast literature cited in [17] the lithostratigraphy of the Tocantins Province results from a long-lived series of events (organized in a chart; the legend for Fig.1b).

Combining much structural evidence (as in [17], [22], and [23]) with the lithostratigraphy, one may envisage the evolution of the Tocantins Province as in Figure 2.

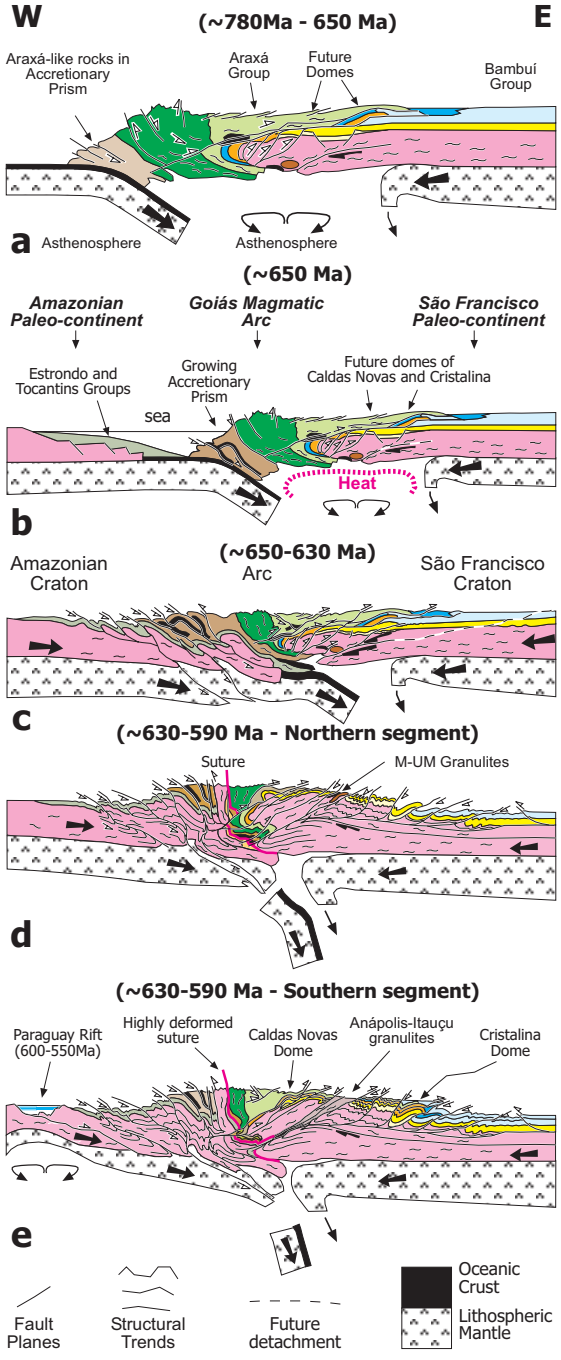

Fig. 2: A series of not-to-scale cartoons (**a**-**e**) to illustrate the tectonic evolution of the Tocantins Province in W-E oriented crustal cross-sections.

2.2 – Tectonic evolution

Before ocean opening, a main event of extension resulted in a ~1.77 Ga continental rift in the São Francisco paleo-continent, as recorded by the metasiliciclastics and metarhyolites (U-Pb zircon ages) of the Araí Group, and the metasiliciclastic-carbonate rocks of the Serra da Mesa Group.

Ocean opening started ~1300 Ma, as recorded by Meso-Neoproterozoic rocks of the Paranoá-Canastra Group and the Estrondo-Tocantins Group. These define passive margins sequences established respectively along the margins of the São Francisco and Amazonian paleo-continents. Mafic-ultramafic rocks intruded the lower crust of the São Francisco margin, ~1300 Ma ago.

An east-dipping B-subduction produced 940-640 Ma island arc intrusive and (Araxá Group) metavolcanic-sedimentary rocks laid down in back-arc basins. Amalgamation of these rocks to the paleo-continental margin resulted in the propagation of nappes of Canastra and Araxá rocks towards the ESE, onto the Paranoá rocks, ca. 750-650 Ma ago.

These events were assisted by the intrusion (~780 Ma) of mafic-ultramafic layered bodies that underwent granulitization (~750 Ma) during the early evolution of the São Francisco active margin (Fig. 2a). A retro-arc foreland-epicratonic basin accounts for the siliciclastic-carbonatic rocks of the Bambuí Group (and other possibly equivalent rocks) that crop out in the External Zone and in the São Francisco craton [24].

The continental collision started ca. 650 Ma ago. It brought the Amazonian paleocontinent into A-subduction (Fig. 2b) and resulted in a Himalayan-type orogen (Fig. 2c). The island arcs and back-arc basins adjacent to the São Francisco paleo-continental margin, and the ~750-650 Ma deformation recorded in rocks of such margin, combined with the fact that rocks in the Araguaia Belt started to deform solely ~650 Ma (data and references in [17] and [22]), strongly indicate the east-dipping subduction.

Deformation is recorded by ~750-630 Ma events (D_1-D_2) of tectonic transport to ESE all across the *BB*. Interlayer shearing produced a layer-parallel foliation (S_1) more penetrative in rocks of the Magmatic Arc and Internal Zone. D_2 event developed ESE-verging F_2 folds associated to a penetrative foliation (S_2) and metamorphism of amphibolite/low-greenschist facies in rocks of the inner *BB* and in the nappes, and to sub-greenschist facies in non-nappe rocks of the External Zone. Continental collision lasted until ~590 Ma (Figs. 2d and

2e) and led to the ~630-590 Ma sub-greenschist facies D_3 event of shortening recorded by the F_3 folds S_3 foliation, as well as contraction faults.

D_3 shortening was oriented WNW-ESE (similarly to D_1-D_2) or WSW-ENE (nearly orthogonal to D_1-D_2) respectively to the north and south of the PZHS (Fig. 1b). As explained in [22] and [17], the change in the direction of shortening and the PZHS relate to the opening and infilling of a rift-oceanic basin (the future Paraguay Belt) within the Amazonian paleo-continent (Fig. 2e). Event D_3 also developed the Maranhão River Thrust and exhumed the belt of granulites found in the inner *BB*. These include (Fig, 2d) bodies of mafic-ultramafic rocks, granulitized (~750 Ma) at the base of the São Francisco paleo-continent, and (Fig. 2e) supracrustals rocks granulitized ~635 Ma in the subduction zone.

3 Crustal Underthrusting

Crustal underthrusting happened in the western and eastern sides of the Tocantins Province.

According to computer modeling for collision-type orogens (e.g. [14]) if the rocks of the Amazonian paleo-margin - in the western side - were attached to the lithosphere, then they must have entered into A-subduction and underwent shortening by underthrusting (Figs. 2b and 2c).

In the eastern side, underthrusting is recorded along the MRT (Fig. 3), a west-dipping, ~630-620 Ma old (U-Pb data of granites along the PZHS) intraplate contractional frontal ramp, along which D_1-D_2 tectonites (mafic-ultramafic layered intrusions and metasedimentary rocks) underwent D_3 top-to-the-ESE shearing and greenschist-facies metamorphism. Actually, exhumation implies to move granulites from point X to point Y (Fig. 3a) along a 30^0 frontal ramp, and displacement of a 35 km-thick crustal wedge for a horizontal distance of ~43 km onto the Paranoá Group rocks. Underthrusting is required because the Paranoá rocks in the MRT footwall exhibit an unexpected much lower metamorphic grade ([19] and [20]).

A very detailed lithostructural analysis in the area labeled *1 (Fig. 1b) led D'el-Rey Silva and co-workers ([17] and [18]) to demonstrate underthrusting during the evolution of the MRT, mainly because:

- The metasedimentary rocks of the MRT hangingwall and footwall belong all to the Paranoá Group, and present the same D_1-D_2 top-to-the-ESE ductile shearing. Farther to the south of area *1 the MRT footwall also includes D_1-D_2 tectonites of the Araxá nappe.

- In the areas to the east of the mafic-ultramafic bodies, the Paranoá rocks exhibit extremely tight and more steeply inclined F_2 folds than elsewhere, and evidence of new shortening (D_3) in the same direction as D_1-D_2.

- Exclusively in the embayment area between the bodies, the Paranoá rocks exhibit abundant and WNW-trending sheath folds due to D_3 shearing superimposed upon the F_2 hinges originally oriented NNE. Moreover, the footwall rocks and the sheath folds underwent further and exclusive shortening in the N-S (D_4) and in the WNW-ESE (D_5) directions.

Underthrusting was likely a consequence of the ductile flow of the lower continental crust to the west, and was initially accommodated along an incipient contractional fault at the base of the bodies of granulite (Fig. 3b).

A scenario involving ductile flow of the lower crust and underthrusting is much expected (see literature review in [17]).

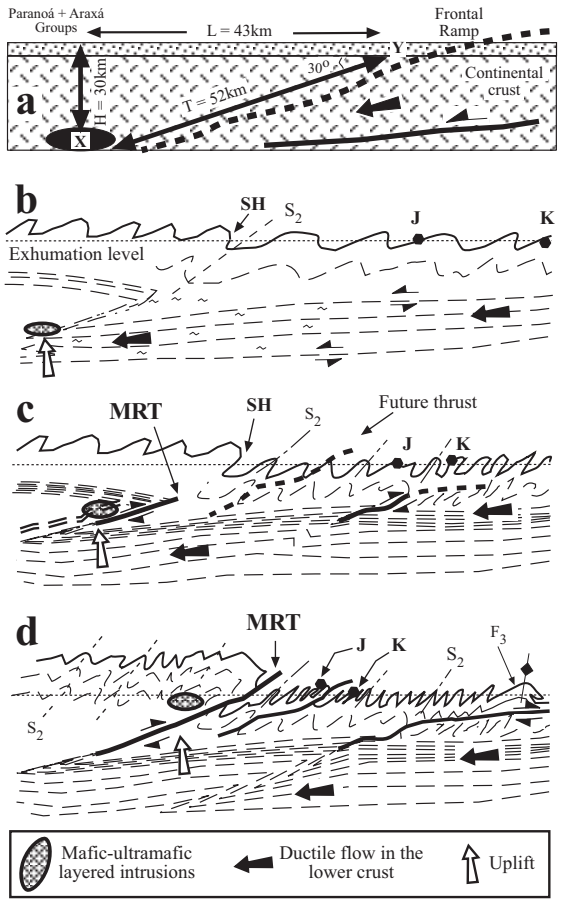

Fig. 3: Not-to-scale cartoons adapted from [17] and [19] for explaining the evolution of the Maranhão River Thrust (MRT). More details in text.

One example of a modern analogue is the Brazilian crust moving down to the west, towards the root of the Andean chain ([5], [4]).

The initial up-lift of the granulitic bodies created an incipient structural high affecting the Araxá and Paranoá rocks on surface (Fig. 3b). As these rocks kept moving from the east to the west, they underthrust below such high. As the mafic-ultramafic granulite bodies were approaching the surface (Fig. 3c) the upper section of footwall rocks located to the east of each body hit against a taller structural high, then experienced the first stages of D_3 shortening and, thus, the F_2 folds started to become tighter and more steeply inclined.

Meanwhile, in the area above the site between the granulite bodies, an incipient embayment formed because the D_1-D_2 tectonites had to move faster and farther to the west, in response to the necessarily faster up-lift of the granulite rocks.

Faster underthrusting gave origin to lateral ramps along the embayment-facing side of each granulitic body, and led to D_3 shearing responsible for developing the sheath folds. The existence of sheath folds also in the MRT hangingwall within the embayment indicates that D_3 shearing started before the tip of the MRT has finally reached the surface.

As the structural high became progressively taller, D_3 shearing continued solely in the MRT footwall. The more the embayment propagated to the west the less was the room available for further underthrusting, so the D_1-D_3 tectonites in the footwall had to shorten in the NNE-SSW direction (event D_4).

When the granulite bodies reached the level of exhumation (Fig. 3d) later underthrusting took place, imprinting D_5 shortening upon the D_1-D_4 tectonites of the embayment area, and turning into isoclinal and nearly up-right the F_2 folds in the area to the east of the two bodies (see movement of points J and K, Fig. 3b-d).

As the F_2 folds became isoclinal and up-right near the two mafic-ultramafic granulitic bodies, they resisted further tightening, and the latest stages of D_3 underthrusting had to be rather accommodated by top-to-the-east shear zones cutting through the F_2 fold hinges (see outcrop 154 described in [17]).

Lately, D_3 underthrusting developed the regional F_3 antiform (right side of Fig. 3d) that affects the Paranoá and Araxá D_1-D_2 tectonites near the middle of the External Zone (Fig. 1b).

Abundant structural data from detailed studies carried out in the areas labeled *2 and *3, and also in the Federal District area (Fig. 1b; two papers in final preparation) leave clear the same D_1-D_3 structural evolution observed in area *1. Further evidence of tectonic transport to the west and underthrusting has been found in the Federal District area and in the footwall of the São Domingos Fault that separates the External Zone from the São Francisco craton.

6 Discussion and Conclusions

Exhumation was facilitated because the final subduction of the Amazonian crust must have created a retro-wedge effect (similar to the one experimentally shown by [11] and [12]) that further pushed the rocks of the Magmatic Arc and Internal Zone to the east [17].

If collision mountain chains actually form above the sites of mantle down welling, the crustal-scale pop-up here described is expected to be rather a rule, and the search for evidence of underthrusting is encouraged elsewhere, in and out of the Tocantins Province.

References:

[1] Oldow, J.S., Bally, A.W., Avé Lallement, H.G., Transpression, orogenic float and lithospheric balance, Geology, Vol.18, No.10, 1990, pp.991-994.

[2] Kominz, M.A. and Bond, G.C., Unusually large subsidence and sea-level events during middle Paleozoic time: New evidence supporting mantle convection models for supercontinent assembly, Geology, Vol.21, No.1, 1991, pp.56-60.

[3] Molnar, P., The structures of Mountain Ranges, in Eldridge M. Moores (ed), Shaping the Earth: Tectonics of Continents and Oceans, Readings from Scientific American, edition, W.H. Freeman & Co., NY, 1990, pp.125-138.

[4] Dalziel, I.W.D., Collision and Cordilleran orogenesis: an Andean perspective, in M.P.Coward & Alison C.Ries (eds), Collision Tectonics, Geological Society Special Publication No. 19, Blackwell Scientific, 1986, pp.389-404.

[5] Suarez, G., Molnar, P. and Burchfiel, B.C., Seismicity, fault plane solutions and active tectonics of the Andes of Peru, Ecuador and southern Colombia, Journal of Geophysical Research, Vol.88, 1983, pp.403-428

[6] Roeder, D. and Chamberlain, R.L., Structural Geology of Sub-Andean Fold and Thrust Belt in Northwestern Bolivia, A. Tankard, R. Suárez and H.J. Welsink (eds)

Petroleum basins of South America, AAPG Memoir, 1995, Vol.62, pp.459-479.
[7] Clowes, R.M., Cook, F.A. and Ludden, J.N., Lithoprobe Leads to New Perspectives on Continental Evolution, GSA Today, Vol.8, No.10, 1998, pp.1-7.
[8] Matte, Ph., Mattauer, M., Olivet, J.M. and Griot, D.A., Continental subduction beneath Tibet and the Himalayan orogeny: a review, Terra Nova, Vol.9, No.5/6, 1997, pp.264-270.
[9] Kosarev, G., Kind, R., Sobolev, S.V., Yuan, X., Hanka, W. and Oreshin, S., Seismic evidence for a detached Indian Lithospheric mantle Beneath Tibet, Science Vol.283, February 26th, 1999, pp.1306-1309.
[10] Mueller, St., Deep-reaching geodynamics processes in the Alps, in M.P. Coward, D. Dietrich and R.G. Park (eds), Alpine Tectonics, Geological Society London Special Publication, Vol. 45, 1989, pp.303-328.
[11] Malavieille, J., Modelisátion expérimentale des chevauchements imbriqués: Application aux chaines des montagnes. Societé Géologique de France, Bulletin, Vol.26, 1984, pp.129-138.
[12] Brown, R.L., Beaumont, C. and Willett, S.D., Comparison of the Selkirk fan structure with mechanical models: Implications for interpretation of the southern Canadian Cordillera, Geology, Vol.21, 1993, pp.1015-1018.
[13] Huiqi, L., McClay, K.R. and Powell, D., Physical models of thrust wedges, in K.R.McClay (ed), Thrust Tectonics, Chapman & Hall, 1992, pp.71-81.
[14] Beaumont, C., Ellis, S., Hamilton, J. and Fullsack, P., Mechanical model for subduction-collision tectonics of alpine-type compressional orogens, Geology, Vol.24, 1996, pp.675-679.
[15] Epard, J-L. and Escher, A., Transition from basement to cover: a geometric model, Journal of Structural Geology Vol.18, No.5, 1996, pp.533-548.
[16] Escher, A. and Beaumont, C., Formation, burial and exhumation of basement nappes at crustal scale: a geometric model based on the Western Swiss-Italian Alps, Journal of Structural Geology, Vol.19, No.7, 1997, pp.955-974.
[17] D'el-Rey Silva, L.J.H, Vasconcelos, M.A.R., Gonçalves, D.V., Timing and role of the Maranhão River Thrust in the evolution of the Neoproterozoic Brasília Belt and Tocantins Province, central Brazil, Gondwana Research, Vol.13, No.3, 2008, pp.352-374; doi:10.1016/j.gr.2007.09.004.
[18] D'el-Rey Silva, L.J.H., Vasconcelos, M.A.R. and Fuck, R.A., Metasediments affected by the Rio Maranhão Fault versus granulite exhumation in the Brasília belt, Central Brazil, XLIII Congresso Brasileiro de Geologia, Aracaju, Anais SBG, S04:P-100, 2006, pp.190.
[19] D'el-Rey Silva, L.J.H., Ferreira Filho, C.F., Nilson, A.A., Oliveira, A.C. de, Silva Jr., C.G., Silva, C.B., Medeiros, E.S., Campos, G.S., Cruz, H.P., Zoby, J.L.G., Almeida, J.C.M., Pinelli, M.P., Mongim, R.M., Algarte, R.D., Bispo, R.S., Souza, R.S., V. Silva, V.V., Uplift of the Barro Alto Mafic-Ultramafic Intrusion by Underthrusting in the Northern Segment of the Brasília Belt, Brazil, VI SNET - Simpósio Nacional de Estudos Tectônicos, Pirenópolis-Go, Anais SBG, 1997, pp.53-56.
[20] D'el-Rey Silva, L.J.H., Fuck, R.A., Ferreira Filho, C.F. and Nilson, A.A., The Niquelândia Layered Intrusion and Underthrusting in The Brasília Fold Belt, XXXIX Congresso Brasileiro de Geologia, Salvador, SBG, Vol.6, 1996, pp.87-91.
[21] Fuck, R.A., Pimentel, M.M., D'el-Rey Silva, L.J.H., Compartimentação Tectônica na Porção Oriental da Província Tocantins, in XXXVIII Congresso Brasileiro de Geologia, Camboriú, SBG, Vol.1, 1994, pp. 215-217.
[22] D'el-Rey Silva, L.J.H., Klein, P.B.W., Walde, D.G.H., The Caldas Novas Dome, Goiás: Structural evolution and implications for tectonics in the Brasília Belt, Brazil, Journal of South American Earth Sciences Vol.17, No. 2, pp. 153-169, 2004, doi:10.1016/j.sames.2004.03.001
[23] D'el-Rey Silva, L.J.H. and Barros Neto, L.de S., The Santa Terezinha-Campos Verdes Emerald District, Central Brazil: Structural and Sm-Nd data to constrain the tectonic evolution of the Neoproterozoic Brasília Belt, Journal of South American Earth Sciences Vol.15, No.6, 2002, pp.693-708; doi:10.1016/S0895-9811(02)00087-1
[24] D'el-Rey Silva, L.J.H., Basin infilling in the southern-central part of the Sergipano Belt, NE Brazil, and implications for the tectonic evolution of the Pan-African/Brasiliano cratons and Neoproterozoic sedimentary cover, Journal of South American Earth Sciences, Vol.12, No.5, 1999, pp.453-470. doi: 10.1016/S0895-9811(99)00034-6

Are we going towards a global planetary magnetic change?

Angelo De Santis and Enkelejda Qamili
Istituto Nazionale di Geofisica e Vulcanologia, Sezione di Roma 2
Via di Vigna Murata 605, 00143 Roma
ITALY
desantisag@ingv.it, qamili@ingv.it; http://www.ingv.it

Abstract: - The dipolar part of the geomagnetic field has been decaying rapidly during the last few hundreds of years. In addition to this classical argument, from Information theory applied to geomagnetism, there are some evidences that the recent Earth magnetic field is showing characteristics typical of a reversal in progress. If this is true, many scientific and environmental questions will arise. For instance, it will be of particular interest to monitor the time-space dynamics the South Atlantic Anomaly, where the magnetic field is strongly reduced (a sort of "planetary magnetic hole"). Here we find one of the most favourite places where Low Earth Orbiting (LEO) satellites are lost or present some damages, due to the vicinity of "clouds" of electric particles (Van Allen belts) to the Earth's surface. The decay of the field will also decrease the screening effect to the solar wind and cosmic charges, so enhancing the cosmic radiation illuminating our planet: possible negative consequences are expected in terms of increase of skin cancers. Also important will be the study of the possible evolution of the core dynamics that will be generating this specific condition of the geomagnetic field.

Key-Words: - Geomagnetic field**,** Geomagnetic reversal, Global change, Information theory, Shannon information

1 Introduction

The geomagnetic field is an important property of our planet. It is generated by turbulent currents in the outer fluid core of the Earth and the study of the variations of the geomagnetic field allows in principle to infer the core dynamics [1]. What is still substantially unclear is the present state of the corresponding dynamical system, i.e., whether the system is stable or instable, random, periodic or chaotic. With this in mind, a series of works led by the first author of this paper faced with this question and tried to give some important answers [e.g. 2, 3, 4]. For instance a fractal interpretation of the geomagnetic spatial spectrum of the last four centuries [3], together with a nonlinear forecasting approach to around 10 geomagnetic observatory time series [4,5], supports the idea of a chaotic regime of the dynamical system generating the field within the terrestrial outer core. In a paper on the study of the temporal and spatial spectral features of the geomagnetic field it has been also shown that the corresponding spectral decaying exponents are simply related confirming a turbulent state of the terrestrial core regime [6]. Although some fundamental equations of the magneto-hydrodynamics are well assessed [7], the whole scenario is rather complex and a sort of holistic approach is demanding. In this paper we will show a short review of some of the previous approaches and another more recently proposed, based on the Information Theory [8]. After this introduction, the next section will describe some of the nonlinear features found for the geomagnetic field, then we will introduce some simple concepts of the Information Theory which will be applied to the case of the recent geomagnetic field. Some possible consequences in case of an imminent magnetic polarity change are briefly described. Finally the conclusions summarise some of the most fundamental concepts and results, together with some possible future development of the work.

2 Nonlinear features of the recent geomagnetic field

A chaotic process usually shows spatial fractal characteristics and temporal long-term unpredictable behaviour. A fractal surface has well defined relations between the fractal dimension D and the exponent of the power-law spatial spectrum [3]. Once found that all available global models of the geomagnetic field for the last four hundred years show a power-law form, we estimated the fractal dimension for all period from the spectrum or with an equivalent generalised ruler method [9] and found that it was practically invariant, with a value of D=2.2. The fractal spatial spectrum of the geomagnetic field could be interpreted as due to a fractal surface of the terrestrial core. One possible explanation of this fractality could be that the dynamical system generating the magnetic field is in a chaotic state. To check whether the field is chaotic we analysed some long time series (of around or more than 100 years) of geomagnetic Observatories applying a nonlinear forecasting approach. Essentially, the method consists of taking the first half part of the time series to make a prediction of the rest; after this, one compares predicted with real values of the geomagnetic field: for a chaotic geomagnetic field the deviation between the two kinds of values is exponential with time, and the exponential exponent is the K-entropy of the field itself. A characteristic of a chaotic process is that, after a time T=1/K the process is no longer predictable. The analysis showed that after around

5 years no reliable prediction was possible, confirming the need of updating the International Geomagnetic Reference Field (IGRF) every 5 years. That the underlying dynamical system producing the Earth's magnetic field is nonlinear was also confirmed by a bispectral analysis of the time series of some geomagnetic Observatories [10]: the results showed a clear quadratic frequency coupling that could be a consequence of the nonlinear behaviour of the generating process of the present geomagnetic field.

Another way to face the problem is to investigate the geomagnetic field in some important regions of the Earth, such as in the South Atlantic or in polar regions [11]. The South Atlantic Anomaly is a large feature of the geomagnetic field placed over South Atlantic where the field is unexpectedly low: it is thought due to an initial magnetic reverse flux at the level of the top of the core. During the last 100 years it seems that this anomaly is getting larger in size and is decreasing in intensity, indicating a possible activation of an internal process of polarity reversal. From recent studies it appears that the field will be zero by around 300 years.

Focussing our attention to Antarctica [11, 12], we found a similar time scale of field reduction, confirming that an imminent geomagnetic reversal is not only a speculation but even possible in short terms.

3 The information analysis of the recent geomagnetic field

Information Theory is an important tool to characterise a dynamical system [13]. It is fundamentally based on the idea that any dynamical system can be thought as a system that produces or loses information; the way the system generates new information (or loses information) can be typical of some classes of processes instead of others.

The geomagnetic field **B**(t) can be defined at and above the Earth's surface as the negative gradient of a scalar potential *V*(t), usually expressed at each time *t* by a spherical harmonic (SH) expansion in space defined by a set of Gauss coefficients ($g_n^m(t)$, $h_n^m(t)$) with n=1, …N degrees and m=0, ...n orders of the expansion; this expansion represents the superposition of N multipoles. We can now define the information content $I(t)$, or Shannon Information of **B**(t) as [10]:

$$I(t) = \sum_{n=1}^{N} p_n(t) \cdot \ln p_n(t), \qquad (1)$$

with the probability, $p_n(t)$, for the n-th multipole given by:

$$p_n = \frac{\langle B_n^2 \rangle}{\langle B^2 \rangle} = \frac{(n+1)q^{2n+4}\sum_{m=0}^{n}(c_n^m)^2}{\sum_{n'=1}^{N}(n'+1)q^{2n'+4}\sum_{m=0}^{n'}(c_{n'}^m)^2}, \qquad (2)$$

where $(c_n^m)^2 = (g_n^m)^2 + (h_n^m)^2$; $q=a/r$, a= 6371.2 km, and $\sum_n p_n = 1$ so that $p_n \ln p_n = 0$ if $p_n = 0$. $<B^2>$ and $<B_n^2>$ are the mean squared amplitudes over the sphere with radius r of the total field and of the field due to the n multipoles, respectively, which also correspond to the total and n-multipole contributions, respectively, to the spatial power spectra. Analogously, we can introduce the probability p_n' for the secular variation (d**B**/dt) = $\dot{\mathbf{B}}$ (also written as **SV**), as in (2) but using $(\dot{c}_n^m)^2 = (\dot{g}_n^m)^2 + (\dot{h}_n^m)^2$ instead of $(c_n^m)^2$. We call the corresponding information content I(SV) to distinguish it from the information content of the geomagnetic field I(B), where the time dependence is implicit in both quantities.

Some synthetic examples with different Shannon information (and Shannon Entropy) are shown in Figure 1 together with the real case deduced from IGRF at 2000. From these examples it is clear that the information content is an objective indicator of the complexity of the system: the lower the information content, the higher the complexity. In these terms we can also consider the Shannon Entropy H defined as H=-I, which has the opposite meaning of I: the higher the entropy, the higher the complexity.

Figure 1 shows the cases in terms of this kind of Entropy, normalised between 0 and 1, (in the figure 1 it is called H*) representing cases from very "smooth" regime to very "complex" one, respectively.

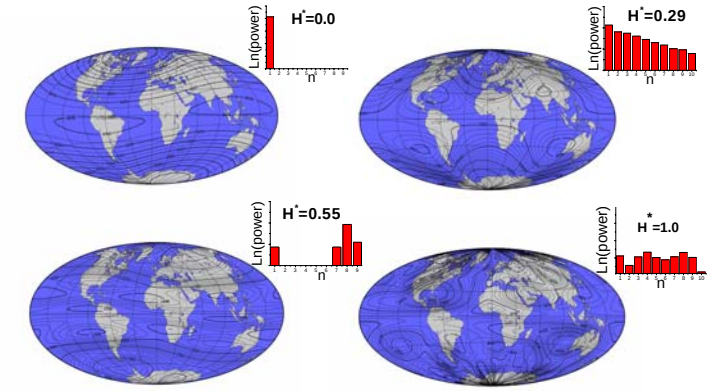

Figure 1. Four examples of geomagnetic field distribution with different Shannon information (indicated here in terms of the Shannon normalised entropy, H*), from left to right and from top to bottom, from high to low Shannon information (or from low to high Shannon entropy). The upper right figure is the only real representing the present geomagnetic field; the others are synthetic. For each case, also the corresponding power spectrum is shown in a smaller frame.

From the analysis of the geomagnetic field and its secular variation over the last few hundreds of years [8, 11] it has been seen that the Shannon information is rapidly decaying for both physical quantities and their characteristic times are of the same order between 400 and 800 years, supporting the idea of an imminent global magnetic change in terms of magnetic polarity change or excursion. This possibility has been suggested also by other authors basing their works on alternative and different approaches and results [14, 15], although some doubts have been arisen against this hypothesis [16, 17]. However if our interpretation is right, the geomagnetic field will reverse by 400-800 years. In addition, if we estimate the probability (2) at the core-mantle boundary, instead of at the Earth's surface, the characteristic time is confirmed to be around 500 years, indicating the time we expect next possible global magnetic change.

4 Some important consequences in case of an imminent geomagnetic reversal

It is thought that a geomagnetic reversal shows a preliminary phase of strong reduction of the geomagnetic field intensity just before the magnetic polarity reversal, such as the magnetic field in the present time (Figure 2). This phase has important consequences on the terrestrial surrounding environment. The low values of the field would contrast the capability of many animal species to use the geomagnetic field for orientation and homing. In particular some problems are potentially expected for some kinds of birds, fishes, turtles, and so on, in their way to reach home, or in their seasonal migrations. Of course, this problem would extend also to humans, because the compass would be practically useless for navigation. Even today the presence of the South Atlantic anomaly produces damages and troubles to low Earth orbiting (LEO) satellites, because their orbits can cross the Van Allen belts, regions containing a significant amount of very energetic charged particles placed at several hundreds km of altitude.

Reduction of the geomagnetic field intensity means a strong reduction in protection against the charged particles forming the so called solar wind and the cosmic rays, coming from the sun and from exploding stars in the outer space, respectively. The consequent increase of cosmic radiation which will reach the Earth's surface will probably imply an increase of expected number of skin cancers or other skin illnesses. If the relationship between incoming radiation and cancers is simply proportional, we would expect two – three times more than the present cases of cancers. However the real connection is not clearly known.

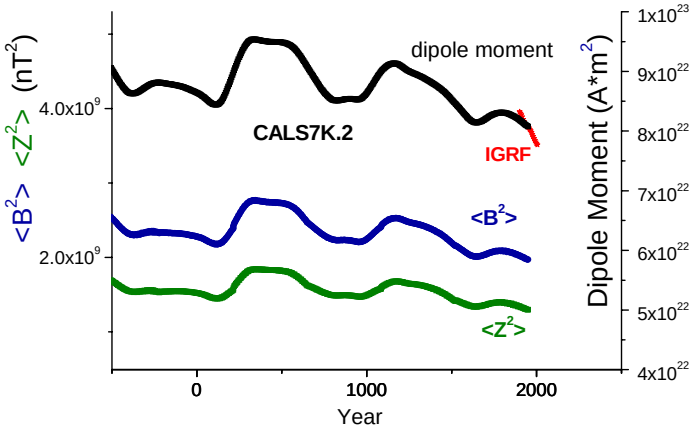

Figure 2. Dipole moment in Am^2 (upper curve), mean squared values in nT^2 of total ***B*** (middle curve) and of vertical ***Z*** intensities (lower curve) from 500 BC to present. The results for the period from -500 to 1900 refer to CALS7K model, whereas the results for the most recent 100 years are from IGRF.

5 Conclusions

There are some evidences that the present geomagnetic field is "special" in many instances. Its intensity is rapidly reducing its intensity in most of the Earth's surface and the origin of this decaying is internal to our planet. This decrease, in turn, will reduce significantly the screen of the magnetic field against external particle and electromagnetic radiations coming from the space. Only this fact would force some attention from the human society in order to protect our activities and life in the days which are coming. However the phenomenon has still its characteristic times as long as several centuries, so the humans have enough time to find all remedies or solutions that will take into account of this possible new global event. However since the field has shown some erratic behaviour during recent epochs [17], nobody can exclude that the present trends of field reduction will stop and the field will increase again. We cannot even exclude some important consequences on climate as recently suggested [18]: this part of the question is of huge importance and we will be required to investigate this aspect much more in the next future.

What is really important and fundamental is to continuously monitor and study the present behaviour of the geomagnetic field, also because we have the unique opportunity to understand its basic processes which are possibly underlying the geomagnetic field generation and variation [7].

Acknowledgments

Most of this work has been funded by the Programma Nazionale di Ricerche in Antartide (PNRA) in the frame of

the Project REM ("Reversing Earth Magnetism?"). One of the authors (EQ) has been supported first by Italian Foreign Office and then by PNRA.

References:

[1] Chiappini M., De Santis A., Magnetic investigation for studying planetary interiors, *Annali di Geofisica*, vol. XXXVII, n. *1*, 3-16, 1994.

[2] De Santis A., Barraclough D.R., A note on two expressions for the spatial power spectrum of the geomagnetic field, *Annali di Geofisica*, vol. XXXIX, n.*3*, 529-531, 1996.

[3] De Santis A. & Barraclough D.R., A fractal interpretation of the topography of the scalar geomagnetic scalar potential at the core-mantle boundary, *Pure and Applied Geophys., 149*, No.4, 747-760, 1997.

[4] Barraclough D.R. & De Santis A., Some possible evidence for a chaotic geomagnetic field from observational data, *Phys. Earth Plan. Inter*., *99*, 207-220, 1997.

[5] De Santis A., Barraclough D. R., Tozzi R., Nonlinear variability of the Recent Geomagnetic Field, Fractals, vol.*10*, No.3, 297-303, 2002.

[6] De Santis, A., Barraclough, D.R., Tozzi, R., Spectral and temporal spectra of the geomagnetic field and their scaling properties, *Phys. Earth Planet. Int*., *135*, 125-134, 2003.

[7] De Santis A., Tozzi R., Observed geomagnetic field and nonlinearity of fluid motions in the Earth's outer core, in *Chaos in geophysical flows*, Visconti et al. (Eds.), Otto Publisher, 339-366, 2003.

[8] De Santis A., Tozzi R., Gaya-Pique' L.R., Information content and K-Entropy of the present geomagnetic field, *Earth Planet. Science Lett*., *218*, 269-275, 2004.

[9] De Santis A., A direct divider method for fractal self-affine profiles and surfaces, *Geophysical Research Letters*, vol. *24*, No. 16, 2099-2102, 1997.

[10] Tozzi, R., De Santis, A., Detecting geomagnetic field nonlinearities by means of bispectral analysis and phase coupling nonlinear technique, *Annals of Geophysics*, vol.*45*, N.2, 279-287, 2002.

[11] De Santis A., How persistent is the present trend of the geomagnetic field to decay and possibly to reverse? Phys. Earth Inter., *162*, 217-226, 2007.

[12] Alfonsi L., De Franceschi G., De Santis A., Geomagnetic and ionospheric data analysis over Antarctica: a contribution to the long term trends investigation, Annales Geophysicae, *26*, 1173-1179, 2008.

[13]Shannon C., A mathematical theory of communication, *The Bell Syst. Tech. J., 27*, 379-423, 623-656, 1948.

[14] Gubbins D., Mechanism for geomagnetic polarity reversals, *Nature, 326*, 167-169, 1987.

[15] Hulot G., C. Eymin, B. Langlais, M. Mandea, N. Olsen, Small-scale structure of the geodynamo inferred from Ørsted and Magsat satellite data, *Nature, 416* , 620-623, 2002.

[16] C.G. Constable , and M. Korte, Is Earth's magnetic field reversing?, *Earth Planet. Sc. Lett., 246*, 1-16, 2006.

[17] D. Gubbins, A.L. Jones, C.C. Finlay, Fall in Earth's Magnetic Field is erratic, *Science, 312*, 900-902, 2006.

[18] Svensmark H., Pedersen J.O.P., Marsh N.D., Enghoff M.B., Uggerhoj U.I., Experimental evidence for the role of ions in particle nucleation under atmospheric conditions, *Proceedings Royal Soc. A*, 463, N.2078, 385-396, 2007.

A Model for the Plate Tectonic Evolution of the Eastern Mediterranean Region that Emphasizes the Role of Transform (Strike-Slip) Structures

RICHARD W. HARRISON
U.S. Geological Survey
MS926A National Center
12201 Sunrise Valley Drive
Reston, VA 20192
USA
rharriso@usgs.gov

Abstract: - A model for the tectonic evolution of the Eastern Mediterranean region from Mesozoic to Present is developed from geological, geophysical, and seismological data on and surrounding the island of Cyprus. This model emphasizes the role of major transform structures in accommodating horizontal plate motions, driven from the west by spreading along the Atlantic-Arctic mid-ocean-ridge system and from the east by escape tectonics related to the movement of the Arabian plate. In particular, this model interprets the African-Anatolian plate boundary as a system of left-lateral transform structures, >75 km wide, that has been active since the early Mesozoic. In this model, Neotethys spreading and closure (subduction and obduction) occurred north of the transform system. Geophysical data indicates that the Troodos ophiolite dips northward; suggesting that subduction was to the north beneath the Anatolian plate. Southward obduction of the Troodos ophiolite was facilitated by contemporaneous left-lateral horizontal shear. The northward sequence of 1) a wide zone of shear containing ophiolites; 2) contracted trench and accretionary prism rocks; and 3) a north-dipping subduction zone is similar to the sequence described across the Arabia-Anatolian plate boundary, indicating commonality in tectonic evolution.

Key Words: Eastern Mediterranean, Plate tectonics, African plate, Mesozoic, Cenozoic, Cyprus, Troodos

1 Introduction

Plate tectonics is one of the Earth's most important dynamic systems in regards to its impact on man and civilization. Seismic, volcanic, and tsunami hazards are all directly influenced by plate movements; the location and genesis of economic mineral deposits, as well as energy resources, are also governed by the various hydrothermal, deformational, and depositional environments associated with past and present plate interactions. A better understanding of present-day settings and the dynamic history of plate interactions are critical to man's future.

The Eastern Mediterranean region has had a complex tectonic history since the early Mesozoic breakup of Gondwana. Between the major plates of Africa and Eurasia, there is a > 1,500-km-wide intervening collage of differing tectonic terranes that is the product of shearing, rifting, subduction, obduction, and contraction over the past 200 Ma. The dynamics of plate interactions is recorded in the assembly of this collage. The E. Med. region encompasses the southern portion of the collage and includes its margin with the African plate. The early Mesozoic opening of the Atlantic basin instigated left-lateral shear along the northern margin of the African plate, as Africa moved eastward relative to the Eurasian plate [1,2]. Neotethys rifting and creation of subduction zones characterizes much of the Mesozoic in the E. Med. region [1,2,3,4]. As Atlantic rifting expanded northward into the N. Atlantic and Arctic, relative motion between these two plates became more convergent and regional stresses along the African plate margin became more transpressive [1,2]. Two other global-scale tectonic events have significantly impacted the E. Med. First, the Eocene collision of the Indian plate with Eurasia enhanced left-lateral movement of Eurasia relative to Africa. And second, the Miocene separation of the Arabia plate from Africa along the Dead Sea transform produced a northward impingement of Arabia into the intervening collage of terranes, in particular the Anatolian microplate; this event initiated escape tectonics of Anatolia [1,2]. Thus, plate tectonics in E. Med. region over the past 5 Ma has been influenced by

the westward escape of the Anatolian microplate; this has been accommodated by strike-slip movement along generally NE-SW- to E-W trending faults along the African-Anatolian and Arabian-Anatolian boundaries [2,3,5,6]. Cyprus is located on the southern margin of the Anatolian microplate (Fig. 1), adjacent to the African plate boundary [1]. Understanding the tectonic evolution of Cyprus is critical to a better understanding of the tectonic evolution of the entire Eastern Mediterranean region.

2 Problem: Competing Plate Tectonic Models for the Eastern Mediterranean Region

The tectonic evolution of the margin between the African and Anatolian plates is controversial [5,6,7], including the present-day tectonic setting (Fig. 1). Much of the controversy centers on (i) the nature of major structures offshore of Cyprus, (ii) the origin of the Troodos ophiolite and its obduction onto continental crust, and (iii) the nature of the crust under the Levantine basin (oceanic vs. attenuated continental). The two competing ideas on the nature of major structures offshore of Cyprus are: 1) that a northerly dipping subduction zone, which has consumed oceanic crust since the Late Cretaceous, exists south of Cyprus [8,9,10,11,12,13], or 2) that a complex system of left-lateral strike-slip faults exists south of Cyprus (Fig. 1) and that there has never been a subduction zone nor oceanic crust south of the island [5,6,7, 14,15,16, 17]. The two competing ideas for the obduction of Troodos are: 1) emplacement from the south after formation over a supra-subduction zone [8,9,10,11, 12,13]; and 2) obduction from the north [5,6,7,18] contemporaneous with left-lateral strike-slip tectonics [7,]. The two competing ideas on the crustal nature of the Eastern Mediterranean are: 1) Cyprus, Eratosthenes Seamount (ES), Nile Delta, and the Levantine basin are all underlain by continental crust, the latter two of which are highly attenuated [19], and 2) the Levantine basin is underlain by oceanic crust [20, 21]. The nature of the crust is beyond the scope of this paper; however, the geophysical evidence that the Levantine basin is highly attenuated continental crust [19] is accepted, otherwise the ES, which is underlain by ~28 km of continental crust [27, 28], becomes an unlikely protrusion off of the African plate.

2.1 Problems with Subduction Zone Models

For the past three decades, the dominant theory for the tectonic setting of Cyprus has been that a northerly dipping subduction zone exists beneath the island [8,9,12,29]. However, several problems exist with the

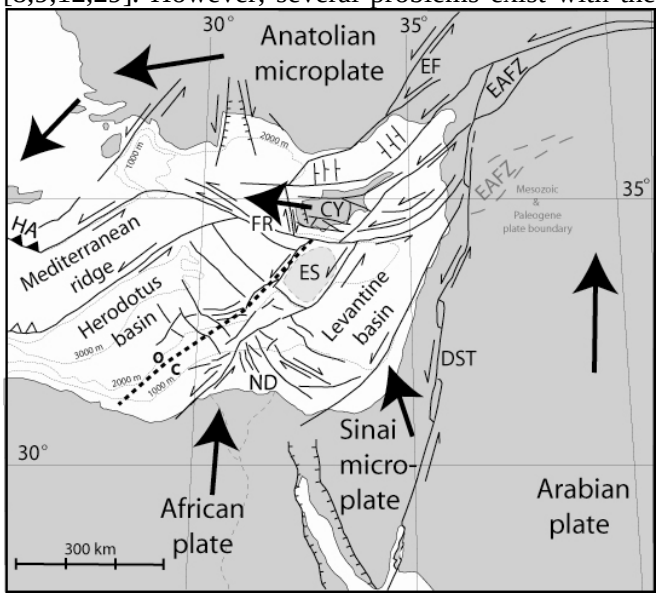

Figure 1. Present-day tectonic map of the Eastern Mediterranean region [after 5,6]. CY- Cyprus, ES- Eratosthenes Seamount, FR- Florence Ridge, which occurs along left-lateral strike-slip structure [22]; EF- Ecemis fault, EAFZ - Eastern Anatolian fault zone (paleo-location to the south during Mesozoic & Paleogene shown by ghost lettering) DST- Dead Sea transform, ND- Nile delta, HA- Hellenic arc; bold dashed line is approximate boundary between oceanic (O) and continental (C) crust [23,24]; large arrows represent relative plate motions [after 25,26]. The fault system between Cyprus and ES is the Cypriot transform, which marks the northern African plate boundary [1,2].

subduction-zone models [5,6,7]. Summarized, these are: **1)** absence of a volcanic arc in the vicinity of Cyprus; the nearest arc rocks are far to the north in the middle and northern parts of the Anatolian plate; **2)** the absence of a Benioff zone beneath Cyprus; rather, a tabulation and plot of the best-constrained recorded seismicity [30] reveals a clustered vertical zone of seismic events (Fig. 2) that extends to depths of greater than 60 km; **3)** known onshore Neogene faults are dominantly strike-slip and transpressive structures [5,6,7,36]; **4)** gravity investigations [27,28] show that Cyprus is underlain by ~35 km of continental crust and that the ES is underlain by ~28 km of continental crust; seismic-refraction measurements support this interpretation[38,39], thus, the plate boundary is a continent-continent interface; **5)** continuous seismic

reflection profiles across the Cypriot transform [40] reveal a complex pattern of braided horst and graben structures that is more characteristic of a transpressive positive-flower structure than a subduction complex; **6)** GPS results [26] show that Cyprus is moving in a westerly direction (Fig. 1) that is orthogonal to the motion of the African plate; this is viewed as inconsistent with subduction-zone models, but is very consistent with a model based on escape tectonics and strike-slip faulting [2,5,6].

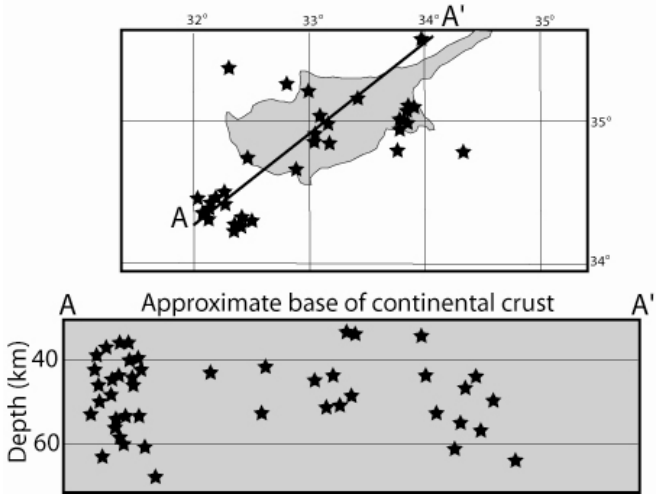

Figure 2. Locations of the best-constrained, recorded deep earthquake epicenters in the Cyprus area [after 30]. Cross section A-A' shows hypocenters projected to the line of section. Note that the top of the cross section is at about 30 km- the approximate base of the crust. Focal mechanisms calculated for larger earthquakes along the Cypriot transform indicate a mixture of faulting styles, but are dominantly of strike-slip faulting [3132,33,34]. Such mixtures of faulting styles are characteristic of strike-slip fault zones [35] and are atypical of subduction zones. If the vertical zone of seismicity offshore Cyprus is a steeply dipping Benioff zone, then the uplift of Cyprus is unexplained and there should be a close-lying volcanic arc (Mariana-type subduction zone).

3 Proposed Solution: A Model Emphasizing Strike-Slip Tectonics

All present-day geologic, geophysical, and seismological data and observations in the Eastern Mediterranean region can be attributed to strike-slip tectonics; active uplift and faulting on Cyprus are attributable to a restraining bend along the Cyprus transform [5,6,7]. One primary premise of this paper is that strike-slip tectonics has played an active role in the geologic history of the region since early in the Mesozoic. The second premise is that obduction of the Troodos ophiolite occurred from the north in concert with strike-slip tectonics.

3.1 Ancestry of Strike-slip Structures

In the vicinity of Cyprus, the northern African-plate margin consisted of parallel strike-slip fault zones in Mesozoic and Paleogene time (Fig. 3). Together with a complex system of associated R, R', and P shears, the Ovgos fault zone, Southern Troodos transform, and the Cypriot transform accommodated eastern movement of the Africa plate relative to Eurasian plate that began with the initial breakup of Gondwana [1]. This zone of strike-slip faulting is >75 km wide; left-lateral shear-coupling across the zone explains the counter-clockwise rotation of Cyprus [41,44,45] and the ES [21] during the Late Cretaceous to Eocene (see Fig. 3).

Across the Ovgos fault zone, differing geologic terranes of Mesozoic and Paleogene age are juxtaposed [6]. North of the Ovgos, accretionary prism and trench rocks, including metamorphosed sediments that contain blocks of pillow basalt and arc-like rhyolite, are overlain by strongly faulted and folded, deep-water turbidites (flysch). South of the Ovgos, platform sediments occur that are comprised of only slightly faulted and un-metamorphosed shallow-water chalk and carbonate rocks with no volcanic rocks [6]. The fact that there is a total mismatch of sedimentary and structural features across the Ovgos until Late Miocene deposition and deformation [5,6] suggests as much as a few hundred kms of transposition.

Beneath Cenozoic sedimentary cover, the entire southern portion of Cyprus is underlain by tectonic mélange and allothonous horizontally sheared rocks of Triassic to Cretaceous age [18,41,42]. Horizontal slip in this zone, the South Troodos transform, was left lateral [18,41,43]; strands of this zone are similarly active today [37]. Also, Late Cretaceous debris-flow deposits in SE Cyprus possess strong, non-penetrative, vertical, E-W-trending shear fabric. Shear was non-abrasive, as there is a total lack of slickenside surfaces, gouge, and other brittle deformation; it is interpreted as having occurred while the deposits were water saturated during deposition.

The Cypriot transform is considered the primary northern African plate boundary during the Mesozoic [1]; extensions to both east and west are known strike-slip crustal boundaries [14,16,22,40,46]. A good modern analogy for this structure in the Mesozoic is the San Andreas fault zone, which runs along the North American plate margin and is inboard to a sequence of allothonous continental crust and mélange, oceanic

crust and spreading center (Pacific plate), and an opposite-facing subduction zone (western Pacific margin). A corollary of this is that the ES lay farther to the west, relative to Cyprus, in the Mesozoic (Fig. 3).

If Neogene motion along the Dead Sea transform is restored in an amount equal to the opening of the Red Sea, then the Eastern Anatolian fault zone at the Arabian-Anatolian plate boundary becomes aligned E-W with faults on and offshore Cyprus described above (see Fig. 1). This indicates a common ancestry, which is also implied by the similar in tectonic packages and history between Arabian-Anatolian boundary [47,48] and the African-Anatolian boundary presented here.

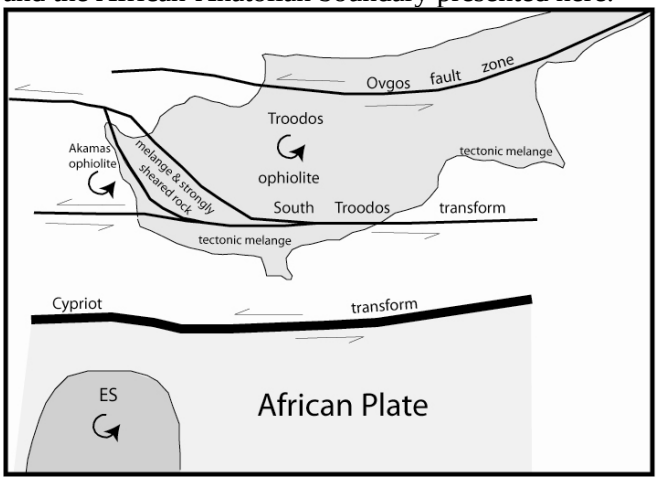

Figure 3. Schematic diagram showing major Mesozoic and Paleogene transform structures along the African plate boundary in vicinity of Cyprus and the Eratosthenes Seamount (ES); in part adapted after [21]. Counter-clockwise rotations after [21,41,43,44].

3.2 Troodos Obduction

Gravity data [18,27] indicate that mantle rocks and oceanic crust dip northward away from the exposed Troodos ophiolite; suggesting a southward-vergence for its obduction in the late Mesozoic (Fig. 4). It is proposed that obduction was facilitated by oblique low-angle slip in a transpressive strike-slip setting (Fig. 5); the same kinematics that produced CCW rotation. A corollary is that the Southern Neotethys becomes a simple uniform sea along the northern margin of the African-Arabia plate, defined by the continuous ophiolite belt from Cyprus eastward.

4 Conclusions:

1) All regional geologic, geophysical, and seismological data are explained through a model that invokes a leading role of strike-slip tectonics along the northern plate margin of Africa. 2) Crustal obduction, 90° CCW rotation of crust, left-lateral shearing, and localized Neogene uplift have occurred across a >75-km-wide tectonic system north of the African plate margin. 3) Neotethys spreading and the creation of oceanic crust (Troodos) occurred north of this strike-slip system. 4) The Troodos ophiolite was obducted from the north, driven by low-angle transpressive stress. 5) Trench, fore-deep, and accretionary prism rocks were over-thrusted from the north by transpressive stress in the Neogene. 6) The northern margins of African and Arabian plates shared a common tectonic evolution prior to Neogene separation along the Dead Sea transform.

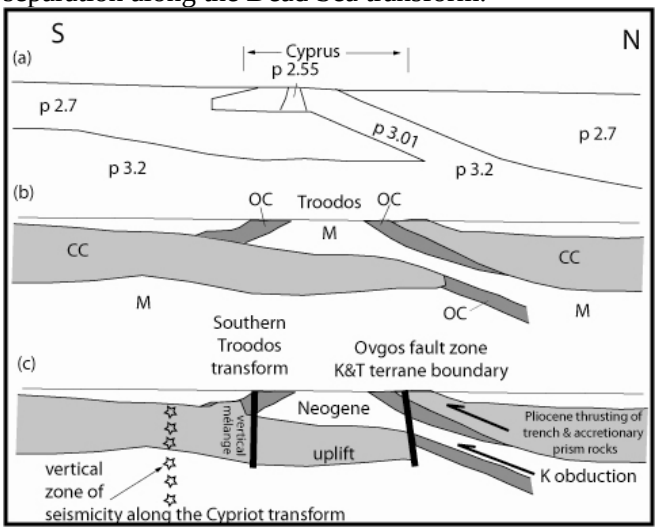

Figure 4. N-S crustal cross sections through Cyprus. (a) Model of gravity data showing rock densities [after 27]. (b) Interpretation of crustal material [after 27]; CC- continental crust, OC- oceanic crust, m- mantle material. (c) Location of seismicity along the Cypriot transform, Also depicted are Neogene uplift do to a restraining bend along the Cypriot transform [5.6] and the direction of Neogene thrusting of trench and accretionary prism rocks [6].

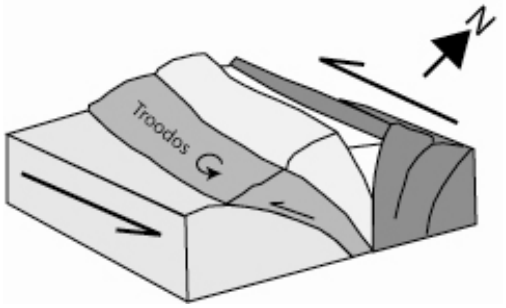

Figure 5. Schematic of Troodos obduction contemporaneous with left-lateral strike-slip faulting, modeled after deformation along the San Andreas transform [35].

References:

[1] Dewey, J.F., Pittman, III, W.C., Ryan, W.B.F., Bonnin, J., Plate tectonics and the evolution of the Alpine system, *Geological Society of America Bulletin*, vol. 84, 1973, pp. 3137-3180.

[2] Şengör, A.M.C., Gorur, N., Saroglu, F., Strike-slip faulting and related basin formation in zones of tectonic escape: Turkey as a case example. In Biddle, K.T., Cristie-Blick, N., eds., *Strike-Slip Deformation, Basin Formation and Sedimentation, Society of Economical Paleontologists and Mineralogists Special Publication*, vol. 37, 1985, pp. 227-264.

[3] Dercourt, J., and 18 others., Geological evolution of the Tethys belt from the Atlantic to the Pamirs since the Lias, *Tectonophysics*, vol. 123, 1986, pp. 241-315.

[4] Robertson, A.H.F., Cliff, P.D., Degnan, P., and Jones, G., Palaeogeographic and palaeotectonic evolution of the Eastern Mediterranean Neothethys, *Palaeo-geography, Palaeoclimotology, and Palaeoecology*, vol. 87, 1991, pp. 289-344.

[5] Harrison, R. and Panayides, I., A restraining-bend model for the tectonic setting and uplift of Cyprus, in Chatzipetros, A.A. and Pavlides, S.B. (eds.), *Proceedings of the 5th International Symposium on Eastern Mediterranean Geology*, Thessalonili, Greece,14 to 20 April, 2004, pp B43-B46.

[6] Harrison R., Newell W., Batıhanlı H., Panayides I., McGeehin, J., Mahan, S., Őzhűr, A., Tsiolakis, E. and Necdet, M., Tectonic framework and late Cenozoic tectonic history of the northern part of Cyprus: implications for earthquake hazards and regional tectonics, *Journal of Asian Earth Sciences*, Vol. 23, 2004, pp. 191-210

[7] Harrison, R.W., and Tsiolakis, E., Change from convergent to collisional transform boundary conditions between the African and Anatolian plates, based on the geology of Cyprus: Geological Society of America Abstracts with Programs, v. 38, no. 7, 2006, p. 277.

[8] Robertson, A.H.F., Kidd, R.B., Ivanov, M.K., Limonov, A.F., Woodside, J.M., Galindo-Zaldivar, J., and Nieto, I., Eratosthenes Seamount: collisional processes in the easternmost Mediterranean in relation to the Plio-Quaternary uplift of southern Cyprus, *Terra Nova*, vol. 7, 1995, pp. 254-264.

[9] Robertson, A.H.F, Tectonic evolution of Cyprus in its Easternmost Mediterranean setting. In: Panayides, I., Xenophontos, C., Malpas, J., eds., *Proceedings of the Third International Conference on the Geology of the Eastern Mediterranean.* Geological Survey Department, Republic of Cyprus, 2000, pp. 11-44.

[10] Robertson A., Tectonic evolution of Cyprus in its easternmost Mediterranean setting, in: Panayides I., Xenophontos C. & Malpas J. (eds.), *Proceedings of the Third International Conference on the Geology of the Eastern Mediterranean*, Geological Survey Department of Cyprus, Republic of Cyprus, 2000, pp. 11-44.

[11] Poole, A., and Robertson, A.H.F., Quaternary uplift and sea-level change at an active plate boundary, Cyprus, *Journal of the Geological Society of London*, vol. 148, 1992, pp. 909-921.

[12] Woodside, J.M., Tectonic elements and crust of the Eastern Mediterranean Sea, *Marine Geophysical Research*, vol. 3, 1977, pp. 317-354.

[13] Woodside, J.M., Disruption of the African plate margin in the Eastern Mediterranean, in M.J. Salem, ed., The Geology of Libya, no. 6, 1992. pp. 2319-2329.

[14] Kempler, D., and Garfunkel, Z., Structures and kinematics in the northeastern Mediterranean: A study of an irregular plate boundary, *Tectonophysics*, vol. 234, 1994, pp.19-32.

[15] Makris, J., Stacker, J., and Kramvis, S., Microseismic studies and tectonic implications of Cyprus. In: Panayides, I., Xenophontos, C., Malpas, J., eds., *Proceedings of the Third International Conference on the Geology of the Eastern Mediterranean,*. Geological Survey Department, Republic of Cyprus, 2000, pp. 137-145.

[16] Neev, D., The Pelusium Line- a major transcontinental shear, Tectonophysics, vol. 38, 1977, pp. T1-T8.

[17] Neev, D. and Hall J.K., A global system of spiraling geosutures, *Journal of Geophysical Research*, vol. 86, 1982, pp. 10,689-10,708.

[18] Gass I.G., MacLeod C.J., Murton B.J., Panayiotou A., Simonian K.O. and Xenophontos C., The geology of the southern Troodos transform fault zone, *Geological Survey Department of Cyprus Memoir 9*, 1994, pp. 218.

[19] Gardosh & Drunkman, Seismic stratigraphy, structure and tectonic evolution of the Levantine Basin, offshore Israel, Geological Society Special Publication, vol. 260, 2006, pp. 201-227.

[20] Ben-Avraham Z., Ginzburg, A., Makris, J., and Eppelbaum, L., Crustal structure of the Levant Basin, eastern Mediterranean, *Tectonophysics*, vol. 346, 2002, pp. 23-43.

[21] Garfunkel, Z., Constrains on the origin and history of the Eastern Mediterranean basin, *Tectonophysics*, vol. 298, 1998, pp. 5-35.

[22] ten Veen, J.H., Woodside, J.M., and Zitter, T.A.C., The enigma of the Hellenic – Cyprus arcs' junction solved, *in* Chatzipetros, A.A., and Pavlides, S.B., eds., 5th *International Symposium on Eastern Mediterranean Geology, Thessaloniki, Greece*, vol. 1, 2004, pp. 201-204.

[23] Dolson J., Shann, M., Matbouly, S., Harwood, C., Rashed, R., and Hammonds, H., The petroleum potential of Egypt, *in* Downey M., Threet, J., and Morgan, W., eds., Petroleum Provinces of the Twenty-first Century, *American Association of Petroleum Geologists Memoir 74*, 2004, pp. 453-482.

[24] Dolson, J.C., Boucher, P.J., Dodd, T., and Ismail, J., Petroleum potential of an emerging giant gas province,

Nile Delta and Mediterranean Sea off Egypt, *Oil &Gas Journal*, vol. 100, no. 20, 2004, pp. 32-37.

[25] Jackson J., and McKenzie, D., The relationship between plate motions and seismic moment tensors, and the rates of active deformation in the Mediterranean and Middle East, *Geophysical Journal*, vol. 93, 1988, pp. 45-73.

[26] McClusky S., and 27 others., Global positioning system constraints on plate kinematics and dynamics in the eastern Mediterranean and Caucasus, *Journal of Geophysical Research*, vol. 105, no. 5, 2000, pp. 5,695-5,719.

[27] Gass I., and Masson-Smith, D., The geology and gravity anomalies of the Troodos Massif, Cyprus, *Philosophical Transactions of the Royal Society of London*, vol. 255, 1963, pp. 417-467.

[28] Makris J., Ben Abraham, Z., Behle, A., Ginzburg, A., Giese, P., Steinmetz, L., Whitmarsh, R.B., and Eleftheriou, S., Seismic refraction profiles between Cyprus and Israel and their interpretation, *Geophysical Journal of the Royal Astrological Society*, vol. 75, 1983, pp. 575-591.

[29] Payne, A.S., and Robertson, A.H.F., Structural evolution and regional significance of the Polis graben system, western Cyprus, *in* Panayides I., Xenophontos, C., and Malpas, J., eds., *Proceedings of the Third International Conference on the Geology of the Eastern Mediterranean*:, Geological Survey Department of Cyprus, Republic of Cyprus, 2000, pp. 45-59.

[30] Algermissen, S., and Rogers, A., Chapter 5. A Cyprus earthquake hazard assessment: Maps of probabilistic peak ground acceleration and uniform-hazard pseudo-absolute acceleration spectral response, *in* DeCoster, M., Zomeni, Z., Panayides, I., Petrides, G., and Berksoy, O., eds., *Seismic Hazard and Risk Assessment of the Greater Nicosia Area*, unpubl. United Nations report available at Geological Survey Department of Cyprus, Lefkosia, Republic of Cyprus, 2004, 73 p.

[31] Arvidsson R., Ben-Avraham, Z., Ekstrom, G., and Wdowinski, S., Plate tectonic framework for the October 9, 1996, Cyprus earthquake, *Geophysical Research Letters*, vol. 25, 1998, pp. 2241-2244.

[32] Pinar A., and Kalafat, D., Source processes and seismotectonic implications of the 1995 and 1996 Cyprus, Eastern Mediterranean region earthquakes, *Tectonophysics*, vol. 301, 1999, pp. 217-230.

[33] Makris J., Stacker, J., and Kramvis, S., Microseismic studies and tectonic implications of Cyprus, *in* Panayides I., Xenophontos C., and Malpas J., eds., *Proceedings of the Third International Conference on the Geology of the Eastern Mediterranean*, Geological Survey Department, Republic of Cyprus, 2000, pp. 137-145.

[34] Jackson J., and McKenzie, D., The relationship between plate motions and seismic moment tensors, and the rates of active deformation in the Mediterranean and Middle East, *Geophysical Journal*, vol. 93, 1988, pp. 45-73.

[35] Sylvester, A.G., Strike-slip faults, *Geological Society of America Bulletin*, vol. 100, 1988, pp. 1666-1703.

[37] Soulas J., Active tectonics studies in Cyprus for seismic risk mitigation: The greater Limassol Area, *unpublished report for the Geological Survey Department of Cyprus*, Nicosia, Cyprus, 1999, 24 p.

[38] Aal A., Barkooky, A., Gerrits, M., Meyer, H., Schwander, M., and Zaki, H., Tectonic evolution of the eastern Mediterranean Basin and its significance for the hydrocarbon prospectivity of the Nile Delta deepwater area, *GeoArabia*, vol. 6, 2001, pp. 363-384.

[39] Ben-Avraham Z., Ginzburg, A., Makris, J., and Eppelbaum, L., Crustal structure of the Levant Basin, eastern Mediterranean, *Tectonophysics*, vol. 346, 2002, pp. 23-43.

[40] Udintsev, G.B., Zverev, A.S., Odinokov, Y.Y., Efremov, V.N., Eleftheriou, S., and Hall, J.K., Structure of the post-Messinian sedimentary cover in the eastern part of the Mediterranean Sea, *in* Krasheninnikov, V.A., and Hall, J.K., eds., *Geological structure of the northeastern Mediterranean (Cruise 5 of the Research Vessel 'Akademik Nikolaj Strakhov')*, Historical Productions-Hall Ltd., Jerusalem, Israel, 1994, pp. 33-74.

[41] Swarbrick, R.E., Sinistral strike-slip and transpressional tectonics in an ancient oceanic setting: the Mamonia Complex, southwest Cyprus, Journal of the geological Society, London, vol. 150, 1993, pp. 381-392.

[42] Geological Survey Department of Cyprus, *Geologic Map of Cyprus*, 1995, 1 sheet.

[43] Spray, J.G., and Roddick, J.C., Evidence for Upper Cretaceous transform fault metamorphism in West Cyprus, *Earth and Planetary Science Letters*, vol. 55, 1981, pp. 273-291.

[44] Moores, E.M., and Vine, F.J., The Troodos Massif, Cyprus and other ophiolites as oceanic crust: evaluation and implications, *Transactions of the Royal Society, London*, vol. A268, 1971, pp. 443-466.

[45] Clube, T.M.M., Creer, K.M., and Robertson, A.H.F., The palaeorotation of the Troodos microplate, *Nature*, vol. 317, 1985, pp. 522-525.

[46] Vidal, N., Klaeschen, D., Kopf, A., Docherty, C., Von Huene, R., Krasheninnikov, V.A.,Seismic images at the convergence zone from south of Cyprus to the Syrian coast, eastern Mediterranean, *Tectonophysics*, vol. 329, 2000, pp. 157-170.

[47] Dilek, Y., Collision tectonics of the Mediterranean region: Causes and Consequences, *Geological Society of America Special 409*, 2006, pp. 1-14.

[48] Robertson, A.H.F., Mesozoic-Tertiary tectonic-sedimentary evolution of a south Tethyan oceanic basin and its margin in southern Turkey, *Geological Society, London , Special Publication*, vol. 173, 2000, pp. 97-138.

On interpreting surface deformations and gravity changes for understanding volcanoes.

PETER VAJDA and LADISLAV BRIMICH
Geophysical Institute
Slovak Academy of Sciences
Dubravska cesta 9, Bratislava 845 28
SLOVAK REPUBLIC
Peter.Vajda@savba.sk, geofbrim@savba.sk

Abstract: We briefly review the topic of monitoring and interpreting the ground deformation and temporal changes of gravity in volcanic regions. We give an overview of techniques used for the monitoring, discuss the interpretation of the observed data, and present our contribution to the field. We aimed at developing a new technique for interpreting temporal gravity changes, the so-called Truncation Filtering Methodology (TFM), that can be characterized as a data enhancement and pattern recognition technique. We tested its applicability on data observed at volcanoes Mayon (Philippines) and Merapi (Indonesia). In the case of Mayon we managed to estimate the depth to the magma chamber of the volcano. In the case of Merapi our technique failed to produce any meaningful interpretation. The topic of monitoring and interpreting phenomena associated with dynamic magma processes leaves the door wide open for further research.

Key-Words: ground deformation, vertical displacements, temporal gravity changes, volcanic hazards, interpretation, geodynamics, Truncation Filtering Methodology

1 Volcanoes as threats

Volcanoes even nowadays in the era of modern technology pose serious threats to human lives and property. Tens to hundreds of thousands people live in the very vicinity of the many active or dormant volcanoes worldwide. Risk assessment, hazard mitigation, and early plus accurate prediction, warning, and evacuation are more than essential. These require a good knowledge of geodynamic processes associated with volcanic activity. Geophysical, geodynamic, geochemical and hydrothermal process linked with magmatic and volcanic activity are very complex. We can typically detect only their surface manifestations. Seismic and geodetic monitoring of these phenomena appears essentially useful. To date, no unifying theory exists to explain the diversity and complexity of magmatic and volcanic systems. The prediction and assessment is thus tied to understanding at least the geological setting of a local system, the composition and state of magma, and the eruptive regimes of that system. Before magma explodes or pours onto the surface, it forms deep within the earth, rises through extreme conditions of pressure and temperature, interacts physically and chemically with crustal rocks, cools, partially crystallizes, degases, may mix, responses to a regional tectonic setting, and interacts with groundwater (Dzurisin, 2007).

2 Monitoring ground deformations and gravity changes

The volcano monitoring techniques may be classified as continuous observations and repeated surveys, both being in the fields of seismology, geodesy, (non-seismic) geophysics, geochemistry, and hydrology (e.g., Dzurisin, 2007). Seismic monitoring is most of the times superior to the rest of the techniques in tracking the awakening of a volcano and predicting an eruption shortly prior to it. Geochemical monitoring of volcanic gasses gives valuable insights into the magma movement and magma state or composition changes. Herein we shall focus at the ground deformations and gravity changes. Magma movement and changes in its physical and chemical state lead to measurable vertical displacements of the ground, and temporal changes of gravity.

Fig.1
Field gravity measurements with the CG5 relative gravity meter

Gravity can be measured in the field with the accuracy of the 8th decimal place (10^{-8} m/s^2 or 1 microGal). Easily portable relative gravimeters (cf. Fig.1) can be used for repeated surveys on monumented gravity points (stations), yielding observed temporal gravity changes that are more or less sparse in both space (on the topographic surface of a volcano and its vicinity) and time. Continuous microgravity measurements can be performed at secured (sheltered) stations using absolute or special (tidal) relative gravimeters.

Ground deformations can be monitored using classical surveying techniques such as leveling, triangulation, trilateration, distance measurements (tape or electronic distance measurements [EDM]), tilt- and strain-meter measurements, and more modern techniques such as GPS or remote sensing: radar interferometry (interferometric synthetic-aperture radar [InSAR]), photogrammetry. The great advantage of remote sensing techniques is the spatial coverage and resolution (Dzurisin, 2007).

3 Interpreting ground deformations and gravity changes

Ground deformations are caused by changing physical and chemical properties of magma and by its movements through the rock environment. Temporal changes of gravity are due to two causes. One is the ground deformation (vertical displacement of the topographic surface), i.e., the change of height of the deforming surface in the ambient gravity field of the earth, the other is the change of subsurface mass distribution due to magmatic dynamic processes associated with the movement and physical and chemical changes in magma. The ascending magma moves through cracks and vents, makes new reservoirs, while stressing and deforming the rock surroundings, the interaction of which also plays its role.

In interpreting temporal gravity changes it is crucial to separate all the signals that contribute to them. We seek to interpret signal at the level of 10 microGal. Thus accurate atmospheric correction at the respective time of observation must be considered, instrument drift must be under perfect control, tidal correction must be accurate, often including ocean loading in the region, the temporal change of the topographic correction, especially due to lava doming (dome building/collapse) must be employed, and perhaps the most tricky to correct for is the effect of ground water changes.

Ground deformations and gravity changes are interpreted most often by modeling, but also by direct inversion. In modeling (e.g., Dzurisin, 2007, chapter 8) the sources of geodynamic magmatic processes are simplified. Point sources or volumetric sources of selected shapes (and their combination) are used to simplify the sources of pressure, heat, and mass change. Then a direct problem is solved analytically, or numerically (especially when topography is considered). The direct problem solution produces model surface deformations and model gravity changes. The parameters of the model (of the sources) are iteratively fine-tuned until a satisfactory match is reached between the observed and the model data (deformation and gravity changes). The problem is non-unique and ill-posed. Several models may produce the same (or too similar) data. Additional information is of great importance in discriminating between possible model solutions.

We have investigated the possibility of applying the so-called Truncation Filtering Methodology (TFM) to interpreting temporal gravity changes at volcanoes. The study was carried out by means of modeling for point sources (Vajda et al., 2000; Vajda and Brimich, 2002). The TFM can be described as a data enhancement and pattern recognition technique (Vajda and Vaníček, 2002). The temporal gravity changes are truncation filtered, i.e., transformed by convolution integrals (with one free parameter – the truncation parameter) into dynamic sequences that are graphically animated with respect to the value of the truncation parameter. These so-called truncation sequences display dynamic patterns. For point sources the onset of the respective pattern depends uniquely (and even linearly) on the depth of the point source and is used to determine the depth of the point source.

3.1 Mayon case

The TFM was tested on real data for the first time when applied to temporal changes of gravity observed at the Mayon volcano, Philippines (Fig.2). Data (kindly provided to us by Prof. Jentzsch) observed in five campaigns between 1992 and 1996 were interpreted. Interestingly, the observed ground deformation was in this period insignificant, while gravity changes reached up to 150 microGals (1500 nm/s^2).

Data (Fig.3) were interpreted in terms of a point source representing the change of masses for a case of an assumed magma injection process. The source mechanisms associated with volcanism are complex processes with combined effects of pressure, heat, and mass transport. For the sake of

our study we made use of two idealizations of the source: first we did not consider the effects of pressure and heat, second we approximated the source of the change of anomalous masses by a point source.

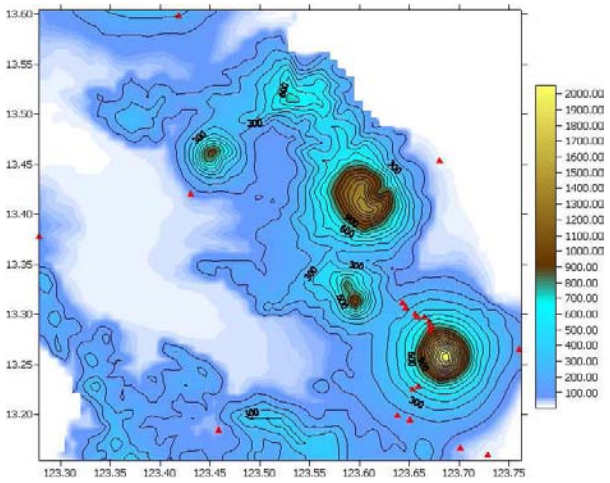

Fig.2
The topography in the region, Mayon is in the bottom-right corner, triangles mark the observed points (stations).

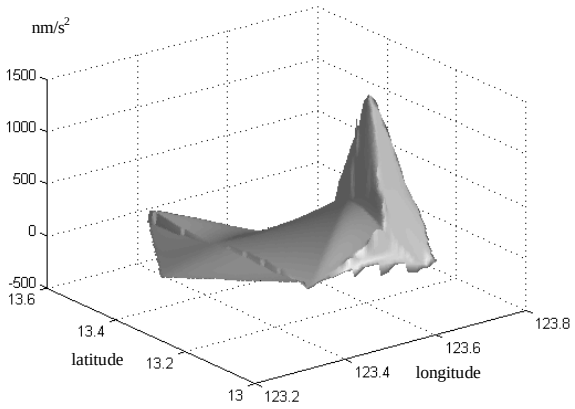

Fig.3
The interpolated (by bicubic splines) observed temporal gravity changes (between campaigns 1 and 4) at the Mayon volcano (nms^{-2} [10 nm/s^2 = 1 microGal]).

Since at Mayon no data have been observed in the summit region, both the magma deflation model (Jentzsch et al., 2001) and the magma inflation model (Fernández et al., 2001) can equally well explain the observations. We chose to assume the magma inflation model in our study.

The source was found (Fig.4) at the depth of 2.4 km (±600 m) below sea level. This result was compared to an interpretation of Fernández et al. (2001), who found a source characterizing the magma inflation at the depth of 1.95 km. The TFM was found applicable to serve as a quick tool for the first "hands on data" interpretation in search for the source, yielding an estimate of the depth to the source. There are several uncertainties still associated with the method: the effect of pressure and heat, the effect of interpolation of the sparse data, and the effect of the upward continuation term. The methodology remains still under development. For more details on our Mayon data TFM-interpretation the reader is referred to (Vajda et al., 2004).

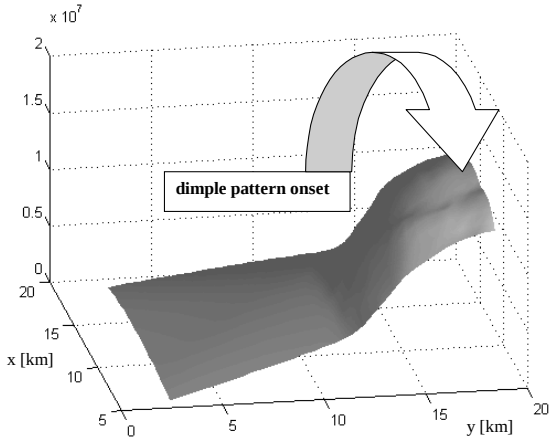

Fig.4
A snapshot of the animated truncation sequence resulting from truncation filtering the observed (and interpolated) temporal gravity changes, at which the so-called dimple pattern sets on. The depth of the magma chamber is estimated from the instant (the value of the truncation parameter) of the dimple pattern onset.

3.2 Merapi case

We have attempted to interpret the temporal gravity changes and vertical surface displacements (kindly provided to us by Prof. Gerstenecker and Carola Tiede) observed at the Merapi volcano, Indonesia in the period 1997–2002 using the TFM. Stratovolcano Merapi is a very active volcano, a so-called dangerous decade volcano, with 11 known fatal eruptions, an active summit lava dome, and frequent pyroclastic flows and lahars. Former evidence and studies were suggesting a deep magma reservoir at 6 km below sea level, and a shallow magma chamber at about 1 km below the summit. Figure 5 shows the location of observation points (triangles) at and around the volcano.

The stations close to the summit were impacted by the gravitational effect of the changing lava dome. Since we did not have detailed data on the shape of the dome at each campaign, we finally had to exclude the summit stations from the analysis and interpretation. For the slope stations we have removed the effect of the vertical displacement of a station using a Bouguer vertical gradient computed

for the density of the volcanic rock. This is an approximation to the actual vertical gradient of gravity at each station. Even then, we were not able to meaningfully interpret the gravity changes at these stations using the TFM.

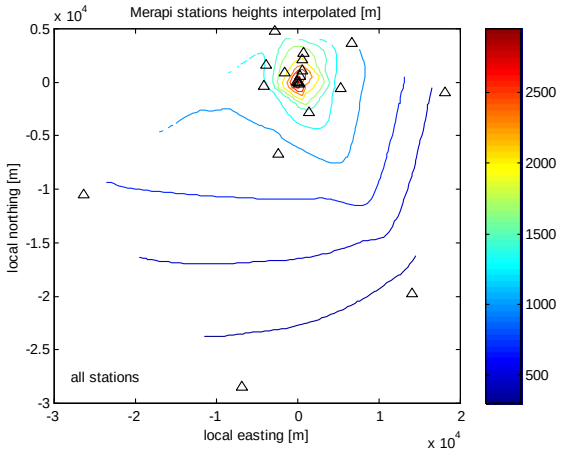

Fig.5
The topography (m) of and around Merapi and the location of observation points (stations).

Merapi is a very active volcano, an open system with ongoing production of lava, dome growth, dome collapses and partial collapses, lava avalanches, lava flows, pyroclastic flows, plumes, eruptions, often with multiple events per year. One year of observational repeat period represents a superposition of several magmatic events. Due to the dome changes, the analysis of temporal changes of gravity requires accurate and detailed DEM of the summit area for each epoch of measurements, otherwise the summit stations are hardly to be interpreted meaningfully. For Merapi we were not able to come up with any reasonable interpretation based on the TFM.

4 Conclusion and Challenges

The changes of gravity at volcanoes are due to a combined effect of all the dynamic processes leading to mass density distribution changes and ground deformation. To acquire such gravity changes from observations one must remove all the other effects on gravity data that have a different origin, such as the effect of atmosphere, tides, instrumental behavior, and especially ground water. The deforming surface of the volcano, the building or collapse of lava domes, the lahars, all produce temporal changes of the gravitational effect of topography, and thus a temporal change of the topo-correction must be considered. To compute it, detailed DEM is required for a given site at each observation campaign. It is very difficult to track in a required resolution the changing ground water level in order to account for its changing gravitational effect.

The terrestrial observations in a repeat survey mode are typically too sparse in both temporal and spatial resolution. The promising improvement can be anticipated from the remote techniques due to their high spatial resolution and coverage, and a good "repeat" regime (temporal resolution). However, terrestrial repeat survey technique may prove very useful at volcanoes that had been dormant for a long time, to check if they are possibly awakening.

We have investigated the possibility of applying a novice methodology, the TFM, to interpreting temporal gravity changes at volcanoes. Although in some situations the TFM interpretation may yield useful insights and estimates of depth for active magma reservoirs, it appears that the methodology suffers tight limitations.

There is vast room and many opportunities for research and technological improvement in the monitoring of volcanoes. Better spatial-temporal data coverage of monitored phenomena would yield improved knowledge of the processes. Of course the cost is a limiting factor. There is plenty room also for research in modeling and interpreting the monitored phenomena associated with volcanic and magmatic processes.

Acknowledgements: The provision of data by and the cooperation of G. Jentzsch, T. Jahr, R.S. Punongbayan, U. Schreiber, G. Seeber, C. Völksen, and A. Weise, in the case of Mayon volcano, and C. Gerstenecker and C. Tiede in the case of Merapi volcano, is thankfully acknowledged. We acknowledge the partial support of the VEGA grant agency, projects No. 2/6019/26 and 1/3066/06.

References:

[1] Dzurisin, D., *Volcano Deformation*, Springer, 2007.

[2] Fernández, J., K.F. Tiampo, G. Jentzsch, M. Charco, and J.B. Rundle, Inflation or deflation? New results for Mayon volcano applying elastic-gravitational modeling. Geophysical Research Letters, Vol.28, No.12, 2001, pp. 2349–2352

[3] Jentzsch, G., R.S. Punongbayan, U. Schreiber, G. Seeber, C. Völksen, and A. Weise, Mayon volcano, Philippines: Change of monitoring strategy after microgravity and GPS measurements from 1992 to 1996. *Journal of*

Volcanology and Geothermal Research, Vol.109, 2001, pp. 219–234

[4] Vajda P., L. Brimich, and P. Vaníček, Geodynamic applications of the truncation filtering methodology: A synthetic case study for a point source of heat: Progress report, *Contributions to Geophysics and Geodesy*, Vol.30, No.4, 2000, pp. 311–322

[5] Vajda P. and L. Brimich, Geodynamic applications of the truncation filtering methodology: A synthetic case study for a point source of force representing the upward pressure around a magmatic body. *Contr. Geophys. Geod.*, Vol.31, No.4, 2001, pp. 683–693 (Correction: *Contr. Geophys. Geod*., Vol.32, No.2, pp. 195–196)

[6] Vajda P., and P. Vaníček, The 3-D truncation filtering methodology defined for planar and spherical models: Interpreting gravity data generated by point masses. *Studia Geophysica et Geodaetica* Vol.46, 2002, pp. 1–16

[7] Vajda P., L. Brimich, G. Jentzsch, T. Jahr, and A. Weise, Towards interpreting gravity changes by means of the Truncation Filtering Methodology: Mayon volcano, Philippines, case study, *Contr. Geophys. Geod*., Vol.34, No.1, 2004, pp. 1–19

The measurements of 4D temperature distribution in Earth Science by distributed optical fiber sensors: an experimental approach to monitoring temperature and heat transfer dynamics at the Campi Flegrei volcano (Italy)

BERNINI R.(1), GRAVINA R.(1), MINARDO A.(2), ZENI L.(2), PETRILLO Z.(3), PIOCHI M.(3), SCARPA R.(4)
(1) IREA – CNR, Naples, Via Diocleziano 328, Napoli, ITALY
(2) Seconda Università di Napoli, Via Roma 29, Aversa, Caserta, ITALY
(3) INGV, Osservatorio Vesuviano, Via Diocleziano 328, Napoli, ITALY
(4) Università di Salerno, Via Ponte don Melillo, Fisciano, Salerno, ITALY

bernini.r@irea.cnr.it,gravina@irea.cnr.it,aldo.minardo@unina2.it,zeni@unina.it,petrillo@ov.ingv.it,monky5@ov.ingv.it,roberto.scarpa@sa.infn.it

Abstract: - We present the first results of long- term monitoring of temperature-depth profiles at the active volcanic area of Campi Flegrei caldera, Italy. The measurements were carried out along a 76 meters-deep borehole already equipped with a borehole strain-meter. We installed a cable containing a loop of optical fiber in order to use a fiber-optics distributed temperature sensor based on stimulated Brillouin scattering. The obtained data are consistent with results of both deep and surface geothermal explorations available in the literature and indicate that the geothermal gradient can be efficiently measured and monitored by the proposed technique.

Key-Words: - Distributed Brillouin optical fibre sensing, temperature-depth profile, thermal monitoring, Campi Flegrei (Italy)

1 Introduction

The knowledge of the three-dimensional distribution of temperature is an important objective of studies in the Earth science focused i) to quantify the geothermal gradient, ii) to determine the heat flux, iii) to define the heat transfer dynamics, iv) to identify the heat source(s). Besides, the analyses of the time series of the temperature-depth profiles allow to gain insights into heat transfer processes as function of the crustal rock strata and the eventual circulating fluids.

In particular, the measurements of 4D temperatures are of great interest at active and quiescent volcanoes where the geothermal gradient combined with geophysical and geochemical observations, can permit to reach a more detailed conceptual model of the volcanic system.

Here we propose the measurement of the thermal gradient by using the Brillouin fiber-optics distributed sensors [1, 2]. The tool is based on the stimulated scattering consequent to the interaction between an acoustic wave, a pump lightwave and a Stokes lightwave, and on the detection of the local Brillouin frequency shift that is linearly dependent on temperature. The technique was applied at the quiescent Campi Flegrei caldera in Italy.

2 Problem Formulation

The Campi Flegrei caldera (Fig. 1) is considered among the highest risk volcanic areas in the World as i) it is inhabited by 1 million people, ii) it produced more than 60 explosive eruptions in the past 15 ky, iii) it is the site of widespread fumaroles and thermal springs connected with a geothermal system and iv) it has been affected by unrest phenomena in the last decades [3]. Its magmatic activity is continuously monitored through seismic, geodetic, gravimetric, magnetic and geochemical monitoring networks [4, 5].

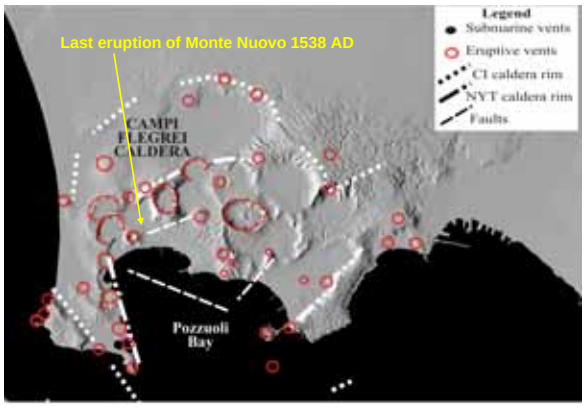

Figure 1. Digital Terrain Modelling (DTM) map of the Campi Flegrei caldera with main volcanic structures.

Measurements of the temperature gradient has been conducted in the past [6, 7] with simple thermo-couple systems. These measurements showed that the thermal gradient is very high (up to 160°C/km). Recent studies suggest that the high temperatures and unrest phenomena are strictly connected with circulation of magma-derived fluids [8]. Therefore, temperature measurements may be a powerful tool in order to i) reproduce the thermal image of the subsurface and its variation through time allowing to

identify heat source(s) and its (their) dynamics and ii) to study the transfer of heat, evaluating the role of the flow versus advective heat transport.
Although the above evidence, 4D-dimension thermal monitoring is still lacking.

3 Problem Solution

Distributed Brillouin optical fibre sensing can provide time-series and spatially resolved measurements of temperature over distances up to a few kilometres. The temperature accuracies are about 1°C, while the system allows the acquisition of temperature profiles with a spatial resolution of about 2 meters.
The advantage of the system is that the fibre has a very low cost, can be installed in the hole, in corrosive and hot (up to 700°C) environment settings, temperature can be measured repeatedly, instantaneously, and without physically disturbing the borehole medium, making it a very good tool for studying transient events.
We installed a cable containing a loop of single-mode optical fiber in order to use a fiber-optics distributed sensor based on stimulated Brillouin scattering (SBS). The two ends of the fiber loop were connected to a prototype for distributed temperature measurements (Fig.2). An acousto-optic modulator (AOM) was used to provide pulses with widths down to 20 ns, whereas the CW probe signal is generated by the electro-optic modulator using the sideband technique [9]. The detector consisted of an InGaAs photodetector and a preamplifier with a sensitivity of 4 mV/μA and an electrical bandwidth of 125 MHz, whereas the data acquisition rate was 625 MS/s. A frequency shift of 300 MHz is induced by the AOM on the pump optical frequency due to acousto-optic effect, so that only one of the two sidebands can effectively interact with the pump wave for Brillouin scattering generation. This occurrence eliminates the need for an optical bandpass filter in front of the detector, differently from the configurations usually proposed in the literature [9], providing an inherent stability to the system, the latter being totally immune to any drift on the source wavelength.

.

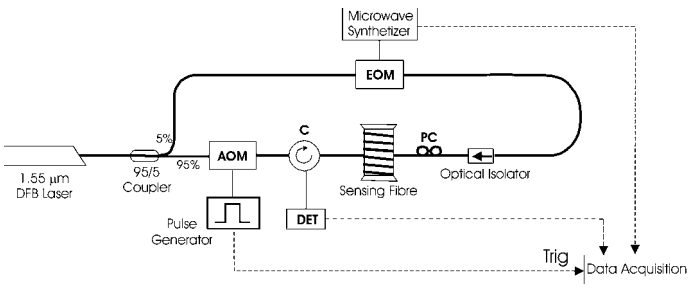

Figure 2. Experimental set-up for distribute temperature sensing. C = optical circulator. PC =polarization controller

Probe amplification was measured for a range of pump-probe frequency shifts, in order to extract the Brillouin gain spectrum at each sensing fiber location.
Finally, each acquired Brillouin gain spectrum was fitted by a Lorentzian function, in order to retrieve the Brillouin frequency shift (which is proportional to the local temperature) at the corresponding fiber position

4 Conclusion

In July 2006, we started an experiment focused to monitor the temperature-depth profile in a borehole drilled into the Campi Flegrei caldera, Italy, using an optical fibre cable as a temperature sensor.
The 4D temperature measurements were carried out along a 76 meters-deep borehole in the centre of the caldera, already equipped with a borehole strainmeter.
Figure 3 shows the obtained results. A progressive increase of temperature with the depth, producing a geothermal gradient consistent with data available in the literature [7, 8] has been registered. Moreover, a general trend of increasing temperatures, within the 1.5 year of observation, is observed at the bottom of the borehole.
The obtained data indicate that geothermal gradient can be efficiently measured and monitored by the proposed technique.

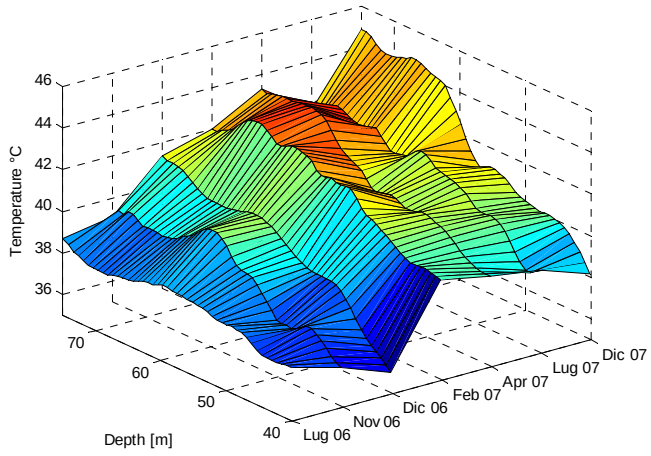

Figure 3. Temperature profile measurements along a borehole in Campi Flegrei caldera. Measurements were taken along a temporal span of about 1.5 years.

References:

[1] R. Bernini, A. Minardo, L. Zeni (2004. Accuracy enhancement in Brillouin distributed fiber-optic temperature sensors using signal processing techniques. *Photonics Technology Letters, IEEE, 16 1143-1145.*
[2] A. Minardo, R. Bernini, L. Zeni, L. Thevenaz, F. Briffod (2005). reconstruction technique for long-range stimulated Brillouin scattering distributed fibre-optic

sensors: experimental results. *Measurement Science and Technology*, 16, 900-908.

[3] A. Parascandola (1947). I fenomeni bradisismici del Serapeo di Pozzuoli. *Genovese, Napoli*

[4] A. Amoruso, L. Crescentini, A. T. Linde, I. S. Sacks, R. Scarpa, and P. Romano (2008). A horizontal crack in a layered structure satisfies deformation for the 2004–2006 uplift of Campi Flegrei. *Geophysical Research Letters, 34, doi:10.1029/2007GL031644.*

[5] F. Barberi, G. Corrado, F. Innocenti and G. Luongo (1984) Phlegraean Fields 1982–1984: Brief chronicle of a volcano emergency in a densely populated area. *Bulletin of Volcanology, 47, 175-185, 10.1007/BF01961547*

[6] AGIP (1987). Geologia e Geofisica del sistema geotermico dei Campi Flegrei, Servizi Centrali per l'Esplorazione, SERG MMESG, San Donato

[7] G. Corrado, S. De Lorenzo, F. Mongelli, A. Tramacere and G. Zito (1998). Surface heat flow density at the phlegrean fields caldera (SOUTHERN ITALY). *Geothermics, 27, 469-484, doi:10.1016/S0375-6505(98)00023-6*

[8] S. Caliro, G. Chiodini, R. Moretti, R. Avino, D. Granieri, M. Russo, J. Fiebig (2007). The origin of the fumaroles of La Solfatara (Campi Flegrei, South Italy). *Geochimica et Cosmochimica Acta (2007), doi: 10.1016/j.gca.2007.04.007*.

[9] M. Niklès, L. Thévenaz, and P. Robert (1997). Brillouin gain spectrum characterization in single-mode optical fibers. *Journal of Lightwave Technology*, 15, 1842–1851.

Occurrence and gas chromatographic determination of volatile fatty acids in landfill leachate. The case of two landfills in Gdansk Pomerania, Poland.

BOGDAN ZYGMUNT[1], ANNA BANEL[1]

[1]Department of Analytical Chemistry

Gdansk University of Technology

11/12 Narutowicza Str., 80-952 Gdańsk

POLAND

e-mail: [1] zygmuntb@chem.pg.gda.pl, banelka@wp.pl http://www.pg.gda.pl

Abstract. In landfills containing biological matter volatile fatty acids (VFAs) are generated at high rate at the early stage of waste disposal and their content in leachate is high as compared to the leachate from old parts of landfill since they are converted to methane gas. Monitoring of the leachate for the content of VFAs can help determine the processes occurring in waste and possible effect of the leachate on the environment in the case of some leakage. The content of VFAs was determined, using the method developed, in inflow and outflow of ground water and in the brook water passing through one landfill upstream and downstream of the landfill. The data show that some, though rather small, amounts of the acids generated in the landfill are transferred to the above waters. VFAs were determined in the two landfills of similar age and waste composition; their contents in the leachate were not drastically different.

Key words: Volatile fatty acids, Landfill, Leachate, Gas chromatography-mass spectrometry, Gdansk Pomerania

1. Introduction

Volatile fatty acids (VFAs) are aliphatic monocarboxylic acids with 2 to 6 or even 7 carbon atoms. They can be found in many environmental matrices due to numerous sources of natural (biological; geological; transformation of other pollutants) and anthropogenic (agriculture, pig farming, food processing, waste disposal) origin. Municipal solid waste (MSW) generation continues to grow and the sanitary landfill method for the ultimate disposal of solid waste material is increasingly accepted and used. It is so because it is cheaper, minimizes environmental insults and some other inconveniences and allows waste to decompose under controlled conditions into relatively inert, stabilized material [1]. However, the leachate formed, when precipitation water percolates through waste, is generally quite strongly polluted wastewater. In young landfills large amounts of free VFAs are released, due to large quantities of biodegradable organic matter which undergoes rapid anaerobic fermentation, and acids content in the leachate is very high [2]. Degradation is strongly influenced by the composition of MSW. Very high percentage of easily putrescible waste produces acid accumulation and an extremely low pH. This inhibits biological process that follows the particulate matter hydrolysis [3] and limits the generation of methane [4]. If leachate treated *ex situ* is used the inhibition problem caused by hydrolysed volatile acids can be resolved [5]. The hydrolysis rate was found out to be the highest when an anaerobically pre-treated leachate was used [6]. Later, VFAs are converted to biogas and organic fraction in the leachate is dominated by non-biodegradable compounds. Organic compounds present in the leachate can be composed of VFAs in up to 80%, 5-30% and only of humic and fulvic acids in recent, intermediate and old landfills, respectively [7]. The relation between the age of the landfill and organic matter composition in the leachate may help select an appropriate treatment process [1]. Moreover, VFAs, when released into the environment, may cause some damages. Therefore, the information on VFAs in the leachate and possibly in ground water and surface water in the landfill neighbourhood is of great importance and the content of individual VFAs should be monitored.

Generally gas chromatography (GC) with polar stationary phases and flame ionisation detection is used for the separation and determination of VFAs in aqueous samples [8, 9]. Before the analysis proper leachate and aqueous leachate-related samples must be prepared to make them compatible with GC. For the purpose Manni and Caron used [10] used extraction

with diethyl ether. In many cases, if the sample is not much contaminated with suspended matter, high molecular organics and some other components, aqueous samples can be injected into GC, after removal of solids, provided that specialty separation columns are applied [11]. When the total content of VFAs is to be known titrimetric [12] and spectrophotometric [13] methods were used.
The aim of this work was to test the procedure of determination of VFAs in aqueous samples based on solvent extraction at the step of sample preparation and gas chromatography coupled with mass spectrometry (GC-MS) as a technique of final analysis and then to apply this procedure for the determination of VFAs in aqueous media in two large landfills situated in Gdansk Pomerania, Poland.

2. Experimental

2.1. Characteristics of the landfills studied

Landfill A situated in the former gravel pit has been operated since 1973. A brook flows through the area of the landfill. About 700 ton municipal and some industrial wastes are delivered every day from the area with ca 600,000 inhabitants. Landfill gas is collected and applied to produce energy on site.
Landfill B situated in the former gravel pit was opened in 1979 and has been modernized quite a few times since then. About 250 ton municipal and some industrial wastes are delivered every day from the area with ca 400,000 inhabitants. Presently a landfill gas is collected and applied to produce energy on site.

2.2. Sample collection

Problems with water sampling from landfills result mainly from non-homogeneity of the aqueous media and certain procedures must be followed to select sampling sites and frequency of sampling in order to collect a representative sample.
Leachate. Samples were collected with a scoop from leachate container. In sampling planning vertical stratification was taken into consideration. Care was taken to collect water without particulate matter depositing all the time at the bottom.
Surface water. Samples were collected with a scoop upstream and downstream of the brook. The sample bottle was rinsed with sampled water twice before filling it with the sample proper.
Ground water. Samples were taken using deep-water pump. Care was taken to pump out stagnant water in well before collection of the sample proper. This can be monitored by measuring pH, conductivity and temperature.

2.3. Sample transport to laboratory

Immediately after collection, samples were transported to the laboratory and subjected to extraction with methyl-*tert*-butyl ether (MTBE). After collection and during transport they were kept at a temperature below 4^0C.

2.4. Sample preparation and GC-MS analysis

After filtering solids and suspended matter sulfuric acid to lower pH and sodium chloride to decrease the solubility of the acids in water were added to the samples. VFAs were extracted from water samples twice with 2 cm^3 methyl-*tert*-butyl ether each time. Then the two extracts obtained were combined and dried with anhydrous sodium sulfate. A Thermo Finningan Trace GC 2000 gas chromatograph coupled with a Trace DSQ mass spectrometer in SCAN and SIM modes were used to determine the content of acids in the extracts. Separation was performed in GC capillary column (30m x 0.32mm x 500nm) coated with Stabilwax-DA stationary phase (polyethylene glycol modified with terephtalic acid). The chromatographic conditions were as follows: flow rate of helium carrier gas – 1.5 mL/min; oven temperature – 60 ^{0}C (2 min), 10 ^{0}C/min to 220 ^{0}C (1 min); temperature of split/splitless injector operated in splitless mode – 250 ^{0}C; transfer line – 250^{0}C. Electron impact ionization was used. The successive steps of the procedure are presented in Fig. 1.

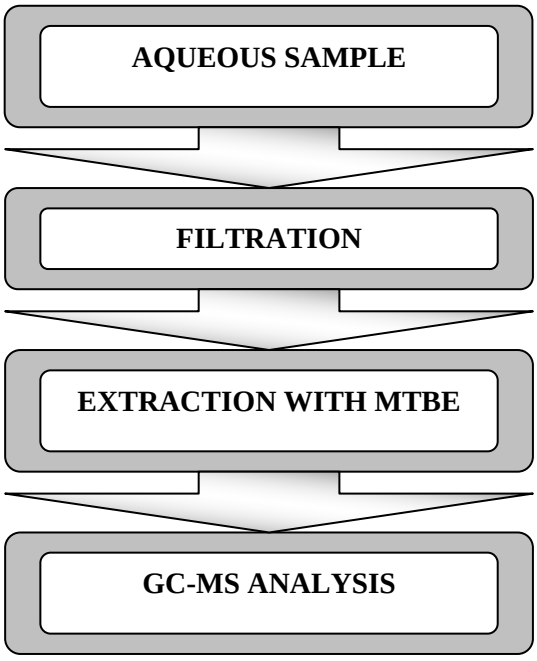

Fig. 1. Successive steps of the procedure of determination of VFAs in aqueous samples.

3. Results

In landfill A VFAs were determined in ground water at the three levels of the upper water-bearing layer in the zone of ground water inflow to the area of the landfill as well as in outflow groundwater; in the brook upstream and downstream of the landfill; and in the leachate. Water in the first level of the upper water layer outflowing the landfill contained acetic acid at a concentration in the range of 0.20-0.50 mg/dm^3. The concentrations of the remaining acids were below detection limit of 0.10 mg/dm^3. Water in the second level of the upper water layer contained acetic acid at a bit higher concentration, i.e. in the range of 0.57-0.80 mg/dm^3 and the remaining acids below the detection limits. In the ground water inflowing the landfill VFAs were not detected. The data indicate that the landfill leachate pollutes the ground water with VFAs to some extent. The acetic acid content in water of the brook downstream was about twice the concentration of acetic upstream, but the concentrations in both cases were close to detection limits of the procedure applied. In the case of Landfill B only the leachate was analyzed.

The comparison of the contents of VFAs in the leachate from Landfill A and Landfill B are presented in Table 1.

Table 1. Comparison of the content of VFAs in the leachate in Landfill A and Landfill B.

Acid	Concentration [mg/dm^3]	
	Landfill A	Landfill B
Acetic	*18.0*	*19.6*
Propionic	*3.37*	*6.84*
Isobutyric	*0.50*	*1.02*
Butyric	*1.36*	*0.67*
Isovaleric	*0.34*	*0.44*
Valeric	*0.28*	*0.39*
Caproic	*n.d.*	*n.d.*
Enanthic	*n.d.*	*n.d.*
Caprylic	*n.d.*	*n.d.*

n.d. – below detection limits

The leachates contain not only acetic acid but also higher VFAs with up to 5 carbon atoms at measurable concentrations which are much higher than in surface and ground water. The differences in concentrations of particular acids in the leachates from these two landfills are not very large. Probably this results from the fact that both landfills are of similar age and the composition of wastes should not differ drastically. In both cases municipal wastes are predominant.

4. Conclusion

Volatile fatty acids are generated in landfills containing municipal solid waste with the rate dependent on age and composition of the waste. Their content is very high in young landfills. Gas chromatography is a convenient and indispensable technique of individual VFAs determination in landfill lechate and leachate-related aqueous samples. When polar stationary phases are used VFAs in a free from can be separated. If aqueous samples are not much contaminated they can be injected into a GC column after filtration. In other cases organic solvent should be used to extract VFAs. MTBE proved to be an effective and convenient solvent. The analytical procedure based on acids extraction with MTBE and GC-MS determination of VFAs in the extracts is characterized by good selectivity and detection limits on the level of 0.1 mg/dm^3. The procedure can be applied to determine VFAs with 2-8 carbon atoms. From the studies of the two landfills in Gdansk Pomerania, Poland results that there can be a slight infiltration of VFAs into ground water and to surface water. The contents of VFAs in the leachates from both landfills are similar. This can be related to the fact that both landfills are of similar age and contain mainly municipal solid waste.

References:

[1]. Renou, S., Givaudan, J.G., Poulain, S., Dirassouyan, F., Moulin, P., Landfill leachate treatment: Review and opportunity, *Journal of Hazardous Materials*, 150, 2008, 468–493.

[2]. Welander, U. , Henryson, T., Welander, T., Nitrification of landfill leachate using suspended-carrier biofilm technology, *Water Research*, 31,1997, 2351–2355.

[3]. Borzacconi, L., Lopez, I., Anido, C., Hydrolysis constant and VFA inhibition in acidogenic phase of MSW anaerobic degradation, *Water Science and Technology*, 36, 6, 1997, 479-484.

[4]. Vavilin, V.A., Jonsson, S., Ejlertsson, J., Svensson, B.H., Modelling MSW decomposition under landfill conditions considering hydrolytic and methanogenic inhibition, *Biodegradation*, 17, 2006, 389–402.

[5]. Kim, J., A Bioreactor Landfill Incorporating Innovations in Leachate and Gas Management with a Dedicated Treatment Zone. PhD thesis. University of Pittsburgh, Pennsylvania, USA, 2001, According to Chemosphere 59, 2005, 837–844.

[6]. He, P.J., Shao, L.M., Qu, X. Li, G.J., Lee, D.J., Effects of feed solutions on refuse hydrolysis and landfill leachate characteristics, *Chemosphere*, 59, 2005, 837–844.

[7]. Chian, E.S.K., DeWalle, F.B., Sanitary landfill leachates and their treatment, *Journal of the Environment Engineering Division*, 103, 1976, 411–431

8. Peldszus, S., Organic Acids (Chapter 13) in *Chromatographic Analysis of the Environment* (Nollet, L.M.L. - editor), Third Edition, Taylor&Francis, 2006.

[9]. Giecewicz J., Zygmunt B., Oznaczanie lotnych kwasów tłuszczowych w ściekach metodą chromatografii gazowej (Determination of volatile fatty acids in waste water by means of gas chromatography), *Chemia i inżynieria ekologiczna (Ecological Chemistry and Engineering S)*, 10(10), 2003, 1125-1138

[10]. Manni G., Caron F., Calibration and determination of volatile fatty acids in waste leachates by gas chromatography, *Journal of Chromatography* A, 690, 1995, 237-242

[11]. Dearman B., Marschner P., Bentham R.H., Methane production and microbial community structure in single-stage batch and sequential batch systems anaerobically co-digesting food waste and biosolids, *Applied Microbiology and Biotechnology*, 69, 2006, 589-596

[12]. Anderson G.K., Yang G., Determination of bicarbonate and total volatile acid concentration in anaerobic digesters using a simple titration, *Water Environmental Research*, 64, 1992, 53-59

[13]. Montgomery H.A.C., Dymock J.F., Thom M.S., The rapid colorimetric determination of AIDS and their salts in sewage-sludge liquor, *The Analyst*, 87, 1962, 949-955

Quality of road and roof runoff waters from an urban region with Gdańsk (Poland) as an example

ŻANETA POLKOWSKA
Department of Analytical Chemistry
Chemical Faculty
Gdańsk University of Technology
11/12 G. Narutowicza St., 80-952 Gdańsk
POLAND
e-mail: zaneta@chem.pg.gda.pl

Abstract: - Runoff water is an important medium transporting various air pollutants from the air to the soil and surface water. This paper presents the results of measurement of removal rates of anions and cations, havy metals and pesticides in the rain, road runoff, and roof runoff near a major urban highway (Gdańsk beltway).

Key-Words: - Precipitation chemistry, Road and roof runoof water, Water quality; Roof coverings Urban area

1 Introduction

In urban environments, most impervious surfaces are sources of stormwater. The three principal categories of impervious area within urban environments are roads, roofs and other paved areas. Roofs are made of a variety of materials and most, with the exception of those made from grass/reed and potentially toxic materials, are suitable as rainwater catchment surfaces. The typical roofing materials are metal sheets, ceramic and clay tiles, rock slate and ferro cement, asbestos cement, gravel, polyester, tar felt.

Runoff water is an important transport medium for various air pollutants from the air to the surface- and ground water, and then indirectly to other environmental compartments [1,2]. Rain water washes dusts away from the atmosphere and the impervious urban surfaces and, in the form of road and roof runoff, carries off dissolved, colloidal and solid constituents in a heterogeneous mixture, which includes organic and inorganic compounds, nutrients, oils, greases and heavy metals [3-5]. The contaminant may remain permanently on the surface, may be removed from the road by resuspension or may be removed in the road runoff waters. The road and roof runoff itself seems to play an important role, both as a pollutant source and a pollutant sorbent [5].

The origin and quantity of pollutants found in highway runoff are site specific and depend on a number of factors, including traffic, highway maintenance, normal depositions on the highway and spillages. Highway surface types (asphalt or concrete) seem to have a minimal effect on the runoff quality [6].

Roof runoff is considered a potential source of pollution for two primary reasons. First, compounds contained in roofing materials (the material used for the roof cover, the guttering, the downpipes and paints, sealants and cleaners) may be leached into runoff (physical washing off or erosion), and airborne pollutants and organic substances, such as leaves, dead insects, and birds' wastes, are added to roofs by interception and deposition. During storms, rainwater not only adds a variety of chemicals and contaminants to the roof watershed, the acidic nature of rainwater will react with compounds retained in or by the roof and cause many elements in the roof runoff to leach out [7,8].

Contamination of runoff water from roads with high traffic intensity and roof runoof in the urban area of Gdańsk, Sopot, Gdynia and Reda in Poland is discussed in this paper.

2. Experimental

2.1 Sampling

Samples of road runoff waters from major highways and roof runoff waters were collected from January 2000 to December 2005 at eight sites with heavy traffic located along a major transportation route - Gdańsk beltway.

2.2 Analytical methods

Samples were collected during or immediately after a precipitation event. They were stored at low temperatures without any chemical preservatives because the analysis was performed either directly on-site or immediately after the samples were delivered to the laboratory. Runoff samples were usually highly contaminated with solids (sand, leaves); therefore, they had to be pre-filtered. The analytical techniques used in this study are summarized in Table 1 and 2.

Table 1. Operating conditions of the analytical techniques used in the study (quantified against synthetic rain standards (RAIN-97, CRM 409))

Analyte	Technique	Analytical parameters	Limit of detection	Precision [% RSD]
Anions/ Cations	Ion chromatography IC	Conductivity detection, AutoSuppression Recycle Mode ASRC®-ULTRA/ CSRS ®-ULTRA, AS9-HC/ CS12A column	0.001 meq/dm^3	1
Metals	Atomic Absorption Spectroscopy (AAS)	AAS, BUCK Scientific model 210-VGP Graphite furnace, BUCK Scientific model 220-GF	0.01 μeq/dm^3	2

Table 2. Parameters of the chromatographic determination of the pesticides in the samples.

	Organochlorine pesticides	Organonitrogen and organophosphorus pesticides
Chromatograph	GC 6180 Vega, Carlo Erba - Fisons	GC 8000 Fisons
Detector	ECD	NPD
Detector temperature	350°C	280°C
Column (length x ID x stationary phase film thickness)	AT-5, 30 m x 0.32 mm x 0.25 μm	HP-5, 30 m x 0.32 mm x 0.25μm
Injector (injection mode)	Cool on-column	Split/splitless (splitless)
Carrier gas	Hydrogen	Hydrogen
Temperature program	80°C → 15°C/min → 180°C → 15 °C/min →280°C → 15°C/min → 300°C (5 min.)	80°C → 15°C/min → 140°C → 10°C/min →280°C → 20°C/min → 300°C (1 min.)
Injector temperature	80°C	80°C
Injected volume	2 μL	2 μL
Data acquisition	Chrom-card	Chrom-card

3. Results and Discussion

3.1. Major anions

Road runoff

Na^+, K^+, Mg^{2+} and Ca^{2+} were detected in all samples, with the highest concentrations found for Na^+ and Ca^{2+}. Among the anions, the highest concentrations were found for Cl^- and SO_4^{2-}. The highest concentrations were observed for chloride, sulfate and sodium in samples from road runoff.In the case of the chloride ions, the extremely high concentrations (4,770 mg/l) can only be explained by the use of road salt to prevent icing in the area.

Roof runoff

Major ion (Cl^-, NO_3^-, SO_4^{2-}) concentrations in rainwater and roof runoff were determined in all samples. For rain, the range of concentrations (in mg/l) of these three ions were contained in the following intervals: Cl^-: 0.25 – 30; NO_3^-: 1.6 - 13; SO_4^{2-}: 3.0 – 11; while for roof runoff Cl^-: 0.05 – 31; NO_3^-: 0.92 – 62; SO_4^{2-}: 0.85 – 432. Concentration of Cl^- in rainwater samples was usually higher than in runoff samples, and only in runoff water from a flat roof covered with thermally bonded tar paper, it was slightly higher. On the other hand, concentrations of Cl^-, NO_3^- and SO_4^{2-} ions in runoff from roofs covered with metal roofing tiles was – in all cases – lower than in rainwater. The highest concentrations of SO_4^{2-} and NO_3^- were discovered in runoff from a roof covered with ceramic tiles that were several tens of years old.

3.2 Heavy metals

Road runoff

Among heavy metals, Zn and Pb exhibited the highest concentrations, as expected for typical pollutants

associated with vehicular traffic. The highest heavy metal concentrations were found in road runoff water. The main source of lead is fuel. However, it appears that only 5% of the lead is removed by runoff water. The largest fraction may, therefore, disperse in the atmosphere or settle on the soil by the roadside. A relatively high level of Zn could be explained by the existence of metallic guardrails. According to Hewitt and Rashed [6], the main sources of zinc are wear and tear from tires and brakes and from the corrosion of galvanized safety barriers, or from an alternative material. As for Pb and Zn, concentrations increase in winter because of the use of chloride-based deicing salts, which generate supply and corrosion phenomen
The pollution load in highway runoff depends on the average daily traffic, air quality and rainfall intensity and duration. Traffic volume would seem to be an important factor for predicting runoff quality. Prior to storm events, roadways with ADT greater than 30,000 vehicles may produce runoff with two to five times the runoff pollutant levels found in that from rural highways. Simple linear regression analysis was performed to evaluate a direct correlation between ADT and the concentration of highway runoff pollutants. The results of this analysis revealed relatively high R values (ranging from 0.49 to 0.70) for all constituents, which may suggest a direct correlation between ADT and pollutant concentrations. However, most of the studies reported in the literature did not confirm strong correlations. For example, Chui et al. [9] found only a weak correlation, and a study conducted by Driscoll et al. [10] suggested that there is no strong and definitive relationship between differences in traffic density and the pollutant concentrations for a site.

Roof runoff

The range of Zn^{2+}, Pb^{2+}, Cu^{2+} and Cd^{2+} concentrations measured in rain samples and runoff water from different roofs. Concentration of heavy metals in roof runoff was mostly higher than in rain. In all rain and roof runoff samples, Zn^{2+} and Pb^{2+} were found. The highest concentration of zinc (4900 µg/l) was noted for runoff from a roof covered with asbestos cement sheets. The highest lead content (102 µg/l) was detected in runoff from a flat roof covered with thermally bonded tar paper. While the highest concentration of cadmium (3,70 µg/l) was noted for runoff from a roof covered with ceramic tiles (old). Cu^{2+} was detected only in runoff samples from roofs covered with tar paper or ceramic tiles. The highest concentration of Zn^{2+} was in runoff from a flat roof covered with thermally bonded tar paper. However, the source of this pollutant was not the roofing material. Zn^{2+} was washed out of the drain pipe, which was made from zinc-coated sheet metal. The highest mean concentration of Pb^{2+} was noted for runoff samples from a roof covered with thermally bonded tar paper. The source of this metal in runoff water is dry deposition, while the low inclination of the roof helps it to accumulate pollutants, which are subsequently washed off by the rain.

3.3 Pesticides

Road runoff

Heptachlor epoxide (metabolite of heptachlor; formed in plants, soil and homeothermic organisms), and o,p'-DDE (DDT metabolite) were the most often detected pesticides in the runoff water samples. The highest value for this sum of pesticide was 1.3 µg/l. Propazine and bromophos, used as selective weed killers, were detected the most often among the pesticides in these groups. The highest value for the sum of the concentrations of organonitrogen and organophosphorus pesticides (14 ng/l) was recorded on the same day (October 27) in Gdańsk-Oliwa. The concentration of organochlorine pesticides in this sample was also relatively high at 81 ng/l. Elevated pesticide concentrations in runoff waters were also observed for samples collected on October 24. This may have been related to the fact that those were the first precipitation events following a prolonged dry spell. Both sites are characterized by very heavy traffic volume.

Roof runoof

The highest total concentration of the organochlorine pesticides (20 ng/l) was found in a sample collected from a roof covered with tar paper in the Gdansk-Przymorze division. The sample with the highest concentration of the sum of organonitrogen and organophosphorus pesticides (52 ng/l) was collected in the same division from a roof covered with metal roof tiles. Most of the samples contained a few thousand ng/L of organochlorine pesticides, and a few tens to a few hundred ng/l of organonitrogen and organophosphorus pesticides. Precipitation samples collected in the same area between October 2000 and March 2001 contained much lower pesticide levels, ranging from 1 to 42 ng/l for organochlorine pesticides and from 2 to 14 ng/l for organonitrogen and organophosphorus pesticides [11].

Pesticides most often detected in runoff samples included heptachlor epoxide (metabolite of heptachlor, synthesized in plants, soil and warm-blooded organisms), p,p'-DDE (DDT metabolite), bromophos,

Table 3. Pesticides (and their concentrations) detected the most often for the individual roofing materials studied.

Roofing material	Analyte (concentration [ng/l])
Tar paper	aldrine (6,020), methoxychlor (430), heptachlor epoxide (19,970), p,p'– DDD (520), o,p '- DDE (540), o,p'- DDD (340), p,p'- DDE (450), o,p'- DDT (190), p,p'- DDT (370), α - HCH (200), γ - HCH (400), propazine (1,070), terbutylazine (120)
Ceramic roofing tiles	aldrine (130), methoxychlor (430), heptachlor epoxide (430), p,p'– DDD (4,610), o,p '- DDE (2,800), o,p'- DDD (1,210), p,p'- DDE (1,360), p,p'- DDT (1,080), α - HCH (740), γ - HCH (600), propazine (1,110), terbutylazine (120), bromophos (2,720)
Asbestos cement corrugated sheets	aldrine (610), methoxychlor (130), heptachlor epoxide (14,540), p,p'– DDD (500), o,p '- DDE (4,640), o,p'- DDD (7,040), p,p'- DDE (1,040), o,p'- DDT (750), p,p'- DDT (8,460), α - HCH (460), γ - HCH (840), atrazine (1,210), terbutylazine (130), bromophos (310)
Metal roofing tiles	Heptachlor epoxide(1,640), o,p '- DDE (920), o,p'- DDD (1,890), p,p'- DDE (680), o,p'- DDT (490), p,p'- DDT (830), α - HCH (320), γ – HCH (500), propazine (400), bromophos (4,912), atrazine (2,980), simazine (620), malathion (1,960), fenitrothion (630), chlorfenvinfos (180)
Painted galvanized steel	aldrine (6,020), methoxychlor (430), heptachlor epoxide (19,970), p,p'– DDD (520), o,p'- DDE (540), o,p'- DDD (340), p,p'- DDE (450), o,p'- DDT (190), p,p'- DDT (370), α - HCH (200), γ - HCH (400), propazine (1,070), terbutylazine (120)
Bituminous membrane	heptachlor epoxide(1,680), bromophos (50)
PTFE	bromophos (40)

malathion (insecticide/miticide used mostly in agriculture) and terbutylazine (broad-spectrum herbicide used in agriculture and forest management). In the case of precipitation samples collected during the same period, o,p'-DDE was detected the most often, followed by p,p'-DDE, γ-HCH (lindane; insecticide used mostly in agriculture) and heptachlor epoxide (Grynkiewicz et al., 2003)

Table 3 lists the pesticides (and their concentrations) detected the most often for the individual roofing materials studied. The highest concentrations were recorded for heptachlor epoxide (tar paper, galvanized sheet metal, asbestos cement corrugated sheets and bituminous membrane), p,p'-DDT (asbestos cement corrugated sheets), o,p'-DDD (asbestos cement corrugated sheets), p,p'-DDD (ceramic roofing tiles), o,p'-DDE (asbestos cement corrugated sheets, ceramic roofing tiles), aldrin (tar paper, galvanized sheet metal), bromophos (metal and ceramic roofing tiles) and atrazine (metal roofing tiles, asbestos cement corrugated sheets). Pesticides were found the most often in runoff from asbestos cement corrugated sheets, ceramic tiles and metal roofing tiles.

4. Conclusions

Road runoff

The analytes determined in road runoff can originate from many different sources, including road deposition (e.g. from tire wear, break wear, fluid leaks), atmospheric deposition (transport of particulates and gaseous pollutants), road wear (cracks and potholes in asphalt and concrete pavements), road maintenance practices (use of de-icers or pesticides) and accidental spills. Overall, road runoff carries with it a substantial load of toxic substances and can be potentially dangerous to the environment. Consequently, it is our opinion that the quality of road runoff should be monitored, especially in large urban agglomerations with heavy traffic.

Roof runoff

Roofs can be a source of water pollution. However, results of roof runoff studies have been variable. The variation reflects differences in roofing materials, industrial treatments, care and maintenance, age, climatic conditions, orientation and slope of roofs, and

air quality of the region. The deposition of various pollutants from the atmosphere into roof surfaces during a dry period greatly influences the runoff water quality from roof catchment systems. The amount of the pollutants deposited on the roof surfaces increases with the age of the roofing material, the increase in the length of the dry period between rainfall events, and ambient temperature, as evidenced by the increase in pollutant concentrations in the water samples collected.

References:

[1] Maltby L., Boxall A., Forrow D., Calow P., Betton C., The effects of motorway runoff on freshwater ecosystems: 1. Field study, *Environ. Toxicol. Chem.*, Vol. 14, 1995, pp. 1079 – 1092.

[2] Hewitt N. C., Rashed M.B., Removal rates of selected pollutants in the runoff waters from a major rural highway, *Wat. Res.*, Vol. 26, 1992, pp. 311-319.

[3] Gnecco I., C. Berretta, L.G. Lanza and P. La Barbera, Storm water pollution in the urban environment of Genoa, Italy' Atmospheric Research, Vol. 77, 2005, pp. 60-73.

[4] Hewitt C.N. and M.B. Rashed, Removal rates of selected pollutants in the runoff waters from a major rural highway, Water Resolution, Vol. 26, 1992, pp. 311-319.

[5] Mangani G., A. Berloni, F. Bellucci, F. Tatano and M. Maione, Evaluation of the pollutant content in road runoff first flush waters' Water, Air and Soil Pollution, Vol. 160, 2005, pp. 213-228.

[6] Hares R.J. and N.I. Ward, Comparison of the heavy metal content of motorway stormwater following discharge into wet biofiltration and dry detention ponds along the London Orbital (M25) motorway, The Science of the Total Environment, Vol. 235, 1999, pp. 169-178.

[7] He W., Odnevall Wallinder I., Leygraf C., A laboratory study of copper and zinc runoff during first flush and steady – state conditions, *Corr. Sci.*, Vol. 43, 2001, pp. 127-146.

[8] Chang M., Matthew W. McBroom, R. Scott Beasley, Roofing as a source of nonpoint water pollution, *J. Environ. Manag.*, Vol. 73, 2004, pp. 307–315.

[9] Chui T. W., B.W. Mar and R.R. Horner, Pollutant loading model for highway runoff, *J. Environ Engineering*, Vol. 108, 1982, pp. 1193–1210.

[10] Driscoll E. D., P. E. Shelley and E. W. Strecker, Pollutant loadings and impacts from highway stormwater runoff. Volume III: Analytical investigation and research report.' Publication No. FHWA-RD-88-008, Federal Highway Administration, Washington, D.C., 1992.

[11] Grynkiewicz M., Polkowska Ż., Górecki T., Namieśnik J., Pesticides in precipitation from an urban region (Gdansk-Sopot-Gdynia Tricity, Poland) between 1998 and 2000, *Water, Air, and Soil Pollut.*, Vol. 149, 2003, pp. 3-16.

Some remarks on mobility, bioavaibility and location of pollutants in sediments.

LIDIA WOLSKA
Department of Analytical Chemistry
Gdańsk University of Technology
11/12 Narutowicza Str, 80-952 Gdańsk, Poland
POLAND
chemanal@pg.gda.pl http://www.pg.gda.pl

Abstract: Some investigation suggest that unavailable pollutants fraction in sediments may pose less risk and therefore can be present only as a contaminant and not a pollutant. Date obtained in these studies show that also immobile fraction of metals may be bioavailable for *Heterocypris incongruens*. majority of the PAHs are associated with coal derived particles
The many field (remediation, analytics, risk assessment) is very important information on PAHs and PCBs location in sediments structures. Majority of the PAHs are associated with coal derived particles in sediment, while PCBs are rather associated with oil fraction.

Key-Words: mobility, bioavailability, heavy metals, PCBs, PAHs, sediments.

1 Introduction

Lake sediments contain thousands of substances of natural and anthropogenic origin. To prevent environment and human health against sediment pollution many remediation methods are used. The approaches include isolation, immobilization, toxicity reduction, physical separation, extraction and bioremediation.
To use appropriate methods and to control remediation process knowledge of the location and nature of pollutants bonded to sediment is needed.
It is well known that pollutants (metals and organic compounds), contained in sediment, can cause significant damage to environment and human life as a result of their mobilities and solubilities [1]. It is thought that only mobile fraction is bioavailable and can be toxic for biota. That means that a major factor influencing successful sediment bioremediation is the availability of contaminants to microorganisms. Therefore better understanding of physicochemical mechanisms controlling site-specific bioavailability of contaminants is very important.

2 Problem Formulation

2.1 Mobility and bioavailability of heavy metals from sediment

To determine the mobility of metals in sediments specific extraction are used. More precise evaluation can be obtained by sequential extraction with solutions of increasing strengths.
The sediment used in this study was obtained from the Turawskie Lake (Poland). The total contents of metals were determined by [3]:

- ✓ inductively coupled plasma - atomic emission spectrometry (ICP-AES) (Cr, Zn, Cu, Ni, V, Fe, Mn, Al, Li);
- ✓ electrothermal atomic absorption spectrometry (ET-AAS) (Cd, Pb);
- ✓ hydride generation atomic absorption spectrometry (HG-AAS) (As);
- ✓ and, cold vapor atomic absorption spectrometry (CV-AAS) (Hg).

Assuming that only water-soluble forms of metals are bioavailable, the speciation of metals was investigated using a sequential extraction technique. The six-step extraction procedure used, distinguishes six specific extraction liquids: I fraction - 1 mol L^{-1} NH_4OAc (pH 7); II fraction - 1 mol L^{-1} NH_4OAc (pH 5); III fraction - 1 mol L^{-1} $NH_2OH{\cdot}HCl$ (pH 2); IV fraction - 0,2 mol L^{-1} $(NH_4)_2C_2O_4$ + 0,2 mol L^{-1} $H_2C_2O_4$ (pH 3); V fraction - 30% H_2O_2 + HNO_3 (pH 2), NH_4OAc (pH 7); VI fraction - 65% HNO_3.
The toxicity of sediments was measured by the acute toxicity test with *Vibrio fischeri* bacteria and chronic toxicity test with *Heterocypris incongruens* crustacean.
If true is the hypothesis, that only mobile fraction is bioavailable, correlation between mobile fraction concentration and toxicity should be observed.

2.2 PAHs and PCBs bioremediation

The unavailable PAHs and PCBs fractions in sediments may pose less risk therefore can be present only as a contaminant and not a pollutant [2]. Little is known about the mechanisms of PAH and PCB sequestration

and aging in soils and sediments and the resulting effect on chemical and biological availability.
In this study certified sediment (Metranal 2) containing PAHs and PCBs was applied. Single and ten fold extraction of sediment with dichloromethane were carried out.

3 Problem Solution

3.1 Mobility and bioavailability of heavy metals from sediment

Table 1 presents a summary of the metal concentration determination results, including heavy metals, in sediment taken from Turawskie Lake (minimal and maximum concentration values). Determinations of metal content were performed in the bulk sediment samples, as well as in the grain size fraction < 63 μm. 250 samples of sediment were tested. The sediment from Turawskie Lake are polluted mainly with Zn, Cd, Pb and Cu, and, to slightly lesser extent, with As, Hg and Cr. Concentrations of Zn, Cd and Pb are approximately 800 times higher than the background level.

Table 1. A summary of the metal concentrations in sediment taken from Turawskie Lake.

metal	As	Hg	Cd	Pb	Cr	Zn	Cu	Ni
metal concentration (total sediment), mg/kg d.m.								
Min	n.d.	n.d.	n.d.	n.d.	n.d.	n.d.	n.d.	n.d.
Max	122	1.21	400	689	121	7599	404	64
Means	7	0.06	15	31	13	399	14	7
metal concentration (fraction < 63 μm), mg/kg d.m								
Min	n.d.	n.d.	n.d.	1.6	2.0	1.02	0.3	0.9
Max	149	2.7	817	1707	105	7174	390	59.2
Means	19	0.2	27.8	73.4	32.7	590	27.8	13.3
Geochem. background	20	0.4	0.3	20	90	95	45	68

n.d. - < LOQ

A sequential analysis showed considerable diversification of mobility of the examined metals from sediment samples. It was observed, for example, that the mobile fraction of Cd constituted up 10% to above 90% its total content.
The studies of the relation between the effect toward *Vibrio fisheri* and *Heterocypris incongruens* indicate that there is no or only very slight correlation between these parameters. However, the studies of the proportion of variability in total metal concentration and toxicity effect toward *Heterocypris incongruens* show the strong correlationbetwee changes in mortality and total concentration of Cd, Zn and slightly weaker correlation in the case Pb and Cu.

Table 2. The square of a correlation coefficient (R^2) between biological effect toward *Heterocypris incongruens* and total metal concentration in sediment.

Heterocypris incongruens	determination coefficient R^2						
effect	sum	Hg	Cd	Pb	Cr	Zn	Cu
means growth after 6 day = f(c/EC50)	0.4563	0.2327	0.4495	0.4289	0.0077	0.3821	0.3890
% growth inhibition = f(c/EC50)	**0.6675**	0.1835	**0.6750**	**0.6686**	0.0001	0.2629	0.3102
% mortality = f(c/LC50)	**0.7108**	0.4450	**0.7015**	**0.5775**	0.0133	**0.6126**	**0.5154**

Such results do not agree with common knowledge that available is only mobile fraction of metals. The data obtained suggest that for *Heterocypris incongruens* immobile metal fractions are also bioavailable.

3.2 PAHs and PCBs

It is very important to known how PAHs and PCBs are sequestrated and aging in sediment. A major factor influencing successful sediment bioremediation is the availability of contaminants to microorganisms for degradation. Table 3 presents the recovery of PCBs and PAHs in single and ten-fold extraction.

Table 3. Recovery of PAHs and PCB from reference material (Metranal 2).

Compound	Recovery [%]		
	A. single extraction	B.10-fold extraction	B-A
PCBs			
PCB 28	85	112	28
PCB 52	64	74	10
PCB 101	60	64	4
PCB 118	37	47	9
PCB 153	76	90	15
PCB 138*	197*	247*	49*
PCB 180	51	62	12
PCB 209	**71**	**102**	**31**
PAHs			
N-d8	**30**	**39**	**9**
Fe	17	67	50
A	20	51	32
Flen	31	55	24
P	30	52	22
B(a)A	25	51	26
Ch	25	50	26
B(a)A-d12	**23**	**46**	**23**
B(b)F	30	59	28
B(k)F	26	49	23
B(a)P	19	37	18
I(123-cd)P	18	30	12
D(ah)A	25	48	23
B(ghi)Pe	22	41	19

* - PCB 138 coeluted with PCB 160

The presented results indicate that, efficiency of single extraction permits to obtain PCBs recovery from sediment on the level of 51-85% (with the exception of PCB 118 for which the recovery was about 37%).
For the internal standard (PCB 209), added to the sediment, the recovery was 71%.

The successive extractions (second to tenth) allowed to recover additional 13% of the original amount of analytes, while the added standard was recovered in 30%. The total recovery of PCB209 in ten extractions is of the order of 102%, while analytes present originally in real samples were recovered in 62% to 112%, with the exception of PCB118, whose recovery was much lower (of the order 47%). These data suggest that the standard was bonded with the sediment in a different way from other analytes present in the sediment. In a single extraction recoveries of standard and the other analytes are very similar.

PCBs reach the aquatic environment with wastewater dissolved in organic phase (small droplets of organic matter (oil) suspended in aqueous phase). In aquatic environment an oil fraction together with PCBs will be bonded to suspended matter and will undergo sedimentation. Oil droplets may attach to mineral sediment structures or organic matter being at different stages of decay.

Conglomerates with mineral matter will not affect the change of the nature of PCBs bonding in oil fraction.

On the other hand, conglomerates with organic matter whose chemical nature is close to the nature of oil fraction, will cause transfer of PCBs to organic matter. This change of bonding nature in time is called sediment aging.

In the case of PAHs the recoveries of standards and original analytes in single extraction (17-30%) and in ten-fold extraction (30-67%) are very close.

The similar results were obtained by other researchers. They compared recoveries of PAHs from reference materials used for monitoring emission of flue gasses and quality of outdoor air [4].

Such results suggest that the proposed method of internal standard addition to sediment sample permits to reconstruct bonding nature of analytes with sediment matrix.

It should be stressed that effectiveness of PAHs extraction from sediment by means of shaking assisted solvent extraction is relatively low.

Recovery in single extraction is only 20-25%, while total recovery in ten extractions is ca. 40-50% (excluding indeno(1,2,3-cd)pyrene, whose recovery is lower - 30%).

Studies on PAHs sorption in sediment were conducted in 1970's [5], but results of increasingly wide studies on mechanism of remediation allowed to find out that adsorption is the main mechanism of bonding PAHs with sediment.

The highest concentrations of PAHs were determined on exterior organic matter patches, where dominant is coal-derived matter, while only negligible amounts were found in the interior.

Similarly, negligible amounts of PAHs were found out on sediment surface of polar nature (e.g. silica) [2].

Additionally the ratios of Flur/(Flur+Pyr) and (An)/(An+Phen) for the studied sediment indicate that PAHs originate from combustion.

There are several significant implications of the finding that majority of the PAHs are associated with coal derived particles.

4 Conclusion

A quite good correlation between biological effect toward *Heterocypris incongruens* and total metals concentration in sediment suggest that for some organizms not only mobile fraction is bioavailable.

The results presented in these studies can be the basis for statement, that PAHs and PCBs are bound in different way to the sediments, depending on the way in which they were introduced to the aqueous environment.

PAHs introduced to aqueous environment by air, are adsorbed mainly on coal and coal-derived particles. While PCBs reach the aquatic environment mainly with oil fraction.

References:

[1] Mulligan C.N., Yong R.N., Gibbs B.F., Remediation technologies for metal-contaminated soils and groundwater: an evaluation. *Engineering Geology* Vol.60, 2001, pp.193-207.

[2] Ghosh U., Gillette S., Luthy R.G., Zare R.N.: Microscale location, characterization, and association of polycyclic aromatic hydrocarbons on harbor sediment particles. *Environ. Sci. Technol.,* Vol.34, 2000, pp.1729–1736.

[3] Simeonov V., Wolska L., Kuczyńska A., Gurwin J., Tsakovski S., Protasowicki M., Namieśnik J.: Sediment-quality assessment by intelligent data analysis, *TRAC - Trends Anal. Chem*., Vol.26, 2007, pp.323-331.

[4] Wnorowski A., Tardif M., Harnish D., Poole G., Chiu Chung.H.: Correction of analytical results for recovery: determination of PAHs in ambient air, soil and diesel emission control samples by isotope dilution gas chromatography-mass spectrometry, *Polycyclic Aromatic Compounds*, Vol. 26, 2006, pp.313-329.

[5] Accardi-Dey M., Goschwend P.M.: Assessing the Combined Roles of Natural Organic Matter and Black Carbon as Sorbents in Sediments, *Environ. Sci. Technol*., Vol. 36, 2002, pp.21-29.

Permian and Triassic wildfires and atmospheric oxygen levels

DIETER UHL
Forschungsinstitut und Naturmuseum Senckenberg
Senckenberganlage 25, D-60325 Frankfurt am Main
GERMANY
dieter.uhl@senckenberg.de http://www.senckenberg.de

ANDRÈ JASPER
Institut für Geowissenschaften
Universität Tübingen
Sigwartstraße 10, D-72076 Tübingen
GERMANY
and
Setor de Botânica e Paleobotânica do MCN/UNIVATES
UNIVATES
Rua Avelino Tallini, 171 – CEP 95.900-000, Lajeado, RS
BRASIL
ajasper@univates.br http://www.yourwebaddress.xx (12pt Times New Roman, centered)

ABDALLAH M.B. ABU HAMAD
Geology Division
The University of Jordan
Amman 11942
JORDAN

MICHAEL MONTENARI
Department of Earth Sciences and Geography
Keele University
William Smith Building, Keele, Staffordshire, ST5 5BG
UNITED KINGDOM
m.montenari@esci.keele.ac.uk http://www.esci.keele.ac.uk/people/staff/montenari/index.htm

Abstract: - Our present knowledge of Permian and Triassic occurrences of fossil charcoal, as direct evidence of palaeo-wildfire, is summarized. These data show that contrary to previous assumptions at least for the Permian a more or les continuous fossil record of charcoal exists. Permian gaps in the fossil record of charcoal are very likely to be explained by taphonomic biases and can not be linked to changes in atmospheric oxygen concentrations. In contrast the record of Triassic charcoal seems to be extremely scarce and this scarcity may be linked, at least to some extent, to rather low oxygen levels. However, parallel to the delayed recovery of terrestrial vegetation after the mass extinction at the Permian-Triassic boundary the fossil record of charcoal improves from the Ladinian up to the Rhaetian, contrary to a drop in atmospheric oxygen concentrations reconstructed by geochemical modeling. Probably a simple correlation between atmospheric oxygen concentrations and the frequency and intensity of naturally occurring wildfires may not be as easily linked to the abundance of fossil charcoal as proposed earlier. Additional factors like taphonomical filters should be taken into account whenever it is attempted to use the frequency and abundance of fossil charcoal as evidence for changes in atmospheric oxygen concentrations.

Key-Words: - Permian; Triassic; charcoal; atmospheric oxygen; taphonomy; vegetation recovery

1 Introduction

It has been predicted for several regions of the world that an increased frequency of wildfires together with their negative impacts on human civilization, will come along with a future climate change [29]. Such a climate change from icehouse conditions to a greenhouse world occurred also during the Permian and the Triassic [7, 23, 25]. Knowledge regarding the development of fire-frequencies as well as the intensities of fire induced devastation during this period is therefore essential for any evaluation of potential effects of a future or contemporary climate change - not only from an ecological, but also from an economical and political point of view.

The occurrence of fossil charcoal in sediments is widely accepted as the direct evidence of palaeo-wildfires [32, 33, 34]. So far, the oldest undisputed charcoal has been described from the Late Silurian of West-England [13], and from this time on there is a more or less continuous fossil record of charcoal [28, 33]. During the last decades special attention has been paid to the Late Carboniferous. For this time very high atmospheric O_2-concentrations have been reconstructed using geochemical modeling methods [1, 4]. Furthermore, widespread evidence exists for very intense fires within various terrestrial ecosystems [9, 10, 33].

Several authors have speculated that fire frequencies, as represented by the abundance and frequency of fossil charcoal, have decreased during the Latest Carboniferous and Permian, because of a drop in atmospheric O_2-concentrations [26, 27, 33]. This assumption is based on experimental data, which indicate a required atmospheric oxygen concentration of at least 13% for sustained biomass combustion [5, 6]. According to the reconstruction by Berner and Canfield [4] the atmospheric oxygen concentration would have dropped below this level during the Late Permian. More recent results from geochemical modeling, however, moved the high O_2-peak forward into the Permian and the acclaimed threshold of 13% atmospheric oxygen has probably not been reached before the Triassic (cf. Fig. 1; [2, 3]). Following this new reconstruction it has to be questioned whether changes in the atmospheric oxygen concentration are indeed the main reasons for the observed decrease of evidence for wildfires during the Latest Carboniferous and the Permian, as well as the Triassic or whether additional reasons have to be taken into account for the low charcoal abundances and frequencies during this period.

Here we present a tentative overview of previously published, as well as hitherto unpublished records of Permian and Triassic charcoals during this periods, to establish a first temporal framework for the causal interpretation of the fossil record of wildfires during this time.

2 Records of Permian charcoal

Most detailed reports on Late Palaeozoic charcoal from the northern hemisphere prior to the extensive review on Pre-Quaternary fires by Scott [33] came from Westphalian and pre-Westphalian deposits. For the Stephanian and the entire Permian, only few investigations had been made on this subject up to this date [30, 31, 35]. Although the occurrence of charcoal has anecdotally been reported from a number of localities from the latest Carboniferous (‘‘post’’-Stephanian C = lowermost Rotliegend of Central Europe) and Permian of Central Europe (cf. [39] and citations therein), no detailed descriptions of the material had been given and no anatomical or petrologic evidence supporting such an interpretation of the respective material had been presented.

Only recently it has been demonstrated that in the rather humid Lower Rotliegend (upper Gzhelian – Asselian) of the Saar-Nahe basin in SW Germany all sedimentary lithologies investigated so far yielded charcoal remains in varying abundance (cf. Fig. 2A) [39]. In contrast most sedimentary facies (i.e. red beds, deposited under strong climatic seasonality) from the more arid Upper Rotliegend (Asselian – Sakmarian) of this area yielded no macroscopically identifiable charcoal remains (cf. Fig. 2B) [39]. Only in volcanically influenced sediments charcoal has been found here. However, in these cases most charcoals were silicified and the few non-silicified charcoals were found in tuffs or tuffites that have been deposited subaquatically [39]. As demonstrated by Skjemstad et al. [36] charcoal breaks down rapidly under semi-arid conditions and it has been assumed by Uhl et al. [39] that this, together with a generally sparse vegetation cover, is also very likely the main reason for the low abundance of charcoal in sediments from the Upper Rotliegend of the Saar-Nahe basin. Additional reports of Early Permian charcoals come from Northern America, where fossil charcoal has been discovered at several localities in lacustrine and marine sediments [30, 31, 33]. Charcoal found in coals [17, 19, 37] and in lacustrine Kungurian sandstones of the Rio Bonito Formation, in the Paraná Basin, South Brazil (Fig. 2C), is proof that during the Early Per-

mian wildfires also occurred in the mid latitudes of Gondwana.

The up to now the published record of Middle Permian charcoal is rather scarce. So far only a few reports of fossil charcoal from this period have been substantiated by anatomical [8] or petrographic evidence [12]. However, records of Middle Permian wildfires are geographically widespread, including the Euramerican floral province [8], Cathaysia [42] and the high latitudes of Southern Gondwana [12].

Plant bearing localities from the Late Permian of the Northern hemisphere, especially from Euramerica, are very rare. An analysis of marine marls from the lower Zechstein (Wuchiapingian) of NW-Hesse (Germany) provided abundant charcoal fragments, not only consisting of charred woods, but also of charred conifer needles (cf. Fig. 2D–E) [38]. Remains of Wuchiapingian charcoal have also been discovered in Zechstein sediments near the abandoned village of Culmitzsch in E-Thuringia (Germany) (cf. Fig. 2F). Further reports of Wuchiapingian charcoals come from Cathaysia, were a lycopsid dominated vegetation experienced more or less regular wildfires during this time [41, 42, 43].

Additional to charcoals from the Late Permian of Central Europe and China also charcoals from the uppermost Permian (Changhsingian) deposits of Jordan have recently been discovered (Fig. 2G), which testify for the first time to the occurrence of palaeo-wildfires in the low latitudes of Northern Gondwana during this period [40]. These charcoals are abundant in facies types, like clays deposited in abandoned channels, which are favourable for the preservation of charcoal, whereas other facies types deposited under more dry conditions yielded no macroscopically identifiable charcoal at all.

3 Records of Triassic charcoal

Charcoal is extremely rare in clastic sediments from the Triassic [33] and only a few reports deal with Triassic charcoal in detail. Substantiated reports on macroscopically identifiable charcoal from the Early Triassic (Indusian – Olenekian) and the Anisian are completely missing so far. Only occasionally shattered remains of charcoal have been reported from studies on the palynofacies of early to middle Triassic sediments [24]. So far the oldest substantiated Triassic record of macroscopically identifiable charcoal comes from the Ladinian of S-Germany [20, 21, 22]. The record of Carnian and Norian charcoal is also extremely scarce, but the occurrence of charcoal has repeatedly been testified for N-America [18, 45], as well as S-Germany [20, 21, 22].

Harris [15, 16] described charcoal from Rhaetian – Liassic fissure fills in Carboniferous limestones of South Wales. Although Harris [15] could give no definitive age assignments for his material he stated that it would be most likely of lower Liassic age, based on taxonomic similarities with Liassic floras from S-Germany. Harris [16] also reported the occurrence of charcoal in Rhaetian – Lower Liassic deltaic deposits of Eastern Greenland. In this case the charcoal has not been identified, but it is abundant and has a widespread occurrence in this area. Later on Scott [33] considered the charcoal described by Harris [15, 16] to be of Early Jurassic age. In S-Germany (Franconia, Bavaria) charcoal has also been recorded from Rhaetian sediments [20, 21, 22]. In SW-Germany charcoal is frequent in Rhaetian sandstones (Fig. 2H–I). This material shows characteristics which are considered to be typical for charcoal by several authors [33], like black streak, silky lustre and homogenized cell-walls when investigated under the SEM, giving proof to the occurrence of wildfires during the uppermost Triassic in Central Europe.

4 Discussion

Our brief overview has shown that the fossil record of Permian charcoals is obviously not as scarce as previously believed by various authors [18, 33], although the fossil record of Permian charcoal is in fact less abundant than that of Carboniferous charcoal [33]. However, according to recent model results the highest atmospheric oxygen concentrations were not reached during the Carboniferous, thus promoting widespread and intense wildfires, but during the Permian and probably did not fall below the assumed crucial threshold of 13% during the entire Permian (cf. Fig. 1), but remained above this level until the Lower Triassic [2]. Instead of low oxygen levels it is therefore necessary to evaluate other potential reasons for the lower abundance of charcoal during the Permian.

One of the potential reasons is a generally scarcer vegetation cover during the Permian in many areas worldwide, than during the Carboniferous. Climatic deterioration as well as tectonic reorganization of landscapes led to the disappearance of coal forming forests in most regions worldwide [23] and probably the potential amount of available fuel for wildfires decreased on a large scale. Regionally such a reason has also been discussed for the scarceness of charcoal in Upper Rotliegend (As-

selian – Sakmarian) sediments from SW-Germany [39]. Another potential reason are taphonomic filters and it has already been proposed that charcoal produced during wildfires has not been preserved due to degradation under the semi-arid and arid conditions prevailing during parts of the Permian [39], like it has been observed in present-day Australia where buried charcoal breaks down rapidly under semi-arid conditions [36]. Both reasons, maybe together with other, so far unidentified reasons, can probably explain the lower abundance of Permian charcoal as compared to the Carboniferous.

In contrast to the Permian the record of Triassic charcoal actually seems to be extremely scarce and this scarcity of charcoal may in fact be linked, at least to some extent, to rather low oxygen levels, which probably dropped below 13% during parts of the Triassic [2, 3]. However, these geochemical model results also suggest that oxygen levels were lowest during the Triassic – Jurassic transition interval. This low-oxygen phase corresponds at least partly to the Rhaetian, a phase with widespread and abundant evidence of palaeo-wildfires. After a global "charcoal gap" from the Indusian up to the Anisian, the fossil record of charcoal seems to increase slowly from the Ladinian up to the Rhaetian, contrary to a modeled drop in atmospheric oxygen concentrations. This seems to contradict a direct relationship between oxygen concentrations and fire-frequencies. However, based on physico-chemical considerations and experimental evidence it has to be assumed that oxygen concentrations [5, 6], together with chemical and physical properties of the fuel [44], have actually an influence on the intensity and frequency of naturally occurring fires. But, why is the fossil record of charcoal increasing from the Ladinian onwards, despite low oxygen levels? A potential explanation may be linked to the recovery patterns of terrestrial vegetation seen after the devastating mass-extinction at the Permian-Triassic boundary.

As Grauvogel-Stamm and Ash [14] have shown, the worldwide fossil record of land plants is extremely scarce during an Early Triassic survival phase and only from the Anisian onward do fossil plant remains become more frequent, pointing to a recovery of terrestrial ecosystems during this period. Considering the fact that most of the potential refugia for many Early Triassic plants, which may have experienced wildfires during this period, were probably far away from the areas were sediments from this period have been deposited [11, 14] it seems likely that no charcoal as direct evidence of wildfires within such potential refugia, has been deposited within sediments from this period. However, the scarce records of charcoal remains in palynofacies samples from the Early Triassic [24] demonstrate that actually wildfires occurred somewhere in the hinterland.

It seems, that we have to consider that the scarceness of charcoal during the Triassic is not only related to the low atmospheric oxygen concentrations prevailing during this period, but also reflects the rather slow recovery of the terrestrial vegetation after the mass-extinction at the Permian-Triassic boundary. Additionally, as considered above for the Permian, taphonomic filters have to be taken into account which may have further decreased the quantity of fossil charcoal within most sediments (i.e. the widespread red beds) deposited during the Triassic.

Our results and interpretations indicate that a simple correlation between atmospheric oxygen concentrations and the frequency and intensity of naturally occurring wildfires may not be as easily linked to the abundance of fossil charcoal as proposed by previous authors [18, 26, 27, 33]. Additional factors like the global or regional density of the vegetation, as well as taphonomic filters, which are independent from oxygen concentrations, should be taken into account whenever it is attempted to use the frequency and abundance of fossil charcoal as evidence for changes in atmospheric oxygen concentrations.

References:

[1] Berner, R.A., Modelling atmospheric O_2 over Phanerozoic time, *Geochimica et Cosmochimica Acta*, Vol. 65, 2001, pp. 685-694.

[2] Berner, R.A., Examination of hypotheses for the Permo-Triassic boundary extinction by carbon cycle modeling, *Proceedings of the National Academy of Sciences*, Vol. 99, 2002, pp. 4172-4177.

[3] Berner, R.A., The carbon and sulfur cycles and atmospheric oxygen from middle Permian to middle Triassic, *Geochimica et Cosmochimica Acta*, Vol. 69, 2005, pp. 3211-3217.

[4] Berner, R.A., and Canfield, D.E., A new model for atmospheric oxygen over Phanerozoic time, *American Journal of Science*, Vol. 289, 1989, pp. 333–361.

[5] Clark, F.R.S., and Russell, D.A., Fossil charcoal and the palaeoatmosphere, *Nature*, Vol. 290, 1981, pp. 428.

[6] Cope, M.J., and Chaloner, W.G., Fossil charcoal and the palaeoatmosphere. Reply, *Nature*, Vol. 290, 1981, pp. 428.

[7] DiMichele, W.A., Pfefferkorn, H.W., and Gastaldo, R.A., Response of Late Carboniferous and Early Permian plant communities to climate change, *Annual Review of Earth and Planetary Science*, Vol. 29, 2001, pp. 461-487.

[8] DiMichele, W.A., Hook, R.W., Nelson, W.J., and Chaney, D.S., An unusual Middle Permian flora from the Blaine Formation (Pease River group: Leonardian-Guadalupian series) of King County, West Texas, *Journal of Paleontology*, Vol. 78, 2004, pp. 765-782.

[9] Falcon-Lang, H.J., The impact of wildfire on an Early Carboniferous coastal environment, North Mayo, Ireland, *Palaeogeography, Palaeoclimatology, Palaeoecology*, Vol. 139, 1998, pp. 121-138.

[10] Falcon-Lang, H.J., and Scott, A.C., Upland ecology of some Late Carboniferous cordaitalean trees from Nova Scotia and England, *Palaeogeography, Palaeoclimatology, Palaeoecology*, Vol. 156, 2000, pp. 225-242.

[11] Gall, J.-C., and Grauvogel-Stamm, L., The early Middle Triassic 'Grès à Voltzia' Formation of eastern France: a model of environmental refugium, *Compte Rendu Palevol*, Vol. 4, 2005, pp. 569-584.

[12] Glasspool, I., A major fire event recorded in the mesofossils and petrology of the Late Permian, Lower Whybrow coal seam, Sydney Basin, Australia, *Palaeogeography, Palaeoclimatology, Palaeoecology*, Vol. 164, 2000, pp. 373-396.

[13] Glasspool, I.J., Edwards, D., and Axe, L., Charcoal in the Silurian as evidence for the earliest wildfire, *Geology*, Vol. 32, 2004, pp. 381-383.

[14] Grauvogel-Stamm, L., and Ash, S.R., Recovery of the Triassic land flora from the end-Permian life crisis, *Compte Rendu Palevol*, Vol. 4, 2005, pp. 525-540.

[15] Harris, T.M., A Liasso-Rhaetic flora in South Wales, *Proceedings of the Royal Society of London, ser. B*, Vol. 147, 1957, pp. 289-308.

[16] Harris, T.M., Forest fire in the Mesozoic, *Journal of Ecology*, Vol. 46, 1958, pp. 447-453.

[17] Holz, M., Vieira, P.E., and Kalkreuth, W., The Early Permian coal-bearing succession of the Paraná Basin in Southernmost Brazil: depositional model and sequence stratigraphy, *Revista Brasileira de Geociências*, Vol. 30, 2000, pp. 420-422.

[18] Jones, T.P., Ash, S., and Figueiral, I., Late Triassic charcoal from Petrified Forest national Park, Arizona, USA, *Palaeogeography, Palaeoclimatology, Palaeoecology*, Vol. 188, 2002, pp. 127-139.

[19] Kalkreuth, W., Holz, K.M., Machado, G., Mexias, A., Silva, M.B., Willett, J., Finkelman, R., and Burger, H., Petrology and chemistry of Permian coals from the Paraná Basin: 1. Santa Terezinha, Leão-Butiá and Candiota Coalfields, Rio Grande do Sul, Brazil, *International Journal of Coal Geology*, Vol. 68, 2006, pp. 79-116.

[20] Kelber, K.-P., Der Nachweis von Paläo-Wildfeuer durch fossile Holzkohlen aus dem süddeutschen Keuper, *Terra Nostra*, Vol. 99/8, 1999, pp. 41.

[21] Kelber, K.-P., Preservation and taphonomy of charcoal from the Upper Triassic of southern Germany, Abstract, *12th Plant Taphonomy Meeting*, 26th of October 2001, Altlengbach, Austria, 2001.

[22] Kelber K-P. Die Erhaltung und paläobiologische Bedeutung der fossilen Hölzer aus dem süddeutschen Keuper (Trias, Ladinium bis Rhätium), In: Schüssler H, Simon T. (eds.): *Aus Holz wird Stein - Kieselhölzer aus dem Keuper Frankens* (Offsetdruck Eppe GmbH), Bergatreute-Aulendorf, 2007, pp. 37-100.

[23] Kerp, H., The modernization of landscapes during the Late Paleozoic-Early Mesozoic, *Paleontological Society Papers*, Vol. 6, 2000, pp. 79-113.

[24] Mangerud, G., and Rømuld, A., Spathian–Anisian (Triassic) palynology at the Svalis Dome, southwestern Barents Sea, *Review of Palaeobotany and Palynology*, Vol. 70, 1991, pp. 199-216.

[25] Retallack, GJ., Permian-Triassic life crisis on land, *Science*, Vol. 267, 1995, pp. 77–80

[26] Robinson, J.M., Phanerozoic O_2 variation, fire, and terrestrial ecology, *Palaeogeography, Palaeoclimatology, Palaeoecology*, Vol. 75, 1989, pp. 223-240.

[27] Robinson, J.M., Phanerozoic atmospheric reconstructions: a terrestrial perspective, *Palaeogeography, Palaeoclimatology, Palaeoecology*, Vol. 97, 1991, pp. 51-62.

[28] Rowe, N.P., and Jones, T.P., Devonian charcoal, *Palaeogeography, Palaeoclimatology, Palaeoecology*, Vol. 164, 2000, pp. 347-354.

[29] Ryan, K.C., Global Change and Wildland Fire. In: *Wildland fire in ecosystems: effects of fire on flora*, USDA Forest Service General Technical Report, RMRS-GTR-42 (2), 2000, pp. 175-184.

[30] Sander, P.M., Taphonomy of the Lower Permian Geraldine bonebed in Archer County, Texas, *Palaeogeography, Palaeoclimatology, Palaeoecology*, Vol. 61, 1987, pp. 221-236.

[31] Sander, P.M., and Gee, C.T., Fossil charcoal: techniques and applications, *Review of Palaeobotany and Palynology*, Vol. 63, 1990, pp. 269-279.

[32] Scott, A.C., Observations on the nature and origin of fusain, *International Journal of Coal Geology*, Vol. 12, 1989, pp. 443-475.

[33] Scott, A.C., The Pre-Quaternary history of fire, *Palaeogeography, Palaeoclimatology, Palaeoecology*, Vol. 164, 2000, pp. 297–345.

[34] Scott, A.C., Preservation by fire, In: Briggs D.E.G. and Crowther P.R. (eds.), *Palaeobiology a synthesis II*. Blackwell Scientific Publ., 2001, pp. 277-280.

[35] Scott, A.C., and Glasspool, I.J., The diversification of Paleozoic fire systems and fluctuations in atmospheric oxygen concentration, *Proceedings of the National Academy of Science U.S.A.*, Vol. 103, 2006, pp. 10861–10865.

[36] Skjemstad, J.O., Clarke, P., Taylor, J.A., Oades, J.M., and McClure, S.G., The chemistry and nature of protected carbon in soil, *Australian Journal of Soil Research*, Vol. 34, 1996, pp. 251-271.

[37] Silva, M.B., and Kalkreuth W., Petrological and geochemical characterization of Candiota coal seams, Brazil – Implication for coal facies interpretations and coal rank, *International Journal of Coal Geology*, Vol. 64, 2005, pp. 217-238.

[38] Uhl, D., and Kerp, H., Wildfires in the late Palaeozoic of Central Europe - The Zechstein (Upper Permian) of NW-Hesse (Germany), *Palaeogeography, Palaeoclimatology, Palaeoecology*, Vol. 199, 2003, pp. 1-15.

[39] Uhl, D., Lausberg, S., Noll, R., and Stapf, K.R.G., Wildfires in the Late Palaeozoic of Central Europe - an overview of the Rotliegend (Upper Carboniferous - Lower Permian) of the Saar-Nahe Basin (SW-Germany), *Palaeogeography, Palaeoclimatology, Palaeoecology*, Vol. 207, 2004, pp. 23-35.

[40] Uhl, D., Abu Hamad, A.M.B., Kerp, H., and Bandel, K., Evidence for palaeo-wildfire in the Late Permian palaeotropics – charcoalified wood from the Um Irna Formation of Jordan, *Review of Palaeobotany and Palynology*, Vol. 144, 2007, pp. 221-230.

[41] Wang Zi-Qiang, Vegetation declination on the eve of the P-T Event in North China and plant survival strategies: an example of Upper Permian refugium in Nortwestern Shanxi, China, *Acta Palaeontologica Sinica*, Vol. 39 (Suppl.), 2000, pp. 127-153.

[42] Wang Zi-Qiang, and Chen An-Shu, Traces of arborescent lycopsids and dieback of the forest vegetation in relation to the terminal Permian mass extinction in North China, *Review of Palaeobotany and Palynology*, Vol. 117, 2001, pp. 217-243.

[43] Wang Zi-Qiang, and Zhang Zhiping, Gymnosperms on the eve of the terminal Permian mass extinction in North China and their survival strategies, *Chinese Science Bulletin*, Vol. 43, 1998, pp. 889-897.

[44] Wildman, R.A., Hickey, L.J., Dickinson, M.B., Berner, R.A., Robinson, J.M., Dietrich, M., Essenhigh, R.H., and Wildman, C.B., Burning of forest materials under late Paleozoic high atmospheric oxygen levels, *Geology*, Vol. 32, 2004, pp. 457-460.

[45] Zeigler, K.E., Heckert, A.B., and Lucas, S.G., Taphonomic analysis of a fire-related Upper Triassic vertebrate fossil assemblage from North-Central New Mexico, *New Mexico Geological Society, 56th Field Conference Guidebook, Geology of the Chama basin*, 2005, pp. 341-354.

Figure captions:

Fig. 1.

Reconstructed atmospheric oxygen concentrations over the last 600 million years (redrawn from Berner, 2002). Permian and Triassic highlighted in grey; PTB = Permian – Triassic boundary

Fig. 2.

SEM-images of charcoal remains from the Permian and Triassic. A) Gzhelian/Asselian, Saar-Nahe basin SW-Germany (from Uhl et al., 2004); B) Asselian/Sakmarian, Saar-Nahe basin SW-Germany (from Uhl et al., 2004); C) Kungurian, Paraná Basin, Rio Grande do Sul, S-Brazil (from Jasper et al., submitted); D – E) Wuchiapingian, Frankenberg, NW-Hesse, Germany (from Uhl and Kerp, 2003), F) Wuchiapingian, Culmitzsch, E-Thuringia, Germany; G) Changhsingian, Wadi Himara, Jordan (from Uhl et al., 2007); H – I) Rhaetian, Tubingen, SW-Germany.

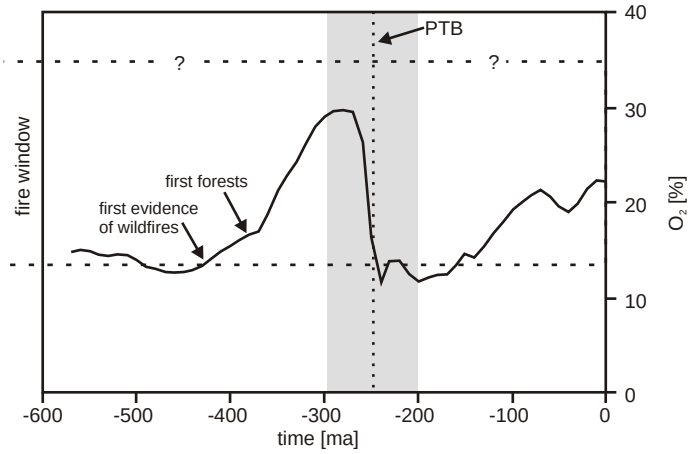

Uhl et al., Fig. 1

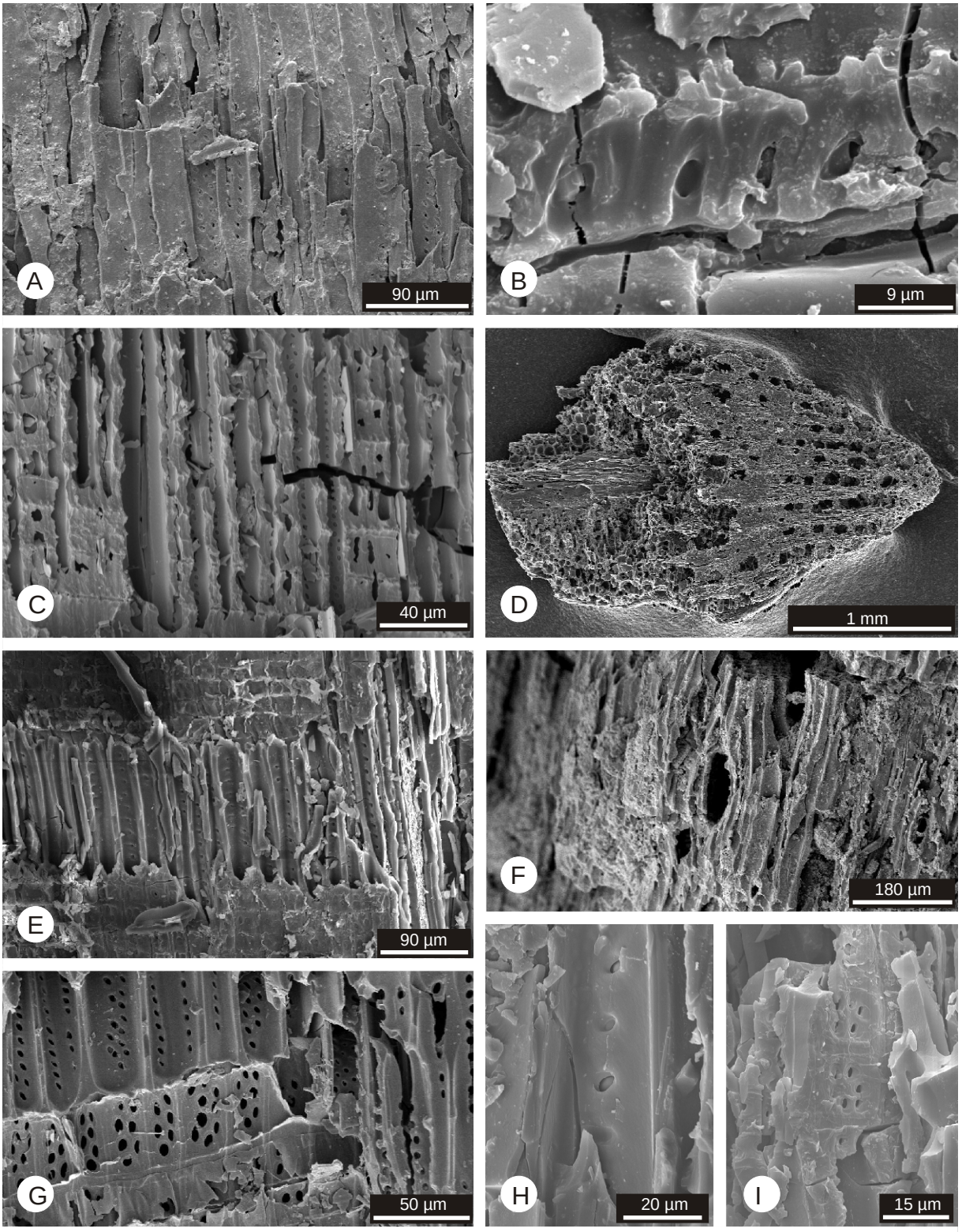

Uhl et al., Fig. 2

The GEOMIND, a new international geophysical information service on the Internet

Greg DETZKY[1], László VÉRTESY[2], László SŐRÉS[3]
Department of Geoinformatics
Eötvös Loránd Geophysical Institute (ELGI)
1145 Budapest, Colombus u. 17-23.
HUNGARY
detzky@elgi.hu[1] vert@elgi.hu[2] sores@almos.vein.hu[3] http://www.elgi.hu

Abstract: Various dispersed geophysical databases exist in European countries, both in public and private organisations in different standards and languages. Thus the usefulness and availability are limited. The existence of particular datasets is often unknown even for geo-experts. The GeoMind system has been developed by 9 European countries (Danmark, Germany, Poland, Lithuania, Czech Republic, Slovakia, Hungary, Greece, Italy) integrating their national databases to meet the needs of different actors in the economy potentially utilising geophysical data on the international level. GeoMind is a web-based information service (an internet portal) opened literally a few days ago for the public use, after a 2 years intensive development, co financed by the eContetPlus programme of the European Committee. It facilitates unified search and display of geophysical information across Europe, providing users with a multilingual interface. System enables a collection of geophysical metadata and submission of orders to obtain related geophysical data from actual data provider members (Fig 1), without any limitation regarding the national boundaries. The potential users of the GeoMind service are governmental- and local authorities; exploration-, mining-, civil engineering-, insurance- and other companies; scientists, researchers, students and of course individual citizens.

A more detailed description about the GeoMind system architecture and the way of its usage are provided below in the recent paper. Additional information about the GeoMind could be obtained at the GeoMind portal: www.geomind.eu.

Key-Words: geophysics, data service, database, metadata, online, Internet, multilingual, standard, ISO, XML

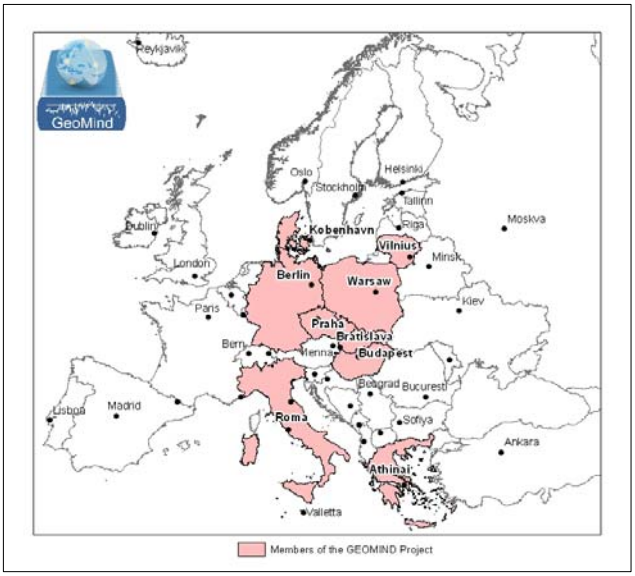

Fig. 1 *Member countries of the GeoMind project consortium*

1 Introduction

There are 3 main data categories comprising hierarchy of the GeoMind data repository. The **ISO-19115 compliant metadata** (general description, distribution, quality, spatial and temporal extent of detailed geophysical data) are on the topmost level. These data are independent from the underlying geophysical methods. **Geophysical metadata** which are specific to related geophysical methods, holding general parameters (instrumentation, measuring conditions, etc.) are on the middle level. The **detailed geophysical data** constitute the base level. The items here are stored in a newly developed XML based inner GeoMind standard form, generally capable to include practically any kind of geophysical data.

Recent data repository of GeoMind covers data types of vertical electrical sounding (VES), time domainian electromagnetics (TDEM), magneto-

tellurics & tellurics, gravimetry, magnetometry, radiometry & gamma spectrometry, seismics & seismologic monitoring, well logging, petrophysical measurements.

2 GeoMind system concept

2.1 Functionality

Internet portal at the site www.geomind.eu provides spatial and thematic search against unified geophysical metadata repositories, giving information on the availability, on the way of distribution and on the quality of the geophysical datasets.

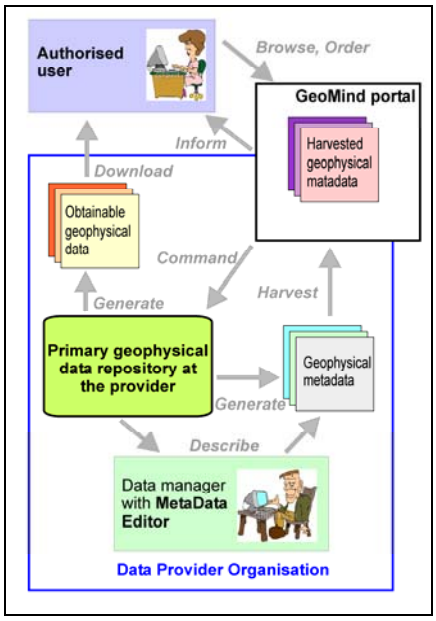

Fig. 2 *Geomind system elements and data flows*

In the usual dataflow (Fig. 2), several organizations provide their geophysical data through the GeoMind portal such a way that the data repositories itself are physically remaining at the data providers' places.

Data managers at the data providers by using the *MetaData Editor* tool are preparing metadata information records for the GeoMind portal about *describing* their geophysical data to be provided. The GeoMind portal is *harvesting* this metadata information in regular basis using appropriate CSW (Catalogue Service Web) application in order to be able to specify particular geophysical objects for the data customer users for *browsing* and *ordering* purposes.

In such a way an individual interested in geophysical data is able to search geographically or textually the GeoMind system (Fig. 3) for types and places of data available from data providers even from different countries. Geographycal search tool provides a topographic window with common GIS capabilities. Search map could be covered by predefined user selectable layers of different geophysical measurement methods (which are independent from selection operation).

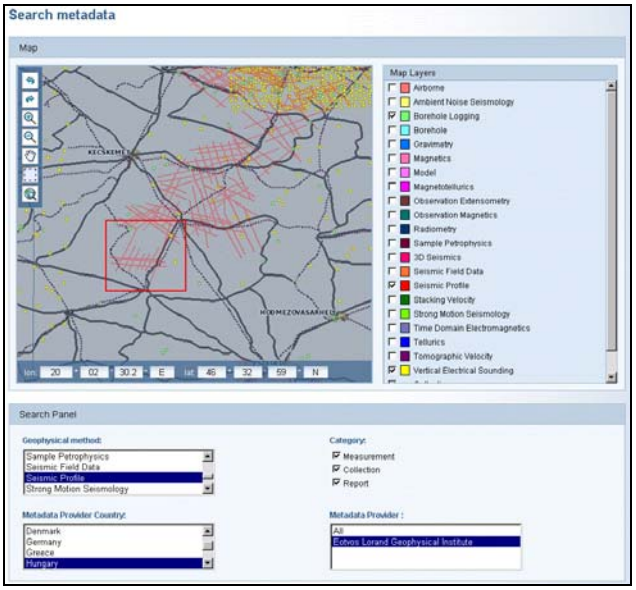

Fig. 3 *Interface for metadata search with GIS capabilities*

(Map fragment of central Hungary with borehole logging data, VE Soundings and seismic profiles shown)

User, by setting the *'area of interest'* (e.g. red rectangle on the map of Fig. 3) specifies a geographic subset of geophysical objects, corresponding to the criteria in the drop down lists for selection of *'Geophysical method'*, *'Category'*, *'…provider country'* and *'…provider organisation'* (which are independent otherwise from the layers switched on the selection map). In case the user does not provide *'area of interest'* the system will search and provide metadata for all the objects with satisfying the criteria without any geographic limitation.

Once the user has found the interested subset of data he/she is able to review a list of metadata and obtain underlying detailed information (geophysical parameter 'headers') of the particular items (Fig.4) to be used for further restriction of the primary selection. Customer user is provided by appropriate online GeoMind portal tools to place a direct order to the data providers to obtain authorisation for the *downloading* of the detailed geophysical data related to the refined metadata selection. GeoMind system *informs* the user upon availability.

Fig. 4 *Metadata list of search selection and a part of 'detailed information' on a particular item*

2.2 Architecture

System architecture has been built for reliable managing beside the aimed functionality of the involved geophysical information in the form defined by **GeoMind metadata Profile** (Fig. 6) and **General Geophysical Model**.

The website is an opened WMS/WFS based GIS portal of geophysical datasets from the data provider partner institutions (see Fig. 4), and from all those, who are willing to join to the system in the future.

The developed system architecture allows future extensions by adding new languages to the GeoMind's multilingual facility (see section 4) and defining new data models for data types to be additionally distributed by the system. New geographic areas, like countries also could be easily included into the current data supplier community.

3 ISO compliant standard extension for inner data representation

New data models have been developed for the geophysical metadata, header data and detailed data as internal standards, based on general use of XML (Extensible Markup Language) format which is widely accepted as a standard for data exchange on the Internet.

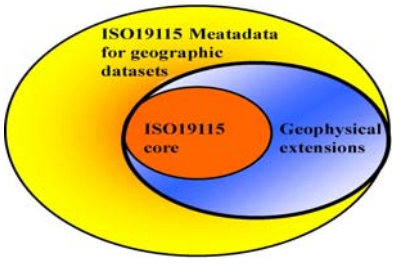

Fig. 5 *Extension principle of ISO-19115 standard*

GeoMind internal metadata standard has been established by removing optional elements not needed for geophysical applications (yellow part on the Fig. 5) and including general mandatory part of the ISO-19115 standard (orange part on the Fig. 5) with extension by special components describing geophysical issues (blue part on the Fig. 5). This way of extension is considered by the ISO-19115 standard itself which is intended for general use in GIS based information applications.

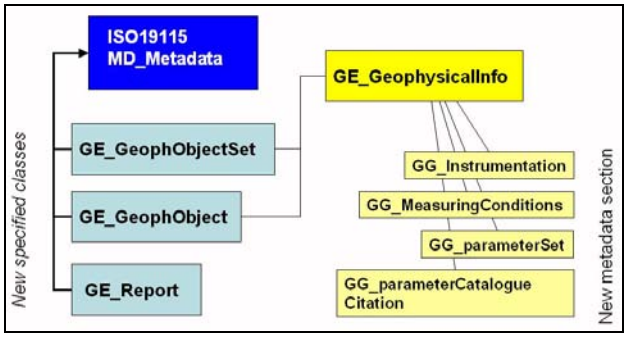

Fig. 6 *New geophysical classes and metadata categories in extended ISO-19115*

These standards are used for transmitting the geophysical data from the national data provider systems to the users during download and to GeoMind information portal to create up-to-date searchable metadata catalogues of provider's systems.

These standards (Fig. 6) are planned to use in possible future data exchange between the participants, and any third party institutions as well.

4 Multilingual functionality

The multilingual (cross-border) approach of the GeoMind project and its outcomes is emphasized. The launched GeoMind portal recently could be reached in 9 different languages of current participants and in English.

Multilingual support covers system interfaces of all software tools, GeoMind metadata profile, and hierarchical geophysical thesaurus with independent usability. Thesaurus helps interactive translation of any textual geophysical content outcoming from the system on any of participants' languages.

The interactive Multilingual Content Manager (Fig. 7) makes available an online preparation and maintenance of the multilingual textual system interface elements. The included Multilingual Geophysical Thesaurus with 3500 geophysical terms provides users a translation help for application of

national geophysical information in any participant's languages.

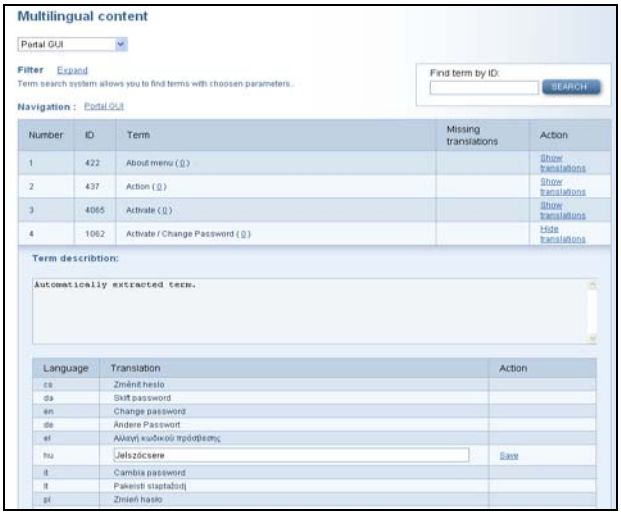

***Fig. 7** Multilingual thesaurus and ML system interface manager*

This part of the GeoMind system allows the easy future extension by adding any other languages (as well as other data providers) from new countries.

5 Data preparation based on XML schemes

Offline MetaData Editor (Fig. 8) is the core tool for providers to manage geophysical metadata & detailed data of their own repositories for standardized description of the central metadata catalogue system in the background of the GeoMind portal.

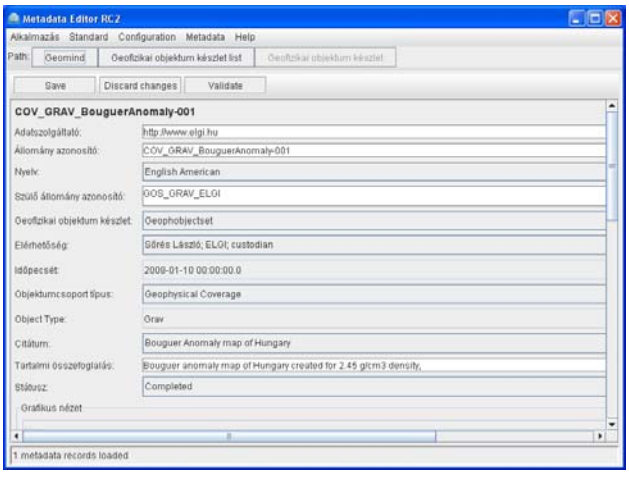

***Fig. 8** Independent MetaData Editor with multilingual (here with Hungarian) user interface*

MDEditor manipulates on the geophysical contents of national data sources, compiling information about them in GeoMind standard XML structures. It provides functions for interactive data editing at the client side and bulk data uploading as well. The user interface of the MDEditor is also multilingual (Fig. 8) and could be extended with new languages at any time by using Multilingual Content Manager (Fig. 7.)

6 Conclusion

The public dissemination and regular running of the established service are the main current activities in the project. (Recent paper serves for this objective as well.) It is expected that the overall effect of the GeoMind system will essentially enhance the cross-border use of geophysical data resources, in multinational manner. The activities related to GeoMind are also intended to contribute the development of European Spatial Data Infrastructure (INSPIRE) and supposed to assist communication and collaboration of different European countries.

The organization taking care of the physical elements of the system core from now is the Geological Survey of Denmark and Greenland (GEUS). The very actual public launching of the system **1st September** had been preceded by transferring its IT elements from the Lithuanian developing information technology company ITG to the current host.

Thus a large part of European geophysical data effectively could be applied, processed and interpreted for a wide variety of such a purposes as exploration for mineral resources and groundwater, studying environmental features for spatial planning, construction works or detection of potential geohazards and various research projects as well.

The GeoMind Consortium kindly encourages all geophysical data owners and potential users of geophysical data to join to the providers' community or just browse the system. Both activities could be initiated right through the GeoMind portal www.geomind.eu. All of them who are interested in more detailed information, it is recommended to attend the system's portal and review the wide variety of documentations available there about the system itself.

References:

[1] INTERNATIONAL STANDARD ORGANISATION, *Geographic information — Metadata*, reference number: ISO/FDIS 1911, 20035(E)

[2] L. SŐRÉS & the GEOMIND CONSORTIUM, *Metadata Hierarchy in Geophysics, and a General Geophysical Model*, EAGE 69th Conference & Exhibition – London, UK, 11 - 14 June 2007

[3] L. VÉRTESY , Á. GULYÁS, G. DETZKY & the GEOMIND CONSORTIUM, *GEOMIND – A Project to Set up a Geophysical Multilingual Internet-Driven Information Service*, EAGE 69th Conference & Exhibition – London, UK, 11 - 14 June 2007

[4] J. SEDLAK, T. MARDAL, G. DETZKY, L. SŐRÉS, L. VÉRTESY, V. HLADIK, R. TOMAS, V. SZALAIOVA, *GeoMind, a Geophysical Multilingual Internet-Driven Information Service*, EAGE 70th Conference & Exhibition – Rome, Italy, 9 - 12 June 2008

[5] GREG DETZKY, LÁSZLÓ VÉRTESY, LÁSZLÓ SŐRÉS & THE GEOMID CONSORTIUM, *The GEOMIND, a new geophysical multilingual internet driven information service, established by 9 European countries, supported by the EC* eContentplus *programme*, 21st International CODATA Conference – Scientific Information for Society from Today to the Future – Kyiv, Ukraine, 5 - 8 October, 2008

[6] KUEHNE, K., KUDER, J. (GGA INSTITIUTE), SLOVAKIEWICZ, M. (POLISH GEOLOGICAL INSTITUTE) & GEOMIND CONSORTIUM *GEOMIND - Find and Obtain Geophysical Data across National Borders*, 33rd International Geological Congress – Oslo, Norway, 6-14 August 2008

Pollutant deposition via snowpack in the context of granite buffering capacity, Western Sudetes, Poland

BŁAŚ MAREK[1)], POLKOWSKA ŻANETA[2)], SOBIK MIECZYSŁAW[1)] and GODEK MICHAŁ[1)]
[1)]Department of Meteorology and Climatology; [2)]Department of Analytical Chemistry
[1)]University of Wrocław; [2)]Gdańsk University of Technology (GUT)
[1)]8 Kosiby St. PL 51-670, Wrocław; [2)]111/12 G. Narutowicza St. PL 80-952, Gdańsk
[1,2]POLAND
[1)]blasm@meteo.uni.wroc.pl, http://www.meteo.uni.wroc.pl [2)]chemanal@pg.gda.pl, http://www.pg.gda.pl

Abstract: - The analysis of the pollutant deposition via snowpack is based on a dataset from Field Meteorological Station of the University of Wrocław at Mt. Szrenica situated in the Giant Mts. (φ=50˚48′, λ=15˚31′, H=1331 m a.s.l.). At the end of each analyzed winter season, the cores of the snowpack profile were collected in the phase of maximum snow water equivalent and a few days later during long spring thaw. Comparison between pH and snow water equivalent allowed to calculate the load of hydrogen ion in the whole snowpack profile. To obtain detailed recognition of the structure of released load of pollutants, the results of determination of chemical composition of snowpack for winter season 2005/2006 are also included. The release of pollutants from snow and their real penetration into soil, ground and surface waters take place during thaw episodes. The initial results indicate however, that the first portions of water penetrating from snow into ground may bring a huge pollutant load and it depends on the amount of snowpack water storage and Total Inorganic Ionic Content value. During one week of continuous ablation in snow season 2005/2006, total load of H^+ accumulated in snowpack show 40% decrease (it means: 16,4 mMoles m^{-2}). The fastest removal via the first portions of melting water occurred in case of H^+, NO_3^-, SO_4^{2-} and Mg^{2+}, which is in contrast with much smaller removal rate of Na^+, Cl^- and NH_4^+. Such mechanism is responsible for significant acidification of soil and water ecosystems because granite bedrock is able to buffer only 20-30 mMoles m^{-2} of H^+ within the whole year. The rate of pollutant deposition released from snowpack is closely related to the number and depth of thaw episodes. It means that the most intense acidification of soil and water ecosystems occurs at areas with deep snowpack during spring thaw events. The growth of snowpack during winter, maximum height and water storage change significantly from one year to another, however the basic mechanisms related to the additional environmental acidification under the influence of snow ablation at the end of each winter season are similar.

Key-Words: - snowpack, pollutant deposition, granite, buffering capacity, Giant Mts., Sudetes, Poland.

1 Introduction

The Giant Mts. constitute the highest massif within the mountain range of the Sudetes, reaching the elevation of 1603 m a.s.l. (Mt. Śnieżka). The main ridge stretch from NW to SE for almost 30 km with mean altitude 1200-1400 m a.s.l. Terrain falls steeply northward on the Polish side and forms a widespread slope (about 1000 m of relative height). The Giant Mts. are represented by a contact zone of a major granitoid pluton and its country rocks that were metamorphosed and deformed by tectonic processes [1].

The Sudetes, as many other middle-size mountain ranges in central Europe, are subjected to air pollution emitted from combustion of sulphur-rich coal in an industrial region on the Polish, German and Czech borderland. During typical westerly wind conditions they are exposed to highly polluted air from heavy industry densely situated at the distance of tens to hundreds kilometers on the windward side of the mountains [2-5].

The average annual load of hydrogen ion (which is an important acidity indice) brought by atmospheric precipitation in the years 1988-95 was estimated at 158,4 mMoles m^{-2} y^{-1} at Szrenica (Giant Mts.). It underwent significant changes resulting from pH variations and the amount of atmospheric precipitation within the year and from one year to another [6]. The maximum load was observed in 1990 (about 242 mMoles m^{-2} y^{-1}). As the result of national scale pollutant abatement policy, since the beginning of the nineties a substantial reduction of gaseous emission has been observed with SO_2 being reduced most [7]. During the last 10-15 years, deposition of hydrogen ion in Sudety Mts. decreased by three times and was estimated at the level of 50-60 mMoles m^{-2} y^{-1} in the years 2004-2006. However one should stress that deposition is still high and remains a serious problem.

The contribution of solid precipitation in the sum of annual atmospheric precipitation is strongly related to altitude and ranges from 27% at the forefield of Giant Mts. to 74% in the upper parts [8]. Thus the role of snowpack in water flux structure increases with

increasing height. Because of wind action the redistribution of snow mass via snow-drift is observed within the earlier deposited snowpack, this process is also accompanied by transfer of pollutants contained by snow from deflation to accumulation areas.Due to the high sum of atmospheric precipitation during winter months, when air temperature is negative, snowpack remains relatively long, has a considerable thickness and density. According to [8,9], the number of days with snowpack annually ranges from 94 (at the height of 600 m a. s. l.) and 170 (1100 m a. s. l.) to 176 (1500 m a. s. l.). Research made by [10] indicated that snow remains in the higher parts along upper tree line at the height of about 1200-1300 m a.s.l., disappearing in June and locally in concave landforms like snow nische and glacial cirques even later.

The greatest water storage in snow occurs a few days after the maximum snowpack depth and ranges from 80 mm at the height of 600 m a.s.l. to over 800 mm at the height of 1200 m a.s.l. In the local concave forms of the upper mountain parts (snow nisches, and glacial cirques), the snowpack water storage might be significantly higher, for example in Szrenica snow nische at the end of winter season 1976, it was 1574 mm [10].

In the Sudetes high chemical concentrations of cloud water is accompanied by very efficient horizontal precipitation through fog and clouds. These are areas situated at wind-exposed mountain summits or ridges covered by forest or at least groups of trees or bushes which are efficient receptors of wind-driven fog/cloud droplets. In such places, high enough to be frequently immersed in orographic clouds, the amount of horizontal precipitation can be comparable with bulk precipitation. It should be taken into consideration that fog water is characterized by lower pH value in relation to atmospheric precipitation, on the average of 0,3-0,4 units. It indicates 3-4 times greater deposited flux of acidic substances, when compared with atmospheric precipitation. The current nitrogen deposition at such hot spots situated in an igneous bedrock environment is around 15 times larger than the relevant critical load of nitrogen deposition. Therefore besides precipitation, also cloud water deposition was the main cause of acidification of natural environment in the Sudetes. These processes led to extensive negative results e.g. edaphic changes and forest decline [2,11,12].

In the regions built of carbonate rocks, which are rich in calcium, potassium and magnesium, buffering of acidic atmospheric deposition is relatively efficient. Significantly lower buffering capacities have igneous rocks, including granite, from which Giant Mts. are built. Carbonate rocks can buffer over 200 mMoles H^+ on the area of 1 m^2 annually. In the case of igneous rocks (granite and gneiss), this capacity is estimated at about 20-30 mMoles $H^+ m^{-2}y^{-1}$ [13]. From that reason, in the Giant Mts., influenced by increased acidic atmospheric deposition, a strong soil acidification covering the whole surface layers up to matrix is observed. As the result pH value decreased by 0,5-1 units and in individual cases even by 1,5 units. Because of acidification, the total number of earthworms and soil bacteria is reduced and that's why decomposition of decaying organic matter is proceeded mainly by fungi [14]. It causes the slowdown of the decomposition rate and the decreasing trend of nutrient substances release.

2 Problem Formulation

The analysis of chemical composition of daily atmospheric precipitation does not reflect the real rate of pollutant deposition. It is particularly related to the colder part of the year, when snow does not melt and the whole pollutant load contained in atmospheric precipitation is accumulated. As the result, both snowpack water storage and pollutant loadincrease. It is particularly significant in the mountains, where snowpack retention can last even a few months [15-17].

The chemical composition of water originated from the melting snow is not only a sum of chemical constituents brought by the following portions of atmospheric precipitation. During a longer period of time, dry deposition and rime formation take place onto the snowpack, snow can be blown from one place to another, partial melting followed by water migration to the ground can also occur. These phenomena lead to permanent changes in the chemistry of snowpack.

The release of pollutants from snow and their real penetration into soil, ground and surface waters take place during snow ablation. Generally, pollutants accumulated in snow do not penetrate into the crystal structure of ice, but they have the tendency to appear in the spaces between crystals in the water solution of increased concentration [15,18]. Thus the portions of water released into the ground during the beginning of snow ablation, are characterized by significantly larger concentration of pollutants, when compared with the average concentration in the whole snow profile. It means that the most efficient release of pollutants and significant acidification of soil and water ecosystems occur in the initial phase of snow ablation. It depends on the amount of snowpack water storage and TIC value (Total Inorganic Ionic Content). The basic goal is to:

- evidence the influence of snowpack on the process of atmospheric deposition of pollutants (taking the Giant Mts. as an example);
- identify the main factors responsible for the diverse release rate of pollutants accumulated in the snowpack to the ground, particularly in the preliminary phase of snow ablation.

3 Experimental

The analysis of the pollutant deposition via snowpack was based on a dataset from Field Meteorological Station of the University of Wrocław at Mt. Szrenica situated in the Giant Mts. (φ=50˚48′, λ=15˚31′, H=1331 m a.s.l.; Fig. 1).

Fig. 1. Location of the Terrain Meteorological Station at the Szrenica Mt.

Among others the dataset incorporates information about HS and daily precipitation totals. Fresh snow samples were collected in the morning after each precipitation event and were analyzed on-site for electrolytic conductivity and pH. The identical measurements in the core of the whole snowpack profile were repeated at a few-days interval. It mainly depended on the significant changes in water reserves in the snow cover (fresh precipitation or ablation) and atmospheric conditions providing measurements. In this research study, the obtained results including measurements of thickness (HS) and water storage (SWE) in the snowpack for two selected winter seasons were presented. Comparison between pH and SWE allowed to calculate the load of hydrogen ion in the whole snowpack profile, which was expressed as mMoles m^{-2}. Winter season 1996/1997 was exceptionally warm and not typical, because snowpack reached inconsiderable thickness and repeatedly disappeared. In contrast, during winter season 1999/2000, there was no deep thawing episode before the final spring ablation. Owing to this fact, thickness and water storage in the snowpack reached then characteristic values for long-term measurements (1961-2008).

In order to obtain detailed recognition of the structure of released load of pollutants, the results of determination of chemical composition of snowpack at Szrenica for winter season 2005/2006 were also included. At the end of winter season, the cores of the snowpack profile were collected in the phase of maximum SWE and a few days later during long spring thaw. Selected anions and cations were determined using ion suppressed chromatography (Dionex Corporation, USA) and quantified against synthetic rain standards: Reference Material No. 409 (BCR-409, Institute for Reference Materials and Measurements, Belgium) and Analytical Reference Material Rain-97 (National Water Research Institute, Environment Canada; [19]).

4 Results and discussion

Formation of the permanent snowpack in the season 1999/2000 began quite commonly as for the conditions prevailing in the Giant Mts. in the first decade of November (Fig. 2A). However, the following portions of atmospheric precipitation were not so big, because the snowpack did not exceed the thickness of 50 cm and the water reserve reached only 150 mm till the half of January. The intensive snow precipitation and the rapid increase of HS and SWE values occurred in the third decade of January and February. The greatest increase of HS was noticed during 17-23 January (39 cm) and during 14-18 March (31 cm), whereas the highest SWE amounted to 690 mm of water layer was observed on the 20th March (Fig. 2A). From that moment, intensive snowpack melting began until snow disappearance on the 24th April. It should be openly stated that significant ablation episodes, which could lead to penetration of water from snowpack into the ground, were not observed during the whole analyzed winter season. It indicates that the whole load of pollutants (including H^+) accumulated in snow since the winter beginning was still present in snowpackon the 20th March and was brought by atmospheric precipitation and in a smaller measure by atmospheric deposits (fog deposition, hoarfrost, dew) and dry deposition. A rapid decrease of H^+ related with penetration of ablation water from the snowpack into the ground took place after a few days of continuous ablation. During one week (18-24 March), the content of hydrogen ion decreased from 30 to 19 mMoles m^{-2}, whereas HS value lowered only from 139 to 119 cm (Fig. 2A). It indicates that the 15% decrease in the HS corresponded to 40% decrease in the load of H^+; this phenomenon is a typical example of the "frontal wave" environmental acidification during spring ablation. During the consecutive days, till the disappearance of snowpack at Szrenica (24th April), a progressive increase of pH value and significantly milder, when compared with the previous period, decrease of H^+ occurred.

Similar variations were also reported during the second half of 2005/2006 winter season (Fig. 3). The stable snowpack was formed in mid November 2005 and then consequently increased in 3 distinct stages until the second half of March 2006. During those 4 months no significant thawing was reported, which could potentially lower the SWE. On two dates the snow cores were sampled to determine snow chemistry.

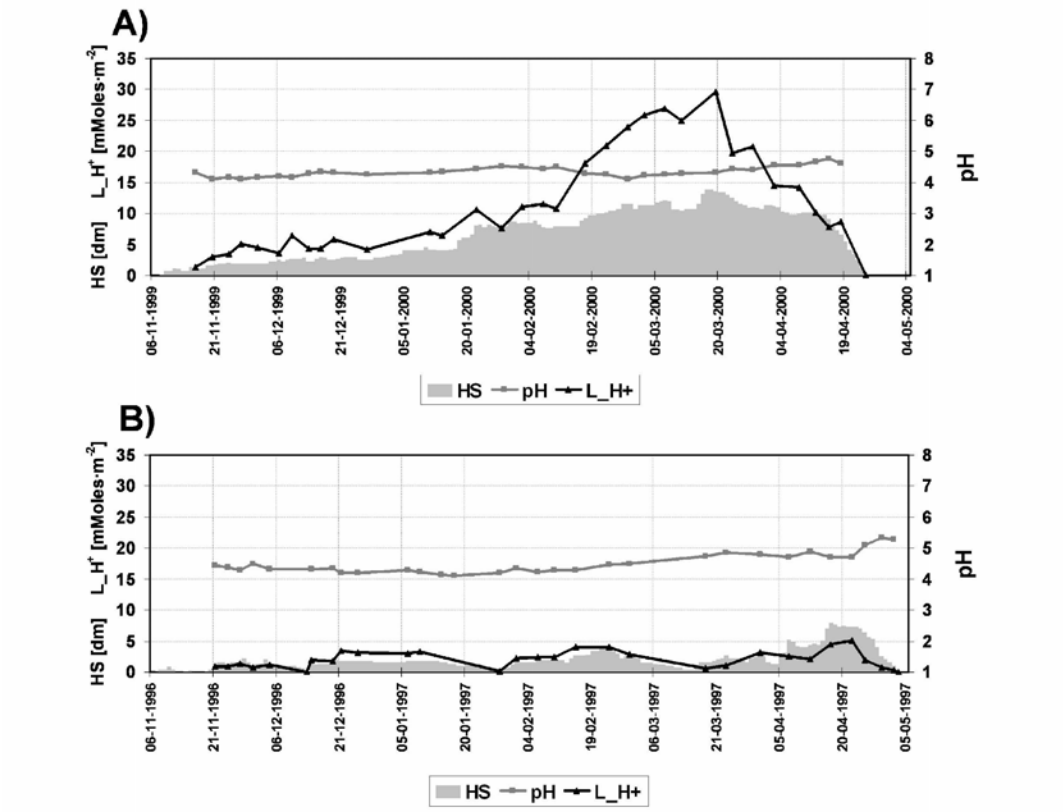

Fig. 2. Course of depth (HS), pH and load of H^+ ion (L_H^+) in snow cover during winter seasons (A) 1999/2000 and (B) 1996/1997 at the Szrenica Mt.

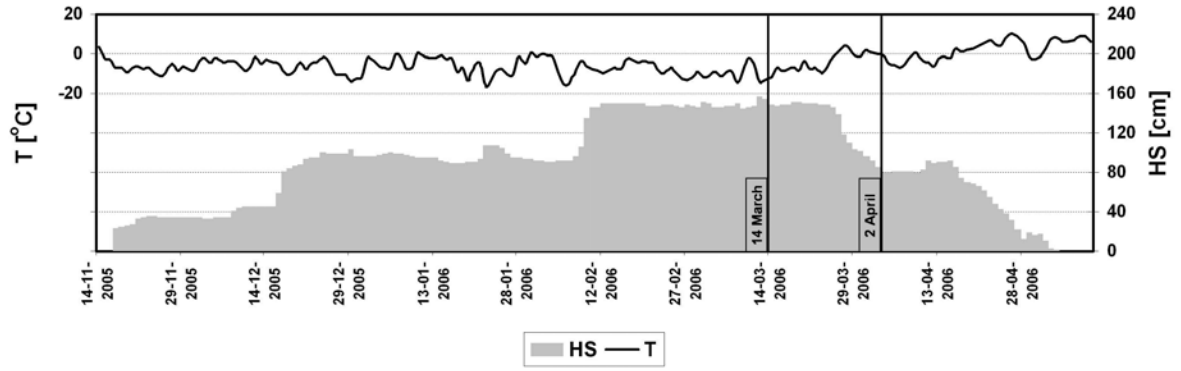

Fig. 3. Course of depth (HS) and average daily temperature (T) during winter season 2005/2006 at the Szrenica Mt.

The first one of 14 III represents the seasonal maximum of HS and SWE (152 cm i 570 mm respectively) accompanied by 23,8 mMoles m^{-2} of hydrogen cation content. The following snow core was taken 26nd April, one week after the beginning of intense spring melting. During that week the snow depth was reduced by 46% from 152 to 82 cm, which caused the release to the ground of 177 mm of liquid water i.e. 31% of the earlier maximum storage. Simultanously TIC was reduced by 52,7 mMoles m^{-2} (45%) and H^+ load by 16,4 mMoles m^{-2} (almost 70%), pH value increased from 4,21 to 4,74, while conductivity was reduced by a half.

Quite distinct differences in particular ions release from snowpack were observed (Table 1). The fastest removal via the first portions of melting water occurred in case of H^+, NO_3^-, SO_4^{2-} and Mg^{2+} (>50%), which was in contrast with much smaller removal rate of Na^+, Cl^- and NH_4^+.

The released, in the first phase of ablation, amount of H^+ had to cause severe decrease of pH value in soil and surface waters, because granite bedrock is able to buffer only 20-30 mMoles m^{-2} of H^+ within the whole year [13]. Such episodes cause the whole chain of negative effects described in the second chapter, from which the

Table. 1. Load of pollutants and some basic quantitative characteristics of snowpack samples collected at the Szrenica Mt. (14 III – maximum of snow water equivalent; 2 IV – middle part of ablation episode and percentage differencec between dates).

PARAMETERS / IONS	14 III 2006	2 IV 2006	Changes [%]
HS [cm]	152	82	46%
SWE [mm]	570	393	31%
pH	4,21	4,74	0,53 unit
L_H+ [mMoles•m^{-2}]	23,8	7,4	69%
Conductivity [µS•cm^{-1}]	19,2	10,1	47%
Cl^-	13,0	10,2	21%
NO_3^-	19,9	7,5	62%
SO_4^{2-}	19,0	9,3	51%
Na^+	6,6	6,0	9%
NH_4^+	11,8	10,1	14%
Mg^{2+} [mMoles•m^{-2}]	11,2	5,4	52%
Ca^{2+}	8,6	4,9	44%
TIC	118,4	65,7	45%

Notes: HS – snow cover depth; SWE – snow water equivalent; L_H+ - load of H+ ion in snow cover; TIC – Total Inorganic Ionic Content.

most important are: leaching the nutrient substances from soil, release of aluminum from the ground and elimination of many plant and animal species from aqueous ecosystems.

The growth of snowpack during winter, its maximum depth and water storage change significantly from one year to another [20,21]. However the basic mechanisms related to the additional environmental acidification under the influence of snow ablation at the end of each winter season are similar to the presented example. The greatest importance of the "frontal wave" phenomenon occurs in the places characterized by the highest and the longest remaining snowpack, thus at the height of 1200-1300 m, near the upper tree line, with the indication to local concave forms of terrain in the upper parts of mountain slope with northern exposition. The most prominent effects of the "frontal wave" phenomenon occur at areas characterized by the deepest and the longest remaining snowpack, thus at the height of 1100-1300 m a.s.l., particularly close to the tree line in local concave landforms with northern aspect. In such sites, the accumulation of wind-blown snow (snowpack reaches a thickness of a few meters) and the increased pollutant deposition during thaw events take place [11].

Winter season 1996/1997, which was exceptionally warm and not typical in terms of snow conditions, is a completely different example (Fig. 2B; [8]). HS exceeded 50 cm at the end of winter season (in the second half of April 1997). Maximum values of HS and SWE were observed on the 18th April 1997 (74 cm and 120 mm) and were much lower than average ones estimated for long-term measurements 1961-2008 (138 cm and 500-700 mm, respectively; Fig. 2B). In the case of such winters, when snowpack is scarse and occurs in a few separated episodes divided by deep thaw events , the above described phenomena proceed several times and with much smaller intensity. Owing to this fact, environmental stress is significantly smaller, because pollutant deposition is distributed over time.

5 Conclusion

The rate of pollutant deposition released from snowpack is closely related to the number and depth of thaw episodes. The initial results indicate that the first portions of water penetrating from snow into ground may bring a huge pollutant load. It means that the most intense acidification of soil and water ecosystems occurs at areas with deep snowpack during spring thaw events. The growth of snowpack during winter, maximum height and water storage change significantly from one year to another, however the basic mechanisms related to the additional environmental acidification under the influence of snow ablation at the end of each winter season are similar. The greatest importance of the "frontal wave" phenomenon occurs in the places characterized by the highest and the longest remaining snowpack, thus near the upper tree line, with the indication to local concave landforms.

References:

[1] Migoń P., Karkonosze – rozwój rzeźby, [in:]Karkonosze, Przyroda nieożywiona i człowiek, edited by M.P. Mierzejewski, *Acta Universitatis Wratislaviensis,* No. 2823, Wrocław 2005, pp. 323-349.

[2] Błaś M., Sobik M., Natural and Human Impact on Pollutant Deposition in Mountain Ecosystems with the Sudetes as an Example, [in:] Man and Climate in the 20th Century, edited by J.L. Pyka, M. Dubicka, A. Szczepankiewicz-Szmyrka, M.Sobik, M.Błaś, *Acta Universitatis Wratislaviensis,* No. 2542, Wrocław 2003, pp. 411-420.

[3] Błaś M., Sobik M., Twarowski R., Changes of cloud water chemical composition in the Western Sudety Mountains, Poland, *Atmopheric Research*, Vol. 87, 2008, pp. 224-231.

[4] Dore A.J., Sobik M., Migała K., Patterns of precipitation and pollutant deposition by rain and snow in the Western Sudete Mountains, Poland, *Atmospheric Environment*, Vol. 33, pp. 3301-3312.

[5] Mill W.A., Schlama A., Twarowski R., Błachuta J., Stasyewski T., Modelling and Mapping of Critical Thresholds in Europe, CCE Status Report 2003, *National Focal Centre Report – Poland*, Bilthoven, Netherlands, 2003.

[6] Sobik M., Meteorologiczne uwarunkowania zakwaszenia hydrometeorów w Karkonoszach, *PhD work*, Departament of Meteorology and Climatology, Wrocław, 1999.

[7] Mańczyk H., The Black Triangle [in:] Reducing air pollution in Central Europe. *International District Energy Association 90th Annual Conference and Trade Show in Boston*, Massachusetts, USA, 1999.

[8] Peryma J., Sobik M., Szczepankiewicz-Szmyrka A., Migała K., Contemporary climatic conditions and topoclimatic differentiation of the Karkonosze Mts., *Acta Universitatis Wratislaviensis,* No. 1950, Wrocław 1997, pp. 75-94.

[9] Kosiba A., Częstotliwość szaty śnieżnej na ziemiach śląskich, *Prace Wrocławskiego Towarzystwa Naukowego*, Vol. 21, 1949.

[10] Głowicki B., Struktura przestrzenna pokrywy śnieżnej w górnej części Potoku Szrenickiego. *Materiały Badawcze IMGW*, 1977, pp. 77-95.

[11] Sobik M., Migała K., The role of cloudwater and fog deposits on the water budget in the Karkonosze (Giant) Mountains, *Alpex Reg. Bull. Swiss Met. Inst.*, Vol. 21, pp. 13-15.

[12] Błaś M., Sobik M., Quiel F., Netzel P., Temporal and spatial variations of fog in the Western Sudety Mts., Poland. *Atmospheric Research*, 64, 2002, 19-28.

[13] Nilsson J., Grennfelt P., Critical loads of Sulphur and Nitrogen, *Nordic council of Ministers*, Report 1988, Denmark, 1988, 8-57.

[14] Bingman I., Thunberg B., Berlekom M., Pleijel H., Agren Ch., Ponadgraniczne Zagrożenie Środowiska. Fakty o zanieczyszczeniu powietrza oraz o zakwaszeniu*, Szwedzko-Polskie Towarzystwo Ochrony Środowiska i Urząd Ochrony Przyrody*, Sweden, Sztokholm, 1989.

[15] Colin J.L., Lim B., Herms E., Genet F., Drab E., Jaffrezo J.L., Davidson C.I., Air-to-snow mineral transfer-crustal elements in aerosols, fresh snow and snowpits on the Greenland ice sheet, *Atmospheric Environment*, Vol. 31, No. 20, 1997, pp. 3395-3406.

[16] Coughlan J.C., Running S.W., Regional ecosystem simulation: A general model for simulating snow accumulation and melt in mountainous terrain, *Landscape Ecology*, Vol. 12, 1997, pp. 119-136.

[17] Mote P.W., Hamlet A.F., Clark M.P., Lettenmier D.P., Declining mountain snowpack in Western North America, American Meteorological Society, 2004, pp. 39-45.

[18] Obled C., Rosse B., Mathematical models of a melting snowpack at an inex plot, *Journal of Hydrology*, Vol. 32. 1977.

[19] Polkowska Ż., Astel A., Walna B., Małek S., Mędrzycka K., Górecki T., Siepak J., Namieśnik J., Chemometric analysis of rainwater and throughfall at several sites in Poland, *Atmospheric Environment.*, 39, 2005, pp. 837-855.

[20] Piasecki J., Pokrywa śnieżna na Szrenicy w latach 1960-1990 i klasyfikacja śnieżności zim, *Acta Universitatis Wratislaviensis,* No. 1705, 1995, pp. 23-57.

[21] Kwiatkowski J., Szata śnieżna, szadź i lawiny, [in:] *Karkonosze Polskie*, edited by Jahn A., Ossolineum, 1985, pp. 117-144.

Guidance for an Effective Biodiesel Environmental Impact Assessment

A.A. Refaat*; S.T. El Sheltawy; H.A. Sibak
Department of Chemical Engineering
Faculty of Engineering
Cairo University
Egypt
aarefaat@hotmail.com

Abstract: - Cooperative global efforts are held to confront climate change threats by measures aiming at the stabilization of greenhouse gas concentrations in the atmosphere at a level that would prevent dangerous anthropogenic interference with the climate system. Biodiesel is a renewable, energy efficient, substitution fuel which reduces net carbon dioxide emissions. By running on biodiesel, vehicles can help reduce GHGs and polluting emissions even more, without impairing their performance or reducing their energy efficiency. This paper presents the main features of the guidelines and the requirements for preparing an Environmental Impact Assessment (EIA) for a biodiesel project together with some guidance comments. The purpose is to provide a clear and detailed advice on carrying out effective EIA for a biodiesel project.

Keywords: - Biodiesel, Environment, Assessment, Guidelines, EIA

1. Introduction

1.1. Background

Since 1751 roughly 315 billion tons of carbon have been released to the atmosphere from the consumption of fossil fuels and cement production. Half of these emissions have occurred since the mid 1970s. The 2004 global fossil-fuel CO_2 emission estimate, 7910 million metric tons of carbon, represents an all-time high and a 5.4% increase from 2003. Globally, liquid and solid fuels accounted for 77.5% of the emissions from fossil-fuel burning in 2004 [1]. The present atmospheric concentration of CO_2 is about 383 parts per million by volume. Future CO_2 levels are expected to rise due to ongoing burning of fossil fuels and land-use change [2].

Biodiesel is a renewable, energy efficient, substitution fuel which reduces net carbon dioxide emissions. By running on biodiesel, vehicles can help reduce GHGs and polluting emissions even more, without impairing their performance or reducing their energy efficiency. Displacing petroleum diesel with biodiesel in urban buses is an extremely effective strategy for reducing carbon dioxide emissions. It has been shown that burning 1 ton of petroleum diesel releases 3.11 tons of CO_2 and burning 1 ton of biodiesel releases almost the same amount. But, because the bio-diesel process recycles CO_2, the replacement of standard diesel by bio-diesel would reduce net CO_2 emissions by approximately a factor of three. A bio-diesel plant producing 1500 tons of fuel each year would therefore help to prevent around 4500 tons of CO_2 emissions [3].

Proposed newly established projects are required to carry out an Environmental Impact Assessment (EIA) as a preliminary step before construction work. Developers should be fully aware of their obligations under all laws and guidelines applicable to their situation. Environmental impact assessment (EIA) is the systematic examination of unintended consequences of a development project or program, with the view to reduce or mitigate negative consequences and capitalize on positive ones. It is a planning and management tool for sustainable development that seeks to identify the type, magnitude and probability of environmental and social changes likely to occur as direct or indirect result of a project or policy and to design the possible mitigation procedure [4].

1.2. Purpose

The purpose of these guidelines is to provide clear and detailed advice on carrying out effective EIA for a biodiesel project. This paper presents the main features of these guidelines and the requirements for preparing an EIA for a biodiesel project. The overarching goal is achievement of ecologically sustainable development which is the object of much of the current legislation that contains EIA processes.

1.3. Scope
EIA guidelines are intended to apply to all proposals that undergo EI for a biodiesel project. They can be used by EIA consultants undertaking studies and reporting, project proponents, stakeholders affected by proposals, and community representatives or interested persons.

2. Requirements for Biodiesel EIA
The specific requirements for an EIA for a biodiesel project are provided below. It should be pointed out, however, that all issues identified will not have the same degree of relevance for all proposals and, depending on the characteristics of the proposal, some of the requirements may be more relevant than others. Each individual EIA should be tailored to the specific proposal and should focus on the key issues.

2.1. Executive Summary
An executive summary should be provided in the EIA and be available separately. The summary should give a short overview of the proposal, the potential environmental impacts and proposed mitigation measures. The summary should incorporate a clear map or aerial photograph showing the location of the project.

Commentary

- The summary should be written in non-technical language and clear manner to facilitate understanding by all readers including non-specialist readers.
- It should be presented on a separate page at the beginning of the EIA report

2.2. Introduction
The introduction should give general information about the project such as the title of the project that will be used in issuing the permit/license, the type of project and the name of the owner (s) of the project.

Commentary

It is recommended to give the name of the consultant or consulting firm that co-operated with the owner in preparing the EIA document.

2.3. Legislative framework
During the preparation of the EIA, the relevant national and international legislation should be considered.

Commentary

All approvals and licenses required for the project must be identified as soon as possible. This will allow the relevant authorities to be contacted and briefed on their involvement and will help ensure an integrated approach to the granting of approvals. Having this list will also avoid delays resulting from missing or incomplete approvals. It will also allow the community to identify authorities responsible for assessment and regulation of the proposal.

2.4. Project Description
The following information should be provided:

2.4.1. Objectives
There should be a clear statement of the objectives of the proposal including a work-plan, timing and lifecycle of the project, in addition to decommissioning methods, if any.

2.4.2. Location and Site description
Describe the exact location of the project and the area to be occupied.
The following information should be provided:

- Existing land uses on the site and the surrounding environment
- The site description documented with maps: plant layout, maps for the projects' components, photographs clearly identifying the location of the proposed project.

2.4.3. Process and associated facilities description
A brief description of the project with the main components, specifications, layout…etc. should be provided with the following information:

- Maximum land area affected by the project
- Identification of the source(s) of water to be used, the quantity and quality of water to be used for different purposes
- Identification of the energy supply required for the project its source and the rate of consumption.
- Number and size of fuel storage tanks, and way of storage and handling

- Type and quantity of chemicals or other hazardous materials, and method of handling, storage…etc
- On-site surface water management systems; identification of drainage lines, pollution control and abatement systems, waste storage and disposal systems.
- Specifications of the municipal or industrial wastewater treatment plants
- Access roads used by trailers, cranes…etc
- Methods for disposing solid and liquid waste, proposed methods and locations for recycling or disposal.

Commentary

The following criteria are to be stressed when preparing an EIA for a biodiesel project:

1. The proposed biodiesel project can be designed to:
   - demonstrate the feasibility of operating urban bus fleet with biodiesel to reduce the amount of conventional diesel used.
   - assess the technical, economic and environmental impacts of this option on urban transportation.

2. Information provided for the location should involve zoning, permissibility and land use constraints. A project based on small-scale batch biodiesel production can be conducted on urban bus main garages.
3. The most commonly used method for biodiesel production is the base-catalyzed transesterification technique as it is the most economical process [5]. The steps performed are the same whether in a small, home-based biodiesel processor, or in large industrial facilities. The chemistry is similar in either case [6]. The criteria for a process to be considered "green-compatible" are the following:
   - Use of renewable or recycled feedstock
   - Use of safer solvents and reaction conditions
   - Increased energy efficiency, or using less energy for the same or greater output
   - Avoidance of persistent, bioaccumulative and toxic substances.

   The economic and environmental relevance of these aspects is self-evident, and this is typically manifested in substituting biodiesel for petrodiesel.
4. The following criteria of the transesterification process are to be stressed from the environmental standpoint:
   - Biodiesel is produced from a renewable feedstock (vegetable oil). Using renewable or recycled feedstock is tantamount to rational management of resources, by maximizing what can be obtained from a given amount of starting raw materials [7]. Biodiesel from the proposed project can be produced by transesterification of recycled waste cooking vegetable oil (WVO), possibly donated by a fast-food chain. Production of biodiesel from used cooking oil is environmentally beneficial inasmuch as it provides a cleaner way of disposing of these products. Substituting biodiesel for other fuels has a positive effect on air pollutants, on greenhouse gas emissions, and on waste streams. Using waste cooking oil as stock material converts an industrial waste into a usable commodity.
   - Since the prices of edible vegetable oils, as sunflower oil, are higher than that of diesel fuel, waste vegetable oils are preferred as potential low-priced biodiesel sources. This product is comparable in composition, similar in calorific value to biodiesel produced from refined sunflower oil [8].
   - The temperature used in transesterification process does not exceed 70°C, and no pressure is applied.
   - Feedstock, chemicals, product and by-product (glycerol) are all environmentally benign
   - WVO biodiesel has a positive fossil energy balance of 7.8:1 compared to 3.2:1 for biodiesel produced from neat vegetable oil [9].
   - Biodiesel is biodegradable, non toxic and safe to handle and transport [10].
5. Applying modern innovative techniques for biodiesel production can make the process more environmentally benign
   - Using heterogeneous catalyst [11].
   - Using Novel solid acid catalysts for esterification made by incomplete carbonization of D-glucose followed by sulfonation [12].
   - An improved process was investigated for methanolysis of vegetable oil. The process comprises solubilizing oil in

methanol by addition of a cosolvent in order to form a one-phase reaction mixture [13].

- Using ultrasonic mixing produced high biodiesel yields at significantly shorter times in comparison to those reported previously using batch systems with external heating and mechanical stirring [14].

2.5. Baseline data

The purpose of this section is to give an overview of the existing environmental conditions in the area of the project, against which the anticipated environmental impacts of the project can be evaluated. With each issue mentioned later, the level of detail should match the level of importance of the issue in decision making. The following information should be provided:

2.5.1. Physical characteristics of the project area:

The topography of the area including landforms, elevations, and other relevant characteristics should be described. It is recommended to include a topographical map of the area.

2.5.2. Climate

A brief description of seasonal weather conditions in the area of the project (temperature, humidity, wind speed and direction, rain) and any seasonal storm data that might affect the area should be given. The information should be based on the most recent meteorological data obtained from the nearest meteorological station. The location of the meteorological station should be identified in relation to the site.

2.5.3. Air quality

- If ambient air quality is likely to change as a result of the project, the existing sources of pollution, either fixed (e.g. machines) or mobile (e.g. cars, etc) should be studied.
- Ambient air analysis is needed.

2.5.4. Noise

If noise is likely to be produced from the project, issues to consider include noise levels from fixed and mobile noise sources.

2.5.5. Land use

Describe the pattern of land use in the area of the project and its surroundings, focusing on:

- The type and size of human settlements in the area (town, village, etc)
- Socioeconomic activity in the area (industry, recreation, agricultural, etc)
- Sites that are valued for their historic, scenic, cultural or archeological significance
- Nearby protected areas
- Other characteristics that might be affected by the project.

2.5.6. Socio-economic issues

Should address the demography, gender issues, and culture. In addition to social issues identified already, issues to consider include:

- Health and safety issues
- Employment issues
- Land displacement

Commentary

The amount of emission reduction, obviously, depends on the emissions that would have occurred without the project. The construction of such a hypothetical scenario is known as the baseline of the project. The baseline may be estimated through reference to emissions from similar activities and technologies in the same country or other countries, or to actual emissions prior to project implementation.

2.6. Environmental Impact Analysis

The following specific issues are nominated as potentially important in the assessment of impacts and for decision-making in relation to the project. The outline of the issues is not exhaustive and the degree of relevance of each will vary. The EIA should only deal with relevant issues as applicable to the particular project. The following should be included for any potential impact that is relevant for the assessment of a specific proposal:

2.6.1. Wastewater

Identify the sources of wastewater to be discharged from the project site municipal and/or industrial wastewater.

The following information should be included:

- Estimate the quantity of wastewater to be discharged per day
- Describe the characteristics of each wastewater stream to be discharged
- Describe any prior treatment to be carried out
- Assess the impact of this discharge on land, surface water body, and ground water aquifers in the receiving area.

- Assess the impact of this discharge on terrestrial and aquatic biota in the receiving area
- Assess the possible biological accumulation of toxic constituents and resulting impacts on human health.

2.6.2. Solid Waste

Identify the sources of solid waste (municipal and industrial wastes) which will be generated from the proposed project. The following information should be considered:

- Describe the composition of each of the solid waste and classify the solid wastes into hazardous versus non-hazardous
- Describe the solid waste handling system which will be utilized from the source to the final disposal
- Estimate the expected quantity of solid wastes that will be generated from the proposed project.
- Describe the final disposal method
- Assess the impact of solid waste on human health, underground water and surface water near the final disposal area.

2.6.3. Gaseous Emissions

Identify the sources of gaseous emissions (sulfur oxides, nitrogen oxides, carbon oxides, total suspended particulate, hydrocarbons, hydrogen sulphide, etc.). The following information should be included:

- Estimates of the expected levels of emissions from each source.
- Estimates of the expected short and long term effects of these pollutants on human health, and ecosystems in the project site and the surrounding area
- Methods of control of such pollutants
- Assess the impact of gaseous emissions on human health and surrounding air environment

2.6.4. Noise

Identify the sources of noise and the exposure time. The following information should be included:

- Baseline data on the existing acoustic environment
- Estimate the expected level of noise from each significant source.
- Estimate the possible impact of noise on human health in the working environment, and on the nearest residential area (if applicable).

2.6.5. Hazardous materials

Issues to consider include:

- Identify all hazardous materials, quantities and proposals for safe storage and handling
- Identify potential hazards from such materials during storage and handling

Commentary

The most important adverse environmental impact of a biodiesel project is wastewater. Water washing of biodiesel results in wastewater containing chemical contaminants including soaps, free glycerin, unreacted oil, residual methanol, residual catalyst and FFA.

Biodiesel is biodegradable, non-toxic and safer in handling and transportation. The avoidance of substances that remain in the environment for a long time (persistent), or accumulate in living organisms (bioaccumulative) or are toxic to living organisms prevents the undesirable effects resulting from the introduction of such substances into the environment. Avoiding their production is the only effective option to prevent their presence in the environment. Biodiesel, the final product, is as biodegradable as dextrose [10].

2.7. Mitigation Measures

The proposed mitigating measures to control impacts and to ensure compliance with relevant standards, including an estimate of how effective this mitigation is expected to be and consequences of failure, segregation of chemicals, fire fighting systems, use of inflammable materials…etc

2.7.1. Waste Water Management and Water Quality

Proposed mitigation controls to waste water

2.7.2. Solid Waste Management

Proposed mitigating measures to be undertaken to dispose or recycle the hazardous solid waste as well as non-hazardous solid waste generated from the project.

2.7.3. Air quality and Noise

Proposed mitigating measures to be undertaken to control air pollution and noise in the area of the project to enhance air quality and to reduce noise effects.

Commentary

Dry washing is far superior to the traditional water washing purification method followed by drying. Magnesol (a form of magnesium silicate) absorbs the impurities left over in the fuel. This method has the following advantages:

- No water consumed (Saves water and money - water is scarce)
- No wastewater disposal.
- No drying (Saves time and energy)
- No risk of emulsion or wasted biodiesel.
- Increases process yield
- Improves storage stability

2.8. Alternatives

The EIA should include an assessment of adopting alternatives of the project (in design, technology, location, etc.), alternative decommissioning methods, as well as alternative mitigating measures. Consideration of alternatives should also be given to the consequences of not carrying out the proposal, the "DO NOTHING" alternative. The preferred alternative should be clearly stated, along with a justification for its choice.

Commentary

The following points are to be stressed:

- In the absence of the project activity, all the vehicles would continue to use diesel oil. Emission reductions from the project are additional to what would have happened in the absence of the project. Greenhouse gas emissions are lower with the project than they would have been without the project (i.e. the baseline situation).
- In the absence of project activities, the amount of used oil employed - the raw material for producing biodiesel - would become a waste, being disposed of in sanitary landfills or discharged into the sanitary sewage system.

2.9. Monitoring Plan

The proposed monitoring plan should be designed to determine the effectiveness of mitigation and to verify predictions and comply with the Egyptian environmental laws. The monitoring system should be outlined to determine whether mitigation actions have been implemented in accordance with an agreed schedule and are working as expected. The monitoring plan could be used for the periodical assessment of the project, to introduce corrective measures if necessary.

2.10. Environmental Management Plan (EMP)

An environmental management plan (EMP) is a document designed to ensure that the commitments in the EIA, subsequent assessment reports, approval or license conditions are fully implemented. It is a comprehensive technical document that is usually finalized during or after detailed design of the project, including any decommissioning measures, following approval of the development application. Although the level of detail required in an EMP is usually not considered necessary for the EIA, an outline of the structure of the EMP with a summary of the environmental management principles should be presented. Two sections should be included during the development phase: one setting out the program for managing the proposal, and the other outlining the monitoring program.

2.10.1. Environmental management outline

This section includes details of:

- Materials management on site, including chemicals and fuel
- Water and air quality management
- Maintenance and site security plans
- Contingency plans to respond to emergencies, incidents or any breakdown in environmental performance
- Strategies to feed information from the monitoring program back into the management practices and action plans to improve the environmental performance and sustainability of all components of the scheme
- Training programs for operational staff and incentives for environmentally sound performance

2.10.2. Monitoring outline

This Monitoring program should be carefully designed and related to the predictions made in the EIA and the key environmental indicators that would demonstrate the potential ecological sustainability of the project. The EIA should outline the need for and use of any proposed monitoring, monitoring intervals and reporting procedures. Parameters that might be relevant include:

- Quality of water discharged or leaching to groundwater, surface water or soil
- Air quality and Noise
- Quantity and quality of wastes

- Any relevant public health indicators
- List of chemicals and their quantities

2.10.3. Emergency Response Plan
An estimate of the probability of potential accidents (e.g. blowouts, oil leaks) should be given, together with a thorough description of the measures to be adapted to contain such accident if they occur, and to address their impacts on the environment.

3. Conclusions and Recommendations

Biodiesel industry needs to be promoted and enhanced. These guidelines are aimed to provide clear and detailed advice on carrying out effective EIA for a biodiesel project. The overarching goal is achievement of ecologically sustainable development which is the object of much of the current legislation that contains EIA processes.
Improvements in the state of the art depend on a variety of factors that embrace capacity building, promote environmental awareness and allow public participation. **Capacity Building** measures include:

- Developing library of EIA reports
- Maintaining database of information collected during EIA
- Strengthening networks between practitioners with experience in EIA or technical analysis
- Collecting examples of good practice
- Certification of consultants
- Training programs
  Politicians, senior administrators, managers in industry and business
  Project managers, technical experts and review experts
  NGOs (Non-Governmental Organizations)
  Consultancies and academic institutions
  General public

References

[1] Marland, G.; Boden, T.A.; Andres, R.J., (2007). Global, Regional, and National Fossil Fuel CO_2 Emissions. In Trends: A Compendium of Data on Global Change. Carbon Dioxide Information Analysis Center, Oak Ridge National Laboratory, U.S. Dept. of Energy, Oak Ridge, Tenn., U.S.A.

[2] Tans, P., (2007). Trends in Atmospheric Carbon Dioxide. Mauna Loa U.S. Department of Commerce, National Oceanic and Atmospheric Administration Earth System Research Laboratory, Global Monitoring Division NOAA/ESRL.

[3] Van Gerpen, J., Biodiesel processing and production, *Fuel Processing Technology*, Vol.86, No.10, 2005, pp. 1097-1107.

[4] Moussa, M.I.; Mohamed, O.H.S., Environmental Impact Assessment Projects and Consultants Information System, *Journal of Applied Sciences Research*, Vol.3, No.2, 2007, pp.130-134.

[5] Singh, A.B.He; Thompson, J.; Van Gerpen, J., Process Optimization of Biodiesel Production using Different Alkaline Catalysts, *Applied Engineering in Agriculture*, Vol.22, No.4, 2006, pp. 597-600.

[6] Guo, Y.; Leung Y.C., Analysis on the biodiesel production using grease trap oils from restaurants, Macro Review. Japan, Japan Macro-engineers Society, Vol.16, 2003, pp. 421-426.

[7] Pinto, A.C.; Guarieiro, L.N.; Rezende, M.J.; Ribeiro, N.M.; Torres E.A., Biodiesel: An Overview, *Journal of Brazilian Chemical Society*, Vol.16, No.6B, 2005, pp. 1313-1330.

[8] Refaat, A.A.; Attia, N.K.; , Sibak, H.A.; El Sheltawy, S.T.; ElDiwani, G.I., Production Optimization and Quality Assessment of Biodiesel from Waste Vegetable Oil, *International Journal of Environmental Science and Technology*, Vol.5, No. 1, 2008, pp. 75-82.

[9] Hoover, S., (2005). A study of energy balance of biodiesel produced from waste vegetable oil, (http://www.biofuels.coop/education/energy_balance.shtml).

[10] Zhang, X.; Peterson, C.; Reece, D.; Haws, R.; Moller G., Biodegradability of biodiesel in the aquatic environment, *American Society of Agricultural and Biological Engineers*, Vol.41, No. 5, 1998, pp. 1423-1430.

[11] Bournay, L.; Casanave, D.; Delfort, B.; Hillion, G.; Chodorge, J.A., New heterogeneous process for biodiesel production: A way to improve the quality and the value of the crude glycerin produced by biodiesel plants, *Catalysis Today*, Vol.106, No.1-4, 2005, pp. 190-192.

[12] Zong, M.H.; Duan, Z.Q.; Lou, W.Y.; Smith, T.J.; Wu, H., Preparation of a sugar catalyst and its use for highly efficient production of biodiesel, *Green Chemistry*, Vol.9, 2007, pp. 434-437.

[13] Meher, L.C.; Sagar, D.V.; Naik, S.N., Technical aspects of biodiesel production by transesterification - a review, *Renewable & Sustainable Energy Reviews*, Vol.10, 2006, pp. 248-268.

[14] Singh, A.K.; Fernando S., Catalyzed Fast-Transesterification of Soybean Oil Using Ultrasonication, American Society of Agricultural Engineers, ASAE Annual Meeting 2006, Paper number 066220.

Using a decision support software in planning a waste management system in Hungary

ANGELIKA CSERNY, ANETT UTASI, ENDRE DOMOKOS
Institute of Environmental Engineering
University of Pannonia
Veszprém, Egyetem u.10. P.O.B. 158. H-8201
HUNGARY
cserny@almos.uni-pannon.hu, domokose@uni-pannon.hu

Abstract: Modernizing and rearrange the waste management system to the norms of the European Union is one of the most important tasks of the environmental protection in Hungary. Connected to this the Middle-Danube Region Waste Management System is one of the biggest infrastructure investments at present. This investment having an effect on six counties could solve the waste treatment problems of the residents for at least 20 years in the settlements affected.
Systems approach mind is needed to complex waste management systems like this, in which beside landfills, plants for separated collection as sorting devices, compost piles, transfer points, waste yards are included and the recultivation of the inconvenient landfills is needed, too. Meeting the systems approach mind is possible only with computational decision support tools.
Parmenides EIDOS is a module-based decision support software, specially developed for the economy and the corporate management. The goal of the research was to adapt these software toolkits to environmental field and to examine how the software could be used in the course of the planning of the Middle-Danube Region Waste Management System.
According to the authors experience some modules of the software are able to apply well to simplify the complex decision situation and to lay stress on the most important problems. Subjectivity is unavoidable of course, but the subjective elements aid rather than hinder the process due to the group decision-making technique. [1] Further advantage is that the data, results are presented visually by this means the time of understanding decreases and keeping in mind become easier than reading naked data or tables. That is why the figures made with EIDOS could be part of a marketing material prepared for the population to increase their support for the investment.

*Keywords***:** waste management, decision support, computer-aided visualization, environmental impact assessment

1 Introduction

The membership of Hungary in the European Union means obligation and at the same time possibility to join up in the respect of environmental protection, since the Union provides financial sources for environmental improvements. Modernizing and rearrange the waste management to the norms of the European Union is one of the most important tasks of the environmental protection. The aim is to expand a comprehensive, up-to-date waste management structure that is to harmonize and widen the available and planned waste treatment plants and capacities and to establish new, regional waste management systems, which cover the whole country. The Middle-Danube Region Waste Management System set the aim to handle the municipal waste of 680 thousand people of 170 settlements affected which includes the creation of the technological, constitutional and the communication conditions. The system contains the treatment of the waste coming from the households, the economy and from the institutions covering the separated waste collection as well. Though public services are developed in the whole of the planning area, the waste elimination is done solely by deposition at present with negligible treatment. That is why the main aim is to produce secondary raw materials from paper, glass, plastic and metal, to compost and to collect the

hazardous material separately in accordance with the Best Available Technology. By this the needed landfill capacity and territorial demand could be decreased therefore the environmental load caused by the landfills would be mitigated. Further aim is to improve the environmental consciousness of the inhabitants for the success of the project.

2 Materials and methods

Parmenides EIDOS is a decision support software, specially developed for the economy and the corporate management. It comprises ten modules, which make up a whole decision cycle and by the visualization techniques could help the decision making process in different fields. There are five core reasoning tools, three support tools and two data visualization tools. These provide an innovative approach to managing the entire decision making process by visualizing complex situations, by helping to reconcile different positions of different decision makers, and supporting the identification of possible courses of action. It also assist in analyzing proposed solutions against established metrics and developing implementation plans. The software uses the group decision making technique, beside which the scientific literature lines many reasons up.

One of its advantages is the incitement, since working in a group encourages greater achievement. The complete group has more information than either of its members alone. The members of the group can learn from each other, with which could improve the performance, too. In groups the evaluation becomes more objective and the creativity develops since the members possess different background knowledge, so they can put to use the information in other way.

The authors used the toolkits of EIDOS to get experiences about its usefulness in the process of the waste management system planning. The work was built on the method of brainstorming leaning on the earlier studies about the waste management condition of the region and taking into consideration the legal requirements of course.

3 Results

The module "Conceptual Overview" is a tool of the software built on the group-technique, which can be used to map complex, multidimensional relationships between project components in a 3D space. Sixteen factors were collected seen in Table 1, which are important in terms of the examined project.

Table1−The collected factors that are important in the process

10: the strongest relationship, 0: no relationship	Getting the highest level of financial aid from the European Union	Meeting the legal requirements	Public support	Separated waste treatment	Minimising the needed landfill capacity	Minimising the organing waste deposition	Leveling up the standard of the public services	Minimising the operational costs	Energy recovery from waste	Minimising the risk on human health and the environment	Enforcement of the pollutant pays principle	Manpower utilization	Modern technology	Minimising the secondary waste production	Searching for a solution which fits to the actual conditions	Environmental sustainability
Getting the highest level of financial aid from the European Union	x	8	6	6	1	5	3	6	5	3	1	3	7	4	0	7
Meeting the legal requirements		x	0	6	0	5	1	0	0	5	1	0	9	2	0	1
Public support			x	8	6	9	5	0	5	8	4	5	9	1	1	3
Separated waste treatment				x	9	7	0	5	2	4	4	0	3	6	10	9
Minimising the needed landfill capacity					x	9	0	7	9	5	3	3	7	10	5	8
Minimising the organing waste deposition						x	0	5	0	0	2	0	5	1	5	8
Leveling up the standard of the public services							x	3	1	6	8	2	10	5	7	7
Minimising the operational costs								x	5	6	5	0	8	3	0	3
Energy recovery from waste									x	5	0	3	8	8	6	10
Minimising the risk on human health and the environment										x	7	0	9	7	0	9
Enforcement of the pollutant pays principle											x	0	0	0	10	6
Manpower utilization												x	0	0	4	0
Modern technology													x	7	7	8
Minimising the secondary waste production														x	8	8
Searching for a solution which fits to the actual conditions															x	6
Environmental sustainability																x

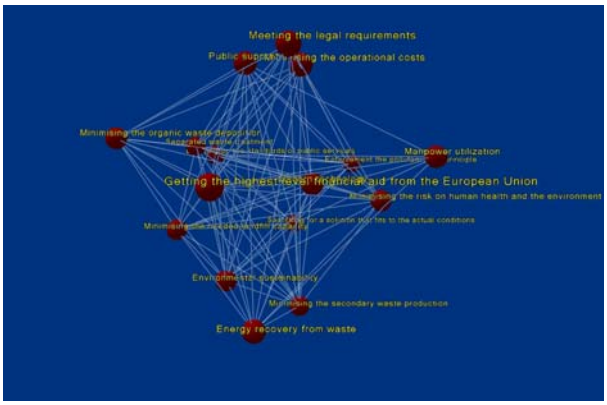

Fig. 1−The tension structuring molecule with the module "Conceptual Overview"

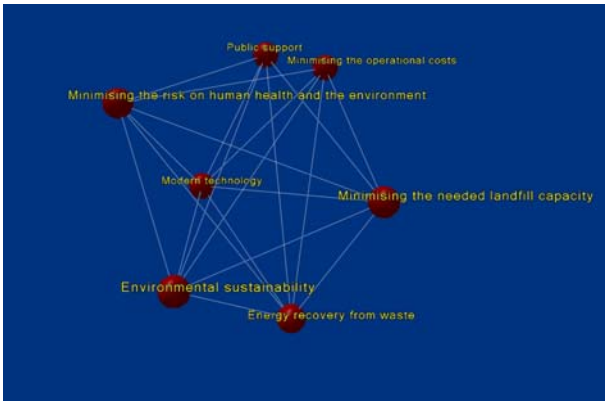

Fig. 2−The simplified decision situation

After defining the factors the relationships were rated between each pair of factors by a value from zero to 10. Negative values were not added, because there were no factors that have a meaning contrary to each other. As a result, the model shows the relationships in a tension-structuring molecule (Fig. 1), with the placement of the elements based on the combined calculation of all relationships, so it evaluates the synergies and tensions among them. Those elements which sticks out from the model were removed thus the decision situation would be simpler (Fig. 2). With the model, the most important fields of the problem brought up can be found easier. In this case, these are the public support, the operational costs, the risk on the human health and the environment, the modern technology, the landfill capacity minimizing, the energy recovery and the sustainability. These are the main goals that have to be fulfilled in the waste management system.

The "Situation Analysis" tool helps to reveal the nature of a problem. In Fig. 3, the situation analysis chart is shown with the barriers and driving forces of the project. These factors are linked with arrows to define the relationships between them. Green arrows show increasing impacts that means relationships that reinforce the target factor. Red arrows indicate decreasing impacts also relationships that counterbalance or mitigate the target factor. Arrow thickness refers to the strength of the impact. Though all factors in the "Situation Analysis" are important to the problem, some of them are likely to be more relevant for further analysis than others. Using the "Active/Passive Map" generated to the chart, key factors are easier to be identified. All of them are represented by a numbered ball in compliance with the chart. These positions are determined by the inputs and outputs of the components. Looking at the figure it becomes unambiguous, which are the key-problems, where effects have to be moderated. In the "Active/Passive Map", factors at the top such marketing are active, they drive other factors. Any actions one take regarding the active factor will have a ripple effect on the other factors. Factors to the right are passive, they are driven by other factors and are therefore likely to be factors that are outcomes or goals, such as public support or the financing in this case. Key factors tend to be both active and passive and are placed especially the upper right section. These have the strongest links to the other factors; changes in those factors will have the most influence on the other barriers and driving forces of the problem. Therefore, concentrating attention on these key factors will have the most significant impact on the project. In this case, the successful competition and the satisfying regional relationship need to be marked as the most important factors since without them the project would not be developed at all. Without successful marketing the regional relationships cannot be improved and the public support would not be reached sufficiently. That is why it is needed to lay more stress on it than earlier. The most important fields of the group decision making are the methods in connected to generating ideas, systematization, analysis for example brainstorming and classification.

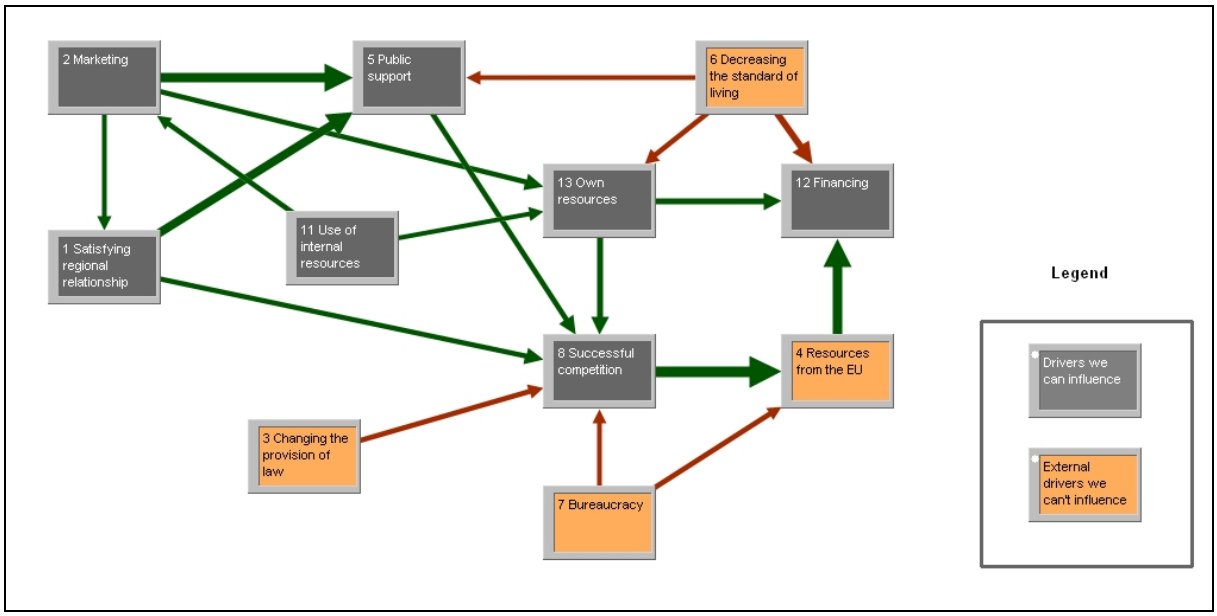

Fig. 3–"Situation Analysis" chart

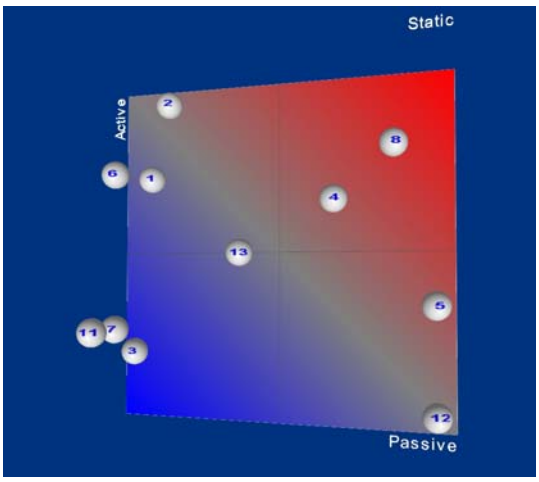

Fig. 4 –"Active/Passive Map"

Those methods are also important, with which the different versions can be evaluated on the strength of several viewpoints simultaneously. The "Option Evaluation" module of the software provides an opportunity to this. Effort to evaluate the alternatives with numbers is a general tendency in the computer-aided decision-making systems. This module evaluates options according to weighted criteria in multiple views and then makes a comparison among the options. By affecting the choice among the options created by generating rankings from the evaluation, it supports an improved decision-making. Three technological alternatives were examined by the developers of the environmental impact study of the Middle-Danube Region Waste Managements System to manage the problems in regional level. The alternatives differ from each other in the treatment technology referring to the municipal waste that constitutes the biggest part of the produced quantity. Mechanical-biological pre-treatment then fractionating are the central elements in version „A". The fine fraction would be used for recultivation; the rough fraction would be deposited in landfills. The municipal waste would be transported directly to incinerator, where waste heat utilization would be possible in case of realizing version „B". While in version „C", fuel material with high heating value would be turned out from the rough fraction received from the fractionating after the mechanical-biological pre-treatment. This fuel material would be used for electric energy production. The technology of treating the smaller waste fractions is the same within the scope of the three alternatives due to their characteristics and the legal requirements. By the reason of these, the green waste would be chipped and classified before recycling and the separate collection of the hazardous waste would be solved, too. [2] In Fig. 5, the evaluation of the alternatives is visible. The criteria are the goals defined with the "Conceptual Overview" and are weighted according to the members' opinion on importance of the goals in 2012, the years by

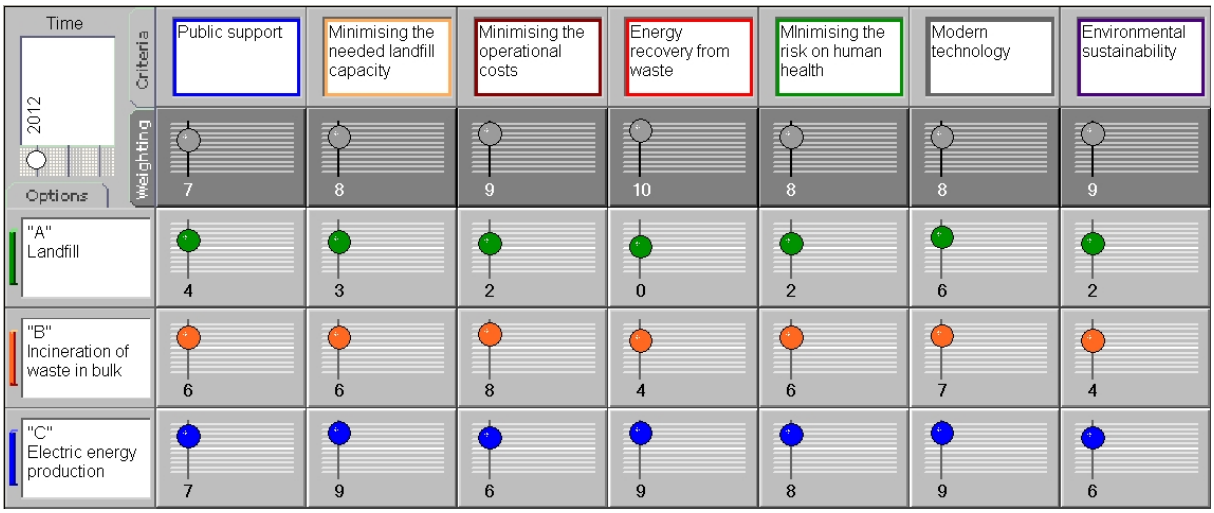

Fig. 5−The evaluation of the alternatives

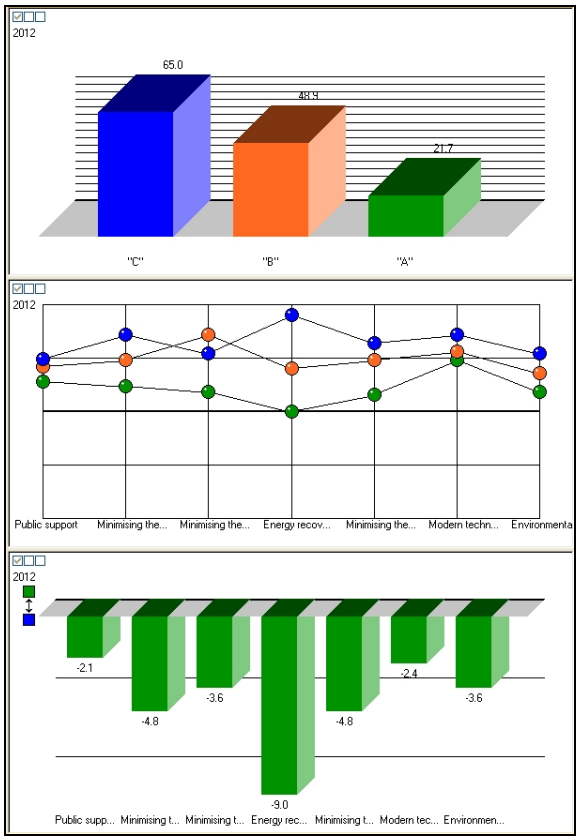

Fig. 6− Ranking among the alternatives

when the investment should have been fully developed. The three alternatives are defined as options in the matrix and rated with a value from -10 to 10 according to each goal. The analysis charts based on the entered data into the matrix present a ranking among the alternatives. These diagrams support the experts' arguments for version "C". The examined software is not able to appoint the gathering headquarters of the zones. It was carried out with cluster-analysis and it does not form the part of this paper.

4 Conclusion

Some of the modules of the software Parmenides EIDOS are presented in this paper which appeared to be useful to support the decision-making connected to Middle-Danube Region Waste Management System procedure. The "Conceptual Overview" tool can be used successfully in the beginning of the process to get a clear overview about the main goals which should lead the decision makers during the implementation planning. The "Situation Analysis" shed light upon the importance of the marketing. It is important particularly in the case of the incinerator that has put up a significant resistance among the population. To convince the population of the necessity of the incinerator and the waste management system in general the "Option Evaluation" tool could be really advantageous due to the expressive visualization.

References

[1] Hugh Wilkins, The need for subjectivity in EIA, Environmental Impact Assessment Review, No. 23, 2003, pp. 401-414

[2] András Diószegi, Middle-Danube Region Waste Management System, Feasibility study, 2008

Role of environmental monitoring, modeling and GIS in the assessment of state of the environment

IMRE MAGYAR, FERENC SPEISER, PÁL BUI, LAURA MAGYAR
Institute of Environmental Engineering
University of Pannonia
8200 Veszprém, Egyetem str. 10
HUNGARY
mim023@almos.vein.hu

Abstract: The goal of the project was to monitoring the complex environmental state of Balatonfüred, a little city near the lake Balaton. In the course of the monitoring the gained data were processed by utilization of a geographical information system. After the data preparation work environment qualifier maps were derived for publishing the measured information. We developed an environment quality maps series and a spatial and time dependent evaluation system for the state of environment. These maps (air quality maps, noise map, water quality map, soil and green-areas affect map) were presented for the inhabitants using Internet.

Key-words: envinmental monitoring, GIS, impact assessment, noise map, environmetal information system

1 Introduction

Nowadays our environment protection getting bigger and bigger role within this topic the protection of the human is even more important. The continuous monitoring of the municipal environment came into foreground in Hungary also through the past years. This control is possible with settle of modern monitoring stations, but the presence of control possibilities by the inhabitants is really limited yet. The best solution for this problem is to publish the environmental data on-line, through the Internet.

Within the Faculty of Engineering of Pannon University a unique economic unit was estabilished called “Ecological Regional Knowledge Base”, "ÖKORET". This centre started an R+D project on the main topic of environmental protection and its technologies. This work is about the environmental informatics sub-program, which targets to work out the measurement methodologies of environmental pollution data, then measuring (monitoring) these. The main goal of the project is to make it possible to build and deploy an information system based on the collected data, that can publish environmental data trough the internet as a web service.

In connection with the information system above, the local government/authority can elaborate an attractive, informative, up-to-date information service that provides data of the state of their environment for the inhabitant's purpose.

2 Monitoring the environmental parameter

2.1 Air

The project monitored and measured the environmental air quality parameters, concentration of air pollutants and meteorological parameters on multiple locations.

The measured values were evaluated considering the correspondent health limits. For the measurements ETL 2000 air-quality monitoring system was used. This technology is based on the change of conductivity of the thick-film semiconductors [1].

The appliance is able to measure CO, NOx, O_3, NO_2 and benzene concentration in the environmental air. We elaborated a so called dynamic measurement procedure that is based on the ETL 2000 device installed into a vehicle. This way the measurement vehicle is able to measure the environmental contamination concentration dynamically even in motion. The measurement device was connected to a data collection unit ensuring the determination of the actual location by a GPS

and the communication by the database of the central computer over a GPRS connection.

The continuous on-line connection provided by the GPRS unit made it possible to visualize the air contamination parameters bounded to a track of movement. Moreover construction of air contamination distribution maps – applied to a given time interval – was permitted based on the spatial-evaluation of the measured information.

We decided to develop a system for measuring environmental parameters that is extremely mobile and capable to measure most of the parameters that a monitoring-container can collect.

The defined requirements of the system are the following:

- it should be significantly better in cost effectiveness,
- it should capable to transmit the collected data to the process server in a reliable way immediately,
- the system should be installable at any site of the country, even if the costs would be serious to establish a monitoring station.

Besides gathering the air quality and meteorological information, we try for applying on-site water-analytical methods that are mostly fast and cost effective and they are suitable to provide reliable information about our surface waters.

It came up by the acquired information that the cheaper absorption measuring procedure is applicable only in the case of two parameters during preparation of the position paper. Moreover its demand of chemicals is high, but it can only provide lack of information about the given parameters. The air-quality monitoring appliances installed into the automatic monitoring containers and the well-equipped monitoring vehicles are precise, providing a lot of data, but they are extremely expensive.

The chemiluminescent measuring of NO and NO_2, the NDIR meter for measuring CO either the gas-chromatograph metering of BTX compounds amounts to serious costs. The definition of PM10 based on discolour of the filter-paper is slow and demanding materials.

It looks good based on these facts that the significant fractions of costs are generated by the imission measure of air quality. Hence first of all we concentrate to the air analytical measuring system during the development.

We seek a method that can make a compromise between the cheap and mobile data collection and the numerous, relative reliable data providing.

The figure below shows the shaped air quality meter system:

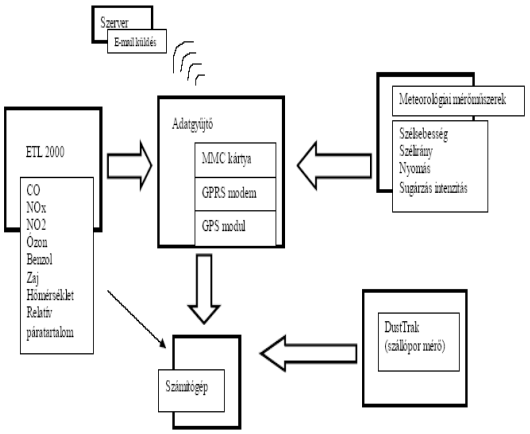

Figure 1. The measuring system

The operation of the system is solvable with relative low specific costs. It is highly mobile and it measures almost any of the air quality and meteorological parameters that are measured by the automatic monitoring containers.

As it visible in the picture above, we can find a meteorological measuring station equipped with conventional tools modem in the system. It is connected to a data-collector which contains a GPS module and a GPRS modem. It is essential to take into consideration the meteorological parameters during the monitoring of the air-pollution. The wind direction, speed, sun radiation intensity could strongly influence our observations. The digital

data-collector collects the data from the ETL2000 and the meteorological sensors and sends them in every hour via e-mail to the central processing server using the GPRS modem of the system.
It marks out from the above that the two key-elements of the system are the air quality monitoring ETL2000 – developed in Italy – and the dust-concentration measuring device the DustTrak aerosol monitor.

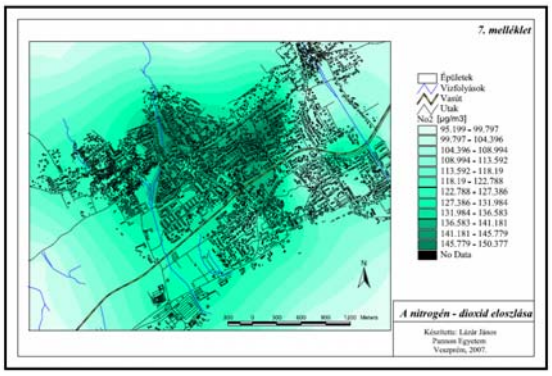

Figure 2. Air quality map

2.2 Noise

Beyond collecting the data mentioned above, it is really important to measure the noise also. Although the noise is not an air polluter, but it has a serious effect on our feel and it is harmful to our health. So the monitoring of it is at mush important as the monitoring of air pollutant compounds. The Brüel & Kjaer 2238 Mediator device was disposable to us to manage the noise monitoring.
On the base of measured noise data, complex survey of the traffic and GIS database (digitalised maps, 3D model) traffic-noise map of the town was constructed. During the preparation of the maps a first class noise measurement device was used to collect the data. These data were used for the calculations that were processed by the SoundPlan noise and air pollution modelling software [2].

Figure 3. Traffic noise map of Balatonfüred

2.3 Drinking water

The drinking water supplement of the town is divided into territory units. The different territory units receive the drinking water from different sources, accordingly a little difference was found in the drinking water parameters too. Based on these parameters drinking-water-quality map was constructed.

2.4 Effects of green-ares

Beyond the examination of the above mentioned environmental parameters, the green-area survey of the town was elaborated also. In this work package we examined the effect of the green-area on the environment.

3 Develop a GIS based environmental evaluation and information system

Based on the maps derived by the examination of individual environmental elements a complex environment evaluation system was elaborated that takes into consideration the quality, the spatial and temporal changes of the environment elements.
The certain layers was aggregated by a mathematical algorithm that using different weights to different environmental parameters. This method is the realization of a map-based environmental quality evaluation system.

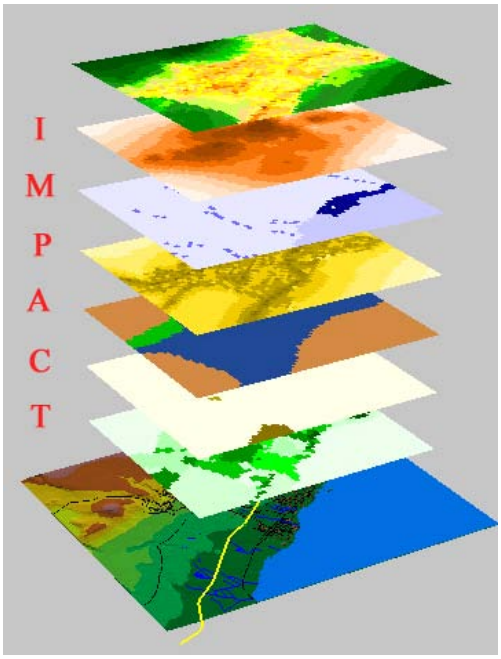

Figure 4. The layers of IMPACT-method

4 Develop a public-information internet portal

The gained map and measurement data were used for establishing a public-information internet portal that is accessible by the inhabitants of the town or by anybody who is interested [5].

The turnout of the open-source mapping services (Google Maps, Yahoo Maps, etc.) ensures effective tools for the publication of environmental information using maps over the Internet. The environmental-evaluation made of the measured data was used to set up a Google Maps mash-up (integration of more services) for Balatonfüred. This mash-up can be placed on any optional Internet-portal.

The mash-up demonstrates the state of the environmental elements, the description of the used measurement devices, the theoretical basis and the preparation steps of the noise and environmental evaluation maps. The established map service is for the demonstration of the possibilities. The present functionalities can be extended corresponding to the further requirements [6,7].

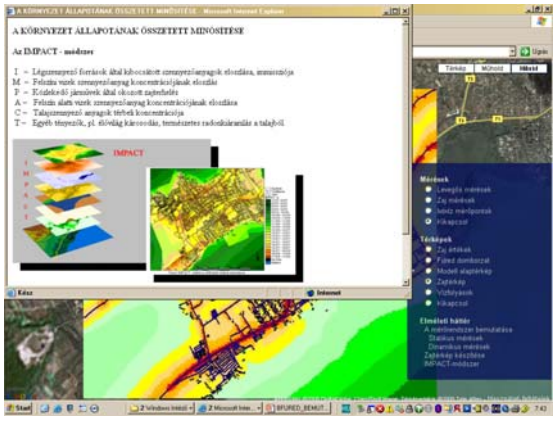

Figure 5. The Internet portal

5 Conclusion

The environmental data displayed on maps provided by an information system is beneficial for the local government and on regional level in environmental protection and for the inhabitants by publishing the information also. At the level of administration the opportunity is given by the data collected by the system using the attached devices to support investment and environmental decisions (determinate, predicate and model environmental risk and load). The population can get guidance about actual environmental information through a continuously available Internet portal. The strengths of the monitoring system is the integration since every measured data of environmental parameters is loaded to the database, so to publish, to retrieve and the later utilization is getting easier [8].

Every of the system produced to the present was specialized to monitor one specific environmental parameter group (air-, soil-, water quality monitoring), hence it was more complicated if someone wanted to monitor all of the components, because of the variety of the user interfaces and data formats. In contrast to this the developed system gives the power of data integration, the user can manages one a uniform user interface all data gained from the environmental measurements of all parameters. The application can process and load in the already extant data also.

References:

[1] UniTec – ETL-Bus Ecological Traffic Light Mobile Version (Dott. Crema Luigi)

[2] Braunstein + Berndt Gmbh / SoundPLAN LLC, SoundPLAN User's Manual.

[3] Sacchi, E, Muller, C: Air quality monitoring at historic sites: Redefining an environmental classification system for gaseous pollution, ASHRAE J 47 (8): 40-46 AUG 2005 WEB of Science/ISI

[4] Gorman, HS, Conway, EM: Monitoring the environment: Taking a historical perspective ENVIRON MONIT ASSESS 106 (1-3): 1-10 JUL 2005 WEB of Science/ISI

[5] Ferenc Speiser – Imre Magyar – Rozália Jamniczky – Dr. Ákos Rédey: Municipal Enverionmental-monitoring System, 12th EC&GI-GIS Workshop, ESDI: From Inspiration to Implementation, 21-23 June 2006., Austria, Innsbruck (poster proceedings

[6] I. Magyar, F. Speiser: Municipal monitoring from University of Pannonia, Geoinformatics 2007/1 (p19-20, in Hungarian)

[7] Ferenc Speiser, Imre Magyar, Rozália Jamniczky, Dr. Ákos Rédey: Municipal Environmental Monitoring-System, EFITA/WCCA 2007. The European Federation of IT in Agriculture and the World Congress on Computers in Agriculture, Glasgow, Scotland 2-5 July 2007

[8] Imre Magyar – Ferenc Speiser – Pál Bui: GIS based environment quality maps for Balatonfüred, Conference of Chemical Engineering '08, Veszprém, 2008. Proceedings p.340-341.

Source Identification Using CMB Models and Effects of Emission Control on Reducing Ambient Air Pollution in Industrial City

DRAGANA ĐORĐEVIĆ
Department of Environment,
Institute for Chemistry, Technology and Metallurgy, Centre of Chemistry
University of Belgrade
Studentski trg 12 – 16, 11001 Belgrade
SERBIA
dragadj@chem.bg.ac.yu

Abstract: Harmful substances in the ambient air can be reduced only on condition that their emitters are kept under control. For that purpose it is necessarily to know key points in technological processes that are emitting specific pollutants, the nature of emitters, the link between the emission fluxes on the emitters, meteorological base of the region and the concentration of pollutants at the receptors of ambient air. Atmospheric surface temperature inversions play a significant role in the problem of ambient air pollution since their upper edge acts as a natural barrier to the vertical dispersion of pollutants. In many cases of pollution, there are no prior knowledge of the emission sources, hence Chemical Mass Balance models (CMB) are applied to extract information concerning the sources using minute by minute continuous measurements data of ambient air pollution at the receptors. The results of calculated fingerprints of possibly sources are connecting to real emission sources. Model of investigation was highly industrial city in Serbia (Pančevo), with over 80.000 habitants, where among the rest industries are located oil refinery, petrochemistry and fertilizer factory. The investigated region is characterized by maximum number of surface temperature inversions of atmosphere during the night times and their furlough during the day times in August. Analysis of daily variations contents of pollutants in ambient air show that concentrations of the pollutants from the low altitude emission sources were higher two times and more during the night than daytimes vice verse for pollutants from the high altitude sources. The daily variations of their concentrations show the minimums in the afternoons when is boundary layer at the top point. NH_3 in this case origin from high altitude source in fertilizer factory, which is only one in the region, therefore was chosen as a tracer of industrial area influence. CMB models showed the highest associations of pollutants that are constituents of volatile organic compounds from low altitude sources in industrial area. The measures of control of identified emission sources, such as extinguishing key sources, planning of emiters' activities in harmony with meteorological conditions, and at a low rate and simple reconstruction one part of sources in both the refinery and petrochemistry had as the result the reduction of VOCs concentrations in the receptor's part of ambient air for more than twice. The benzene concentrations at the receptors which are under high influence of industrial sources reached in the years 2004 and 2005 the values acceptable with regard to the limit value of the Directive 2000/69/EC.

Key-Words: - Source identification, CMB models, emission control.

1 Introduction

Today, no region of the global atmosphere is unaffected by anthropogenic pollution. Urban regions are affected by inorganic, light organic and heavy organic gases [1] and aerosols. Import heavy organics in urban air, such as toluene and xylenes, break down chemically over hours to a few days; thus, most of the free troposphere is not affected directly by these gases, although it is affected by their breakdown products.

Understanding the chemical and physical processes in the atmosphere and emission sources of various technologies is the key to the development of cost-effective and health-protective air pollution control strategies. A number of species have been designated "hazardous air pollutants" or toxic air contaminants. Most are directly emitted into the air, but some also have significant secondary sources, i.e., are formed by chemical reactions in air. Furthermore, the ultimate health impacts are determined not only by the emission and formation of such compounds in air but also by their atmospheric fates. In short, some pollutants react in

air to form less toxic species, whereas other form more toxic compounds [2].

The mathematical models based on fundamentals of atmospheric chemistry and physics are essential tools in tracking emissions from many sources, their atmospheric transport and transformation, and finally their contribution to concentrations at a given location (receptor). The receptor models are enabling to attack the source contribution identification problem in reverse order, proceeding from particulate concentrations at the receptor site backward to responsible emission sources. The corresponding tools, named receptor models, attempt to relate measured concentration at a given site to their sources without reconstructing the dispersion patterns of the material [3].

2 CMB Model UNMIX

The idea that multivariate data analysis of air quality data could be give quantitative information on the sources of air pollution was very much in the air during the late 1960s and 1970s [4]. Mathematical models based on fundamental of atmospheric chemistry and physics are essential tools in tracking emissions from many sources, their atmospheric transport and transformation, and finally their contribution to concentrations at the given location (receptor). It is possible to attack the source contribution identification problem in reverse order, proceeding from pollutants concentrations at the receptor site backward to responsible emission sources. The corresponding tools named receptor models attempt to relate measured concentrations at a given site to their sources without reconstruction the dispersion patterns of the material.

If s_j is the total contribution (in μg m^{-3}) of the pollutants from source j to their concentration at the receptor site, the concentration c_i of pollutant i at the site is:

$$c_i = \sum_{j=1}^{m} f_{ij} a_{ij} s_j \qquad i = 1, 2, \ldots\ldots n \tag{1}$$

where $f_{ij}a_{ij}$ is the fraction of species i in the pollutants concentration from source j at the receptor.

Number of approaches based on (1) has been used to develop our understanding of source-receptor relationship for nonreactive species in an airshed. These methods include the *chemical mass balance* (CMB) for source apportionment and *principal component analysis* (PCA) for source identification [3].

Assume that N air quality samples are analyzed for n species which come from m sources. If these species are conservative, then mass balance on each species requires that:

$$C_{ij} = \sum a_{ij} S_{ik} + errors \tag{2}$$

where C_{ij} is the concentration of the j_{th} (j = 1,…. N) species in the ith sample (i = 1, …. , N), a_{jk} is the mass fraction of species j in source k (k = 1, … m), and S_{ik} is the total mass of material from source k in the i_{th} sample. The equation (2) includes errors which may be the result of analytical uncertainty and variations in the sources' composition [4,5].

In this study, an attempt was made to identify the main contributions of the emission sources in industrial town (Pančevo – Serbia) using UNMIX multivariate model Version 2.4. by Ronald C. Henry which runs under the high level language Matlab version at list 6.x.

2.1 Air pollution problem in Pančevo

Pančevo (20^0 40' N, 44^0 53' E) an industrial town of about 80,000 inhabitants is located about 20 km northeast of Belgrade. The investigated region is characterized by maximum number of surface temperature inversions of atmosphere during the night times - 26 and their furlough during the day times in August [6].

A major industrial complex includes petrochemical plant a fertilizer plant and a major oil refinery. Industries for refining oil and for the production of petroleum derivatives and fertilizer manufacture are situated in the South Industrial Zone of Pančevo. In the South Industrial Zone industrial furnaces and oil refinery torches, which are emission sources of SO_2 and NO_x and other products of burning are situated. The dominant wind flows from the south-eastern segment, i.e. from the direction of the Southern Industrial Zone, towards the town of Pančevo.

The factories for refining oil are emitting oil-type NMVOCs, including benzene, toluene, xylenes, as well as sulphur compounds, methyl-mercaptan and TRS (total reduced sulphur). NMVOCs are also emitted from sources of technological processes for the production of petroleum derivatives. However, non-hermetic equipment and installations at the oil refinery and the petrochemical industry, from which NMVOCs can freely evaporate, contribute more significantly to the emissions. These are mainly non-hermetic oil- and oil derivative-tanks, dispatch facilities for petroleum products at the oil refinery,

dispatch facilities for pyrolytic gasoline at the petrochemical industry and open-air waste water treatment plants at the oil refinery and petrochemical industry, where NMVOCs freely evaporate from the surface of the waste water. There is also a significant contribution of NMVOCs from traffic.

The fertilizer plant produces NH_3 using natural gas, which is first desuphurized with ZnO and subsequently, after mixing with water vapour, reformed and methanized to give a mixture with following composition: CO and CO_2, CH_4, H_2, N_2 and Ar. This gas mixture is compressed for the synthesis of NH_3 from the H_2 and N_2. One part of the recycled gas is driven to the reforming section, as a fuel, to keep the partial pressures of N_2 and H_2 constant. The production of NH_3 and its use in the manufacture of synthetic fertilizers is an only one emission source of NH_3 to the ambient air of Pančevo, while the combustion of the recycled gas is one of emission source of NO_x, besides traffic and other industrial furnaces [6,7].

2.2 Limits of concentration values for organic pollutants in ambient air

The huge problem in Pančevo is high concentration of organic pollutants of oil origin; hydrocarbons from raw oil as well as their derivates are appearing in ambient air simultaneously.

According to EU low regulation the concentration of benzene which is component of oil and their derivates is limited.

Valid limited value of benzene concentration in the ambient air is defined by Directive 2000/69/EC, ANNEX I, as a value for the protection of human health. Limit value is 5μg/m^3 on the averaging period of calendar year with margin of tolerance of 5 μg/m^3 (100%) on 13 December 2000, reducing on 1 January 2006 and every 12 months thereafter by 1 μg/m^3 to reach 0% by 1 January 2010. Date by which limit value of 5μg/m^3 on the averaging period of calendar year, is to be met is 1 January 2010, except within zones and agglomerations within which a time-limited extension has been agreed in accordance with Article 3(2).

3 The control of the identified sources

Results of continuous monitoring, of near ground concentrations of ambient air pollutants for August 2004, were obtained from the municipal monitoring system of the industrial town Pančevo. In order to detect and record minute-by-minute fluctuations of the concentrations of pollutants, the following methods were employed: for ammonia, a chemiluminescent type NH_3 analyser; for SO_2 a pulsed UV fluorescent type analyser; for Total Reduced Sulphur (TRS) a UV Fluorescent type TRS analyser; for NO_x, a chemiluminescent type NO_x analyser; for PM_{10}, a dichotomous model sampler on gravimetric methods; for organic pollutants GC/PID and for NMVOCs GC/FID.

It is postulated that high emission sources are the dominant contributors to the concentrations of SO_2, NO_2 and NH_3, while low sources are the dominant contributors to the benzene, toluene, xylenes, Me-Me and TRS concentrations to their contents in the near ground ambient air, investigated in this study.

Analysis of daily variations contents of pollutants in ambient air show that concentrations of the pollutants from the low altitude emission sources were higher two times and more during the night than daytimes vice verse for pollutants from the high altitude sources. Fig. 1 shows daily variation of pollutants originating from low level altitude of emission sources.

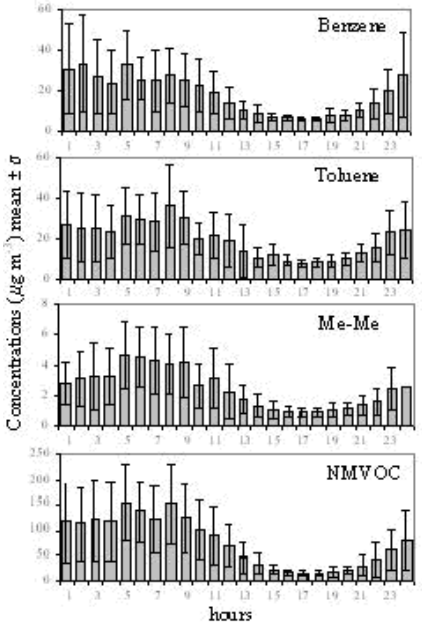

Fig. 1 Daily variation of concentration of pollutants that are originating from from the low altitude emission sources

The concentrations of the pollutants from the low altitude emission sources were higher two times and more during the night than daytimes vice verse for pollutants from the high altitude sources like NH_3, which has only one emission source. The daily variations of their concentrations show the minimums in the afternoons when is boundary layer at the top point.

Trough legislative and administrative action, health-protective and cost-effective risk management decision made and regulatory action implemented, that directly affected the starting point of Pančevo's urban atmosphere, that is, primary emissions and their sources. Main emiters of pollutants have been identified, on application of CMB model UNMIX, upon analysis of technological processes in factories of the South industrial zone in Pančevo (Refinery, Petrochemistry and Fertilizer factory), by measurement of pollutants' concentrations in the ambient air and meteorological base of the area. The measures of control of emission - such as extinguishing key sources (pouring station of pyrolytic oil in the Petrochemistry), planning of emiters' activities in harmony with meteorological conditions, and reconstruction of one part of sources in both the Refinery and Petrtochemistry – had as the result the reduction of benzene concentrations in the receptor's part, in ambient air, for more than twice.

The dominant emission sources were analysed using chemical mass balance model (UNMIX v.2.4). Results showed in Tab. 1.

Table 1. Profiles of identified emission sources

	Profile of Source 1 (%)	Profile of Source 2 (%)	Profile of Source 3 (%)	Profile of Source 4 (%)
SO_2	9	10	**72**	9
Benzene	9	**43**	0	**48**
Toluene	13	12	16	**59**
Me-me	16	18	10	**56**
NH_3	**100**	0	0	0
NO_2	21	20	**59**	0
NMVOC	7	**81**	<1	12
S_{ij}	16	48	17	19
Assumptioned emission sources	Fertilizer + Petrochemical plants	Traffic	Industrial furnaces	Oil rafinery

UNMIX showed the highest associations of pollutants that are constituents of volatile organic compounds, which signify strong influences of emission from low altitude sources e.g. evaporation of organic pollutants from low altitude devices in the oil refinery and petrochemical plants as well as traffic.

The dominant contribution to air pollution in Pančevo is from low-lying emission sources, such as the loading facilities for *van*- and *truck*-decanters and oily waste water treatment plants.

4 Conclusion

The measures of control of identified emission sources, such as extinguishing key sources, planning of emiters' activities in harmony with meteorological conditions, and at a low rate and simple reconstruction one part of sources in both the refinery and petrochemistry had as the result the reduction of VOCs concentrations in the receptor's part of ambient air for more than twice. The benzene concentrations on the measurement site which is under high influence of industrial sources reached the values acceptable with regard to the limit value of the Directive 2000/69/EC in the years 2004 and 2005.

Acknowledgements

I am very grateful to Prof. R. Henry for UNMIX model. Also I am grateful to the Ministry of Science and Environment of the Republic of Serbia for financial support. I would also like to thank the Municipality of Pančevo for the measurement data used in this paper, as well as the Oil refinery, and the factories Petrochemical and Fertilizer "Azotara" from Pančevo for the technological data.

References:

[1]Jacobson, Mark, Z., *Atmospheric Pollution, History,Science, and Regulation*, Cambridge University Press, ISBN 0 521 01044 6, United Kingdom, 2002.

[2]Finlayson – Pitts Barbara J.; Pitts, Jr.,James N., *Chemistry of the Upper and Lower Atmosphere, Theory, Experiments and Applications*, Academic Press, ISBN 1-12-257060-x, California, USA, 2000.

[3]Seinfeld, J.H., Pandis, S.N., Atmospheric Chemistry and Physics From Air Pollution to Climate Change, John Wiley & Sons, Inc., New York 1998.

[4]Henry, R.C., History and fundamentals of multivariate air quality receptor models, Chemometrics and Intelligent Laboratory Systems 37, 37-42, 1997.

[5] Henry, R.C., Multivariate receptor models – current practice and future trends, Chemometrics and Intelligent Laboratory Systems 60, 43-48, 2002.

[6] Dragana Đorđević and Tatjana Šolević, The contribution of high- and low altitude emission sources to the near ground concentrations of air pollutants, Atmospheric Research 87, 170-182, 2008.

[7] Đorđević Dragana, Chapter 4: Emission Sources and Their Contributions to Ambient Air Concentrations of Pollutants in: Environmental technologies New Developments, Edited by Burcu Özkaraova Güngör, I-Tech Education and Publishing, ISBN 978-3-902613-10-3, 2008.

A Reputation based Trust Model for Geospatial Web Services

D. UMUHOZA[1], J.I. AGBINYA [2], D MOODLEY[3], A VAHED[1]

[1]Meraka Institute, PO Box 395, Pretoria 0001,
South Africa; ({dumuhoza, avahed}@csir.co.za);

[2]Information and Communication Technology Group, University of Technology, Sydney, NSW 2007,Australia;
(agbinya@eng.uts.edu.au);

[3] School of Computer Science, University of Kwazulu-Natal , Private Bag X54001,Durban, 4000 ,
South Africa; (moodleyd37@ukzn.ac.za)

Abstract : Geospatial semantic web services are typically used to process sensory data and produce results for the end user. There are many web services available, providing data products of varying quality. The reliability of services that process or provide this data is of concern since it influences the quality and usefulness of this data.
Trust can be used as a means to filter Geospatial Semantic Web services, based on their descriptions and data they provide. Many definitions of trust are provided in the literature and these definitions usually depend on the context and the purpose for which trust is used. We provide a definition of trust for a Web service in a dynamic, open and distributed environment such as the Geospatial Semantic Web.
This paper presents progress in developing an ontological representation of trust for Geospatial Web services. The paper highlights challenges in processing geospatial data and presents concepts of a trust ontology for Geospatial Semantic Web services in this context. The paper proposes a reputation based trust model that is dynamic and that takes the service requester's constraints as inputs to the trust function. The trust estimation function presented in this paper is based on direct evidence and indirect evidence of the quality of data produced by the service.

Key-Words: Trust, Geospatial Web services, Reputation, geospatial data, Semantic Web

1 Introduction

The Geospatial Semantic Web is a specialisation of the Semantic Web which allows for the formal definition of the meaning of concepts about geographical entities and their relations [1]. These definitions permit reasoning and querying of information required through geospatial services by applying analytical methods to geospatial data.

These services provide different capabilities like visualization, editing and analysis of geospatial information on the Internet. An example of such a service is one that provides geographic information that represents real-world geographic features, such as a building or a road, and their attributes like height or width

Real-time access to geospatial data is not always possible because of the need to transfer large volumes of data that would consume a lot of bandwidth and computing resources. Geospatial Web services are advantageous in this respect, as they can significantly reduce the volume of data and the computing resources required at the end-user side [2].

The dependability of the Semantic web, expressed in terms of privacy, trust and confidentiality, has been addressed in [3]. We address the dependability problem from two perspectives, namely, the usefulness of data produced by Web services and quality of service (QoS) of Web services.

The geospatial processing and analyses of data is complicated by the characteristics of geospatial data. Geospatial data is spatially dependent and autocorrelated. For example, the intensity of a phenomenon observed depends on the phenomenon on neighbouring locations. Spatial data is dynamic since it reflects the reality of the world as it evolves with time. Heterogeneity is another characteristic of spatial data since different sources of datasets for a given geographical feature may have to be integrated.
In this paper we address the dependability issue by providing mechanisms to measure trust for Geospatial Semantic Web services based on the quality of data produced by the Web services.
Our contribution is to propose an ontological representation of trust for a Geospatial Semantic Web service that allows for the judgement of the Web service based on quality of data produced. We introduce concepts of the trust ontology hatrepresent variables whose values are used in computing the trust

function. We propose a trust function based on direct experience and recommendations resulting from indirect experience.

The remainder of this paper is organized as follows. Section 2 will provide a brief review of existing trust models for Web services in Semantic Web. In section 3 we present our view of trust and in section 4 we introduce concepts for an ontology for representing trust of a Geospatial Web service. We present the relationships of concepts in trust estimation in section 5. We conclude and state future research issues in section 6.

2 Related work

Trust as it is known in social networks, is a fundamental concept on which we base our interactions in our daily life. It is important for all agents utilising a trust computation system to realise that trust is a subjective measurement and is dependent on many factors. One such factor is the prior successful and dependable utilization of a service for specific applications. Trust is just an indication and it does not provide any guarantee of a successful outcome of an interaction.

The notion of trust has been addressed variously in different areas of research, with the adopted definition of trust typically based on the context and purpose for which it is applied. Providing a level of confidence in a selected servicetrust has also been used as an approach to filter discovered services, e.g., [4,8,9,10,11].

Trust in the content of statements describing a service has been linked to trust in the source of the service. In [10] a model is introduced that establishes a degree of belief in the statement asserted on the Semantic Web. The model suggests that a user's belief in a statement is a function of the user's trust in one or many sources of the statement. This model sets the belief of a service to zero if there is no information available on the belief in that statement. We argue that the absence of information about belief does not necessarily mean that there is no belief. On the contrary, if there is no information about belief, then any value in specified range could be applicable to belief. There should be a distinction between belief with a minimum value and belief being unknown.

Trust has been addressed as a common interpretation of policies on Semantic Web. In [4], it is proposed that each participant involved in the system must have a trust policy and that there must be a means of common interpretation of different policies. A policy is defined as a trust requirement or trust guarantee. A trust ontology, WSTO (Web Services Trust Ontology), has been proposed [4]. In WSTO, a shared vocabulary is developed to map the descriptions of different policies and for participants to specify their trust requirements. This approach provides a good starting point in providing a common way of interpreting trust policies in the Semantic Web, but it does not have mechanisms to verify and validate trust described in the policy.

Research has focused on different aspects of Web service selection based on QoS. A quality driven Web service selection model that considers service selection as a multiple attribute decision making problem is introduced in [5]. The proposed model takes into consideration, QoS user requirements.This model measures QoS based on execution cost, execution time, availability and reliability in terms of historical information about the performance of a Web service. It is important to evaluate QoS on multiple criteria, but the model does not indicate how to evaluate QoS at the initial stage where there is no historical data available to use to predict reliability and availability. The model introduces an interesting concept of measuring the fidelity of each QoS criterion. This concept adds value to the computation of QoS of a Web service and to measuring the trustworthiness of a Web service.

Authors in [6] have argued that a reputation based system is not sufficient for optimal Web service selection. The authors introduced a QoS broker based scenario which can be compared to the model in [7], where QoS advertised by provider is checked and validated. [6] proposes a trust model, which includes a QoS model, decision model and trust correction. This model does not consider cases where trust could be derived from a combination of QoS and trust information available from previous agents or other services that interacted with the service in question. We believe that it is important to consider the prior experience of other services or agents that interacted with a given service, particularly at the initial stage of engaging that service.

3. A view of trust

Our view of trust is based to the definition of trust in the Cambridge International Dictionary of English,*Cambridge International Dictionary of English*, 1995) which defines trust as having: "...belief or confidence in the honesty, goodness, skill or safety

of (a person, organization or thing)" [18]

We define trust for a Web service as *the degree of confidence in a Web service of being able to provide dependable results within a specific period of time and under specified constraints set by the entity requesting the service.*

Reputation based approaches for rating trust based on social networks have been studied in the literature for on-line systems or distributed networks [12,13,14,15]. The same approaches are suitable for rating trust geospatial Web services as both Geospatial Semantic Web and mobile ad-hoc networks are dynamic, open and distributed environments.
However, the inference of trust for Geospatial Semantic Web services using reputation based system is more complex due to the nature by which geospatial data is collected and used. Such data is collected usually with a specific purpose in mind; when shared amongst different users or organizations, they may have different opinions about the usefulness of the data because of how it is marked up, the amount of detail in the data, the format in which the data is in, etc.

We argue that the requester of a service should specify the constraints under which the service must be provided in order to set the context and to allow for a reasonable comparison of different views about the same service. Currently we consider the constraints identified in [16] which are as follows:

i) Completeness, which means that there are no omissions in datasets provided by the service.
ii) Resolution, which refer to the level of detail about geospatial objects and details of spatial and temporal entities involved in the process of describing the data.
iii) Accuracy, which refer to the degree of distortion in the values of attributes of geospatial data.
iv) Data format: which can be referred to as data type since the data may be in a format that a requester cannot interpret or decode.

4. Concepts of trust ontology

The use of ontologies is one way to formally describe existing concepts and relationships among these concepts in order to have a shared and processable specification of knowledge within a given domain.
We propose following concepts and instances for a Geospatial Semantic Web trust ontology:

- *Data_characteristics:* A service must produce data that has some degree of *accuracy*, is *complete*, and that has a specified *theme*, with a well specified *location* and *time.*
- Interacting_entities will establish a level of communication between themselves. A *service_requester* will want to predict the degree of success with which a web service provides the required quality of data. Past records about the performance of a *target_service* will be used. A *trust_recommender* entity which is a service, an agent or an organization that interacted with the target_service provides evidence about its experience with the target_service on criteria that a requester specifies. The criteria will be based on one or many of the data_characteristics and QoS of target_service.
- A target_service will be described by its *service_descriptions.* A service may have a textual description. Typical descriptions would include a summary of what the service offers and any requirements that the service has.
- A *service_provider* entity could be a service, an agent or an organization owning agents. The trust of a service provider will influence the trust of the service it provides. The trust of a service provider will be computed based on *QoS* it provides
- *Evidence* will be used as the basis for predicting the expected results of a service.
  - We introduce the term *evidence_type.* A requester itself could have had some interaction with the target_service and it could have *direct* evidence contrary to evidence provided by a third party entity which is *indirect* evidence.
  - Evidence has an evidence_value as one of *positive*, *neutral* or *negative*.
  - Evidence has an *evidence_status* as *current* or *past* evidence. This is because evidence peratins to the performance of a service within a specific period of time. The values of evidence changes with time since the QoS of Web services depend on changes in the QoS infrastructure that these services run on.
- There might be cases where there is limited or no past records available about the target service. In that case the uncertainty about the past performance of the target service on each criteria will be estimated.

5 Relationship amongst concepts

Trust can be estimated differently but understanding the relationship between the main concepts is key in deciding how to estimate trust. We consider these relationships:

5.1 Direct evidence and indirect evidence

The fact that indirect evidence introduces a third party, namely a recommender, for which trust must be estimated independently of the evidence it provides. Clearly, such evidence should have less weight than direct evidence. The notion of levels of indirect evidence reflects the number of recommenders that the same evidence passed through. Trust about the recommender itself influences the trust in the evidence the recommender provides. We say that the weight of indirect evidence reduces with the increase in the number of recommenders in the chain of passing on the evidence.

5.2 Evidence and uncertainty

It is important to distinguish ignorance about the past performance of the target_service and neutrality resulting in positive and negative reports being of equal values. Uncertainty and evidence are in exponential relationship where when evidence value increases, uncertainty value decrease and vice versa.

5.3 Past evidence and current evidence

We say that evidence should evaporate (decays) after a length of time T which we define as the life time of the evidence. We are cautious not to jump into conclusions about how past evidence evaporates or decays in this paper. However, bearing in mind that the quality of service (QoS) upon which many of the parameters here are defined also changes, the nature of the decay of evidence is linked to the dynamic nature of the QoS. The nature of how an evidence decays can also be modelled as exponential and using a negative linear function and/or depreciating functions. A simple depreciating evidence is one in which the value of the evidence is reduced by its historical age. For example in a chain of five recommendations the first recommendation has the most value and the fifth the least value. The decay rates therefore are:

$$Rate_{decay} = \left\{ \frac{1}{5} \quad \frac{2}{5} \quad \frac{3}{5} \quad \frac{4}{5} \right\} or\ Rate_k = \frac{k}{age}$$

Where in this expression "age" refers to how old the evidence is and k the position in the sequence of recommendations. Thus the value 1/5 means the most current recommendation for a sequence of 5 recommendations and 4/5 refers to the first recommendation received. This depreciating function assumes that the first recommendation is most likely the most important and more likely to be less diluted by extraneous opinions. This is similar to passing on gossip and the further it is passed on, the more false evidence is likely to be inserted. We can improve upon this concept by relating the evidence to the trust value of the entity giving this evidence. Better still consider the following chain of evidence:

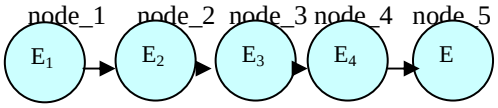

Figure 1: Chain of evidence

In this chain of evidence, if node 1 is the first to give evidence, the evidence at each node is given by the expression:

$$E_1 = E_1;\ E_2 = \frac{4E_1}{5};\ E_3 = \frac{3E_1}{5};\ E_4 = \frac{2E_1}{5} \quad (1)$$

$$E_5 = \frac{E_1}{5}$$

Thus the evidence provided by node 1 has decayed so much due to its age that when node 5 hears it, it has reduced to one fifth in value of its original.

5.4 Trust Function

This paper reports on quality of data that a service produces, present and past are used as the evidence. These reports are either obtained directly or through recommendation. Let Q(S) be the total quality of data produced by a service S. It has been shown in [17] that QoS can be summed in general. Hence

$$Q(S) = \sum_k q_k(S) \qquad (2)$$

$q_k(S)$ are the individual QoS components derived as either direct or indirect evidence (recommendation). These components include data completeness, data resolution, data accuracy, data format and other parameters. Following the example in [12, the trust function is:

$$T(S) = \frac{1 + [Q_d(S) + Q_r(S)]}{2 + [Q_d(S) + Q_r(S)] + [Q_{df}(S) + Q_{rf}(S)]} \quad (3)$$

The letters "d" and "r" are used to designate direct evidence and recommendations. The letter "f" in the denominator is used to designate the value of QoS

when the service fails with the caveat that it is possible for this value to be negative and usually is when a service fails or a negative recommendation is given.

6. Conclusion

In this paper we have presented progress in developing trust for Geospatial Semantic Web services. Trust ontology concepts presented in this paper are used to collect information about the past performance of a Geospatial Semantic Web service. It is designed for Geospatial Semantic Web services where spatial characteristics of data produced by Web services are detailed, which allows comparison of performance of a same service without ambiguity.

The taxonomy of the presented concepts allow for the extension of concepts and additions of more concepts as a service requester may require it.

The evidence status and evidence type introduced allow automatic and dynamic maintenance of the ontology. In addition to that, the fact that it is possible to capture both negative and positive evidence allows estimation of trust with more accuracy.

We have provided functional relationships between evidence and uncertainty. This function is important for decision making before a service is selected. Trust changing rate can also be used as an indication to predict the successfulness of subsequent interactions. Uncertainty concept is used to measure trust in case of partial or missing data required to compute trust. The concepts presented can be easily integrated with other ontologies like policy based ontology and provenance and topic based ontologies as they may be added as concepts linking to provider and service concepts.

In our future work we will implement the ontology and evaluate its performance in a real world example in a specific use case. We have a goal to extend the ontology by adding other aspects used to measure trust in literature like trust of communication policies, trust of information source, trust of content and others we will identify. We will propose a trust function and a decision model that takes into account all trust concepts and their relations.

Bibliography

[1] Jonathan Lowe, *A Geospatial Semantic Web*,http://www.geospatialsolutions.com/geospatialsolutions/article/articleDetail.jsp?id=163883, Accessed June 2008

[2] Yue Peng et al. , *Semantics-based automatic composition of geospatial Web serice chains*, Computers & Geosciences 33 (2007) 649-665. Elsevier.

[3] Thuraisingham B., *Building trustworthy semantic webs*, Auerbach Publications. Taylor & Francis Group. ISBN 0849350808.

[4] Galizia S. et al., *A Trust Based Methodology for Web Service Selection*, http://kmi.open.ac.uk/people/stefania/publications/ICSC07_Galizia.pdf Accessed March 2008.

[5] Hu J. et al., *Quality Driven Web Services Selection*, Proceedings of the 2005 IEEE International Conference on e-Business Engineering (ICEBE'05) 0-7695-2430-3/05.

[6] Zedan P. and J. Baik, *QoS Broker-Based Trust Model for Effective Web Service Selection*, Cambridge, Massachusetts, USA: IASTED SEA 2007.

[7] Shuping R., *A Model for Web Services Discovery with QoS*, ACM2003.

[8] Gil Y. and D. Artz, *Towards content trust of web resources*, In Proceedings of the 15th International World Wide Web Conference.

[9] Kim J. et al., *Provenance Trails in the Wings/Pegasus workflow systems*, Journal of Computation and Concurrency: Practice and Experience, Special issue on the First Provenance Challenge, L. Moreau and B. Ludaescher(Eds).

[10] Richardson M. et al., *Trust Management for Semantic Web*, Sanibel Island, Florida: Proceedings of the Second International Semantic Web Conference.

[11] Shaikh A. et al., *A Cognitive Trust-Based Approach for Web Service Discovery and Selection*, In Proc 3rd European Conference on Web Services. (ECOWS'05)0-7695-2484-2/05.

[12] Sun Y et al., *Defense of Trust Management Vulnerability in Distributed Networks*, IEEE Communications Magazine.

[13] Josang A. , Ismail R., and Boyd C., *A survey of trust and reputation systems for online service provision*, Decision Support Systems, Vol.43, No.2, pp.618 - 644, 2005.

[14] Wang Y. and Vassileva J., . *A review on trust and reputation for web service selection*, In Proceeding of the 1st Int. Workshop on Trust and Reputation Management in Massively Distributed Computing Systems, Toronto, Canada, June 2007.

[15] Buchegger S. and Boudec J. L. , *Coping with false accusations in misbehavior reputation systems for mobile ad-hoc networks*, EPFL Technical Report IC/2003/31, EPFL-DI-ICA, 2003.

[16] Subbiah G et al., *Geospatial Data Qualities as Web Services Performance Metrics*, Proceedings of the 15th International Symposium on Advances in Geographic Information Systems. ACM GIS 2007

[17] Agbinya I. J., *QoS Functions and Theorems for Moving Wireless Networks*, Sydney Australia: In Proc. International Conference on Information Technology and Application.

[18] Cambridge International Dictionary of English, Cambridge University Press, 1995. ISBN 0521 588359

Control simulations and design of ISOGLIDE3 medical parallel robot

SERGIU-DAN STAN, RADU BĂLAN, VISTRIAN MĂTIEŞ, CIPRIAN LAPUSAN, TUDOR VLAD
Department of Mechatronics
Technical University of Cluj-Napoca
C. Daicoviciu no. 15, 400020, Cluj-Napoca
ROMANIA
sergiustan@ieee.org http://www.mecanica.utcluj.ro/mmfm/index.html

Abstract: - The paper presents the design and control simulations of ISOGLIDE3 parallel robot. An innovative user interface for high-level control of a 3 DOF parallel robot is also presented. The robot interface using virtual reality was verified and tested, and results in MATLAB, Simulink, and SimMechanics were presented. The ISOGLIDE3 robot offers the superior characteristics with regards to the other parallel manipulators, such as the light weight construction.

Key-Words: - ISOGLIDE, decoupled motions, parallel robot, design, control.

1 Introduction

The structure of the 3 DOF Isoglide3 parallel robot is shown in Fig. 1, where a mobile platform is coupled with the fixed base by three legs of type PRRR (Prismatic Revolute Revolute Revolute).

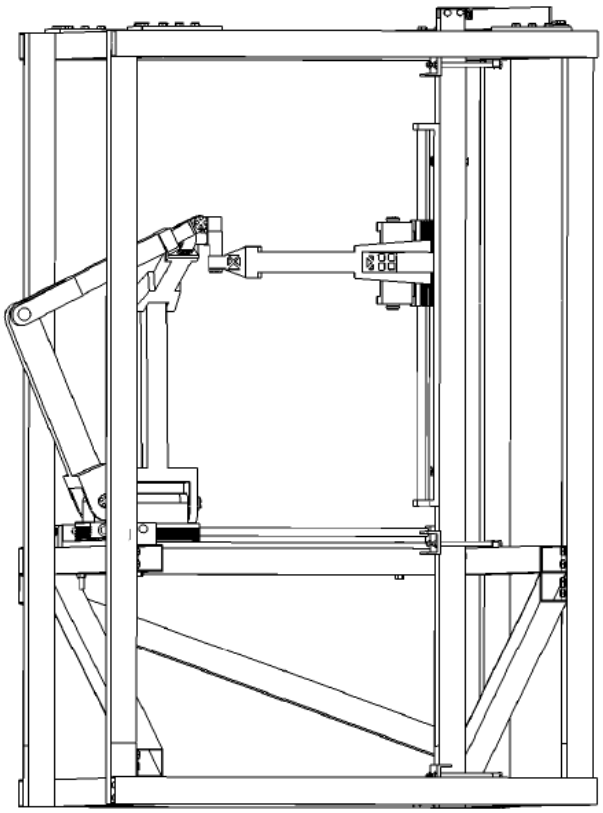

Fig. 1. CAD design of 3 DOF Isoglide3 parallel robot.

The mobile platform can be visualized as a square whose side length 2L is defined by B_1, B_2, and B_3 points. The fixed base is defined by three guide rods that passing through A_1, A_2, and A_3 points, respectively (Fig. 3).

Fig. 2. 3 DOF Isoglide3 parallel robot realized at Mechatronics Department.

Fixed coordinate frame originates at the point O. In Fig. 4, the reference frame XYZ is attached to the fixed base.

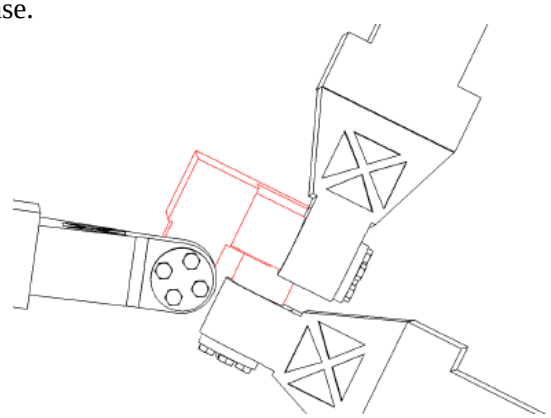

Fig. 3. The mobile platform of 3 DOF Isoglide3 parallel robot.

The three revolute joint axes at each of these links are parallel to the ground connected prismatic joint axis, and are located at points A_i, M_i, and B_i, respectively. Also, the three prismatic joint axes passing through points A_i, for i = 1, 2, 3, are parallel to the X, Y, and Z axes, respectively.

The first prismatic joint axis lies on the X-axis; the second prismatic joint axis lies on the Y axis; while the third prismatic joint axis is parallel to the Z axis.

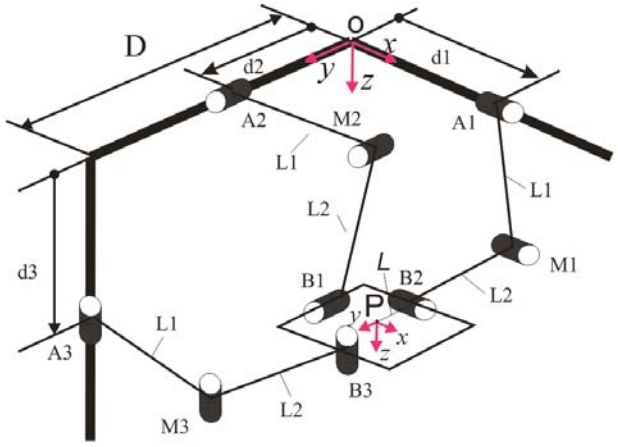

Fig. 4. Kinematic scheme of 3 DOF Isoglide3 parallel robot.

Consequently, the location of point P is determined by the intersection of three planes. The forward and inverse kinematic analysis is trivial. A simple kinematic relation can be written as (1).

$$\begin{bmatrix} x \\ y \\ z \end{bmatrix} = \begin{bmatrix} d_1 \\ d_2 \\ d_3 \end{bmatrix} \tag{1}$$

This robot architecture was also implemented and known in the literature under the name of Isoglide3-T3 (Gogu 2004, 2008), Orthogonal Tripteron (Gosselin et al. 2004), or CPM (Kim and Tsai 2002).

2 Trajectory planning

Path is defined as sequence of robot configurations in a particular order without regard for timing of these configurations while trajectory is concerned about when each part of the path must be obtained thus specifying timing.

The control of the robot is implemented using a joint-based control scheme. In such a scheme, the end effecter is positioned by finding the difference between the desired quantities and the actual ones expressed in the joint space.

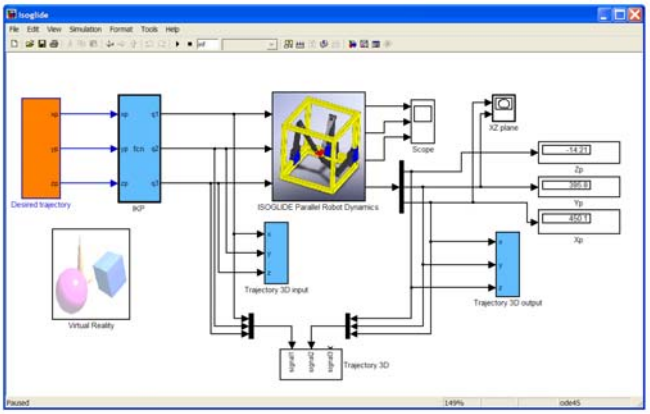

Fig. 5. Simulink model of the ISOGLIDE3 parallel robot.

The first tests on the prototype encourage the direction of the research: the chosen control algorithms emphasize the peculiar characteristics of the parallel architecture and, in particular, the good dynamic performance due to the limited moving masses, and advantageous robot behaviour.

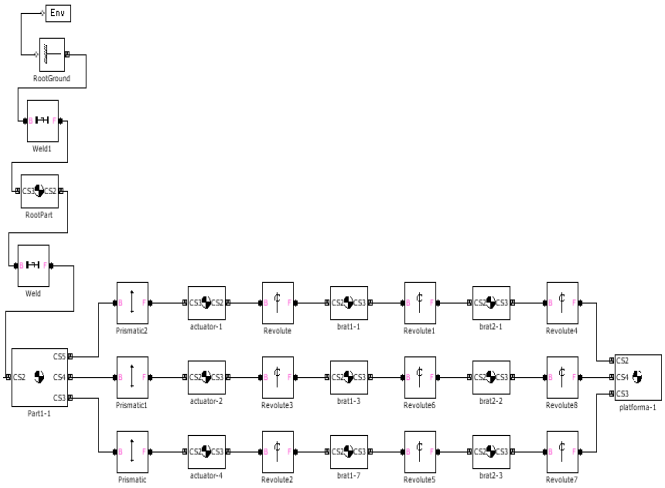

Fig. 6. SimMechanics generated model of the ISOGLIDE3 parallel robot.

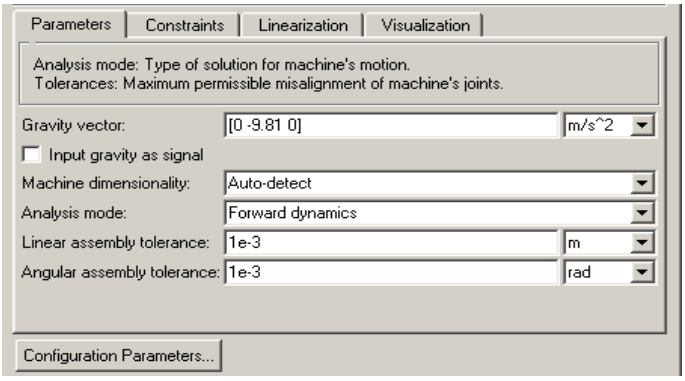

Fig. 7. Configuration parameters of the ISOGLIDE3 parallel robot.

The interface is based on a virtual reality approach in order to provide the user with an interactive 3D graphical representation of the parallel robot.

The interface was designed to give a novice user an intuitive tool to control any kind of mechanical structure (serial, parallel or hybrid), requiring no programming skills. Computer based simulation allows mimicking of a real life or potential situations.

SimMechanics models, however, can be interfaced seamlessly with ordinary Simulink block diagrams. For example, this enables user to design the mechanical and the control system in one common environment.

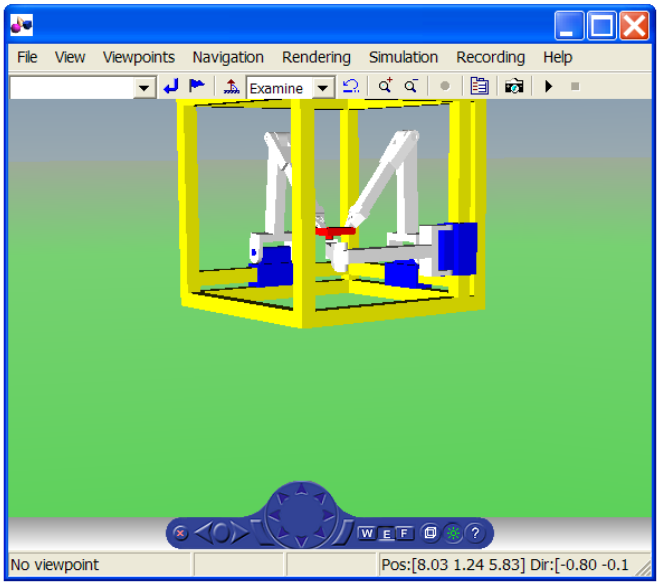

Fig. 8. ISOGLIDE3 virtual reality robot interface.

In addition, Virtual Reality Toolbox for MATLAB makes possible a more realistic rendering of bodies. Arbitrary virtual worlds can be designed with Virtual Reality Modeling Language (VRML), and interfaced to the SimMechanics model.

3 Simulation results

The sample trajectory of the end-effector is chosen to be a circular path with the radius of 0.3 meters and its center is O(0 , 0, 0).

This path is designed to be completed in 7 seconds when the end-effector reaches the starting point P1 (0.3, 0, 0) again with constant angular velocity $\omega = 0.5\pi$ rad/sec. The end-effector path is shown in figure 7.

The desired force obtained from the actuators to move the end-effector of the Isoglide3 parallel robot along the desired trajectory is shown in figure 8.

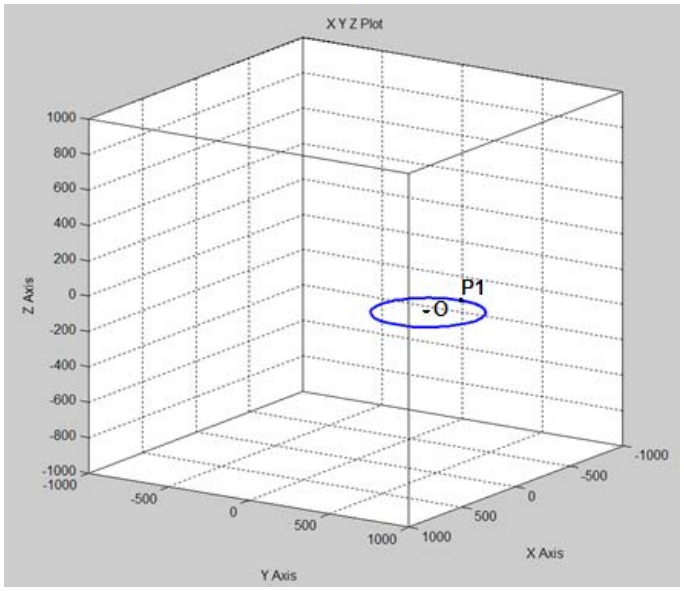

Fig. 9. End-effector path for the circular trajectory.

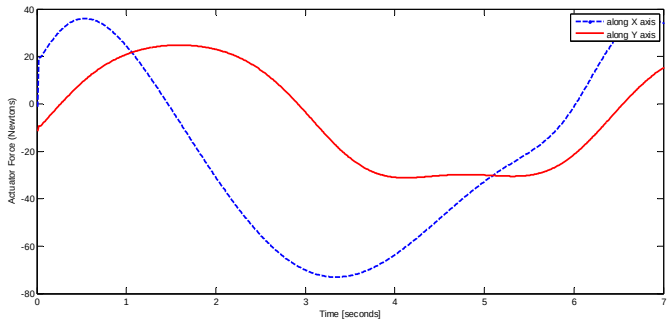

Fig. 10. The desired force obtained from the actuators.

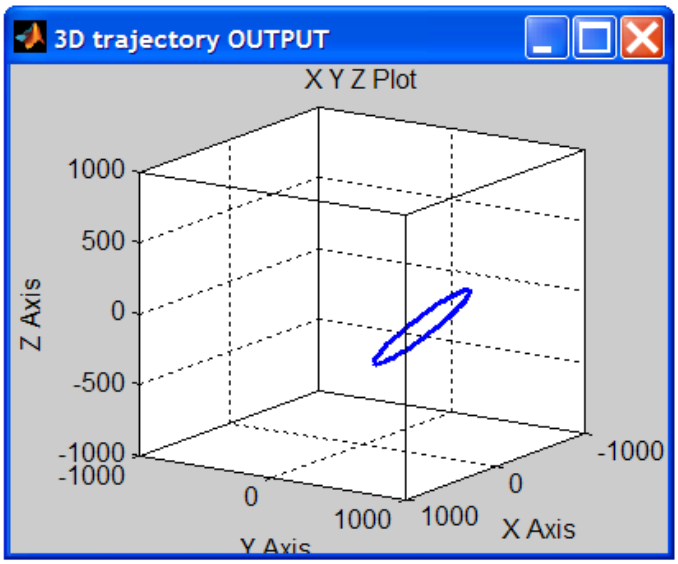

Fig. 11. End-effector path for the circular trajectory.

The desired force obtained from the actuators to move the end-effector of the Isoglide3 parallel robot for the trajectory presented in Fig. 11 is shown in Fig. 12.

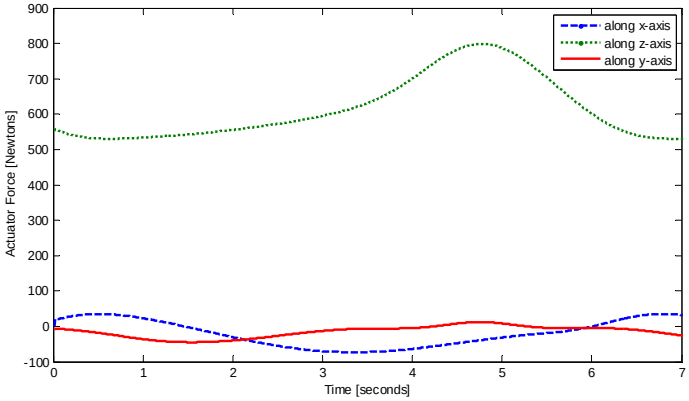

Fig. 12. The desired force obtained from the actuators.

4 Conclusion

The paper presents the design and control simulations of Isoglide3 parallel robot. Also is presented a Virtual Reality Interface for the 3 DOF Isoglide3 parallel robot (IG3PR) control. An evaluation model from the Matlab/SimMechanics environment was used for the simulation. An interactive tool for dynamics system modeling and analysis was presented and exemplified on the control in Virtual Reality environment of this Isoglide3 parallel robot. The main advantages of this parallel manipulator are that all of the actuators can be attached directly to the base, that closed-form solutions are available for the forward and inverse kinematics, and that the moving platform maintains the same orientation throughout the entire workspace. By means of SimMechanics, the authors considered robotic system as a block of functional diagrams. Besides, such software packages allow visualizing the motion of mechanical system in 3D virtual space. Especially non-experts will benefit from the proposed visualization tools, as they facilitate the modeling and the interpretation of results.

References:

[1] Gogu, G., Structural synthesis of fully-isotropic translational parallel robots via theory of linear transformations, European Journal of Mechanics / A –Solids, vol. 23, pp. 1021-1039, 2004.

[2] Gogu, G., Structural synthesis of parallel robots, Part 1: Methodology, Springer, 2008.

[3] Stan, S.-D, Manic, M., Măties, M., Bălan, R., "Evolutionary Approach to Optimal Design of 3 DOF Translation Exoskeleton and Medical Parallel Robots", HSI 2008, IEEE Conference on Human System Interaction, Krakow, Poland, May 25-27, 2008.

[4] Stan, S.-D, Manic, M., Măties, M., Bălan, R., "Kinematics Analysis, Design, and Control of an Isoglide3 Parallel Robot (IG3PR)", IECON 2008, The 34th Annual Conference of the IEEE Industrial Electronics Society, Orlando, USA, November 10-13, 2008.

[5] Kim, S.H., Tsai, L-W., "Evaluation of a cartesian parallel manipulator", In: Lenarčič J, Thomas F (eds) Advances in robot kinematics. Kluwer Academic Publishers, pp 21-28, 2002.

[6] Gosselin, C.M., Kong, X., Foucault, S., Bonev, I.A., "A fully-decoupled 3-dof translational parallel mechanism", In: Parallel Kinematic Machines in Research and Practice, 4th Chemnitz Parallel Kinematics Seminar, pp 595-610, 2004.

[7] S. Stan, V. Maties, R. Balan, „Optimal Design of a 2 DOF Micro Parallel Robot Using Genetic Algorithms", Proceedings of the 2007 IEEE-ICIT 2007, IEEE *International Conference on Integration Technology*, March 20 - 24, 2007, Shenzhen, China, p. 719-724. IEEE Catalog Number: 07EX1735, ISBN: 1-4244-1091-6, ISBN: 1-4244-1092-4.

[8] S. Stan, *Workspace optimization of a two degree of freedom mini parallel robot*, 2006 IEEE-– AQTR 2006 (THETA 15), May 25-28 2006, Cluj-Napoca, Romania, IEEE Catalog number: 06EX1370, ISBN: 1-4244-0360-X, pp. 278-283.

[9] J. Hesselbach, H. Kerle, M. Krefft, N. Plitea, (2004) The Assessment of Parallel Mechanical Structures for Machines Taking Account of their Operational Purposes. In: Proc. of the 11th World Congress in Mechanism and Machine Science-IFToMM 11, Tianjin, China.

[10] Lăpusan, Ciprian; Măties Vistrian; Bălan, Radu & Stan, Sergiu: Mechatronic approach for control of 2 dof mini parallel robots, The 18th International DAAAM Symposium "Intelligent Manufacturing & Automation: Focus on Creativity, Responsibility and Ethics of Engineers", 24-27th October 2007, University of Zadar, Zadar, Croatia (ISI Proceeding), pag. 415-416.

[11] Merlet, J-P., The Parallel Robots, Kluwer Academic Publ., The Netherland, 2000.

[12] Craig, J., Robotics, Mechanics and Control, Addison-Wesley Publishing Company, USA, 1995.

[13] Isermann, R., Mechatronic Systems, Fundamentals, Springer, Londra, Anglia, 2005.

Application of Membrane Filtration for Reuse of Bleaching Plant Effluent in the Process

SUDHEER KUMAR SHUKLA, VIVEK KUMAR, M. C. BANSAL
Department of Paper Technology, Indian Institute of Technology Roorkee, Saharanpur Campus,
Saharanpur-247001(INDIA) Phone +91-132-2714003, Fax +91-132-2714011
E-mail: sudheertejasvee@yahoo.co.in, shuklasudheer@rediffmail.com

Abstract:

Membrane filtration technology is being adopted increasingly in the paper mills for closing of process water streams. E- Stage bleaching effluent is very well suited for ultrafiltration process because of its comparatively small volume and high molecular –weight –substances in it. In the present study extraction stage (E- stage) bleach plant effluent of an integrated paper mill employing CEH bleaching sequence for bleaching of hardwood pulp was treated in the Ultrafiltration (UF), Nanofiltration (NF) and Reverse osmosis (RO) in series. Concentrate of each stage is recycled back and permeate of ultrafiltration is fed to nanofiltration, and permeate of nanofiltration is fed to RO. Molecular weight cut-of (MWCO) were 1000, 300 and 50 Dalton, for UF, NF and RO respectively. Initial inlet pressure was 6.8 bar for UF, NF and 10.3 bar for RO. All membranes performed well as per expectation and water recovery was 86.4 %, 95.28 % and 95.95 % for UF, NF and RO membrane respectively.

Key Words: Membrane Filtration; E-stage Effluent; System Closure, Bleaching plant Effluent

1. Introduction:

The water processed in pulp and paper industries cannot be recycled, because some of its components are enriched, causing either direct or indirect problems. Slime and deposit formations, which affect the paper quality, are some of these problems. Therefore, specific purification technologies are required (J. Nuortila-Jokinen, M. Nyström, 1996). Membrane filtration is being adopted increasingly in the paper mills for closing their mill process water. Application of membrane technology is one such option which can improve the recycled water quality by removal of heavy metal contaminates, COD, TDS, AOX (Adsorbable organic halides) and color.

This shall reduce the load on conventional recovery evaporation system with no significant loss of inorganic compounds.

E- Stage effluent is very well suited for ultrafiltration process because of its comparatively small volume and high molecular –weight –substances in it. Some extensive work has been done in removal of impurities from E- stage effluent through membrane filtration. Lundahl H. et. al. (1980) found total removal of color 90%, 40%, reduction in COD, and 10% reduction in BOD_7. M. Nystrijm et. al (1988) observed that sufficient chlorolignin removal can be achieved if ultrafiltration is carried out at pH 10, which is approximately the pH of the first caustic stage in the bleach process.

Jansson, A. S. (1987, 1989) observed that ultrafiltration of plant E- stage effluent contribute can reduce TOCl (Total organic chlorides) by 60-80%, COD by 50-80%, AOX (absorbable organic halides) by 90%, color by 90%, BOD_7 by 25-50%. Rosa et. al. (1995) studied color removal experiment of E-stage effluent through ultrafiltration, and found 85% color removal efficiency by the ultrafiltration with a thin- film composite (TFC) membrane of 10.8 kDa, while total color removal was achieved using a TFC Nanofiltration membrane of poly (transe-2,5-dimethyl) piperazinthiofurazanamide. Richard Greaves (1999) achieved 50% reduction in COD in oxygen bleaching by ultrafiltration in the pilot scale study. De Pinho M.N. et. al (2000) carried out flotation / ultrafiltration experiments to treat E_1 stage effluent and achieved the removal efficiencies in terms of conductivity, TOC, color, TSS, 40%, 65%, 90%, and 100% respectively. Fredrik Filth, et. al. (2001) found that the retention of the substances causing the COD is approximately 40%. Dube et al. (2000) reported that 88% and 89% removal of BOD, and COD, respectively was achieved by reverse osmosis (RO). Merrill et al. (2001) stated that membrane filtration (MF), and granular membrane filtration (GMF) was suitable for removing heavy metals from the pulp and paper mill wastewaters.

In the present study E- stage bleach plant effluent was treated in the Ultrafiltration (UF), Nanofiltration (NF) and Reverse osmosis (RO). The extraction -stage bleaching plant effluent was taken from an integrated paper mill. The CEH sequence is being used for bleaching of hardwood pulp. Spiral wound membranes were used for the purpose, total membrane area is 2.51 m^2 membrane material is polysulphone for UF, NF and polyamide used in RO. The molecular weight cut-off (MWCO) is 1000 Dalton for UF, 300 Dalton for NF, and 50 Dalton for RO.

2. Material and Methods:

In the present study extraction- stage bleaching effluent was taken from an integrated paper mill employing conventional CEH sequence for bleaching of hardwood pulp Effluent was treated in a system consisting of Ultrafiltration (UF), Nanofiltration (NF) and Reverse osmosis (RO) membrane modules in series, specifications are given in Table 1. Before introducing the effluent to the ultrafiltration membrane, some primary treatments were applied as coagulation, bag filtration and microfiltration. Scheme of the treatment is given in Fig.1.

2.1 Pre treatment:

In most cases when membrane filtration is used it cannot be used without some kind of pretreatment of the feed. The reason is that the feed channels in the modules get blocked in most types of elements. Especially spiral modules are very sensitive to this type of blocking. In order to avoid this different types of pretreatments or pre-filters have to be used, (Cactus 1, 1998-2000). To minimize blocking of pores following pretreatment were applied before feed to UF.

2.1.1 Coagulation:

Coagulation and flocculation is normally employed in the tertiary treatment in the case of pulp and paper mill wastewater treatment and not commonly adopted in the primary treatment. Tong et al. (1999) and Ganjidoust et al. (1997) carried out a comparative study of horseradish peroxide (chitosan) and other coagulants such as ($Al_2(SO_4)_3$), hexamethylene diamine epichlorohydrin polycondensate (HE), polyethyleneimine (PEI), to remove adsorbable organic halides (AOX), total organic carbon (TOC), and color. The authors indicated that modified chitosan was far more effective in removing these pollutants than other coagulants**.** Dilek and Gokcay (1994) reported 96% removal of COD from the paper machine, 50% from the pulping, and 20% for bleaching effluents by using alum as a coagulant. For the purpose 0.5 g/l coagulant ASCP (Trade name, procured from Aastropure, electrosystems Pvt. Ltd. Naroda, Ahmedabad INDIA) was used and retention time given was 20 minutes. After the settling of solids for 20 minutes, effluent was fed to bag filtration and micro filtration.

2.1.2 Anti scaling agents:

For prevention scale on surface of membranes anti-scalant is used. In the present study 6 ml/100L sodium-hexa-meta-phosphate was used while adding coagulants.

2.1.3 Bag filtration and microfiltration:

The solid particles are harmful to the membrane process. They are removed by the pretreatment screen filters like bow screen, multilayer filter, sand filter, bag filter (MF). After coagulation effluent was passed through bag filter and micro filter. Micro filtered water was collected in a tank and was fed to UF membrane plant.

2.2 Membrane experiments:

Membrane treatment experiments were performed for the similar kind of effluent at room temperature. For ultrafiltration and nanofiltration treatment, initial inlet pressure was 6.8 bar and for reverse osmosis treatment 10.3. Retentate of each experiment was recycled back to the feed and retreated till inlet pressure increased up to the maximum cut-of pressure for each membrane (indicated by the manufacturer). Ultrafiltration permeate was fed to the nanofiltration, and permeate of nanofiltration was again fed to the reverse osmosis as shown in Fig 1.

2.3 Water quality assessment:

Feed wastewater samples, the retentate samples and the permeate samples of the UF, NF and RO were collected in clean and dry canisters. All samples were analyzed for their ionic content (pH, Conductivity), total dissolved solids (TDS), total suspended solids (TSS), chemical oxygen demand (COD, Hach reactor**,** dichromate oxidation method), Color (Hach DR/4000) and adsorbable organic halides (AOX analyzer ECS 1200 using column method).

2.4 Membrane performance assessment:

Performance of each membrane was assessed with time for each initial inlet pressure on the basis of variation in the three parameters namely, trans-membrane pressure (Eq.no1), permeate flux (Eq.no2).

Trans-membrane pressure in (bar) = Pi + Po/2 - Pp (1)

Where Pi is inlet pressure, Po is outlet pressure and Pp is permeate pressure

Permeate Flux in (L m^{-2} h^{-1}) = volume of permeate in the given time/ membrane area (2)

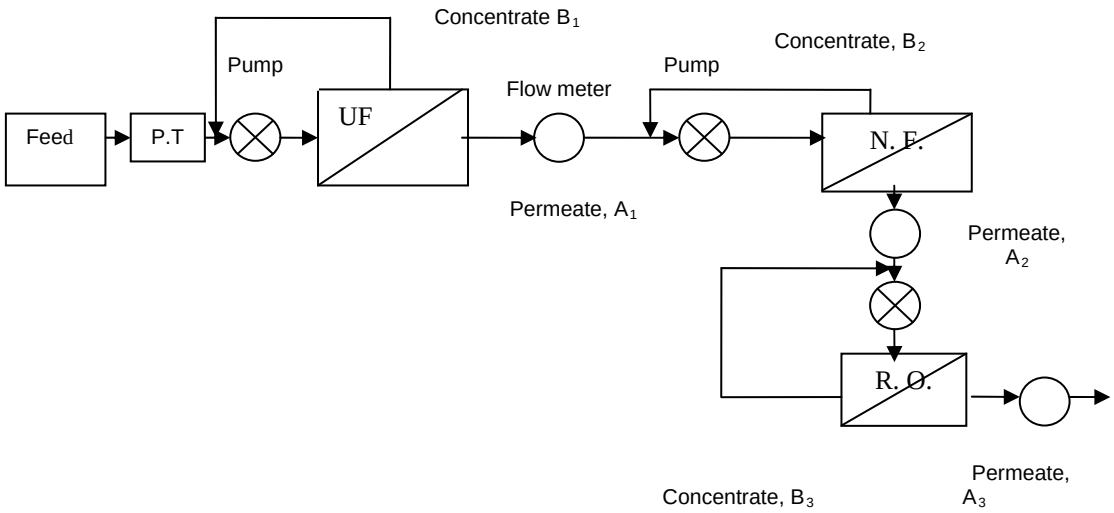

Fig: 1 Scheme of Pilot membrane treatment plant

Abbreviations:
P.T.: primary treatment unit, UF: ultrafiltration, NF: nanofiltration, RO: reverse osmosis

Table 2 Specifications of the membranes used in the study

Module	Membrane	Membrane material	MWCO	Area (m^2)	Manufacturer
UF, spiral bound	AP-01	Thin film polyamide/ polysulphone blend	1000 Da	2.51	Aastropure, India
NF, spiral bound	AP-02	Thin film polyamide/ Polysulphone blend	300 Da	2.51	Aastropure, India
RO, spiral bound	AP-03	Thin film Polyamide	50 Da	2.51	Aastropure, India

3. Result and Discussion:

3.1. Pollutants removal:

It can be seen from the figure: 2 that COD and color removal from the ultrafiltration is 50% and 84.34% respectively and 86.85% TSS removal was observed which are very good. TDS removal was just 40.05% which may be due to the fact that ultrafiltration removes high fraction. The color importing high molecular weight dissolved organic compounds. AOX removal was 38.62% observed.

It can be seen from the figure: 3 that COD and color removal after the nanofiltration is 77.1% and 96.79% respectively. 95.7% TSS removal was observed, TDS removal was also 70.83 %. AOX removal was 88.94%. The color removal is very high and permeates seams literally colorless.

It can be seen from the figure: 4 that TDS and AOX removal after the reverse osmosis were 99.77% and 98.51% respectively, which is excellent. All other pollutants like TSS, COD and Color removal was found to be 100%. Permeate seems transparent after the treatment, and it can be recycled at adequate point.

3.2 Membrane performance:

During the course of study it was found that TMP increases slowly for each membrane (Fig; 5, 6, 7). In the RO TMP was found more stable than UF and NF at this particular initial inlet pressure. TMP in the membranes shows linear pattern. Permeate flux decreases rapidly in UF treatment and shows linear pattern, in the NF membrane, initially permeate flux was stable, which slowly decreases later, it also shows linear pattern. As far as RO membrane is concerned permeate flux is almost stable initially but after some time of run rapid decrease was observed, and shows polynomial pattern. As retentate is being recycled and mixed to the feed so it increases the trance – membrane pressure, and due to

concentration polarization decline in permeate was observed for each membrane.

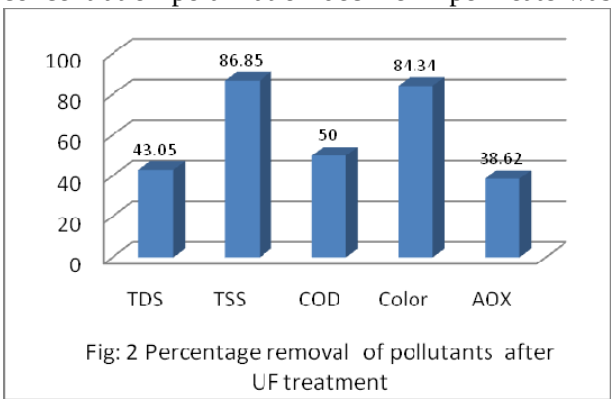

Fig: 2 Percentage removal of pollutants after UF treatment

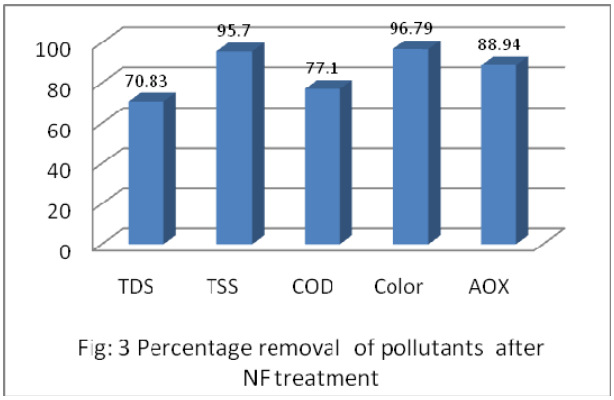

Fig: 3 Percentage removal of pollutants after NF treatment

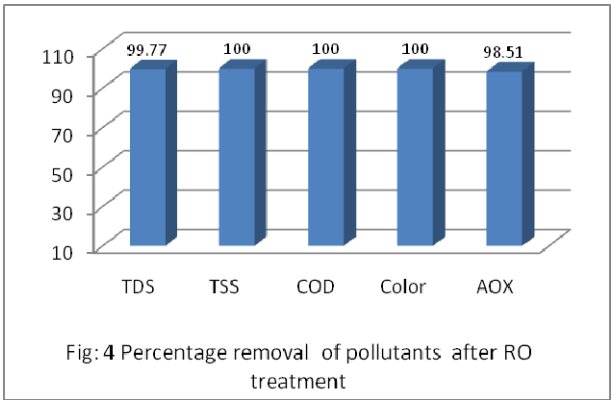

Fig: 4 Percentage removal of pollutants after RO treatment

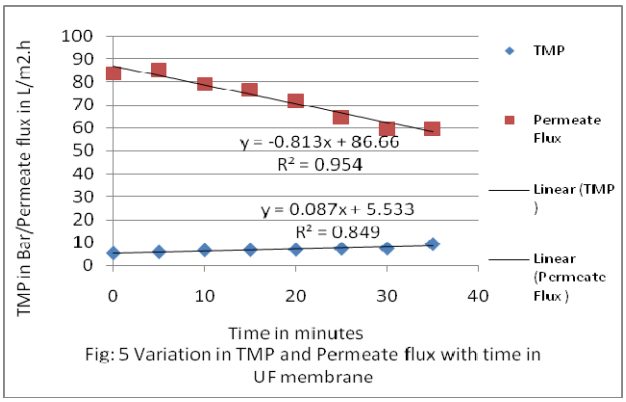

Fig: 5 Variation in TMP and Permeate flux with time in UF membrane

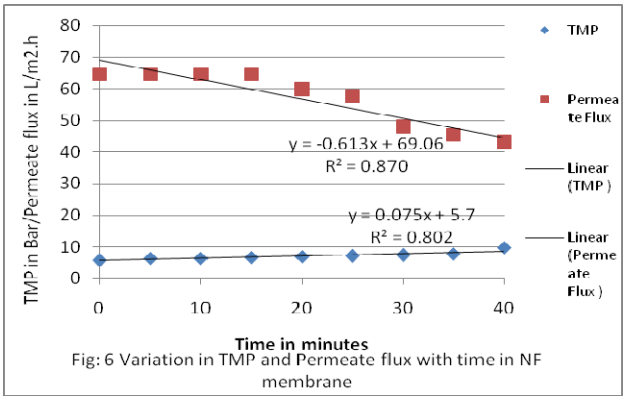

Fig: 6 Variation in TMP and Permeate flux with time in NF membrane

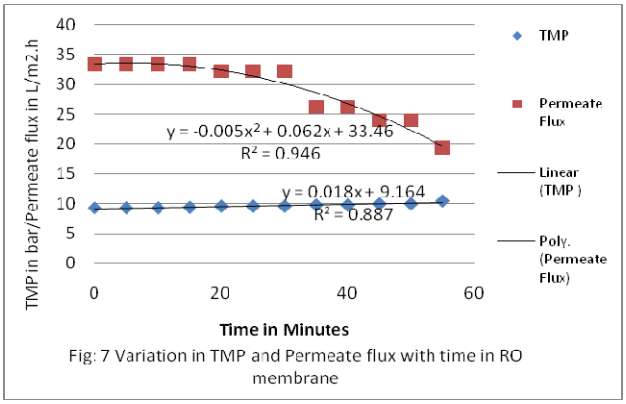

Fig: 7 Variation in TMP and Permeate flux with time in RO membrane

4. Conclusion:

During the course of study removal efficiency of UF, removal of COD, TSS and color was 50%, 86.85% and 84.34% respectively. TDS and AOX removal is not very good in that particular treatment. After NF treatment COD, TSS and color removal was 77.1%, 95.7% and 96.79% respectively. TDS removal was also 70.83 %. AOX removal was 88.94%. Nanofiltration has smaller pore size than UF that is 300 Da make it more efficient for removal of TDS and AOX. Whereas after RO treatment TDS and AOX removal was 99.77% and 98.51% respectively, that can be said excellent. All other pollutants like TSS, COD and Color removal was found to be 100%. TMP in the all studied membranes was found almost stable. Slow decrease in permeate flux was observed at 6.8 bar initial inlet pressure for UF and NF and at 10.3 bar initial inlet pressure for RO. As for as reusability of E- stage treated water is concern membrane treatment is best available process, one hand it removes organic matters like COD and AOX and other hand it removes solid like TDS and TSS significantly. After the treatment water recovery was 86.4 % for UF 95.28 % for NF and 95.95 % for RO membrane respectively. Permeate seems transparent after the treatment, and it can be recycled at adequate point.

Reference:

1. Cactus1, "The influence of pretreatment on membrane processes in pulp and paper process water purification" Marianne Nystrom, Jutta-Jokien, Mika Manttari, Samantha Patt, Tina Huuhilo, Pasi Vaisanen, Liisa Puro, Pekka Olin, Helvi Turka, Laboratory of Membrane Technology and Technical Polymer Chemistry, LUT, 1998-2000.
2. De Pinho M.N, Minhlma M., Rosa .M.J. and Taborda F., "Integration of flotation/ultrafiltration for treatment of bleached pulp effluent" Pulp and Paper Canada, (2000)101:4, p.50-54
3. Dilek FB, Gokcay CF. "Treatment of effluents from hemp-based pulp and paper industry: waste characterization and physicochemical treatability" Water Sci Technol (1994)29(9):161– 3.
4. Dube M, McLean R, MacLatchy D, Savage P. "Reverse osmosis treatment: effects on effluent quality" Pulp Pap Can (2000)101(8):42– 5.
5. Filth Fredrik, Ann-Sofi J & won, Roland Wimmerstedt "Ultrafiltration of effluents from chlorine-free, Kraft pulp bleach plants" Desalination 133 (2001) 155-165
6. Ganjidoust H, Tatsumi K, Yamagishi T, Gholian RN. "Effect of synthetic and natural coagulant on lignin removal from pulp and paper waste water" Water Sci Technol (1997) 35(2– 3):291– 6.
7. Jonsson A.S. "Treatment of bleach plant effluent" Nordic pulp and paper Res. J. (1987) 2(1):23.
8. Jonsson A.S. "Treatment of effluent from alkali extraction with ultrafiltration and reverse osmosis" Nordic pulp and paper Res. J., (1989) 4(1) 33.
9. J. Nuortila-Jokinen, M. Nyström, Comparison of membrane separation processes in the internal purification of paper mill water, J. Membr. Sci. 119 (1996) 99–115.
10. Lundahl H. and Inge Mansson "Ultrafiltration for removing color from bleach plant effluent" TAPPI, 63(1980) (4):97.
11. M. Nystrijm and M. Lindstrij "Optimal removal of chlorolignin by ultrafiltration achieved by pH control" Desalination, 70 (1988)145-156
12. Merrill DT, Maltby CV, Kahmark K, Gerhardt M, Melecer H. "Evaluating treatment process to reduce metals concentrations in pulp and paper mill wastewaters to extremely low values" Tappi J (2001)84(4):52.
13. Richard Greaves. "The use of ultrafiltration for COD reduction in pulp mill effluent" TAPPI International environmental conference proceedings (1999).p.1167.
14. Rosa, M.J., De Pinho, M.N. "The role of ultrafiltration and nanofiltration on the minimization of the environmental impact of bleached pulp effluent" Journal of membrane science (1995)102:155.
15. Tong Z, Wada S, Takao Y, Yamagishi T, Hiroyasu I, Tamatsu K, "Treatment of bleaching wastewater from pulp-paper plants in China using enzymes and coagulants" J Environ Sci (1999) 11(4):480–4.

How a horizontal surface is traced

PETR VANICEK
Department of Geodesy and Geomatic Engineering,
University of New Brunswick,
Fredericton, NB,
CANADA
vanicek@unb.ca

Abstract: - What is a horizontal surface and who needs it? Whoever is determining or using heights uses it, implicitly or explicitly: one particular horizontal surface, the geoid, is the reference surface for heights, the "heights above the sea level". These heights are used exclusively in engineering practice as well as in other applications. A horizontal surface is realized, more or less, by a surface of a water body, but how about dry land; what is needed for tracing a horizontal surface on land? What is needed, are gravity data observed on the surface of the earth, earth topography, some idea about topo-density, some idea about long-wavelength features of gravity field (derived from satellite tracking), and a conventional reference system with respect to which the tracing and the display should be done. The tracing is done through solving a non-linear boundary value problem for gravity potential with the boundary (the geoid) being itself a function of the potential. The solution is obtained by finite element or finite difference techniques, after transforming the boundary value problem into Green's form. The solution uses a vast amount of data irregularly distributed on the surface of the earth.

Keywords: - level surface, gravitation, gravity, geoid, reference surface, topography, disturbing potential, normal potential, gravity anomaly, Poisson's upward continuation,

1 Introduction

What is a **Horizontal surface**? Who needs a horizontal (level) surface and why should anyone be interested in determining a horizontal (level) surface? And how do we go about determining a horizontal surface anyway?

A surface is horizontal when fluid on the surface does not flow anywhere, when the fluid is in equilibrium. In the terminology of physics, a horizontal surface on the Earth is a surface of equal gravitational potential. Since the Earth is spinning around its instantaneous spin axis, the gravitational force is not the only force acting on the fluid: we have to consider also the centrifugal force caused by the Earth spin. The sum of these two forces is called gravity force. In fact, any of these three forces depends linearly on the mass of the physical body we use to measure the force with. It is thus more simple and more convenient, to work with the kinematic equivalent of a force, i.e., with acceleration. We can thus say that a horizontal surface on the spinning Earth is an equipotential surface of gravity potential *W*, where the term "gravity" stands for "gravity acceleration". In fact, we have to consider other time varying forces such as the tidal force.

There exist infinitely many horizontal surfaces that satisfy the above definition. There is one particular horizontal surface, however, which is of the utmost importance in geodesy (for the definition of "geodesy" see, for example [Vanicek and Krakiwsky, 1986]), the horizontal surface that represents the mean sea level globally. This particular horizontal surface is known as the geoid [Listing, 1873] and it is so important because it is the reference surface for all practical heights, heights used in engineering, surveying and mapping practice. These heights are used exclusively in practice and anyone who needs them should be aware of how they are defined, cf., [Vanicek and Krakiwsky, 1986]. They are known, popularly, as "heights above the sea level". In fact, they should be called "*H*, the heights above the geoid".

Geoid is thus the equipotential surface

$$W(\Omega) = const. = W_0 \qquad (1)$$

of gravity potential W that best represents the mean sea level globally; it is however not coincident with the mean sea level. The symbol Ω in Eq.(1) stands for geocentric direction. Actual mean sea level departs from the geoid by at most 1.5 metres in each direction due to the fact that sea water is not homogeneous: it has different density at different places, in different geocentric directions Ω. The departures of mean sea level from the geoid are called the sea surface topography (SST) [Montgomery, 1937-38].

If we could have a look at the shape of the geoid globally, it would resemble a somewhat smooth potato, oblate (flattened) in the direction of the spin axis of the earth. Regionally, the geoid is again bumpy, yet with the curvature being everywhere positive: there are no valleys and depressions in its surface, only patches of larger or smaller convection.

While it is easy to visualize the geoid over the ocean, it is rather difficult to trace the geoid on, or rather under the dry land, under the topography. It cannot be measured (observed) and has to be derived indirectly using mathematical tools. As the geoid is a uniquely defined equipotential surface of the actual gravity potential, it would seem to suffice to compute the actual gravity potential everywhere within topography and connect all the points of the required potential W_0. But how can we compute the actual gravity potential under and in topography? We cannot, unless we knew the exact value of mass density σ within the Earth.

2 Setting up the boundary value problem

The closest observable thing to gravity potential is gravity (acceleration) $g(\Omega, H)$. It can and is observed (measured) by gravimeters on the surface of the earth, at sea ($H(\Omega) \sim 0$), in space by monitoring the motion of satellites, and at some places within topography (in wells, mines, tunnels, etc.) again using gravimeters. If we knew gravity at all the "required" points on the geoid, then we can formulate a boundary value problem (with the geoid as the boundary) for resolving the gravity potential $W(\Omega, H)$ on and above the geoid, i.e., for $\forall\Omega$, and $H \geq 0$.

The most obvious partial differential equation to use (easiest to solve) in the geodetic boundary value problem is the Poisson potential equation [Kellog, 1929]

$$\nabla^2 W(\Omega, H) = -4\pi G\rho(\Omega, H) + 2\omega^2 , \qquad (2)$$

where G is the Newtonian gravitational constant and ω is the angular spin velocity of the Earth, i.e., one revolution per sidereal day. Here, the mass density ρ is that of topographical masses (masses between the surface of the Earth and the geoid) and the Earth atmosphere. The rest of the masses in the universe do not contribute to the Earth gravitation.

The Poisson equation can be transformed to a much simpler Laplace (homogeneous) equation by working with an Earth's model that is not spinning and is stripped of the topography and atmosphere. This model has the mass density ρ above the geoid equal to 0 everywhere above the geoid and the spin velocity ω is equal to 0 everywhere.

At the same time the problem can be reduced numerically, to work with a potential that is several orders of magnitude smaller, the disturbing potential T. The disturbing potential is defined as follows:

$$T(\Omega, H) = W(\Omega, H) - U(\Omega, H) , \qquad (3)$$

where $U(\Omega,H)$ is the potential of a spinning reference ellipsoid called normal potential.

The stripping of topography is best done [Vanicek and Martinec, 1994] by condensing the topography onto an infinitesimal layer on the geoid: in the first step the measured gravity values are reduced by the attraction of topography (and the atmosphere, which is much smaller and we shall not discuss it here) then increased again by the attraction of the condensed topography (and atmosphere) as follows

$$\frac{\partial W^H(\Omega, H)}{\partial H} = \frac{\partial W(\Omega, H)}{\partial H} - \frac{\partial W^t(\Omega, H)}{\partial H} + \frac{\partial W^{ct}(\Omega, H)}{\partial H} , \qquad (4)$$

where W^t is the gravitational potential of the topography and W^{ct} is the potential of the condensed topography. This particular model of the Earth is known as the Helmert model [Helmert, 1884] and the disturbing potential that uses this model is called the Helmert disturbing potential T^H [Vanicek and Martinec, 1994]

$$T^H(\Omega, H) = W^H(\Omega, H) - U(\Omega, H) . \qquad (5)$$

Note that the subscript *H* has nothing to do with height *H* above the geoid. There are other scenarios used in geodesy, but the author believes that the here described strategy is the best.

3 Derivation of boundary values

Helmert's disturbing potential obeys the Laplace equation and is thus harmonic everywhere above the geoid

$$\forall (H > 0 \vee r > R): \quad \nabla^2 T^H(\Omega, H) = 0 \qquad (6)$$

and also [Martinec, 1998]

$$\forall (H \vee r \to \infty): T^H = \frac{c}{r} + O\left(\frac{1}{r^3}\right). \qquad (7)$$

Now, the gravity anomaly Δg is defined as follows [Vanicek and Krakiwsky, 1986]

$$\Delta g(\Omega, H) = grad\, W(\Omega, H) - grad\, U(\Omega, h) = \\ = grad\, W(\Omega, H) - \gamma(\Omega, h) \qquad ,(8)$$

where γ is the normal gravity and h is the height H above the geoid augmented by the height N of the geoid above the reference ellipsoid

$$h(\Omega) = H(\Omega) + N(\Omega). \qquad (9)$$

Thus h can be regarded as height above the reference ellipsoid, known as geodetic height (called incorrectly ellipsoidal height by some people). Helmert's gravity anomaly Δg^H is given by a formula identical to Eq.(8), except that the actual potential W is replaced by Helmert's potential W^H. We can thus write

$$\Delta g^H(\Omega, H) = \Delta g(\Omega, H) - grad\, W^t \\ + grad\, W^{ct} = \Delta g(\Omega, H) + \delta A(\Omega, H) \qquad ,(10)$$

where the small gravitation effect of the atmosphere is, once more, left out.

Here, the *grad W* can be observed by a gravimeter and the rest of the terms, $\gamma + \delta A$, have to be evaluated mathematically from normal potential and the digital model of topography *H*. The formula for δA, Helmert's direct topographical effect on gravity anomaly, is given by the following expression

$$\delta A(\Omega, H) = G \iint_{\Omega' \in \Omega_0} \frac{\partial}{\partial r} \left[\int_{r'=R}^{r+H'} \rho(\Omega', H') \frac{r'^2}{L(r, \psi, r')} dr' - \right. \\ \left. - \frac{\partial}{\partial r} \int_{r'=R}^{r+H} \rho_{ct}(\Omega) \frac{r'^2}{L(r, \psi, r')} dr' \right] \qquad (11)$$

where $L(r, \psi, r')$ is the distance between the point of interest (Ω, r) and the dummy point (Ω', r') and $\rho_{ct}(\Omega)$ is the density of the condensation layer on the geoid.

Helmert's anomaly on the Earth surface can also be written as

$$\Delta g^H(\Omega, H) - \varepsilon_h[T^H(\Omega, H)] - \varepsilon_\gamma[T^H(\Omega, H = 0)] = \\ = \Delta g^H *(\Omega, H) \\ = -\left.\frac{\partial T^H(\Omega, r)}{\partial r}\right|_{r=r_e} - \frac{2}{r} T^H(\Omega, H = 0) - \varepsilon_h - \varepsilon_\gamma \qquad (12)$$

where ε_h and ε_γ are called ellipsoidal corrections and r_e is the geocentric radius of the reference ellipsoid mentioned above [Martinec, 1998]. The modified Helmert's gravity anomaly Δg^H* is given as a linear combination of Helmert's disturbing potential with Helmert's "disturbing acceleration". It can be used as a boundary value on the boundary (the geoid) and the triplet of equations, (6), (7) and (12) define uniquely the BVP of third kind that we have been trying to formulate. Well, not quite: Eq.(12) is valid on the surface of the Earth, while we need to know this linear combination on the geoid. The last step is then the derivation of the values of the linear combination on the geoid.

As T^H is harmonic everywhere above the geoid, the linear combination we wish to investigate is also harmonic when multiplied by *r* [Heiskanen and Moritz, 1967]. Hence $r\Delta g$* can be continued downward from the surface of the Earth to the geoid using Poisson's upward continuation [Kellog, 1929]:

$$\Delta g^H *(\Omega, H) = \frac{R}{4\pi(R+H)} \iint_{\Omega' \in \Omega_0} K(R+H, \psi, R) \times \\ \times \Delta g^H *(\Omega', H = 0) d\Omega' \qquad (13)$$

where the Poisson kernel is given by

$$K(R+H,\psi,R) = \\ = \sum_{n=0}^{\infty}(2n+1)\left(\frac{R}{R+H}\right)^{n+1} P_n(\cos\psi) . \qquad (14)$$

For the downward continuation, the integral equation (13) has to be solved for $\Delta g^*(\Omega,H=0)$ on the geoid.

We note that the boundary values $\Delta g^*(\Omega,H=0)$ are themselves functions of the unknown potential T^H which is present in the ellipsoidal corrections ε_h and ε_γ. As these corrections and thus the non-linearity of the BVP are very small, the present knowledge of T^H is good enough to guarantee sufficient accuracy already with the first iteration.

4 solution to the bvp

Laplace's equation (6) is a more simple equation to solve than Eq.(2). Its solution was first conceived by Sir Gabriel Stokes [1849], for a spherical boundary of radius R, with boundary values consisting of gravity anomalies Δg. Stokes's solution is of Green's kind in the form of a convolution integral (over the boundary) of the boundary values with Stokes's integration kernel:

$$\forall\Omega \wedge \forall r - R > 0: \quad T^H(\Omega, H=0) = \\ = \frac{R}{4\pi} \iint_{\Omega'\in\Omega_0} \Delta g^H{}^*(\Omega') S[\psi(\Omega,\Omega')] d\Omega'' \qquad (15)$$

where r is the geocentric distance of the point of interest $(\Omega,H) \equiv (\Omega,r)$, S is the Stokes (isotropic) kernel and ψ is the geocentric angular distance between the point of interest Ω and the dummy point Ω' in the integration. The formula for Stokes's kernel reads

$$S(\psi) = \sum_{n=1}^{\infty} \frac{2n+1}{n-1} P_n(\cos\psi) = \\ = 1 + \frac{1}{\sin\frac{\psi}{2}} - 6\sin\frac{\psi}{2} - 5\cos\psi - 3\cos\psi\ln(\sin\tfrac{\psi}{2} + \sin^2\tfrac{\psi}{2}) \\ . \qquad (16)$$

Now, the boundary values Δg^H * are reckoned to be on the geoid, i.e., at points of H = 0. In addition to that, for the purpose of the integration, the geoid is approximated by a sphere of radius R, the mean radius of the Earth. To reduce the effect of this spherical approximation, we reformulate the BVP on a reference spheroid (sphere-like body) of a specific order, considered known by definition. The best choice, in our opinion, is the low order part of the geoid as determined from satellite orbit analysis, perhaps augmented by the information from one or several of the modern satellite gravity missions, e.g., GRACE. The low order P (think for example of an order of 20) expression for the Helmert disturbing potential

$$\forall\Omega \in \Omega_0 : T_\ell{}^H(\Omega, H) = T_\ell{}^H(\Omega, r_t) = \\ = \frac{GM}{R} \sum_{n=0}^{\ell} \left(\frac{R}{r_t}\right)^{n+1} \sum_{m=-n}^{n} A_{nm}(T^H, R) Y_{nm}(\Omega) \qquad ,(17)$$

where M is the mass of the Earth, $r_t(\Omega)$ is the geocentric radius of topography and A_{nm} are the satellite derived disturbing potential coefficients. This expression can be easily converted to the low order part of the geoid by means of Bruns's formula [Bruns, 1878]

$$N(\Omega, r) \approx \frac{T(\Omega, r)}{\gamma(\Omega, r)} . \qquad (18)$$

We then have, in particular,

$$\forall\Omega \in \Omega_0 : N_\ell{}^H(\Omega, H=0) = \\ = \frac{GM}{R\gamma(\Omega, r_g)} \sum_{n=0}^{\ell} \left(\frac{R}{r_g}\right)^{n+1} \sum_{m=-n}^{n} A_{nm}(T^H, R) Y_{nm}(\Omega) \\ , \qquad (19)$$

where the symbol $N_P{}^H$ stands for Helmert's geoid, usually called Helmert's co-geoid, of order P. This is then used as the reference spheroid, which is the boundary for the reformulated BVP.

The Stokes solution of the reformulated BVP is of the same form as Eq.(15) except that the gravity anomaly is referred to the reference field of order P so that it becomes $[\delta\Delta g^\ell]^H(\Omega)$ [Vaníček and Sjöberg, 1991]:

$$[\delta\Delta g^\ell]^H(\Omega) = \Delta g^H(\Omega) - \Delta g_\ell{}^H(\Omega) , \qquad (20)$$

where $\Delta g_\ell{}^H(\Omega)$ is the reference field of order P. Similarly, the Stokes kernel retains only the higher order components to become [*ibid.*]

$$S^{\ell}(\psi) = \sum_{n=\ell+1}^{\infty} \frac{2n+1}{n-1} P_n(\cos\psi) = \\ = S(\psi) - \sum_{n=0}^{\ell} \frac{2n+1}{n-1} P_n(\cos\psi) \quad . \qquad (21)$$

It is interesting to note that the higher the order of the reference field the closer the modified Stokes kernel comes to a Dirac distribution.

The result of the Stokes integration is, of course, $[\delta T^{\ell}]^H$ which can be transformed, by means of Eq.(18) to the Helmert co-geoid height above the reference spheroid

$$[\delta N^{\ell}]^H(\Omega, H=0) = \frac{[\delta T^{\ell}]^H(\Omega, H=0)}{\gamma(\Omega, H=0)} . \qquad (22)$$

This residual co-geoidal height is then added to the reference spheroid (Eq.(19)) to get the complete co-geoidal height N^H above the reference ellipsoid. A simple correction, called Primary Indirect Topographical Effect [Martinec and Vaníček, 1994] is then added to N^H to give us the final geoidal height above the reference ellipsoid. Its magnitude is at most a couple of decimetres.

5 Numerical evaluation

The numerical evaluation consists of the evaluation of several 2D integrals, these shown in this paper and some others. The "data" we are talking about here are the gravity anomalies, heights of topography (Digital Terrain Model, DTM) and mass density of topography. For different reasons, the rules for collecting these data vary among the kinds of data: for instance, while it is generally easy to get a DTM on a relatively dense regular grid (DTMs on a one arcsec geographical grid are not uncommon), it would be prohibitively expensive to do the same for gravity anomalies and it would be outright foolish to require the same data coverage for the topo-density. Fortunately, the gravity anomaly field is quite smooth, compared to topography and as far as topo-density effect is concerned, it is quite small (see below), so much sparser coverage is still enough to give us the required accuracy of the resulting geoid.

There are some very important issues involved in the data collection and preparation. First and foremost there is the question as to whether we should collect point values or mean values (in the integral sense)

$$\mu(x) = \mathrm{A}^{-1} \iint_{\Omega' \in \mathrm{A}} x(\Omega') d\Omega' , \qquad (23)$$

where A is the area for which we seek the mean value? Clearly, for the evaluation of an integral it is much easier to use mean values in the form of finite elements. Point values have to be used with the scheme of finite differences, which is always somewhat tricky. In some cases it is not even clear if the collected data are point values or mean values. Fortunately, however, the difference between the two gets obliterated with regularly decreasing separation between adjacent points.

Should the data be collected in a haphazard way or should it be collected on a regular geographical grid? In the nature, it is very difficult, if not impossible, to collect observations on a regular (we speak typically of rectangular) grid. That can be done easily when data are prepared with an office instrument, as a DTM generally is. Data collected in nature reflect the vagaries of morphology: gravity is measured by highways and railways, where the access is relatively easy, and on flat tops of hills and mountains, where helicopter can land easily. Irregularly distributed data can be either used as they lay or they can be gridded; usually the latter.

Averaging and gridding have one thing in common: in both procedures one has to predict values in locations where they have not been observed. It is a *maxim* in approximation theory that using whatever prediction technique one wishes to use, the prediction is always better when the field to be predicted is as smooth as possible. This is quite strictly followed in geodesy when averaging or gridding gravity anomalies. The procedure is done on the smoothest variety of gravity anomaly (i.e., complete spherical Bouguer anomaly) that can be obtained from other varieties by applying a rigorous correction, which is not a function of gravity.

The last point we wish to make here concerns the topo-density introduced above. Topo-density is well known only at a few locations on Earth. Elsewhere, we have to rely on modelling of one kind or another. So far, computations have shown that modelling only the lateral in-homogeneities (as seen on the earth surface) the effect, which is at most a few decimetres, can express the effect to perhaps 5 cm. To get a geoid accurate to one centimetre, would require employing a three-dimensional topo-density model.

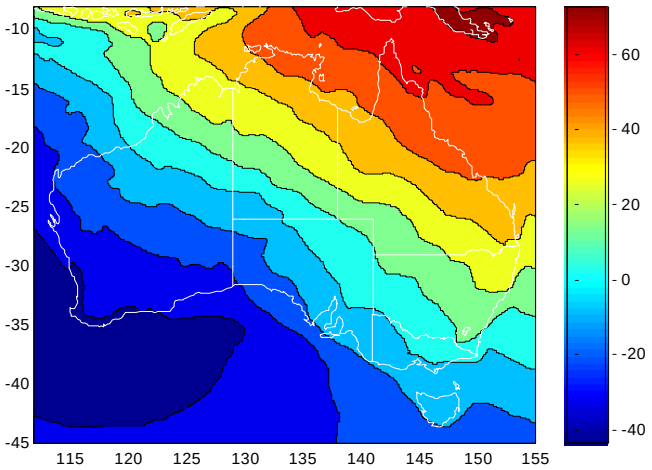

Figure 1 – geoid in Australia

References:

Bruns, H., 1878. *Die Figur der Erde*, Publikacion des Koniglichen Preussischen Geodatischen Institutes, Berlin, Germany.

Heiskanen, W. and H. Moritz, 1967. *Physical Geodesy* , Freeman, San Francisco.

Helmert, F.R.,1884: *Die mathematischen und physikalischen Theorieen der Höheren Geodäsie*. II. Teil: Die physikalischen Theorieen, B.G.Teubner, Leipzig (reprinted 1962 by Minerva GMBH, Frankfurt/Main).

Kellog, O.D., 1929. *Foundations of potential theory*, Springer, Berlin, Heidelberg, New York (reprinted by Dover, New York in 1953).

Listing, J. B., 1873. Ueber unsere jetzige Kenntniss der Gestalt und Grösse der Erde, *Nachrichten von der Königl. Gesellschaft der Wissenschaften und der G. A. Universität zu Göttingen*, No. 3, pp. 33-98.

Martinec, Z., 1998. *Geodetic Boundary Value Problem*, Springer.

Martinec, Z. and P. Vanicek, 1994. The indirect effect of Stokes-Helmert's technique for a spherical approximation of the geoid. *Manuscripta Geodaetica* 19, pp.213-219.

Montgomery, R.B., 1937-38. Fluctuations in monthly sea level on eastern U.S. coast as related to dynamics of western North Atlantic ocean. *J. Mar. Res.*, 1(2), pp. 165-185.

Stokes, G.G., 1849. On the variation of gravity on the surface of the Earth, *Trans. Camb. Phil. Soc.* 8, pp. 672-696.

Vaníček, P. and E.J. Krakiwsky, 1986. *Geodesy: The Concepts.* 2nd rev. ed., North-Holland, Amsterdam.

Vaníček P. and L. Sjöberg, 1991. Reformulation of Stokes's theory for higher than second-degree reference field and modification of integration kernels, *J Geophys Res* 96(B4): pp. 6529-6540.

Vanicek, P. and Z.Martinec, 1994. Stokes-Helmert scheme for the evaluation of a precise geoid *Manuscripta Geodaetica* 19 pp. 119-128.

Author Index